The primary structures and fabrics of the upper mantle and lower oceanic crust from ophiolite complexes

Thesis

The Primary Structures and Fabrics of the Upper Mantle and Lower Oceanic Crust from Ophiolite Complexes.

A thesis presented for the degree of

Doctor of Philosophy

by

Iain Douglas Bartholomew,
B.Sc. Hons., University of Edinburgh, 1980.

Department of Earth Sciences,
The Open University,
December, 1983.

VOL2

-RESTRICTED ACCESS-

I, Iain Douglas Bartholomew, am willing that my thesis be made available to readers, and, subject to the discretion of the Librarian, may be photocopied.

Iain D. Bartholomew

Abstract

The structures and textures of areas from the lower sequences of the Oman Ophiolite, the Troodos Ophiolite, Cyprus, and the Shetland Ophiolite have been studied in order to gain an understanding of the structural and kinematic history of the upper mantle and lowermost oceanic crust at accretionary margins.

In all areas the mantle has similar petrological features. It is composed largely of harzburgite which is often compositionally banded into orthopyroxene-rich and olivine-rich segregation layers. Dunitic sheets and pods are common in some of the areas studied. They are highly variable in size and shape (up to 1½km diameter in Troodos) and some contain concentrations of chromite ore.

The mantle is strongly foliated in all areas, the foliations being defined by the alignment of chrome-spinel and orthopyroxene grains. The foliations cross-cut all the mantle petrological features except for a few late-stage dykes, and in some areas extend into the lowermost crustal cumulates. Lineations are sometimes measurable on the foliation planes. Emplacement of the different ophiolite sequences has caused only localised shearing and brittle faulting, these structures being clearly identifiable from the primary, ocean-spreading related foliations.

In some areas two primary foliations (S1 and S2) are measurable from the same outcrop. A detailed crystallographic and shape fabric analysis shows that they have been formed by two different ductile shearing episodes. (D1 and D2). Both D1 and D2 are essentially simple shearing events. Individual olivine and orthopyroxene crystals deform by a combination of slip along discrete slip planes and by recrystallisation processes. In many

specimens which have undergone D2 deformation, some olivine grains preserve a partially rotated relict D1 crystallographic orientation. Changes in the D2 shear sense form a shear folding pattern of the S1 planes. The shapes and orientations of the petrological features are strongly controlled by the intensity of D1 and D2 shearing.

Both the D1 and D2 shearing events are the remnants of mantle asthenospheric flow at an oceanic spreading centre which have been fossilised into the lithospheric mantle at the asthenosphere-lithosphere boundary. This fossilisation occurs during the off-axis, dominantly horizontal, flow of the asthenosphere. A study of the orientations of the D1 and D2 shearing structures from the different areas shows that they have similar orientations within a single area but that their orientations are highly variable between areas. This can be related to the horizontal flow of mantle material away from diapiric uprise centres along a ridge-axis. The interaction between the diverging flow from an earlier diapiric centre (S1 planes) and those from a later centre (S2 planes) will cause the earlier flow lines to be deformed.

Acknowledgements

This work was funded by the Natural Environment Research Council. I would like to express my thanks to the following individuals for their help and advice during the research and writing of this thesis:

My supervisor, Professor Robert Shackleton, for suggesting this project and for reading the first draft of this thesis.

Members of the EEC Chromite Project, especially Steve Roberts, Flemming G Christiansen and Thierry Auge for many hours of fruitful discussion.

Members of the Open University Oman Ophiolite Project, especially Professor Ian Gass, Steve Lippard, Dave Rothery, Tony Shelton and John Smewing for advice in the field and in the department.

The Department of Petroleum and Minerals, Muscat; specifically Mohammed Kassim, for permission to work in the Sultanate of Oman.

Bob Cheeny (University of Edinburgh) for the use of his computer programme 'Ellipfit' and a large amount of advice, and Nigel Woodcock (Cambridge University) for the use of his computer programme 'Statis'.

Roy Gill, John Dixon and Brian Upton of Edinburgh University for their stimulating discussions.

For accommodation and good fun I would like to thank Mrs Johnson and Gilda of Baltasound Post Office, Unst, Shetland, and Mr Papapeitrou of the Troodos Hotel, Cyprus.

I am indebted to my typists, Carole Fulcher, Debbie Skeats and Frances Thomas for their speed and patience, and also to Helen Boxall, Julia Massey and Alan Stevenson for their hours spent in preparing some of the diagrams. Many thanks also to John Taylor for cartographic advice and Ian Chaplin and Moira Staerck for the rapid production of a large number of thin sections.

Finally, I would like to thank my wife, Mandy, for her support and patience over the last three years, and for extensively editing this thesis, for preparing the references, and helping to draw many of the diagrams.

List of Contents

List of Figures

List of Plates

Chapter 2 The Oman Ophiolite

List of Tables

Chapter 8 Crystal Size and Shape Orientation Studies.

Chapter 9 Kinematic Interpretation for Each of the Areas Studied.

Appendices

List of Enclosures

Chapter 1

Introduction

CONTENTS

1.1 Ophiolites and Oceanic Lithosphere.

The term "ophiolite" was used in geology as far back as 1827 by Brongniart (1827). However, the typical "ophiolite" sequence of the association of serpentines and gabbros with amphibolites and diabases was not defined until 1905 by Steinmann (1905). Before the advent of the theories of plate tectonics an ophiolite was described as "basic and ultrabasic lavas and minor intrusions associated with the infilling of a geosyncline". (Whitten and Brooks, 1972.) Only in the last 30 years have ophiolite complexes been studied and described in detail; it is now widely accepted that such complexes represent remnents of oceanic lithosphere.

In 1972 the G.S.A. Penrose Conference (Anon, 1972) defined an ophiolite as "a distinctive assemblage of mafic to ultramafic rocks", and "in a completely developed ophiolite the rock types occur in the following sequence, starting from the bottom and working up:

1) Ultramafic complex consisting of variable proportions of harzburgite, lherzolite and dunite, usually with a metamorphic tectonic fabric (more or less serpentinized).

2) Gabbroic complex, ordinarily with cumulus textures commonly containing cumulus peridotites and pyroxenites and usually less deformed than the ultramafic complex.

3) Mafic sheeted dyke complex.

4) Mafic volcanic complex, commonly pillowed".

The conference further reported that "an ophiolite may be incomplete, dismembered, or metamorphosed", and that "although an ophiolite is interpreted to be oceanic crust and upper mantle, the use of the term should be independant of its supposed origin".

Hess (1955) first proposed a peridotite-serpentinite model for the oceanic crust; and in 1960 he interpreted the serpentinites of Puerto Rico as uplifted oceanic material (Hess, 1960) and soon afterwards arrived at the concept of sea-floor spreading which was then rapidly developed (Hess, 1962; Dietz, 1961; Gass and Masson Smith, 1963; and Vine and Matthews, 1963). It was proposed that new oceanic crust is created at mid-ocean ridges and spreads laterally. The crust is supplied and driven by convection currents in the mantle below. Gass (1968) developed this theory further, proposing that diverging cells in the mantle would produce crustal tension and thus a mechanism for the intrusion of the sheeted dyke complex. He also suggested a 'riding' of the ocean crust on top of the mantle away from the spreading centre. An alternative hypothesis put forward by McKenzie (1969) was that the tensional forces in the crust are caused by subduction processes and that the crust and upper mantle are pulled by the sinking lithospheric slab.

In recent years the seismic properties of ophiolite complexes have been investigated (Christensen and Smewing, 1981). The seismically distinguished layers closely correspond to the petrological units in the ophiolites. Ophiolitic seismic

velocities have been found to be very similar to those measured from oceanic regions but the layers are often thinner (see Figure 1.1). This is attributed to emplacement of the ophiolites soon after formation, either from back-arc marginal basins or from zones of ocean floor close to the spreading zone. The seismic velocities in ophiolites are slightly lower than in oceanic crust. This has been attributed to hydrothermal metamorphism. (Review in Brown and Mussett, 1981.)

Many ophiolite sequences have now been recognised throughout the world (Reviews in Coleman, 1977, and Gass and Smewing, 1980) and their study has led to a generally accepted oceanic spreading model which was developed by Cann (1974) and more recently by Gass and Smewing (1980). (Figure 1.2.) In this model a two stage process is represented. Firstly, the mantle partially melts and the magma rises to occupy a convecting magma chamber in the ocean crust. Secondly, crystallization in the magma chamber forms the cumulates; this is accompanied by the occasional ejection of magma to the surface. The upper mantle residuum is the harzburgite and dunite.

The oceanic crustal sequence has now been studied in great detail within ophiolite complexes and much more is understood of the processes occurring within it. (Reviews in Hargraves, 1980.) The mantle sequences, however, have been relatively neglected, due mainly to their apparent homogeneity and lack of geological features. Structurally, very little can be seen in the field apart from a prominent pervasive foliation which usually has remarkably constant trends within individual ophiolite complexes.

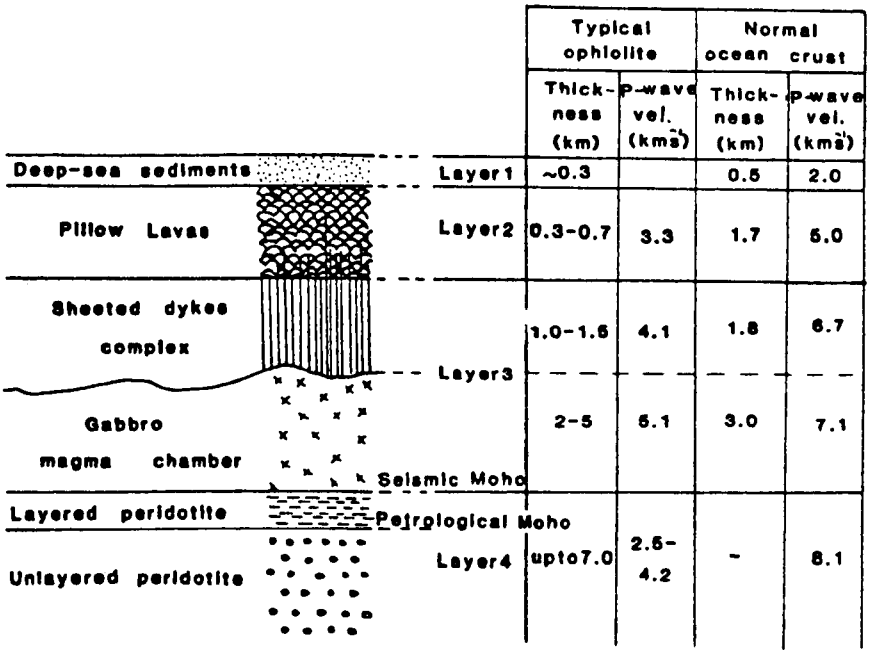

	Typical ophiolite		Normal ocean crust	
	Thick-ness (km)	P-wave vel. (kms⁻¹)	Thick-ness (km)	P-wave vel. (kms⁻¹)
Layer1	~0.3		0.5	2.0
Layer2	0.3-0.7	3.3	1.7	5.0
	1.0-1.5	4.1	1.8	6.7
Layer3				
	2-5	5.1	3.0	7.1
Layer4	upto7.0	2.5-4.2	-	8.1

Figure 1.1 Petrological, seismic and thickness data compared between a typical ophiolite sequence and seismic layers for the ocean crust. (Not to scale). (From Brown and Mussett, 1981).

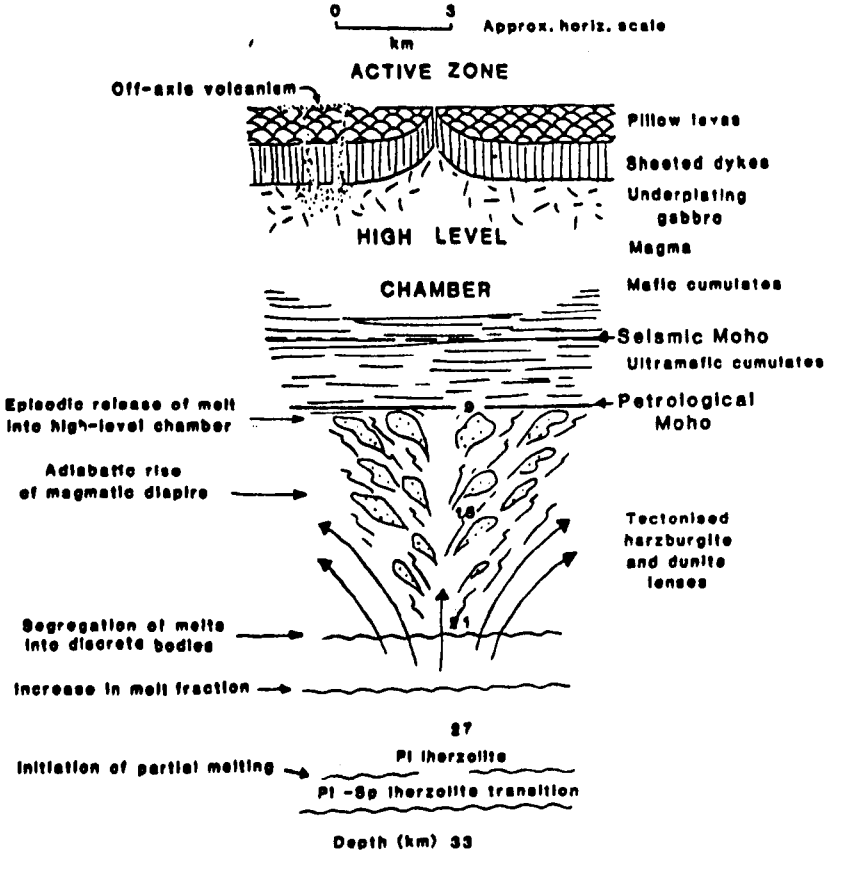

Figure 1.2 A consensus ocean-spreading model. (From Gass, 1980).

1.2 The Ophiolite Mantle and Lower Crustal Sequence - Previous Work.

Only a few mantle and lower crustal ophiolite sequences have been mapped and studied in any detail. These areas include the Bay of Islands Complex, Newfoundland (Malpas, 1977; Girardeau and Nicolas, 1981); the Troodos Massif, Cyprus (George, 1975, 1978; Violette, 1980); the Semail Ophiolite, Oman (Boudier and Coleman, 1981; Smewing, 1979) the Antalya Complex; Turkey (Juteau et al, 1977); the New Caledonian complex (Prinzhoffer et al, 1980); and the Zambales complex, Philippines (Nicolas and Violette, 1982).

The upper part of the ophiolite sequence is absent in the New Caledonian complex due to thrusting during emplacement, and it must therefore be termed a 'dismembered' sequence. However, because of its huge area of over 6,000km^2 and the lack of correlation between the structural trends within the sequence and those in the surrounding areas, it can be assumed to have been relatively undeformed by obduction processes. All the other ophiolites mentioned are complete.

It is striking that most features recorded in the field are common to all the complexes mentioned above. The predominant upper mantle rock is harzburgite containing dunitic layers and pods (varying from cm scale to km scale). The harzburgite grades upwards into dunite, which grades into clinopyroxene-rich dunite, wehrlites, and finally into the layered gabbros. Each of the complexes, however, do have certain unique features. The similarities and differences of each complex are briefly described below.

For descriptive purposes the lower ophiolite sequence will be divided into three units: the Peridotite Unit; the Transition Zone Unit, and the Gabbro and Mafic Cumulate Unit. The main features of each unit are summarized in Figure 1.3 and described below.

1.2.1 The Peridotite Unit

The harzburgites are strongly foliated and lineated. Both foliations and lineations have been measured by a study of the alignments of orthopyroxene and chrome-spinel grains in the field. In most ophiolites the foliation and related lineations have a consistent orientation over large areas of the Peridotite Unit. In a few ophiolites, however, the foliation changes rapidly in dip. (Prizhoffer et al, 1980; Nicolas and Violette, 1982.)

The olivine and orthopyroxene grain size usually increases downwards from the moho area (Girardeau and Nicolas, 1981; Prinzhoffer et al, 1980). This is an indication of a progressive decrease in stress downwards. (Ross et al, 1980.) The texture is usually porphyroclastic (Harte et al, 1977) but sometimes grades upwards into a mosaic porphyroclastic texture (Harte et al, 1977) where stress is greatest along the moho as in New Caledonia (Prinzhoffer et al, 1980). In the Bay of Islands Complex, Newfoundland, however, Girardeau and Nicolas (1981) reported an increasein stress downwards. In the 5km depth of mantle measured, the stress in the upper 2½km varied from 175 to 275 bars, and from 300 to 400 bars in the lower 2½km.

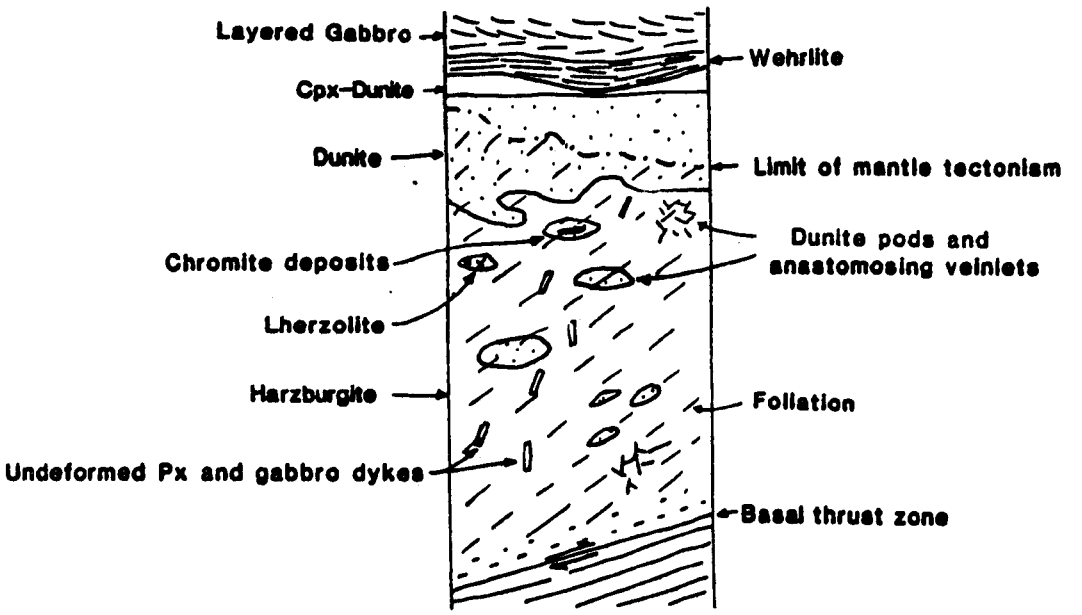

Figure 1.3 A simplified section through a typical lower ophiolite sequence showing some of the main petrological and structural features that have been observed by previous workers. (See text).

In Cyprus, George (1975, 1978) reported the existence of a second foliation in a small area of the Troodos harzburgites. He does not relate it to any mechanisms of deformation, but does state that it was formed in an ocean spreading environment. No other author has reported a second foliation.

Shear sense studies of the Peridotite Unit have been carried out on the Antalya complex (Juteau et al, 1977), Bay of Islands (Girardeau and Nicolas, 1981), Oman (Boudier and Coleman, 1981) and New Caledonia (Prinzhoffer et al, 1980). (See Chapter 6 for review of shear sense studies.) Juteau et al (1977) and Boudier and Coleman (1981) found only one shear regime in the areas that they studied. Their measurements, however, are of a very limited extent: Juteau et al (1977) only record 18 measurements, and Boudier and Coleman (1981) only 13. The Bay of Islands and New Caledonia complexes, however, were studied in greater detail (Girardeau and Nicolas, 1981; Prinzhoffer et al, 1980) and in both complexes two zones of opposite shear sense were mapped in addition to those associated with emplacement (see below).

Dunite within the harzburgite usually occurs as centimetre scale layers in areas greater than 3km depth from the moho. Pyroxene-rich layers are closely associated with these dunitic layers. Dunite pods ranging from a few metres to a few kilometres in diameter are common in areas just below the moho. The main economic chromite deposits occur in these pods. Boudier and Coleman (1981) report an abundance of

large dunite bodies as deep as 9km below the moho in the SE Semail ophiolite. The foliation in the harzburgites extends through the dunite layers and pods. The olivine and pyroxene rich layers tend to be parallel to the foliation, but the larger dunite bodies are often slightly discordant to the foliation. Little explanation has so far been given for the centimetre-scale olivine and pyroxene rich layering. Dick and Sinton (1979) propose that they are formed during anatexis and are essentially derived from metamorphic differentiation accompanying mantle deformation processes.

Two different mechanisms have been proposed for the formation of the dunite bodies. The bodies are either residual from which all other phases have been removed (Allen, 1975) and define channels along which melts were carried to the surface (Prinzhoffer et al 1980; Girardeau and Nicolas, 1981); or are the primary crystal fractionation products of a rising melt (O'Hara et al, 1975; Gass, 1980). Boudier and Coleman (1981) and Smewing (1979) support the cumulate theory for the Samail ophiolite. Smewing (1979) notes that the shape of the bodies is controlled partly by their original shape as they rise upwards towards the ridge, and partly by horizontal flattening within the foliation plane. Juteau et al (1977) report layering and orbicular textures in the dunite and chromite pods all of which point to their probably magmatic origin.

In the top few kilometres of harzburgite, dunite has also been reported as occurring in patches and anastomosing veinlets. (Loney et al, 1971; Cassard et al, 1981; Girardeau and Nicolas, 1981; Smewing, 1981.) These have a diameter of up to several metres and have irregular and digitated contacts with the surrounding harzburgite. Both the foliation and dunite layers cut straight through these features. Dick and Sinton (1979) have proposed a similar metamorphic differentiation process for their origin to that which they used to explain the olivine and pyroxene rich layering.

Small lherzolite bodies have also been reported within the harzburgite sequences (Girardeau and Nicolas, 1981; Gass, 1979; Prinzhoffer et al, 1980). These are thought to be the residue left after only a small degree of partial melting (Suen et al, 1979) or mantle material that has not undergone partial melting at all (Gass, 1980).

Pyroxenitic and gabbroic dykes are common in mantle harzburgites which cross-cut the layering and foliation. They are usually undeformed but occasionally are strongly folded with their fold axial planes parallel to the main foliation direction. Boudier and Coleman (1981) have shown, from field relations, that the gabbroic dykes are later than those rich in clinopyroxene. In most complexes, the dykes have either a random or strongly preferred orientation. Most authors have not related these trends to mantle deformation, but Nicolas and Jackson (1982) propose that the orientation of

the dykes relative to the main foliation trends can be directly related to the magnitudes of magma pressure and applied deviatoric stresses. Comparitively low magma pressure and high applied deviatoric stress result in shear fractures (at low angles to the foliation); high magma pressure and moderate applied stress result in tension fractures (at high angles to the foliation). Nicolas and Jackson (1982) also suggest that the olivine and pyroxene rich layering described above originates in this way. In all the complexes these dykes are nowhere described as cutting into the Gabbros and Mafic Cumulates Unit, although Juteau et al (1977) have observed late diabase dykes which do penetrate into the cumulate sequences above the harzburgites.

The harzburgite sequences in all of these ophiolites are remarkably undeformed by emplacement structures. In Semail, Bay of Islands, and Antalya, a 1km thick basal zone is the only evidence of emplacement. This zone shows lower temperature deformation in the olivines (Nicolas et al, 1980) and an abundance of dunite layers (tens of metres thick). This has been termed the 'banded unit' in the Semail ophiolite (Smewing, 1981). Isoclinal folding is abundant and the texture is fine-grained porphyroclastic (Harte et al, 1977). In the Bay of Islands the shear sense has been reversed from that in the overlying harzburgites in this basal unit. (Girardeau and Nicolas, 1981.)

1.2.2 The Transition Zone Unit

There has been considerable controversy over the origin of the Transition Zone. In all the ophiolites reviewed, the zone is a progressive transition from the residual harzburgite, through

dunite to wehrlite and finally olivine gabbro and gabbro. The thickness of each of these lithologies is highly variable both within and between different complexes.

Generally the harzburgite becomes more and more scarce upwards with dunite lobes extending down into the harzburgite (Boudier and Coleman, 1981), and harzburgite bodies isolated within the dunite (Prinzhoffer et al, 1980). In both the Troodos massif (George, 1975, 1978; Gass, 1980) and the Acoje section of the Zambales massif (Nicolas and Violette, 1982) the authors have interpreted this lobing phenomenon as an interfolding between dunite and harzburgite. This folding is thought to have post-dated the main deformation event of the Peridotite Unit as the fold axes bear no systematic relationship to the lineation directions in the harzburgites. (Nicolas and Violette, 1982.)

The deformation in the harzburgites usually dies out somewhere in the Transition Zone. In the Troodos Massif the deformation extends about 500m into the dunites (George, 1975); in the S.E. Semail section Boudier and Coleman (1981) report that the harzburgite and dunite in the transition zone only shows deformation in some places; in New Caledonia the foliation dies out at the harzburgites - dunite boundary (Prinzhoffer et al, 1980); and in both the Bay of Islands complex (Girardeau and Nicolas, 1981) and in the Antalya complex (Juteau et al, 1977) the foliation dies out within the harzburgites.

The main controversy is whether the dunites have a residual or a cumulus origin. Field relations, structures, spinel types (Nicolas et al, 1980) and the chemistry have all been used as evidence for or against a cumulus origin for the dunites.

In the Troodos massif, George (1975, 1977) postulated a cumulus origin for all the dunites above the dunite - harzburgite contact on the evidence of both relict textures and the gradational contact between the underformed and deformed dunite. He also found spinels and pyroxenes that showed no evidence of deformation in the top 500m of harzburgites. He attributed this to the harzburgite being contact-metamorphosed by the overlying cumulate dunites. Gass (1980) supported the cumulus origin of the dunites by geochemical evidence: a high Cr/Al ratio.

Malpas (1977) found cumulate textures throughout the dunites in the Bay of Islands, but Girardeau and Nicolas (1981) favoured a residual origin. This was because of the lack of stratiform chromites with magmatic spinel, the transitional contact between the harzburgites and dunites, and also the extreme thickness of the dunite pile (up to 3km). Nicolas and Prinzhoffer (1983) have proposed that most dunites in transition zones are residual in origin with the wehrlites and feldspathic dunites resulting from magmatic impregnation. They based this proposal on the comparative study of transition zones from eight ophiolite complexes.

The exact position of the Petrological Moho is thus unclear. Nicolas and Prinzhoffer (1983) place it at the base of the layered gabbros above the Transition Zone. Most previous authors, however, located it at the top of the Peridotite Unit, and infer that the Transition Zone dunite is cumulate and not residual in origin. In this thesis the boundary between the harzburgites (Peridotite Unit) and the dunites will be referred to as the "Petrological Moho" or just "moho".

1.2.3 The Gabbro and Mafic Cumulate Unit.

In all the complexes studied the lower cumulate sequence is strongly layered with sharp isomodal layers suggesting fractional crystallisation processes (Jackson et al, 1975) and/or successive magma injections (Cambell, 1977). Girardeau and Nicolas (1981) suggest an open system magma chamber with a continuous or semi-continuous injection of magma.

Slump, channel and cross-bedding structures are fairly common in all the complexes.

Post-Peridotite Unit deformation shear zones have been reported in the layered gabbros of the Semail ophiolite (Smewing, 1979) and the Bay of Islands Complex (Girardeau and Nicolas, 1981). Even though each zone is of a small lateral extent, because of the abundance of zones in some places, the movement within the gabbros could have been quite large. These shear zones have variable orientations in different areas. Smewing (1979) proposed a 30km wide zone within the Semail gabbros in which sinistral shear zones are abundant. This he attributes as the response of the gabbro to simple shear caused by the intersection of the ridge with a 'leaky' transform fault system (see Chapter 2). Girardeau and Nicolas (1981) interpret the more dispersed shear zones in the Bay of Islands gabbros as evidence of hydrothermal circulation and the subsidence of the magma chamber during spreading as proposed by Dewey and Kidd (1977). Further evidence of hydrothermal circulation is shown by the late pegmatitic dykes which are common in the gabbros from all the complexes.

Generally, the gabbro layers are discordant with the underlying tectonites, the angle between the layering and moho plane being up to 30° in the lower cumulate sequences. It is proposed by Girardeau and Nicolas (1981) and Boudier and Coleman (1979) that the cumulate layering dips towards the spreading axis. Browning (1982) further develops this for the Oman ophiolite by proposing that the variation in inclination and direction of dip of the cumulate layers indicate the existence of sequentially developed magma chambers of finite length beneath the ridge axis (see Chapter 2).

1.3 The Mechanisms of Deformation of the Peridotite Unit.

Most authors agree that the foliations and lineations present in the Peridotite Unit of ophiolite complexes have been formed by ductile flow processes. These processes are thought to have occurred at an ocean-spreading centre and mainly involve inter- and intracrystalline slip and recrystallisation of olivine and pyroxene grains in a simple shear environment.

An extensive review of ductile deformation processes in olivine-rich rocks comprises Chapter 6 of this thesis.

1.4 The Structural Behaviour of the Upper Mantle and Lower Oceanic Crust at a Spreading Centre - Evidence from Ophiolite Complexes.

Various authors have related the deformational structures observed in lower ophiolite sequences to the structural and kinematic behaviour of the upper mantle and lower oceanic crust at a spreading centre.

Even though the cumulates, on the whole, are undeformed, Juteau et al (1977) pointed out that in both the tectonites and the cumulates, the whole structure is largely controlled by the ductile flow direction (mantle and crust lineations are very similar in orientation). Juteau et al (1977) also noted that the orientation of mantle foliations were not consistent with a continuous length of spreading ridge at mantle depths, but were more likely to have been formed by diapiric intrusion of mantle rocks beneath the ridge.

Prinzhoffer et al (1980) obtained a lineation pattern from the New Caledonia ophiolite which exhibited a divergence of flow lines away from the ridge. This they attributed to mantle flow diverging from a hot spot and channelled by transform faults as modelled by Vogt (1975). Nicolas and Violette (1982) have related the structures of eleven ophiolite complexes to the Vogt (1975) model. (See Chapter 10 for details.)

Detailed theoretical models for the kinematic behaviour of the upper mantle at a spreading centre are considered in Chapter 10, as well as a comparison of the seismic anisotropy studies of the present day oceanic lithospheric mantle with the structures observed in the Peridotite Unit of ophiolite complexes.

It is clear that many of the structural and petrological features of the lower sequences of ophiolite complexes are common to all those described above. The structural orientations of these features with respect to a spreading axis, however, is highly variable between ophiolite complexes. Much ambiguity therefore remains as to the exact processes occurring in the uppermost

mantle at an oceanic spreading centre. There is still considerable scope for the development of oceanic spreading models from the study of the structures of the upper mantle and lower oceanic crust that have been preserved in ophiolites.

1.5 Present Study

1.5.1 Aims of This Study

The overall aim of this work was to reach a better understanding of the primary structural processes occurring in the uppermost mantle and lower oceanic crust at plate accretionary margins.

In order to achieve this, it was decided to study three separate ophiolite complexes and to compare and contrast the structures of each. Very detailed structural mapping, combined with specimen collection and optical and crystallographic analysis, of the lower ophiolitic units of each complex was completed in order to:-

(i) Record the structural styles and their variation within each mantle complex and between complexes.

(ii) Record the structural styles and their variation within each lower crustal sequence from each complex and between complexes.

(iii) Record the structural significance of the crust-mantle boundary (the Petrological Moho) within each complex.

and (iv) Discern accretion and spreading related structures from emplacement related structures within lower ophiolite sequences.

1.5.2 The Choice of Areas of Study

In order to choose suitable areas for detailed study, four factors were taken into consideration. Firstly, the area should have been previously mapped in some detail in order that basic regional mapping is not required. Secondly, the ophiolite complex should be as complete as possible and have little or no emplacement-related or later deformation. Thirdly sufficient exposure of the mantle and lower crustal units was required in order that detailed mapping could be carried out; and fourthly the area should be logistically a realistic proposition.

The areas finally selected were chosen with the above considerations in mind and also because of their strong links with the Open University Earth Sciences department. The areas are the northern part of the Oman (or Semail) Ophiolite, the Troodos Massif of Cyprus, and the ophiolite complex on the islands of Unst and Fetlar, Shetland. Brief visits were also made to the Vourinos and Othris Complexes of Greece, and the Lizard Complex of Cornwall.

1.5.3 Layout of Thesis

In the first section the regional geology and detailed field observations from the mantle and lower crustal regions of each area are described. This section of the thesis will be mainly descriptive except for minor field-based and petrological interpretations. Methods of structural analysis are then described and performed on each area of study. Finally, the field observations are combined with the various structural

data to propose models for the behaviour of the upper mantle and lower oceanic crust at an accretionary margin.

1.6 Rock Classification and Description

The rocks in this study have been classified using the schemes of Streckeisen (1976). Figure 1.4 shows the categories used from both the ultramafic and gabbroic rocks.

The description of textures is based mainly on the textural classification schemes of Harte (1977) with modifications after Nicolas et al (1980) and Augustithis (1979). Table 1.1 summarizes the textural classification scheme used.

1.7 A Note on the Presentation of Data.

In order to gain a full understanding of the structural styles and their distributions, most of the field and specimen data is presented on large scale map enclosures of each of the areas studied. Equal area projections are included on these maps instead of within the thesis itself.

The symbols in each of the enclosures have been standardised so that different features from different areas can be directly compared. Enclosure 32 is a legend of all the symbols used in Enclosures 1-31.

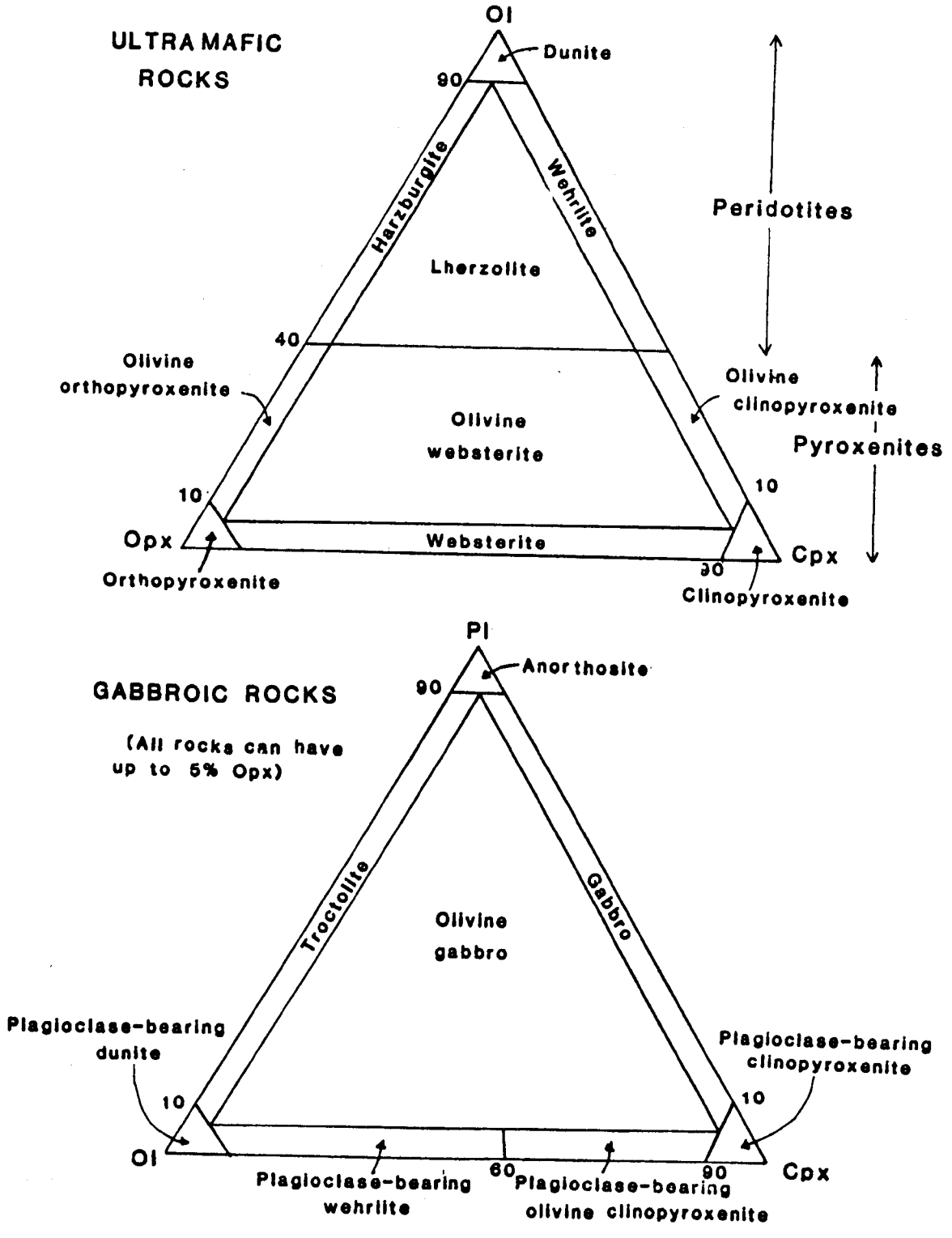

Figure 1.4 Ultramafic and gabbroic rock nomenclature. (Modified from Streckeisen, 1976).

Textural Type	Porphyroclasts (> 2mm diam.)	Matrix Comments
Coarse	None	Grains all greater than 2mm diameter. Variable strain.
Coarse-porphyroclastic	> 50% porphyroclasts	Polygonal or tabular sub-grains and neoblast formations in matrix.
Porphyroclastic	10-50% porphyroclasts	
Mosaic-pophyroclastic	< 10% porphyroclasts	
Granuloblastic	< 5% porphyroclasts	Small size range with extensive recrystallisation.

Table 1.1 Summary of textural classification schemes.

PART 1

Regional Geology, Field Descriptions, and Petrological Features of the Lower Ophiolite Sequences Studied.

Chapter 2

The Oman Ophiolite

CONTENTS

2.4.1.2 The Distribution and Orientation of Intrusive and Cumulate Features.

(a) Dunitic Intrusions within the Peridotite Unit.

(b) Pyroxenitic and Gabbroic Dykes and Sheets.

(c) Cumulate Features of the Lower Cumulate Unit.

2.4.2 The Salahi Block

2.4.2.1 Structural Trends.

2.4.2.2 The Distribution and Orientation of Intrusive and Cumulate Features.

2.4.3 The Sarami Block

2.4.3.1 Structural Trends.

(a) Early Tectonic Foliations and Lineations.

(b) Later Structures.

2.4.3.2 The Distribution and Orientation of Intrusive and Cumulate Features.

(a) Dunitic Intrusions within the Peridotite Unit.

(b) Pyroxenitic and Gabbroic Dykes and Sheets.

(c) Cumulate Features of the Lower Cumulate Unit.

2.4.4 The Haylayn Block

2.4.4.1 Structural Trends.

(a) Earlier Tectonic Foliations and Lineations.

(b) Later Structures.

2.4.4.2 The Distribution and Orientation of Intrusive and Cumulate Features.

(a) Dunitic Intrusions within the Peridotite Unit.

(b) Pyroxenitic and Gabbroic Dykes and Sheets.

(c) Cumulate Features of the Lower Cumulate Unit.

2.4.5 The Rustaq Block

2.4.5.1 Structural Trends.

(a) Early Tectonic Foliations and Lineations.

(b) Later Structures.

2.4.5.2 The Distribution and Orientation of Intrusive and Cumulate Features.

(a) Dunitic and Olivine Gabbroic Intrusions within the Peridotite Unit.

(b) Pyroxenitic and Gabbroic Dykes and Sheets.

(c) Cumulate Features of the Lower Cumulate Unit.

2.5 Summary of the Structural Trends and Distribution of Petrographic Features of the Peridotite and Lower Cumulate Units of the Northern Oman Ophiolite.

2.1 Geographical and Geological Setting - Previous Work.

The Oman (or Semail) Ophiolite is one of the largest and best preserved ophiolites in the world. It has an area of over 30,000 km² and forms most of the 700km long mountain chain of the Oman Mountains.

The Sultanate of Oman lies on the north-eastern corner of the Arabian Peninsula and the Oman Mountains form an arcuate chain parallel to the north-eastern coastline. (Figure 2.1) The mountains are bounded on the east by the gravel plains of the Batinah coast and by the Gulf of Oman, and on the west by the great sand-seas of western Arabia - the Rub al Khali.

Previous work on the regional geology, geological setting and detailed ophiolite geology of the Oman Mountains has been recently reviewed in detail by Browning (1982) and Rothery (1982). It is not the purpose of this section to re-review previous work, but to present a synthesis of the data in order to describe the consensual geological history of the Oman Mountains.

2.1.1 Regional Geology.

The regional geology of the Oman Mountains was first described in detail by Lees (1982), but the most significant work on the understanding of the stratigraphy and structure is that by Glennie et al (1973,74). This has been further refined by Gealey (1977), Graham (1980), Searle (1980), Woodcock and Robertson (1982) and Robertson and Woodcock (1983). A simplified

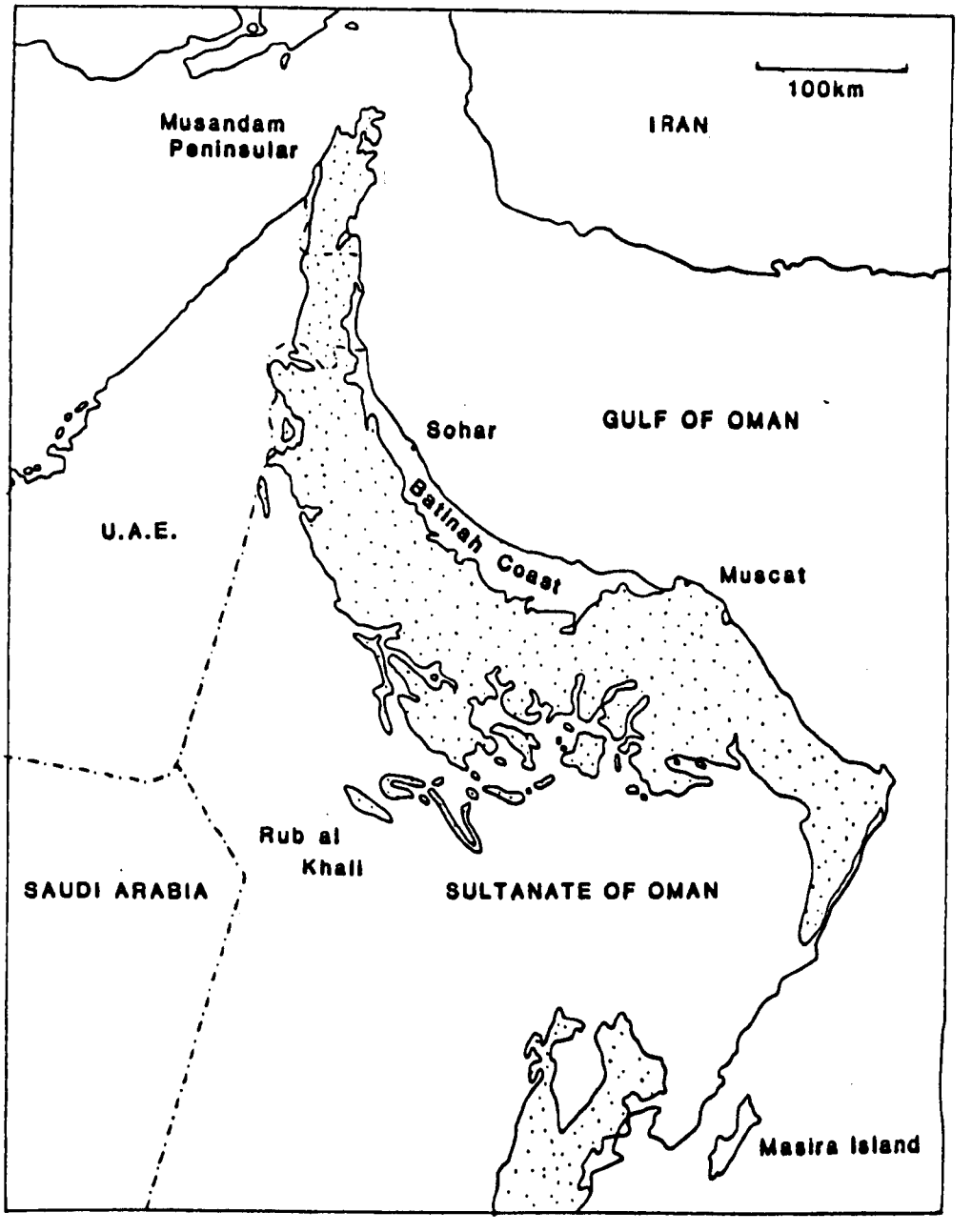

Figure 2.1 The geography of Northern Oman showing the outcrop area of the Oman Mountains. (From Graham, 1980).

geological map of the Oman Mountains based on Glennie et al (1973,74) is shown in Figure 2.2. The tectonostratigraphic sequence of the Oman Mountains based mainly on the work of the authors mentioned above, is shown in Figure 2.3. The main units recognised which outcrop above the mainly continentally derived Mid Permian basement are :-

1) The Hajar Supergroup; Mid Permian to Cenomanian autochthonous sequence of shallow marine carbonates lying unconformibly on the Arabian continental margin. Thrust southwards onto this Hajar Supergroup, from Upper Permian to Upper Cretaceous times, is a series of allochthonous thrust sheets ; -

2) The Sumeini Group; the lowermost allochthonous unit of Upper Permian to Cenomanian shelf edge and slope carbonates.

3) The Hawasina Complex; an imbricated nappe pile of Permian to Cenomanian basinal and deep water marine sediments.

4) The Haybi Complex; a melange of Hawasina sediments, volcanics, metamorphics and serpentinite.

5) The Semail Ophiolite; Upper Cretaceous oceanic crust and mantle sequence.

6) The Batinah Melange; an extremely complex melange of mainly Hawasina-type sediments.

Each of these thrust sheets is separated by major thrust zones. Successively higher sheets are progressively more distal indicating the "telescoping" of a continental shelf sequence onto a continental margin. The Batinah Melange unit is an exception to this as it lies structurally above the Semail Ophiolite Unit. It is proposed by Robertson and Woodcock (1983)

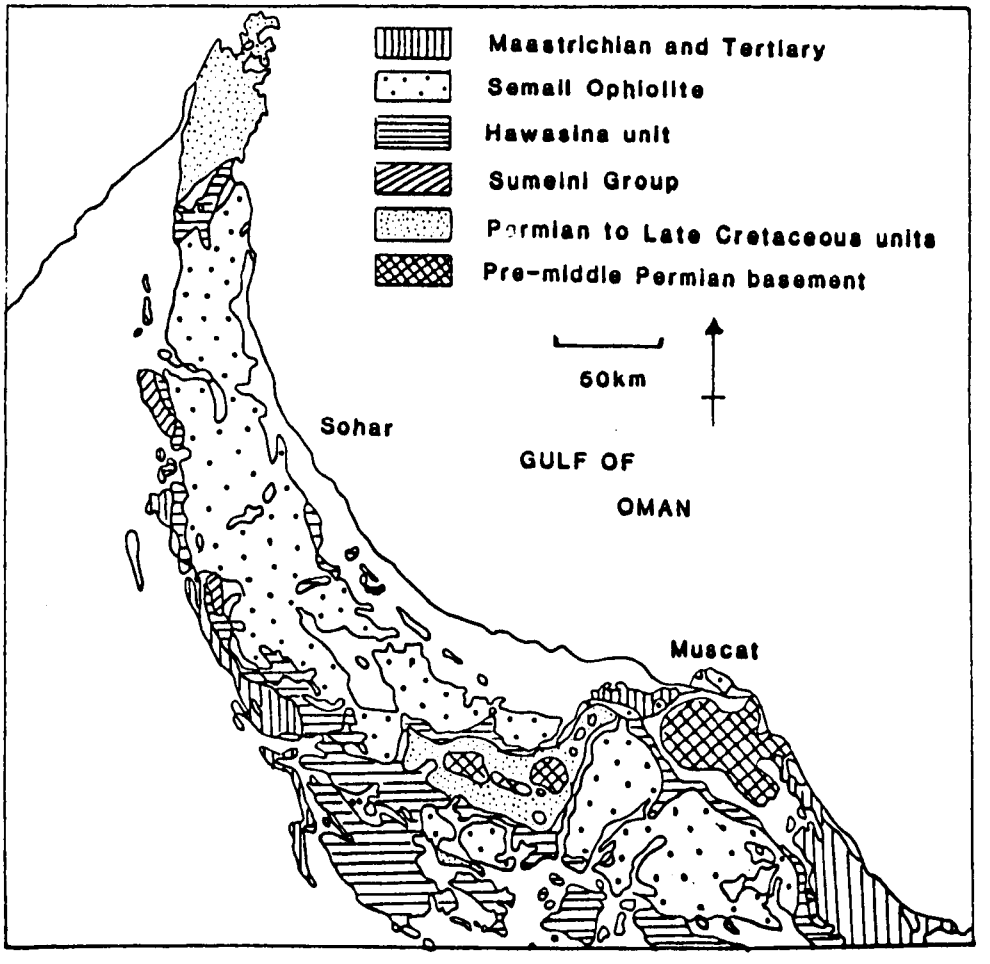

Figure 2.2 Simplified geological map of the Oman Mountains (Modified after Glennie et al, 1974).

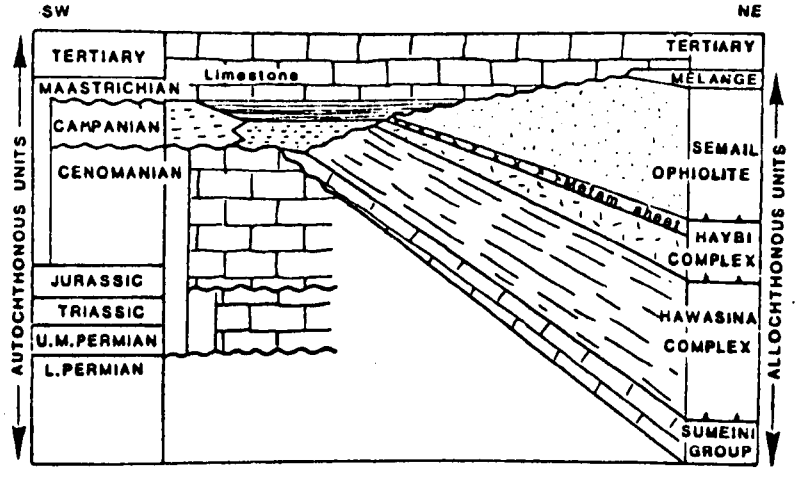

Figure 2.3 Generalised tectonostratigraphic section of the Oman Mountains. (Modified from Rothery, 1982).

that this Melange formed when the Semail Ophiolite broke into separate blocks during its tectonic emplacement over the Arabian continental margin; sub-ophiolitic rocks moving up through fault-bounded corridors and redistributed above the ophiolite by gravity-driven mechanisms.

7) Maastrichtian and Tertiary Limestones: shallow water carbonates overlying unconformably all the above units.

2.1.2 Ophiolite Geology

Reinhardt (1969) first recognised and described the ophiolitic units of the Oman Mountains. They conform well to the Penrose Conference definitions (Anon, 1972) and the Oman Ophiolite can be classed as a complete ophiolite sequence.

Detailed studies of the Oman Ophiolite have been carried out by the Open University Oman Ophiolite Project led by Prof. I.G. Gass and the United States Geological Survey (U.S.G.S.) led by Dr. R.G. Coleman. The Open University Group has mapped the northern and central section of the ophiolite to a scale of 1:100,000 (Smewing, 1979; Lippard, 1980; Lippard and Rothery, 1981; Browning and Lippard, 1982) and the U.S.G.S. team an area in the south-east Oman Mountains at a scale of 1:60,000 (Hopson et al, 1981; Bailey, 1981).

Figure 2.4 shows the Oman Ophiolite stratigraphy developed by the Open University research group for the northern and central Oman Ophiolite.

The units are those of a typical ophiolite sequence; a few of

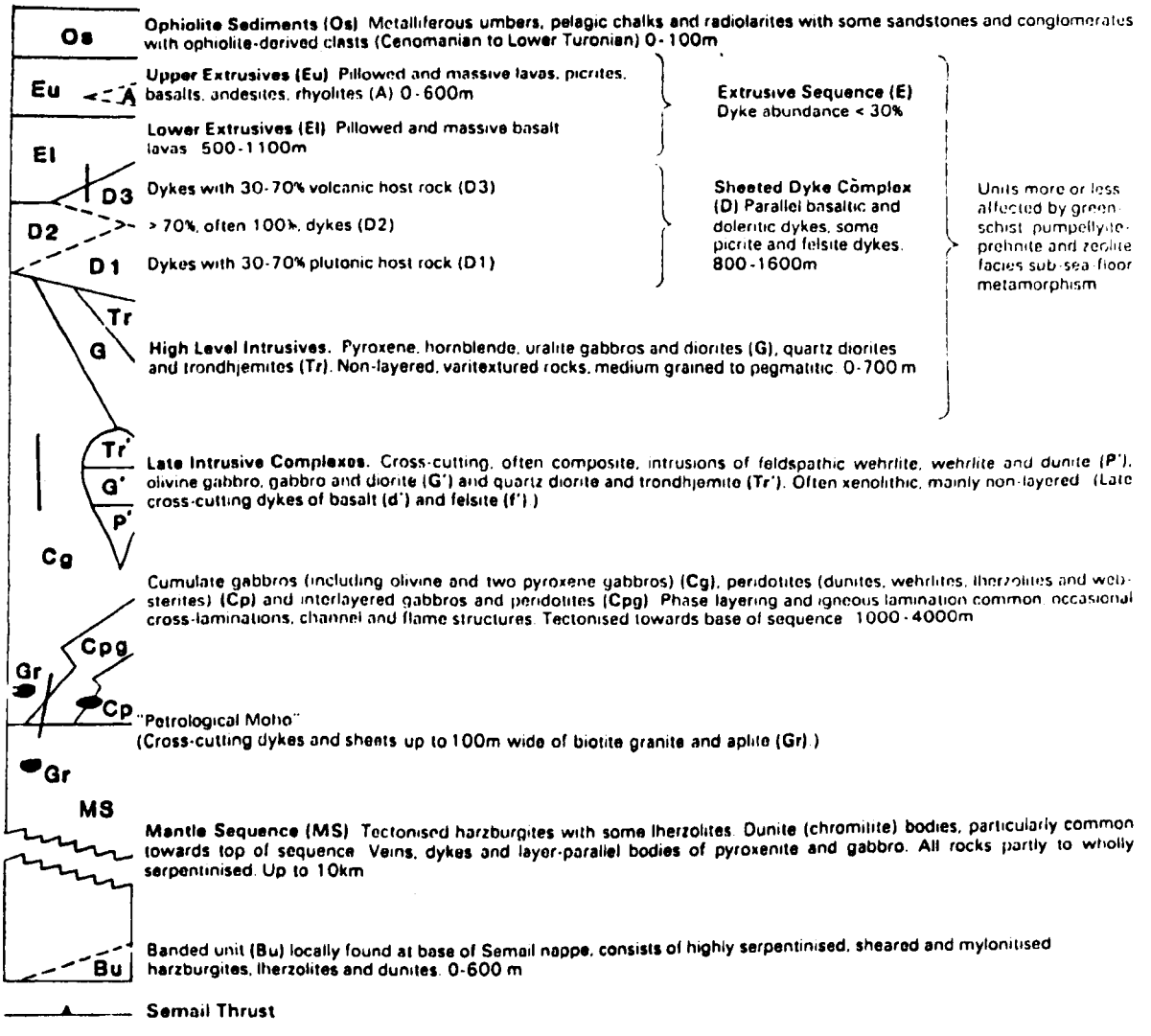

Figure 2.4 The Oman Ophiolite stratigraphy. (From Lippard and Rothery, 1983).

the more detailed relationships are discussed below.

The lava stratigraphy is complex with three subdivisions (Alabaster et al, 1980). The lowest unit, the Goetimes Unit, is of mainly basaltic pillow lavas which directly overlie the Sheeted Dyke Complex. They are related to the main cumulate sequence and high level intrusives (Browning, 1982), and are thought to have been produced by the creation of oceanic crust by back arc spreading (Pearce et al, 1981).

Late Trondhjemite - Gabbro complexes have been intruded into this newly formed ocean crust (Browning and Smewing, 1981; Browning, 1982); these producing the off-axis seamount activity attributed to the lavas of the Lasail Unit (Alabaster et al, 1980; Pearce et al, 1981).

A later submarine rifting phase is thought to have initiated further intrusion of fracture-controlled peridotite-gabbro complexes which extrude the stratigraphically youngest Alley Unit lavas (Pearce et al, 1981).

An even later areally restricted lava unit has been recognised by Alabaster et al (1982). This was named the Salahi Unit and has been related to a syn-emplacement volcanic event.

In the south eastern Oman Mountains, the U.S.G.S team found no evidence for the 'off-axis' sequence of lavas reported from the central and northern areas of the ophiolite (Hopson et al, 1981).

The strike of the Sheeted Dykes generally follow the arcuate shape of the Oman Mountains except for a pronounced variation

in trend in the northern area of the ophiolite. Smewing (1980) has proposed the existence of a "leaky" transform zone to explain this, but Pearce et al (1981) argue that some of the Sheeted Dyke Complex was injected during the "off-axis" episodes of igneous activity, and that the trends of the sheeted dykes vary in relation to the position of the seamounts.

From the chilling directions on individual sheeted dykes in the south eastern ophiolite area, Pallister (1981) inferred a palaeo-ridge axis to the south west of the outcrop. Lippard (1981), however, in a more detailed study of the northern and central axis-related sheeted dykes, showed that the chilling relationships between dykes is very complex and that statistical evidence places the palaeo-ridge axis to the north east of the northern and central Oman Ophiolite. Browning (1982) backed this up by using the relationships between the inclination of the cumulate layering and the petrological moho.

The lower Cumulate Sequence of the Oman Ophiolite shows a strong layering which is believed to have formed in situ within a long-lived, dynamic, compositionally stratified, open system magma chamber. (Reviewed in Browning, 1982). Pallister and Hopson (1981) noted that the base of the cumulate sequence of the southern Oman Ophiolite area has been subjected to a hypersolidus deformation. The deformation is localized and this is related to the differing behaviour of the various cumulus layers near the seismically active palaeo-spreading axis.

The Mantle Sequence has been described from the south eastern Oman Mountains by Boudier and Coleman (1981), and they concluded that the pervasive, constantly trending tectonic foliations,

lineations and other structures have been formed at or near solidus temperatures.

Boudier and Coleman (1981) also infer that both the homogeneous chemistry and the extreme depletion of the harzburgite show that it is a highly refractory residue. Discordant dunite, websterite and gabbro dykes record crystal fractionation products of ascending basaltic liquids derived from partial metling at greater depths. Boudier and Coleman (1981) attribute the websterite and gabbro dykes to 'off axis' processes.

Christensen and Smewing (1981) show from seismic studies that the compressional and shear wave velocities of the ophiolite units from the northern Oman Ophiolite correspond well with the wave velocities measured from the different seismic layers of the oceanic lithosphere. In the Mantle Sequence the velocities have a large anisotropy with the fast wave direction parallel to the tectonic lineations measured from the field.

Boudier and Coleman (1981), and Searle (1980) describe mylonitic textures from the ½km thick basal contact zone of the Mantle Sequence. These die out upwards and are an imprint of a superposed deformation at lower temperatures and higher deviatoric stresses than the ridge-related mantle structures; they are related to the thrusting and detachment of the Oman Ophiolite during emplacement. This zone of emplacement deformation has been termed the 'Banded Unit' by the Open University research group.

2.1.3 Regional Setting and Emplacement Models.

The Oman Ophiolite is the largest of the Tethyan chain of ophiolites and ophiolite related rocks extending from the Alps through the eastern Mediterranean and Iran to the Himalayas. (Figure 2.5).

The Oman area of the Tethys Ocean is thought to have been obducted as a result of a complex series of collisions between successive microcontinents or island arcs due to a general northward shift of fragments into the Asian continent and away from Gondwanaland (Review in Rothery, 1982).

Metamorphic studies in the rocks directly underlying the Semail Ophiolite by Searle (1980) show that the residual heat within the overlying mantle rocks was the main cause of metamorphism of the underlying sheet. Thus, the Semail Ophiolite was displaced from an oceanic environment very soon after its formation. This has also been shown from radiometric and palaeontological dating (Review in Rothery, 1982).

Most of the reconstructions reviewed by Rothery (1982), of the obduction of the Oman Ophiolite suggest a tectonic setting just prior to ophiolite obduction as shown in Figure 2.6, with a north eastward dipping subduction zone. Oceanic crust was subducted north eastwards and formed a back-arc basin and island arc complex, part of which eventually became the Oman Ophiolite. When the Arabian Continent and passive margin approached the subduction zone, subduction could not continue and so obduction processes began. Thus the

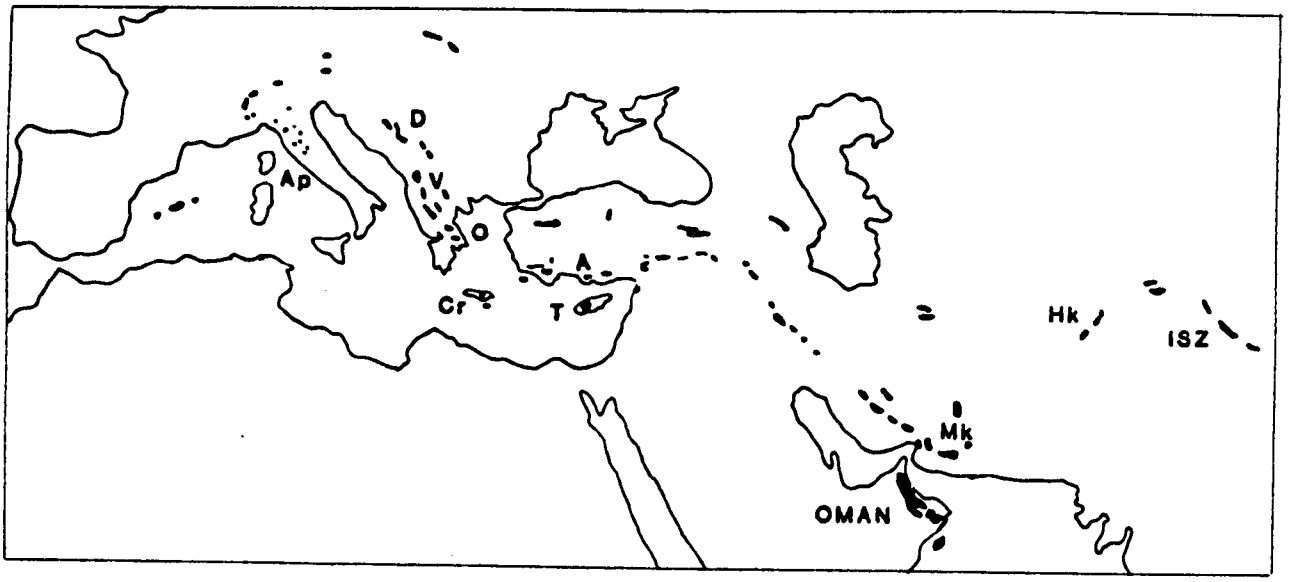

Figure 2.5 The Distribution of Tethyan Ophiolites.

A - Antalya, Ap - Appenines, Cr - Crete, D - Dinarides, HK - Hindu Kush, ISZ - Indus Suture Zone, Mk - Makran, O - Othris, T - Troodos, V - Vourinos.

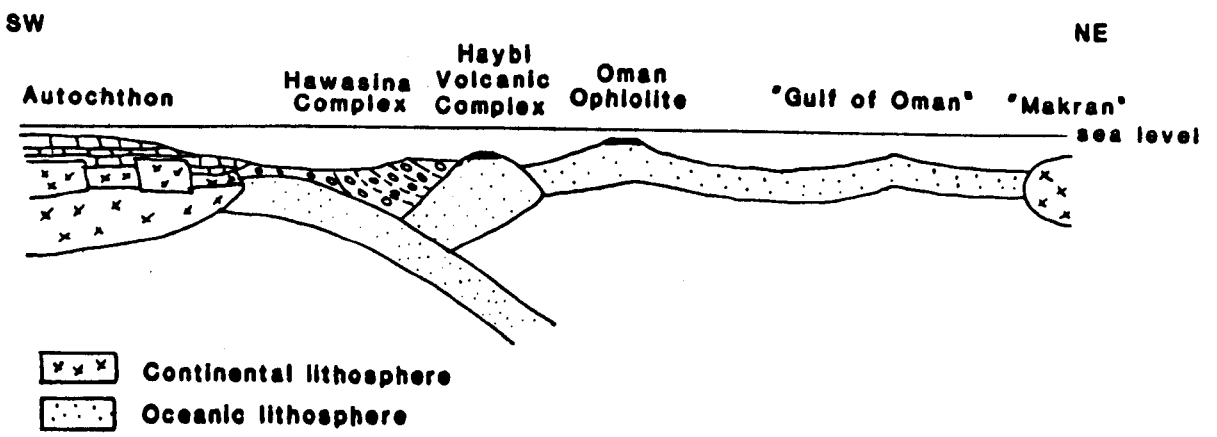

Figure 2.6 Hypothetical section showing the tectonic setting of the Oman Ophiolite just prior to obduction. (Modified from Pearce, 1982 and Rothery, 1980).

allochthonous units of the Oman Mountains were thrust in a south westerly direction onto the Arabian continental margin.

Searle (1980) and Searle and Malpas (1981) divided the obduction of the ophiolite sequence into two stages. Firstly an initial "displacement" stage involving compressional deformation with underthrusting of the Haybi and Hawasina Units. This caused the formation of the metamorphic sheet underlying the ophiolite sequence. Secondly a final "emplacement" stage, most probably by gravity sliding or spreading of the relatively underformed ophiolite complex. This was accomplished on a thin basal decollement layer of ductile basal serpentinite which also formed the tectonic melange zone of the Haybi Complex. During emplacement, the Oman Ophiolite broke into separate blocks by fracturing (Graham, 1980; Robertson and Woodcock, 1983). (Figure 2.7).

2.2 Logistics and Areas Studied in Oman

A three month field season was spent in the Sultanate of Oman from November - March, 1980/81. One-to-two week field excursions were made into the Oman Mountains by landrover from a base in Sohar (Figure 2.1). The rugged lower crustal and mantle sequences are highly inaccessible with very few mountain tracks reaching the petrological moho; this restricted the areas which could be studied. The Open University 1:100,000 geological maps (Referenced in Section 2.1) were used to identify suitable areas for study. These areas needed to have a motorable track reaching close to the area selected for possible study. The

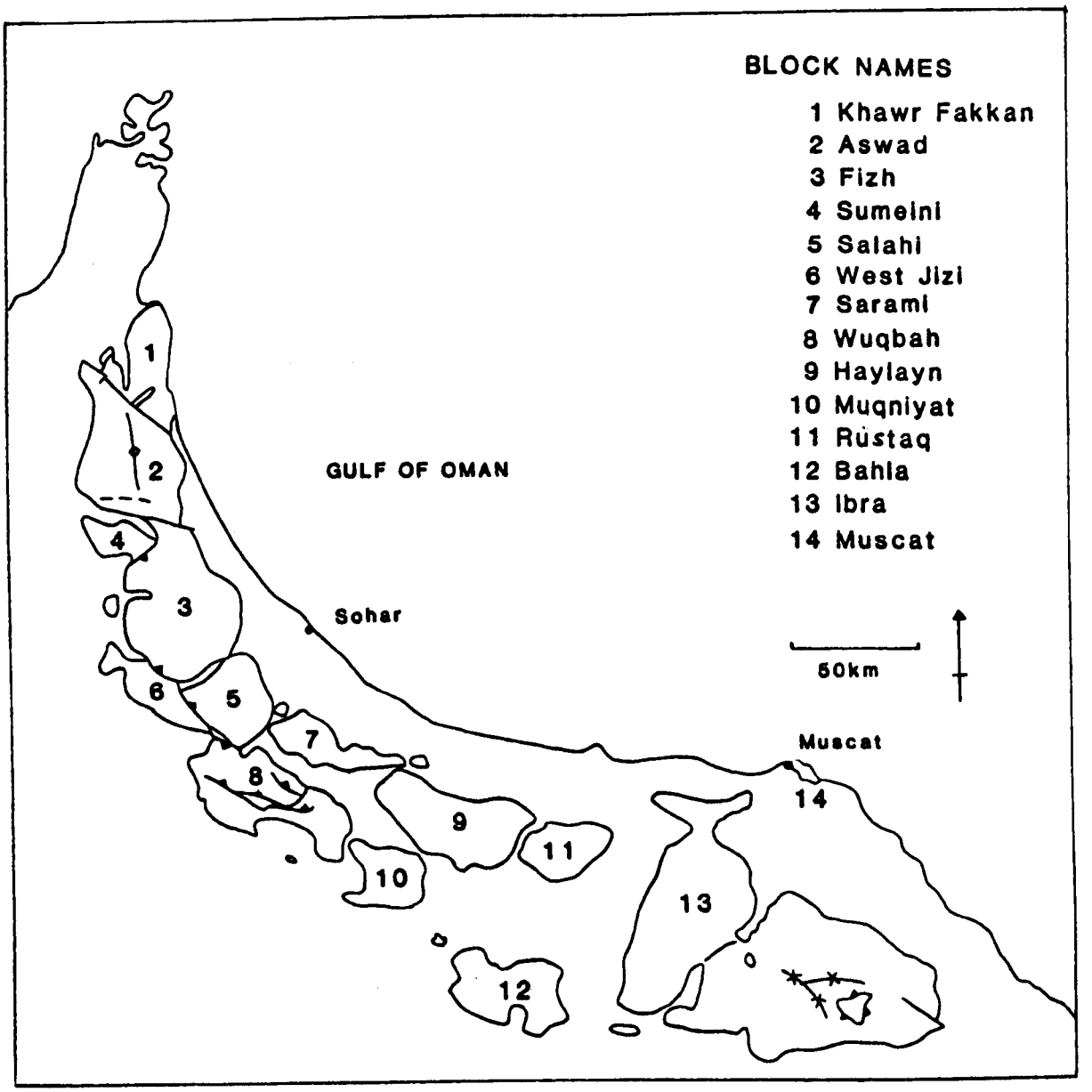

Figure 2.7 Outcrop extent and structural blocks of the Oman Ophiolite.

areas should not be in the vicinity of fault zones or the basal contact zone of the ophiolite with the underlying thrust sheets; this constraint minimizing the effects of emplacement events on the primary mantle structures.

On the basis of the above considerations, it was decided to map four major traverses through the lower crust and mantle sequences as well as many smaller traverses. All traverses mapped are at a scale of 1:10,000.

Each major ophiolite block containing large amounts of mantle was studied in order to obtain a full picture of the behaviour of the mantle and lower crust throughout the northern Oman Ophiolite, Figure 2.8 shows the outcrop extent of mantle sequence for each of the structural blocks of the Oman Ophiolite and the areas which were studied. The four major traverses from north to south were

1) The Wadi Rajmi traverse. (Fizh Block)
2) The Wadi Sarami and Kanut traverse. (Sarami Block)
3) The Wadi Hajir traverse (Haylayn Block)

and 4) The Wadi Al Abyad traverse. (Part of Wadi Bani Kharus in the Rustaq Block).

The mantle and lower crustal features common to all the areas studied in Oman are described below.

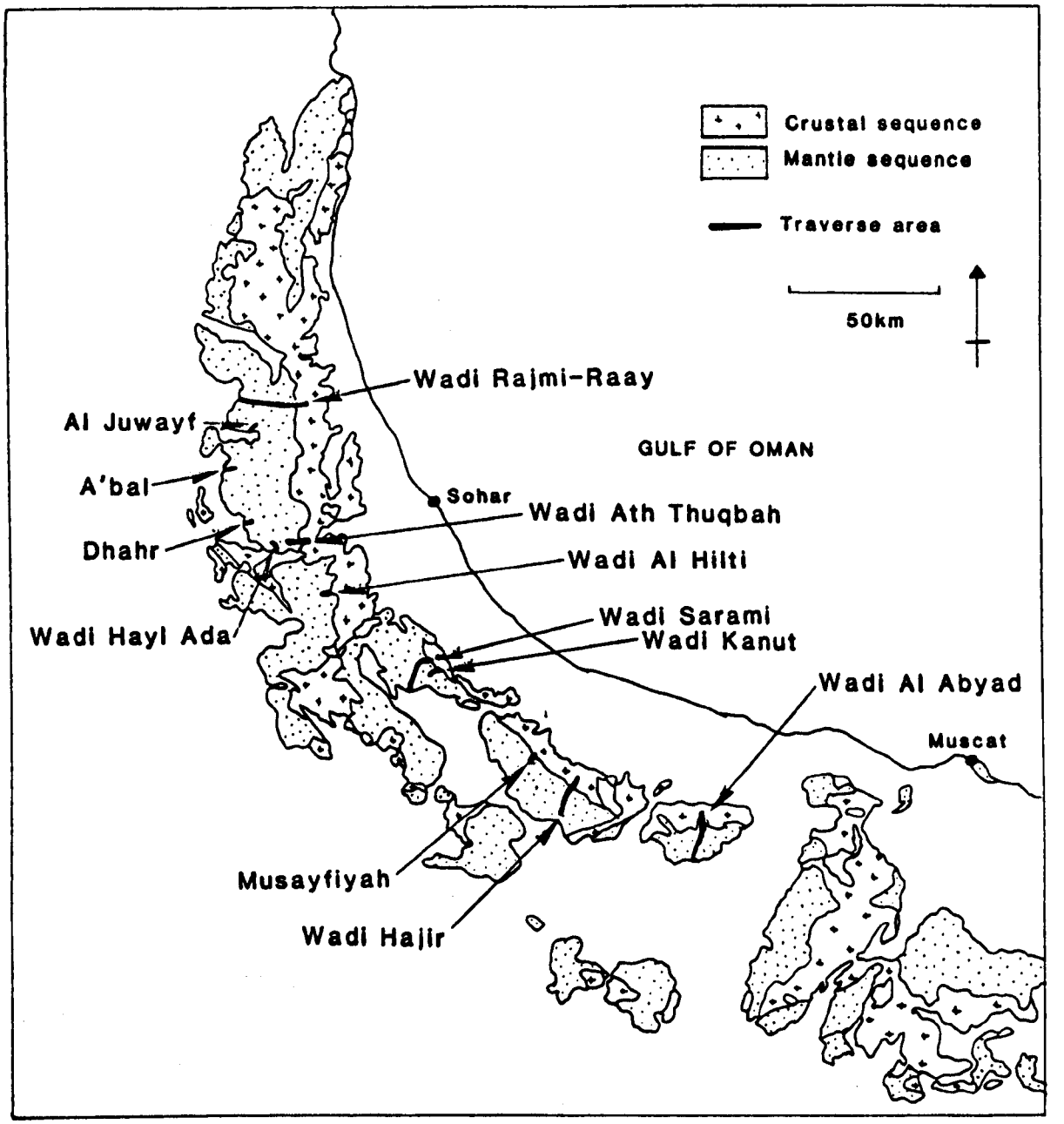

Figure 2.8 Outcrop extent of the Mantle Sequence and location of the areas studied.

2.3 General Mantle and Lower Crustal Petrological Features of the Oman Ophiolite.

2.3.1 Appearance of Rock Types in the Field.

The Mantle Sequence varies in colour from a light-orange brown to black pending on the degree of serpentinisation and the minerals present. The harzburgite, when fairly fresh, is green-yellow in colour in hand-specimen with the orthopyroxene green and the olivine yellowish green. More commonly, however, it is moderately serpentinised and gives an overall deep red-brown appearance.

On a weathered surface olivine is a smooth brown groundmass from which individual crystals cannot be distinguished. Individual orthopyroxene crystals are usually distinct and are yellow-brown in colour. Clinopyroxene is greener and more vitreous than orthopyroxene. Spinel grains occur as black elongate specks.

As serpentinisation increases, the overall colour of the harzburgite darkens towards a serpentinite with a dark brown-black desert varnish. On a freshly broken surface the harzburgite has a green-black granular appearance on which it is difficult to identify individual grains.

Within the Mantle Sequence, and especially within the Transition Zone, dunite is highly serpentinised and weathered in Oman. It is usually yellow-brown in colour and crumbles when hit with a hammer. Spinel grains occur as black specks but are often obscured by the high degree of weathering.

The Lower Cumulate Sequence varies from light shades of brown to light grey depending on the relative proportions of ultramafics

and gabbros present. These rocks tend to be fresher in appearance than the mantle rocks but are locally highly weathered, especially in areas close to joint and fault zones.

2.3.2 Petrological Features of the Peridotite Unit

The Peridotite Unit is composed predominantly of harzburgite with minor bodies of other ultramafic type rocks. These have been intruded into the harzburgites as liquids, and have formed either dyke-like or magma-chamber-type bodies.

The massive tectonised harzburgites are described below proceeded by a description of the intrusive features within the Peridotite Unit. It is intended that this section should be descriptive, the genetic origins of the major structural features described will be discussed in Chapters 9 and 10.

(a) The Tectonised Harzburgites Harzburgite has a remarkably constant composition over the whole of the Peridotite Unit studied in Oman. Olivine is the most abundant mineral present (75-90%) with orthopyroxene the only other abundant phase (25-10%). Clinopyroxene is fairly common in trace amounts and it rarely exceeds 3% of the modal composition. Chrome spinel is always present as an accessory phase. Each mineral phase present has a fairly constant chemical composition as shown by Christensen and Smewing (1981). (Olivine Fo_{91}, orthopyroxene En_{91}, and clinopyroxene $Wo_{45}En_{51}Fs_{04}$.) On the outcrop scale the modal proportions of olivine and orthopyroxene

present is, in some areas, fairly variable, and gives rise to layering.

These layers have highly diffuse ratio contacts and vary from olivine to orthopyroxene-rich (Plates 2.1 and 2.2). They are up to 10cm thick but more commonly vary from a few mm up to 5cm. They are laterally discontinuous on the outcrop scale. This layering has been termed a 'segregation layering' by Dick and Sinton (1979), and is thought to have been formed 'in situ' by mainly chemical diffusion-type processes. The orientation of the segregation layers is strongly related to the deformational fabrics within the harzburgites (see below).

A pervasive tectonic foliation is developed throughout the Peridotite Unit. It varies from a strong to only a weak trace in some areas and is sub-parallel to the segregation layering. It is best picked out in the field by studying the preferred orientation of the elongate spinel grains on more than one adjacent rock faces (Plate 2.3). Individual orthopyroxene crystals, when clearly visible, are also aligned parallel to the foliation (Plate 2.4). A tectonic lineation is associated with the foliation plane but is difficult to identify in the field or in hand specimens; only in areas where the foliation is strongly developed is a lineation measured with confidence.

In a typical thin section of the tectonized harzburgite, serpentisation has partially marked the original textures present (Plate 2.5). Olivine crystals have been partially altered to serpentine along internal fractures to give a mesh-texture. In sections of strong serpentinisation,

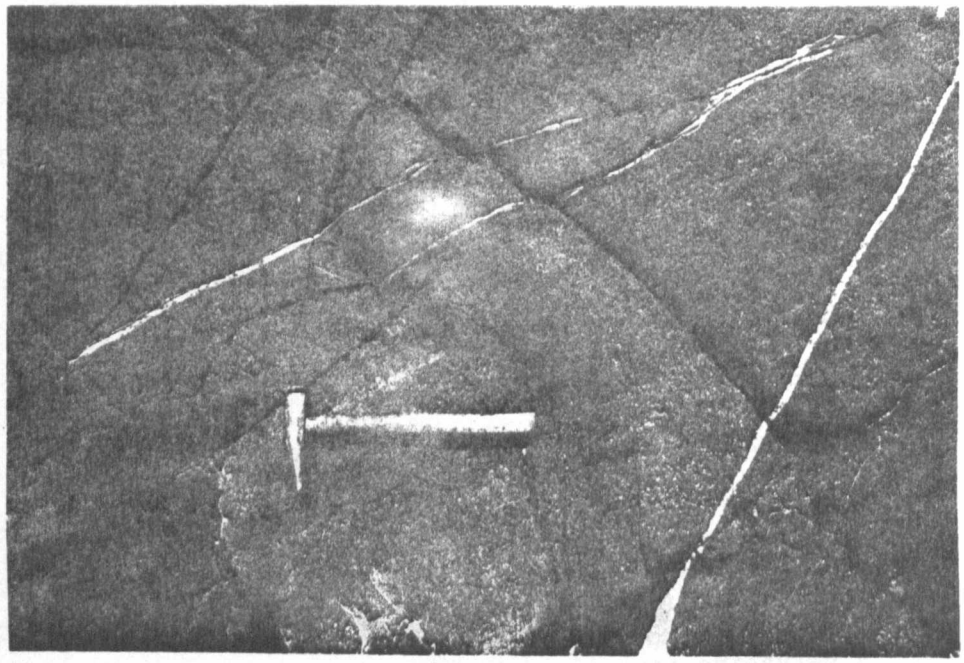

Plate 2.1 Orthopyroxene-rich segregation layers in tectonised harzburgite. (Hammer 40 cm in length).

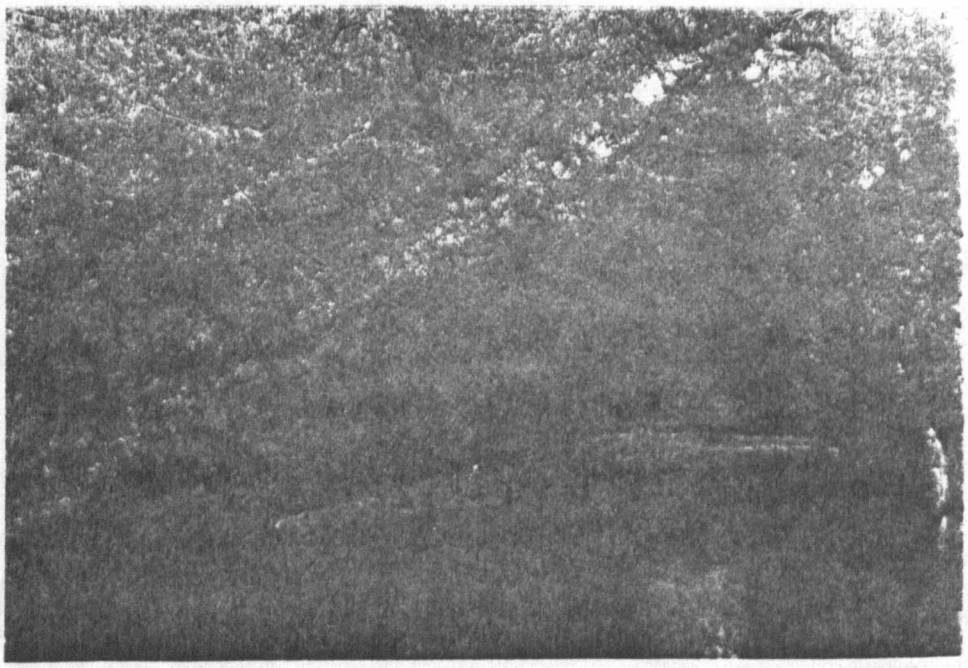

Plate 2.2 Orthopyroxene-rich and olivine-rich segregation layers in tectonised harzburgite.

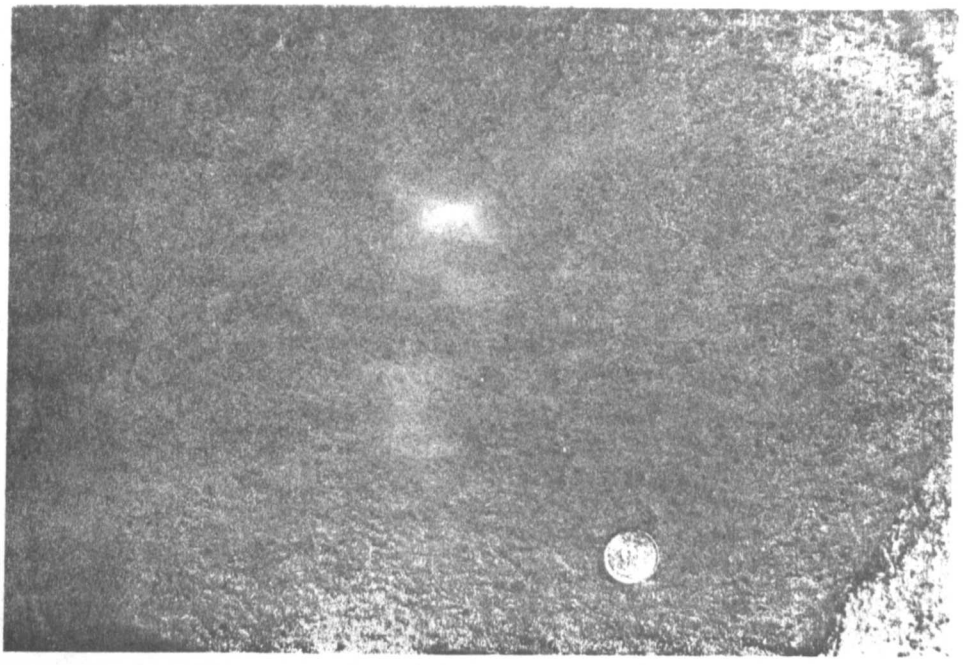

Plate 2.3 Chrome-spinel grains defining a foliation trace in tectonised harzburgite. (Coin 2.5 cm diameter). —— = foliation trace.

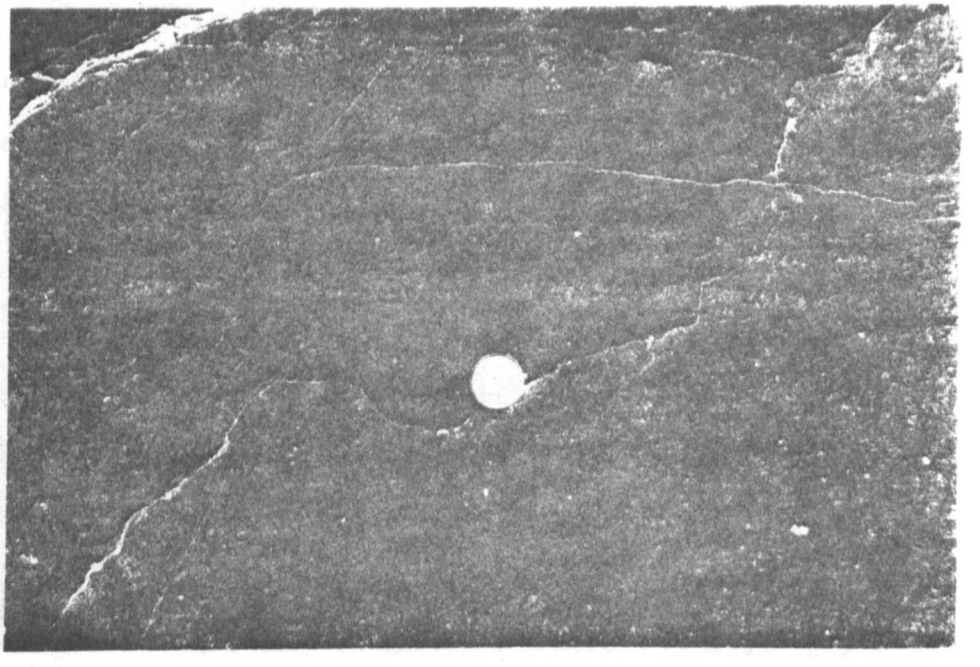

Plate 2.4 Orthopyroxene grains defining a foliation trace in tectonised harzburgite.

mesh-serpentine completely replaces olivine (Plate 2.6). The preservation of this mesh texture, even in rocks that have been 100% serpentinised, indicates that very little movement occurred during or after the serpentinisation event: ie. serpentinisation occurred well after the Peridotite Unit had been pervasively deformed. In moderately serpentinised sections original olivine crystals can be discerned by 'piecing together' relict pieces of equal birefringence to produce a 'composite' of an original crystal.

Olivine varies considerably in its appearance both within a single specimen and between different areas. Olivine grains vary from being highly strained porphyroclasts with undulose extinction to unstrained and recrystallized neoblasts with straight extinction. Both porphyroclasts and neoblasts vary considerably in grain size from a groundmass of grains less than 0.1mm in diameter up to grains of over 1cm in diameter. A detailed study of the grain shapes, crystallographic orientations and deformation states of olivine is discussed in Chapter 8. This study shows that as deformation proceeds in the Peridotite Unit, olivine undergoes a cyclical behaviour of: crystallization with grain growth - crystal strain with breakdown of larger grains to a groundmass of strained grains - recrystallization of favourably oriented grains; and so on. In any one section, olivine grains in all stages of this cycle will be present. This cyclical pattern has been described by Harte (1977). The rate at which an individual olivine crystal will grow in a strain environment will depend on the strain

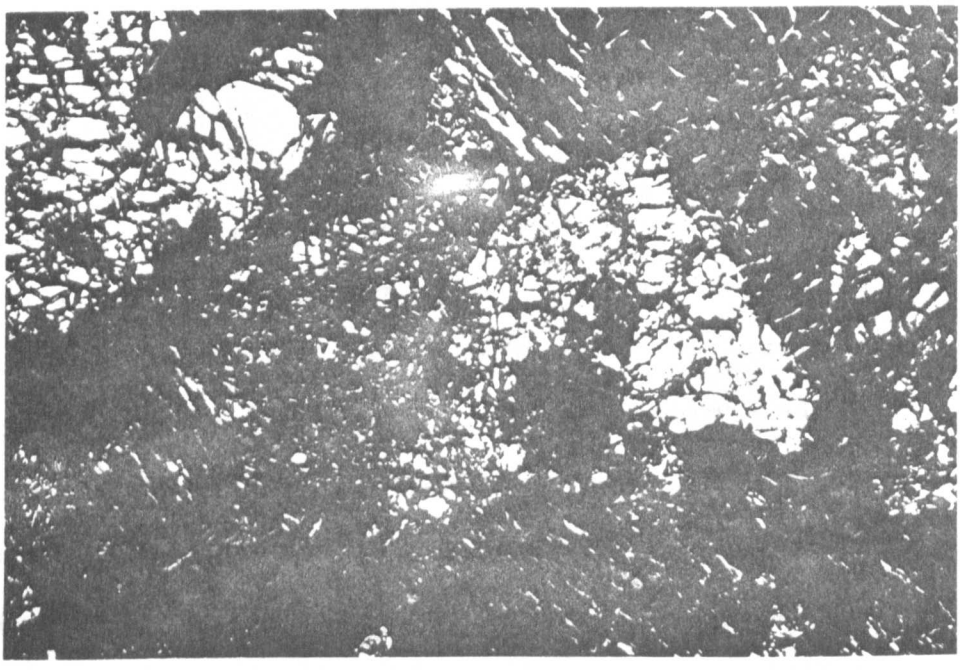

Plate 2.5 A typically serpentinised thin-section. (Cross polarised light). Length of plate = 5 mm.

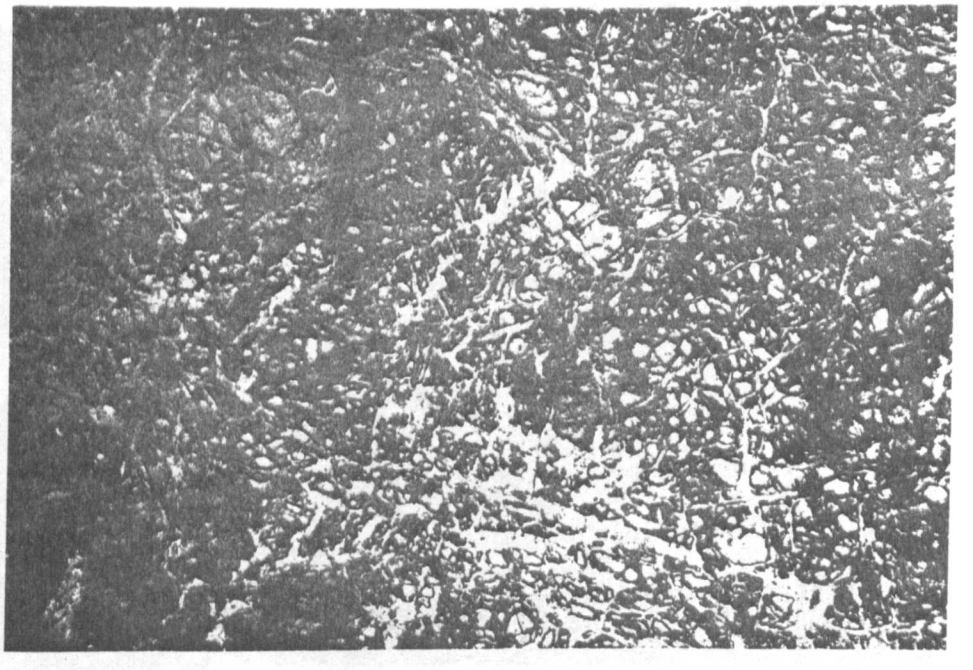

Plate 2.6 Serpentinite mesh texture in thin-section. (Plane-polarised light). Length of plate = 5 mm.

rate and intensity, and also on the initial crystallographic orientation of the crystal. (See Chapter 6 for review of olivinedeformation.) Each crystal will act independently and thus at any one time some crystals will be growing whilst others are being broken down. The overall rock textures (in thin section) have been classified by Harte (1977) on the basis of the distribution and type of olivine crystals present. This classification is shown on Table 1.1 (Chapter 1). The harzburgite textures in Oman vary from coarse through to mosaic porphyroclastic (Plates 2.7 - 2.9), with most rocks having a porphyroclastic to coarse-porphyroclastic texture. The distribution of the different textural types over the areas studied in Oman is discussed below (Section 2.4).

Orthopyroxene shows little alteration in this section. It most commonly occurs as large porphyroclasts of up to 4mm diameter or as 'clot-like' groups of porphyroclasts. It reacts in a more brittle manner to strain than olivine and does not recrystallise so readily. With an increase in strain, orthopyroxene porphyroclasts break down into groups of sub-grains (Plate 2.10) which then become more dispersed throughout the rock. Clinopyroxene, where present, behaves in a similar manner to orthopyroxene. (Plate 2.11).

Small groups of olivine neoblasts are commonly associated with the orthopyroxene 'clots' (Plate 2.12), as well as unstrained olivine inclusions within individual orthopyroxene grains Larger olivines also poikiloblastically enclose

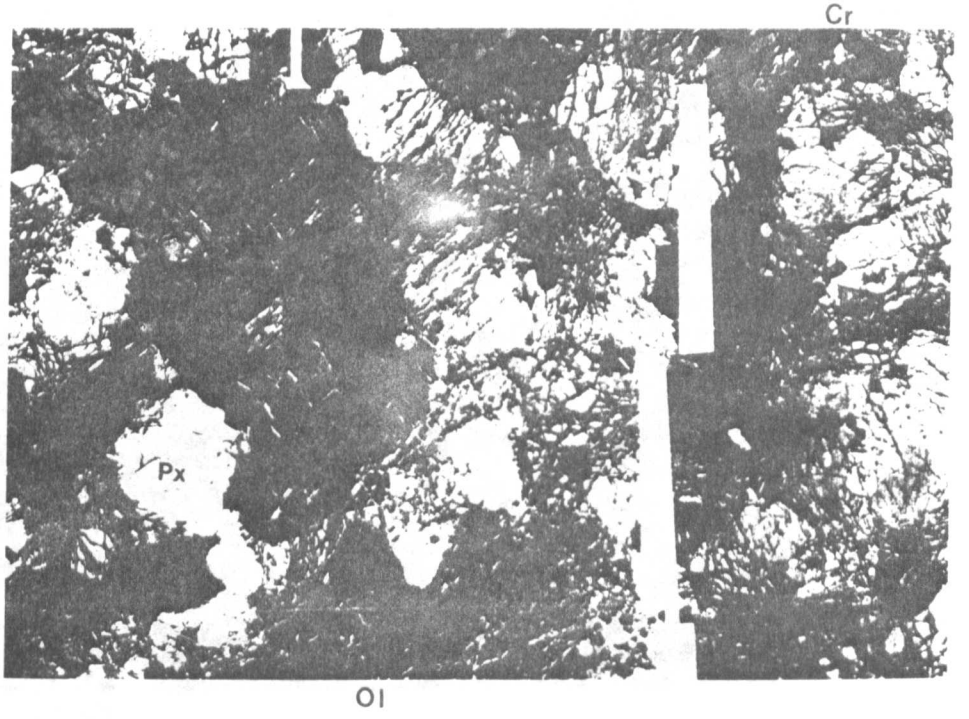

Plate 2.7 Coarse textured harzburgite. (Cross-polarised light). Length of plate = 2 cm. Ol = Olivine, Px = Orthopyroxene, Cr = Chrome-spinel.

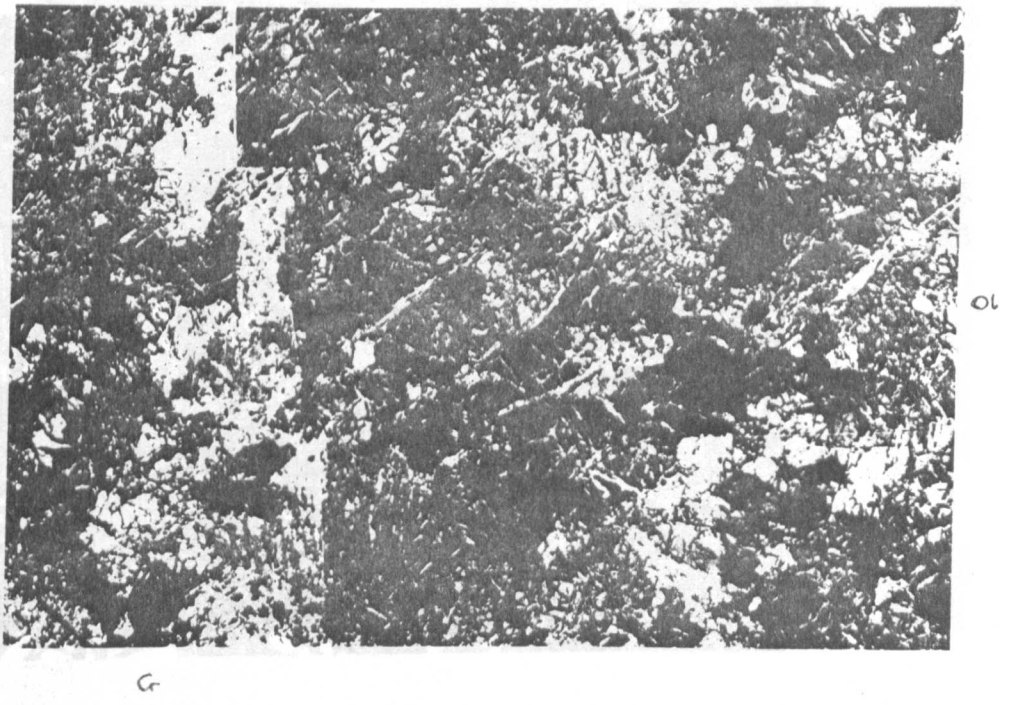

Plate 2.8 Porphyroclastic textured harzburgite. (Cross-polarised light). Length of plate = 2 cm. Ol = Olivine, Px = Orthopyroxene, Cr = Chrome-spinel.

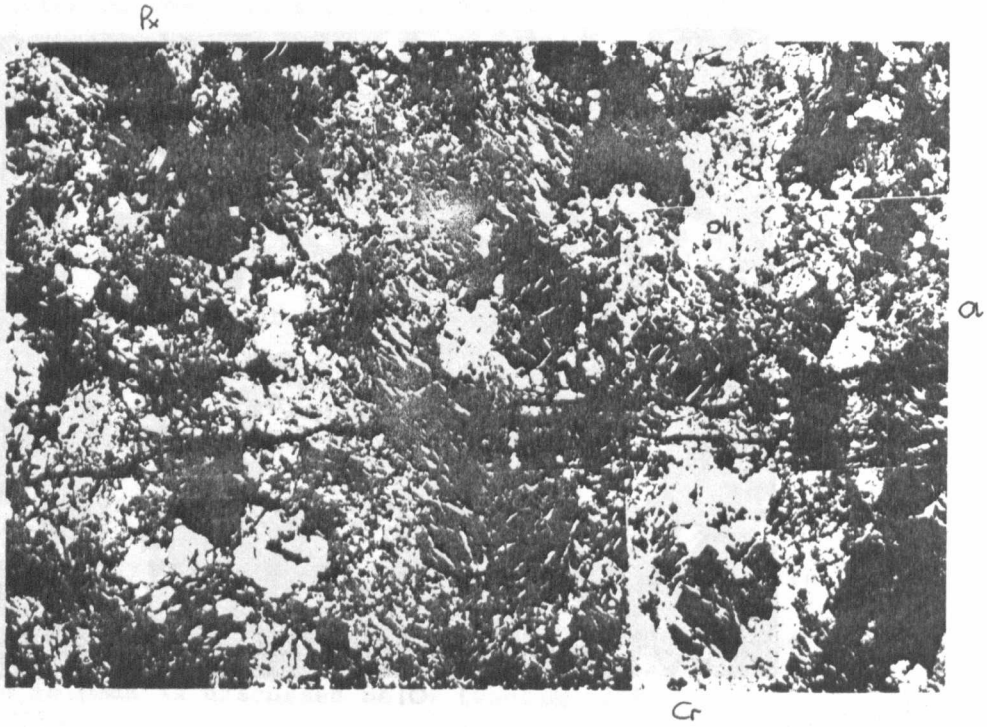

Plate 2.9 Mosaic porphyroclastic textured harzburgite. (Cross-polarised light). Length of plate = 2 cm. Ol = Olivine, Px = Orthopyroxene, Cr = Chrome-spinel.

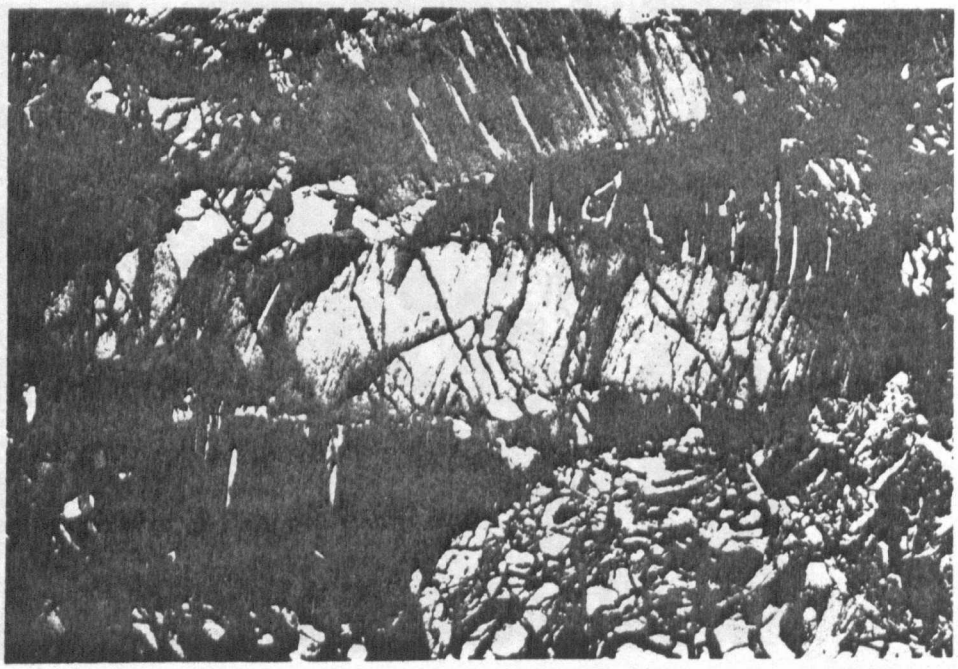

Plate 2.10 Sub-graining of orthopyroxene porphyroclasts. (Cross-polarised light). Length of plate = 5 mm.

Plate 2.11 Sub-graining of clinopyroxene porphyroclasts. (Cross-polarised light). Length of plate = 5 mm. Cpx = Clinopyroxene.

Plate 2.12 Olivine neoblasts associated with orthopyroxene clots. (Cross-polarised light). Length of plate = 5 mm. n = olivine neoblasts.

orthopyroxene grains. These observations imply that there was more than one olivine recrystallization phase in some areas of the harzburgites. (See Chapter 8.)

The textures of chrome-spinel in the Peridotite Unit are highly variable. Spinel grains of less than 0.5mm diameter are dispersed interstitially throughout the groundmass and also as inclusions within olivine and orthopyroxene grains (Plate 2.13). These spinels have been deformed and are elongate and wormy, their long dimensions orientated parallel to the tectonic fabric. In thin section they are the only clear indicators of the orientation of the foliation plane trace. In some thin sections, elongate spinel grains show two preferred orientations. A few grains are parallel to one trend whilst most others are parallel to another trend. This implies that some grains are still aligned parallel to a relict earlier foliation plane whilst most have been rotated into a later foliation plane. Two foliation planes can be defined by studying 3 orthogonal thin sections and can be related to field foliation measurements. In the areas where two foliation planes have been observed, it is clear that evidence has been preserved of two separate deformational events. These events have been termed D1 and D2 and their associated structures and their orientations are discussed in detail below. (Section 2.4.)

Spinel also occurs as much larger grains, up to 2mm in diameter. Grains vary from being euhedral to anhedral and are commonly associated with the pyroxene clots. Inclusions of olivine,

orthopyroxene and other accessories are sometimes present in the larger spinels. The anhedral grains often show a 'holly-leaf' texture (Plate 2.14). This implies that the chrome spinel has recrystallized 'in situ' like poikilocrysts in orthocumulates which have crystallized from the intercumulus liquid. The euhedral spinel grains are most likely to be cumulate in origin as proposed by Dick (1977) and are the result of the crystallization of trapped droplets of magma.

Within a single specimen there is commonly a complete sequence of spinel textures from minute wormy spinel to euhedral spinel. Leblanc (1978), attributed this to spinel growth during incongruent melting of orthopyroxene along interfaces with olivine and used the term 'Impregnated Residual Peridotites' to describe the Peridotite Unit. Nicolas et al (1980) proposed that as strain increased, residual mantle spinel became more evenly distributed throughout the rock and recrystallised into 'holly-leaf' type grains. They noted that residual mantle spinel is more aluminous, and thus dark red-brown in thin section; compared to the less aluminous opaque cumulate-type spinel formed by impregnation and crystallisation of trapped magma droplets.

In the mantle areas studied in the Oman Ophiolite the minute wormy spinel is present at all levels in the mantle and its distribution does not correspond to the variations in strain discussed in Chapter 7. The larger grain-sized spinel, however, does vary: euhedral grains become more elongate with an increase in strain and recrystallisation causes the formation

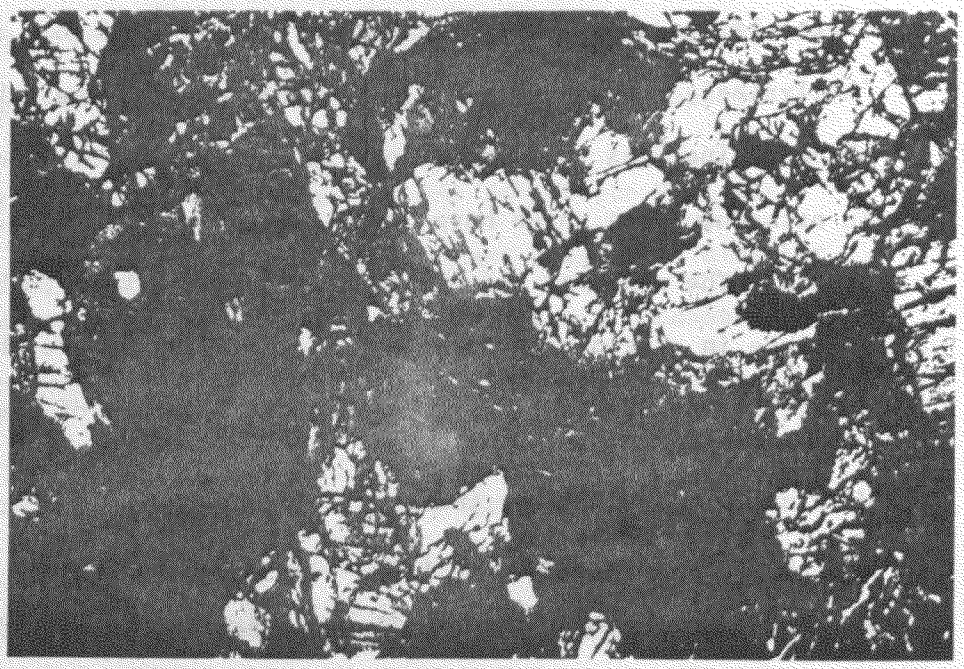

Plate 2.13 Chrome-spinel and olivine grains included in orthopyroxene porphyroclast. (Cross-polarised light). Length of plate = 5 mm.

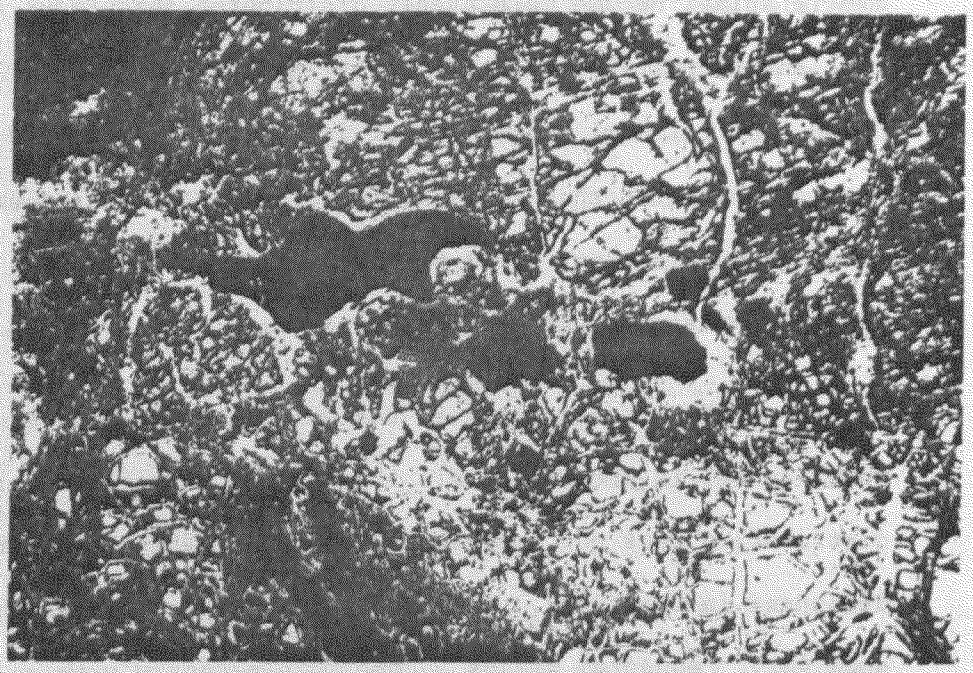

Plate 2.14 'Holly-leaf' chrome spinel texture in harzburgite. (Plane polarised light). Length of plate = 5 mm.

of the 'holly-leaf' type textures. (See section 2.4.) Christiansen (pers. com.) has proposed that deformation of these larger euhedral spinels by pressure solution may have formed the 'holly-leaf' textures.

Euhedral spinels occur in the same section as highly deformed elongate 'holly-leaf' grains. This indicates that droplets of magma were impregnating the Peridotite Unit in more than one event. Early impregnated droplets would have crystallized when the Peridotite Unit was still being deformed; these spinel crystals would quickly be deformed and recrystallised as shown in Figure 2.9. Droplets impregnated after deformation had ceased would form euhedral spinels or possibly poikilocrysts with 'holly-leaf' type textures.

In areas rich in segregation layers, similar textures and petrologic features are observed in thin-section as in the more massive harzburgies. The layers are always sub-parallel to the most prominent foliation which is defined from the alignment of both spinel and orthopyroxene grains. The lack of sharp ratio contacts, and the similarities of textural and petrologic features between these layers and the surrounding harzburgites, along with their parallelism to the major foliation, all support the hypothesis that they were formed by metamorphic segregation processes taking place during deformation. (Dick and Sinton, 1979.) Olivine-rich layers appear undeformed in the field because of the small contrast in competency between mantle dunites and harzburgites.

(Compositionally, they are very similar.) More orthopyroxenitic layers, on the other hand, behave in a more brittle fashion and are often slightly boudined when orthopyroxene forms over 70% of the rock (Plate 2.15).

(b) Intrusive Features Within the Tectonised Harzburgites

Various sheet-like and podiform bodies are present within the Peridotite Unit of the Oman Ophiolite. They represent either dyke-like intrusions or relict magma-chambers within the mantle sequence. They are all termed intrusive features as the original liquid which formed them has clearly not been derived from the crystallization of the harzburgites (ie. in situ) but from later liquid infiltration events, as the evidence below shows. These intrusive features have been divided into three groups on the basis of their composition and field relations:-

(i) Dunite Pods and Sheets: Bodies of dunite outcrop sporadically within the Peridotite Unit of the Oman Ophiolite. In contrast to the metamorphic layering, the contacts between these bodies and the surrounding harzburgites are always sharp (Plate 2.16). The bodies vary from discontinuous layers or sheets a few centimetres thick to large pod-shaped bodies as large as 200 × 600 metres. Associated with some of these dunites are concentrations of chrome-spinel which form thin layers parallel to the intrusive contacts. The spinel layers are usually found in the centres of the bodies (Plate 2.17).

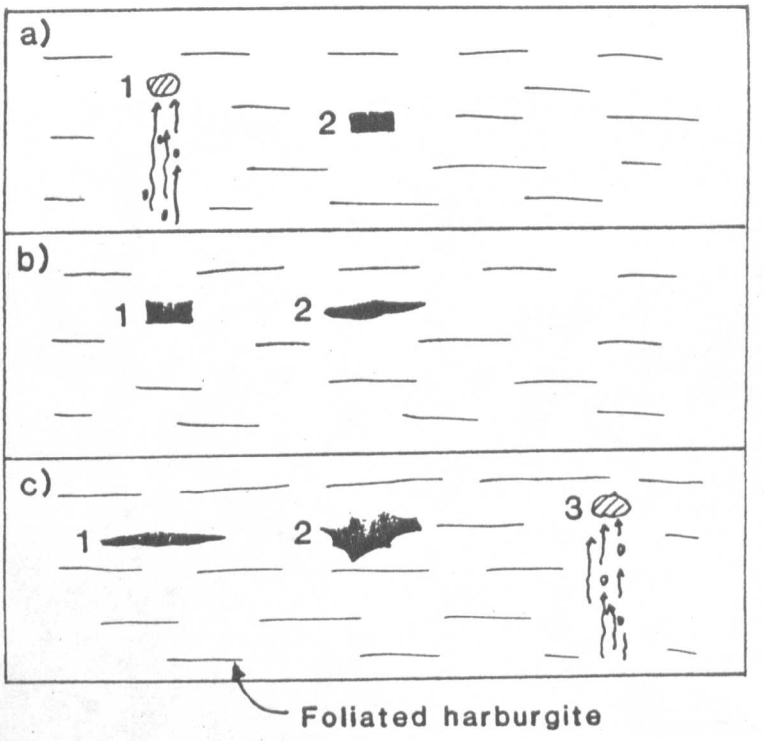

Figure 2.9 The suggested deformation of chrome spinel in the Peridotite Unit. a) Infiltration of droplet 1, grain 2 crystalllised; b) Grain 1 crystallised, grain 2 elongates; c) Grain 1 elongates, grain 2 regrows to holly-leaf shape, grain 3 infiltrates.

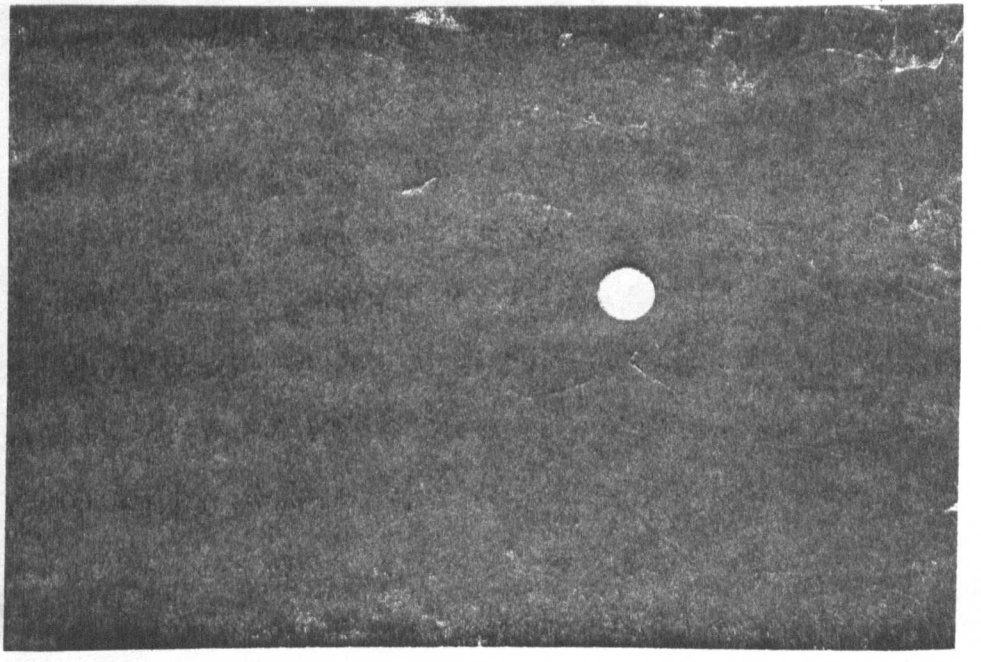

Plate 2.15 Boudinage of orthopyroxene-rich layers and stretching of orthopyroxene-poor layers in harzburgite. (Coin 2.5 cm diameter).

Plate 2.16 The sharp contact between a dunite sheet and harzburgite. (Length of plate = 100 cm).

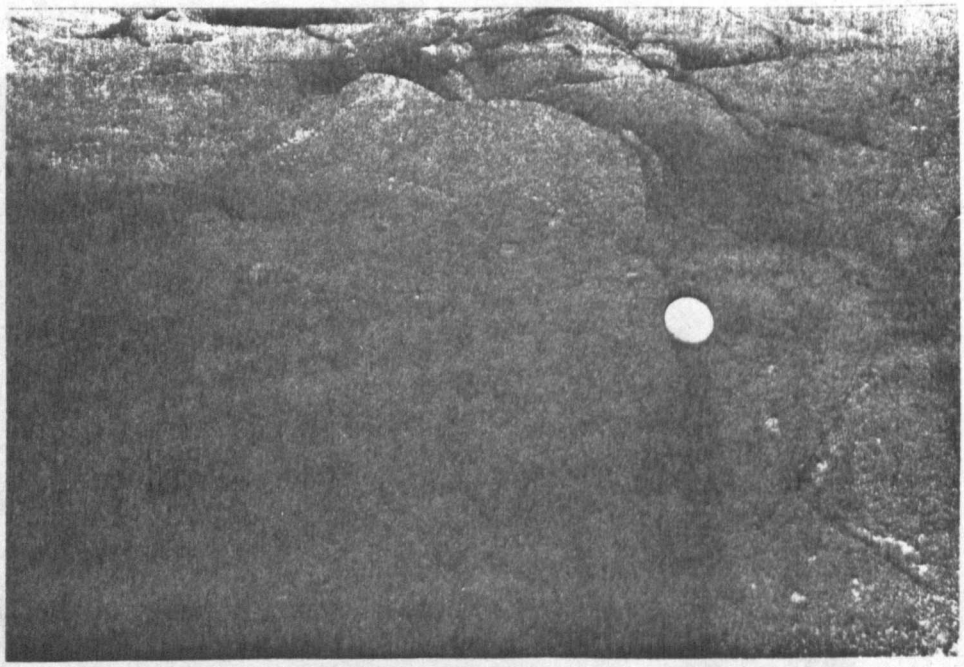

Plate 2.17 Chrome-spinel horizons in a dunite sheet and their relationship to the surrounding harzburgite. (Coin 2.5 cm diameter).

In thin section the olivines in the dunites show similar textures to those in the harzburgites, with porphyroclasts and neoblasts in various states of strain. The dunites tend to be coarser-grained than the harzburgites: either because they were intruded later in the deformation history of the harzburgites, and have thus undergone less deformation; or because they behave slightly differently from the pyroxene-containing harzburgite in that the olivine porphyroclasts are more easily rotated into a favourable position for grain growth in monomineralic rocks where pyroxene is absent. As already noted, small olivine neoblasts are often associated with orthopyroxene clots in harzburgites (Plate 2.12). However, in some areas of pyroxene-poor harzburgites (< 10% Pyroxene), where the pyroxene present is locally concentrated into clots, the texture of the rock is fine-grained porphyroclastic; whereas nearby dunitic bodies have a coarse texture. This indicates that the dunitic bodies have undergone less deformation than the surrounding harzburgites and were intruded into the harzburgites later in the whole deformation process.

The pervasive tectonic foliation developed throughout the Peridotite Unit cuts straight through all of the dunite pods and sheets. This indicates that the dunite intruded into the residual harzburgites before or early during the foliation-producing deformation, which is itself a late event in the mantle deformation history. (See section 2.3.3 and Chapter 9.)

The shape of the dunitic bodies is controlled partly by their original intrusive shape and partly by the deformation. They most probably originated either as feeder conduits or as cumulate chambers within the rising mantle diapir and were subsequently deformed. Where deformation is low the original intrusive relationships are preserved: the feeder conduits are sharp sided 4-10cm thick dykes and the foliation is often sharply discordent to them; the dunite cumulate chambers are centimetres to metres thick, have sharp contacts and are commonly connected by feeder conduits. In some areas this results in a net-like pattern of dunitic sheets and bodies - these features are termed "anastomosing dunites" in this thesis (Plate 2.18). In these areas of low deformation, the margins of the dunite cumulates interfinger with the residual harzburgite in a direction parallel to the foliation (Plate 2.19). Chromitites form large coherent bodies in some of the larger of these dunites. Possible cumulate textures have been observed in some of these bodies: layering, graded bedding and possible layer slumping (Brown, 1979). Possible 'harrisitic'-type textures of olivines associated with chromitite layers described by Brown (1980) have now been re-interpreted as aggregates of olivine neoblasts within tectonically folded chromitite layers (Christiansen and Roberts, in prep.).

These relict cumulate-type textures, the deformation textures in thin section and the sharp-sided boundaries of the dunite bodies with the surrounding harzburgites all point towards either an intrusive origin or a cumulus origin in both large and small cumulate

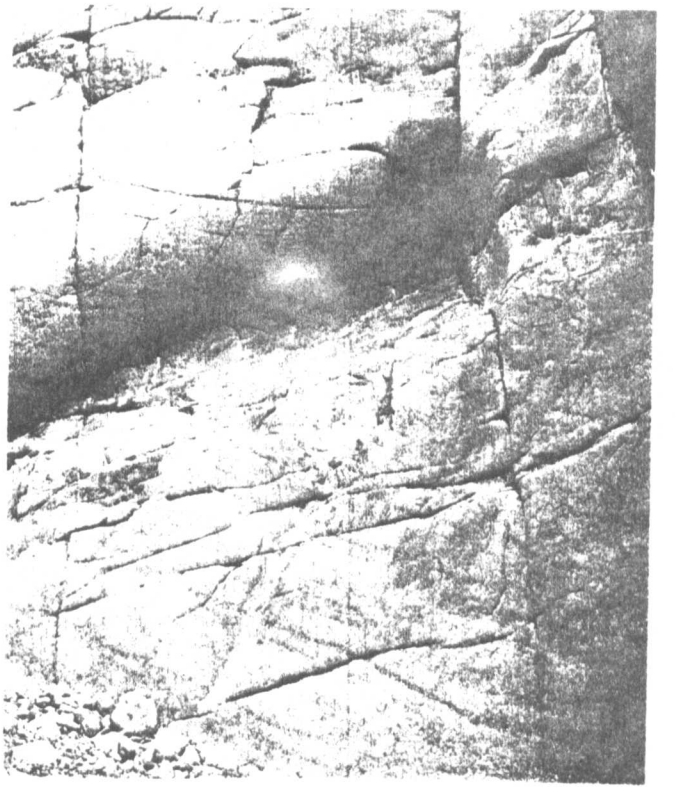

Plate 2.18 Anastomosing dunite sheets in a weakly deformed harzburgite.

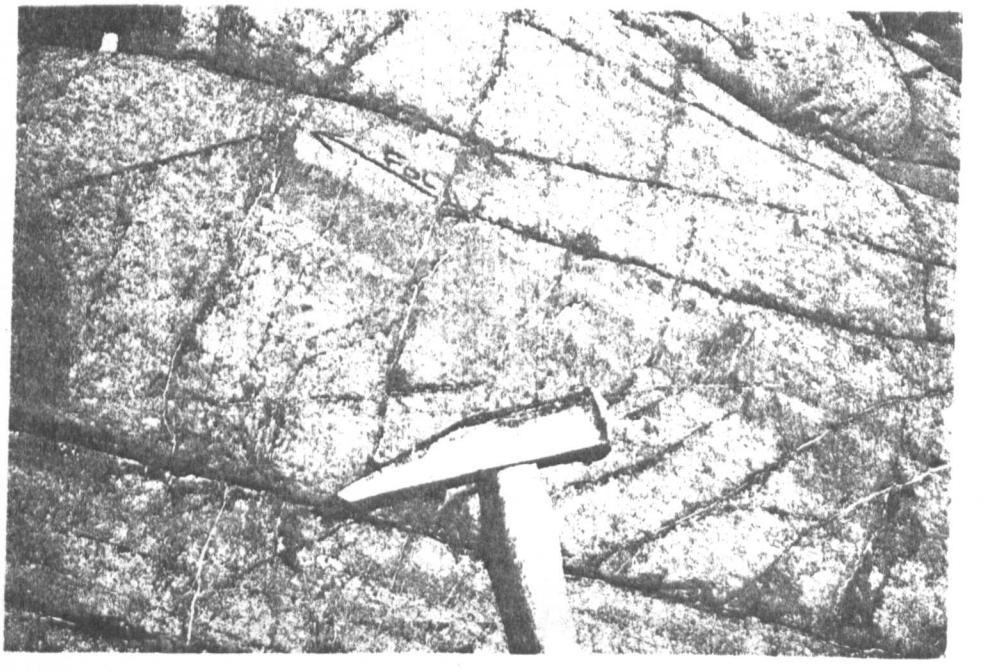

Plate 2.19 Dunite sheets interfingering with harzburgite. (Hammer 40 cm in length).

chambers. Their characters contrast strongly with the segregation layers described above, and it is difficult to explain their origin as part of the residuum of the massive harzburgites.

In areas of more intense deformation the dunite cumulates are more podiform and are concordant or sub-concordant with the more strongly developed foliation. The dunite feeders are also sub-parallel to the foliation and the anastomosing structures of the dunites in areas of low deformation are destroyed. Chromitites occur as thin strung-out layers a few centimetres thick (Plate 2.17) and rarely show isoclinal to tight folding (Plate 2.20).

The viscosity contrast between these dunitic bodies and the surrounding harzburgites was very small. The bodies are therefore not folded as they acted as a single unit with the harzburgites.

Figure 2.10 summarises the different features of dunite intrusives in the Mantle Sequence.

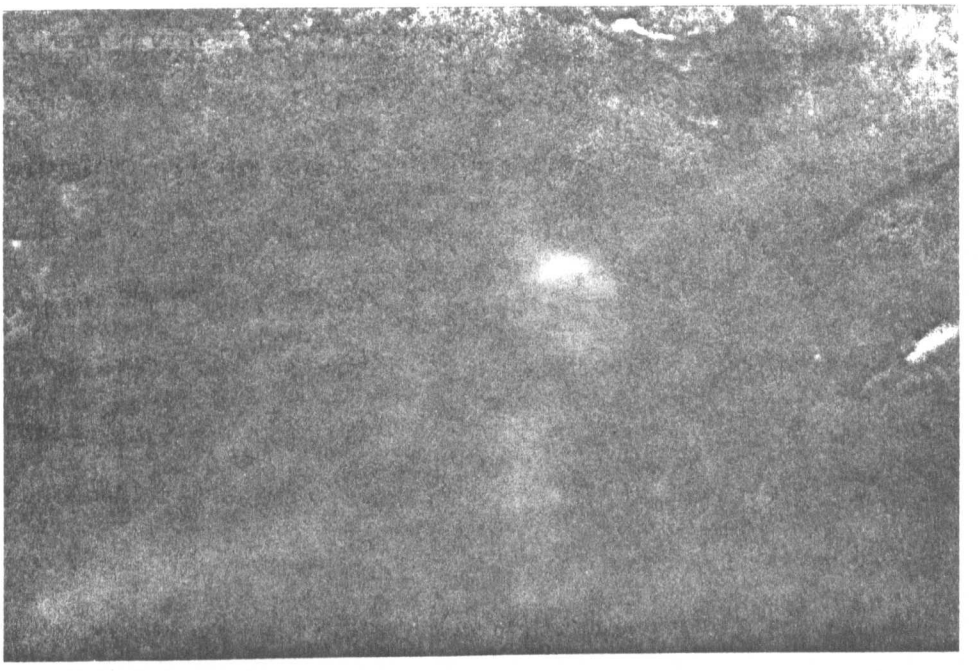

Plate 2.20 Tightly folded chromite layer within a dunite sheet. (Length of plate 25 cm).

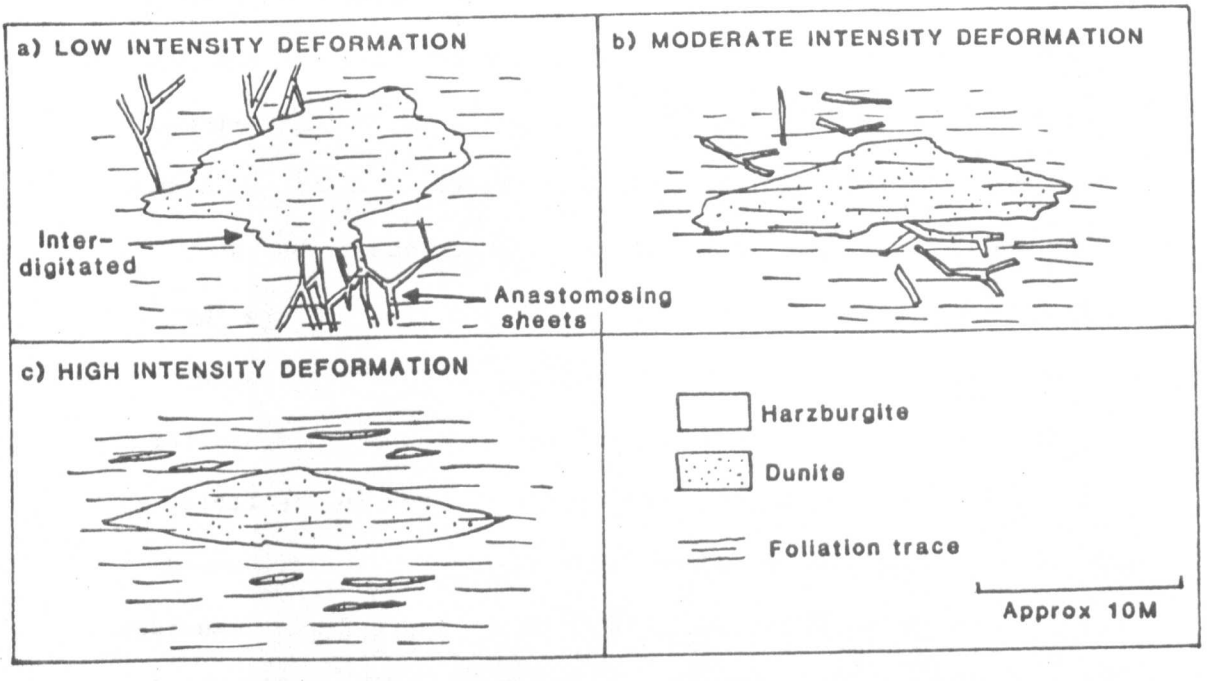

Figure 2.10 The progressive deformation of dunitic bodies and sheets within the Peridotite Unit.

(ii) Deformed pyroxenitic and gabbroic sheets:

These dyke-like sheets have sharp contacts and are laterally discontinuous on the outcrop scale. They are rarely more than 5cm thick. Compositions vary from clinopyroxenitic, wehrlitic, olivine gabbroic to gabbroic. Some dykes have substantial amounts of orthopyroxene giving websterites and gabbronorites, but clinopyroxene is usually the main pyroxene present. Individual grains are elongate and define a foliation which is sub-parallel to the main harzburgite foliation. The dykes have thus been deformed during the main Periodite Unit deformation event.

Two deformation styles are shown by the dykes. The more competent pyroxene-rich dykes have been deformed by flexural shear processes and have formed either tight folds (Plate 2.21) or boudins (Plate 2.22) depending on their original orientation within the strain ellpsoid (Figure 2.11). The pyroxene-poor dykes of a lower competency, closer to that of the harzburgites and dunites have been deformed not by folding but instead have been rotated by shearing towards the foliation plane. Plates 2.23 and 2.24 show that the dykes have been sheared along discrete shear planes parallel to the foliation. It is tentatively suggested here that the massive harzburgites and dunites deform in a similar manner by shearing, but on a much smaller scale, so that no evidence for a shearing deformation in the harzburgites is seen in the field. The detailed crystallographic and shape fabric studies discussed in Chapters 6-8 show that this is the case. Figure 2.11 summarises the styles of deformation in the deformed pyroxenitic and gabbroic sheets.

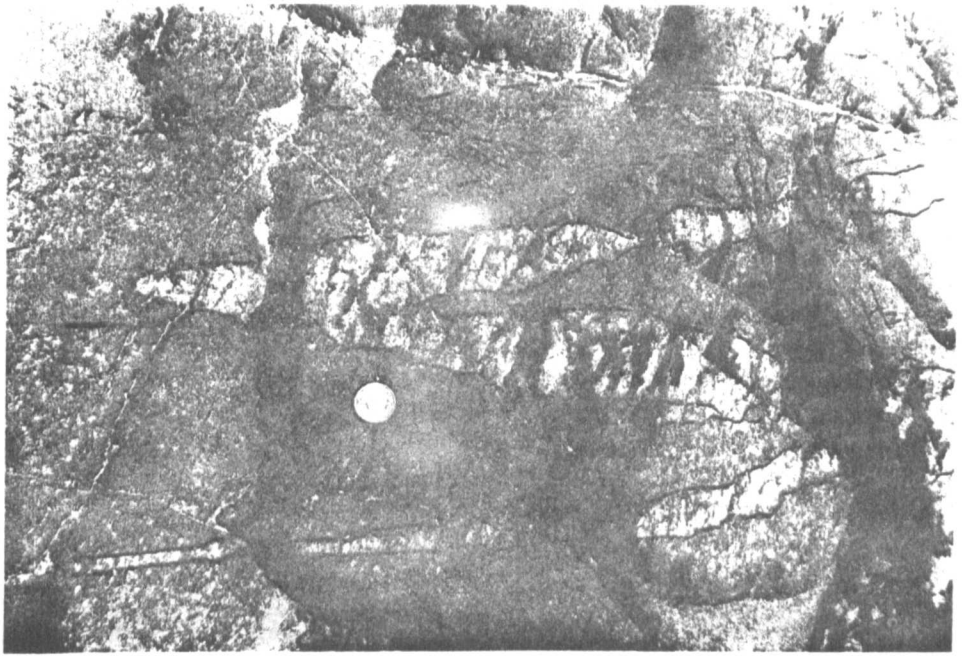

Plate 2.21 Tightly folded clinopyroxene dyke in harzburgite. (— = S2 foliation in harzburgite). (Coin 2.5 cm diameter).

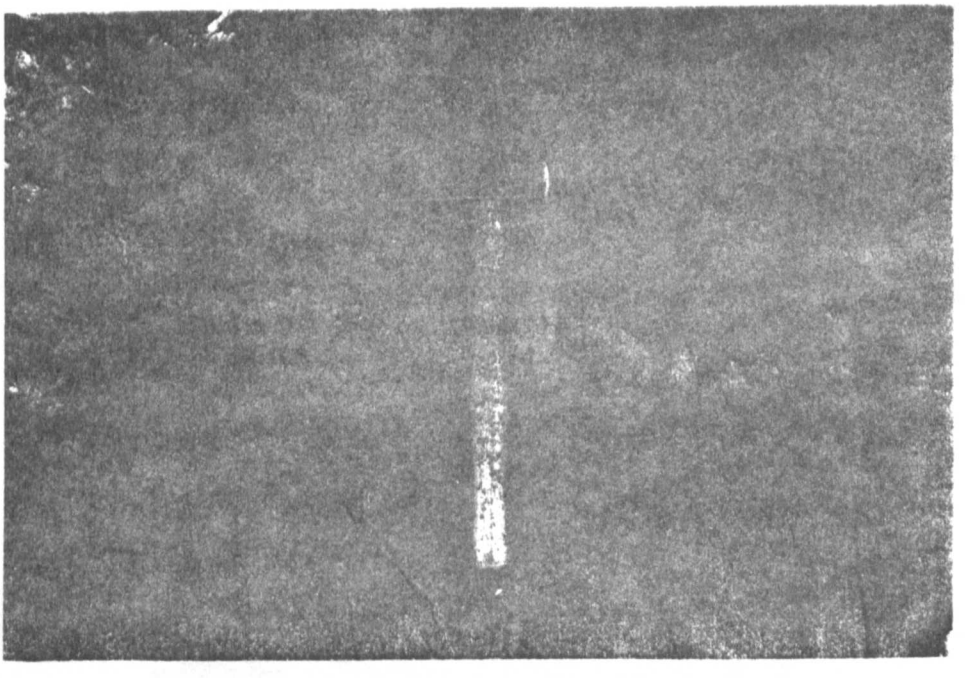

Plate 2.22 Boudined clinopyroxene dyke in harzburgite. (— = S2 foliation in harzburgite). (Hammer 40 cm length).

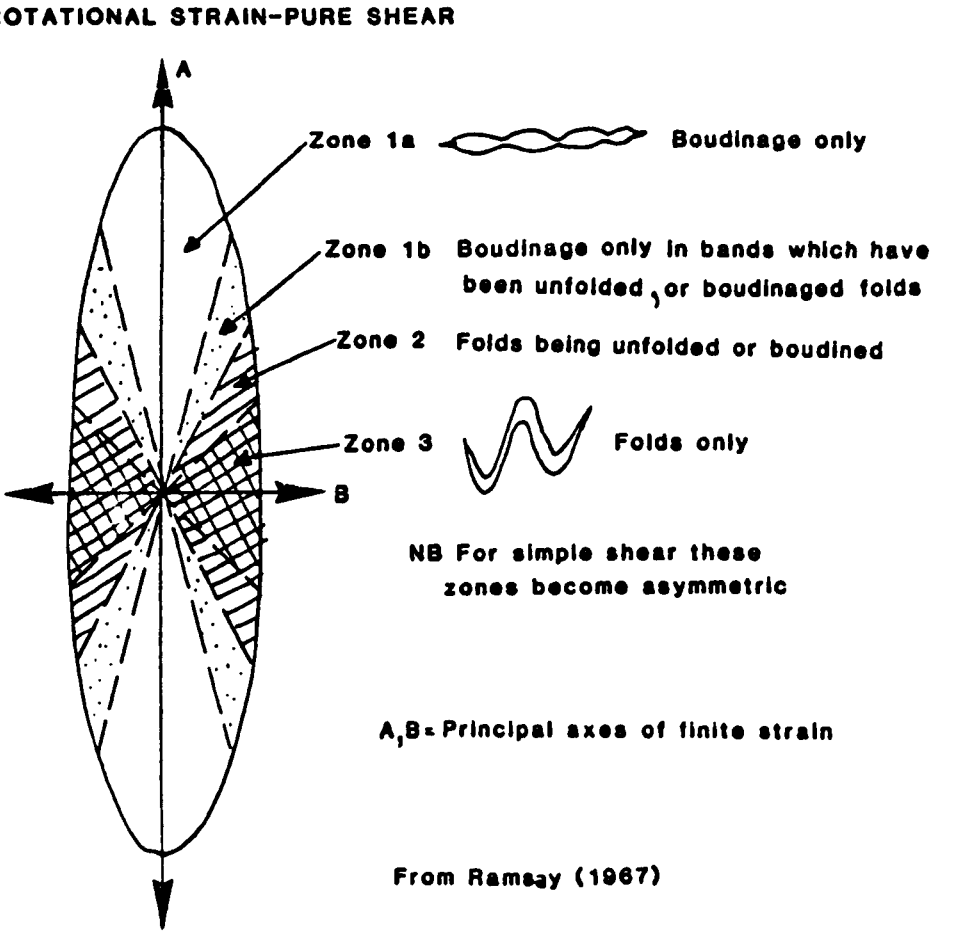

Figure 2.11 Deformation of competent pyroxene-rich dykes. Flexural shearing forming folds or boudins.

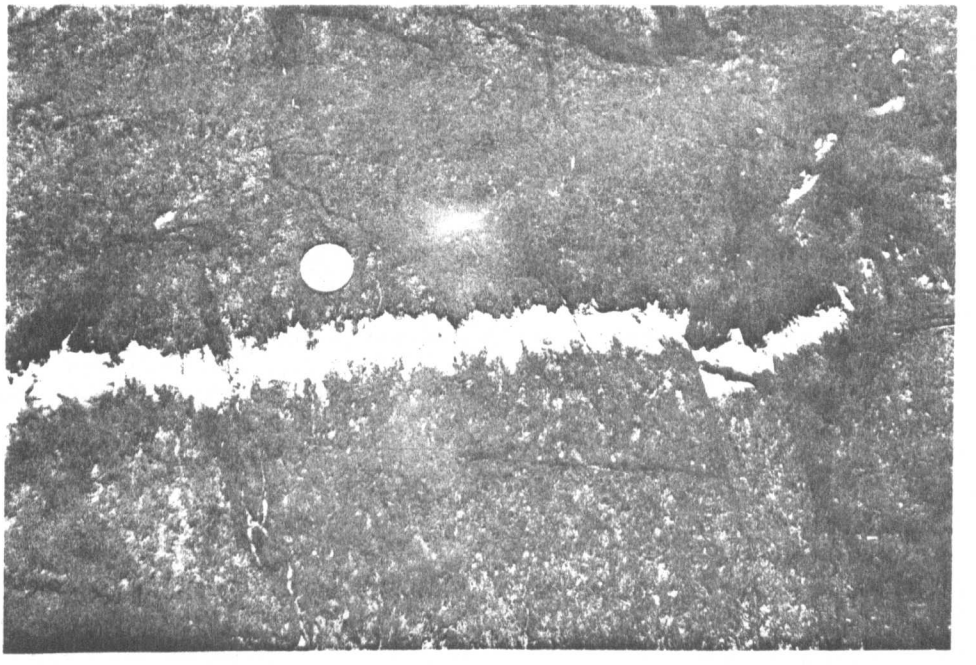

Plate 2.23 Small scale shearing of a plagioclase-rich dyke. (—— ⊨ S2 foliation in harzburgite). (Coin 2.5 cm diameter).

Plate 2.24 Larger-scale shearing of a plagioclase-rich dyke. (—— = S2 foliation in harzburgite). (Coin 2.5 cm diameter).

In all cases these deformed sheets cut the dunite pods and sheets; they were therefore intruded later than the durites and consequently very late in the deformation history of the Peridotite Unit.

(iii) Undeformed pyroxenitic and gabbroic sheets:

These sharp-sides dyke-like sheets are similar in composition to the deformed pyroxenitic and gabbroic sheets. They vary from 1cm to 1.5m in width and are often pegmatitic (Plate 2.25) with individual pyroxene crystals up to 30cm in diameter. Some dykes show marginal chilling against the harzburgites. In general the pyroxenite dykes are the earliest of the undeformed dykes to be intruded into the Mantle Sequence. Cross-cutting relationships between pyroxenite dykes however, show that there is more than one dyke generation in the Oman Peridotite Unit. Composite dykes of pyroxenite intruded by gabbroic dykes (Plate 2.26) and cross-cutting relationships indicate that most of the gabbroic dykes were intruded after the pyroxenites. As with the pyroxenites, there was more than one generation of intrusion. (Plate 2.27) Occasionally clinopyroxenite grades laterally into gabbro along the same dyke. This implies that a number of gabbroic dykes are from the same source as some of the pyroxenitic dykes.

The undeformed dykes have not been seen to cross-cut any of the deformed pyroxenitic and gabbroic sheets, but they do intrude into all the other Peridotite Unit petrographic features described above. The orientation of the different dyke types is described in section 2.4 below; there is no relationship between these trends and the earlier structural trends.

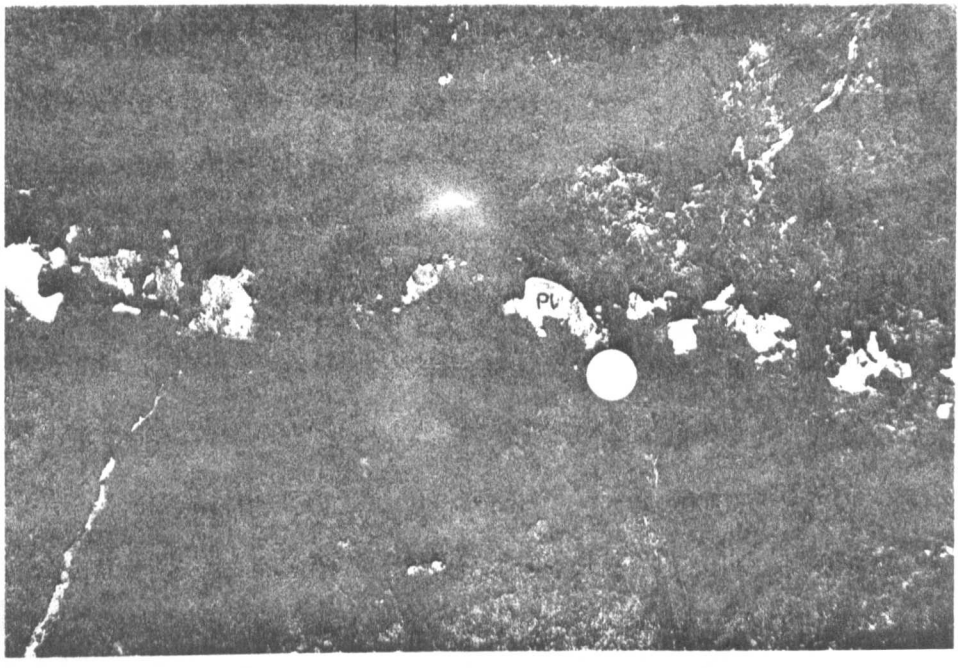

Plate 2.25 Undeformed pegmatitic dyke in harzburgite. Pl = plagioclase, Cpx = Clinopyroxene. (Coin 2.5 cm diameter).

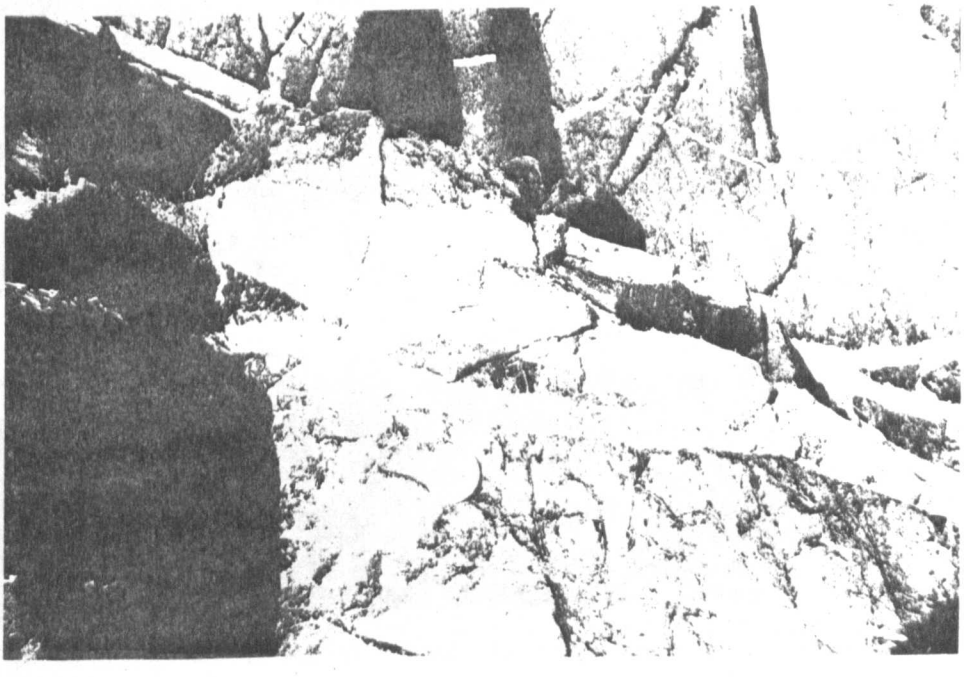

Plate 2.27 Cross-cutting gabbroic and pegmatitic dykes in harzburgite. (Coin 2.5 cm diameter).

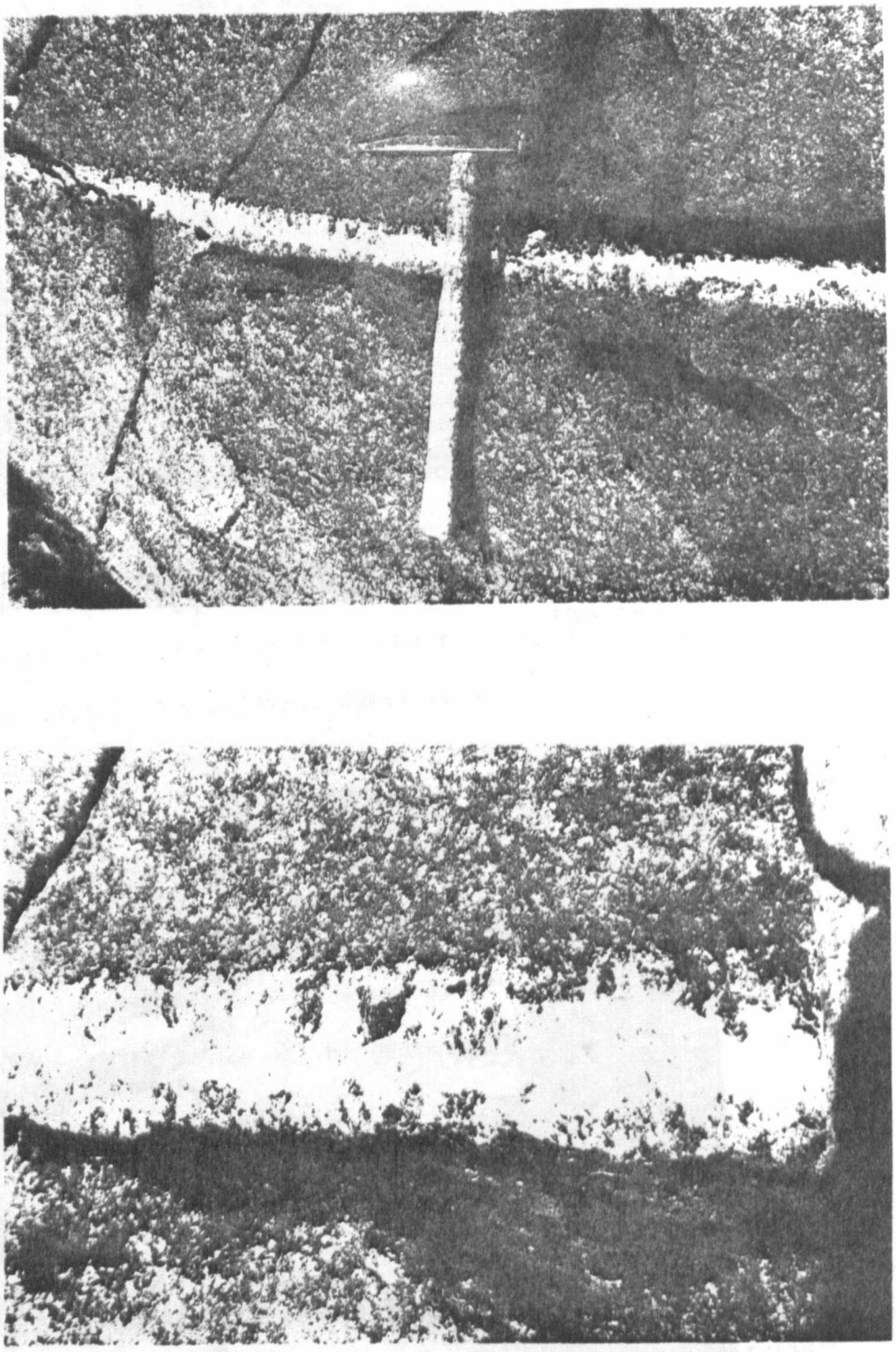

Plate 2.26 Composite dyke in harzburgite with a clinopyroxene-rich rim and plagioclase-rich centre. (Length of hammer 40 cm).

For the purposes of mapping, the pyroxenitic and gabbroic dykes have been divided into the following groups: deformed pyroxenites, deformed gabbros, undeformed pyroxenites, undeformed gabbros, and undeformed pegmatite gabbros. These divisions are used in section 2.4 where specific areas from the Oman Ophiolite are described in detail.

2.3.3 General Features of the Transition Zone and the Gabbros and Ultramfic Cumulates Units

In the Oman Ophiolite the contact between the Peridotite Unit and the cumulates is sharp and planar in all of the areas studied. The pattern of harzburgite becoming more and more scarce upwards with dunite lobes extending down into the harzburgite as described from many ophiolite complexes (see Chapter 1.3.2) is not present in Oman. Accordingly there is no distinctive Transition Zone Unit: all of the rocks from the top boundary of the Peridotite Unit (the Petrological Moho) upwards are therefore taken together as a single unit - the Cumulate Unit.

The upper limit of the Cumulate Unit is taken as the level at which regular layering disappears. It is not the purpose of this thesis to discuss the Cumulate Unit in detail: the following section is restricted to a description of the lower few 1000 metres of the unit which has been termed the Lower Cumulate Unit.

The Lower Cumulate Unit consists of layered gabbroic and ultramafic rocks in a cumulate sequence. The distribution of the different rock types is highly variable between areas, with the ultramafic rocks characterising the lower parts of the Unit and the gabbroic rocks the upper parts. The lateral and vertical variations of

the assemblages developed in the Lower Cumulate Sequence is described for each area in section 2.4.

In a few areas the olivine gabbros are in direct contact with the Petrological Moho, but normally there is a thin (0-200m) ultramafic sequence between the moho and the gabbros.

The major rock types of the Lower Cumulate Unit are dunites, wehrlites, plagioclase-bearing wehrlites, olivine gabbros and gabbros. The phase assemblages developed from the moho upwards depend on the crystallisation order displayed. This is variable between areas (see Section 2.4).

In all areas the Lower Cumulate Unit is strongly layered with layer thicknesses between 10cm and 100cm. The layers can be laterally continuous for over 1km, (Plate 2.28) but are also more discontinuous in some areas (Plate 2.29). The attitude of the compositional layering is highly variable from area to area (see section 2.4). In some areas it is constant over the whole area studied, with a low to moderate angle between the moho plane and the layering; but in other areas the attitude of the layering varies rapidly within a small area. This change in layering attitude has been attributed by Browning (1982) to the existence of fairly small magma chambers which closed and opened along the ridge strike, with highly variable layering attitudes at the ends of the magma chambers.

The rhythmic layers are predominately mineral-graded (Plate 2.30) with isomodal layers sometimes present. The layers are defined

Plate 2.28 Cumulate layers of over 1 km lateral extent in the Wadi Ath Thuqbah area. Du = dunite, G = olivine gabbro.

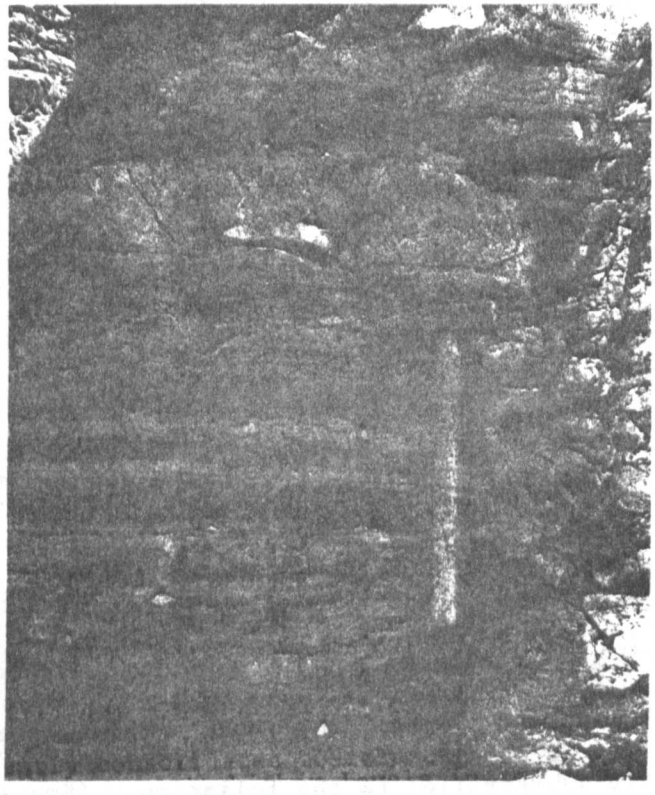

Plate 2.29 Discontinuous cumulate layers in the layered gabbros adjacent to Wadi Jizi. (Length of hammer 40 cm).

by sharp ratio contacts, and in some areas layer truncation and overstepping is fairly common (Plate 2.31). This occurs on both small (cm) and large (10m) scale (Plates 2.32 and 2.33). These small scale features are possibly analogous to sedimentary erosional structures common in an aeolian environment. Other such structures are possibly channel scour and fill type features (Plate 2.34) and slump folds (Plate 2.35). The larger scale layer trucation structures may represent the bases and sides of individual magma chambers within the Cumulate Sequence.

In a few areas of layered cumulates a magmatic lineation can be discerned from the alignment of the plagioclase grains on a layering surface (Plate 2.36). A igneous lamination can often be measured on faces perpendicular to the layering surface (Plate 2.37).

In thin section the cumulates either have adcumulate or mesocumulate textures (Plate 2.38). The grain size is variable with grains from 1mm to 1cm in diameter with a grain size of between 1½ -3mm the most common. In some rocks a strong igneous lamination is seen in thin section (Plate 2.38).

In a few of the areas studied, the pervasive tectonic fabric in the Peridotite Unit extends into the Lower Cumulate Unit. It rapidly dies out upwards in most areas but in the Wadi Al Abyad traverse (Figure 2.8) the foliation extends at least 1km into the cumulates. The trends of the foliation and lineation are uninterrupted by the change in lithology between the Peridotite Unit and the Lower Cumulate Unit, and they maintain a constant orientation in both units. The layers of the Lower Cumulate Unit are usually sub-parallel to the foliation. (See section 2.4)

Plate 2.30 Mineral graded rhythmic layer in the Rajmi area. Clinopyroxene-rich base grading to an olivine-rich top. (B = base, T = top). (Coin 2.5 cm diameter).

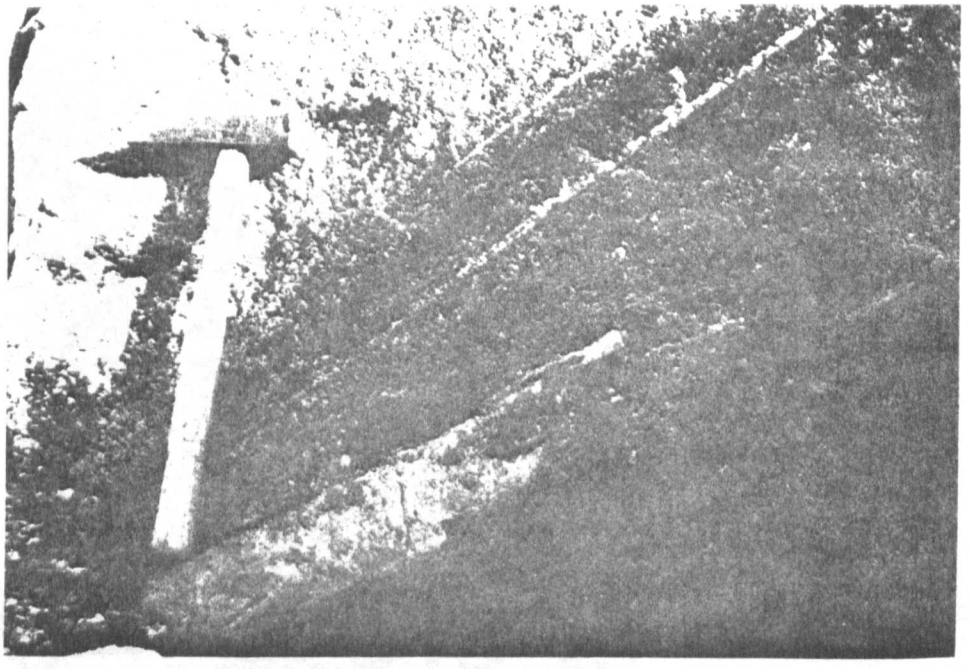

Plate 2.31 Truncation of plagioclase-rich cumulate layer. (Length of hammer 40 cm).

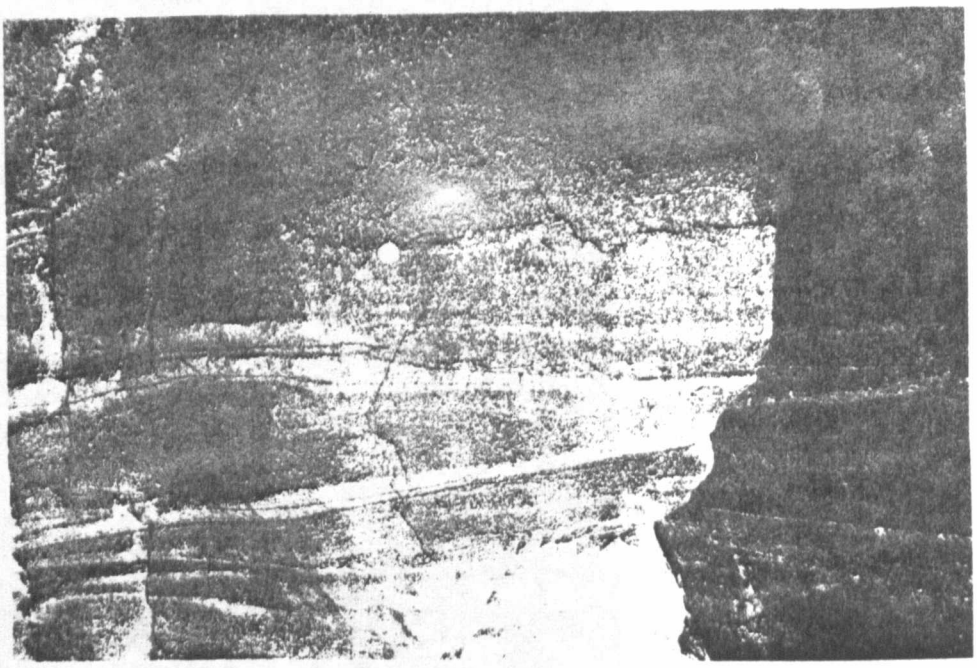

Plate 2.32 Small-scale cumulate layer overstepping in Wadi Al Hilti. (Coin 2.5 cm diameter).

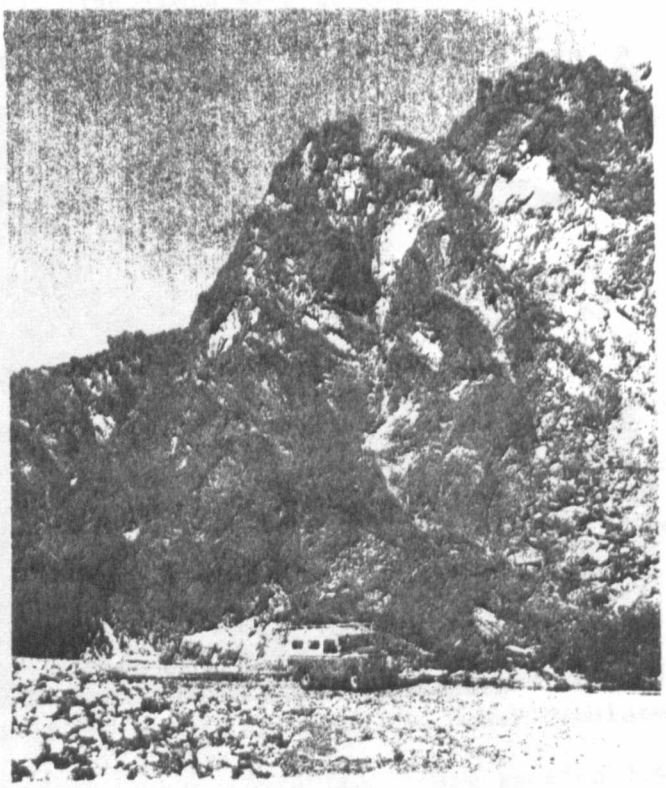

Plate 2.33 Large-scale cumulate layer overstepping in Wadi Al Abyad. Dotted line marks overstepping layer.

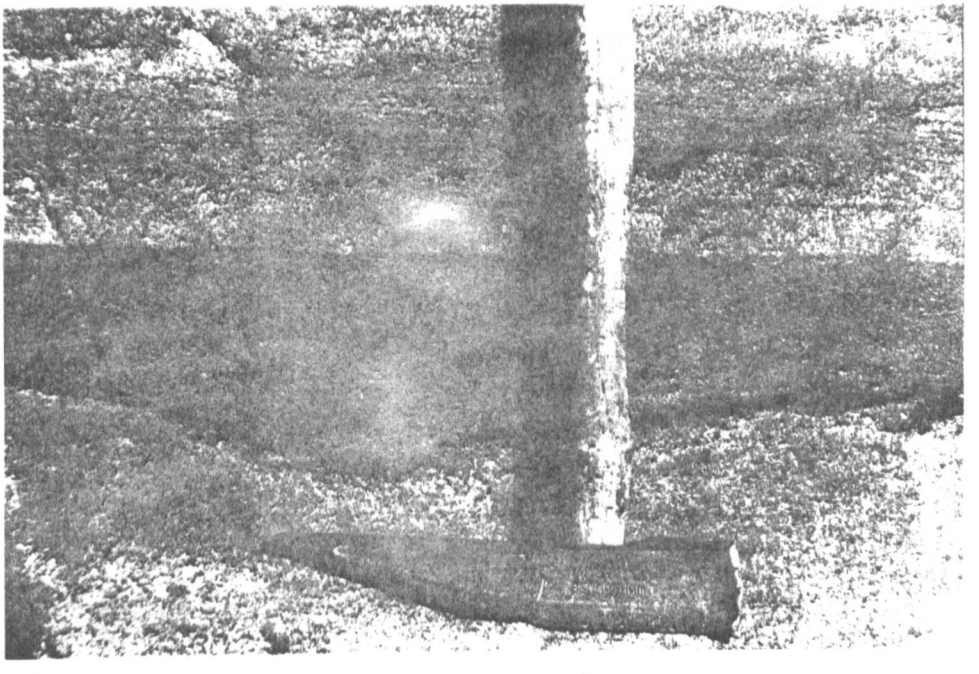

Plate 2.34 Possible channel scour feature at the base of a cumulate layer, Wadi Al Abyad. (Length of hammer head 17 cm).

Plate 2.35 Slump-folding of a cumulate layer, Wadi Al Abyad. (Length of plate 30 cm).

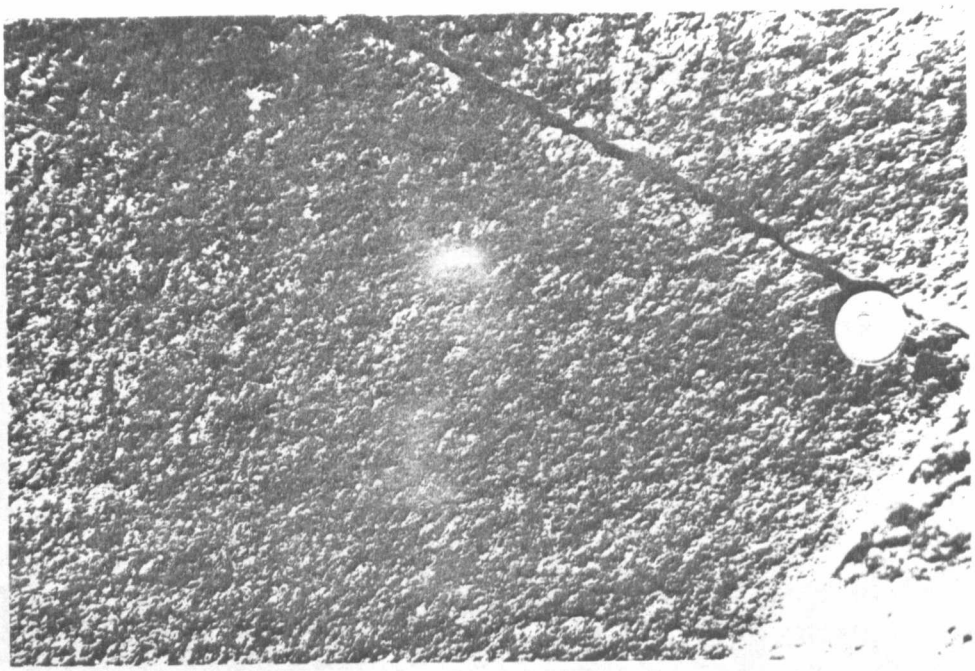

Plate 2.36 Plagioclase grains defining a magmatic lineation on the layering plane, Wadi Al Abyad. (— = lineation trace). (Coin 2.5 cm diameter).

Plate 2.37 Plagioclase grains defining an igneous lamination on a face perpendicular to the layering plane. (Coin 2.5 cm diameter).

There is some difficulty in distinguishing in the field between a strongly laminated and a tectonically foliated layered gabbro where a three-dimensional outcrop is not available. In a tectonically undeformed gabbro the laminations are always parallel to the layers, except where layer truncations are present. The lineations on the layering surfaces are only poorly developed, with the plagioclase feldspar grains often having an irregular shape and only slightly elongate (Plate 2.37). In a deformed gabbro the lineation on the layering surface is much more apparent with the plagioclase grains more elongate and having a more regular shape. (Plate 2.39). There is always a very small angle (usually not more than 10^{o}) between the tectonic foliation and the layering when measured on a face perpendicular to the layering and parallel to the lineation. Figure 2.12 summarizes the differences between tectonised and non-tectonised cumulates.

In thin section it is fairly easy to distinguish between tectonised and non-tectonised rocks. Where olivine is present in tectonised gabbros it is commonly strained with undulose extinction. With an increase in deformation, clinopyroxene also exhibits undulose extinction and some olivine recystallises as neoblasts. In general, tectonised gabbros are finer grained than their non-tectonised equivalents. Recystallisation partially destroys the original adcumulate textures. (Plate 2.40).

Tectonism of the cumulates has clearly taken place during or slightly after formation of the cumulate layer. Only in the lowermost cumulates of the Wadi Al Abyad section have the gabbro layers been sufficiently consolidated to form tight folds with an axial planar foliation. Elsewhere only a foliation and lineation has been formed which dies out upwards. This either

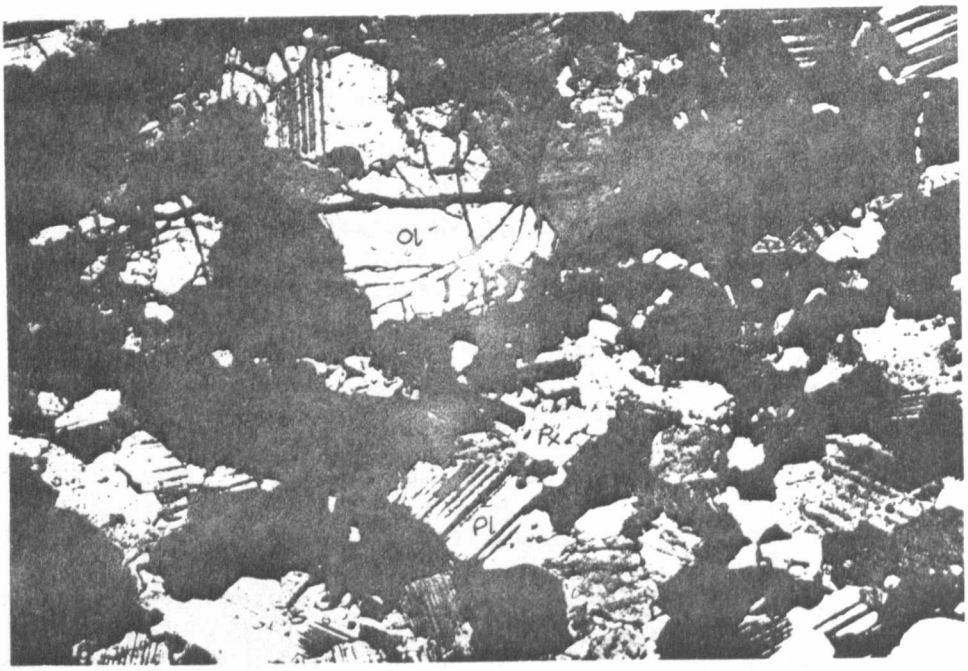

Plate 2.38 Thin-section of tectonically undeformed olivine gabbro showing the alignment of grains defining an igneous lamination. (Cross-polarised light). Pl = plagioclase, Px = Clinopyroxene, Ol = Olivine. (Length of plate 5 mm).

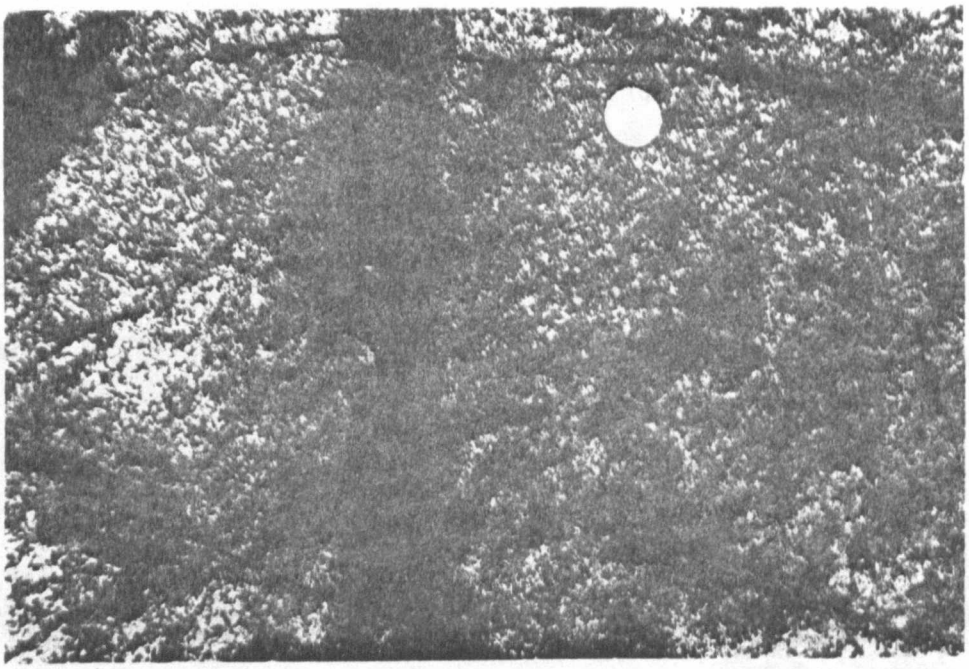

Plate 2.39 Plagioclase grains defining a tectonic lineation on the foliation plane. (Coin 2.5 cm diameter).

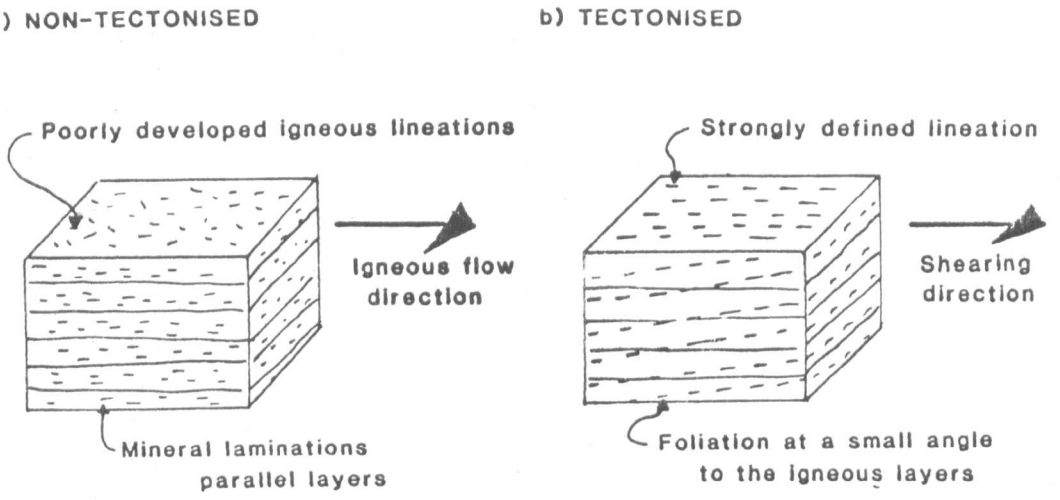

Figure 2.12 The differences in hand specimen between tectonised and non-tectonised cumulate gabbros.

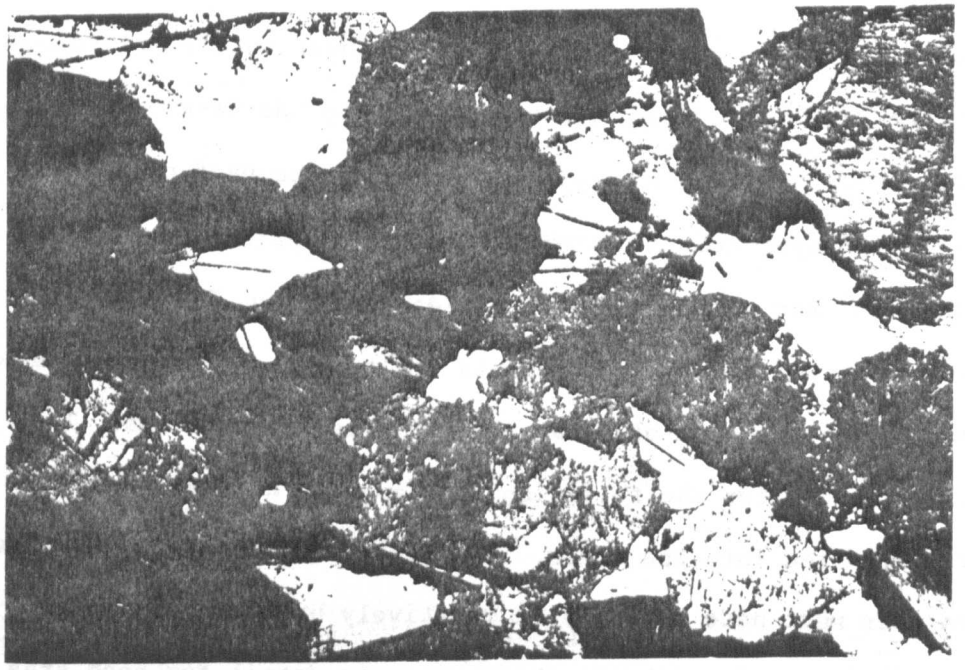

Plate 2.40 Thin section of a tectonised olivine-gabbro showing a strong mineral alignment. (Length of plate 5 mm).

indicates a limit of the deformation after the gabbro consolidated; or the limit up to which a tectonic fabric was impressed and above which the layered cumulates were still crystallizing and consolidating, and thus only deforming by 'crystal mush' flow processes (Reviewed in George, 1975). This latter hypothesis is favoured as the crystallographic studies discussed in Chapters 7 and 8 show that olivine is deforming by slip along high temperature slip planes (above 800°c). Non-tectonised cumulate layering close to tectonised areas is sub-parallel to the layering within tectonised areas. The parallelism of the tectonic foliation to this layering in all areas suggests a close relationship between the layering and tectonism which also favours the latter hypothesis. In some highly tectonised areas of the Lower Cumulate Unit, clinopyroxene rich layers show evidence of boudinage (see section 2.4).

In some areas of the Lower Cumulate Unit small-scale ductile shear zones have been observed (Plate 2.41). These rarely exceed 1 metre in length. They occur only locally and have only been measured in the two wadis where the Peridotite Unit tectonism extends an appreciable distance into the Lower Cumulate Unit - Wadi Rajmi and Wadi Al Abyad (see Section 2.4). The shear zones have only very small displacements (mm to cm) and in both areas show variable senses of shear and variable orientations. They were formed after the foliation and layering as these features are deflected into the zones. Shearing is still ductile however, and thus must have occurred at relatively high temperatures. Section 2.4 deals with the shear zones in detail for each area studied.

A few cross-cutting bodies are present in the Lower Cumulate Unit; fine aphyric basaltic dykes, wehrlitic dykes, gabbroic dykes, horblende-gabbro dykes and pegmatitic sheets and veins. In the areas of tectonism the wehrlitic and gabbroic dykes have been deformed by the main foliation-forming event. In Wadi Rajmi undeformed gabbroic dykes cross-cut the moho. The fine aphyric basaltic dykes appear undeformed except by the later small-scale shear zones. The hornblende gabbroic dykes were intruded much later and are undeformed. In Wadi Al Abyad they are also present in the Peridotite Unit and here they cross-cut the moho. The pegmatite sheets and veins are undeformed except for one locality in Wadi Rajmi where a vein is isoclinally folded. (See Section 2.4.)

Figure 2.13 summarises the different cumulate and intrusive relationships of a general section through the Lower Cumulate Unit of Oman.

The purpose of this thesis is not to describe the detailed stratigraphy of the Cumulate Unit, but to determine the extent of the tectonism within the Unit. Thus only those areas which are tectonised or are at the boundary between tectonism and non-tectonism of the cumulates are described in the following section. (Section 2.4)

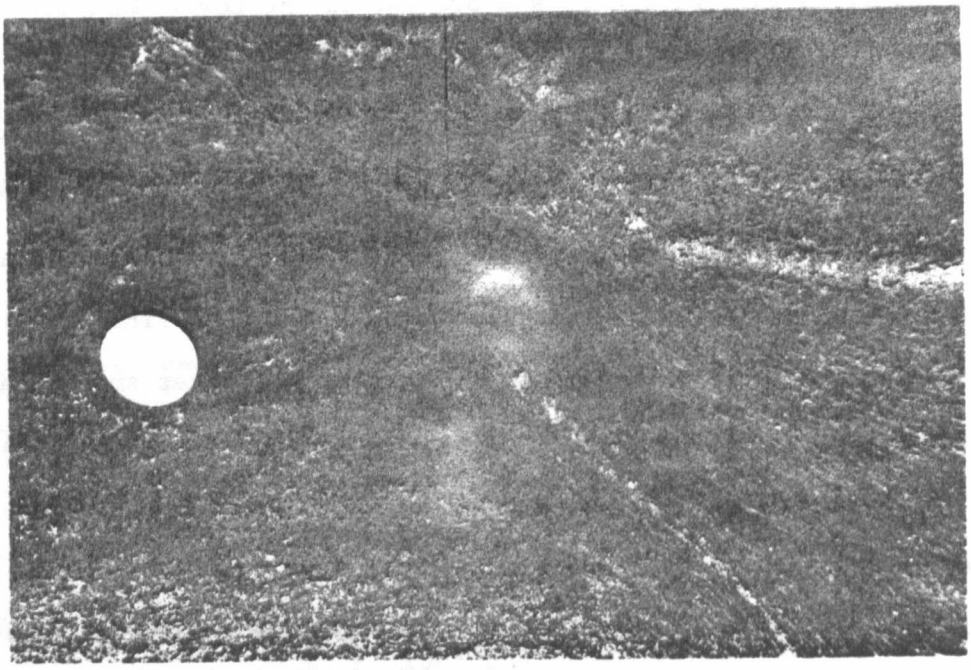

Plate 2.41 Small-scale ductile shear zone in the cumulate gabbros of the Wadi Al Abyad area. (Diameter of coin 2.5 cm).

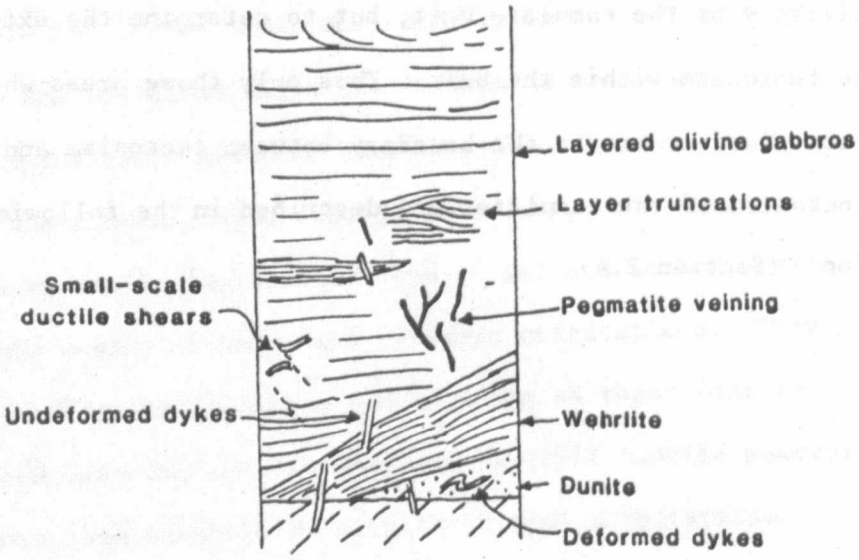

Figure 2.13 A generalised section showing the cumulate and intrusive relationships in the Lower Cumulate Unit of the Oman Ophiolite.

2.3.4 Late Stage Tectonic Features

All of the areas studied in Oman have been affected by a late-state mainly brittle deformation. The only late-stage ductile deformation is in the Banded-Unit at the base of the Peridotite Unit where mylonitic features are present and extensive later shearing has occurred. The fabric developed is parallel to the thrust contact at the base of the Peridotite Unit and has been related by Searle (1980) to the emplacement of the ophiolite. These areas of emplacement related structures have not been studied in detail. The orientation of the structures in the areas unaffected by ductile emplacement structures is unrelated to the structural trends of emplacement affected areas. (See Section 2.4)

Brittle fracture and fault zones are present throughout the Peridotite and Lower Cumulate Units. These usually dip steeply and have been formed late in the emplacement stage of the ophiolite: they are probably related to the final brittle break-up of the ophiolite into the present day configuration of tectonic blocks separated by major fault zones. (Figure 2.7). It is not possible to determine displacements along fracture zones because of the homogeneity of the Peridotite Unit rocks. It is clear, however, that most fractures involve very little or no movement and that major displacements only occur between the ophiolite blocks and along a few major faults within each of the blocks. At higher levels in the Peridotite Unit the larger faults displace the moho by up to 10km and extend into the crustal sequences (Figure 2.14).

In some areas of the Peridotite Unit, the rocks show a strong cm scale fracture jointing (Plate 2.42), the orientation of which is parallel or perpendicular to the larger fracture zones. (See section 2.4). Thin section studies show that this fracturing involves no detectable movement and that serpentinisation trends are associated with and parallel to the fracture jointing trends.

In the smaller ophiolite blocks, thrust and fault zones have disrupted the ophiolite units (Figure 2.14); but in the areas of the larger blocks studied for this thesis, the structural trends of the primary mantle fabrics show that the blocks have remained as stable, relatively intact bodies during and after emplacement. (See section 2.4).

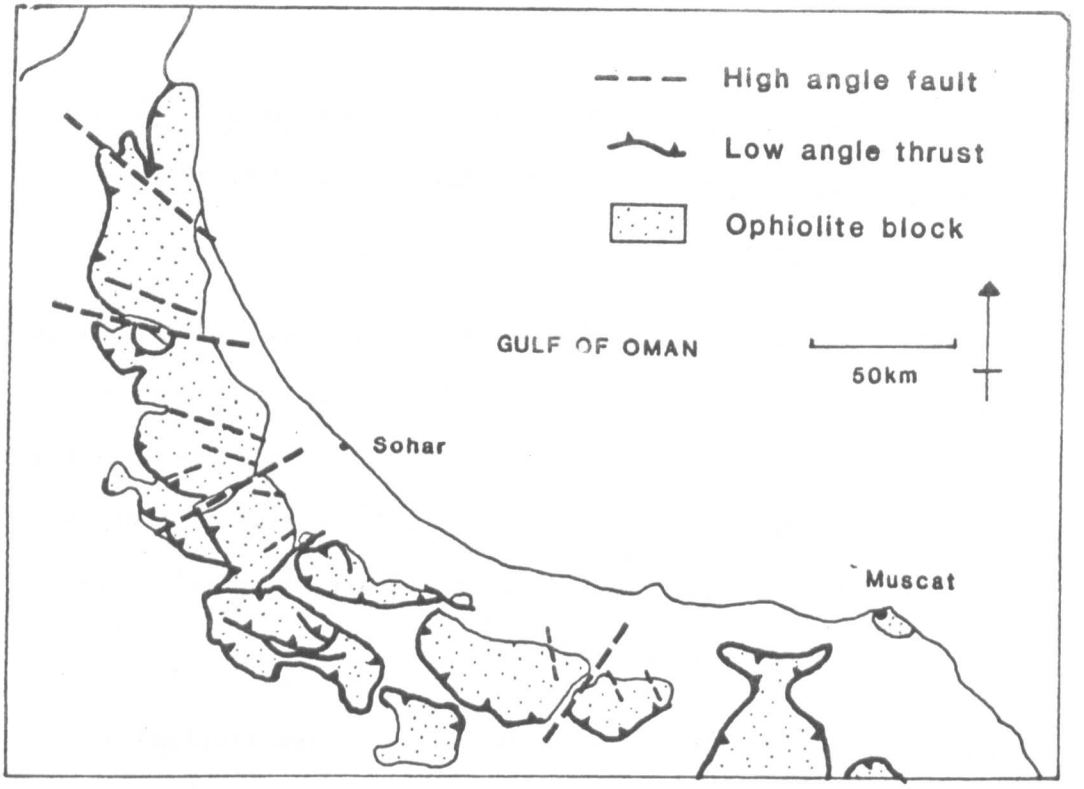

Figure 2.14 Major thrust and fault orientations and distributions in the northern Oman ophiolite blocks.

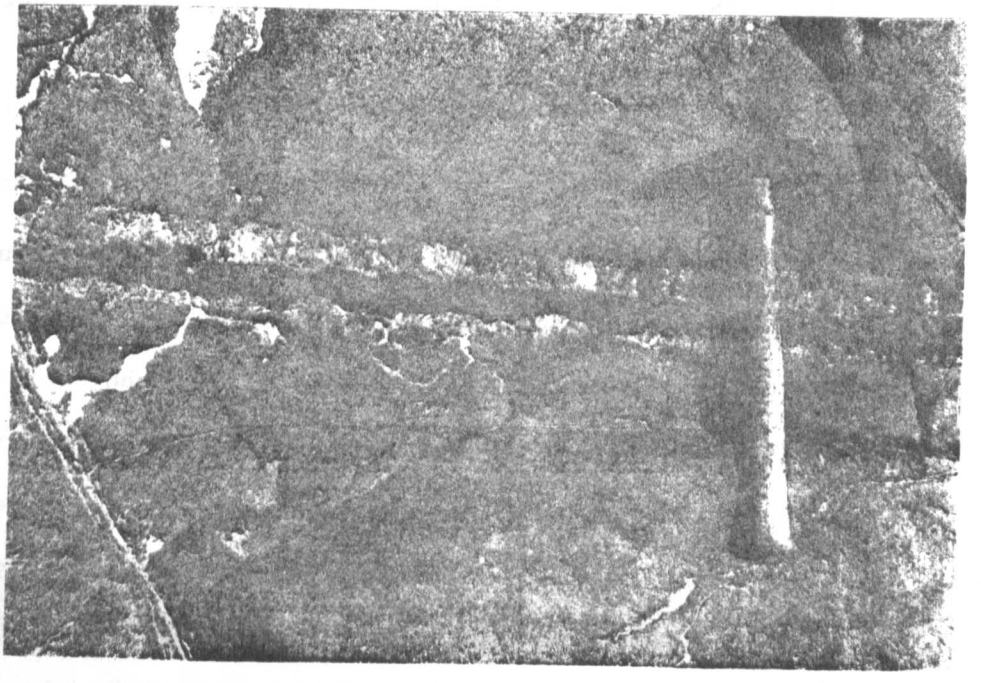

Plate 2.42 Centimetre-scale fracture jointing in pyroxene rich layers in harzburgite. (Length of hammer 40 cm).

2.4 The Distribution and Orientations of the Structural and Petrological Features in the Areas Studied from the Oman Ophiolite.

In this section the distribution and orientations of the features covered in section 2.3 are described for each of the ophiolite blocks studied. For each block firstly the structures and their trends and then their effects on and the distributions of the various intrusive and cumulate features are discussed. The blocks are considered from north to south.

For each area studied, the traverses have been divided into 1-2 km lengths. Selected measurements are plotted on 1:20,000 maps enclosures showing localised variations of the structural trends. All of the field measurements taken are represented on lower hemisphere equal area projections for each area. The maps also show lithological variations in the Peridotite and Lower Cumulate Units.

2.4.1 The Fizh Block

The Fizh Block is the largest of the ophiolite blocks studied. (Figure 2.7) The Peridotite Unit is up to 25 km thick from its basal contact with the Banded Unit to the Moho contact. For this reason this block has been studied in more detail than the others. One traverse was completed through the whole Peridotite Unit:- the Rajmi-Raay traverse. A few fairly accessible areas were visited in the lower sections of the Peridotite Unit as well as areas closer to the Moho and into the Lower Cumulate Unit. (See Figure 2.15.)

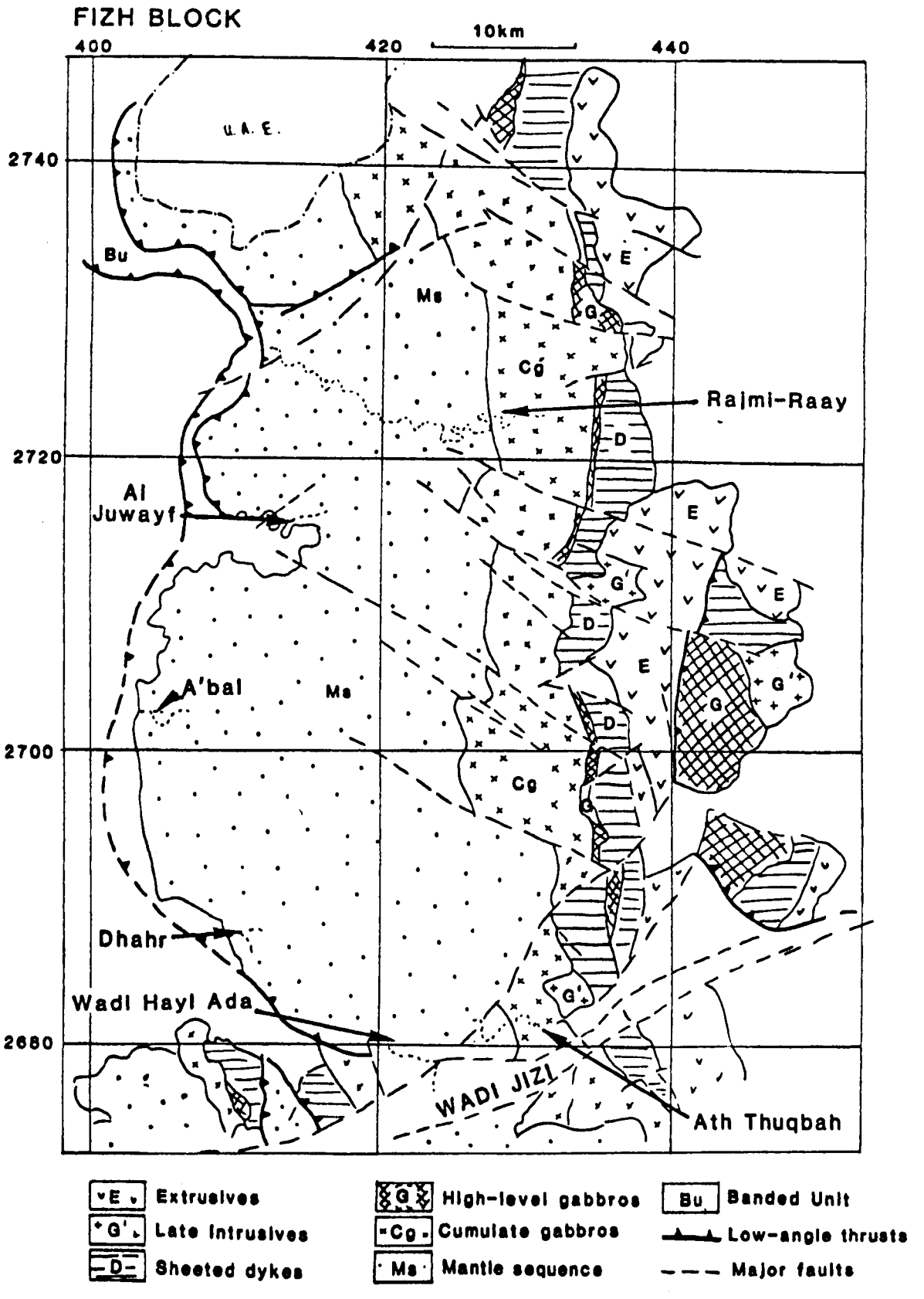

Figure 2.15 Geological map of the Fizh Ophiolite Block. (Modified from Lippard and Rothery, 1983).

2.4.1.1 Structural Trends

These are summarised on Enclosures 1-3.

(a) Early Tectonic Foliations and Lineations

The foliation pole plots show two alternative patterns for the Fizh Block; either a fairly strong cluster pattern or a great-circle trend.

In all of the areas in the lower section of the Peridotite Unit the foliations are easily measurable in the field and their poles show a cluster pattern. Within a single area and between areas the foliation trends are highly consistent. The foliation generally dips steeply towards the ENE striking NNW-SSE. In all of these areas the texture of harzburgite in thin section is either porphyroclastic or mosaic porphyroclastic. The tectonic lineations associated with this strong foliation all have shallow plunges either to between NNW and N or between SSE and S. In the area between eastings 160 and 180 in the Rajmi-Raay section a few foliation planes dip gently to ENE. Their strikes and lineation trends, however, are the same as that of the steeper foliations. This implies a gentle flexuring of the foliation plane with a fold axial trace parallel to the lineation direction. This is the only area where this feature has been observed in the Fizh Block.

In the lower Rajmi-Raay traverse the strikes of the foliations and trends of the lineations gradually rotate from a NNW-SSE foliation strike and lineation trend at the western end, to

a N-S foliation strike and lineation trend at easting 190. East of easting 190 the cluster pattern of foliation poles is no longer present in all areas; in many areas the foliation is not well developed in the field and the lineation can be measured with confidence in only a very few localities. The poles to foliations give plots ranging from dispersed clusters to girdle patterns. Some areas give a fairly strong foliation pole cluster pattern, the foliation striking N-S and dipping steeply towards the east - an orientation analagous to the foliation trends lower in the traverse. These areas with foliation pole clusters (Eg. the area between eastings 220 and 240) also have a few more dispersed foliations with poles plotting in a great circle and all with a very steep dip. In some areas (eg. the km square of easting 240 and northing 240) the girdle trend is more prominent than the cluster. In the Peridotite Unit of the km square of easting 250 and northing 230 the foliation poles give a two cluster pattern with a dispersed cluster of planes dipping steeply ESE and another of planes dipping steeply SW.

The textures in thin section of the harzburgites vary with the orientation of the foliation plane: in areas where the foliation strike is roughtly N-S the rock texture varies from mosaic porphyroclastic to laminated - and disrupted-porphyroclastic; and in areas where the foliation strike is more variable the harzburgite texture varies from porphyroclastic to coarse-porphyroclastic. The shape of the large spinel grains (greater than 0.5mm) within the rocks corresponds well to the overall texture and foliation trends. In areas

of mosaic-porphyroclastic to porphyroclastic textures with a roughly N-S foliation strike, the large spinel grains are generally highly elongated parallel to the foliation trace whether they were originally euhedral or 'holly-leaf' type grains (see Section 2.3.2)(Plate 2.13). In specimens which have a less evolved texture (ie. Coarse-porphyroclastic to porphyroclastic) and a foliation plane which is divergent from the prominent N-S strike, the larger spinel grains are much less elongate with good euhedral and holly-leaf textures (Plate 2.14). With these spinel textures, the foliation planes are difficult to measure in the field.

This textural evidence indicates that deformation has been more intense in the lower half of the Rajmi-Raay traverse. In this area of more intense deformation the foliation has a constant trend. In the areas of less intense deformation the constantly trending N-S foliation is still present but an earlier foliation is also preserved in some areas. The only evidence from the field and thin-section that one foliation is earlier than the other, is based on the textures observed and the relative orientations of the foliations. With an increase in the intensity of deformation which produces the N-S strike of the foliation, the earlier foliation is progressively rotated by shearing from its original orientation towards the later N-S direction. Where the N-S foliation stike is only very weakly developed, the earlier foliation poles form a dispersed cluster pattern as in the km square of easting 250 and northing 230 where a two cluster pattern is present (see above). In areas where the N-S striking foliation is stronly developed, the earlier foliation trend

has been destroyed by a total rotation into the later trend and also by extensive recrystallization of the mineral phases with regrowth in the later foliation direction. A single-cluster foliation pole pattern is developed in these areas.

At most localities only one foliation plane is measureable, but, as mentioned in Section 2.3.2, two distinct foliation planes can sometimes be discerned in the same specimen by the careful study of the spinel orientations in three orthogonal thin-sections. This is only possible in areas where the earlier relict foliation trend has not been destroyed by the deformation which produced the N-S striking foliation. This evidence of two foliations being present in the same specimen shows that they must have been formed by two seperate deformational events. The earlier and later deformational events will be referred to as D1 and D2 respectively and their associated foliations and lineations S1 and S2, and L1 and L2.

The D1 and D2 structures are distinguishable from each other after a careful study of their orientations, their related textures in thin section, and their relative intensities in the field. In the Rajmi area,the lower half of the Peridotite Unit traverse has undergone an intense D2 deformation and only the D2 structures are preserved: any relict D1 structures have been destroyed or rotated into parallelism with the D2 structures. All the S2 foliations and L2 lineations are easily measurable in the field, have a constant orientation and are present in rocks with either porphyroclastic or mosaic porphyroclastic textures. At higher levels in the Rajmi traverse the D2 deformation has been less intense and in some

localities an S2 foliation is not easily measurable: instead a relict S1 foliation has been preserved. In these areas, the S2 foliation, where measurable, has a constant orientation, whereas the S1 foliation has a variable attitude and shows a folding pattern. (See foliation pole projections on Enclosure 2.) In this area the thin section textures vary from coarse to porphyroclastic depending on the intensity of the D2 deformation. In areas where both S1 and S2 foliations are present, lineations defined from spinel grain alignments are difficult to measure and relate to either D1 or D2.

In the Rajmi area both S1 and S2 foliations extend into the Lower Cumulate Unit. S2 foliations predominate, S1 foliations only being prominent in the tectonised Lower Cumulate Unit between northings 220 and 230. The zone of tectonism extends from 150 to 350 metres into the Lower Cumulate Unit. Lineations are difficult to measure in the layered gabbros, but where made recognisable by elongate feldspars and pyroxenes, they show a trend similar to that of the more easily measurable L2 lineation in the more strongly deformed parts of the Peridotite Unit.

In the Zaymi area (see Enclosure 1) the foliation poles plot as a dispersed cluster-girdle pattern. The strike of the foliation planes is roughly E-W with a steep dip to the north. The lineations plot on a great-circle as a dispersed cluster-girdle pattern with a shallow plunge towards the NE to SE, the L2 lineations trending to the east as a cluster and L1 the dispersed girdle. These structural trends are completely different from the Wadi Rajmi trends; they may represent the

relict D1 structures which have only been very slightly reorientated by D2 events. Only the lowermost dunites of the Lower Cumulate Unit show appreciable tectonic deformation, the foliations and lineations of which have a similar orientation to the Peridotite Unit. (See Enclosure 1.)

The Ath Thuqbah area is situated on the southernmost end of the Fizh Block. The area studied is separated from the main block by a major fault - part of the Wadi Jizi fault system (Figure 2.15). The foliations and lineations give similar patterns to the Rajmi-Raay traverse area with cluster and girdle trends. The orientations of the structures are, however, quite different from the Rajmi area (Enclosure 3). In the Peridotite Unit north of northing 828 the foliation poles plot as a cluster with the foliation dipping moderately towards the east. The associated lineations have a moderate eastwards plunge. South of northing 828, the foliation poles have a more girdle-like pattern. The pi-pole girdle of foliations contains a fairly strong cluster with a similar orientation to the foliation pole clusters of the area north of northing 828. The lineations from the southern area also plot as a more girdle-like pattern. Where the foliation dips and the lineation plunges are moderately towards the east, the thin section textures are porphyroclastic. In the areas with more variable foliation and lineation trends, the textures are more variable; from coarse-porphyroclastic to porphyroclastic.

The varying structural trends and textures indicate that the D2 deformation is variable in its intensity: in the area north of northing 828 it is fairly strong and the earlier D1 structures are not preserved. In the southern area, the D2 deformation is much less intense in places and S2 foliations and L1 lineations have been reoriented more or less completely into the D2 trends.

In the Ath Thuqbah area, the Peridotite Unit D2 deformation extends for up to 250m into the Lower Cumulate Unit, and is essentially confined to the dunitic and plagioclase-wehrlite rocks of the transition zone area.

(b) Later Structures In the Fizh Block Peridotite Unit all other structures are related to the emplacement of the ophiolite. The only late ductile structures are within the Banded Unit where a strong foliation has been developed. This is parallel to the foliations in the metamorphic sole beneath the ophiolite block and is clearly later than the D1 and D2 ductile structures observed in the Peridotite Unit (Enclosure 2). The metamorphic sole and adjacent areas have been studied by Graham (1980).

In areas away from the Banded Unit, all the late-stage structures are brittle. In the Fizh Block the larger-scale faults and fractures generally dip steeply and strike WNW-ESE. The sense of their movement cannot be determined in the homogeneous Peridotite Unit, but where they extend into the Lower Cumulate Unit some of the faults can be shown to have a major (up to 5km) strike-slip component. Rarer NE-SW vertical faults are restricted to the lower sections and the areas adjacent to Wadi Jizi in the Fizh Block (Figure 2.15).

In some of the areas studied a prominent small-scale fracture jointing is present. It is restricted to pyroxene-rich rocks, as only the pyroxenes were competent enough to fracture in a brittle manner; olivine is easily serpentinised if fractured, forming sub-grains surrounded by a serpentinite matrix. The fracture jointing is most easily measurable in either pyroxene-rich segregation layers or in the pyroxene-rich dykes (see below). Enclosures 1, 2 and 3 show the orientations of the small-scale fracture joints measured in the Fizh Block. In most areas, the fracture joints are sub-parallel or perpendicular to the larger-scale fractures and faults. In the areas studied in the lower sections of the Fizh Block the main orientation of the fracture jointing is parallel to the NE-SW striking faults. In the higher level Ath Thuqbah area the fracture jointing is parallel to the Wadi Jizi faults. The higher levels of the Rajmi area have fracture joints parallel to the WNW-ESE striking faults, as well as a number of flat-lying fracture joint planes. These may be a conjugate set of joints formed during fault movements. Their trends clearly differ from those produced by the earlier deformations.

In the Lower Cumulate Unit of the Fizh Block the faults have similar trends to those in the Peridotite Unit but no associated fracture joints were recognised. No later structures have been observed in the Lower Cumulate Unit except in the Wadi Rajmi area. Here there are small-scale ductile shear zones in the layered gabbros. These formed after the D1 and D2 structures, since the foliations are reoriented in the shear zones, but before the brittle faults and fractures as the shear zone

deformation was ductile and must have occurred at a higher temperature than the later brittle movements associated with the ophiolite emplacement. Smewing (1979) has described similar ductile shear zones from the layered gabbros in the vicinity near Rajmi village (for location see Enclosure 1). These shears are sub-vertical and strike NW-SE. All the shears measured by Smewing (1979) had a sinistral sense of displacement when observed on a horizontal surface. In the areas of the Lower Cumulate Unit studied for this thesis (see Enclosure 2) a much wider range of shear zone orientations has been observed. The main area and the orientations of the shear zones is shown on Enclosure 4. There are evidently conjugate sets, one subvertical, with WNW-ESE strike and sinistral displacement sense (similar to those of Smewing (1979)); the other subvertical with NNW-SSW strike and dextral displacement sense. These dextral shear zones were not recognised by Smewing (1979) in the higher-level layered gabbros near Rajmi village. The shear zones mapped in the area of Enclosure 4 are generally much smaller than those of Smewing,having a lateral strike of between 1 and 5 metres and a thickness of up to a few centimetres. The relative displacement along both sinistral and dextral shears is very small with a maximum displacement of 5cm. The gabbro layers (and foliations in tectonised areas) are deflected by the shear zone movements and,in the more major shear zones,are sub-parallel to the shear zone itself.

Smewing (1979) interpreted the sinistral shear zones as Riedel-type shears. These are shear zones which develop at a small angle (between 15° and 20°) to the principal plane of movement in a shearing environment. (Riedel, 1929). Figure 2.16 summarizes the orientation and sense of movement of Riedel shears in relation to the orientation and movement sense of the main shear direction. Smewing (1979) correlated the movement of the small-scale Riedel shears with larger-scale movements along a possible transform fault zone. In his preferred model, however, he proposed a transform fault with a dextral shear sense which does not agree with the senses of movement expected from the experimental work of Riedel (1929). For Riedel shears with a sinistral sense of shear making a small angle with the main shear direction, the sense of movement of the main shear direction should also be sinistral.

Cloos (1955) showed experimentally that for a major slip surface two conjugate sets of Riedel type shears can be formed. (See Figure 2.16.) One set, of a similar displacement sense to the major slip surface, lying at a small angle to the major slip surface; and the other set, with opposite shear sense, lying at a high angle to the major slip surface. The conjugate shear zones measured in the area of Enclosure 4 would give two possible orientations of the major slip surface as shown in Figure 2.16. These two possible orientations are clearly not in agreement with Smewing (1979). His interpretation gives both the wrong sense of shear and the wrong angular relationship between the supposed Riedel shears and the major slip surface.

a)

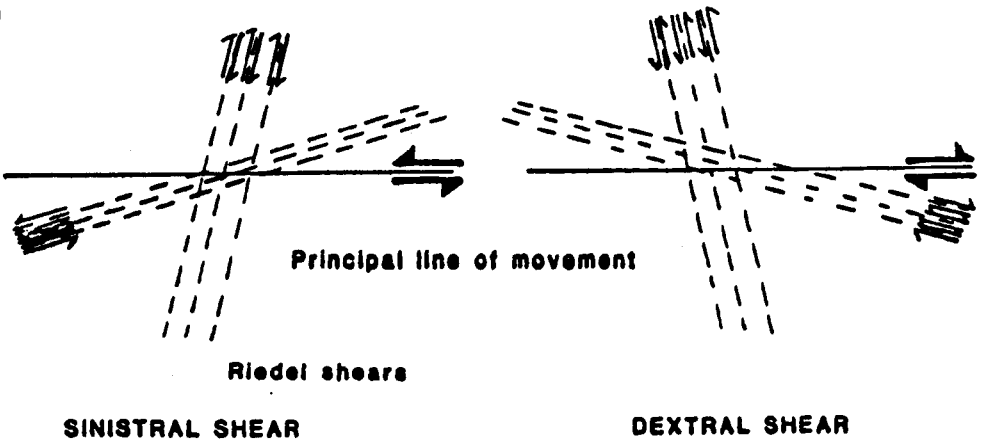

b) RAJMI AREA

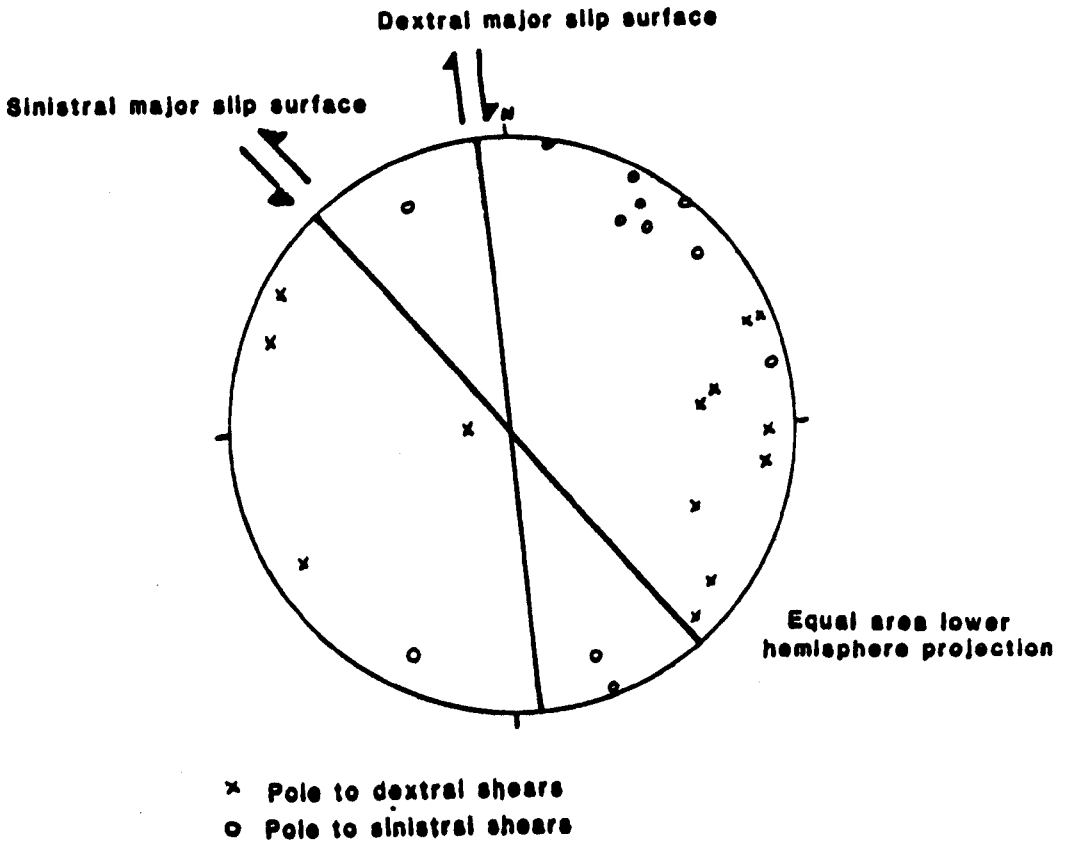

Figure 2.16 a) Riedel shears - their relationship to stress and sense of movement. b) The orientation of the major slip surface from the Riedel shears of the Rajmi area.

The orientation of the shear zones in relation to an ocean spreading environment is discussed in Chapter 9.

2.4.1.2 The Distribution and Orientation of Intrusive and Cumulate Features.

(a) Dunitic Intrusions within the Peridotite Unit

In the Fizh Block the only large dunite bodies mapped were in the Rajmi-Raay traverse. Elsewhere, the bodies do not exceed 10m in diameter and are very sparsely distributed. In the lower areas of the Fizh Block where the D2 deformation is fairly intense the dunitic bodies are podiform and strongly aligned parallel to the S2 foliation trends. (See Enclosures 1 and 2.) In higher levels of the Peridotite Unit of the Rajmi-Raay traverse the dunites are much more irregularly shaped and generally larger (up to 200m diameter). The shapes of the dunitic bodies cannot be accurately defined in most areas because of their extremely inaccessible outcrops on the wadi walls. Areas of anastomosing dunite sheets are commonly associated with the larger dunite pods. (See Enclosure 2.) In the traverse areas west of easting 200, the anastomosing sheets are all at small angles to the S2 foliations. In the areas east of easting 200, where the D2 deformation has been generally less intense, the anastomosing sheets are at more variable angles to the outcrop foliations (eg. Plate 2.18). In the area between eastings 240 and 250 anastomosing sheets are particularly common in the Rajmi area. They are not, however, associated with any large scale dunitic bodies. Anastomosing dunite sheets are not common in any of the other areas studied from the Fizh Block.

In a locality at grid ref. 257224 in the area adjacent to the Rajmi moho, a small 5m² area of harzburgite contains a number of anastomosing sheets of plagioclose wehrlites. Their field relations are identical to those of anastomosing dunitic sheets and they most probably represent a remnant of a slightly more evolved infiltrating liquid. Such plagioclase-rich anastomosing sheets have not been observed elsewhere in Oman.

(b) Pyroxenitic and Gabbroic Dykes and Sheets.

Dykes have been observed in all areas of the Fizh Block except for the Wadi A'Bal and Dhahr areas at the base of the Peridotite Unit. The trends of the various types of dyke in each area are shown in Figure 2.17. The dykes are only deformed in areas where D2 deformation has been fairly intense (ie. mainly in the lower sections of the Peridotite Unit). These deformed dykes approach parallelism with the S2 foliation planes which implies that they have undergone a fairly high strain.

In the Rajmi-Raay traverse all the dykes west of easting 190 are of pyroxenite and they are all deformed. As mentioned in section 2.3.2 the pyroxenite dykes are either boudinaged or folded depending on their orientation relative to the two planes of maximum shearing stress during D2 deformation. East of easting 190 the dykes are pyroxenitic, wehrlitic, gabbroic and pegmatite gabbroic and are usually undeformed. They mainly dip steeply but have no common strike. Seven pairs of undeformed dykes from the upper sections of the Rajmi Peridotite Unit show cross-cutting relationships. Figure 2.17 shows their various trends. At least three dyke orientation

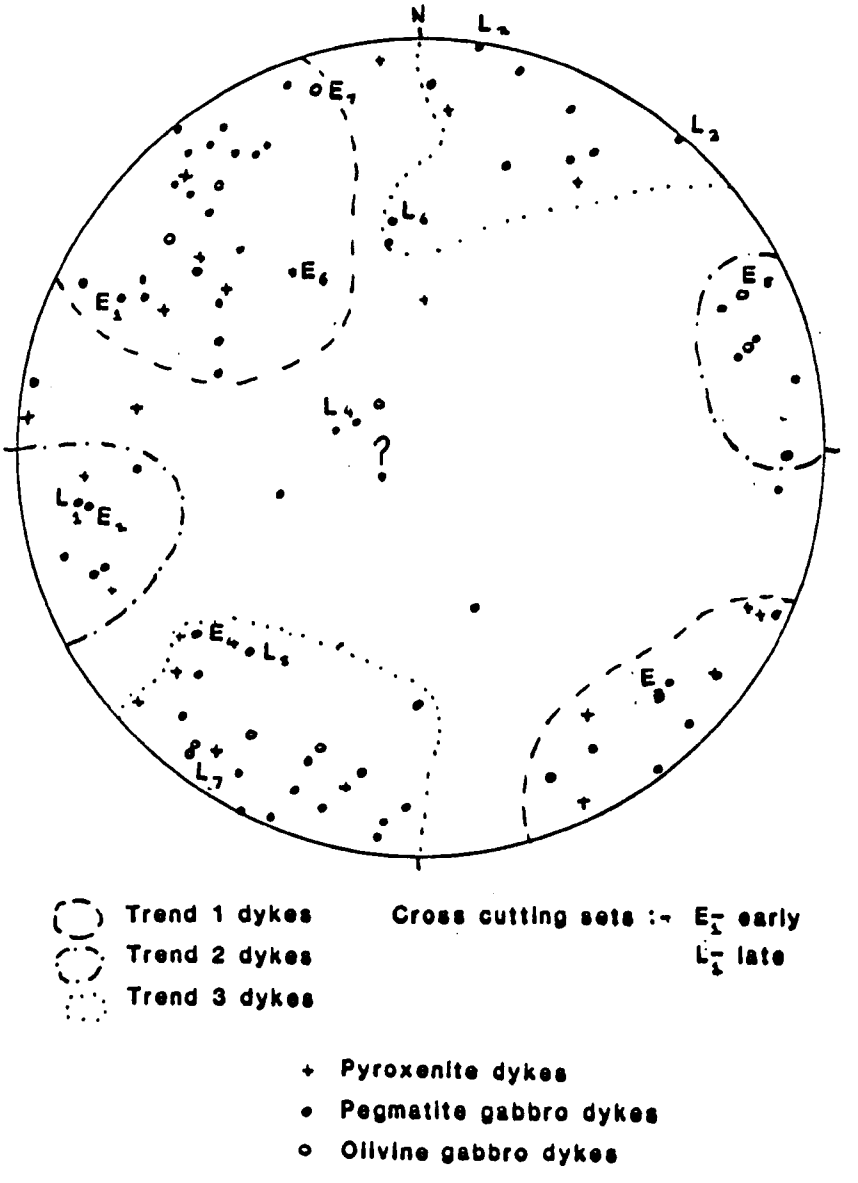

Figure 2.17 The orientations of cross-cutting dykes from the Rajmi Peridotite Unit.

pairs can be discerned, the earliest set striking NE-SW (trend 1), the next striking NNW-SSE (trend 2), and the youngest striking WNW-ESE (trend 3). The dips are all steep except for the youngest WNW-ESE set of few dykes with much shallower dips. (See Figure 2.17). As noted in section 2.3.2, pyroxenite grades into gabbro along the same dyke: this shows that a specific dyke set will not necessarily be restricted to a single composition. Figure 2.17 shows that this is so for the Rajmi dykes; all dyke compositions having all three orientations.

The dykes with trend 1 and trend 3 also occur within the Lower Cumulate Unit in the Rajmi area. Pyroxenitic dykes are absent from this area but all other types are present, including hornblende-gabbro dykes which only trend in the trend 3 dyke set direction and are not present in the Peridotite Unit. No cross-cutting relationships were observed in the dykes of the Lower Cumulate Unit.

In some areas adjacent to the Rajmi moho area where the D2 deformation is fairly intense, all three types of dykes were slightly sheared during the D2 event. This is evident in both the Peridotite and Lower Cumulate Units.
Dyke rotation by shearing is only minimal as the deformed dyke trends still plot in one of the three dyke-set fields. The fact that dykes with all three trends have been deformed in some localised areas implies that the D2 deformation was a fairly late event. It was also a fairly long-lived event as in the areas a few km below the Rajmi moho S2 foliations are

fairly prominent but all three dyke sets are undeformed: whereas in a few areas adjacent to the Rajmi moho all the dykes are deformed by D2. (But only very slightly.) Thus the D2 event must have started prior to local dyke intrusion and continued locally in a few areas after three dyke intrusion events had occurred.

In the moho area at grid reference 254239 the D2 deformation is very weak. Here an undeformed gabbroic dyke with trend 3 intrudes both the Peridotite Unit and the Lower Cumulate Unit.

In the Ath Thuqbah and Zaymi areas there are undeformed dyke-set trends similar to those in the Rajmi area. (See Enclosure 3). No dykes were seen in the Cumulate Unit and none of the dykes in the Peridotite Unit are deformed. Most of the dykes are of pegmatitic gabbro. The similar trends of the undeformed dykes in the Rajmi Zaymi and Ath Thuqbah areas indicate that there has been very little relative rotation between them; and thus the major difference in the S2 orientations between the areas must be a primary feature. In the Zaymi area hornblende-gabbro dykes with trend 3 outcrop in the Peridotite Unit, and are similar to those in the Rajmi area.

The Rajmi-Raay traverse and the Wadi Hayl Ada area are the only areas mapped in the Fizh Block in which a of the dykes in the Lower Peridotite Unit are deformed. In the Al Juwayf area none of the dykes are deformed: they are both pyroxenitic and gabbroic and are all parallel to the trend 3 Rajmi dykes. This implies that the duration of the D2 deformations varied over areas of the lower Peridotite Unit as well as near to the moho areas as described above.

In all the areas, the dykes vary in thickness from 1 to 10cm, and extend no more than 5m laterally. In the upper part of the Peridotite Unit in the Rajmi-Raay traverse area the dykes which trend in the earliest dyke-set directions (trend 1) often occur in swarms of centimetre thick sheets, these are the major dyke trends present. In other areas no dyke trend is dominant.

In the Rajmi area of the Lower Cumulate Unit one wehrlitic dyke (grid ref/ 255230) was seen to be affected by late Riedel-type shear zones as described in section 2.4.1.1. The shear sense on this dyke is dextral (Plate 2.43). The dyke is undeformed by the D2 deformation present in the surrounding layered gabbros and its orientation is that of the trend 1 dyke-sets. No other dykes were seen to be affected by Riedel type shears. This dates the late shearing of the Lower Cumulate Unit as after the intrusion of the type 1 dykes.

(c) Cumulate Features of the Lower Cumulate Unit.

The cumulate assemblages in the Lower Cumulate Unit are highly variable between and within the areas studied in the Fizh Block. Figure 2.18 summarizes the cumulate successions from the moho upwards for each area. In the Rajmi area itself the sequence varies from dunite to olivine gabbro, wehrlite to plagioclase wehrlite to olivine gabbro, and just olivine gabbro.

Wehrlitic pods of up to 100m in length outcrop sporadically in the first 300m thickness of olivine gabbros in the Rajmi area. A major unit of interbanded wehrlites and dunites outcrops above this gabbro zone in the area shown on Enclosure 2.

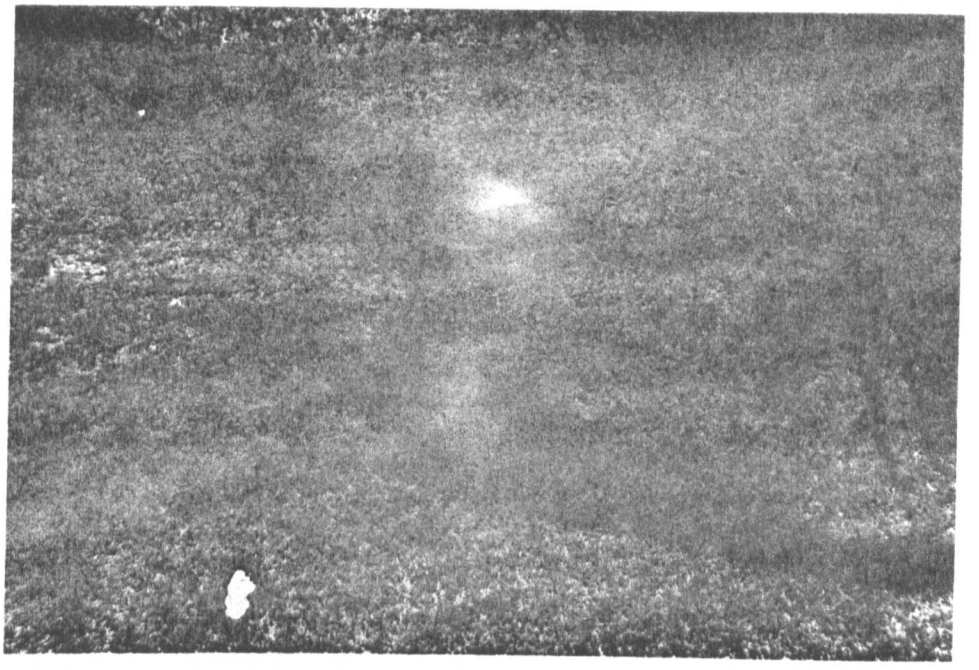

Plate 2.43 Dextral shearing of a wehrlitic dyke in the Wadi Rami Lower Cumulate Unit. (Coin diameter 2.5 cm).

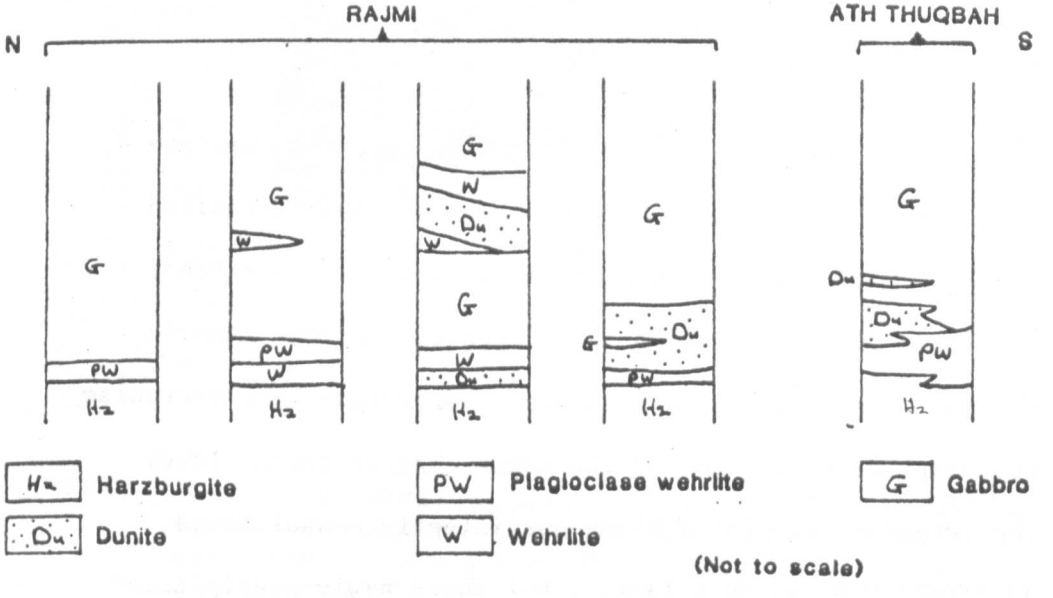

Figure 2.18 The cumulate successions of the Lower Cumulate Unit areas studied from the Fizh Block.

These are all tectonically undeformed and show good graded-bedding features with one metre thick layers of clinopyroxene rich bottoms grading to wehrlitic tops. (Plate 2.44.) In Sheet 1 of the Oman Geological Ophiolite Project Maps (Smewing, 1979) a major fault zone is inferred between the wehrlite/dunite unit and the underlying gabbros. In the field, however, there is no evidence for a fault zone. The dip and strike of the cumulate layers changes rapidly from the gabbros into the dunites and wehrlites, the contact between the two being roughly sub-parallel to the moho plane. The contact is thus more likely to be a relict magma chamber floor, formed by a fresh influx of magma into an already partially consolidated magma chamber, than a relict fault zone.

In the Ath Thuqbah area the cumulate sequence varies from dunite-olivine gabbro and from plagioclase wehrlite-dunite-olivine gabbro. (See Enclosure 3.) The plagioclase wehrlite horizon is up to 200 m thick and the dunite horizon up to 300m. The two rock-types interfinger with each other and also with the olivine gabbros above.

In the both the Rajmi and Ath Thuqbah areas, the cumulate layers in both the tectonised and adjacent non-tectonised areas are parallel to the tectonic foliation. As already mentioned in section 2.3.3 this suggests a strong genetic link between tectonism and cumulate formation: the tectonism occurring as cumulation of the magma chamber takes place; the lowermost cumulates being sufficiently consolidated to preserve a tectonic fabric, but those newly precipitated

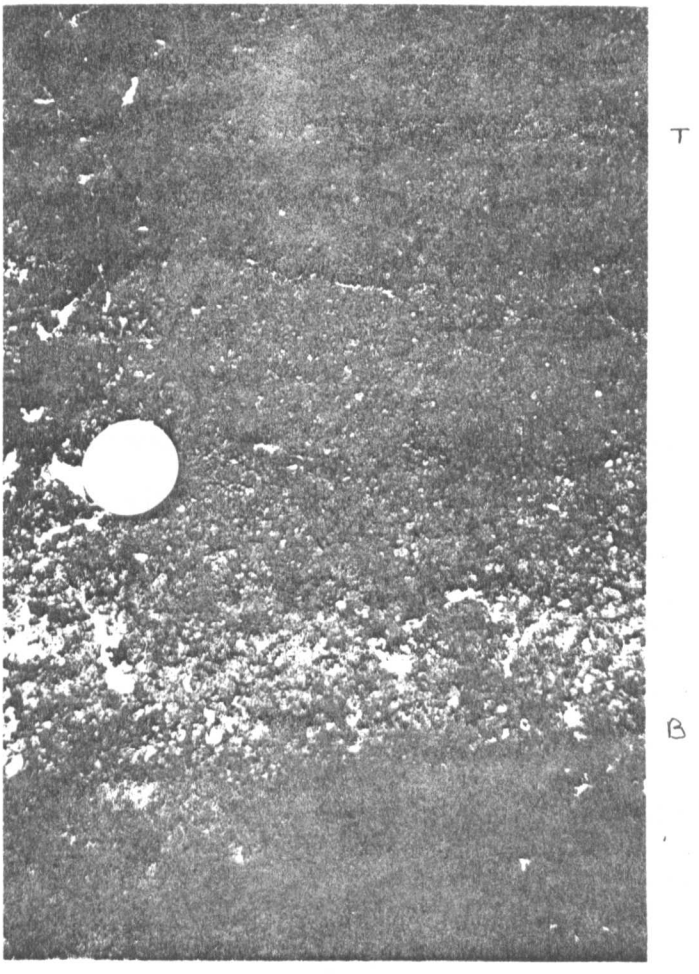

Plate 2.44 Mineral graded rhythmic layer in the Rajmi area. Clinopyroxene-rich base grading to an olivine-rich top. (B = base, T = top). (Coin 2.5 cm diameter).

only deforming by crystal-mush flow thus not giving a strong fabric development but a layering orientation parallel to the tectonic flow directions. It might be possible that a strong layering could control the orientation of the tectonic fabric and not vice-versa. However, because the tectonic fabric of the lowermost tectonised cumulates is distinct from the non-tectonised area, where a flow fabric which only results in a shape orientation exists, the hypothesis of tectonism occurring during cumulation is more probable.

In areas more distant from the zone of tectonism, the cumulate layers have more variable attitudes and are no longer sub-parallel to the underlying tectonic foliations. As already mentioned the layer attitudes sometimes rapidly change in the Rajmi area (see Enclosure 2) and usually make a fairly high angle with the moho plane (up to 60°). These areas can best be interpreted as the ends of different localised magma chambers as proposed by Browning (1982) for the Wadi Al Abyad section in the Rustaq Block (see section 2.4.5). In the Ath Thuqbah area individual layers in the gabbros can be traced for over 1km with remarkably constant thicknesses (10cm-100cm). The layer attitudes are sub-parallel to the moho plane. This is interpreted as a more central area of a single magma chamber, in contrast to the Rajmi area.

The orientation of the gabbro layers with respect to the moho plane and the Peridotite Unit tectonism are considered in detail in Chapters 9 and 10 in relation to the oceanic spreading environment.

2.4.2 The Salahi Block

The Salahi Block is about half the size of the Fizh Block. It is bounded by the Wadi Jizi fault zone to the north and the Wadi Ahin fault zone to the south (Figure 2.7). The Peridotite Unit is particularly inaccessible in this block and only one area was studied - the Wadi al Hilti area (Figure 2.8). Figure 2.19 summarizes the geology of the Salahi Ophiolite Block.

2.4.2.1 Structural Trends

The different structural trends of the Peridotite and Lower Cumulate Units are summarized on Figure 2.20.

The tectonic foliations and lineations of the Peridotite Unit show a similar orientation pattern to those in the Peridotite Unit south of northing 828 in the Ath Thuqbah area of the Fizh Block (see Enclosure 3). The foliation poles plot in a dispersed cluster within a girdle, and the lineations plot as a girdle with a strong cluster plunging gently towards the EESE. Associated with this strong lineation cluster are foliations dipping moderately ENE. If the S2 orientation is assumed to be similar to that of the Ath Thuqbah area, then these NNW-SSE striking foliations are from the D2 event, and the strong lineation cluster represent the L2 lineations. If this is the case then the other foliation and lineation trends are D1 structures which have been rotated to various degrees by the D2 deformation. Since the D1 structures are partially preserved the D2 event must have been very weak.

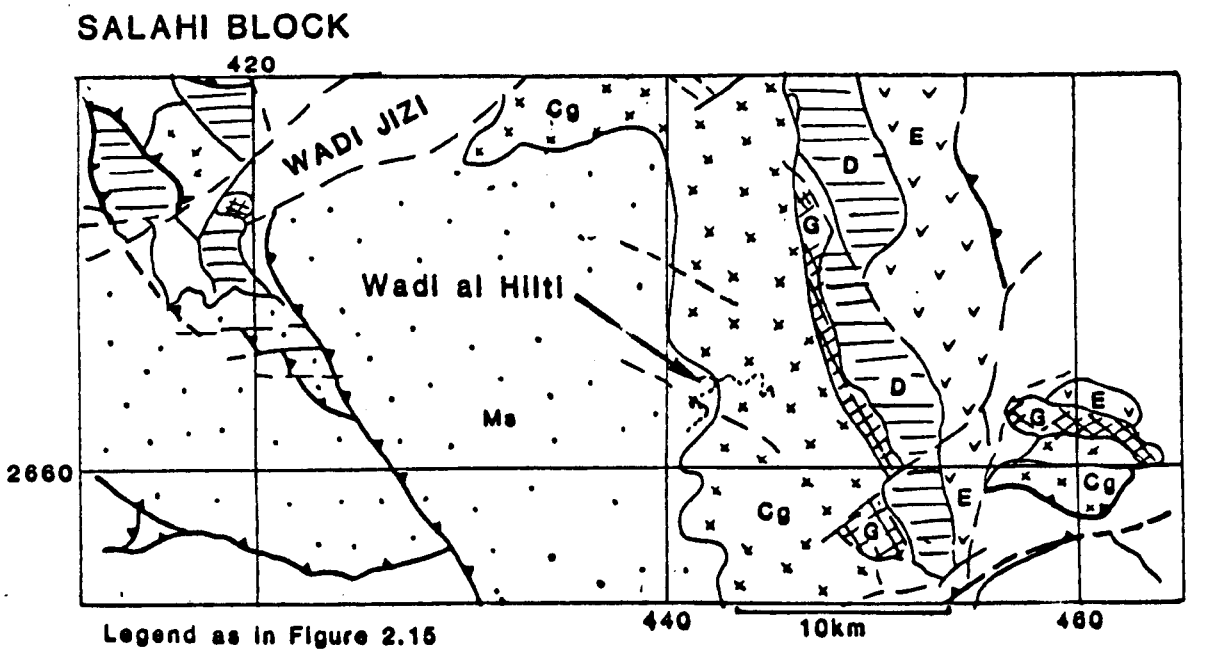

Figure 2.19 Geological map of the Salahi Ophiolite Block. (Modified from Lippard and Rothery, 1983).

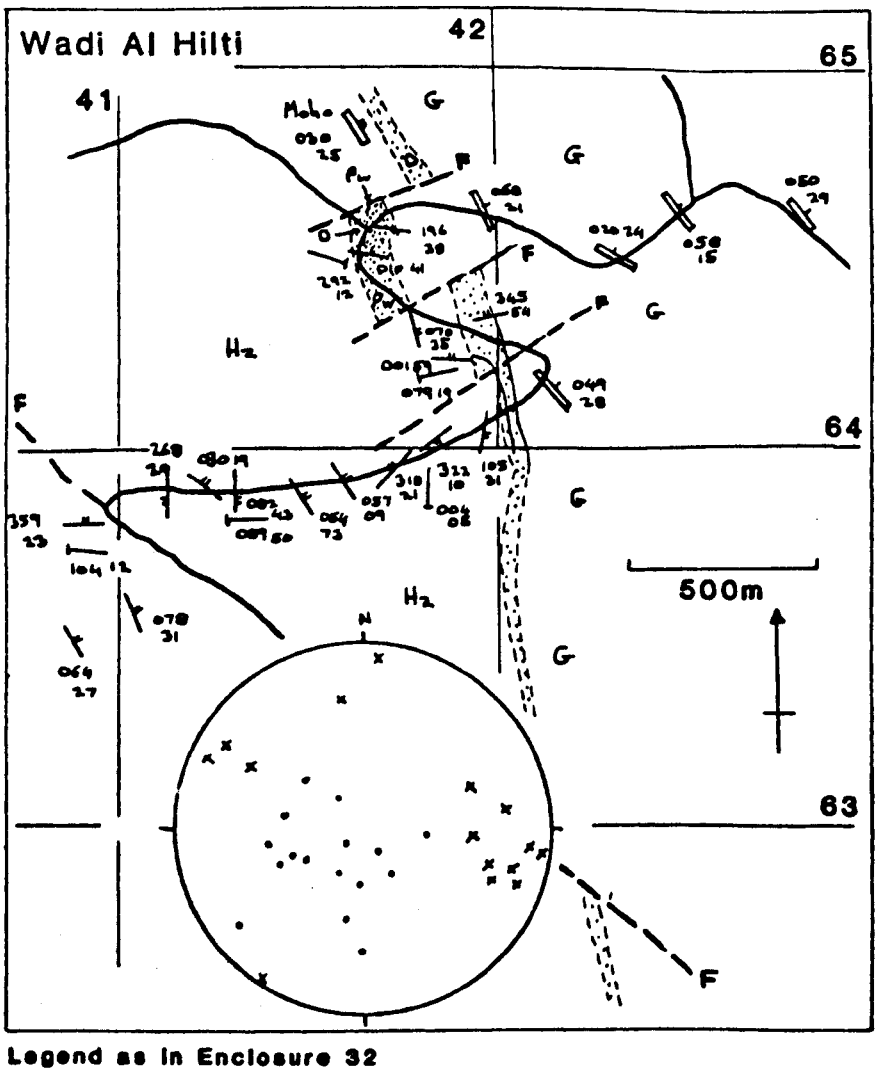

Figure 2.20 1:20,000 map of the Wadi Al Hilti area.

The Wadi Al Hilti harzburgites are all too serpentinised to allow any primary harzburgite textures to be distinguished.

The D1 and D2 deformations only extend into the Lower Cumulate Unit to a maximum of 50 metres. The D1 trends are more commonly observed and extend further than the D2 trends (see Figure 2.20) but poor exposure and later brittle faulting obscure their detailed relationships.

The brittle faults and fractures have a dominantly NE-SW strike and are sub-vertical. The maximum strike-slip displacement measured from the displacement of the moho plane is 300 metres and both senses of movement are present in the area mapped. These faults are parallel to the major Wadi Jizi and Wadi Ahin fault zones. There are also vertical faults trending NW-SE. A fracture jointing is present in the pyroxene-rich rocks near the NW-SE striking fault. (See Figure 2.20.)

2.4.2.2 The Distribution and Orientation of Intrusive and Cumulate Features.

The Peridotite Unit of the Wadi Al Hilti area is remarkably homogenous and no dunitic bodies or anastomosing sheets are present in the area mapped. All the late dykes are of gabbro or pegmatitic gabbro. They are all undeformed and have a fairly constant NNE-SSW trend with a moderate to steep dip to the east. These dykes are nowhere seen to cut the Lower Cumulate Unit. If it is assumed that very little or no relative rotation has taken place between the Fizh and Salahi Blocks, (the moho plane dips and late fault and fracture trends are very similar), then the Al Hilti dyke trends are the same as the trend 1 dykes of the Rajmi area.

The cumulate assemblage of the Lower Cumulate Unit is similar to that of Ath Thuqbah: either dunitic or wehrlitic units at the base of the sequence rapidly changing to gabbroic and olivine gabbroic in about 50 metres. (Figure 2.20.) The wehrlitic rocks contain plagioclase-rich horizons parallel to the gabbro layering above and sub-parallel to the moho plane. About 300 metres into the layered gabbros at grid ref. 423645 there is a 20 metre thick zone of strongly cross-laminated layers (see Plate 2.31). Unfortunately, the steep wadi sides and the only sporadic exposure, made it impossible to study either the lateral extent or the underlying layers, of this laminated zone. It most probably represents an area of channel fill during a major episode of rapid magma movement within the magma chamber. It may either be part of the cumulation process, or possibly due to a further magma influx into the system. The olivine gabbros are more melanocratic in this area with a few plagioclase wehrlitic layers which could imply an influx of less evolved magma. Above this zone the layered gabbros resume their constant layering orientation and their more normal leucocratic nature.

2.4.3 The Sarami Block

The location of the Sarami Block is shown on Figure 2.7. The block is smaller than the Fizh and Salahi Blocks, the Peridotite Unit being only 10km thick. (Figure 2.8.) The central areas of the block are, however, fairly accessible and there is no indication of any major tectonic breaks between the Lower Cumulate

and Peridotite Units. (Figure 2.21.) One traverse was completed trhough the whole Peridotite Unit - the Wadi Sarami traverse; as well as a further moho area traverse in the Wadi Kanut area.

2.4.3.1 Structural Trends

The structural trends for both the Wadi Sarami and Kanut areas are summarized on Enclosure 5.

(a) Early Tectonic Foliations and Lineations

In the Sarami traverse two distinct structural trends are present. In the Peridotite Unit north of northing 443 the foliation poles plot as a fairly strong cluster with the planes dipping fairly steeply to the NE. The corresponding lineations plunge gently NW or SE. In the Peridotite Unit south of northing 443 the foliation poles plot as a girdle. In the area between northing 425 and 443 the girdle of foliation poles is fairly dispersed. There is, however, a distinct cluster pattern of poles of foliation planes which dip steeply with a NNE-SSW strike. The lineations associated with these foliations have a shallow SSW plunge. The differently oriented lineations present in this area dip moderately to the east and form a girdle pattern with the SSW plunging lineations. In the area south of northing 425 the lineations plot as a similar girdle pattern but also show a fairly strong cluster parallel to the lineation direction of the Peridotite Unit area north of northing 443. The foliation poles of this lowermost area plot in a girdle with a fairly strong pole cluster parallel to the foliations of the area north of northing 443.

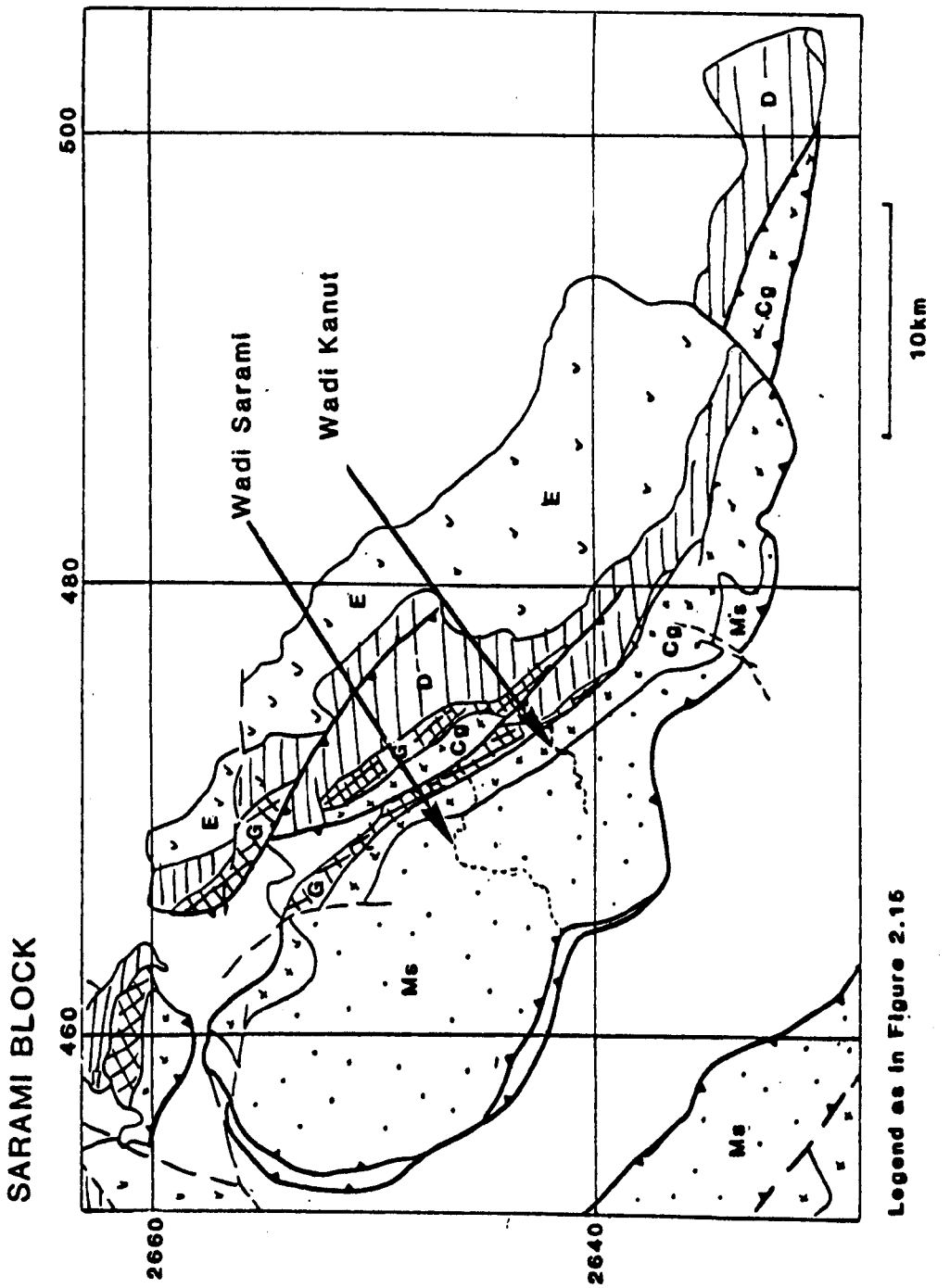

Figure 2.21 Geological map of the Sarami Ophiolite Block. (Modified from Lippard and Rothery, 1983).

The fabrics associated with the different structural orientations are distinct when studied in thin section. In the area north of northing 443 the thin section textures are all coarse with large unstrained olivine grains (Plate 2.45). A detailed crystallographic study of these thin sections shows that they have undergone only D1 deformation (see Chapter 7).

In the area between northings 443 and 425, D2 deformation has been intense producing an S2 foliation of NNE-SSW strike and L2 lineations gently plunging to SSW. The textures in these areas of intense D2 deformation are either disrupted porphyroclastic or mosaic porphyroclastic; as would be expected from the discussions in section 2.3.2. The larger spinel grains are elongate in these rocks. In this structural area the D1 structures are fairly strongly rotated by the D2 event. In the area south of northing 424, however, the D2 deformation has been much less intense with the D1 structures hardly rotated in some areas. Specimen 02/99 is from an area where D2 has been very slight: it has a tabular porphyroclastic texture - a texture inbetween the coarse textures of harzburgites deformed by only D1, and the mosaic porphyroclastic textures of strongly D2 deformed harzburgites.

In the Wadi Kanut area only D1 structures and textures are present in the Peridotite Unit except for very small areas, mainly near to the moho in grid square northing 72 easting 40, where D2 structural trends and textures are present. (See Enclosure 5.) In the area at grid reference 710405 the D1 structures are slightly flexured. This is probably due to

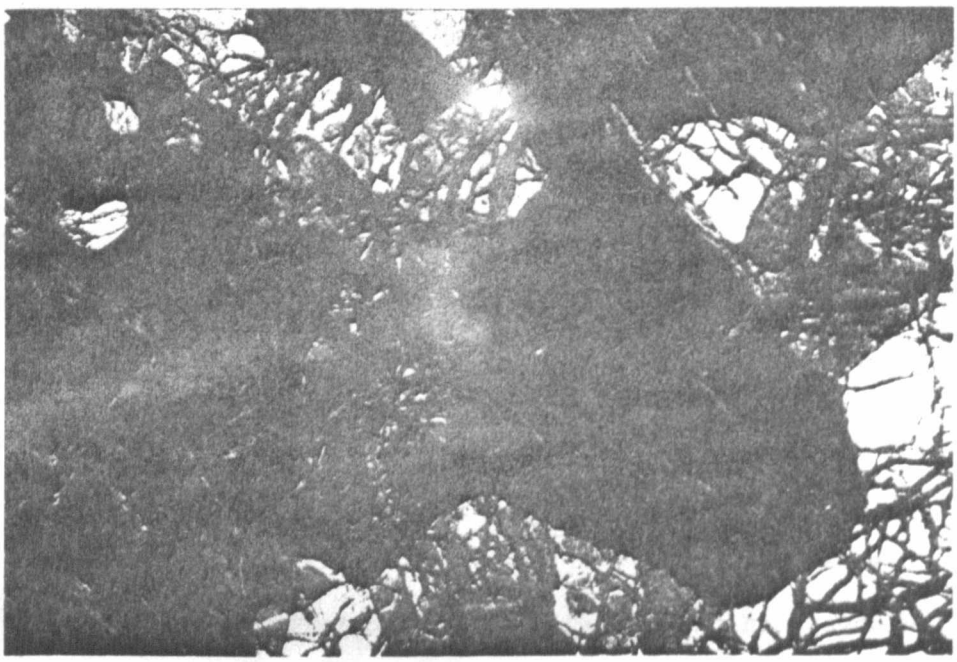

Plate 2.45 Specimen 02/88. Coarse textured with large, unstrained olivine grains. (Length of plate 5 mm). (Cross-polarised light).

very minor D2 deformation. This area thus represents the upper limit of the area of rocks affected by the D2 event similar to that in the Wadi Sarami traverse. Unfortunately, the area south of this locality was not mapped - the D2 structures should become more intense southwards.

In both the Sarami and Kanut areas the Lower Cumulate Unit is undeformed by either D1 or D2.

(b) Later Structures The Banded Unit is exposed at the base of the Wadi Sarami traverse. It has undergone a strong ductile deformation with the development of a foliation. This foliation is parallel to the thrust contact between the main Peridotite Unit and the Banded Unit, and is clearly different from the foliation orientations within the Main Peridotite Unit.

The late brittle faults and fractures in the Sarami area have two general trends - NW-SE and NE-SW. Both sets have sub-vertical dips. Only the NE-SW set is seen to cross-cut and displace the moho or basal thrust.

In the Kanut area the fracture joints have a similar trend to those in the Sarami area. No major fractures or faults were observed in the Peridotite Unit except for a zone of localised serpentinisation which strikes NNE-SSW within the harzburgites and also runs along the moho boundary with a N-S strike in the area south of northing 417 (see Enclosure 5). The moho is unserpentinised in the area north of northing 417. This implies that very little movement has taken place within these serpentinite zones.

In both of the areas minor NE-SW striking faulting is present in the Lower Cumulate Unit. Otherwise the cumulates are undeformed by later structures.

2.4.3.2 The Distribution and Orientation of Intrusive and Cumulate Features.

(a) Dunitic Intrusions within the Peridotite Unit.

In the areas mapped in the Sarami Block there are very few dunitic intrusions within the Peridotite Unit. The only area in which a sizeable dunitic body with associated anastomosing veinlets exists, is at grid ref. 670438 in the Sarami traverse. The inaccessibility of the wadi sides makes it impossible to determine the exact shape and dimensions of the body - it is at least 100 metres thick.

(b) Pyroxenitic and Gabbroic Dykes and Sheets.

The dykes in the Sarami and Kanut areas have highly variable trends with a predominant strike direction of NW-SE. They are restricted to the Peridotite Unit and are of pyroxenite, gabbro and peridotite-gabbro. In a few dykes in the Kanut area there is a gradation from pyroxenite to gabbro.

In the Sarami area two of the measured dykes have been deformed by D2 deformation. No dykes have been deformed by D1 deformation in either of the areas studied.

The cross-cutting relationships between different dyke trends gives no coherent pattern (Enclosure 5). In the Sarami area the earlier and later trends cannot be separated on the basis of the dyke trends. In the Kanut area the NW-SE striking dykes are the latest set to be intruded: earlier trends are, however, difficult to distinguish.

In both of the areas, the dykes vary in thickness from a few mm to 50cm. At grid reference 670460 an E-W pegmatite gabbro sheet dips gently towards the north; it is one metre thick in places. A clinopyroxene crystal 30cm in diameter was measured from this sheet.

In the Sarami traverse the top kilometre of the Peridotite Unit is void of dykes and sheets, as is the Lower Cumulate Unit. In the Wadi Kanut area a NW-SE striking gabbroic dyke is present in the lowermost dunites of the Lower Cumulate Unit (grid ref. 718423), and a fine-grained doleritic dyke with a N-S strike outcrops higher in the gabbro sequence (grid ref. 729423).

(c) Cumulate Features of the Lower Cumulate Unit.

The cumulate successions of the Lower Cumulate Unit are very simple in both the Sarami and Kanut areas. The succession is either dunite to olivine gabbro, or just olivine gabbro. The dunites vary in thickness along the moho strike; they are up to 200 metres in the Kanut area.

In detail, however, the cumulate units in the Sarami area are more complex, with the dunites grading into olivine gabbros containing wehrlitic and dunitic layers and horizons of more melanocratic olivine gabbros. In the area of gabbros west of northing 696 the layers are highly disrupted and reworked by magma chamber processes. Metre scale slump folds are present as well as numerous cross-laminated and truncated layers. (Plate 2.46). This area of extreme disruption within the magma chamber close to the moho, dies out along moho strike to an area of layered gabbros containing no igneous disruption

structures (Figure 2.22). Here the layers dip moderately towards the NE with the dip shallowing slightly up section to become sub-parallel to the underlying moho plane which dips at an angle of 50° towards the NE. (Enclosure 5 and Figure 2.22.) The petrological succession is the same in both the disrupted and non-disrupted area. This implies that the disruption features are more likely to have been formed within a single chamber by density flow or convection currents, than at the interface between two different magma chambers as in the Wadi Al Hilti cumulates (see section 2.4.2.2).

In the Kanut area the cumulate layers have a similar dip to those of the undisrupted areas of Wadi Sarami, and dip more steeply towards the NE than the moho plane (see Enclosure 5). The layers in both areas are oriented parallel to the S1 foliation trends in the tectonised Peridotite Unit below. This suggests that the D1 shear stresses extended into the Lower Cumulate Unit while it was still unconsolidated; flow of the crystal mush would thus have orientated the crystallizing layers parallel to the Peridotite Unit S1 foliations without any internal crystal deformation. (See Chapter 7.) The fact that the Lower Cumulate Unit is tectonically undeformed implies that D1 deformation took place before the cumulate layers had become sufficiently consolidated to show any deformation structures. This contrasts with the areas of D2 Peridotite Unit shearing in the Rajmi area of the Fizh Block where the lowermost gabbros show a strong tectonic fabric, and thus must have been solid before deformation. The change from deformed layers to layers aligned by crystal-mush flow occurs at a higher level in this sequence (see section 2.4.1.2).

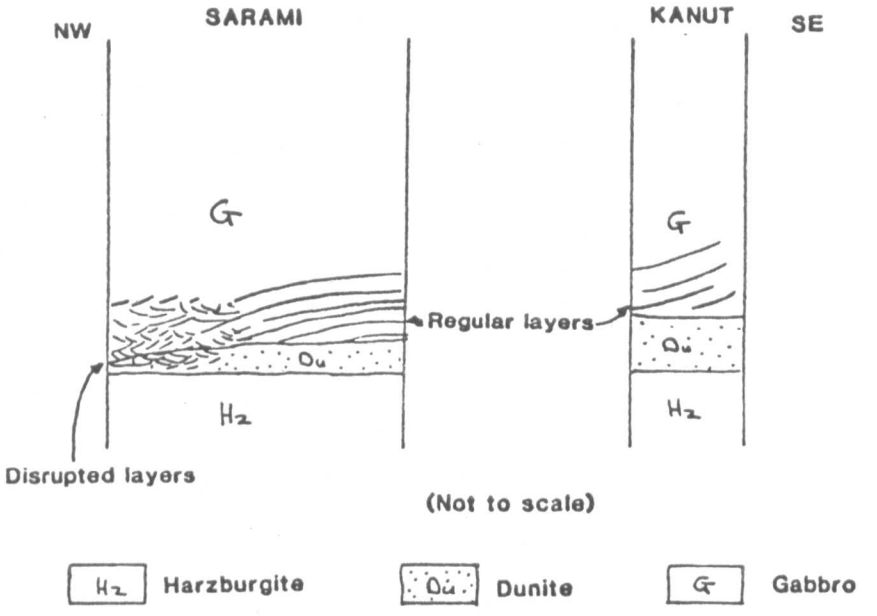

Figure 2.22 The cumulate successions of the Sarami and Kanut Lower Cumulate Units.

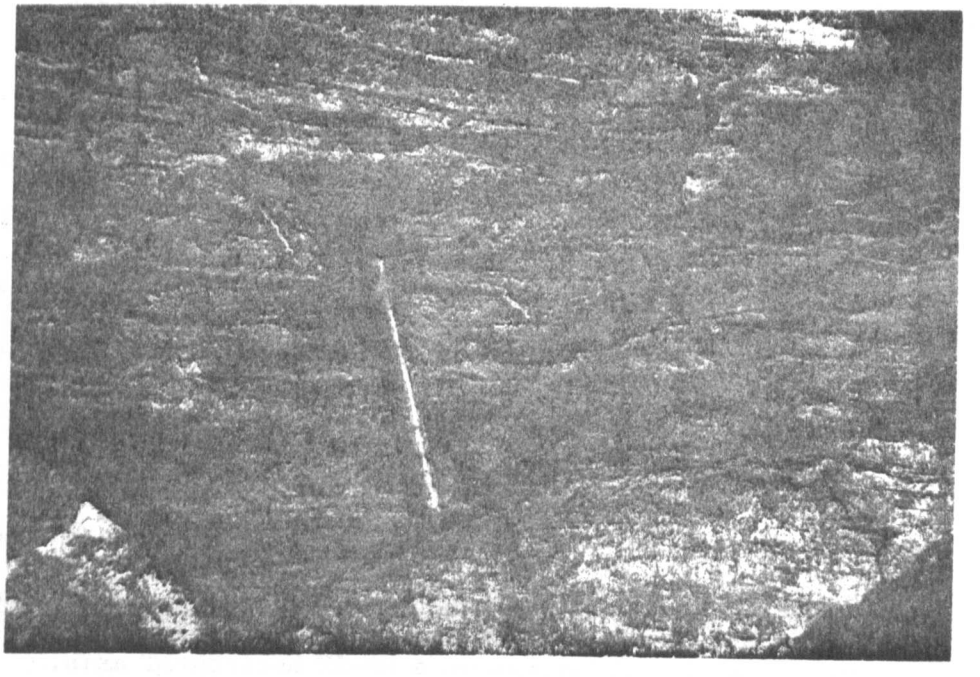

Plate 2.46 Small-scale truncated and cross-laminated layers in the Wadi Sarami Lower Cumulate Unit. (Length of hammer 40 cm).

Late pegmatitic veining is fairly common in the cumulate gabbros in the Sarami and Kanut areas. Pegmatisation tends to be concentrated in specific zones within the gabbros, and occurs as irregularly orientated veins of varying widths (few mm up to 50cm). In the larger veins individual plagioclase and clinopyroxene crystals have grown up to diameters of 10cm.

A detailed study of the relationships between the orientations of the cumulate and tectonic features in relation to an ocean-spreading environment is discussed in Chapters 9 and 10.

2.4.4 The Haylayn Block

The Haylayn Block occupies over 1200km² (Figure 2.7). The Peridotite Unit has a maximum thickness of 20km from the moho to the basal thrust sheets. It is mostly inaccessible except for the Wadi Hajir area through which a traverse was completed. Another area close to the moho was studied at Musayfiyah (Figure 2.8).

Figure 2.23 summarizes the geology of the Haylayn Block. As well as extensive faulting, Browning (1982) has mapped large-scale, emplacement related open folds with NW-SE trending axial traces within the lower ophiolite units in the SE corner of the block. This folding causes outcrop repitition of the Peridotite and Lower Cumulate Units. The Wadi Hajir traverse is not significantly close to these areas of open folding but, as is shown in section 2.4.4.1 below, the orientations of the Peridotite Unit structures are affected by slight rotations on a NW-SE horizontal axis.

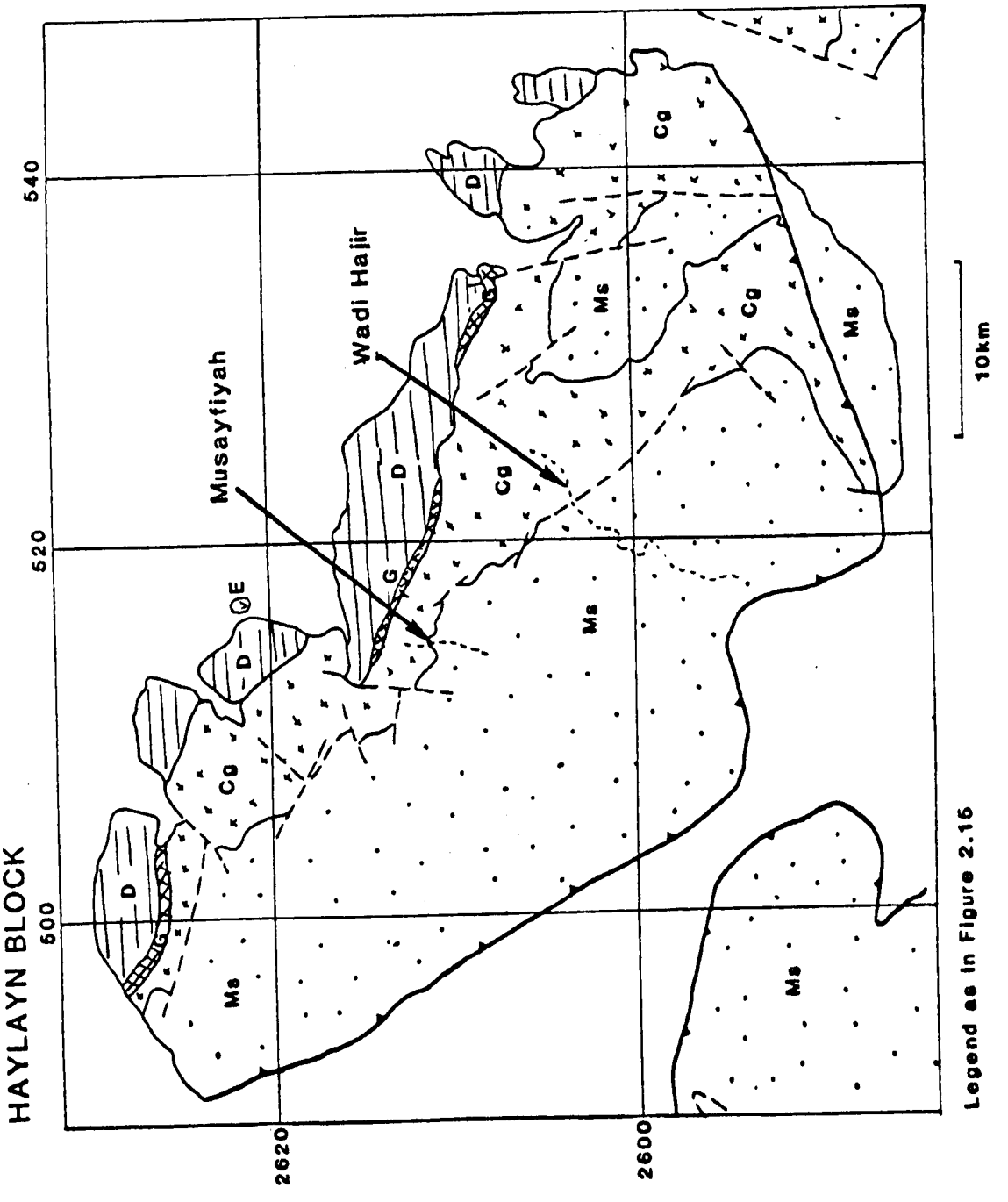

Figure 2.23 Geological map of the Haylayn Ophiolite Block. (Modified from Lippard and Rothery, 1983).

2.4.4.1 Structural Trends

The structural trends for the Wadi Hajir Traverse are summarized on Enclosure 6, and those for the Musayfiyah area on Figure 2.24.

(a) Earlier Tectonic Foliations and Lineations

The foliation poles of the Hajir and Musayfiyah areas show similar distributions to the other Peridotite Units described above. The foliation poles either plot as clusters or girdles. The lineations have similar distributions.

In the Peridotite Unit north of northing 010 in the Hajir Traverse, the foliation poles plot as a girdle with a point concentration of planes steeply dipping northwards. Lineations are difficult to measure in the field: the few measured plot as a two cluster pattern, those associated with the E-W striking foliations having a shallow plunge to the west, and those in the other cluster a moderate plunge to the NE. All of the specimens collected in this area have a coarse porphyroclastic texture with the larger spinel grains only slightly elongate.

In the area between northing 010 and 990 the foliation poles plot as a more dispersed cluster pattern, the main cluster giving a steeply dipping foliation plane with a WNW-ESE strike. The lineations are still difficult to measure in the field and give a possible two cluster plot as shown on Enclosure 6.

The stratigraphically lowest part of the Peridotite Unit studied south of northing 990 gives a fairly strong foliation pole cluster representing a moderate dip to the SSE. The

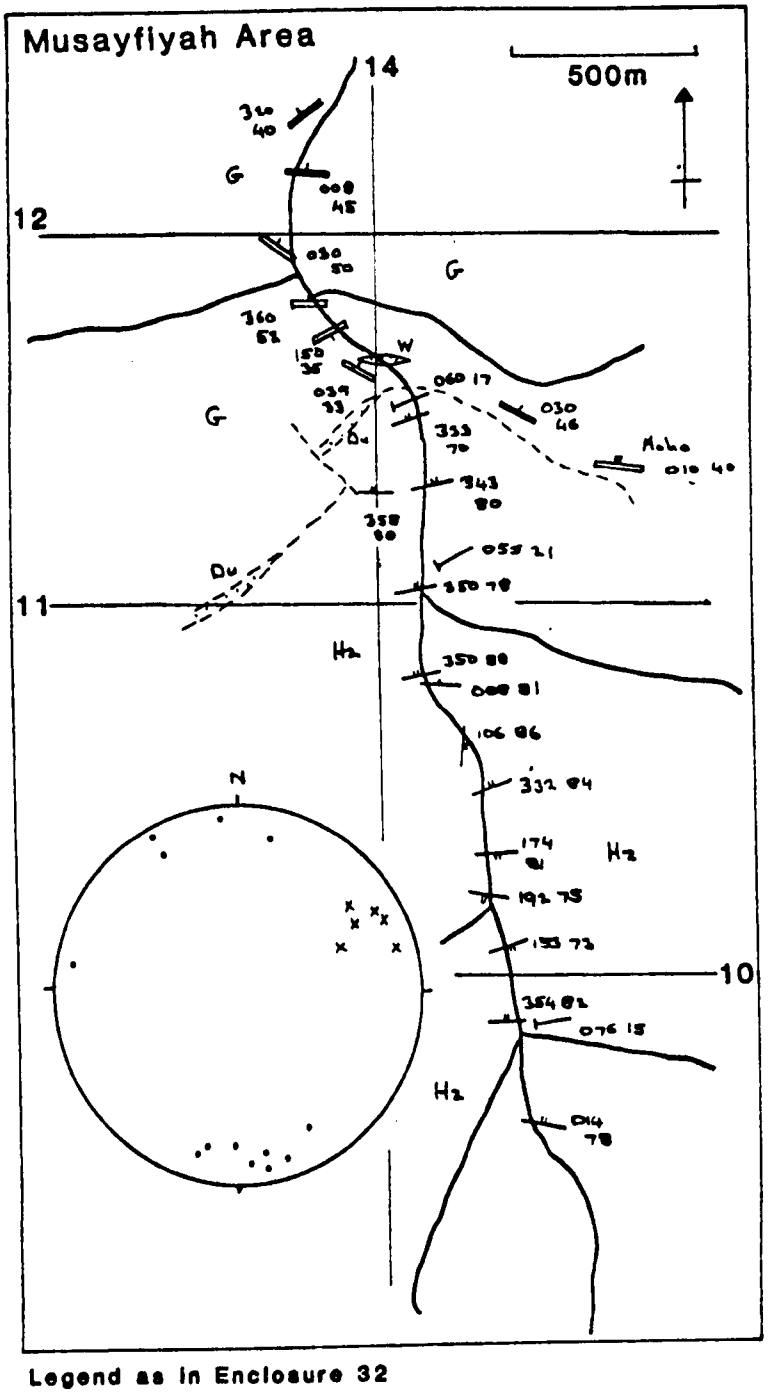

Figure 2.24 1:20,000 map of the Musayfiyah area.

associated lineations plot as a dispersed cluster giving a gentle plunge to the WSW to SSW. In the area around grid reference 192962 the foliation dips steeply to the WNW. The associated lineation plunges very gently towards the south. The textures of thin sections from this area are either coarse porphyroclastic or porphyroclastic. The larger spinel grains in the porphyroclastic textured specimen 02/73 are moderately elongated parallel to the WNW-ESE foliation trace. In the coarse porphyroclastic specimen (02/69) the larger spinels are only slightly elongate.

The foliations of the Hajir traverse do not show the obvious two deformational trend recognised in the other areas. This is thought to be due to the large-scale flexurings in the south eastern corner of the Haylayn Block mentioned above. In the areas south of northing 010 the foliation generally has a fairly constant attitude with a steep to moderate dip and a WNW-ESE strike. Both the textural evidence and the crystallographic evidence discussed in Chapter 7 suggest that this foliation has been formed by the D2 event. The associated L2 lineation has a shallow SW plunge. D1 structures are sporadically preserved, as in the area around grid reference 192961.

In the area north of northing 010, D2 deformation is clearly less intense with the foliation poles forming a girdle. The crystallographic evidence discussed in Chapter 7 suggests that the S2 foliation trends have a more E-W strike implying that there has been a minor late stage rotation between the

different areas of the Peridotite Unit. The corresponding L2 lineations have a moderate plunge to the NE. As discussed in section 2.4.4.2 the late dykes from small areas give a dispersed pattern, and thus cannot be used to show whether there has been a late rotation between different areas.

In the Musayfiyah area the Peridotite Unit foliations all dip steeply with an E-W strike (except for one locality at grid reference 107142). (See Figure 2.24.) The associated lineations plunge gently ENE. The cluster patterns of foliation poles and lineations have a similar orientation to the D2 fabrics of the upper Hajir traverse. This fabric extends at least 200 metres into the Lower Cumulate Unit in the Musayfiyah area. It has similar trends to the Peridotite Unit (see Figure 2.24).

The Peridotite Unit is in fault contact with the Lower Cumulate Unit in the Wadi Hajir area. The cumulate rocks adjacent to and above the fault zone are all tectonically undeformed.

(b) Later Structures Appart from the major NW-SE vertical fault between the Peridotite Unit and the Lower Cumulate Unit in the Hajir section, late brittle-type structures are uncommon in the part of the Haylayn Block studied. Minor fractures and fracture joints are only locally developed and trend either NW-SE or NE-SW and are generally sub-vertical.

The Lower Cumulate Unit of the Musayfiyah area was only briefly studied. One small-scale shear zone, similar to the Riedel

shears of the Wadi Rajmi cumulate sequence, was measured at grid reference 117139. It dips 50° to the NE and has a dextral shear sense with a maximum 10cm displacement of the layering and foliations.

2.4.4.2 The Distribution and Orientation of Intrusive and Cumulate Features.

(a) Dunitic Intrusions within the Peridotite Unit.

No large bodies of dunite were mapped in either area studied in the Haylayn Block. The only dunitic intrusive feature within the Peridotite Unit is a small area of anastomosing veinlets at grid reference 182980 in the Hajir traverse.

(b) Pyroxenitic and Gabbroic Dykes and Sheets.

In the Wadi Hajir area there are both pyroxenitic and gabbroic dykes. Most have a moderate to steep dip and roughly NW-SE strike (Enclosure 6). There is, however, no obvious pattern of dyke trends. No cross-cutting relationships between dykes was seen and so no intrusive history can be discerned. None of the dykes are deformed which implies that they were all intruded after D2 deformation had ceased. There are no pyroxenitic or gabbroic dykes in the Lower Cumulate Sequence of the Hajir traverse.

In the Musayfiyah section the late intrusive dykes are undeformed and similar in composition to the Hajir dykes. They do, however, have two different trends, both steeply dipping, one set striking E-W and the other NNW-SSE. No cross-cutting relationships between the sets were seen. There are also pegmatite gabbro dykes in the Lower Cumulate Unit with similar trends to those in the Peridotite Unit.

(c) Cumulate Features of the Lower Cumulate Unit.

In the Musayfiyah area the cumulate succession varies from dunitic to olivine gabbroic. Wehrlitic pods and layers are fairly common in the largely melanocratic olivine gabbros. (Up to 50m in length.) In the tectonised area the layers are sub-parallel to the tectonic foliation. The apparently curving moho trace on Figure 2.24 is entirely due to the effect of topography - the moho plane has a constant dip of 45^{o} towards the NNE. Outside the areas of tectonised cumulates, the layering is sub-parallel to the moho plane. No sedimentary-type cross lamination or slump structures were seen in the cumulates of the Musayfiyah area.

The dip and strike of the undeformed cumulates in the Hajir area is highly variable. The composition of all of the cumulate sequence studied is olivine gabbroic except for a few wehrlitic horizons. Intruded into the cumulate sequence are biotite rich granitic bodies of up to 200 metres thick. These bodies were first recognized by Browning (1982) as part of a late plutonic suite and are associated with the late stage NW-SE faulting. The area of cumulates mapped was not large enough to provide an explanation for the large variation in orientations of the cumulate layers.

2.4.5 The Rustaq Block

The most southerly area studied is in the Rustaq Block. (Figure 2.7) Although the area of this block is approximately 400 km^2, the exposed thickness of the Peridotite Unit is over 15km. The higher ophiolitic units; the sheeted dykes and pillow lavas are generally absent. (Figure 2.25)

The block is affected by an open folding, like that in the Haylayn Block, which is restricted to the western edge of the Rustaq Block. The area studied is in the centre of the block and is unaffected by this late-stage folding (see below). A traverse was completed through the Wadi Al Abyad section of the Lower Cumulate and Peridotite Units (Figure 2.25). (This section is part of the Wadi Bari Kharus section mapped by Browning (1982).)

2.4.5.1 Structural Trends

The structural trends of the Wadi Al Abyad traverse are summarised on Enclosure 7.

(a) Early Tectonic Foliations and Lineations

As in all the other areas studied, the foliation poles from the Al Abyad area show two different patterns: either a girdle or a cluster. In the main traverse area (approximately following easting 680) the northernmost area of the Peridotite Unit north of northing 910 has a fairly well developed girdle of foliation poles and also a girdle of lineations. Within the foliation pole girdle there is a discrete cluster of planes dipping moderately to the NE. The lineations associated with these foliations have a general E-W trend and a shallow plunge. In the adjacent area between northings 910

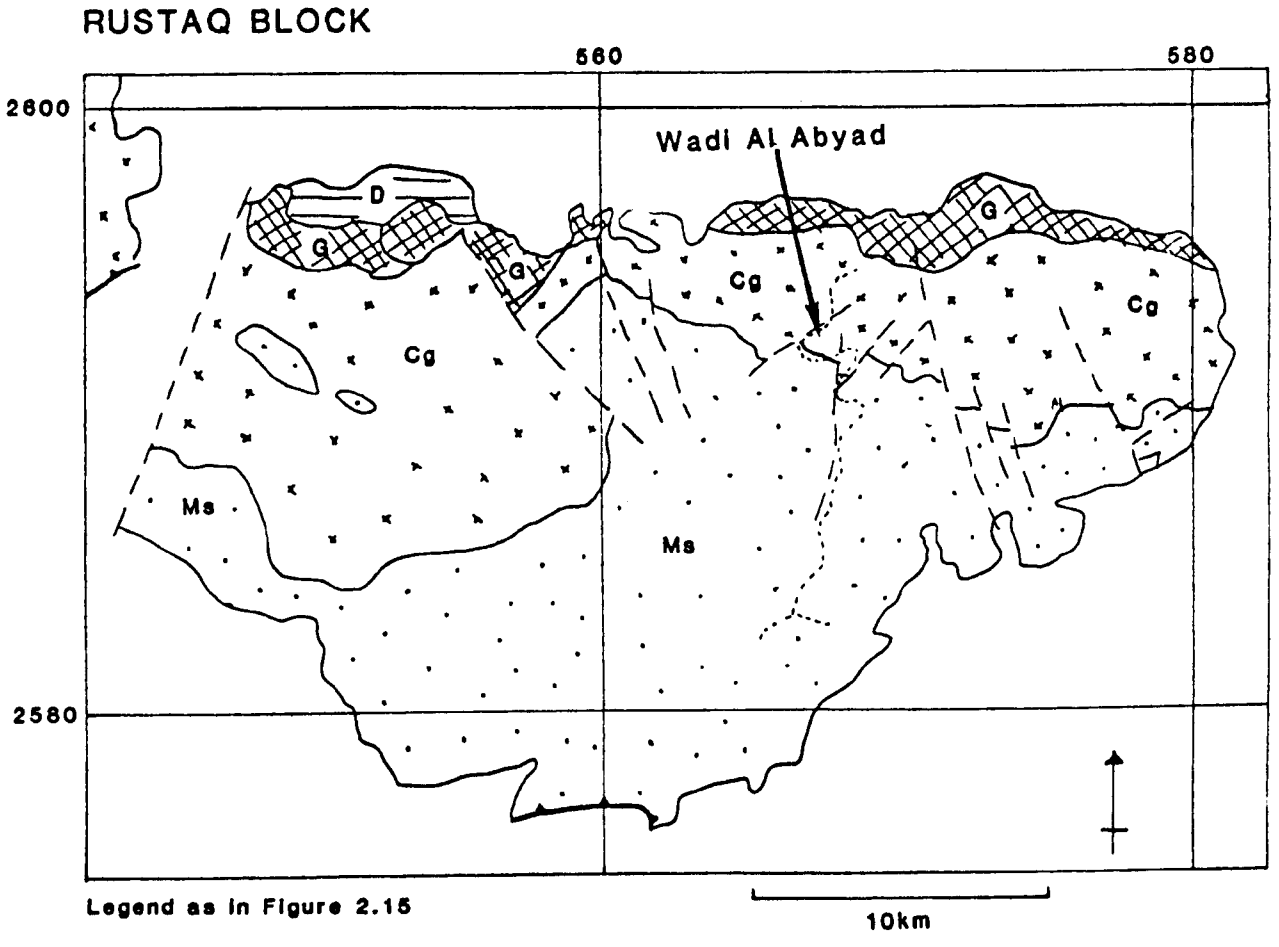

Figure 2.25 Geological map of the Rustaq Ophiolite Block. (Modified from Lippard and Rothery, 1983).

and 890 a similarly oriented cluster pattern of foliation poles is well developed; the girdle of foliation poles is only slightly developed. The lineations plot on a gently inclined girdle, with the lineations associated with the E-W striking foliations plunging gently east or west. The harzburgite textures from these two areas vary from coarse porphyroclastic with slightly elongate spinels to mosaic porphyroclastic with highly elongate spinels. The detailed crystallographic work discussed in Chapter 7 shows that the textures relate well to the intensity of D2 deformation as in the Wadi Rajmi area: i.e. low intensity D2 deformation produces coarse porphyroclastic textures grading to mosaic porphyroclastic textures as the intensity of D2 increases. In these areas the D2 deformation froms the NE gently dipping foliation and the E-W gently plunging lineation. The relict D1 deformation structures have variable trends depending on the intensity of the D2 deformation.

The area between northings 890 and 870 shows similar structural trends to the areas above except that the S2 foliations dip more steeply to the north east and the D2 lineations have a steeper dip to the east. (See Enclosure 7) The textures of the harzburgite thin sections are porphyroclastic to mosaic porphyroclastic with highly elongate spinel grains; this fact and the dispersed cluster pattern of the foliation poles suggests that the D2 deformation was fairly intense.

In the area south of northing 870 the S2 foliations dip more gently towards the north. There is a fairly pronounced girdle of foliation poles and most of the lineations do not show the expected D2 trend.

Harzburgite textures are porphyroclastic with moderately elongated spinel grains. This evidence suggests that D2 deformation has been less intense here than in the area to the north.

The Peridotite Unit adjacent to the moho, between eastings 660 and 682, has a much more complex structure. This area is subdivided into sub-units as shown in Enclosure 8. The small area east of easting 670 and north of northing 920 has a strong foliation pole cluster and lineation cluster pattern. The orientations are similar to those of the D2 deformation in the areas already described. In the sub-area to the south the foliation poles plot as a cluster/girdle pattern. The pole cluster has a significantly different trend from the sub-area to the north. The pi-pole girdles of each area are sub-parallel (See the equal area projection on Enclosure 7 which shows the foliation poles from both sub-areas on the same projection). The lineations of this southern area plot as a great circle with only a few plotting in the expected L2 direction. The structural trends for this area are intepreted as showing only minor D2 deformation. The original S1 foliation planes dipping moderately to the SE, and the associated lineations plunging gently to the SSW, have undergone only a slight D2 deformation and thus only a little rotation. S2 foliations and L2 lineations have only been formed in a few localised areas where D2 has been slightly more intense. In these areas the S1 foliation has been rotated more than in areas where D2 structures are absent. (See Enclosure 8).

The area west of easting 670 and north of northing 920 has been moderately deformed by D2 shearing, with localized D2 structures oriented as in the adjacent areas, and a dispersed girdle pattern of D1 structures showing a large variation in the intensity of D2 deformation. This area is bounded on the west by a large fault with a sinstral strike-slip displacement of about 1200 metres. This faulting may have locally disrupted the adjacent areas; this could explain the few foliation poles which give the overall girdle pattern a rather dispersed appearance. The area south of northing 920, also adjacent to this fault, gives a similar dispersed girdle pattern implying a similar deformational history.

The D2 deformation extends into the Lower Cumulate Unit. In the area east of easting 682 it dies out approximately 300 metres into the cumulate unit; in the area west of easting 682 the D2 deformation extends at least 1000 metres into the Lower Cumulate Unit. The foliation pole and lineation plots show strong clusters parallel to the D2 trends of the Peridotite Unit; the foliations dip moderately to the NE, and the lineations plunge moderately to the east. (Enclosures 7 and 8) In the lowermost areas of the Lower Cumulate Unit traces of a possible S1 foliation have been measured. In three localities in the vicinity of grid ref.675923 this S1 foliation trace is tightly folded with the fold axial planes parallel to the S2 foliation planes. Figure 2.26 shows a detailed map of these localities and the moho boundary. In the two eastern localities the folds are asymmetrical with dextral vergence on the horizontal surface. (Plate 2.47) The trends of the S2 foliation between these two fold localities

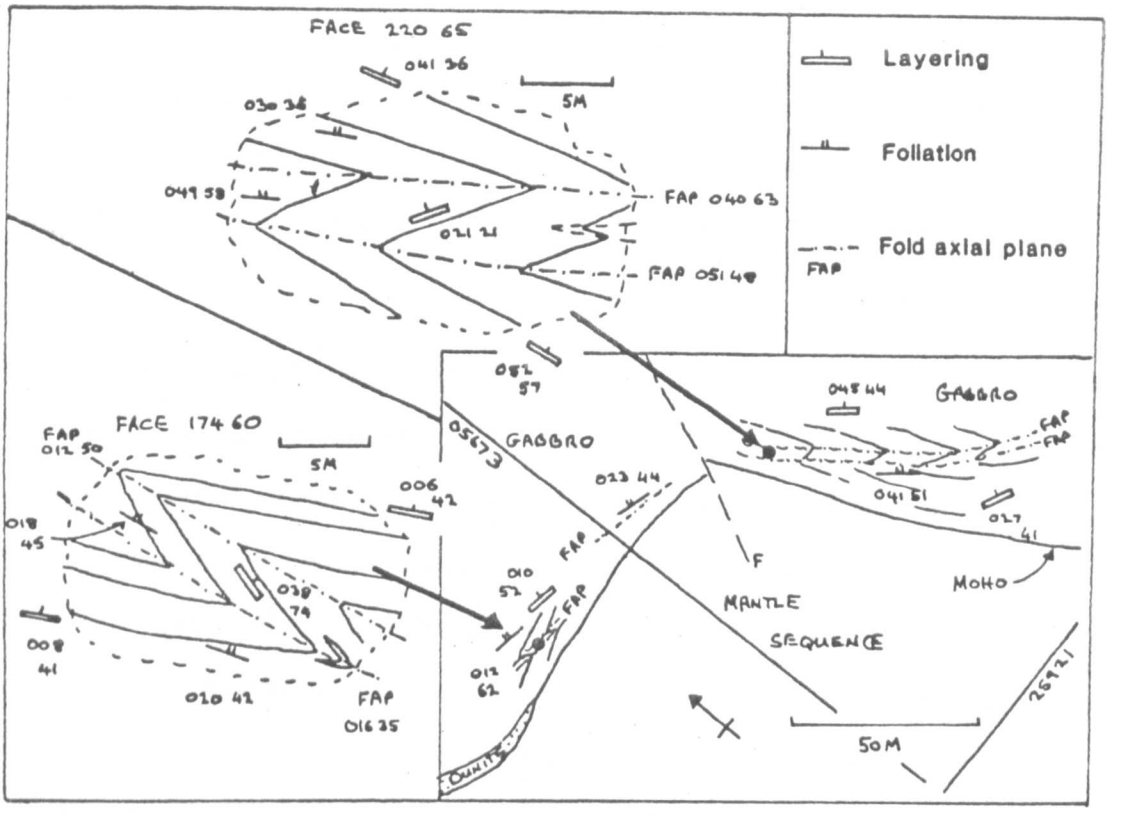

Figure 2.26 Sketch map of the Lower Cumulate Unit gabbro folding localities.

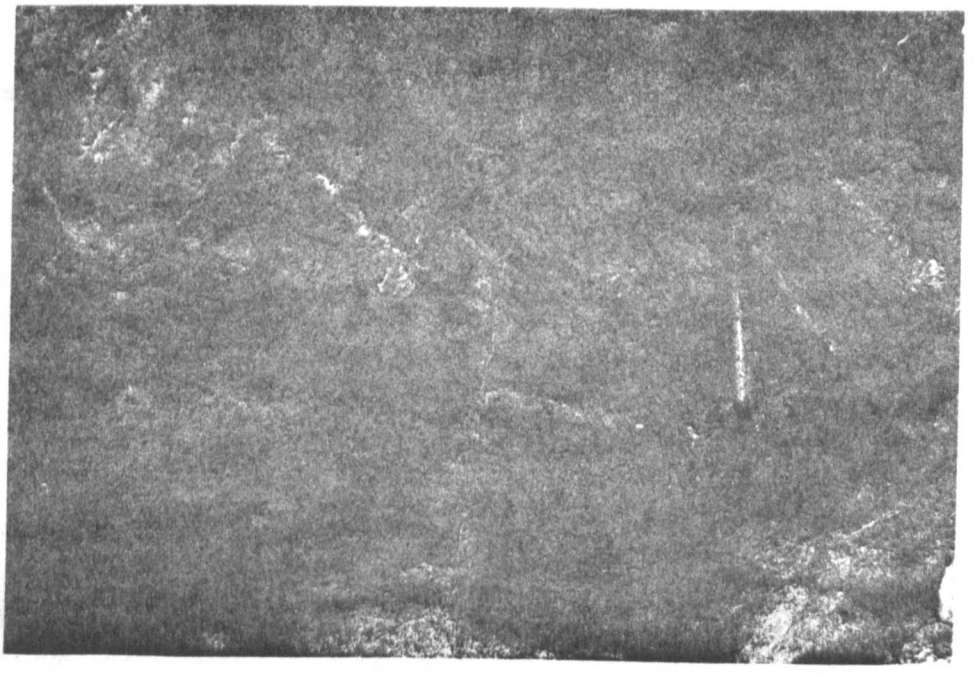

Plate 2.47 Tight folding of cumulate layers at the base of the Al Abyad Lower Cumulate Unit, (— =S2 foliation trace). (Length of hammer 40 cm).

indicate that they are both on the same fold limb (Figure 2.26). The western fold locality has asymmetrical folds with a sinistral vergence as seen on the horizontal surface. The S2 foliation plane trends show that this fold is structurally beneath the eastern fold localities.

Deformation in the cumulates is mainly by shear processes as in the Peridotite Unit (See Chapter 7). The different vergence senses of the folds indicates a change in the sense of shearing of the deformation between different areas. No fold closures of D1 foliations have been observed in the Peridotite Unit. This is probably due to its extreme homogeneity in constrast to the highly variable cumulate sequence.

(b) Later Structures

In the areas mapped of the Peridotite Unit all the later structures are brittle. There is large-scale faulting in the northern parts of the studied area. The faults are all sub-vertical and strike either NE-SW or N-S. As already mentioned above, the NE-SW striking faults have a major strike-slip component with a sinistral displacement of up to 1200 metres. A N-S trending fault, which bisects the northern part of the area, has a dextral strike-slip displacement of at least 400 metres in the moho area. (Enclosure 7)

Despite this major faulting, a fracture jointing is only very locally developed in the Peridotite Unit. The poles to the fracture joints plot as a girdle, the joint planes all having sub-vertical dips. These trends cannot be directly

related to localized fracture and fault zones because of the small number of measurements taken.

Small-scale ductile shear zones are faily common in the lower 400 metres of the Lower Cumulate Unit. They are very similar to those described in the Rajmi area of the Fizh Block. (See section 2.4.1.1). They deflect the cumulate layers and the S2 foliations. In the areas of gabbro folding the shear zones locally displace the fold axial planes and limbs. They are rarely more than 2 metres in length and have displacements of only a few centimetres; both shear senses have been measured and their orientations are shown on Figure 2.27. The shear plane poles plot as a girdle pattern and do not show such an obvious conjugate relationship as the Rajmi shears. Shear zones with a sinistral displacement sense, as measured on a horizontal surface, generally dip moderately towards the NW-NNW, and those with a dextral sense to the NE.

If these shear zones are Ridel shears, they imply that the orientation of a possible major slip surface should either be a dextral or sinistral zone striking roughly east-west, the exact orientation depending on the shear sense. (See Figure 2.27)

The orientation of these shear zones in relation to an ocean spreading environment is discussed in Chapter 9.

In the area west of the major N-S trending fault there is a zone of serpentinization which roughly parallels the boundary between the Lower Cumulate and Peridotite Units. Minor movements have occurred along this zone. This is shown by the brittle buckling

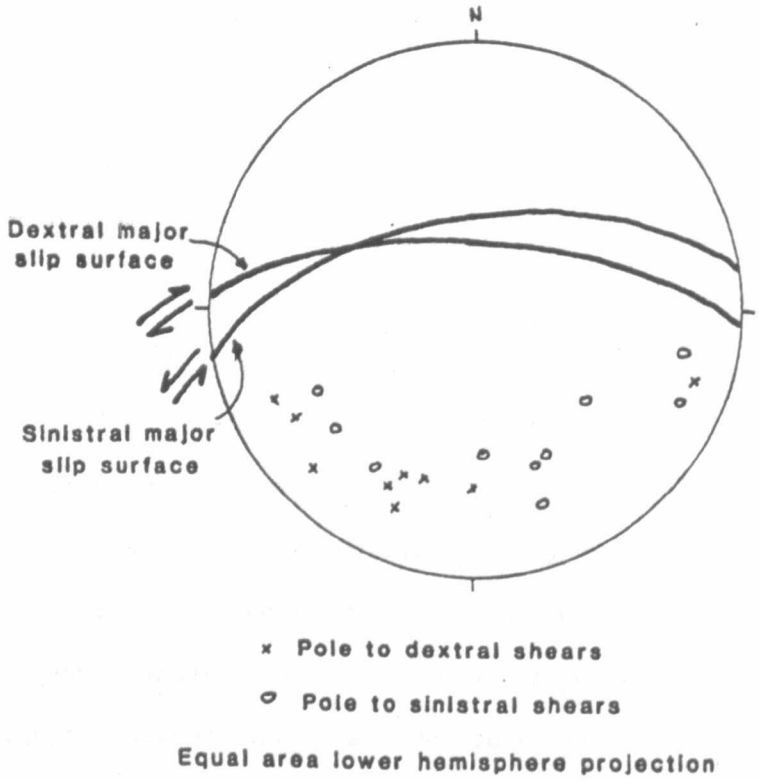

Figure 2.27 The possible orientation of a major slip surface for the Al Abyad area as determined from Riedel shears in the Lower Cumulate Unit.

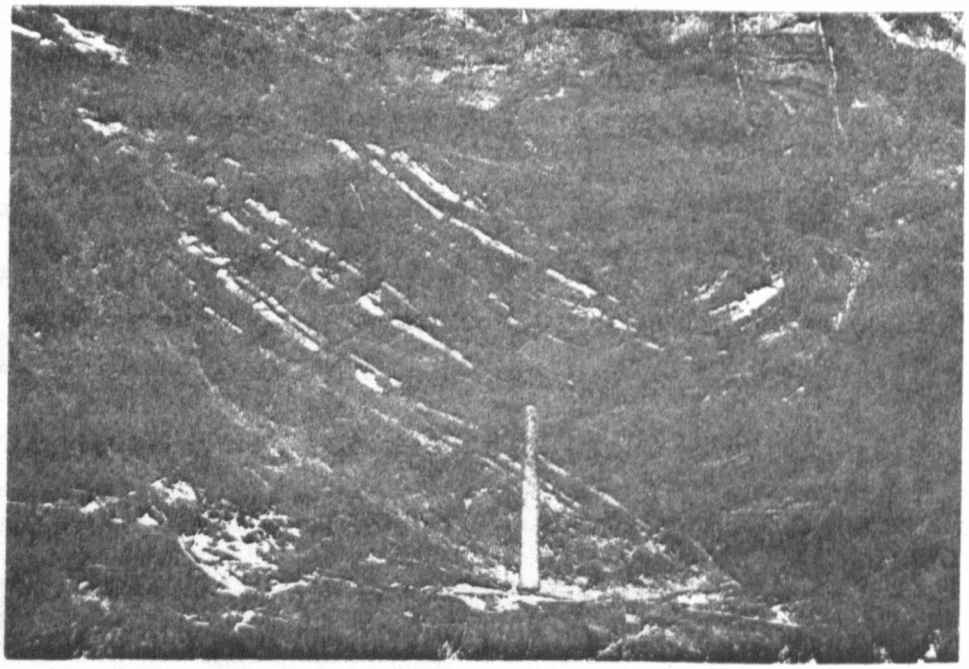

Plate 2.48 Brittle buckling of plagioclase rich horizons in the uppermost Peridotite Unit associated with minor movements along the moho boundary. (Length of hammer 40 cm).

of some of the plagioclase-rich horizons within the Peridotite Unit (Plate 2.48), and the off-setting of late-state hornblendic gabbro dykes (both described in section 2.4.5.2) which cross-cut all other petrological and structural features apart from the late faults mentioned above. The sense of movement along the serpentinite zone is sinistral when measured on the surface horizontal with a displacement of 1½ metres.

The displacement relationships observed from the field would suggest that, in places, a minor decoupling took place between the Peridotite and Cumulate Units during the early stages of obduction and emplacement of the Oman Ophiolite: this occurred before the break-up of the ophiolite into separate blocks by faulting and thrusting.

2.4.5.2 The Distribution and Orientation of Intrusive and Cumulate Features

(a) Dunitic and Olivine Gabbroic Intrusions within the Peridotite Unit

No large dunitic bodies were mapped in the Peridotite Unit of the Al Abyad area. Near northing 900 there is a fairly extensive area of anastomosing dunitic sheets. Elsewhere in the Peridotite Unit, apart from areas immediately adjacent to the moho, there is a noticeable absence of intrusive dunites. (See Enclosure 7) In some areas near to the moho, to a depth of about 300 metres, there are small dunitic pods up to 30 metres in extent.

Plagioclase wehrlite and gabboric rocks outcrop in the topmost few metres of the Peridotite Unit harzburgites in all areas of the Al Abyad moho section. These vary from being discrete strung out plagioclase and clinopyroxene clasts (Plate 2.49) to more definite layers up to 50cm thick. (Plate 2.50) Browing (1982) has related these layers and discrete stringers to the intensity of deformation. He suggests that as deformation progressed, the layers and dykes become more dispersed deforming into flaser gabbros and finally into diffuse blebs.

The area containing these plagioclase and clinopyroxene-rich rocks within the harzburgites has been subjected to fairly extensive D2 shearing. The crystallographic study of a harzburgite specimen within this zone (Specimen 02/46) indicates that the D2 deformation had only a moderate intensity (see above and Chapter 7). With only moderately intense shearing it would not be possible to deform a massive dyke-like body into a completely strung out and disrupted body. In other areas of intense D2 shearing, gabbroic dykes have been rotated into the foliation plane and slightly boudined or folded but not disrupted on the scale inferred above. (See Plate 2.23)

Instead of being variably deformed dyke-like bodies, a more plausible explanation of these features would be that they are similar in nature and origin to the dunitic bodies of the Peridotite Unit: i.e. they are a more and variably evolved equivalent, some sheets being more dunitic, evolving to wehrlitic to plagioclase wehrlitic and finally to olivine gabbroic. They

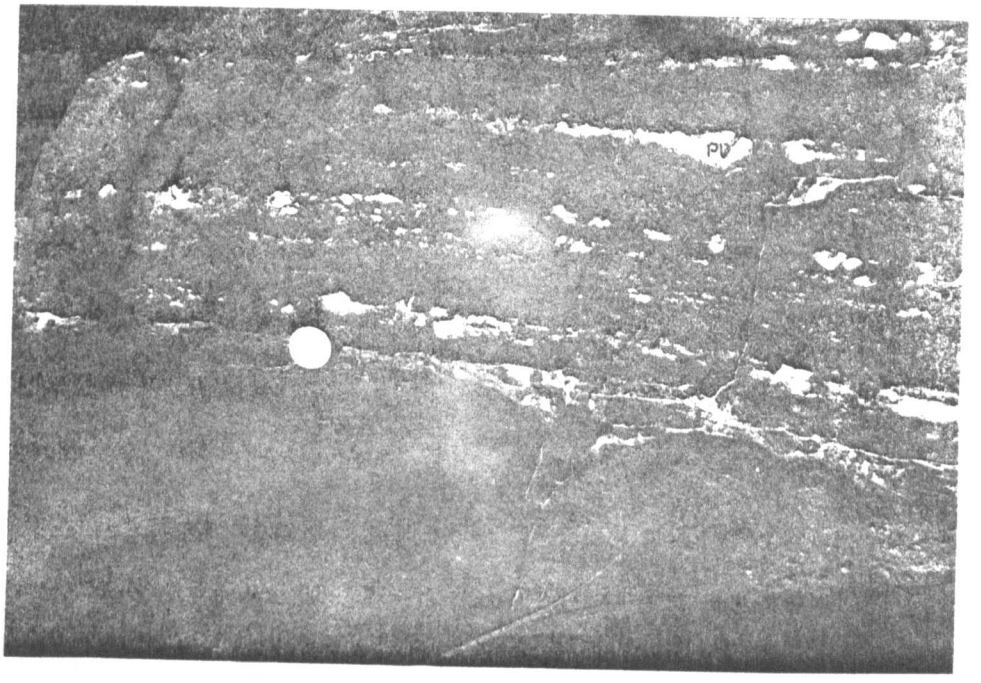

Plate 2.49 Strung out plagioclase (Pl) and clinopyroxene (Px) clasts in harzburgite. (Coin diameter 2.5 cm).

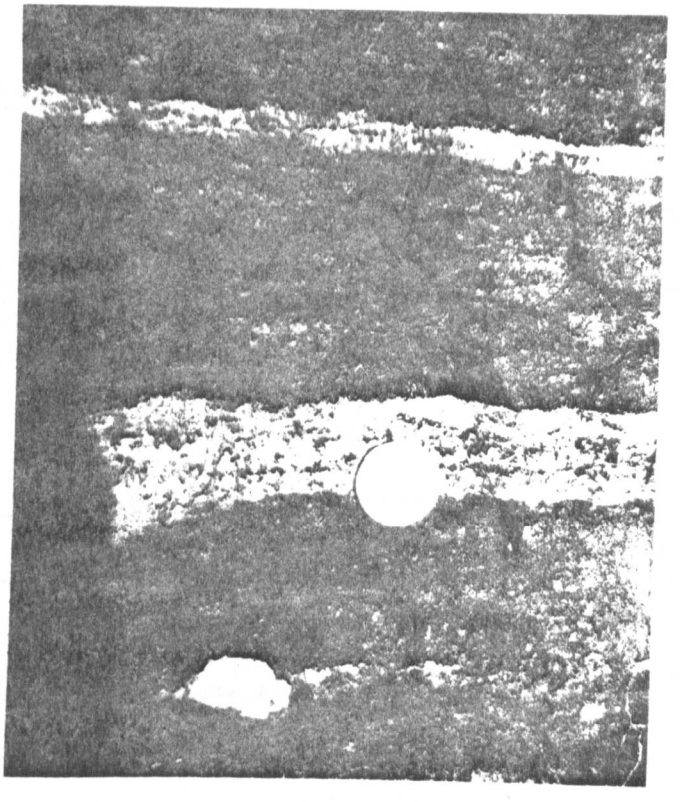

Plate 2.50 Plagioclase- and clinopyroxene-rich layers and clasts in harzburgite. (Coin diameter 2.5 cm).

were formed essentially prior to D2 deformation and had a primary variation in mineralogical compositions. This affected the style of deformation of each individual sheet: those which were olivine gabbroic in character, and thus more competent, were rotated and slightly boudined but remained as identifiable sheets; the competency of plagioclase-and clinopyroxene-poor sheets was lower and more comparable with that of the surrounding harzburgites and so they were defomed with the main harzburgite mass instead of independently. Figure 2.28 summarises the above relationships.

These plagioclase- and clinopyroxene-rich sheets have not been observed elsewhere in Oman. In the Wadi Rajmi area one small similar body of olivine gabbro has already been described (see above) but elsewhere plagioclase is only abundant in the Cumulate Unit.

(b) Pyroxenitic and Gabbroic Dykes and Sheets

In the parts of the Wadi Al Abyad traverse studied, gabbro and pegmatite gabbro dykes are abundant. None are deformed by D1 or D2 except for a few near to the Moho. Only two pyroxenite dykes were measured.

All the dykes have fairly steep dips but their strike is highly variable. Cross-cutting relationships imply that NE-SW striking dykes were intruded first (trend 1); with a series of WNW-ESE dyke intrusions next (trend 2). A few of the dykes from both of these trends are slightly deformed by D2;

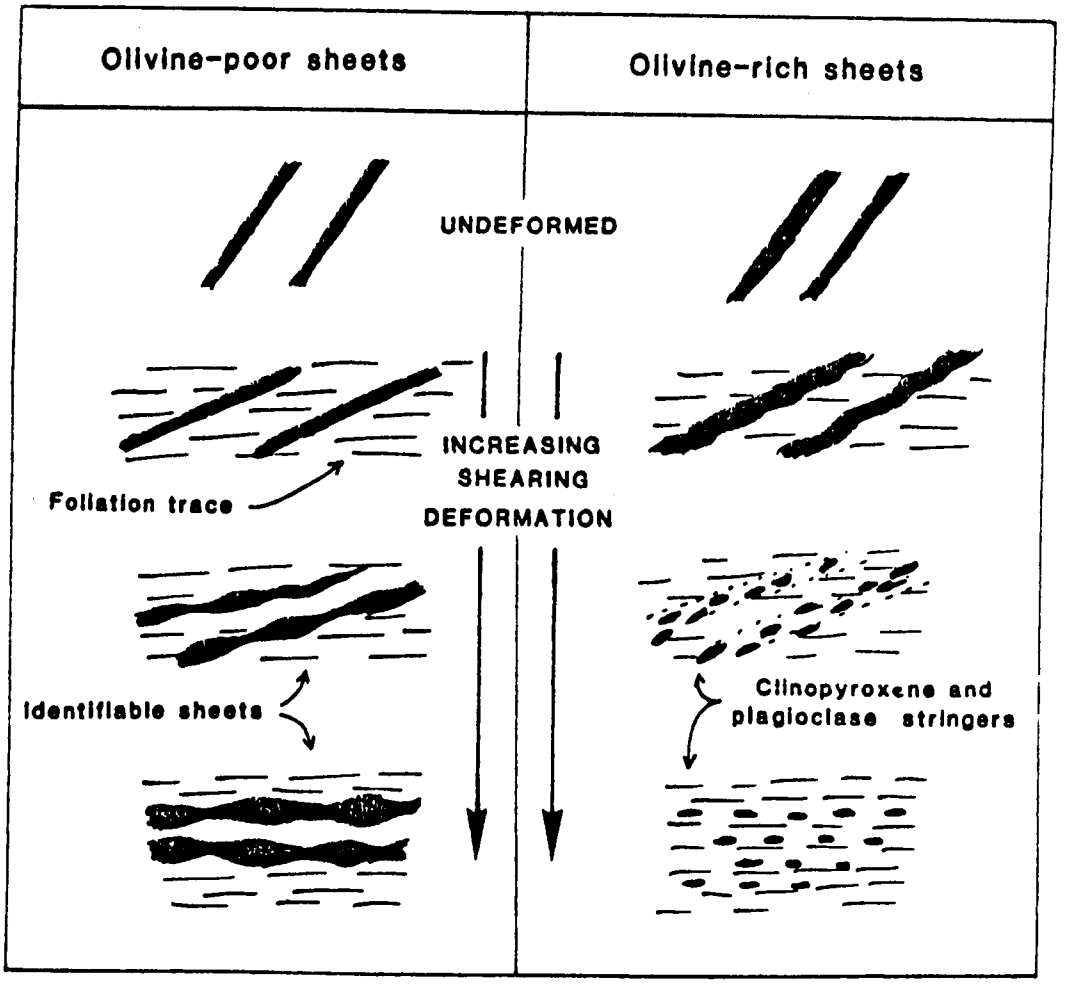

Figure 2.28 The deformation of plagioclase-, clinopyroxene- and olivine-rich sheets in the uppermost Peridotite Unit of the Al Abyad area.

this suggests that dyke intrusion started as D2 was dying out.

In the top two kilometres of the Peridotite Unit, later-stage hornblende gabbro dykes intrude the sequence (trend 3). They all dip steeply and strike N-S (Plate 2.51). At the moho at grid ref. 672923 these dykes are up to 3 metres thick and cross-cut the moho. As mentioned above, the minor late-stage serpentinite shearing at the moho displaces these hornblende gabbro dykes.

Trend 3 hornblende gabbro dykes only extend a few hundred metres into the Lower Cumulate Unit. No other dykes are present in this unit except for fine-grained doleritic dykes at grid ref 671925. These also strike approximately N-S and are deflected by the small scale sheer zones described in section 2.4.5.1.

Late-stage pegmatisation is common within the Lower Cumulate Unit of the Al Abyad area. The veining is random but in some areas, where small-scale shear zones are abundant, the pegmatite veins are strongly associated with, and parallel to, the shear planes.

(c) Cumulate Features of the Lower Cumulate Unit

In the areas adjacent to the moho, a narrow band of dunite, not more than 5 metres thick, is present in some areas. This rapidly grades into an area of interbanded dunites, wehrlites and olivine gabbros. This zone is up to 20 metres thick. Above it, olivine gabbros are predominant, with a few more melanocratic bands and layers.

In the moho areas studied in the eastern side of the traverse, olivine gabbros lie directly on top of the moho plane. In the area east of easting 683 the sequence of olivine gabbro layers include a 100 metre thick zone of dunitic and wehrlitic pods and bands as well as isolated ultramafic pods within the gabbros (See Enclosure 7).

The layers and ultramafic pods are all sub-parallel to the tectonic fabric in those areas which have undergone the Peridotite Unit tectonism (Enclosure 8). This implies the same relationship between deformation and layer formation as deduced for the other areas studied in Oman.

Above the zone of tectonism, the cumulate layers are still sub-parallel to the foliation below; but good layer truncations, cross-laminations and slump folds are also present on the centimetre to metre scale. Browning (1982) studied the entire Lower Cumulate Unit and High-level Intrusive Unit in detail. He notes that the layering within the Cumulate Unit steepens towards the top of the Unit and passes upwards into the massive, usually isotropic gabbro of the High-level Intrusive Unit. The change in dip of the cumulate layers and their truncations and rapid mineralogical changes have been related by Browning (1982) to the interactions between localized magma chambers, and also magma chamber processes within individual magma chambers.

The High-level Intrusive Unit is fairly well exposed in the Wadi Al Abyad section. In most areas it is composed of massive isotropic gabbros, but in some localised areas the gabbros have large-scale slump folds. Figure 2.29 shows a typical locality of large-scale slump folding and associated features. As can be seen by comparing Figure 2.29 with Figure 2.26, the structures formed in the gabbros

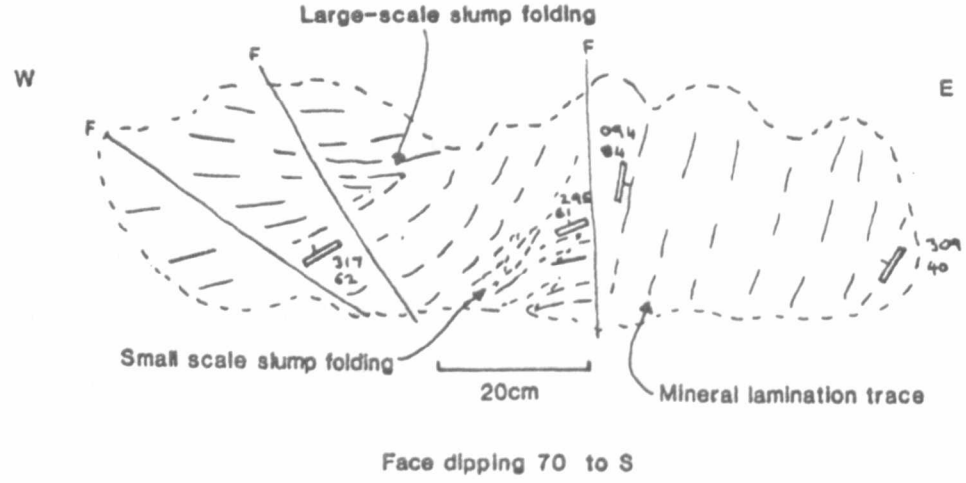

Figure 2.29 Sketch map of slump-folded gabbros in the High-level Intrusive Unit.

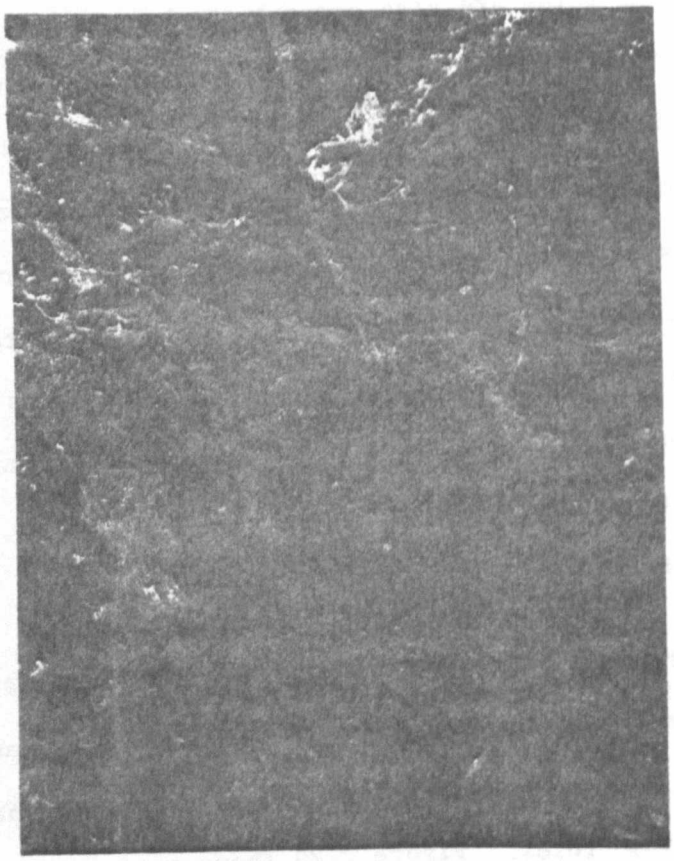

Plate 2.51 Late-stage hornblende gabbro dykes intruding harzburgite. (Plate 10 m across).

by a tectonically induced folding are entirely different from those due to slumping.

The orientation of the gabbro layers with respect to the moho plane and the Peridotite Unit tectonism are considered in detail in Chapters 9 and 10.

2.5 Summary of the Structural Trends and Distribution of Petrographic Features of the Peridotite and Lower Cumulate Units of the Northern Oman Ophiolite

The distribution of the D1, D2 and later structures and the different petrographic features for each area studied are summarised on Enclosure 9.

As can be seen there is a large variation in the structural trends both within and between the different ophiolite blocks studied. The angle between the S2 foliations and the moho plane is highly variable between areas:in some areas they are almost sub-parallel (e.g. Wadi Al Abyad), but in other areas the angle between the two is large (e.g. Wadi Sarami). The L2 lineations show a similar large variation in trends.

The intensity of the D2 deformation is highly variable both within and between areas, D2 deformation being absent from small areas of a few of the sections studied (e.g. Wadi Sarami). In these areas the S2 foliation is sub-parallel to the moho plane.

In Chapters 6 and 7, crystallographic studies are described which enable the mechanisms of the D1 and D2 deformations to be determined. The orientation of the D1 and D2 structural elements with respect to a spreading axis and the moho plane are considered in detail in Chapters 9 and 10. The petrographic data and its variation between the different areas is also put into an ocean-spreading context in these chapters.

CHAPTER 3

The Troodos Ophiolite, Cyprus.

CONTENTS

Chapter 3.

3.1 Geographical and Geological Setting - Previous Work.

The island of Cyprus is situated in the north eastern corner of the Mediterranean Sea, approximately 100 km west of Syria and 70 km south of Turkey. (Figure 3.1).

The ophiolite complex of Cyprus covers an area of approximately 2,700 km^2 and forms the major part of the Troodos Massif in southern Cyprus.

3.1.1 Regional Geology.

The geology of Cyprus can be divided into five major geological units. (Figure 3.2). These are :-

1) The Kyrenia Range: this mountain range extends along the northern coast of Cyprus. It is composed of upthrust masses of Permian to Cretaceous limestones and basic volcanics, and is flanked on both sides by Miocene Flysch deposits (the Kythrea Formation).

2) The Mamonia Complex: located in the south of Cyprus this complex forms an allochthonous sequence of thrust slices of Triassic to Mid Cretaceous age composed largely of continental margin type sediments (mainly pelagic) and includes a Triassic alkaline volcanic series. In Upper Cretaceous times this complex was juxtapositioned against Upper Cretaceous ocean crust which now forms the Troodos Complex. A large-scale strike-slip movement probably caused the formation of the Kathikas Formation - a melange composed largely of sediments but also including serpentinite slices. This mélange zone is classed as part of the Mamonia Complex (Swarbrick, 1980). Another mélange zone occurs in the south of Cyprus - the Moni Melange. It is thought

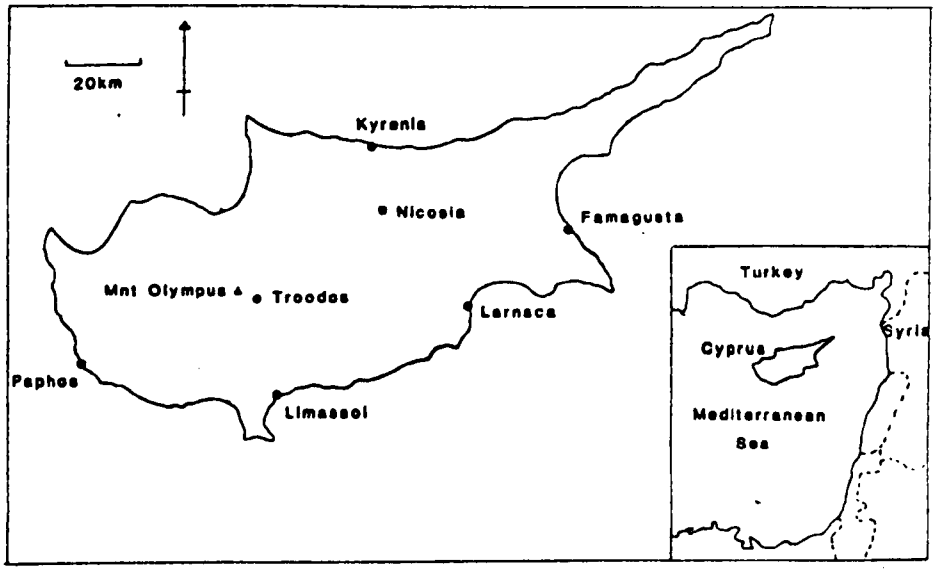

Figure 3.1 The location and geography of Cyprus.

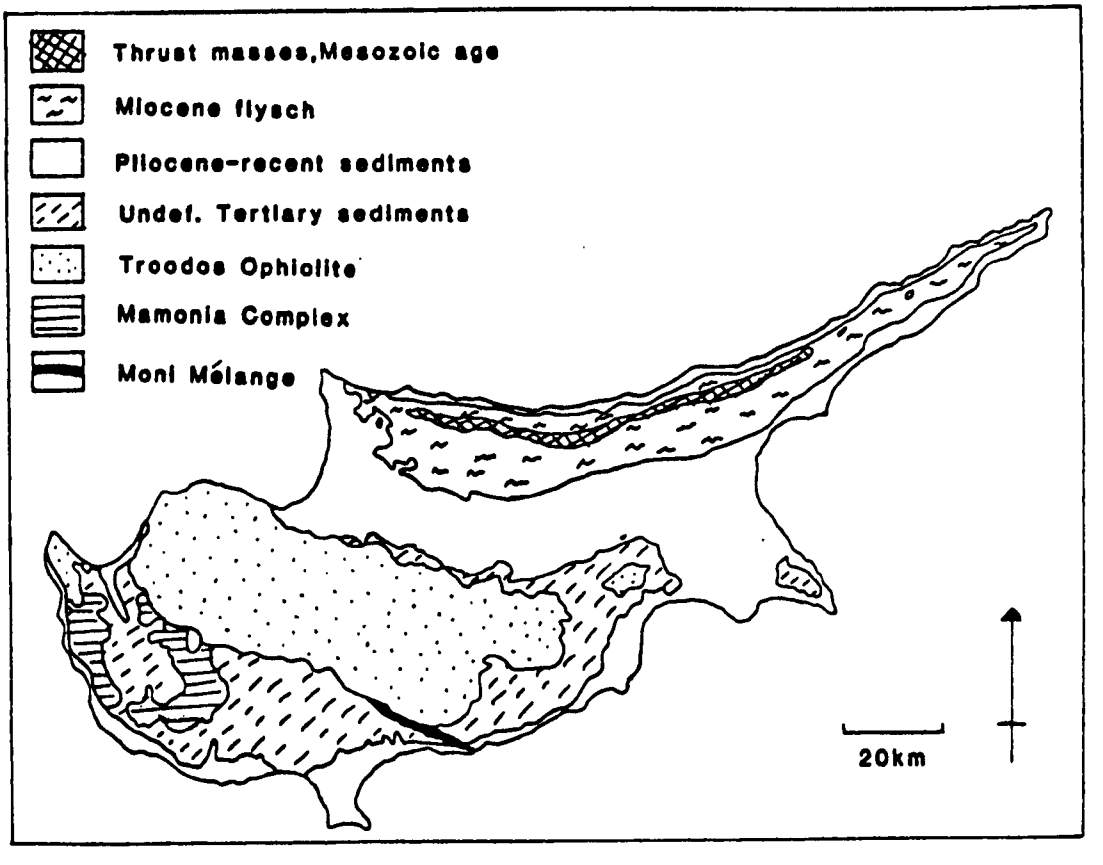

Figure 3.2 The general geology of Cyprus.

Robertson, 1977a) to have been formed in the Cretaceous by gravity sliding of detatched blocks of continental margin rocks into a deeper water oceanic environment.

3) The Troodos Complex: and Upper Cretaceous oceanic crust and mantle sequence.

4) Maastrichtian - Tertiary Sediments: gently folded highly calcareous sediments which unconformably overlie the Mamonia and Troodos Complexes.

5) Messaoria Plain Sediments: undeformed sediments of Pliocene to Recent age which unconformably overlie both the Maastrichtian - Tertiary Sediments in the south and the Miocene Flysch deposits in the north.

Extensive late Tertiary uplift of the Troodos area of Cyprus by some 2000m has been proposed from both gravity anomaly (Gass and Masson-Smith, 1963) and geological evidence (Reviewed in Robertson, 1977b). This uplift is thought to have been centred on a serpentinite diapir beneath the summit of Mount Olympus which caused tilting and block-faulting of the surrounding rocks (Searle and Panayiotou, 1980). (See Figure 3.3). As a result the geologically lowest units of the ophiolite sequence - the harzburgites - now outcrop at the highest topographic levels. The Maastrichtian - Tertiary calcareous sediments have a gentle radial inclination which is imposed, along with the gentle folding, by this late Tertiary uplift.

3.1.2 Ophiolite Geology

The Troodos Ophiolite is probably the most studied of the world's ophiolite complexes. It is here that the concept of ophiolites being remnants of oceanic crust and mantle and the theories of

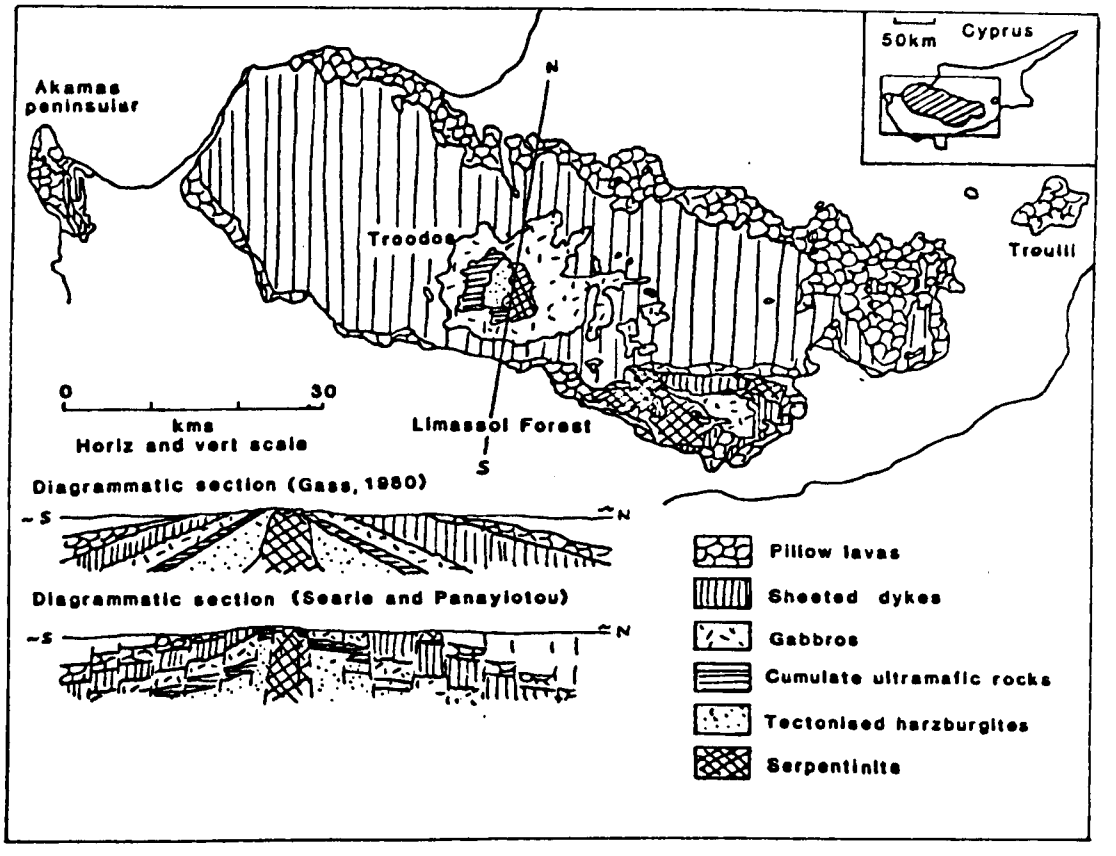

Figure 3.3 Geological sketch map and section of the Cyprus Ophiolite. (Modified from Gass (1980) and Searle and Panayiotou (1980)).

the generation of new crust at oceanic ridges were developed.

Most of the early work on the Troodos Massif was completed by members of the Cyprus Geological Survey, including the compilation of geological maps of the massif on a scale of 1:31,680. This work has been reviewed extensively by Smewing (1975). Figure 3.4 shows the stratigraphy of the Troodos Ophiolite which conforms to the Penrose Conference definition of a complete ophiolite sequence. (Anon, 1972).

The ophiolite occupies a roughly oval area with two small inliers - Troulli and Akamas. The Arakapas fault belt separates the southern Limassol Forest Complex from the main Troodos massif. (Figure 3.3).

The general geology of the ophiolite has been reviewed in detail by Gass (1980). A few particular geological relationships are discussed below.

The Pillow Lavas have been divided into three distinct units by various workers. (Upper Pillow Lavas, Lower Pillow Lavas and Basal Group Lavas), the precise definitions and boundaries of each unit being different depending on the author. (Wilson, 1959; Gass, 1960; Gass and Smewing, 1973; Smewing, 1975; Searle and Panayiotou, 1980; and Gass, 1980).

The Sheeted Dyke Complex make up a large proportion of the Troodos Ophiolite. Early workers reported a north-south vertical strike for large areas of the dyke swarm. Kidd and Cann (1974) and Kidd (1977) use the preferential one-way chilling in the dykes to infer that the Troodos spreading axis lies to the present-day west of the massif. Gass (1980), however, points out

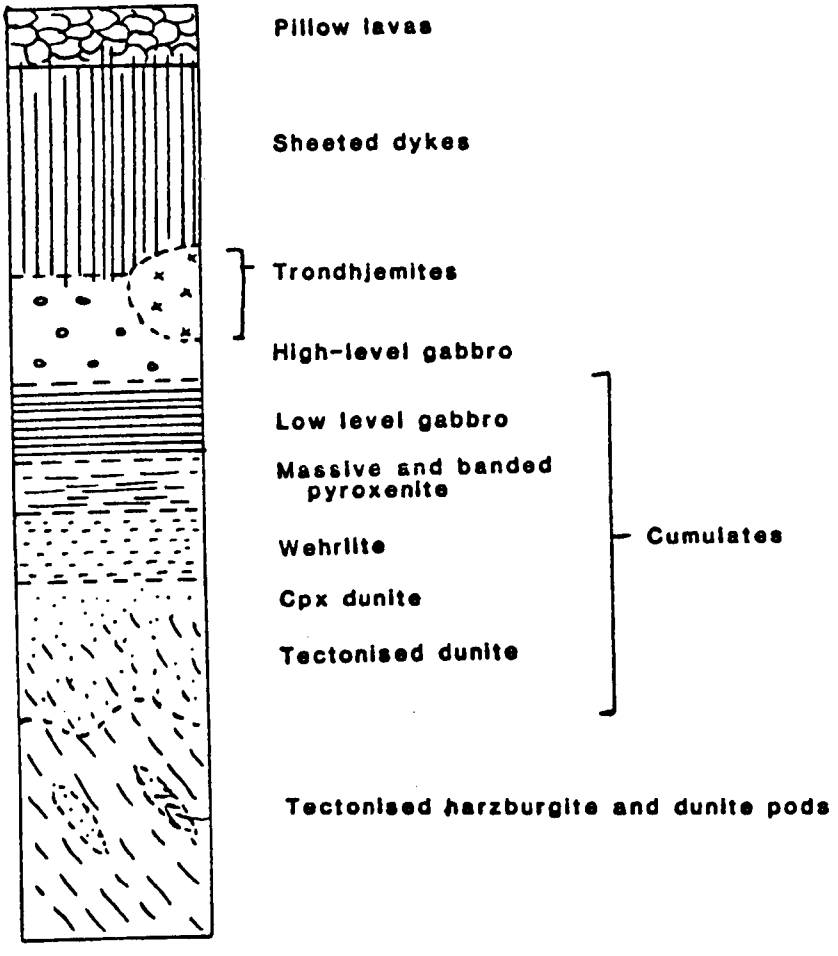

Figure 3.4 General stratigraphy of the Troodos Ophiolite. (From Smewing (1975) and George (1975)).

that only a small sample of dykes were measured and that ... "the differences in the number of chills in each direction is rarely more than one or two dykes per section".

Searle and Panayiotou (1980) dispute the north-south strike for most of the Sheeted Dyke Complex. Mainly on field evidence, they related dominently east-west trending dykes to the Basal Group Lavas; and north-south trending dykes to the Upper Pillow Lavas, Lower Pillow Lavas related dykes having a trend between these two extremes. They do not, however, provide a satisfactory explanation for these differences in dyke trends. Simonian and Gass (1978) recognize that the trend of the Sheeted Dyke Complex bends through almost 90^{o} close to the Arakapas fault belt. They propose that the Arakapas fault zone is a fossil transform zone separating the main Troodos Massif from the Limassol Forest complex. (See Section 3.1.3).

For the purposes of this study it will be accepted that the Troodos spreading axis had a north-south strike in relation to the present day orientation of the ophiolite. Sufficient evidence, however, is not available to calculate the palaeo-spreading direction of the complex.

Recent studies on the High Level Gabbros and the Cumulate Sequence (Moores and Vine, 1971; Smewing et al, 1975; Allen, 1975; Greenbaum, 1977) have shown evidence of many different magma imputs and thus infer multiple magma chamber models: i.e. younger magma bodies injected into solidified older magmas and also the possibility of several magma bodies existing at one time. The base of the Cumulate Sequence is marked by a 200-400 metre band of cumulate dunite. This contains a tectonic fabric which is

thought to be a continuation of the fabric within the harzburgites below and which dies out upwards into the dunites. (George, 1975). In the overlying, tectonically undeformed, cumulates George (1978) reported slump folding and other igneous 'deformation-type' features.

The hypothesis that harzburgite is a residuum of partial fusion of upper mantle peridotite was applied to Cyprus by Greenbaum (1972) and Menzies and Allen (1974), and has been backed up by George (1975 and 1978) in his detailed structural study of the Troodos Ultramafic Complex. The mantle harzburgites show a pervasive tectonic fabric attributed to processes of syntectonic recrystallisation. (George, 1975). The main dunite-harzburgite contact has been described as interdigitated. George (1975) notes that the main mantle foliation is roughly parallel to these interdigitations. He postulates that they were formed by a combination of large-scale folding (Greenbaum, 1972), and gravitational sinking of dense chromite-rich pods of the dunite into the underlying hot and weak harzburgite (Dickey, 1975). Gass (1980) supports this internal folding model.

The mantle sequence is composed of about 80% harzburgite which encloses irregular lenticular masses of dunite which form the remaining 20%. The dunitic lenses have a length of up to 1km and the smaller ones are aligned parallel to the foliation. Greenbaum (1972 and 1977) suggests that these bodies have formed as small cumulate chambers within the diapirically rising, partially melting asthenospheric mantle. This cumulate origin is now generally accepted in the consensus oceanic spreading model. (Figure 1.2). Small bodies of gabbroic and lherzolitic composition also occur within the mantle sequence.

3.1.3 Regional Setting and Emplacement Models.

The Troodos Ophiolite lies on the same Tethyan chain as the Oman Ophiolite (Figure 2.5). Palaeomagnetic studies by Moores and Vine (1971) and Shelton and Gass (1980) have shown that the Troodos Complex was rotated anticlockwise by 90° in post-Middle Miocene times. Thus, at the time of formation of the Troodos oceanic crust, the spreading-ridge strike was most probably east-west with the Troodos crust on the northern flank of the spreading ridge. To the west lay a transform fault - now the east-west trending Arakapas fault zone - with the Limassol Forest complex to the west of the transform. Turbiditic sediments were deposited into the transform zone along which primitive lavas were erupted and serpentine masses emplaced.

Gravity data collected by Gass and Masson-Smith (1963) show that Cyprus is underlain by a northerly inclined slab of high density mantle. (Figure 3.5). Unfortunately it is not yet known if the underlying basement is continental or oceanic in origin. Gass and Masson-Smith (1963) relate this geophysical structure to the northward movement of the African continent and its subduction beneath the Turkish Continental margin.

It is possible to explain the emplacement of the Troodos Ophiolite onto the Turkish continental margin either by obduction of part of the northwards subducting oceanic slab, or by uplift of a back-arc basin formed on the northern margin of the northerly dipping subduction zone. (Figure 3.6).

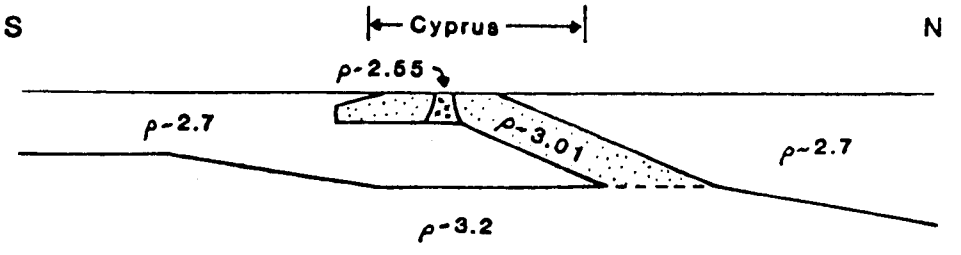

Figure 3.5 Gravity data model for Cyprus. (From Gass and Masson-Smith, 1963).

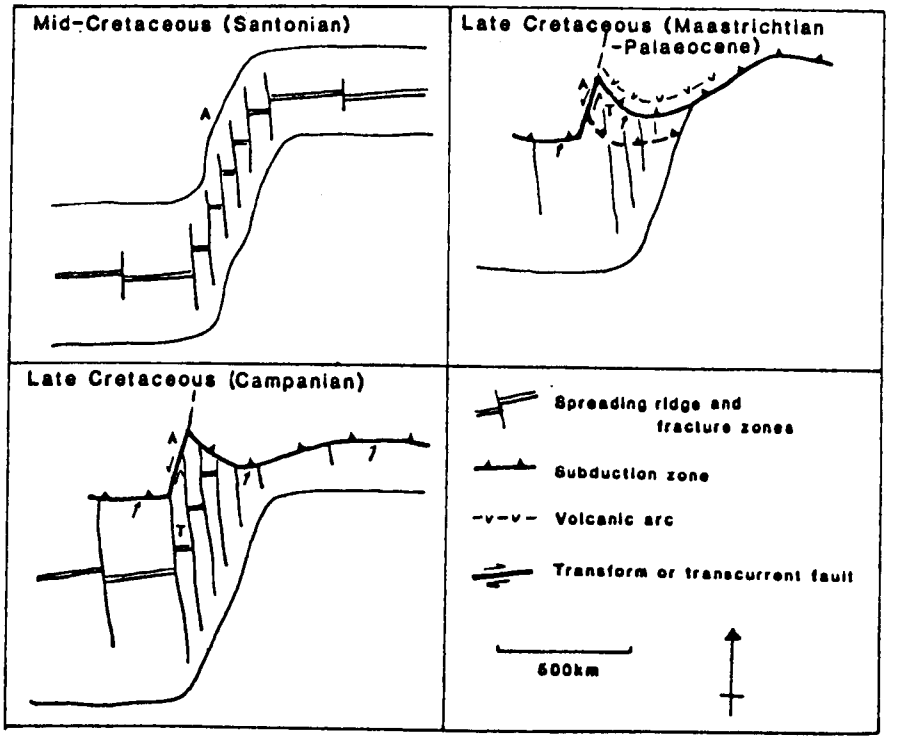

Figure 3.6 The possible formation of the Troodos oceanic crust during Late Cretaceous times and north-south strike-slip faulting along the Antalya margin. (From Robertson and Woodcock, 1980). T = Troodos, A = Antalya.

Robertson and Woodcock (1980) favour the allochthonous origin for the Troodos ophiolite by proposing that it formed as part of a large ocean basin, attached to the African continent by a passive margin and being subducted beneath the northern continental margin. They relate the geology of Cyprus to other areas of the eastern Mediterranean; and, because of the geometry of the various plates, infer that major north-south strike-slip faulting occurred along the Antalya (Turkey) - Cyprus margin. (Figure 3.6). This caused the allochthonous emplacement of the Troodos Complex to its present position.

Chemical, sedimentalogical and seismic data, however, (reviewed by Gass, 1980), strongly suggest that the Troodos Ophiolite was part of a back-arc basin. This would favour the more autochthonous model for its emplacement. The ophiolite was either emplaced as the African continental crust reached the subduction zone as proposed by Gass and Masson-Smith (1963), or as subduction of oceanic crust proceeded. (Figure 3.7).

At present, it is impossible to say whether the Troodos Ophiolite has purely been uplifted, or has been obducted in a similar way to the Oman Ophiolite (See Chapter 2.1.3). The evidence available points to a back-arc origin for Troodos but its exact method of emplacement remains unsolved. It is clear from the gross structure of the ophiolite that a major amount of uplift has occurred but it is not possible to say whether this was associated with a major allochthonous movement or not.

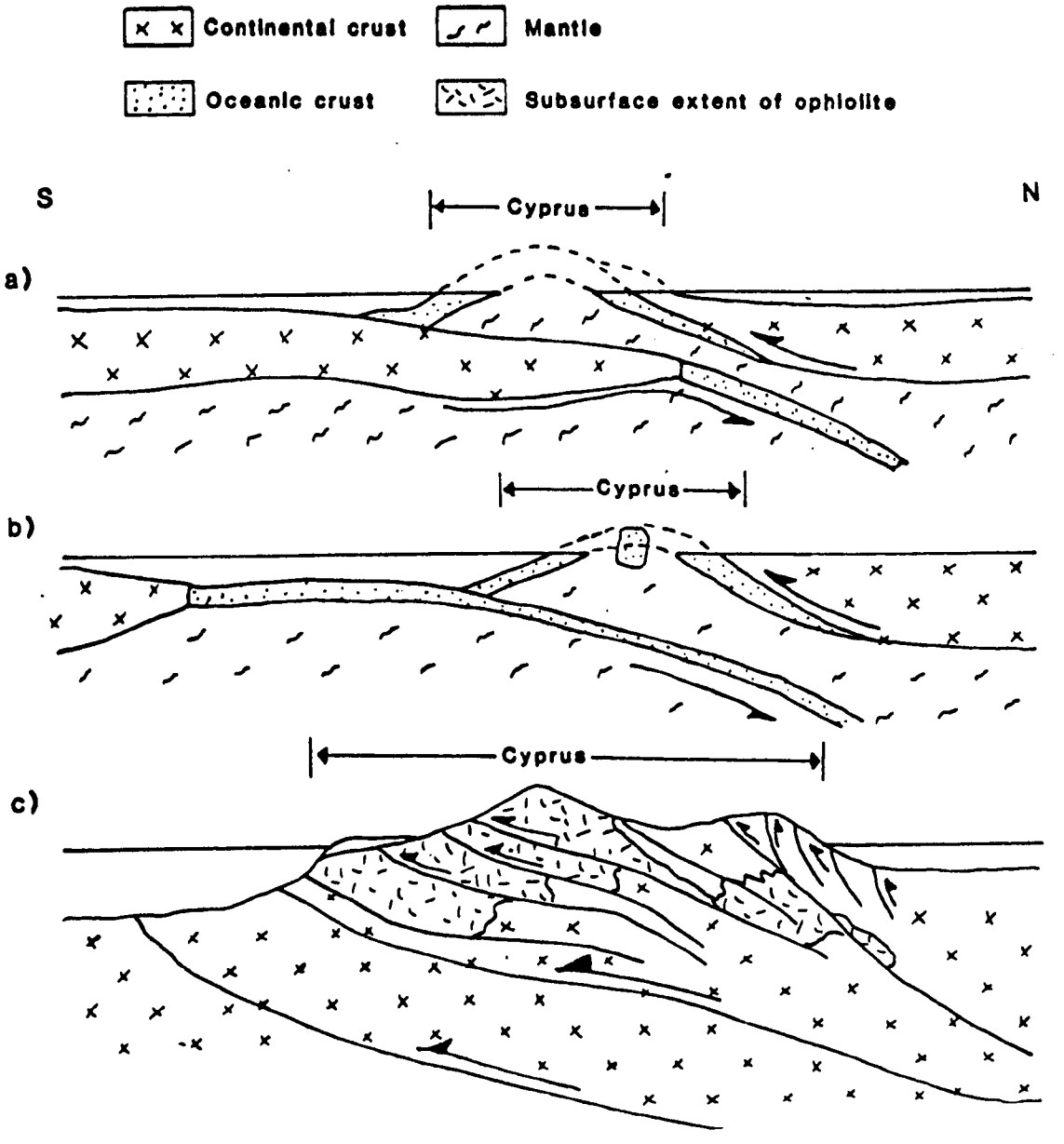

Figure 3.7 Various models for the emplacement of the Troodos Ophiolite. a) Subduction of continental crust autochthonous model. (Gass and Masson-Smith, 1963); b) Subduction of oceanic crust autochthonous model. (Gass, 1980); c) Allochthonous model after Biju-Duval et al, 1976. Modified from Gass (1980).

3.2 Logistics and Area of Study in Cyprus.

Cyprus was visited for 5 weeks in September-October, 1981. Daily field excursions were made by private car from a base in Troodos village. The area selected for study were the main harzburgite and dunite units to the west of the serpentinite diapir. Figure 3.8 shows the area mapped. The whole area has a good network of surfaced and unsurfaced tracks making it easily accessible. The topography is fairly rugged and steep in places, but everywhere is accessible by foot.

The field maps of George (1975) and Wilson (1958) were used as an aid to location in the field as well as 1:6000 aerial photographs kindly lent by the Cyprus Geological Survey. Mapping was carried out at a scale of 1:10.000 and 1:250 for a small area on the harzburgite-dunite boundary.

The detailed field relationships mapped will now be described.

3.3 General Mantle and Lower Crustal Petrology of the Troodos Ophiolite.

3.3.1 Appearance of Rock Types in the Field

The harzburgite varies from a dark-red brown to black colour depending on the degree of serpentinisation. In highly serpentinised black harzburgites, pyroxenes have broken down to antigorite making it difficult to distinguish between wehrlite and harzburgite. In less serpentinised rocks the orthopyroxene is yellow-brown to grey in colour; clinopyroxene in moderately serpentinised wehrlites is much greener in colour. On a weathered surface of moderately serpentinised

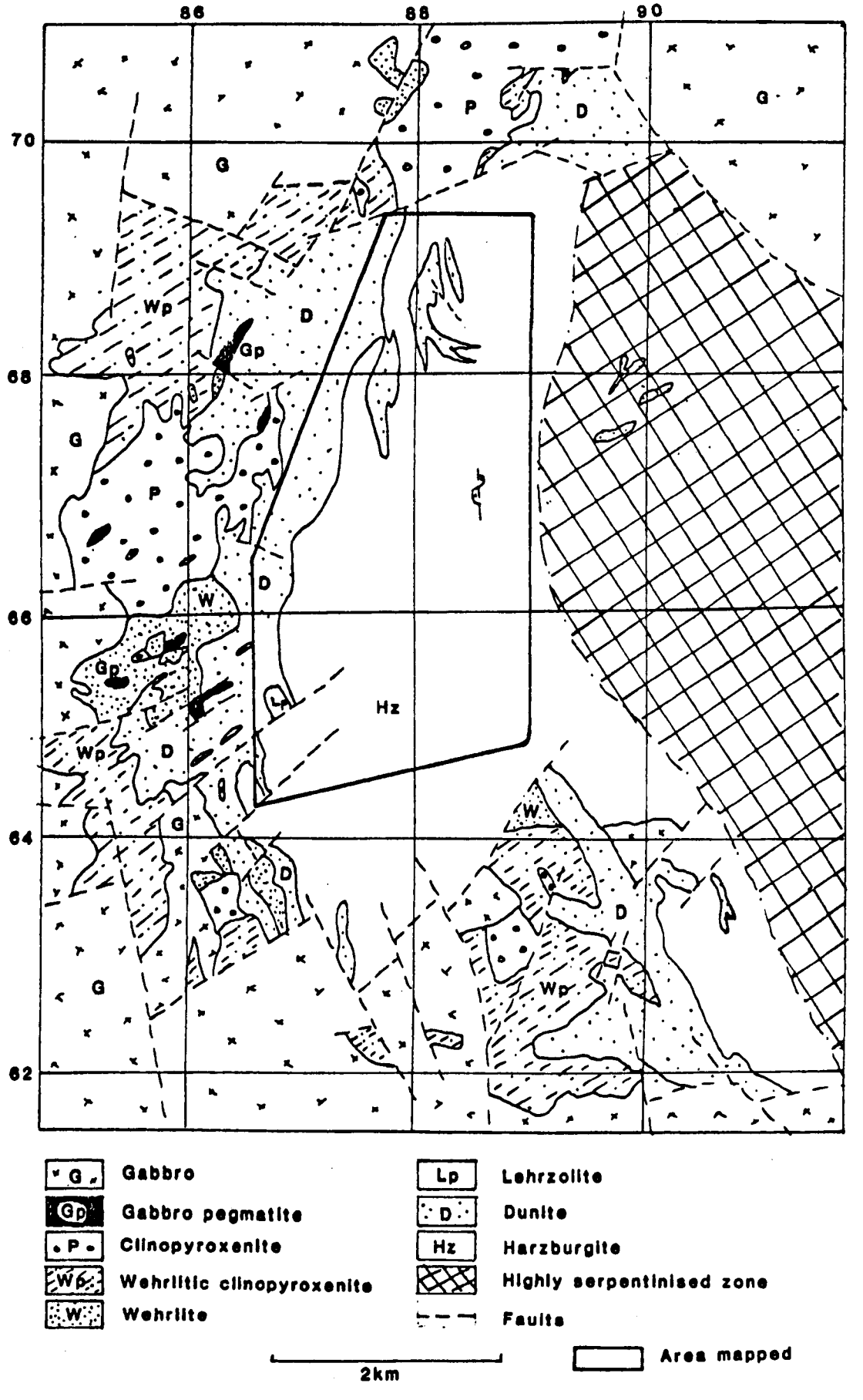

Figure 3.8 Geological map of the Troodos area showing the area mapped for this study. (From Wilson, 1958).

harzburgite the orthopyroxenes commonly stand-out as more resistant grains to the olivine and give a pockmarked appearance to the rock (Plate 3.1). This enables harzburgite to be easily distinguished from dunite in the field. The weathered surface of dunite is smooth and coloured dark yellow-brown. The massive dunites have stood up to weathering much better in Cyprus than in the desert climate of Oman. In Cyprus the dunites are as well preserved as the harzburgites in the field, and foliations can easily be measured from the alignment of spinel grains in both the dunites and harzburgites.

The exposure of the Peridotite Unit and the dunite and wehrlitic -rich areas of the Lower Cumulate Unit is remarkably good in the areas studied. Exposure varies from 100% to 20% with an average of 35-40% exposure. The good accessibility and exposure of the whole area enabled detailed area mapping to be completed giving a more three dimensional picture than in Oman where most mapping was restricted to two dimensional traverses.

The layered gabbros are highly weathered in most areas visited in the Troodos Ophiolite. Outcrops crumble easily and features are difficult to make out.

3.3.2 General Petrology of the Area Studied.

Within the area mapped, the Peridotite Unit is composed predominantly of harzburgite. However, in some areas, dunite is a major component of the Peridotite Unit, and forms bodies of up to 1000 x 300 metres extent. Enclosure 10 shows the distribution

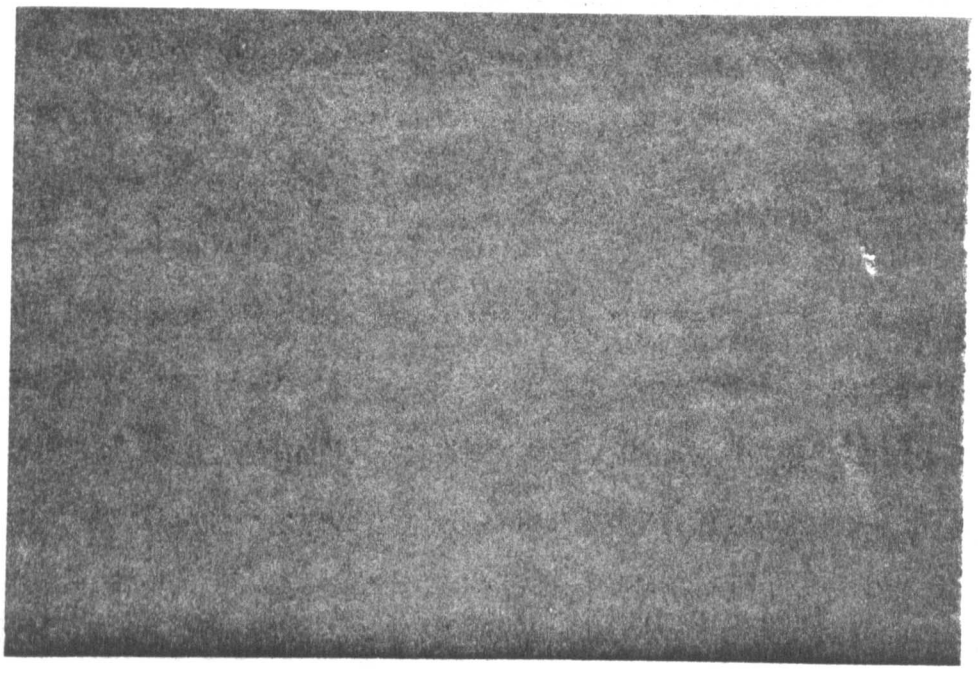

Plate 3.1 Orthopyroxene and chrome-spinel grains showing a pockmarked appearance of the harzburgite from Troodos.

of dunite within the Peridotite Unit.

The base of the Lower Cumulate Unit is composed of a 300-400 metre thickness of dunites with minor occurrences of plagioclase - wehrlites, wehrlites and clinopyroxenites. The rocks become richer in clinonyroxene and plagioclase above the dunite-rich basal layer of the Cumulate Unit, and grade into layered gabbros and olivine gabbros. (Figure 3.8). These higher-level rock-types were not studied in detail as they have not been subjected to the tectonism seen in the Peridotite Unit and the dunites of the Lower Cumulate Unit. (See below). George (1975) and Allen (1975) described the higher levels of the Cumulate Unit in detail.

a) The Peridotite Unit

The harzburgites of the Peridotite Unit have a very similar modal composition to those of the Oman Peridotite Unit. Olivine varies from 75% to 95% modal percentage, with orthopyroxene between 25% and 5% and clinopyroxene from trace amounts to 2%. Chrome-spinel is present as trace amounts in all specimens. Chemically the harzburgites have the same composition as the Oman harzburgites. (George, 1975).

Segregation-type layers rich in olivine or orthopyroxene are not common in the harzburgites. Where present they are similar in character to the segregation layers in the Oman harzburgites, with diffuse boundaries; they rarely exceed a few centimetres in width. The segregation layers are sub-parallel to either of the tectonic foliations described below and are thought to have formed by similar mechanisms to those in Oman (See Chapter 2.3.2).

A pervasive tectonic foliation is measurable in all areas of harzburgites. It is defined mainly by the alignment of the spinel grains, and also, in specimens where individual pyroxenes are discernable, by pyroxene grains which are aligned parallel to the spinel grains. In many localities two foliation planes have been identified from the spinel grain alignments from the same outcrop. The angles between these two foliation planes vary from outcrop to outcrop. The trends of each of the foliations is discussed in detail below. (See Section 3.4).

In some thin sections two distinct alignments of elongate spinel grains can be seen. In specimens where three roughly perpendicular orientated sections were cut, two foliation planes can often be defined from the different spinel traces; both of which are parallel to the foliations measured in the field.

The thin section textures vary from coarse through porphyroclastic to mosaic porphyroclastic. Crystallographic and grain shape studies discussed in Chapter 7 show that almost all of the textures are related to the constantly trending foliation that strikes NW-SE with a sub-vertical dip (See Section 3.4). The coarse textured specimens indicate that this deformation has been a shearing of only slight intensity: this enables an earlier fabric to be partially preserved and only slightly rotated by the later shearing deformation. (See Section 3.4).

A lineation was not usually measurable in the field. Once two foliation planes had been discerned from the spinel grain alignments it was difficult to be confident about measuring a lineation direction on either of the foliation planes. In Chapter 7 the crystallographic orientations of the grains are used to determine the slip directions of the deformational events.

In thin section most specimens are highly serpentinised with an average of 60-70% serpentinite. However, as in Oman, 'composites' of the original olivine crystal shapes can easily be constructed from relict pieces of equal birefringence. Pyroxenes and spinel grains show a similar range of textures as in the harzburgites of Oman. (See Chapter 2.3.2).

As mentioned above, the intrusive dunite in the Peridotite Unit is fairly common in some areas. All dunitic bodies are sharp sided and vary in size from centimetre thick anastomosing sheets to 300 metre thick massive bodies. The larger bodies occur mainly in the northern sector of the area mapped. (See Enclosure 10). In thin section the dunites have similar olivine textures to the harzburgites. The spinel alignments show a similar two foliation pattern to the harzburgites and have similar trends (See Section 3.4 below).

Chrome-spinel layers occur in both the anastomosing dunite sheets and the large dunite bodies. The larger chromitiferous deposits within the dunite bodies have been extensively mined, the largest deposit being over 50 metres thick with a lateral extent of 300 metres and a vertical extent of at least 600 metres. This is the Kokkinorotsos mine at grid ref 875680. (See Figure 3.9). The orientations and shapes of the dunitic and chromite rich bodies in relation to the foliation and other petrologic trends is discussed in Section 3.5 below.

b) <u>The Moho Plane</u>

The lithological contacts of the lower ophiolite sequence of the Troodos Massif were originally mapped in detail by Wilson (1959) and subsequently by Greenbaum (1972). George (1975) used the

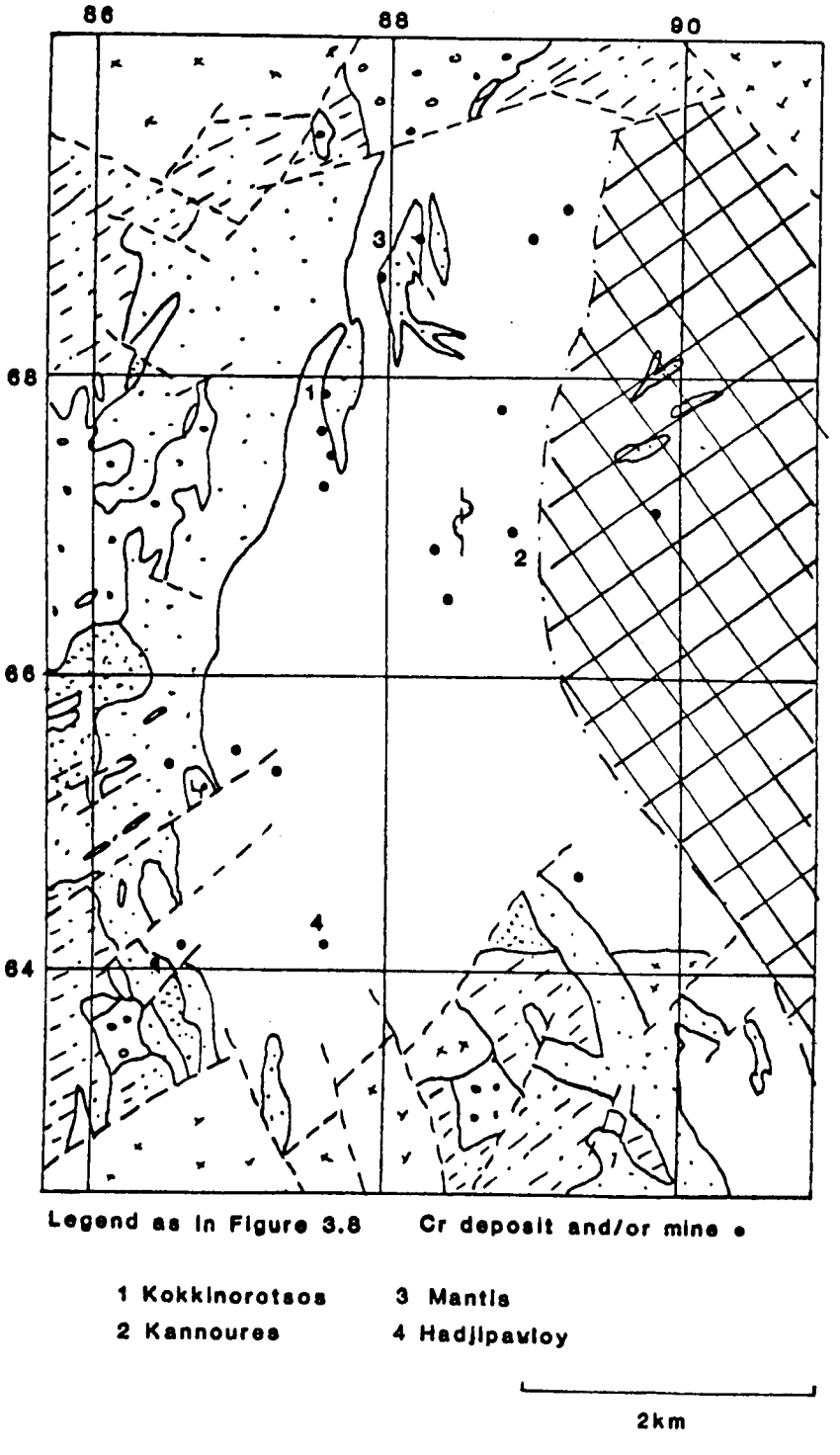

Figure 3.9 The location of Chromite Mines on the Troodos Massif. (Modified from Violette, 1980).

base maps of these two workers for his structural study and did not re-map any of the lithological contacts. This present study involved extensive re-mapping of the central part of the area studied by George (1975). This is shown on Enclosure 10.

In the southern part of the area mapped, extensive faulting of the moho plane explains many of the apparently major fluctuations in the trace of the moho plane reported by George (1975). (See Enclosure 10). In the northern area, a large proportion of the area around the moho has been extensively serpentinised making rock identification difficult. Some areas mapped as dunite by Wilson (1958) and Greenbaum (1972) have been re-mapped as harzburgite in this study. (See Enclosure 10).

This re-mapping has made the moho a much more constantly orientated plane with a NNE-SSW strike and sub-vertical dip with only minor embayments. In the north of the area mapped, one of these minor embayments connects with a large dunite body contained within the Peridotite Unit (Grid ref. 877684). These embayments have previously been related to an infolding of the crustal dunites with the harzburgites by strong deformation along the area of the moho. (See George, 1975). It will be shown in Section 3.5, however, that no large-scale infolding has occurred along the moho, and that the large dunitic bodies within the harzburgites were most probably formed by in situ cumulation processes.

The two foliations measured in the Peridotite Unit extend through the moho in all areas into the base of the Lower Cumulate Unit.

c) The Lower Cumulate Unit.

As already mentioned, the base of the Lower Cumulate Unit is composed of a 200-300 metre thickness of dunites. In hand specimen chrome-spinel grains are easily identifiable. They pick out a similar two foliation pattern as that seen in the Peridotite Unit. Further away from the moho plane only the constantly striking NW-SE foliation is measurable. This itself dies out upwards into non-tectonised rocks. In all of the areas mapped the tectonism dies out in the lowermost dunites and nowhere extends more than 200 metres west of the moho plane. (See Section 3.5 below).

In the non-tectonised dunites the spinel grains are euhedral and rarely define a measurable plane. In thin section the undeformed dunites show anhedral to subhedral olivine grains of up to 5mm diameter. In higher levels of the dunites (i.e. further west of the moho plane), clinopyroxene becomes a more abundant plase. In the non-tectonised dunites, clinopyroxene takes the form of fine to medium grained (1-6mm) equant or tabular anhedra. In rocks where clinopyroxene is less than 5% of the modal constituents, the clinopyroxene commonly occurs as dispersed oikocrysts (up to 3cm in diameter) which enclose olivine crystals. These oikocrysts are sub-rounded to slightly ovoid in shape in non-tectonised rocks. In areas of tectonism the oikocrysts are more elongate and sub-parallel to the foliation traces.

Where clinopyroxene is abundant the rocks are commonly layered with sharp contacts between clinopyroxene-poor and clinopyroxene -rich layers. Layer thicknesses are highly variable but are

usually in the 5-20 centimetre range. More massive wehrlites and clinopyroxenites are also present which exhibit no discernable layering or laminations. George (1975) has differentiated the wehrlites into either 'banded wehrlites' (layered) or 'poikilitic wehrlites' (massive). The same differentiations were used in the areas mapped for this thesis.

Economic chromite deposits in the Lower Cumulate Unit are only found in the areas of dunites immediately adjacent to the moho plane. They are similar in size and shape to the chrome-rich bodies found in the dunite pods in the Peridotite Unit. The orientations of these bodies will be discussed in detail in Section 3.5. In the areas of dunites further from the moho, chrome-spinels occur either as discrete dispersed grains or as millimetre thick layers. The orientation of these layers has been strongly controlled by the tectonism of the Peridotite Unit and lower areas of the Lower Cumulate Unit (See below).

In the vicinity of grid reference 869660 there is an area of 200 metres thickness of plagioclase-rich rocks. Their modal minerology is: 73% Olivine, 9% orthopyroxene, 6% clinopyroxene, 10% plagioclase and 2% spinel (Allen, 1975). These plagioclase lherzolites are strongly layered with plagioclase-poor wehrlites and pyroxenites interbanded within the plagioclase-rich rocks. These layers are sub-parallel to the clinopyroxene-rich layers in the adjacent dunites. Both the plagioclase lherzolites and the adjacent dunites are strongly foliated with similar orientations to the nearby Peridotite Unit. The plagioclases, especially, are highly flattened and show very similar 'stringer' textures to the plagioclase-bearing wehrlites of Oman described in Chapter 2. (Plate 3.2).

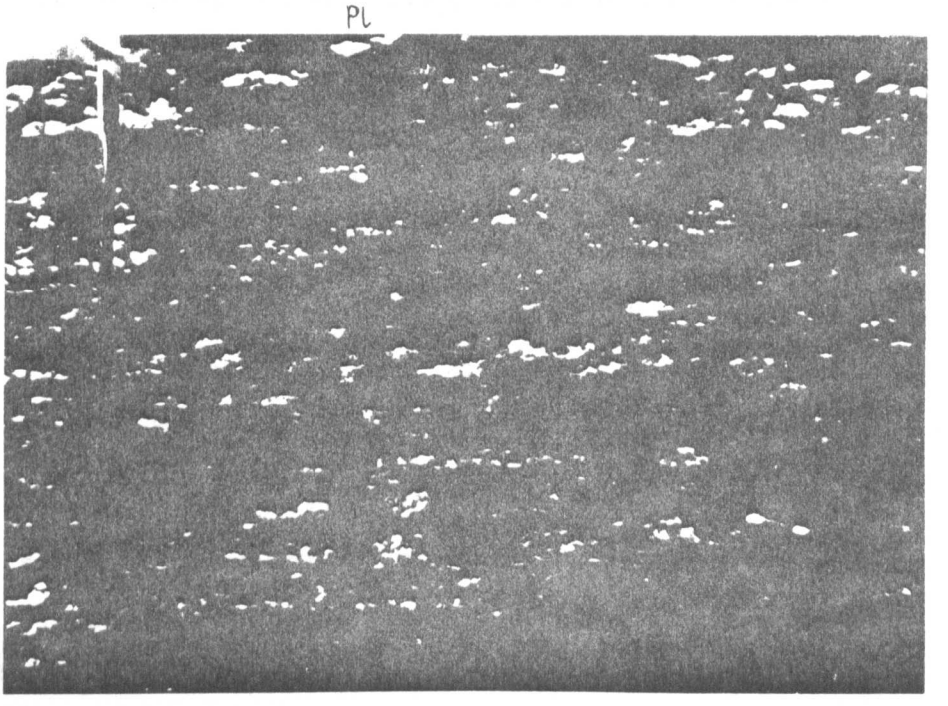

Plate 3.2 Hand-specimen of plagioclase lherzolite showing a plagioclase stringer texture. Pl = plagioclase. (Length of plate 6 cm).

There has been some dispute as to the origin of this plagioclase lherzolite unit. Menzies and Allen (1974) suggest that it represents primary aluminous peridotite mantle which has undergone limited basalt extraction. George (1975), however, contends, that from a study of the fabrics and textures, it is of cumulate origin. A detailed geochemical study (Allen, 1975) failed to demonstrate either a mantle or cumulate origin for the plagioclase lherzolites. Allen (1975) states that the parameter most strongly favouring a cumulate origin is the high chromium content (0.65% Cr_2O_3) compared to that of the harzburgite (0.30% Cr_2O_3). The results of the detailed field mapping carried out in this study support the cumulate origin for the plagioclase lherzolites. There is a 20m layer of dunites and then 10m of wehrlite separating the plagioclase lherzolites from the Peridotite Unit, except at the southern contact of the plagioclase lherzolites which is faulted against the harzburgites. (See Enclosure 10). The pervasive parallel layering would also strongly support a cumulate origin (as compared to the non-parallel anostomosing dunites or diffuse segregation layers of the Peridotite Unit).

In the field there are very few cumulate features in the Lower Cumulate Unit except for the layering. No cross-lamination or channel type structures have been observed.

Detailed petrological studies of the whole Cumulate Unit of the Troodos Ophiolite are given by both George (1975) and Allen (1975).

d) Intrusive Pyroxenite Dykes.

All of the pyroxenitic dykes measured in the Troodos lower ophiolite sequence are sharp-sided and undeformed. They cross-cut the foliations of both the Peridotite and Lower Cumulate Units and

rarely exceed 5cm in thickness. The dykes are nowhere abundant: they are absent from the Peridotite Unit except for the areas immediately adjacent to the moho.

3.3.3 Late-stage Tectonic Features.

a) The Intrusive Serpentinite Diapir.

The eastern area of the ultramafic centre of the Troodos ophiolite is composed of a large serpentinite body (Figure 3.3). This is thought to be diapiric in origin and to have caused the uplift of the central areas of the ophiolite. (See Section 3.1.3). The area of serpentinite was not studied in detail for this thesis.

In the areas studied close to the main area of serpentinisation, the harxburgites rapidly become serpentinised within a 100 metre zone. This roughly follows the valley of the Khionistras stream. (See Enclosure 10). The main foliation trends of the harzburgites rotate from their regular NW-SE trends to more variable orientations within this zone of increasing serpentinisation. They become roughly parallel to the margins of the serpentinite diapir and only a single foliation is measurable from each individual outcrop. The high degree of serpentinisation make it impossible to identify a linear fabric associated with the diapir.

b) Late-stage brittle structures.

In areas away from the serpentinite diapir the only late-stage structures are brittle fault zones. In the south of the area mapped the faults are vertical and strike NE-SW with dominantly dextral strike-slip components. In the north of the area mapped where the faults stike NW-SE to WNW-ESE, it is not possible to determine their senses of movement. The fault zones within the

harzburgites consist of up to 5 metre thicknesses of serpentinite breccia. The movement along the fault zones has caused no deflection of the adjacent foliations indicating a purely brittle deformation style.

These fault zones were probably formed as a response to the diapric uplift of the serpentinite mass.

3.4 Earlier Structural Orientations of the Troodos Massif.

This section deals with the orientations of the penetrative structures measured in the Peridotite and Lower Cumulate Unit.

a) Foliations.

As already mentioned, two foliation planes have been measured from most localities by studying the alignment of spinel and orthopyroxene grains on three-dimensional surfaces. In the field, both the orientations and the relative intensities of the two foliations have been used to discriminate between an earlier or later foliation.

The area of the Troodos Ophiolite mapped has been divided into smaller areas, as in the Oman traverses. These areas are shown on Enclosure 10.

In all of the areas, the structural trends are remarkably similar (See Enclosure 10). In each there is a constantly NW-SE striking foliation with a sub-vertical dip. The plots of the poles of these foliation planes have a fairly strong cluster pattern. The other foliation planes also have a sub-vertical dip but have a highly variable strike in all areas. The poles to these foliations form distinct girdle patterns.

The various equal area projections on Enclosure 10 show that the orientation of the NW-SE striking foliation does not differ from the trends in the harzburgites either in the large dunite bodies within the Peridotite Unit or in the dunites of the Lower Cumulate Unit. Both of the foliations cut straight through the boundaries between harzburgite and dunite. This implies that both the Lower Cumulate dunites and the Peridotite Unit dunites had crystallised and been consolidated before either of the foliations were formed. The reaction of the dunite bodies to the foliation related deformations is discussed in Section 3.5.

In many areas the NW-SE striking foliation is more strongly developed than the other foliation (i.e. most spinel grains are aligned parallel to the NW-SE striking foliation and only a few are aligned parallel to the other foliation.); in a few localities it is the only foliation present. This and the constant orientation of the NW-SE striking foliation over the whole of the area studied, suggest that this is the younger foliation, the other being an earlier formed foliation which has been variably rotated during the later foliation-forming event. The mechanisms of this apparent folding of an earlier foliation by a later deformation are considered in Chapters 6-8.

From now onwards the constantly NW-SE striking foliation will be termed S2, and the earlier foliation S1, with the related deformational events D1 and D2.

To determine the detailed field relationships between S1 and S2, a small area of 4000m^2 was mapped at a scale of 1:250 at grid reference 874677. This is shown on Enclosure 11. The S2 planes

have a constant orientation, similar to the whole of the Troodos area studied. The poles to the S1 planes form a distinct girdle pattern. The orientation of the S1 planes change rapidly from outcrop to outcrop in the 1:250 area giving a folded pattern with the S2 planes parallel to the fold axial planes. This folding relationship is fully described in Chapter 7 (and see Enclosure 28). In this small area the distance between the fold axial plane traces varies from 5m - 25m.

The variation of S1 strike over the whole Troodos area suggests a similar D2 fold amplitude to that present in the 1:250 area. This is discussed in Chapter 7 (and see Enclosure 27).

b) Lineations.

In outcrops where only the S2 foliation is measurable, a lineation has occassionally been discerned from the alignment of spinel grains on the S2 plane. These lineations plot as a dispersed cluster pattern along the S2 plane with the commonest trend plunging steeply to the SE.

It will be shown in Chapters 6-8 that these lineations are sub-parallel to the D2 crystal slip directions.

3.5 The Orientation of the Petrological Features of the Peridotite Unit and Lower Cumulate Unit in Relation to the Orientations of the D1 and D2 structures.

3.5.1 The Peridotite Unit.

a) Large Dunite Bodies.

There are two large dunite bodies within the Peridotite Unit in the area mapped. They are situated close to the moho boundary between

eastings 675 and 692. (See Enclosure 10). Both of the bodies have long diameters parallel to the moho strike (i.e. NNE-SSW) of approximately 1000 metres. The main contacts of the bodies with the adjacent harzburgites are sub-vertical, and sub-parallel to the moho dip. The southern dunite body has a thickness of up to 300 metres, and the northern body up to 150 metres.

The overall shapes of these bodies are not controlled by the D2 deformation as the long axes of the bodies are not sub-parallel to the S2 foliation strikes. However, it is clear that in places the boundary between the harzburgite and dunite has been folded on a small scale. (E.g. Grid reference 877678). The fold axial trace is sub-parallel to the S2 foliation trace. The small scale of this folding is similar to the folding pattern determined from the detailed study of S1 orientational changes in the 1:250 area, and the fold trace is the same for the folding of the S1 foliations and the folds in the dunite body.

If the folding is on such a small scale as suggested by the detailed study of the 1:250 area, then the overall shape of a large dunite body will not have been drastically altered from its original shape.

As is discussed in Chapter 2, dunite has a very similar mineral composition to harzburgite (i.e. mainly olivine) and thus a very similar competency. It will thus behave as a single unit with the harzburgites during deformation. The mechanisms of deformation and how apparent folds are formed is discussed in detail in Chapters 6-8.

Near grid reference 882683 the southern dunite body extends as an eastwards-thinning mass to 300 metres below the base of the

main dunite body. This tongue-like body is not orientated parallel to the S2 foliation. The harzburgites surrounding it contain abundant dunite sheets which decrease in number away from the body in a 150 metre thick zone. The S1 foliation traces through this body show no obvious fluctuations (see Enclosure 10) which implies that there are no major D2 folds through the area: i.e. the whole body is on a single fold limb and its shape must be a relict of the original shape before D1 and D2 deformation. (Also see Enclosure 27 and Chapter 7).

The dunite sheets adjacent to the tongue-like body all have an east-west strike sub-parallel to the tongues. This orientation and the overall shape of the dunite body suggests that this area is a relict 'feeder zone' of a large dunite chamber at sub-moho level, and certainly not an expression of large-scale folding as has been previously suggested. (George, 1975 etc.).

The more southerly dunite body appears to connect with the main Lower Cumulate Unit dunites at grid reference 877683. It is difficult to propose that this body has been formed by large-scale infolding of the main Cumulate Unit dunites as the S1 traces here too imply only small-scale folding during the D2 deformational event. The S2 foliations have a fairly constant trace over the whole area of both the dunite bodies, which shows that there has been no large-scale folding after D2.

The abundance of dunite sheets in the harzburgites adjacent to the dunite-rich zone between the dunite body and the main Cumulate Unit dunites suggests the presence of a 'feeder-zone' similar to that at the base of the more northern dunite body. (See Enclosure 10).

b) Smaller Dunite Bodies and Sheets.

The distribution of the smaller dunite bodies and sheets is summarized on Figure 3.10. The sheets occur in distinct zones which are connected either to the large dunite bodies in the north of the area, or to zones of smaller dunite pods as near grid reference 876672.

A detailed study was made of the orientations of the dunite sheets and small bodies in areas where exposure was suitable. (Localities marked on Figure 3.10). Sketches from these localities are shown of Figure 3.11 and also on Enclosure 11.

In the areas where the S2 foliation is strongly developed, as in localities 1, 2, 7 and 11, the sharp-sided boundaries of the dunite bodies and sheets are sub-parallel to the S2 foliation. Where S2 is weaker, as in localities 4, 5 and 8, the dunite sheets have a more random anastomosing pattern. A similar relationship between S2 intensity and dunite sheet orientations has been observed in Oman. (See Chapter 2.4.).

Most of the dunite sheets and pods are sub-parallel to the S2 foliation traces which indicates either that the deformation was sufficiently intense in most areas to rotate them into the S2 foliation plane or that their original orientations were sub-parallel to the later superimposed S2 foliations. The zones of dunite bodies and sheets are generally aligned at only small angles to the S2 foliation traces. This suggests that these zones are close to their original pre-D2 orientations, since, if they had been at high angles to the S2 plane before D2 deformation, the small dunite bodies would not lie with their long axes sub-parallel to the overall axis of the zone of dunite bodies and

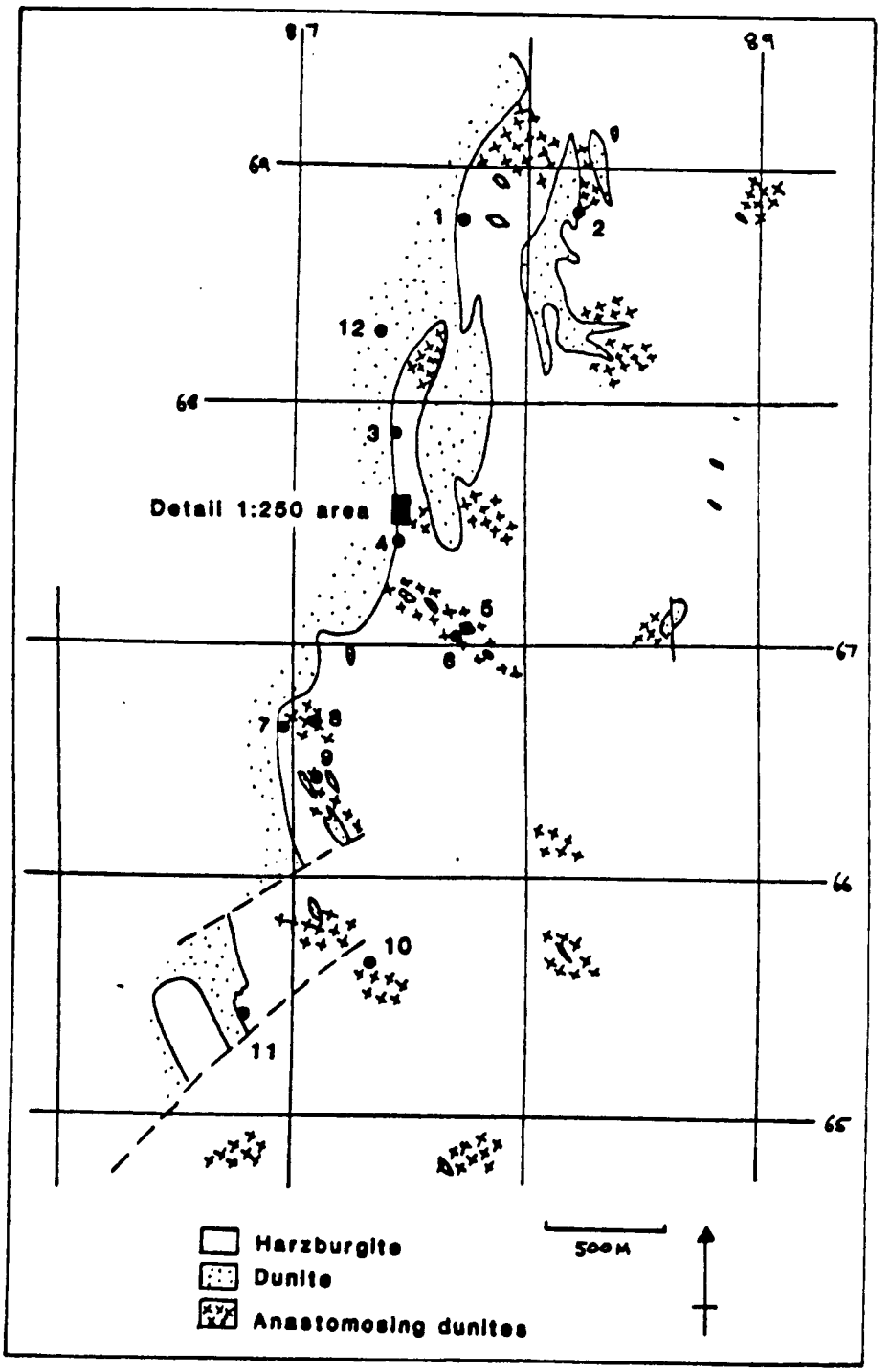

Figure 3.10 The distribution of dunite bodies and sheets within the Peridotite Unit of the Troodos Massif. Numbers refer to the localities sketched in Figure 3.11.

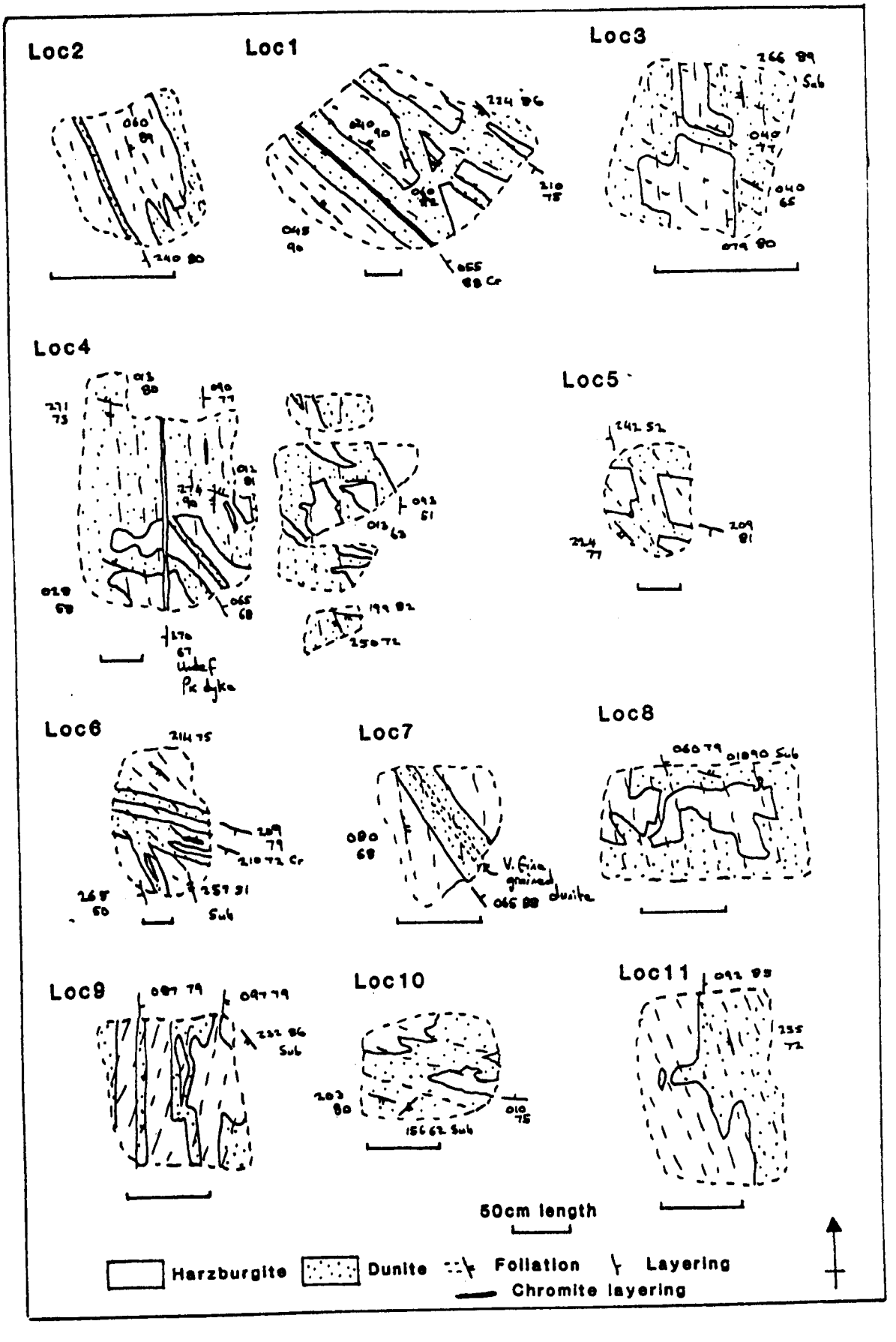

Figure 3.11 Locality sketches of dunite sheet and harzburgite relationships.

sheets. (Figure 3.12). This is assuming that the deformation was by shearing, as will be shown in Chapters 6-8.

Locality 4 is located at the junction of a zone of dunite bodies and sheets with the main Cumulate Unit dunites. (Grid reference 874675). It is clear that although the moho boundary is a fairly planar feature of constant orientation on the scale of 1:5,000, at much smaller scales it is an extremely irregular boundary; especially in areas where dunite sheets and bodies are numerous in the Peridotite Unit. In these areas the dunite sheets are wider and more anastomosing in character than in deeper levels of the Peridotite Unit. On outcrops the harzburgite occurs as irregularly shaped blocks within a 'mesh'-like pattern of dunites. (Figure 3.11 and Plates 3.3).

These anastomosing shapes and strong zonal concentrations of the dunite sheets and bodies suggest that these areas rich in dunite are relict magma feeder zones supplying material to either sub-moho cumulate chambers or the main Cumulate Unit. The deformational events forming the S1 and S2 foliations only slightly rotated the sheets and pods and the pre-deformational relationships between the harzburgite and dunite are thus preserved.

c) Chromite Deposits.

As already mentioned in Section 3.3.2 the main chromite deposits of the Troodos area occur within dunite bodies in the Peridotite Unit. Violette (1980) has summarised their occurence and general structural trends. The orientations of the major deposits in the area studied for this thesis are shown on Figure 3.13.

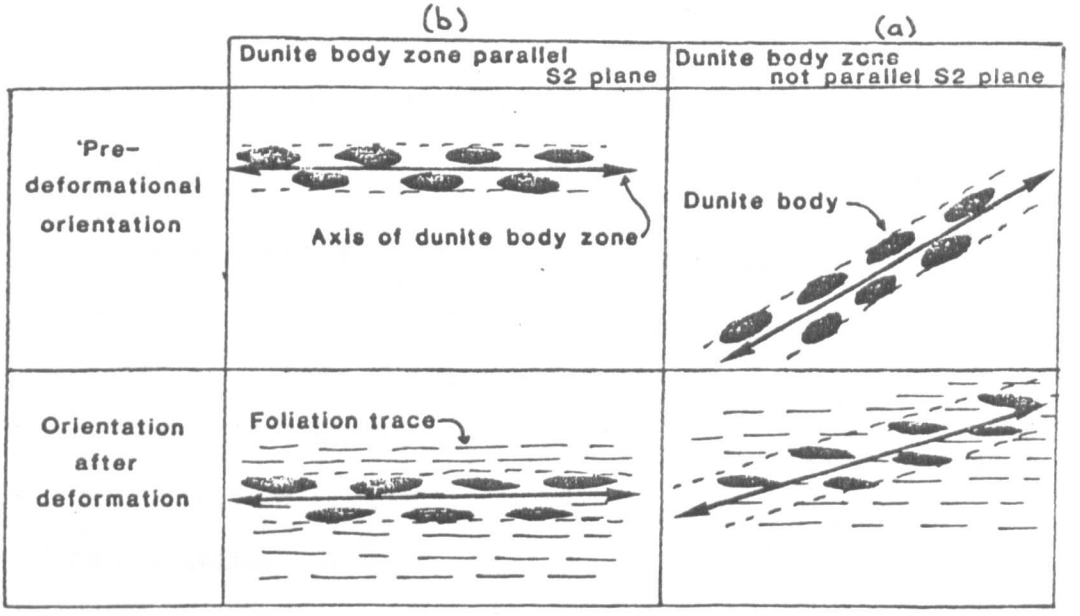

Figure 3.12 The relationship between the initial orientation of dunite bodies before D2 deformation and their orientations after D2 deformation. a) Initial orientation at a high angle to the S2 plane; b) Initial orientation at a small angle to the S2 plane.

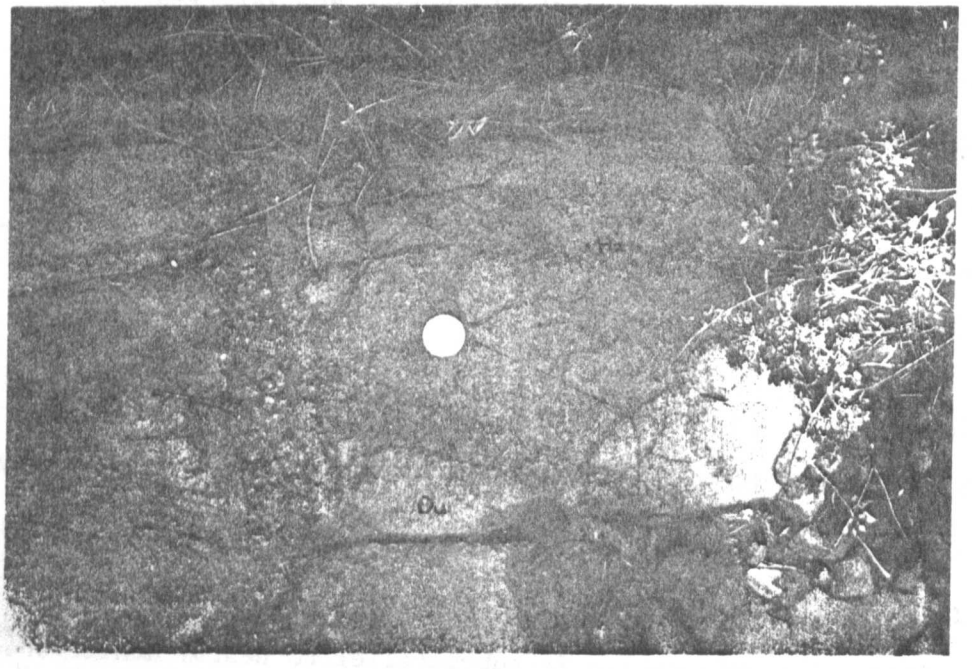

Plate 3.3 Anastomosing dunite sheets in harzburgite. Du = dunite, Hz = harzburgite. (Coin diameter 2 cm).

All the chromite ore bodies are sheet-like but vary in size and orientation depending on the intensity of the deformation and their original orientation.

The Hadjipavloy ore bodies in the south of the area mapped are contained within a series of dunite pods of not more than 70 metres in length and 10 metres in width. This area has undergone fairly intense D2 deformation with a well developed S2 foliation, and both the dunite pods and the ore bodies are sub-parallel to and elongated in the S2 plane. Little can thus be determined on the original orientation of the ore bodies.

In the area north of easting 670, deformation is much less intense and the chromite ore bodies have two orientational trends. The ore bodies of Kokkinorostos, Kannoures and Mantis B all have a north-south strike and vertical dip, even though on a small scale the chromite grains are strongly aligned parallel to S2. This north-south strike and vertical dip is sub-parallel to the main boundaries of the two large dunite bodies described above (Section 3.5.1a). These ore bodies vary in horizontal strike length from 500 metres for the Kokkinorostos body to 9 metres for the Mantis B deposits (See Figure 3.13).

In contrast to this north-south strike, the Mantis A chromite ore body has an ENE-WSW strike with a sub-vertical dip. This body is situated at the base of the northern large sub-moho dunite body. It has a thickness of only 2.5 metres and a maximum length of 20 metres. Its orientation is sub-parallel to nearby dunite sheets and not to the S2 foliation trace (See Enclosure 10), as is the tongue-like body at the base of the southern large dunite body.

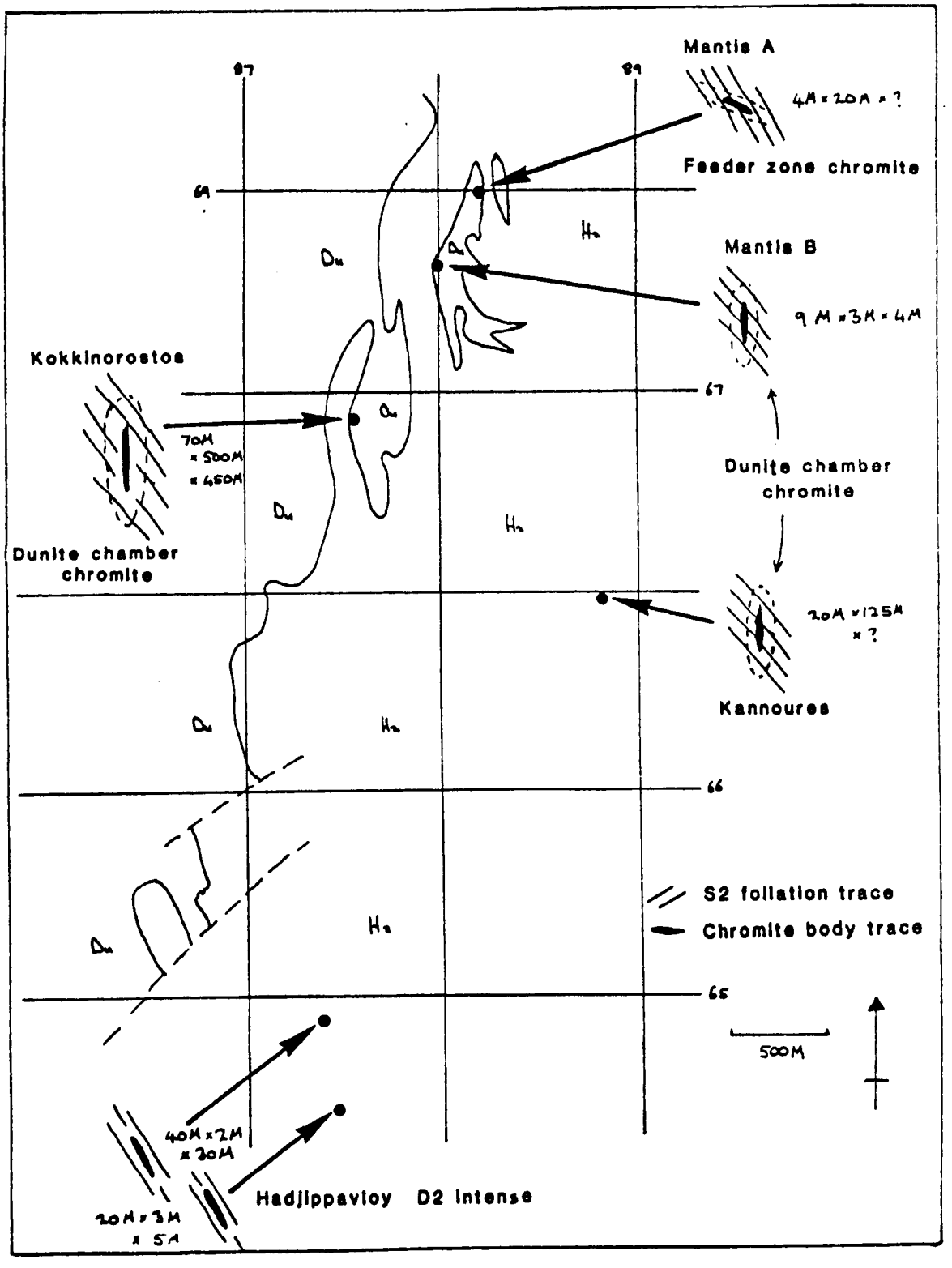

Figure 3.13 The orientations of the major chromite ore bodies in the area studied. (Data collated from Violette, 1980).

(Grid reference 882683). Some of the small dunitic sheets within the dunite-rich 'feeder'zones have thin chromite-rich seams running parallel to the dunite sheet. (E.g. Locality 1).

These two orientational trends, one at a high angle to the bases and tops of the large-scale dunite bodies, the other sub-parallel to these boundaries, can best be explained by the ore bodies being formed by different mechanisms. The ore bodies that are sub-parallel to the bases of the large scale dunite bodies formed as cumulate-type layers within a dunite-rich sub-moho cumulate chamber. The bodies at a high angle to these bodies (E.g. the Mantis A deposit) crystallised within the dyke-like zones feeding either the sub-moho cumulate chamber or the main crustal magma chambers as proposed by Lago et al, (1982).

3.5.2 The Lower Cumulate Unit.

The extent of the D1 and D2 tectonism into the Lower Cumulate Unit is shown in Enclosure 10. In all areas the S2 foliation extends further into this unit than the S1 foliation. Within the zone of tectonism most of the centimetre scale chromite and clinopyroxene rich layering is sub-parallel to the S2 planes.

Where deformation has been only weak, the various petrographic features within the dunites of the Lower Cumulate Unit have two different trends similar to the chromite deposits within the Peridotite Unit. Locality 12 (Grid reference 875684) shows these two trends well. Figure 3.14 summarises the relationships observed at locality 12.

The cumulate-type layers of dunite, wehrlite and clinopyroxenite at locality 12 have a north-south strike and a steep dip to the

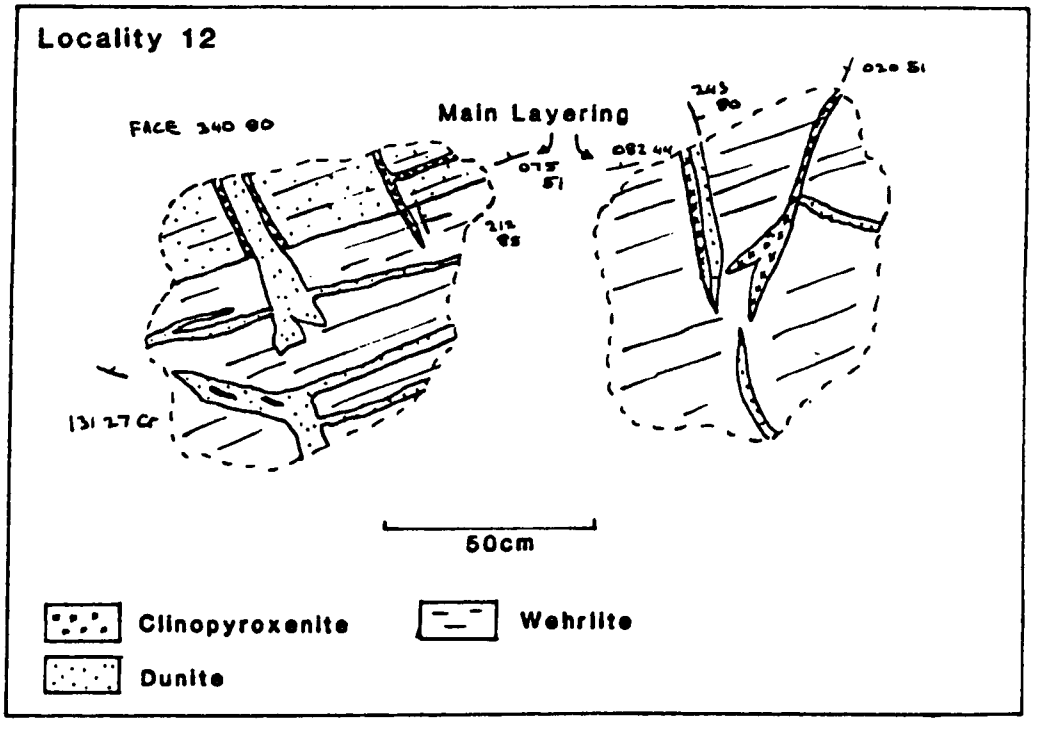

Figure 3.14 Sketch of locality 12. Dunitic intrusive relationships in the Lower Cumulate Unit.

east which is roughly sub-parallel to the moho boundary. After formation these layers have been intruded by olivine-rich and clinopyroxene-rich sheets which cut the layers at varying angles. At locality 12 the intrusive sheets have two dominant orientations: a dyke strike of WNW-ESE with a sub-vertical dip, and a sill-like intrusive relationship with the sheets sub-parallel to the earlier layers. Due to the high degree of alteration it is not possible to see whether these sheets have chilled boundaries against the adjacent layered rocks. Where the adjacent rock is olivine-rich, an olivine-rich intrusive sheet commonly has a clinopyroxene-rich rim which may be a chilling affect (See Figure 3.14).

One of the dunitic intrusive sheets has a less thick chromite seam parallel to the sheet boundaries. This is similar to the feeder-zone type of chromite deposits within the Peridotite Unit.

This late intrusive history of some of the dunitic and clinopyroxenitic bodies observed at locality 12 is the most likely explanation of the variability in the orientation of some of the larger metre-scale bodies of clinopyroxene-rich rocks within the Cumulate Unit dunites. (See Enclosure 10). These bodies are especially common near the Peridotite Unit dunite-rich feeder zones; they extend at least 500 metres upwards from the moho boundary.

The Cumulate Unit dunites become richer in clinopyroxene upwards and finally grade into layered gabbros. The major lithological boundaries all strike roughly north-south, sub-parallel to the moho. These boundaries are all outside the zones of D1 and D2 tectonism and have not been studied in detail for this thesis. George (1975) and Allen (1975) have both studied these areas in detail.

3.6 Summary of the Primary Structural Trends and Distribution of Petrological Features of the Peridotite and Lower Cumulate Units of the Troodos Ophiolite.

The various petrographic and structural features of the areas studied in the Troodos Ophiolite are shown on Figure 3.15.

The moho strikes NNE-SSW and dips sub-vertically in the area studied. The S2 planes have an almost constant orientation over the whole area and make an angle of approximately 45 degrees with the moho plane. (See Figure 3.15). The D2 event caused only small-scale folding of the S1 foliation planes and the boundaries of the sub-moho dunite chambers. The S1 planes all have sub-vertical dips and variable strikes.

The overall intrusive and layering relationships between the various petrological features have been preserved in most areas. It is clear that there are relict dunite cumulate chambers with chromite seams parallel to the cumulate layering below the moho plane. These are connected from deeper levels in the Peridotite-Unit and to the main Cumulate Unit dunites by a series of feeder zones which contain dunitic sheets at a high angle to the moho plane. Minor chromite seams are found within these dunitic sheets.

At least some of these feeder zones must have been active after others as there is strong evidence of olivine-and clinopyroxene-rich rocks intruding the cumulate dunites and wehrlites of the Lower Cumulate Unit. The cumulate layers and the boundaries of the main lithological units of the Lower Cumulate Unit are sub-parallel to the moho plane and also to the cumulate layer-type chromite deposits within the sub-moho dunite chambers.

Diagrammatic section through the Peridotite Unit and Lower Cumulate Unit (Moho rotated to horizontal)

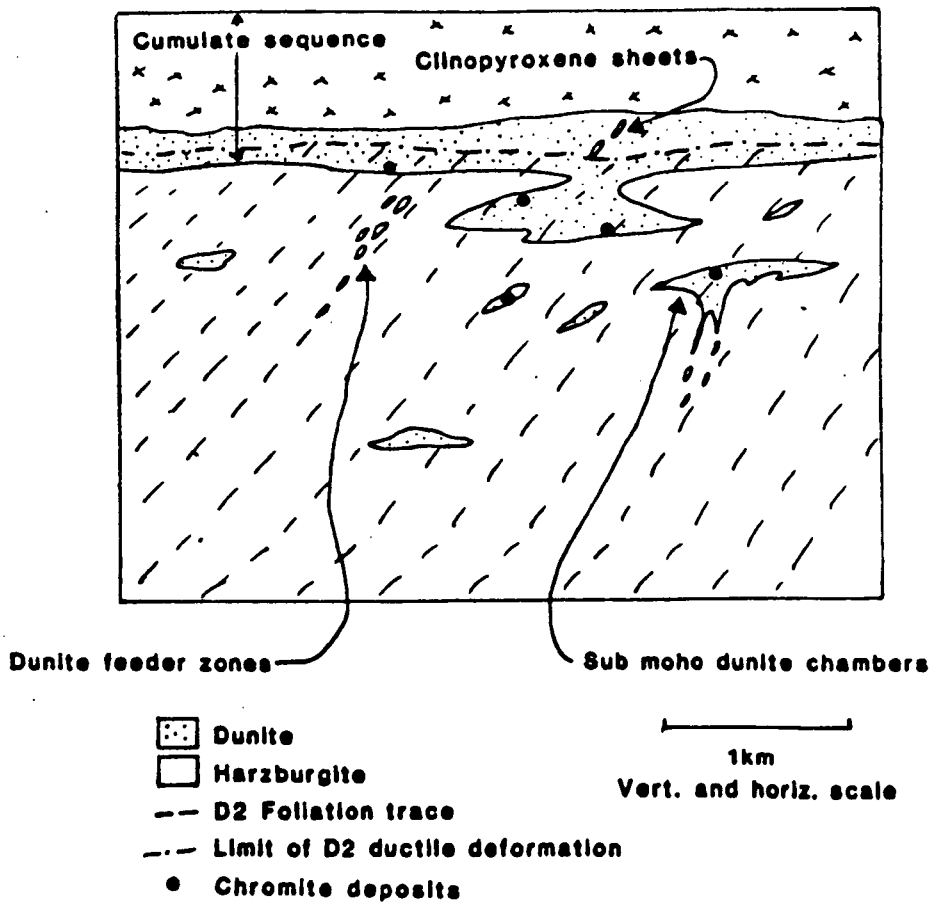

Figure 3.15 General relationships between the various petrological and structural features of the Peridotite and Lower Cumulate Units of the Troodos Ophiolite.

A detailed study of the styles of the D1 and D2 deformations and the directions of movement and shear senses is described in Chapter 7.

The structures of the Troodos Ophiolite are considered in an ocean-spreading context in Chapter 9.

Chapter 4

The Shetland Ophiolite

CONTENTS

4.5 The Orientation of the Petrological Features of the Peridotite and the Lower Cumulate Units of Unst and Fetlar, Shetland.

4.5.1 The Peridotite Unit.

(a) Dunite Pods.

(b) Dunite Sheets.

(c) Chromite Concentrations.

(d) The Clibberswick Hill Block.

4.5.2 The Moho Plane.

4.5.3 The Lower Cumulate Unit.

4.6 Summary of the Primary Structural Trends and Distribution of the Petrological Features of the Lower Ophiolite Blocks of Shetland.

4.1 Geographical and Geological Setting - Previous Work.

The Shetland Islands lie about 165km north-east of the Scottish mainland and about 340km west of Bergen in Norway (Figure 4.1).

The Shetland ophiolite complex covers an area of approximately 95km² on the islands of Unst and Fetlar. The island of Unst is the most northerly of the Shetland Islands. It is fairly undulating in its topography with 100 metre sea-cliffs on the west coast and sheltered voes on the east. Fetlar lies 6km to the south of Unst and has a similar topography (Figure 4.1).

4.1.1 Regional Geology

The Shetland Islands are composed mainly of ancient sedimentary rocks which were metamorphosed, and intruded by igneous rocks during the Caledonian Orogeny. A fairly large part of the mainland is composed of Devonian sedimentary and volcanic rocks laid down at the end of this orogenic period. The general geology of the Shetland Islands has been well summarized in the 'Orkney and Shetland' volume of the British Regional Geology series. (Mykura, 1976.) The following review of the general geology will be restricted to the three islands of Unst, Yell and Fetlar (Figure 4.1).

These islands can be divided geologically into two major units (Figure 4.2).

(1) The Western Unit. This comprises the whole of Yell, the western half of Unst and the most westerly peninsula of Fetlar. It is divided into sub-units by Mykura (1976):-

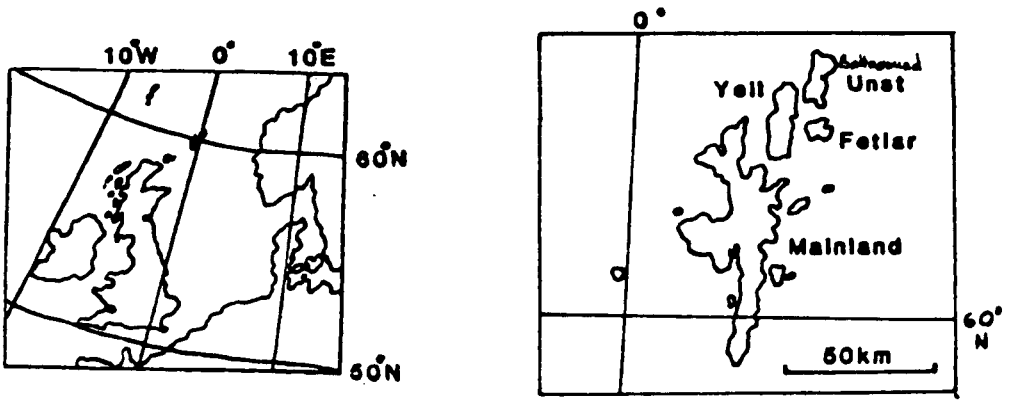

Figure 4.1 The location and geography of the Shetland Islands.

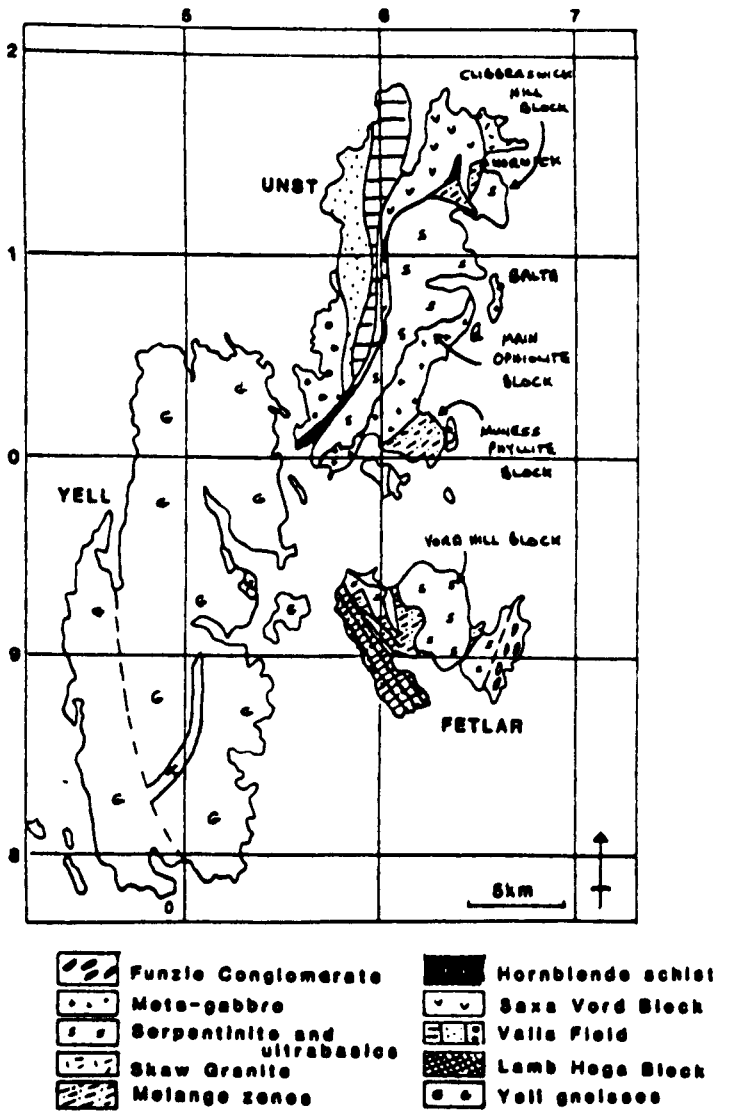

Figure 4.2 General geology of Unst, Yell and Fetlar. (Modified from Phemister (1963).)

(a) A steeply foliated north-south trending sequence of rocks dominantly garnetiferous mica-plagioclase-gneiss. This sub-unit only outcrops on Yell. It also includes garnetiferous mica-schists and is traversed by pegmatite veins. A major vertical brittle dislocation separates this complex from the second sub-unit (Figure 4.2).

(b) A more pelitic unit of schists and gneisses with bands of more calcareous rocks grading into impure limestones. The foliation dips at varying angles towards the east. This sub-unit has been called the Valla Field Block on Unst, and the Lamb Hoga Block on Fetlar. Only minor outcrops of this sub-unit are present on Yell (Figure 4.2).

A major thrust zone separates the Western Unit from the Eastern Unit in all areas except Fetlar, where a major fault separates the Lamb Hoga Block from the rocks to the east.

Read (1934) recognised three metamorphic events within the Valla Field Block of Unst. The first event produced, throughout the Western Unit, a regional prograde metamorphism of moderate grade. It caused widespread migmatisation in the Valla Field and Lamb Hoga Blocks. The second event was a retrograde metamorphic episode affecting the southern half of the Valla Field Block and the whole of the Lamb Hoga Block. Miller and Flinn (1966) related the third dislocation type metamorphism to the westwards upthrusting of the Eastern Unit over the Western Unit. It is confined to the immediate vicinity of the major thrust and shear zone separating the two units.

(2) The Eastern Unit. This unit comprises the eastern half of Unst and a large proportion of Fetlar. It has been termed a 'Nappe Pile' by Flinn (1958) and consists of a series of thrust sheets which have been emplaced onto the Western Unit - the basement. In Unst these allochthonous thrust sheets are:-

(a) The Saxa Vord Block: a southward-thinning sheet composed of pelitic schists and more psammitic rocks. The sheet dips moderately to the east. Key (1972) recognised regional prograde and retrograde metamorphisms within the Saxa Vord Block similar to those in the underlying basement. He also recognised a dislocation event which was only present next to the major dislocations.

(b) The Main Ophiolite Block: (termed the 'Main Serpentinite and Greenstone Block' by previous authors, eg. Flinn (1958), Mykura (1976).) This block forms a large part of eastern Unst and is composed of the lower section of an ophiolite sequence as defined at the Penrose Conference (Anon, 1972). The rock units present are harzburgites, dunites, clinopyroxenites, wehrlites and gabbros. The base of this ophiolitic sequence has been subjected to extensive dislocation metamorphism with a zone of talc-schists, antigorite serpentinites and locally chlorite-schists. Dislocation also occur within the block itself. Gravity and magnetic surveys have shown that the basal thrust of the Main Ophiolite Block dips steeply eastwards (McQuillin and Brooks, 1967).

(c) Muness Phyllitic Block: exposed on the south east of Unst, this block is composed of phyllite with rare bands of schistose conglomerate. Phyllitic rocks are also found within the thrust zones between the thrust sheets particularly at Norwick (Figure 4.2). Flinn (1958) showed that these phyllitic rocks, termed the Phyllite Group, were deposited as the thrust sheets were exposed at the surface. As thrusting continued these sediments were extensively recrystallized and deformed and incorporated into the thrust zones forming mélanges. (Flinn et al, 1979.) Prichard (1982) describes a dynamo-thermal 'aureole' within this mélange zone, reaching amphibolite grade, immediately beneath the Main Ophiolite Block.

A small outcrop of serpentinite and gabbro lies to the east of the Muness Phyllitic Block on the Muness Peninsula. (Figure 4.2.) Both Read (1934) and Flinn (1958) suggest that this is part of the Main Ophiolite Block, and that the Muness Phyllite Block is a synform. Gravity survey results have supported this by showing that the phyllite thins rapidly in depth and only extends to a maximum of 300 metres. (McQuillin and Brooks, 1967.)

(d) Clibberswick Hill Block: this block is composed largely of harzburgites with minor occurrences of dunite. It lies to the north of the main ophiolite block and is separated from it by a major thrust zone. This block has a similar steeply dipping basal dislocation zone to the main ophiolite belt. Geological (Read, 1934; Finn, 1958) and geophysical

evidence (McQuillin and Brooks, 1967) clearly shows that the Clibberswick Hill Block belongs to a separate tectonic unit from the Main Ophiolite Block.

(e) Skaw Granite Block: a pink foliated augen-granite with xenoliths of metasediment. A thrust zone separates this block from the adjacent Saxa Vord Block. Shearing within the granite close to this thrust zone shows that the block is an integral part of the nappe pile (Read, 1936) and is thus allochthonous.

In Fetlar the blocks which have been emplaced onto the Western Unit (the Lamb Hoga Block) are now separated from it by a fault zone (Figure 4.2). There are three serpentinite blocks which are separated by mélange zones. The most westerly serpentinite block - the Hamars Ness Block - is composed largely of serpentine with a small amount of meta-gabbro. Gravity survey results (McQuillin and Brooks, 1967) show a strong positive anomaly axis between the Main Ophiolite Block of Unst, the island of Uyea and the Hamars Ness Block of Fetlar. This supports the correlation by Flinn (1958) between these two blocks.

The largest ophiolite block in Fetlar is the Vord Hill Block (Figure 4.2). It, however, only contains the Peridotite Unit of an ophiolite complex. It structurally overlies the Hamars Ness Block and has a dynamo-thermal aureole associated with its emplacement and exposed on its eastern side (Prichard, 1982).

The Hesta Ness Block in north-east Fetlar is completely altered to antigorite and steatite. Flinn (1958) suggests that the Vord Hill Block forms the core of a synform and that the Hesta Ness Block represents the reappearance of the Hamars Ness Block on the eastern limb of this synform (Figure 4.3).

Between these three serpentinite blocks there are a number of highly complex shear-bounded mélange zones. These consist of varying proportions of phyllite, graphite schist and schistose conglomerate with highly elongate pebbles. Sheared slices of serpentinite and metagabbro are also present. These mélanges are similar to the Phyllite Group discribed from Unst.

Most of the eastern peninsula of Fetlar is composed of a strongly deformed conglomerate at least 1200 metres thick - the Funzie Conglomerate. Pebbles are mainly of quartzite with a few of granitic-type and basic igneous rocks. The conglomerate is faulted against the serpentinite and mélange blocks to the west. However, because the pebbles are more strongly deformed close to this fault zone (Flinn, 1956), this block has clearly been an integral part of the nappe pile.

4.1.2 Ophiolite Geology

The ultrabasic rocks of Unst and Fetlar were first recognised by Garson and Plant (1973) as part of a possible ophiolite complex. The complex was mapped on the scale of six inches to the mile by the Geological Survey of Great Britain from 1929-34 and their findings published by Read (1934 and 1936).

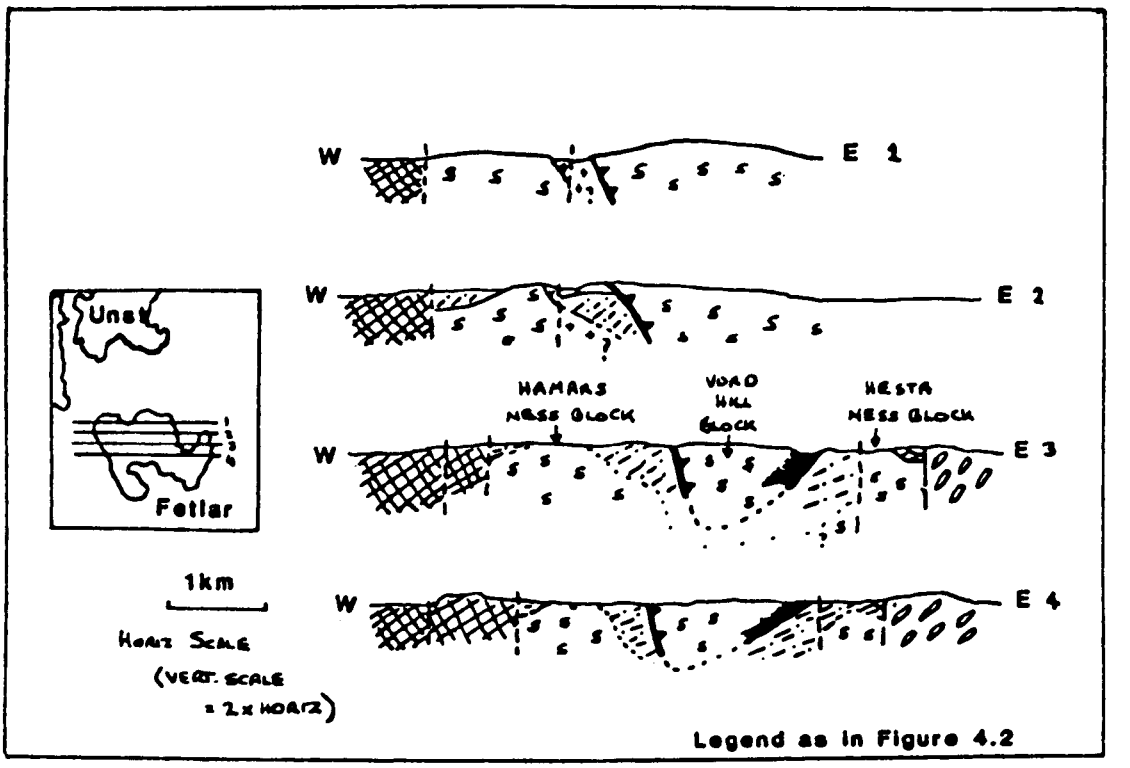

Figure 4.3 A possible cross-section through Fetlar. (After Flinn, 1958).

Since then, little work has been published on the complex except by Amin (1954) and Flinn (1970). Recently, an EEC project was set up to investigate chromite deposits within the Unst and Fetlar ophiolite complexes; this has involved the re-mapping of the 'Serpentinite and Greenstone' Blocks with the use of ophiolite terminology for the lithological units. (Prichard, 1982). Figure 4.4 summarizes the geology of the Shetland Ophiolite as mapped by Prichard (1982).

The Shetland Ophiolite is dismembered with the upper ophiolite units absent. Lavas are totally absent and no major sheeted dyke complex is evident. Prichard (1982) describes swarms of doleritic dykes intruding the highest levels of the gabbro unit along the east coast of Unst. These, however, occur only sporadically and it is not certain that they are remnants of a sheeted dyke complex. Prichard (1982) used geochemical discrimination techniques on a few of the dykes and suggested that they were of island arc affinities.

The gabbro unit is highly altered with original plagioclase and clinopyroxene replaced by albite and actinolite respectively. In places, layering is still discernable, but much of the unit is massive. Prichard (1982) recognised net veining and cross-cutting of the higher-level main gabbros by late felsic differentiates and intrusions. Pods of wehrlite altered to amphibolite are present at all levels within the gabbros (Figure 4.4).

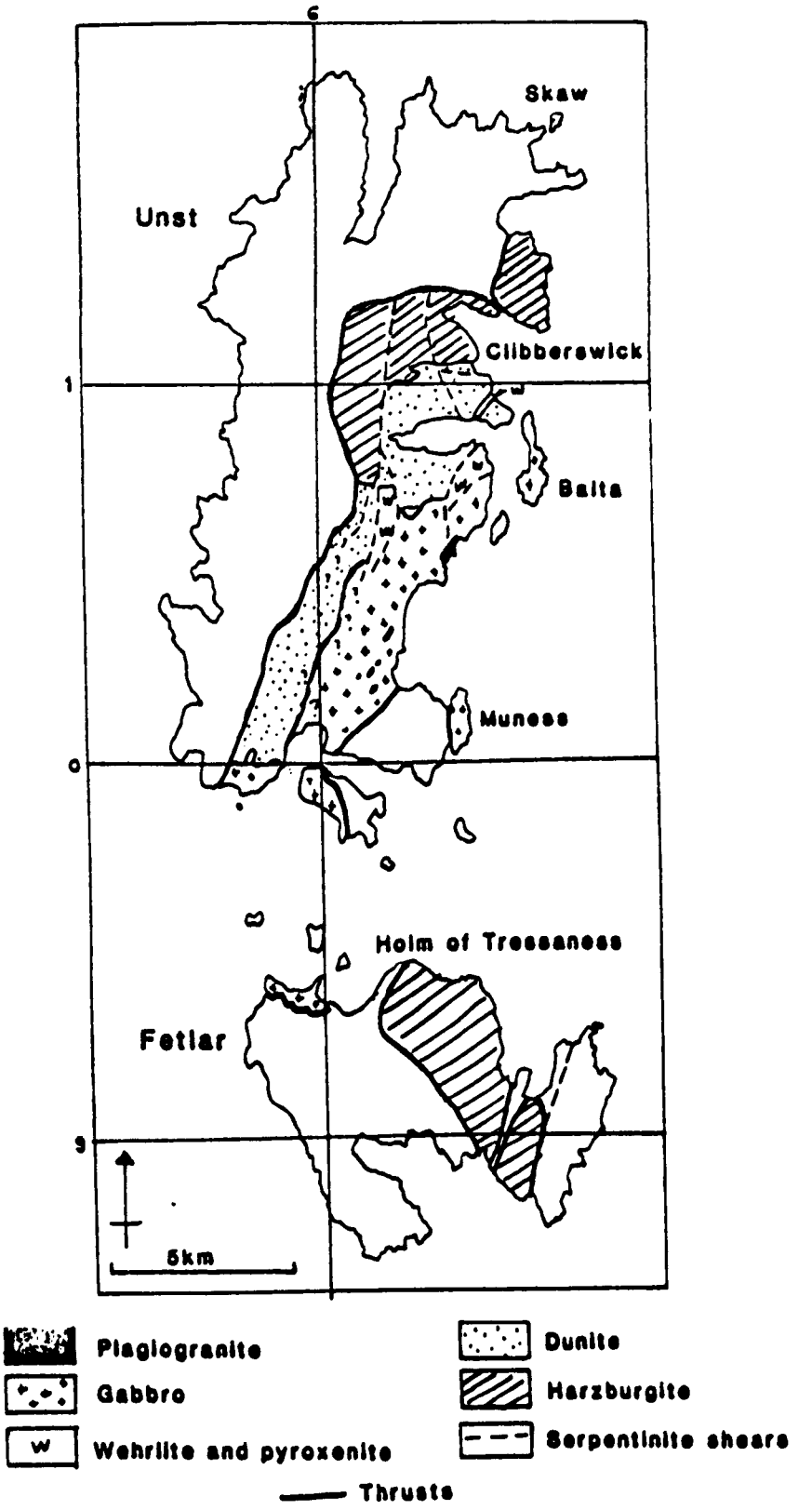

Figure 4.4 The geology of the Shetland Ophiolite. (Modified from Prichard, 1982).

The rock units between the harzburgites and gabbros are predominantly of dunite. Discontinuous layers of wehrlite and clinopyroxenite outcrop in the higher levels of this zone (Figure 4.4). A strong tectonic fabric is present within the harzburgites which extends into the dunite and wehrlite units.

No detailed structural analysis of the ophiolite blocks of Unst and Fetlar has been performed by previous authors.

4.1.3 Regional Setting and Emplacement

The Shetland Ophiolite Complex was formed as oceanic crust before, or at an early stage of the Caledonian Orogeny. (Cambrian - Middle Devonian). Various rocks have been dated (Miller and Flinn, 1966) from Unst and Fetlar. The Western Unit gives a K-Ar age of about 480 ± 30 m.y. for the main regional metamorphic event, and a K-Ar age of 420 ± 30 m.y. for the emplacement of the Eastern Unit onto it. Within the Eastern Unit, the Muness Phyllites gave a K-Ar age of 425 ± 30 m.y. which would support the suggestion that they were deposited and metamorphosed as thrusting took place (Flinn, 1958).

The 'Nappe Pile' of the Eastern Unit has been interpreted by Flinn (1958) as three major thrust sheets separated by mélange zones. (Figure 4.5):-

(a) The Saxa Vord Block: this block has not been dated. It either is an early thrust sheet of the Nappe Pile or could have been emplaced separately at an earlier date (Mykura, 1976).

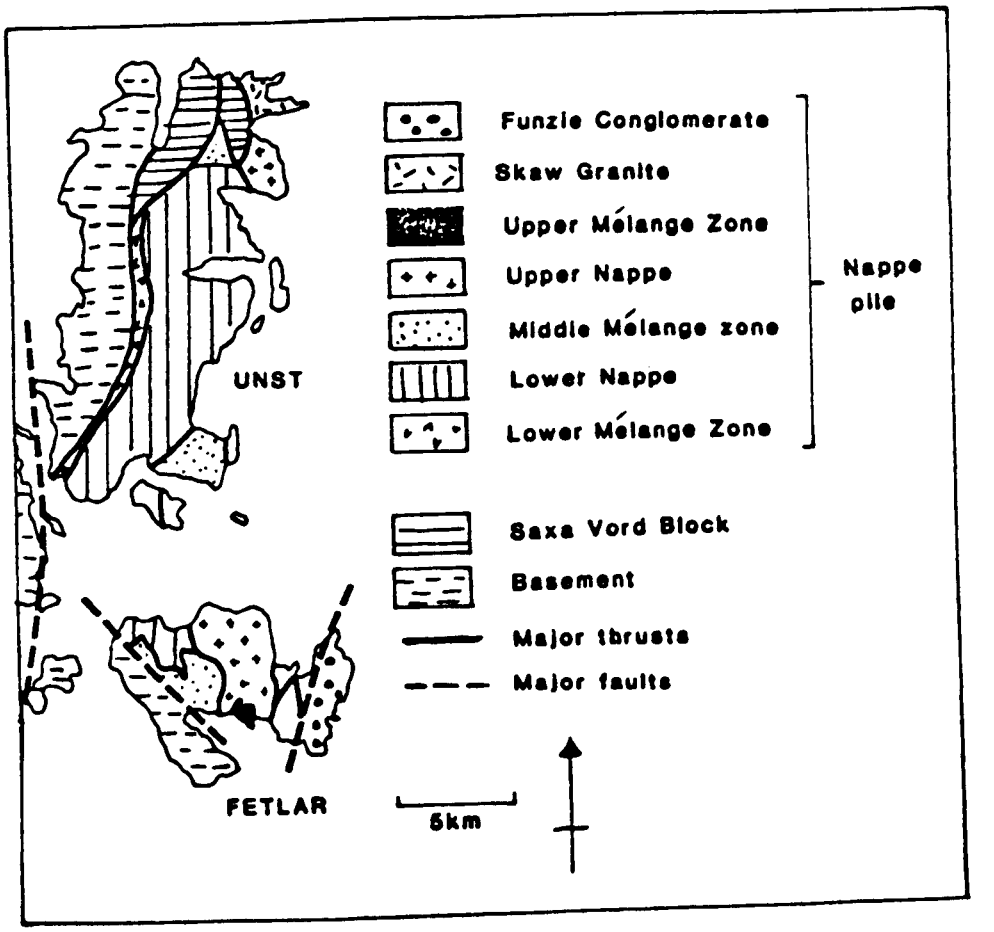

Figure 4.5 The nappe piles of Unst and Fetlar. (Modified from Mykura, 1976).

(b) The Lower Nappe: this is represented by the Main Ophiolite Block and the small outcrop on the Muness Peninsula on Unst, and the Hamars Ness and Hesta Ness Blocks on Fetlar. As already discussed in section 4.1.1, Flinn (1958) proposes that the nappe is folded into a south-south-west-plunging synform in the south of Unst and on Fetlar. This nappe is underlain by the Lower Mélange Zone which is absent in Fetlar because of faulting. The Middle Mélange Zone separates the Lower Nappe from the Upper Nappe. It comprises the phyllitic-type rocks at Norwick and the Muness Phyllites in Unst, and almost all the phyllites of Fetlar.

(c) The Upper Nappe: this comprises the main harzburgite block of Fetlar - the Vord Hill Block. Flinn (1958) has also correlated the Clibberswick Block of Unst with the Upper Nappe, although there is little structural or geophysical evidence for this correlation. Gravity anomalies show that the serpentine composing Gruney Island (see Figure 4.5) extends southwards to the Vord Hill Block and northwestwards towards Muness but probably no further north.

On Fetlar, the remains of an Upper Mélange Zone may be preserved (Figure 4.5). (Flinn, 1958.)

The dynamo-thermal aureole within the mélange zones of both the ophiolite nappes is most probably formed by the over-thrusting of a still hot and thus relatively young mantle, similarly to the aureole below the Oman Ophiolite (Chapter 2). Williams and Smyth (1973) suggested this origin for the hornblendic schists in the Norwick area.

Flinn et al (1979) summarize the history of the Nappe Pile as:

(a) Underthrusting causing emplacement of a still hot slice of upper mantle and lower oceanic crust on top of strongly metamorphosed Caledonian metasediments.

(b) Erosion of this nappe with deposition of locally derived sediments.

(c) Emplacement of a further ophiolitic slice causing incorporation of the newly deposited sediments into the Middle Mélange Zone.

The forces leading to the emplacement of the nappes may also have locally folded them.

The direction of emplacement is difficult to determine. Flinn et al (1979) suggests an ESE-WNW emplacement assuming that emplacement causes the folding observed in Fetlar and in the south of Unst. Measurements of the sense of movement on joint drags in the Muness Phyllite Block by Flinn (1952) suggests that the Upper Nappe has moved south westwards over the Lower Nappe. The elongate pebbles of the Funzie conglomerate give a similar SW-NE trend. (Flinn, 1956.)

A late-stage greenschist metamorphism has affected the whole of the Nappe Pile and the underlying metasediments.

Garson and Plant (1973) correlated the ophiolite blocks of Unst and Fetlar with their Highland Border Ophiolite Belt and also the Ballantrae Ophiolite on the mainland of Scotland.

Flinn (1959) correlates the Shetland Ophiolite with the Jotun nappe pile in Norway. The emplacement age for the Shetland Ophiolite of 420 ± 30 m.y. (Miller and Flinn, 1966) corresponds well with time of closure of the Iapetus Ocean and the collision of the northern and southern continents. (Review in Anderton et al, 1979.) Prichard and Spray (in prep.) propose that the Shetland Ophiolite is an obducted part of a back-arc basin associated with the Iapetus Ocean. A similar back-arc basin history has been suggested for all the ophiolite complexes of a similar emplacement age in Norway (Sturt et al, 1983).

4.2 Logistics and Areas of Study in Shetland.

Two field seasons were spent in Shetland; four weeks in July and August, 1981; and three weeks in April and May, 1982. Daily field excursions were made from a base in Baltasound village (Figure 4.1). The areas selected for study were the Main Ophiolite Block and Clibberswick Hill Block on Unst and the Vord Hill Block on Fetlar (Figure 4.6). Access to most areas in Unst is fairly good but in Fetlar there is no road at the northern end of the island and access is only possible on foot.

Aerial photographs on the scale of 1:4500 and the geological maps of Prichard (1982) and the "One-Inch Series" Institute of Geological Sciences Northern Shetland sheet were all used as an aid to mapping. Regional mapping of the lower ophiolite sequences was carried out at a scale of 1:10,000, with more detailed mapping in selected areas at the scales of 1:5000 and 1:250.

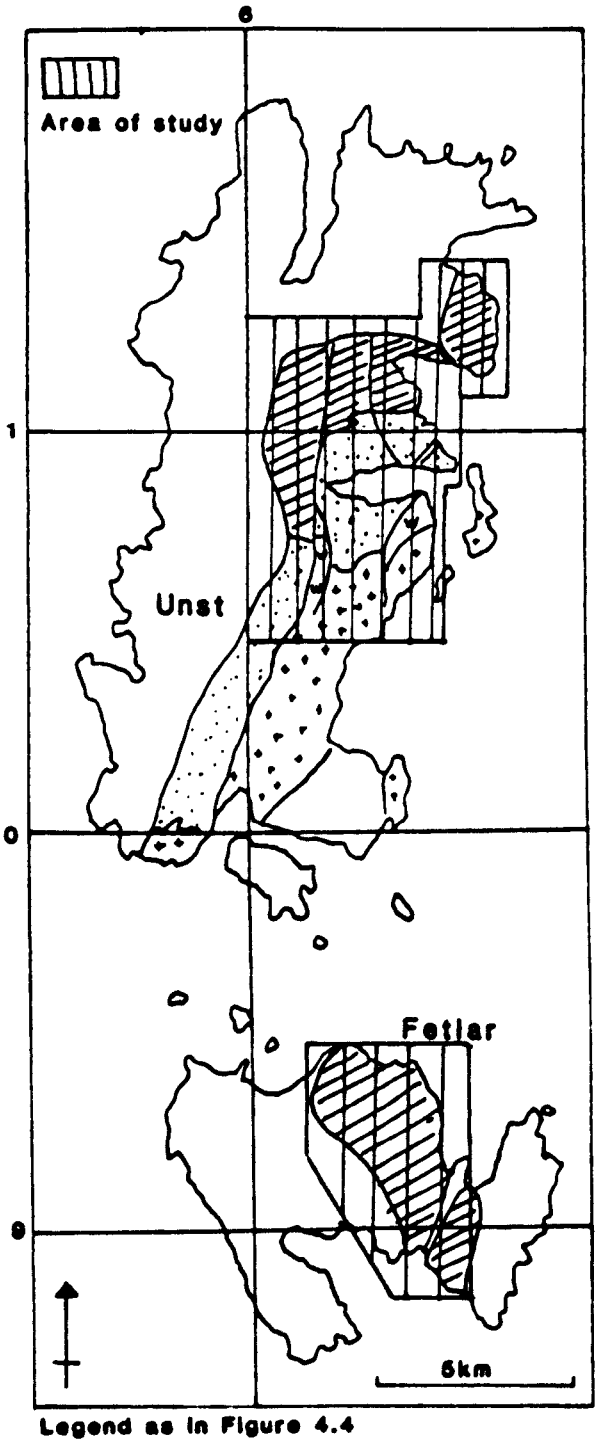

Figure 4.6 Areas of study of the Shetland Ophiolite.

The field relationships mapped from each area will now be described.

4.3 General Mantle and Lower Crustal Petrology of the Shetland Ophiolite.

4.3.1 Appearance of Rock Types in the Field.

The various rock types of the Shetland Ophiolite have a very similar field appearance to those of the Troodos Ophiolite (see Chapter 3.3.1).

The exposure of the Shetland Ophiolite is highly variable. Most of the low lying and some of the higher level areas are covered with extensive peat-bog which gives a very poor exposure. The hillsides of Muckle Heog and Little Heog, however, have an exceptionally good exposure for Shetland, with a large area of harzburgites and dunites having over 50% exposure. This enabled accurate mapping of the moho boundary to be completed.

Coastal exposure is usually 100% but steep cliffs make a large proportion of the coast inaccessible for mapping.

4.3.2 General Petrology of the Area Studied.

The lower ophiolite sequences of Unst and Fetlar have many similar petrological features to the Troodos and Oman Ophiolites. The geology of the areas mapped is shown on Enclosures 12 and 13 (Unst) and Enclosure 14 (Fetlar).

(a) The Peridotite Unit. In both Unst and Fetlar the Peridotite Unit is composed predominantly of harzburgite. The harzburgite has a similar modal composition to Troodos and Oman with 75% - 95% olivine, 25% - 5% orthopyroxene, and trace amounts of clinipyroxene and chrome-spinel.

Olivine and orthopyroxene-rich segregation layers are fairly common in most areas of harzburgite outcrop (Plate 4.1). These diffuse layers are sub-parallel to the main foliation as in Oman and Troodos.

In almost all areas, two foliations have been measured from the same outcrop. The alignment of spinel and orthopyroxene grains define the different foliation planes. These show similar relationships to the two foliations in Cyprus with the more strongly defined foliation having a fairly constant orientation, and the other one varying in its orientation over small areas (see Enclosure 12). For the same reasons as in Cyprus (see Chapter 3.4), the constantly striking foliation will be termed S2 from now onwards, and the earlier foliation with variable strike, S1. The D1 and D2 structural orientations of Unst and Fetlar are described in Section 4.4.

The harzburgite thin section textures vary from coarse to mosaic porphyroclastic with the most common textures between coarse and porphyroclastic. Most of the specimens studied are highly serpentinised.(up to 90%) which makes their textural classification difficult. However, in most sections, sufficient relict olivine and orthopyroxene grains are preserved to show that the textures are related to the S2 orientationns. This will be further shown in Chapter 7 when the olivine crystallographic orientations are discussed.

As in the Troodos Ophiolite, it was not possible to measure lineations on either S2 or S1 planes in the field.

Dunitic bodies are fairly common in the Peridotite Unit of both Unst and Fetlar. They are podiform in shape and have a maximum dimension of 250 metres. (See Enclosures 12 and 14.) Sharp-sided dunite sheets are also common and are anastomosing in some areas. The distribution of the dunite bodies and sheets will be considered in section 4.5 of this chapter. Both the S1 and S2 foliations cut straight through the Peridotite Unit dunitic sheets and bodies, and the dunite textures are the same as in the harzburgites.

(b) The Lower Cumulate Unit. The Lower Cumulate Unit is only exposed on Unst. (See Figure 4.4.) It is composed of dunites at its base which become more clinopyroxene rich and grade upwards from the moho into wherlites and clinopyroxenites and finally gabbros.

In some areas a distinct layering is present in the dunites of either pyroxene-rich or chrome-spinel-rich horizons (Plate 4.3.) The chromite layers are restricted in their distribution to the lowermost kilometre of the Lower Cumulate Unit. The clinopyroxene-rich layers are present close to the wehrlite horizons which are themselves strongly layered in some areas.

All the layering features are sub-parallel to the moho plane which has a fairly constant orientation except for minor localised fluctuations. These orientations are discussed in section 4.5.

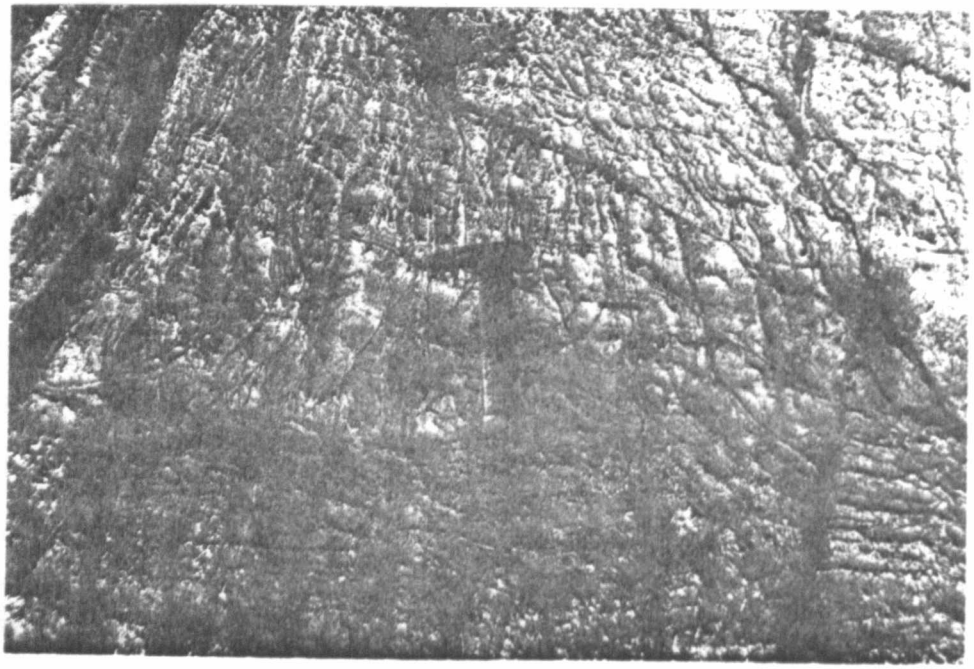

Plate 4.1 Olivine- and orthopyroxene-rich segregation layers in the harzburgites from Fetlar. Ol = olivine-rich, Px = pyroxene-rich. (— = foliation trace). (Length of hammer 40 cm).

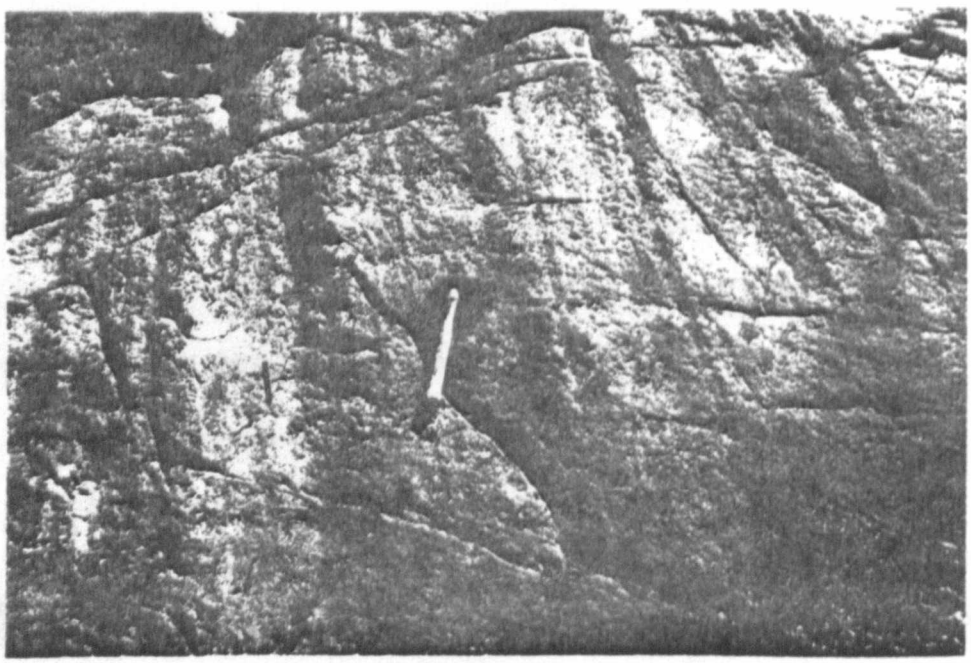

Plate 4.2 Dunitic layering in harzburgites. (— = foliation trace). (Length of hammer 40 cm).

The S1 and S2 foliations of the Peridotite Unit extend across the moho boundary into the Lower Cumulate Unit. They both extend at least 2½ kilometres into the Lower Cumulate Unit. Due to the lack of exposure and high degree of serpentinisation, it is not possible to define accurately the boundary at which either the D1 or D2 deformational episodes die out. In the lower kilometre of the Lower Cumulate Unit there are fold closures between chromite-rich layers, with fold axial planes parallel to the S2 foliation (Plate 4.3). The orientations of the D1 and D2 structures are discussed in section 4.4 and 4.5.

In thin section the tectonised dunites and wehrlites have similar textures to the Peridotite Unit. Because of the high degrees of serpentinisation and poor exposure, only a few samples were collected. These show a trend with the texture becoming coarser away from the moho. (ie. Deformation is less intense in higher levels of the dunites.)

The gabbros are poorly exposed and highly altered. In thin section original plagioclase and clinopyroxene have been replaced by albite and actinolite respectively. Olivine may have originally been present but has now been totally altered. Any relict cumulus-type structures have been destroyed in thin section.

A layering is measurable in some gabbro localities from either plagioclase-or clinopyroxene-rich horizons. The layers are not more than 10 centimetres thick and are usually difficult to discern because of the high degree of alteration.

The high degree of alteration also makes it unclear whether some of the gabbros have been tectonically deformed by the Peridotite Unit D1 and D2 deformations. Two foliation planes have been measured in some outcrops which have similar orientations to the S1 and S2 orientations.

(c) Pyroxenite Dykes. Clinopyroxene-rich dykes are present in the Peridotite Unit of the Shetland Ophiolite but rarely in the dunites of the Lower Cumulate Unit of Unst. Most of the dykes are undeformed and have no dominant orientation. At one locality in Unst (NGR 636107) one clinopyroxene dyke cross-cuts another indicating at least two phases of dyke intrusion.

An earlier pre-D2 pyroxene dyke intrusion event is also evident in the Peridotite Unit of both Unst and Fetlar. These dykes are tightly to isoclinally folded by the D2 deformational event. (Plate 4.4.)

The presence of undeformed pyroxenite dykes indicates that the S1 and S2 foliations are probably related to ocean-spreading processes and not emplacement processes. These dykes may be similar to the off-axis related pyroxene-rich dykes in the Oman Ophiolite Peridotite Unit.

4.3.3 Emplacement Related Structures

As already mentioned in section 4.1.3, the Shetland Ophiolite forms part of a nappe pile which has been formed by extensive thrusting with emplacement roughly from the east to west.

Plate 4.3 Fold-closures in chromite-rich layers. (▬ = trace of fold axial plane). (Cap diameter 2.5 cm).

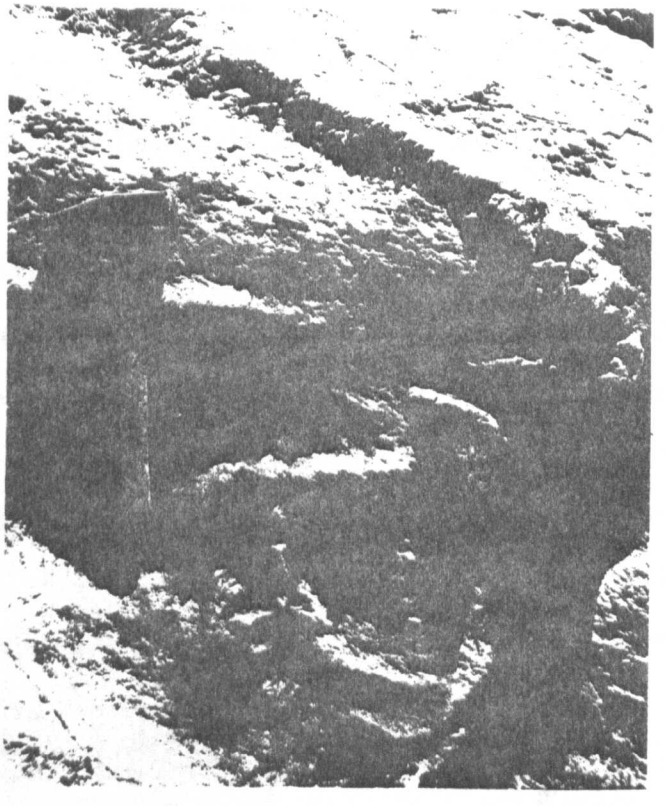

Plate 4.4 Tightly folded clinopyroxene-rich dyke in the harzburgites of the Crussa Field Block, Unst. (▬ = trace of S2 foliation). (Hammer length 40 cm).

This thrusting has caused the ophiolite to be dissected by shear-zones into various blocks. The shear zones are composed of highly sheared serpentinite and talc-rich rocks. Figure 4.7 shows the location of the various shear zones and the ophiolite blocks and their names.

All the shear zones are strongly foliated with the foliations parallel to the shear zone boundaries (Plate 4.5). The adjacent ultramafic rocks of the Peridotite Unit and Lower Cumulate Unit have been locally serpentinised, fractured and occasionally rotated with the fractures sub-parallel to the shear zone foliations. Serpentinisation is particularly intense in Unst along the basal thrust zone of the Crussa Field Block and also the basal thrust zone of the Clibberswick Hill Block. Talc is being actively quarried from both of these shear zones (NGR 613122 and 651121).

The ophiolite blocks have been displaced relative to each other by the various shear zones. Within each block of Unst the S2 orientations do not vary in attitude (Enclosure 12). This fact and the presence of undeformed pyroxenite dykes indicate that the emplacement related structures are restricted to the near vicinity of the shear zones, and that each block has preserved its original ocean-spreading related structures. In Fetlar the main ophiolite block may have been folded on a large-scale by emplacement processes as the orientation of the S2 foliations is not constant over the whole area mapped. These orientations are discussed in detail in section 4.4.

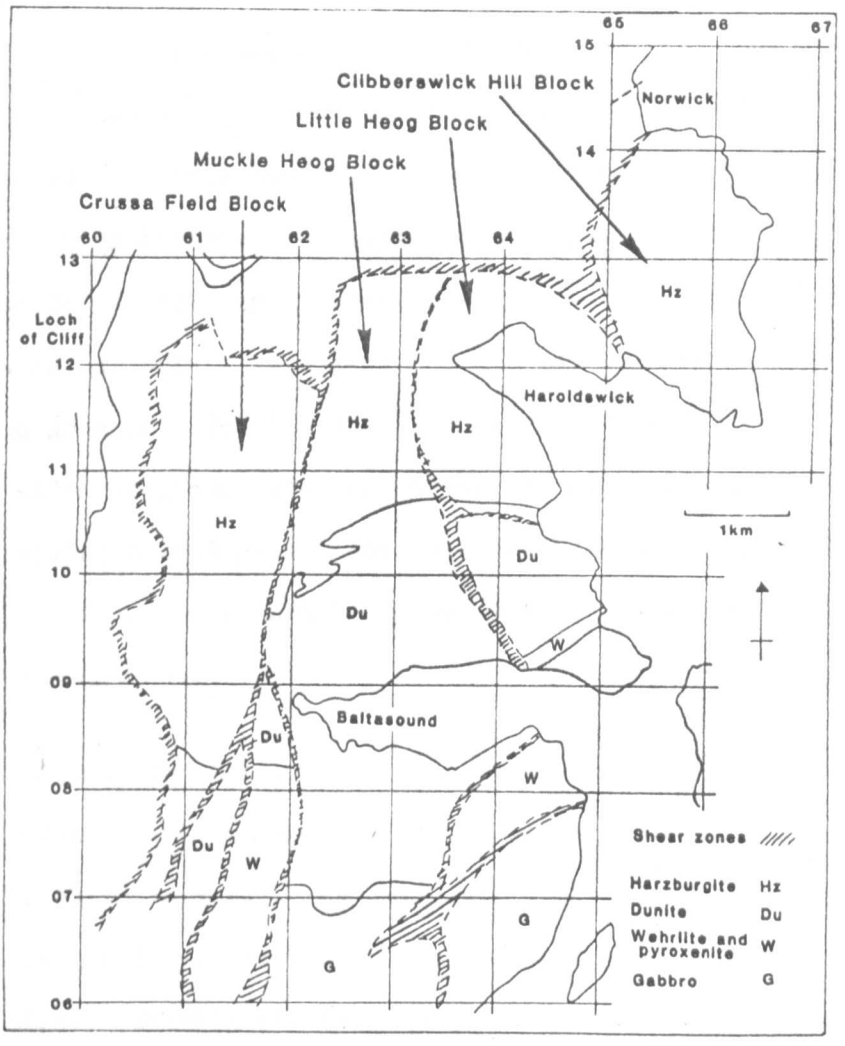

Figure 4.7 The major shear zones mapped in the ophiolite units of Unst and Fetlar and the division of the ophiolite into blocks.

Plate 4.5 Exposure of highly foliated serpentinite shear zone on Unst. (Hammer length 40 cm).

The recognition of shear zones within the ophiolite complex of Unst and their related displacements has necessitated alterations from the mapping of Prichard (1982). The map of Prichard omits the shear zones, and, accordingly, the moho boundary in the northern part of the Unst Ophiolite appears to swing round from an east-west strike in the east to a north-south strike in the west. Careful mapping of poorly exposed areas has shown that what was originally mapped as north-south striking moho is in fact a fairly major shear zone (see Enclosures 12 and 13).

4.4 Earlier Structural Orientations

The S1 and S2 orientations have a consistent pattern for each of the ophiolite blocks studies. Each block will be considered separately in this section.

4.4.1 S1 and S2 Foliations of the Muckle Heog and Little Heog Blocks.

The Muckle Heog and Little Heog Blocks are the best exposed blocks of the Unst lower ophiolite sequence. The shear zone between the blocks is only a minor displacement zone and the two blocks can be considered together.

Within these two blocks the most obvious foliation has a constant east-west strike and sub-vertical dip over the whole area - this is the S2 foliation. (See Enclosure 12). The S1 foliation poles plot as girdle patterns with the planes having a sub-vertical dip but highly variable strike. (See Enclosure 12).

To determine the detailed relationships between S1 and S2, two areas, one of 7,500m^2 and the other of 1,250m^2, from the Muckle Heog Block, were mapped at a scale of 1:250. (See Enclosure 15). As in the whole Muckle Heog Block area, both 1:250 areas show a constantly striking east-west S2 foliation and a variably striking S1 foliation.

The relationship between the S1 and S2 foliations is very similar to that of Troodos (See Chapter 3.4). The S1 foliation planes change rapidly in strike from outcrop to outcrop, and give an overall folded pattern for both of the 1:250 areas with the fold axial traces parallel to the S2 traces. This is further discussed in Chapter 7 (and also see Enclosure 30).

The pattern of S1 folded around S2 is evident from the entire area of tectonism of both the Muckle Heog and Little Heog Blocks. This is discussed in Chapter 7 and shown on Enclosure 29.

Both the S1 and S2 foliations cut through the moho into the Lower Cumulate Unit and are unaltered in attitude through the moho boundary into the Peridotite Unit. The dunitic bodies of the Peridotite Unit also show the S1 and S2 foliations cutting straight through them. This indicates that the moho boundary and the Lower Cumulate Unit and Peridotite Unit dunites had been formed before the D1 and D2 deformational events. The affect of D1 and D2 on the Peridotite Unit and Lower Cumulate Unit dunites and the moho boundary itself is considered in Section 4.5.

In the northern area of the Little Heog Block in the vicinity of Haroldswick and Clibberswick the S2 foliations have been rotated to a NW-SE strike direction. (See Enclosures 12 and 20 and Chapter 7). This localised rotation was most probably caused by the emplacement of the Shetland Ophiolite and has been termed a D3 deformational event.

4.4.2 S1 and S2 Foliations of the Crussa Field Block.

The most westerly ophiolite block of Unst is the Crussa Field Block. (See Figure 4.7). The S1 and S2 orientations of this block are the same as the S1 and S2 orientations of the Muckle Heog Block. There are some localised zones where the structural trends have been slightly rotated because of late stage D3 related thrusting. The S1 and S2 orientations are summarised on Enclosure 29 (see Chapter 7).

4.4.3 S1 and S2 Foliations of the Clibberswick Hill Block.

The whole of the Clibberswick Hill Block has been rotated with respect to the rest of the northern Unst ophiolite blocks. The S2 foliation strikes WSW-ENE with a steep dip instead of east-west as in the other blocks. S1 is folded by D2 in a similar manner as in the Muckle Heog Block. (See Enclosure 12).

In the north and south of the Clibberswick Hill Block the S2 foliations have been locally rotated to a more north-south strike. These zones are fairly linear and D3 fold axial plane traces have been constructed for this localised deformation. The D3 axial planes are roughly parallel to the NW-SE striking shear zone at the southern boundary of the block.

4.4.4 S1 and S2 Foliations of the Fetlar Ophiolite Blocks.

The geology and S1 and S2 orientations of the Vord Hill Block are summarised on Enclosures 14 and 31. (See Chapter 7). The block is divided into two areas by a large serpentinite shear zone extending from the Wick of Aith to the Wick of Gruting. (See Enclosure 14).

The smaller southern Peridotite Unit block has a constantly NE-SW striking, steeply dipping S2 foliation with the S1 foliation giving a folded pattern similar to that of the Unst blocks.

The 2km x 5km northern Peridotite Unit block has been deformed on a large scale by D3 folding. This affects the S2 orientations. In the eastern area of the block the S2 foliations strike NW-SE with a sub-vertical dip. Towards the

central area in the vicinity of Rooin (NGR 633924) the dip progressively shallows to give S2 planes with a similar NW-SE strike but a shallow dip towards the NE. The dip does not shallow in the northern area. West of a line joining the Holm of Tressaness to Rooin to the Waters of Cruss (see Enclosure 14) the S2 planes have a completely different strike. In the vicinity of this line, the NW-SE S2 strike of the eastern area rapidly changes to NE-SW strike with a sub-vertical dip. This strike trend gradually rotates to a N-S direction further to the west.

The zone of rapid change in S2 strike strikes roughly NNW-SSE. It is simplest to interpret this line as a D3 fold axial trace of a large scale folding event. (Figure 4.8). The separate eastern and western limbs have been internally unaffected by this D3 folding and the constant S2 strike trends with the related S1 folding patterns have been preserved in both limbs. (See Enclosure 31 and Chapter 7). No D3 related structures have been identified.

The lack of exposure in most areas and especially in areas close to the serpentinite shear zones makes it impossible to determine either the attitude of the NNW-SSE striking D3 fold-axial trace, or its relationship to the shear zones. Its strike is sub-parallel to the western shear zone bounding the ophiolite block which may indicate a temporal relationship to the shearing.

The shallowing of the dip of the S2 planes on the eastern limb of the D3 fold towards the D3 fold axis suggests that the fold is an antiform and not a synform as proposed by Flinn (1958). (See Figure 4.8).

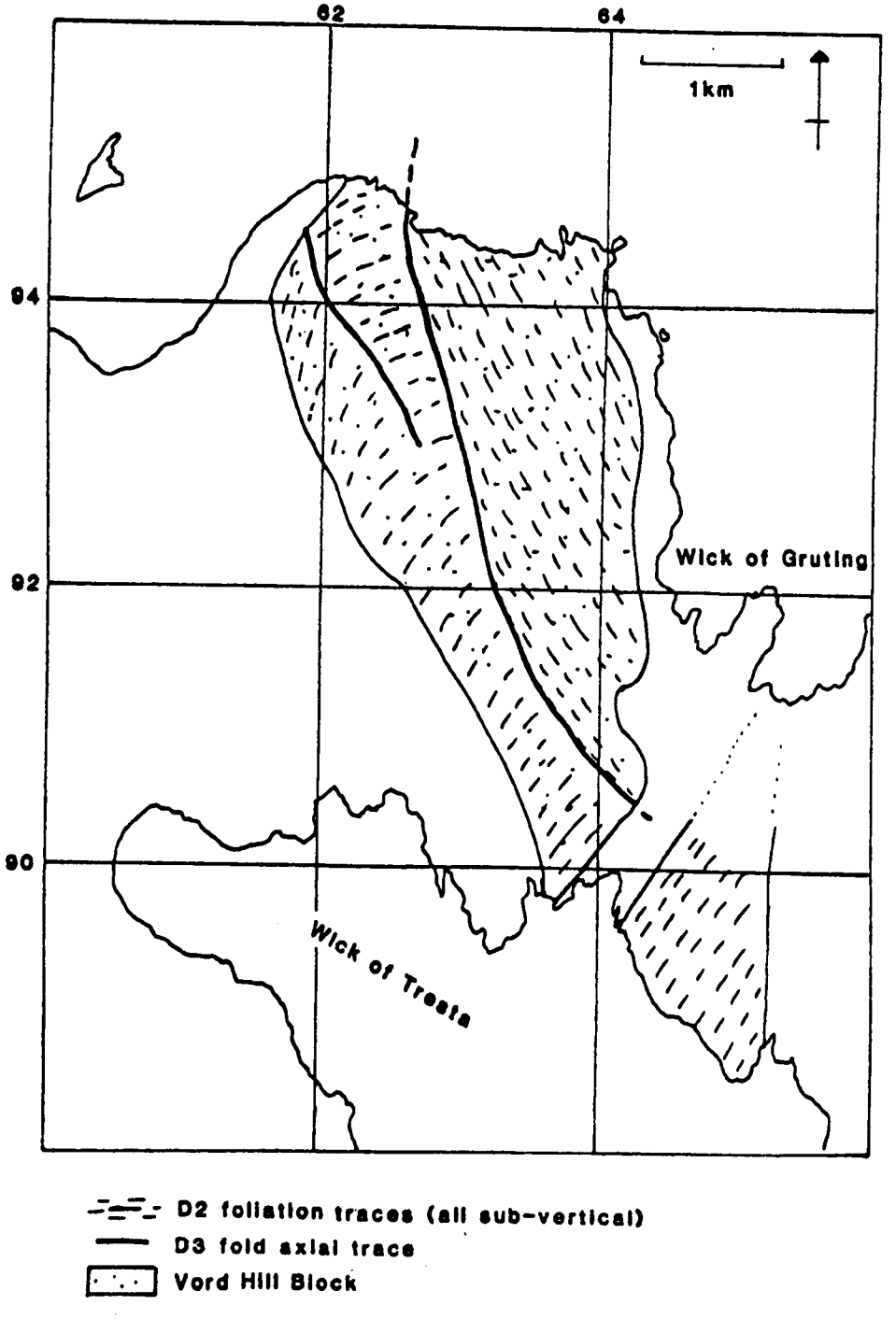

Figure 4.8 Sketch showing large-scale D3 folding of the Vord Hill Block, Fetlar

The orientation of the dunite bodies within the Vord Hill Block in relation to the S1 and S2 orientations is discussed in Section 4.5 below.

4.5 The Orientation of the Petrological features of the Peridotite and the Lower Cumulate Units of Unst and Fetlar, Shetland.

4.5.1 The Peridotite Unit.

a) Dunite Pods.

In the Peridotite Unit areas of both Unst and Fetlar dunite pods are fairly common. The pods are elongated and in all areas are sub-parallel to the S2 foliation planes.

In Fetlar there is no exposure of the moho plane and thus the orientation of the dunite pods and S2 planes with respect to the moho plane and the crustal layers cannot be determined.

In the Crussa Field, Muckle Heog, and Little Heog Blocks of Unst the moho plane is exposed. In all these areas the S2 planes and the dunite pods are sub-parallel to the vertical, approximately east-west striking moho plane.

Even though the dunitic pods are sub-parallel to S2, the shear deformation has not been particularly intense as the commonest Peridotite Unit textures are coarse or porphyroclastic. This suggests that the pods are close to their original pre-deformational orientation, (i.e. sub-parallel to the moho), which is coincidentally sub-parallel to the S2 foliation planes.

As already discussed in Chapters 2 and 3, the dunites and harzburgites of the Peridotite Unit have very similar mineralogical compositions (mainly olivine). Thus at upper oceanic mantle type conditions (see Chapter 6) they will have very similar competencies and will behave essentially as a single unit during deformation. Because of this, folds between the dunite and harzburgites should only be expected where the S1 orientations indicate the presence of a D2 fold, by a sudden change in strike. Most of the dunite pods do not cross these D2 fold axes. Two of the pods mapped, however, do have a possible folded shape and these may easily have D2 fold axes cutting through them. (Figure 4.9). One of these pods is in the Crussa Field Block and is only 50 metres in length (NGR 615097); the other pods is on the shore-line of the Little Heog Block (NGR 645109) and is at least 300 metres in length.

b) Dunite sheets.

In the Muckle Heog and Little Heog Blocks the exposure is particularly good in the top kilometre of the Peridotite Unit. In these areas dunite sheets of up to one metre thick are abundant.

The sheets are usually sub-parallel to the S2 planes as well as to the dunite pods described above. In some localities, however, there are anastomosing relationships, especially in the area close to the Moho boundary at the western edge of the Muckle Heog Block. (Around NGR 620102). Some of the anastomosing relationships seen are shown in Figure 4.10. In these areas the dominant orientation of the dunite sheets is still sub-parallel to the moho.

In the Shetland Ophiolite there are no distinct 'feeder' zones of dunite sheets as in Cyprus. Instead the dunite sheets and pods have a more dispersed distribution over most areas of the Peridotite Unit.

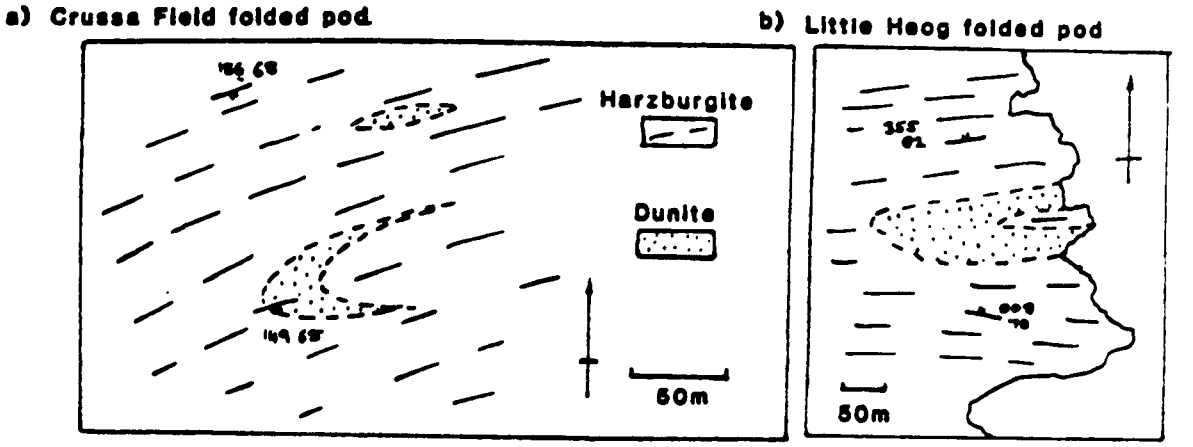

Figure 4.9 Sketch of dunite pods folded by the D2 deformation.

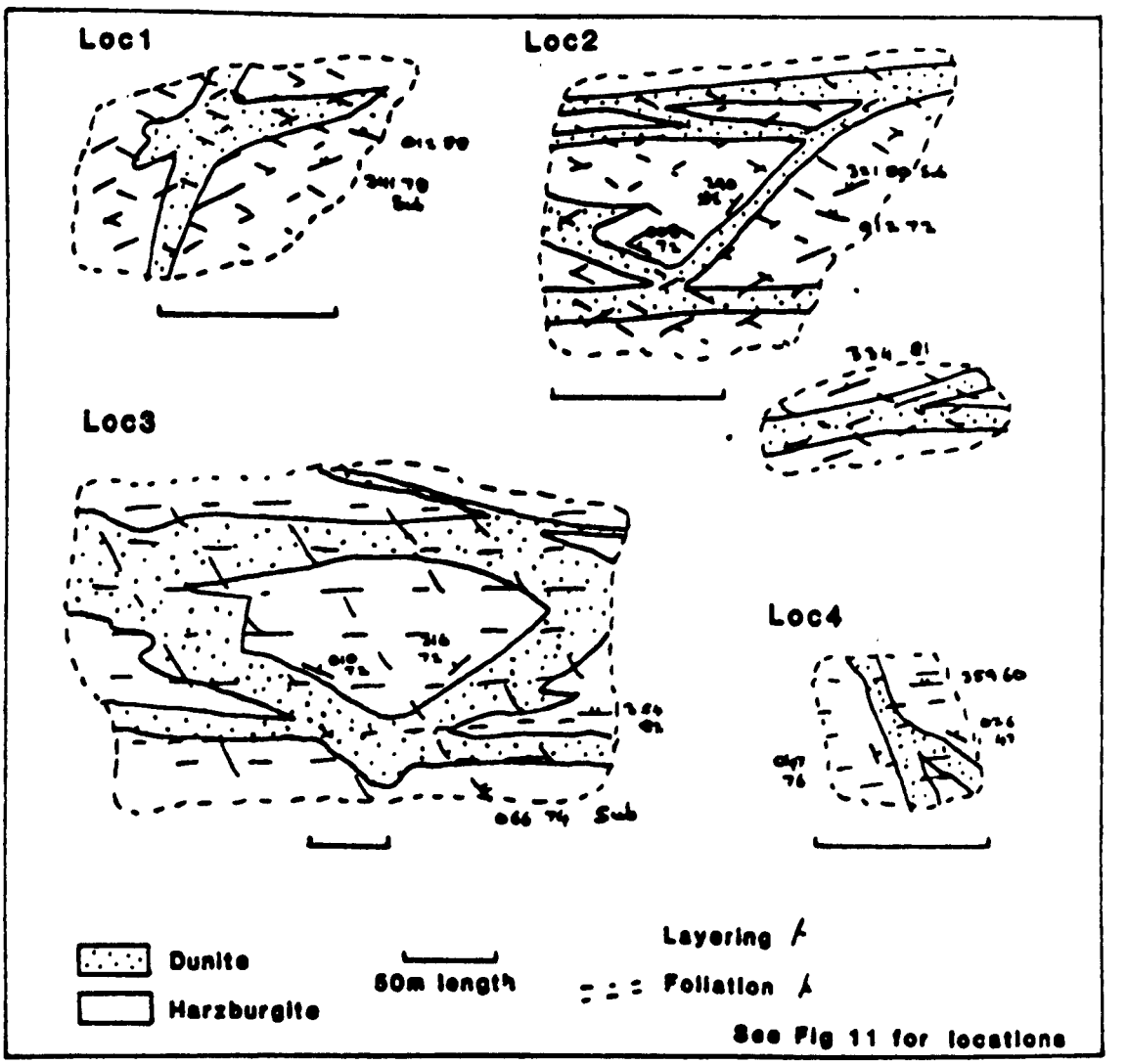

Figure 4.10 Sketch of some anastomosing dunite localities in the Peridotite Unit of the Shetland Ophiolite. See Figure 4.11 for localities.

c) Chromite Concentrations.

The location of chromite deposits in the Peridotite Unit of Unst are shown on Figure 4.11. They all occur within dunite pods and are mainly restricted to those pods within 500 metres of the moho boundary. In the Crussa Field Block there are two exceptions to this pattern with sizable chromite deposits in dunite pods at NGR 616120 and NGR 608111. No major chromite deposits have been found on Fetlar.

The more sizable deposits are composed of massive chromitites with the layering always sub-parallel to the dunite pod boundaries and the S2 trends. A full description of the Peridotite Unit chromite deposits is given in Prichard (1982).

d) The Clibberswick Hill Block.

Unlike the other blocks containing the Peridotite Unit in both Unst and Fetlar, the Clibberswick Hill Peridotite Block is largely devoid of either dunitic pods and sheets or chromite deposits.

This may indicate a deeper origin for the Clibberswick Hill Block, especially as no moho boundary or Lower Cumulate Unit is present.

4.5.2 The Moho Plane.

The area in the vicinity of the moho plane has been especially well exposed in the Muckle Heog Block. This area is shown on Enclosure 12.

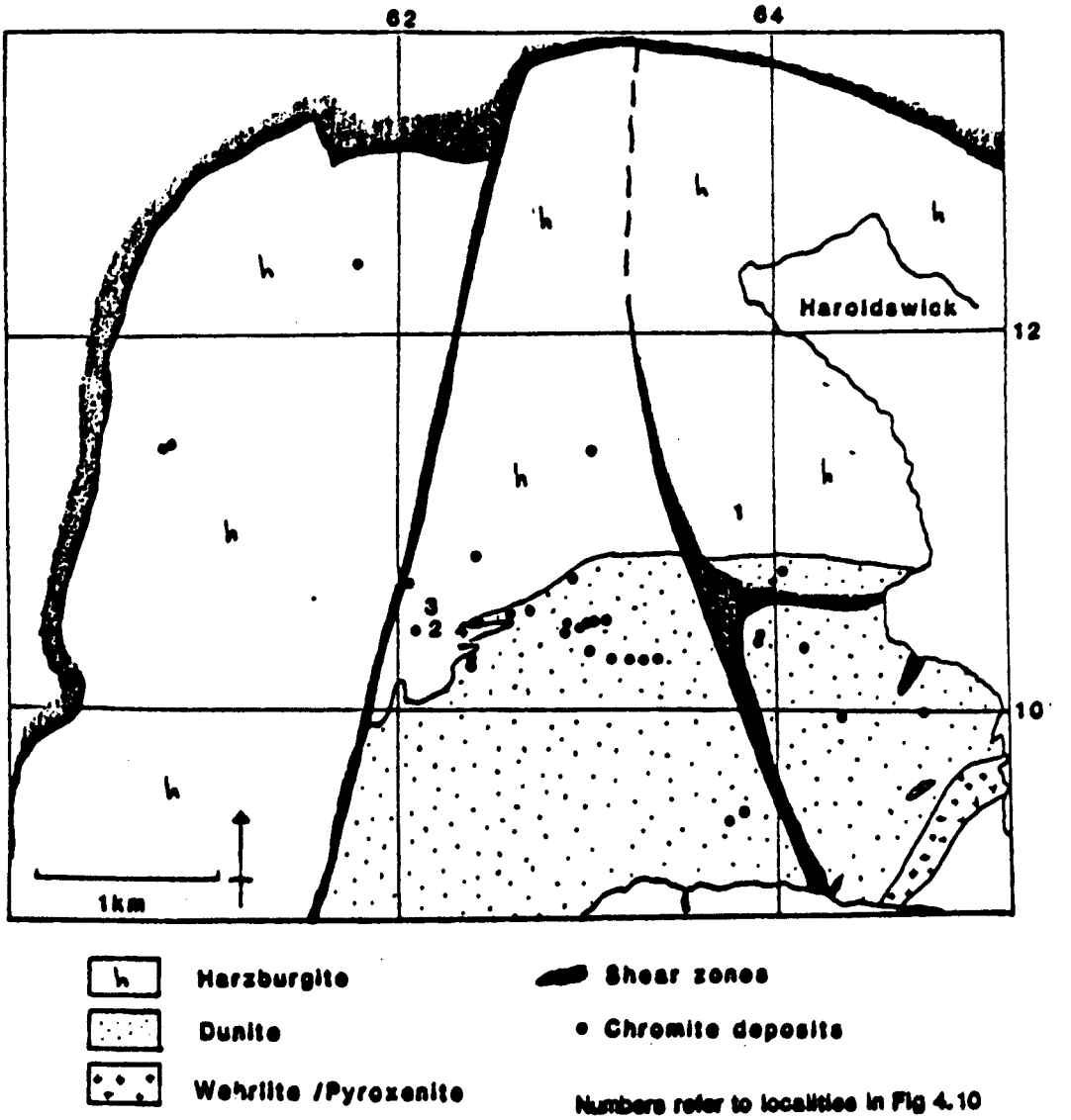

Figure 4.11 The localities of chromite deposits on Unst (after Prichard, 1982). Numbers refer to localities in Figure 4.10.

The moho plane has a sub-vertical dip along its entire length in the Muckle Heog Block. Its strike however, is highly variable on a small scale in the western side of the block.

In the east the moho plane has an east-west strike which gradually veers to a more ENE-WSW strike towards the west. There is no such strike change of the S2 planes which have a fairly constant approximately east-west strike over the entire moho area of the Muckle Heog Block.

In the vicinity of NGR 624103, the moho plane changes rapidly in attitude to give a folded type of pattern (See Enclosure 12). An examination of the S1 and S2 trends in this vicinity shows that the areas of rapid moho plane orientation change may possibly correspond to D2 fold axial plane traces. (See Enclosure 29 and Chapter 7). This is strong evidence for the small scale folding of the moho plane. (See Figure 4.12).

Further to the west of this zone of moho folding there is an embayment of Lower Cumulate Unit Dunite which extends 200 metres into the Peridotite Unit. The southern 1:250 area was mapped from this embayment zone. (See Enclosure 15).

Enclosure 15 indicates that even though the strike of the S1 planes varies, it is dominantly NW-SE and only N-S in thin zones. This implies that there are no major D2 folds through this area. The dunite-harzburgite boundaries may possibly be folded on a very small scale by minor D2 folding shown by the thin zones of variable S1 strike. (Figure 4.13).

This embayment feature is thus most probably a relict pre-deformational feature. It may be due to the intersection of a dunite pod of the

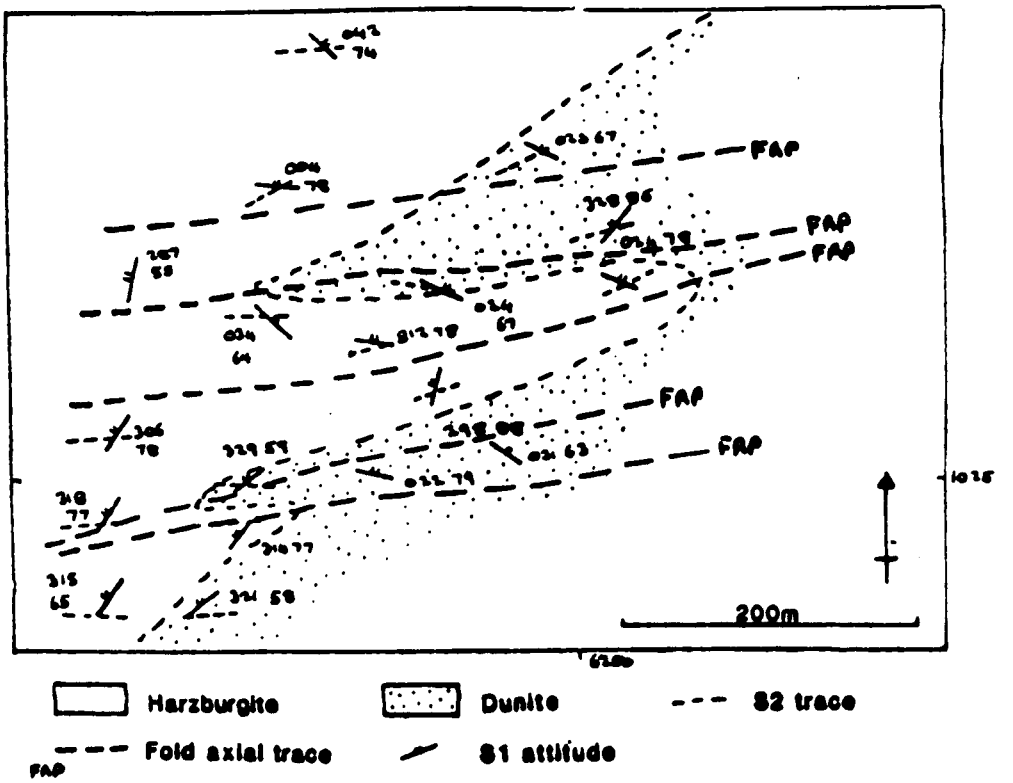

Figure 4.12 Sketch map of an area of small-scale folding of the moho plane in the Muckle Heog Block.

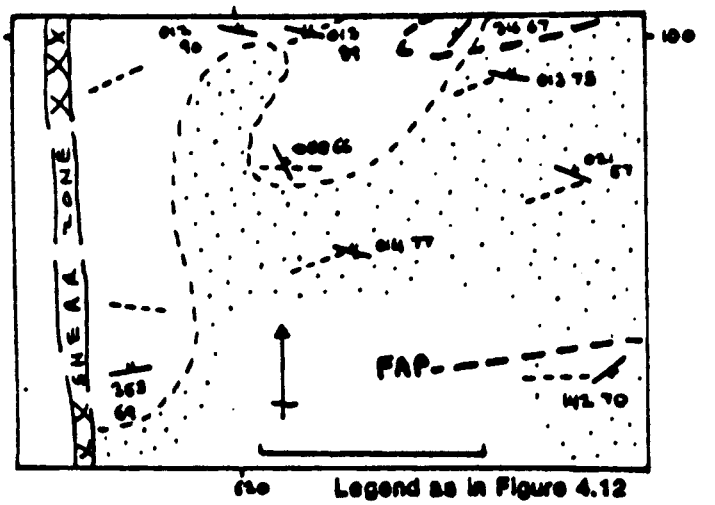

Figure 4.13 Sketch map of the dunite embayment of the Muckle Heog Block showing a possible small-scale folding of the dunite-harzburgite contact.

Peridotite Unit with the main Cumulate Unit dunite - similar to the relationships observed on the Troodos Ophiolite but on a much smaller scale. (See Chapter 3.5.1). Unfortunately no chromite layers were found within this dunite embayment, the orientations of which might point to a possible origin of the embayment (i.e. whether it could have been a sub-moho cumulate chamber or a vertical feeder zone).

Elsewhere in Unst the moho plane has a constant strike for each of the blocks studied, but is poorly exposed.

4.5.3 The Lower Cumulate Unit.

In the Muckle Heog and Little Heog Blocks chromite has been extensively quarried from the dunites of the Lower Cumulate Unit. The location of these deposits is shown in Figure 4.11. All the deposits are within the zone of D1 and D2 tectonism. They all have an east-west strike and are sub-parallel to the S2 strike. (Prichard (1982) discusses the detailed petrography of these chromite deposits.)

The chromite layers in the dunites have been measured in detail from the Muckle Heog Block by Prichard (1982). They all strike east-west but have a fairly variable dip. (See Figure 4.14). This implies that the layers have been folded by the D2 deformation. The fold axial planes being parallel to the S2 planes. In the 400 metres of dunite adjacent to the moho the chromite layers are all sub-vertical. A few localities in this area show possible fold-closures of the chromite layers with a tight to isoclinal fold pattern. (Figure 4.15). It was not possible to measure any fold hinges.

In the dunites more than 400 metres south of the moho plane the dip angle of the chromite layers is highly variable with rapid changes of dip at fold closures (Figure 4.16, Plate 4.3). This large variation in dip angle may be relatable to a less intense D2 deformation in some areas, causing less rotation of the layering. The deformation mechanisms and S1, S2 and chromite layering relationships will be considered in greater detail in Chapters 7 and 8.

The best layering type features in the Lower Cumulate Unit are present on the Swina Ness peninsula at the eastern end of Balta Sound (NGR 650092) The layers are of dunite and wehrlite and comprise centrimetre thick bands as well as 100 metre thick units. They are all sub-parallel to each other and also to local chromite-rich layers within the dunite. They have a NE-SW strike and sub-vertical dip. Unfortunately the block containing these layers is separated from the Little Heog Block to the north by a fairly major east-west striking shear zone (See Enclosure 13). It is thus not clear whether these layers do in fact have a different strike to the moho plane or whether the block in which they are contained has been rotated with respect to the main Little Heog Block.

The S2 orientations from this block have a roughly NE-SW strike as compared to a more east-west strike for the Little Heog Block: This most probably indicates that there has been a rotation during emplacement between the two blocks, and that the layers were originally sub-parallel to the moho plane.

The contact between the ultramafic cumulates and the gabbros is an emplacement related shear zone in most of the areas mapped.

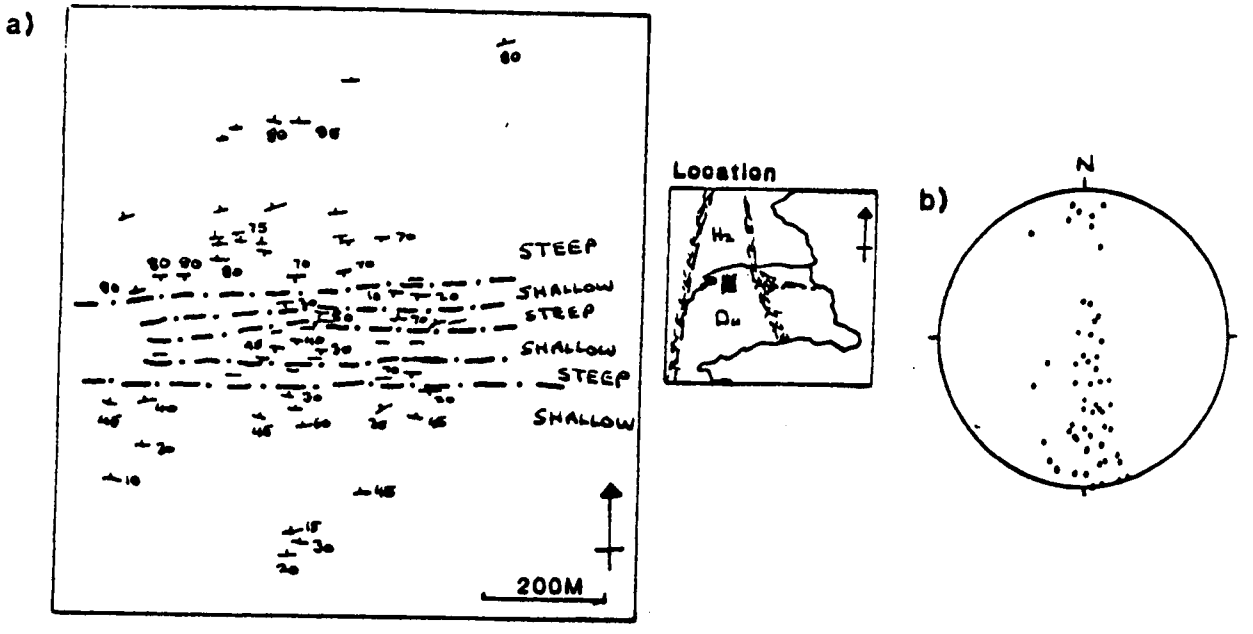

Figure 4.14 Chromite layer orientations in the Lower Cumulate Unit of the Muckle Heog Block. a) Sketch map; b) Equal area lower hemisphere projection of poles to layers. (After Prichard, 1982).

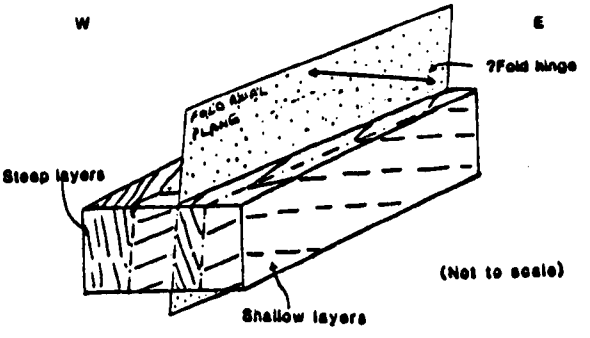

Figure 4.15 Folding pattern deduced from chromite layer orientations in the Lower Cumulate Unit of the Muckle Heog Block.

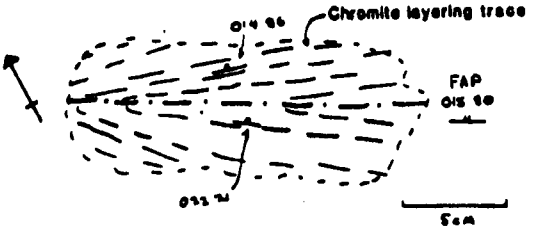

Figure 4.16 Sketch of locality 7. Open folding of chromite layers.

The only area where no shearing appears to have occurred is along northing 070 and between eastings 620 and 633. The exposure, however, is very poor near this contact and it is not clear whether its fluctuations are due to the presence of further shear zones or if they are a primary feature. (See Enclosure 13.)

As already mentioned in Section 4.3.2 the gabbros themselves are highly altered and poorly exposed. On most outcrops a mineral alignment or relict layering is measurable. The layering usually dips steeply but has a highly variable strike. In the area close to the contact with the dunites the layering is sub-parallel to the east-west contact in some localities but in others is at a high angle to this contact. (See Enclosure 13). The mineral alignment in the dunites below this contact have similar variable trends. Neither the dunites nor the gabbros in this area have undergone D1 or D2 deformation.

Further south into the gabbros the relict layers have a more constant NE-SW strike. (See Enclosure 13). There are many NE-SW striking later shear zones running through this area with a prominent associated NE-SW striking fracturing. Because of the poor exposure and high degree of alteration, the relationships between the gabbro layers and these shear zones is uncertain.

It is not possible to state whether the variation in gabbro layering orientations define the geometry of relict magma chambers as is possible in Oman. (See Chapter 2).

4.6 Summary of the Primary Structural Trends and Distribution of the Petrological Features of the Lower Ophiolite Sequences of Shetland.

The various petrographic and structural features of the areas studied in the Shetland Ophiolite are shown on Figure 4.17.

The constantly orientated S2 planes are sub-parallel to the moho boundary, which strikes roughly E-W and has a vertical dip, in all the areas studied. The moho plane has been locally deformed on a small scale by the D2 folding, the fold axial planes of which are defined by the areas in which the S1 planes rapidly change in their orientation.

Dunitic bodies within the Peridotite Unit are sub-parallel to the moho plane, as are layering features in the lowermost Lower Cumulate Unit. The Peridotite Unit immediately below the moho has an abundance of dunite pods and thinner layers, some of which show anastomosing relationships. These layers and pods decrease in abundance away from the moho plane.

Massive chromite is found in a few of the Peridotite Unit dunites, but is more abundant in the lowermost kilometre of the Lower Cumulate Unit dunites. The chromite layers are sub-parallel to the S2 planes and occasionally define fold closures.

In Unst the degree of alteration of the ophiolite blocks gradually increases from north to south. This alteration and extensive late stage shearing obscures the ultramafic - gabbro boundary, and also the primary layering orientations of the gabbros and adjacent ultramafic cumulates.

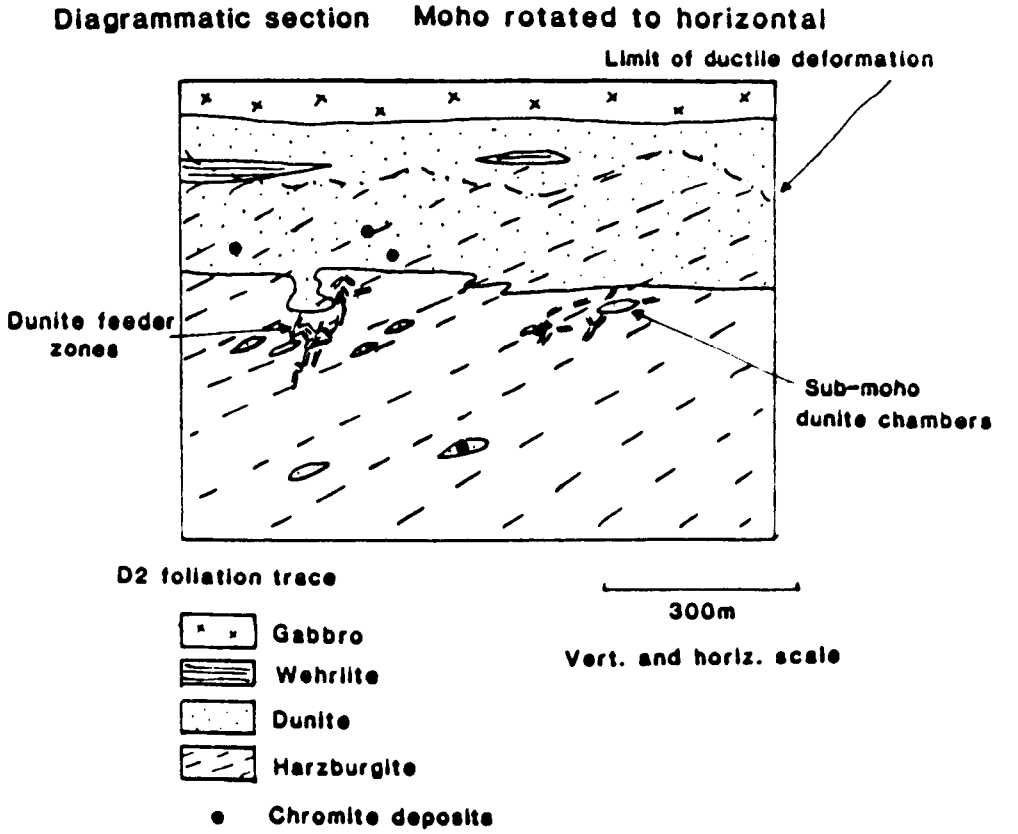

Figure 4.17 Summary of the petrological and structural features of the Shetland Ophiolite.

The Clibberswick Hill Block of Unst is composed entirely of Peridotite Unit and thus its original structural orientations with respect to the moho plane cannot be seen. This also is the case in Fetlar. In both areas, however, the parallelism of the S2 planes with the dunitic pods and layers suggests a relationship similar to that in the other ophiolite blocks of Unst.

The D1 and D2 deformational styles and directions are studied in detail in Chapter 7. These studies and the results from this chapter are considered together in an ocean-spreading context in Chapter 9.

Chapter 5

The Structural and Petrological Features of the Three Lower Ophiolite Sequences - Similarities and Differences.

CONTENTS

A comparison of the last three chapters shows that each of the lower ophiolite sequences studied have similar petrographic and structural features, but that their detailed relationships and orientations are unique to each complex, and for Oman, within each area studied of the Oman Ophiolite.

5.1 Structural Features

In each of the areas studied, ductile tectonic structures are present throughout the Peridotite Unit. These structures extend into the Lower Cumulate Unit by various amounts which vary from area to area. The ductile structures are mainly foliations and lineations as defined from the three-dimensional attitudes of minerals in the field. There are no folds in the massive harzburgites and dunites of the Peridotite Unit except for in a few of the more competent pyroxene rich dykes.

In the three complexes studied the ductile foliations and lineations present in the Peridotite Unit and parts of the Lower Cumulate Unit are ocean-spreading related features. The structures related to the emplacement of the different ophiolite sequences are restricted to localized zones within each ophiolite. These structures are mainly brittle fracture and fault zones but also include more ductile-type shear zones in the Oman and Shetland Ophiolites. They are all much later structures than the pervasive ductile foliations and lineations of the Peridotite Unit.

The pyroxene-rich dykes, the number of which vary in each of the three Peridotite Units, are largely undeformed by the pervasive shearing deformations. In Oman these dykes have been attributed to 'off-axis' magmatic activity (Boudier and Coleman, 1981) which formed late intrusive and extrusive complexes within higher levels of the ophiolite sequence. In Cyprus and Shetland the undeformed pyroxene-rich Peridotite Unit dykes most probably have a similar relationship to those in Oman. The fact that these dykes are undeformed and are relatable to slightly off-axis magmatic activity implies that the deformations forming the pervasive foliations and lineations must have occurred at or very close to an accretionary margin. (Either an oceanic or back-arc basin spreading centre.)

The deformational conditions at an accretionary margin within the Peridotite Unit will be ideal for ductile flow processes to occur within the ultramafic rocks. Temperatures and pressures will be high relative to crustal areas and mantle areas not in the near vicinity of an accretionary margin. These high temperatures and pressures combined with fairly low strain rates are most likely to cause a ductile shearing deformation of the mantle rocks.

In order to study the deformation styles and mechanisms which have been active in the Peridotite Unit rocks, detailed thin section and crystallographic studies have been performed on various specimens from the three areas of study. Previous work on the experimental and natural deformation of mantle type rocks in the ductile state is firstly described in Chapter 6,

and is then used in the studies on the specimens collected from the three field areas; the methods and results of these studies are described in Chapters 7 and 8.

In the three areas studied, the field structures indicate that two ductile deformational events have been active in most of the Peridotite Unit areas. The intensity of shearing is highly variable within and between each area, with no common relationship between shearing intensity, deformational event, and depth from moho. The detailed small-scale relationships between the two deformational events are considered in Chapters 7 and 8.

5.2 Petrological Features

Apart from the late pyroxene-rich dyke intrusions which are mainly undeformed, all of the petrographic features of the Peridotite Units studied were either formed pre-or syn-deformationally.

Similar petrographic features are present in the Peridotite Units of the three ophiolites studied. However, their size, shape and distribution are highly variable between the different ophiolites.

5.2.1 Segregation Layers.

In all the complexes these diffuse olivine-and orthopyroxene-rich layers are always sub-parallel to either the S2 foliation or the S1 foliation in areas where there has been no D2 deformation. The layers are rarely more than 10cm thick in all areas.

In Oman and Shetland segregation layers are fairly common in all the Peridotite Units areas studied. In Cyprus, however, the harzburgites are more massive with a distinct segregation-type layering being largely absent.

In all areas the Peridotite Unit segregation layers are only present within the harzburgites and nowhere extend into the dunitic bodies and sheets. This could imply that they have been formed prior to the intrusion of the dunites; but as dunite is composed only of olivine and trace amounts of spinel, it is not possible for segregation type layers to form within the dunites. However, the sharp and regular contacts between the intrusive dunites and the massive harzburgites that have been observed from all areas within the Peridotite Unit suggests that the layers have indeed formed prior to the intrusion of the dunites.

The strong parallelism to S1 or S2 foliations and the diffuse nature of the segregation layers suggests that they are not intrusive features but have been formed in situ. It appears unlikely that the layering is solely the product of a mechanical segregation accompanying deformation (ie. a 'flow layering'), as the layering is only sporadically developed in some areas whereas a similar deformational style is found throughout the Peridotite Unit. The most likely mechanism for the origin of the layering is that proposed by Dick and Sinton (1979) of a metamorphic differentiation accompanying deformation and anatexis of the harzburgite. Orthopyroxene undergoes dissolution and precipitation during pressure solution creep and partial

melting, and forms pyroxene-rich and poor layers by the development of low and high strain domains. Figure 5.1 shows the schematic representation by Dick and Sinton (1979) of metamorphic differentiation in harzburgites which is analgous to similar processes in low grade metamorphic rocks.

5.2.2 Dunitic Bodies and Sheets.

The sharp contacts between the dunites and the surrounding harzburgites indicates that they have a different origin from that of the segregation layers.

The thickness of the dunitic sheets is highly variable, and in areas of low ductile deformation they have variable attitude, are not sub-parallel to the S1 or S2 foliations, or to the moho plane, and occasionally have an anastomosing relationship. An intrusive origin is the most likely explanation for these dunitic sheets which occur in distinct zones in each Peridotite Unit studied.

In areas of more intense deformation the sheets still have sharp boundaries but they have been rotated into sub-parallelism with the foliation planes.

In areas of low deformation the zones of dunitic sheets often connect up with larger dunitic bodies which are ellipse shaped with their long dimensions sub-parallel to the moho plane. As deformation becomes more intense the dunite bodies become more elongate and are rotated by various degrees into the foliation plane.

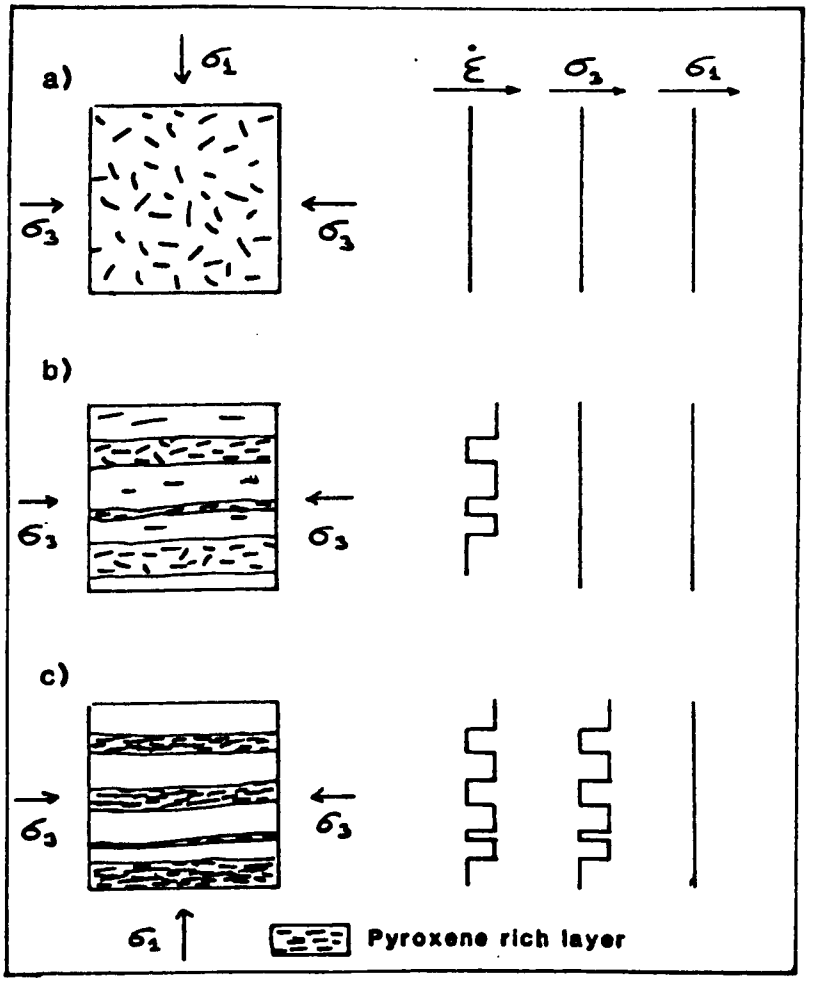

Figure 5.1 A schematic representation of metamorphic differentiation in harzburgites.. (After Dick and Sinton,1979). a) State of stress (σ) and strain rate ($\dot{\epsilon}$) prior to metamorphic differentiation; b) Formation of alternating pyroxene-rich and pyroxene-poor layers following the development of high and low-strain domains; c) Extreme enrichment and depletion of pyroxene accompanied by a local stress drop in the more mechanically resistant pyroxene-rich layers.

The large size of some of these dunite bodies (up to 1500 × 300 metres in Cyprus) and their parallelism to the moho plane in areas of low deformation, unlike the smaller dunitic intrusive sheets, makes it difficult to propose an intrusive origin for them. Their sizes and shapes are more like cumulate chambers in which magmatic settling processes could have occurred.

Unfortunately, all the dunite bodies have undergone some degree of deformation and no cumulate-type textures have been observed in them. In some of these bodies, especially in Cyprus, large chromite deposits have been formed. These form layers which are sub-parallel to the base of the dunite body and moho plane in areas of low deformation. Mineral grading is occasionally preserved in the chromite rich layers which may be a relict feature of a magmatic settling type process.

Thin seams of chromite (up to 4cm thick) are sometimes present in the centres of the intrusive sheet dunites. These are parallel to the dunite sheets and do not show a mineral grading.

It is clear that chromite can form layers either as thin seams within intrusive sheets or as thicker deposits within possible cumulate chambers below the moho plane. A detailed study of the chemistry, textures and structures of chromite deposits is at present being carried out by an E.E.C. funded group. They will hopefully provide strong evidence for the cumulate origin of some Peridotite Unit chromite deposits.
(Pers. Comm, S. Roberts.)

In all areas the dunite sheets have been intruded and the dunite bodies have crystallized either during or before ductile deformation. In areas of fairly intense ductile shearing the shapes and orientations of the dunites are strongly controlled by the orientation of the foliation planes. In areas of less intense shearing the dunites have been less rotated and elongated by shearing, but the foliation planes still cut straight through both the dunites and harzburgites (Figure 5.2).

It is not possible to determine the intrusive relationships between different dunitic bodies and sheets from most areas, but in Cyprus temporal intrusive relationships have been observed between different dunitic sheets both in the Peridotite and Lower Cumulate Units. This implies that there has been more than one dunitic intrusive event, all events occurring before or during shearing deformation.

5.2.3 Petrological Features of the Lower Cumulate Unit

The lithologies of the Lower Cumulate Unit are highly variable in each ophiolite complex studied. In each ophiolite the Lower Cumulate Unit is not a simple layered sequence but a complex series of both temporally and spacially related cumulate chambers and later intrusive features.

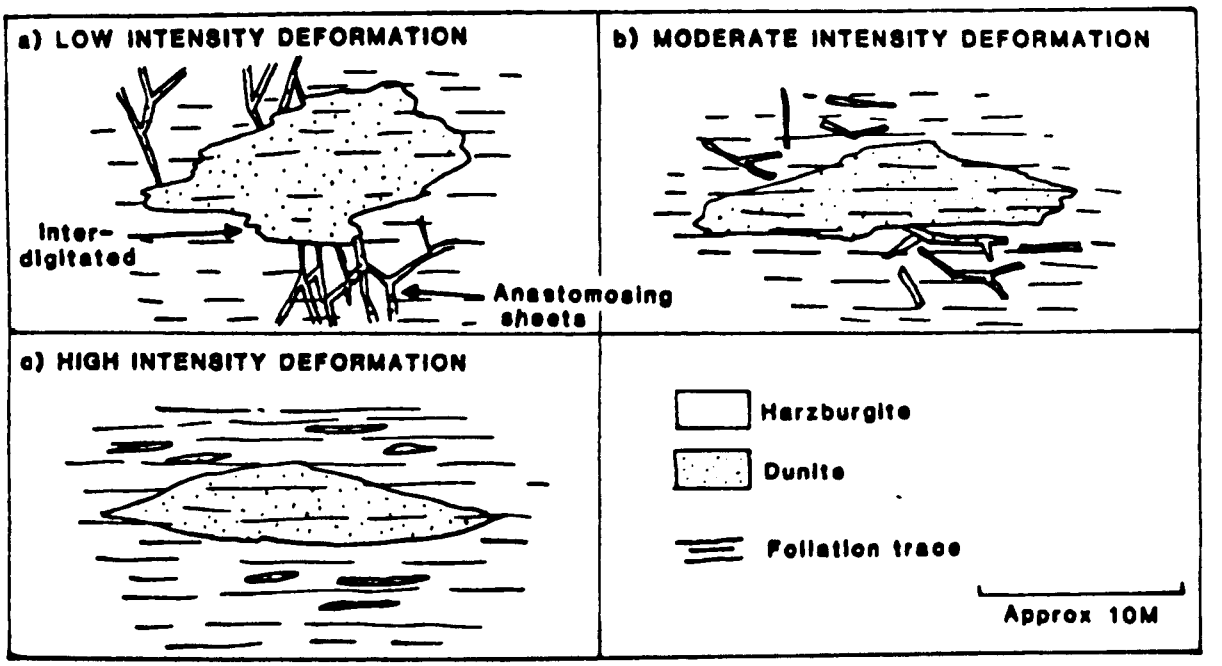

Figure 5.2 The progressive deformation of dunite bodies and sheets within the Peridotite Unit.

In all areas within the zone of ductile tectonism, all of the layered and intrusive feature have been deformed; ie. deformation occurred after the cumulates had formed. This fact is important when relating the deformational events to an ocean spreading situation. (See Chapters 9 and 10.)

5.2.4 The Moho Boundary

The moho boundary is purely a petrological feature of the boundary between the Peridotite Unit and the Lower Cumulate Unit. In all areas studied the moho is a constantly dipping plane once the presence of sub-moho cumulate chambers has been taken into account.

Both the D1 and D2 structures cut straight through the moho boundary in all areas, and in no area is there any intense ductile shearing localized along the moho plane. In Oman there has been some minor brittle movement along the moho plane associated with the Oman Ophiolite emplacement.

5.3 Main Conclusions

In the three areas studied it is clear that similar events have occurred to form the petrological and structural features observed from the field and thin sections.

Within the Peridotite Unit there is an intrusive relationship between the dunites and harzburgites, which most probably took place while deformation processes were active.

The ductile structures measured from the ophiolite complexes are the only relicts of what was probably a complex deformational history, and it would be more realistic to define the two shear deformational events recognised as D(x+1) and D(x+2). In other words they are the last two events of a whole series of deformations.

The next section of the thesis is an attempt to define more accurately the mechanism of plastic shear deformation within the Peridotite Unit, and the directions of senses of, and interactions between the different shear deformational events. In order to do this specimens were studied in detail from all of the ophiolites studied. As the deformational styles are very similar, each area is not considered individually, as in the previous chapters, but all are considered as a whole.

PART 2

Methods and Results of the Structural Analysis of Specimens.

Chapter 6

Plastic Deformation of the Upper Mantle and Lower Crust - a Review of Theoretical, Experimental and Observational Studies.

CONTENTS

Chapter 6.

The D1 and D2 field structures and thin section textures of all the three areas studies indicate that they were formed by plastic deformation processes. Before reviewing the experimental and natural studies of upper mantle type rocks and minerals, a brief summary of the theoretical aspects of plastic deformation is presented below.

6.1 The Theoretical Aspects of Plastic Deformation.

6.1.1 General Relationships.

It is easiest to consider plastic deformation as a flow process when considering the plastic deformation of rocks. Flow is a process of transport of matter which is driven by stress. At a constant volume, the flow of plastic solids is analagous to that of viscous fluids and is essentially a shear process.

The velocity of flow or shearing is expressed as the strain rate (or rate of shear): $\dot{\varepsilon} = \frac{d\varepsilon}{dt}$, where ε is the strain and t is time. Hart (1970) has shown that it is possible to write an equation of state:

$$f(\sigma,\dot{\varepsilon},\varepsilon,T) = 0$$

where σ is the applied stress, $\dot{\varepsilon}$ is the strain rate, ε is the strain and T is the temperature.

The mechanical parameters describing plastic flow are thus the applied stress (σ) and the strain rate ($\dot{\varepsilon}$). In experimental studies one of these parameters must be kept constant. In

compression tests the sample is forced to deform at a constant $\dot{\varepsilon}$, and in creep tests a constant σ is applied.

In both of these tests the physical parameters (temperature (T) and pressure (P)) are held constant. If in a creep test with constant σ, the $\dot{\varepsilon}$ is also constant, then the system is in a steady-state flow condition. This is an important condition of flow and will be considered below. Steady-state flow is achieved in a compression test when the σ reaches a constant value.

At high temperatures, various flow models have been proposed. The models rely on the competition between two elementary processes: work hardening and recovery.

Work hardening occurs when the material being deformed does not behave in a perfectly plastic manner as is the case for most geological materials. It is the process in which the more a material is deformed the more difficult it is to deform. This occurs because the plastic limits of a pre-strained solid is higher than the elastic limit it had when first strained.

For a given strain or stress, work hardening is defined by the work hardening coefficient (h):

$$h = \frac{d\sigma}{d\varepsilon} \tag{6.1}$$

and represents the slope of a stress-strain curve at a point (σ,ε) (Figure 6.1). A positive work hardening coefficient means that deformation at a given strain rate can go on only

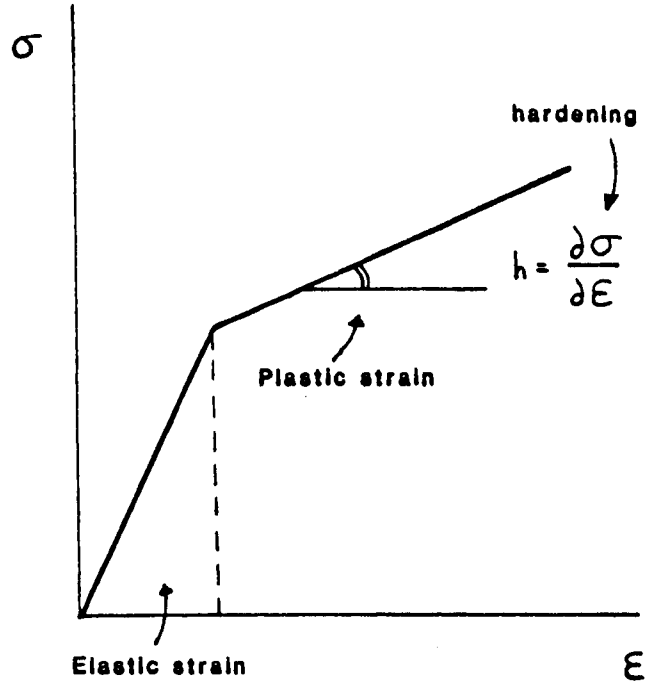

Figure 6.1 Stress-strain curve at constant strain rate.

if the applied stress increases with time at an instantaneous rate:

$$\text{i.e.} \quad \left(\frac{d\sigma}{dt}\right)_h = \frac{d\sigma}{d\varepsilon} \cdot \frac{d\varepsilon}{dt} = h\dot{\varepsilon} \tag{6.2}$$

Recovery is the process which works against work hardening. It allows deformation to proceed by relieving the internal stresses that lead to work hardening, mainly by thermally activated processes. The continuation of crystal slip processes is thus possible at a lower stress when recovery as well as work hardening is taking place.

A recovery rate (r) can be defined as:

$$r = \left(\frac{d\sigma}{dt}\right)_r \tag{6.3}$$

i.e. The rate at which the flow stress will decrease with time for zero strain rate. In general, the recovery rate increases with temperature and decreases as hydrostatic pressure increases.

The overall effect of the competition between work hardening and recovery in a rock deforming by plastic flow can be deduced from the sign of the expression:

$$h\dot{\varepsilon} - r$$

From equations (6.2) and (6.3) the expression $h\dot{\varepsilon}-r$ gives the relationship:

$$h\dot{\varepsilon}-r = \left(\frac{d\sigma}{dt}\right)_h - \left(\frac{d\sigma}{dt}\right)_r = \frac{d\sigma}{dt} \cdot \tag{6.4}$$

Four main cases of the overall effect of work hardening and recovery have been distinguished by Nicolas and Poirier (1976) (Table 6.1).

i) $h\dot{\varepsilon}-r>0$. This regime occurs at low relative temperatures (i.e. Temperature of solid (T) divided by temperature of melting of solid (T_m) is less than 0.3) as the recovery rate is low. The strain rate must be high in order to keep the $h\dot{\varepsilon}-r$ expression at a positive value. This low temperature, high strain rate type of plastic deformation occurs mainly in superficial crustal rocks. Nicolas and Poirier (1976) have compared this with the domain of cold working in metallurgical language.

ii) $h\dot{\varepsilon}-r=0$. This regime corresponds to the balance between strain hardening and recovery. It is the condition of steady-state flow and in constant applied stress conditions, the strain rate remains constant (steady-state creep). It typically occurs at high temperatures (high T/T_m ratio) and low strain rates, conditions that most probably prevail in the lower crust or upper mantle.

iii) $h\dot{\varepsilon}-r<0$. In this regime the recovery rate exceeds the strain hardening rate. Thus a material will offer less and less resistance to deformation. This is an unstable regime and will lead to catastrophic failure of the material being deformed.

iv) $\underline{h\dot{\varepsilon}-r\cong 0}$. In a material undergoing plastic deformation at high temperatures and high strain rates, the strain rates are high enough to increase the strain energy sufficiently.for recrystallisation to take over from recovery. The process of strain induced recrystallisation is also known as annealing. The newly crystallised grains are rapidly strain hardened and the process repeats itself again and again. Thus periods of strain hardening alternate with periods of recrystallisation which causes minor oscillations in both compression test and creep test plots. (See Table 6.1). On average, however, the flow is in a steady-state condition as in case ii). This condition is also most likely to occur in the deformation of lower crustal and upper mantle rocks. Nicolas and Poirier (1976) have compared this to the domain of hot working in metallurgical language.

Thus for plastic deformation conditions in the lower oceanic crust and adjacent upper mantle close to spreading axes, it is most probable that a steady-state flow regime has been present throughout plastic deformation, a steady-state being achieved by the interaction of strain hardening, recovery and recrystallisation processes.

		$\dot{\varepsilon}$ Constant	σ Constant
COLD WORKING Low T/T_M High $\dot{\varepsilon}$	$h\dot{\varepsilon} - r > 0$ Strain hardening, recovery	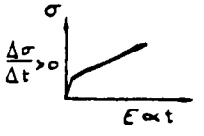	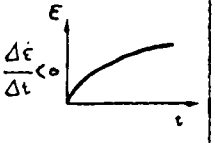
STEADY STATE FLOW High T/T_M Low $\dot{\varepsilon}$	$h\dot{\varepsilon} - r = 0$ Strain hardening, recovery	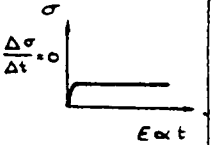	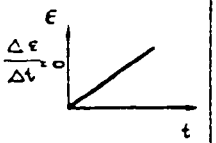
UNSTABLE FLOW High T/T_M Low $\dot{\varepsilon}$	$h\dot{\varepsilon} - r < 0$ Strain hardening, recovery	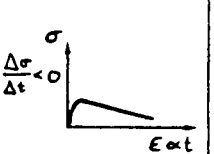	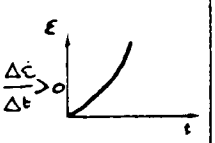
HOT WORKING High T/T_M High $\dot{\varepsilon}$	Strain hardening, recovery + Recrystallisation	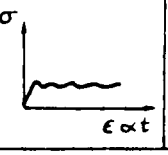	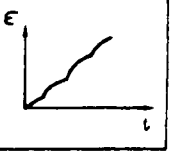

Table 6.1 Deformation regimes from the 'hε̇-r' relationship (From Nicolas and Poirier, 1976).

6.1.2. Steady-state Flow - Regimes of Flow (Creep).

As mentioned at the start of section 6.1.1, at a constant volume, the flow of plastic solids can be considered to be the same as that of viscous fluids.

In a steady-state environment the expression:

$$\dot{\varepsilon} = \alpha\sigma$$

is valid for constant temperatures. α is the fluidity of the material which is $\frac{1}{\eta}$ where η is the viscosity.

$$\text{i.e.} \qquad \eta = \frac{1}{\alpha} = \frac{\sigma}{\dot{\varepsilon}}$$

There are two main cases of steady-state flow or creep depending on the relationship between the fluidity and the shear stress (applied stress):

i) α = constant. α is independent of σ. This is the state of Newtonian viscous flow where the creep rate is directly proportional to the shear stress. On a stress-strain rate plot, the gradient (n) (or slope) of the line relating shear stress to strain rate in a Newtonian behaviour is equal to 1. (See Figure 6.2). This condition only occurs at low stresses, and at high relative temperatures. (T/T_m close to 1.).

ii) $\alpha = f(\sigma)$. At higher stresses the fluidity (or viscosity) depends on the shear stress. In general as the shear stress increases the fluidity increases (the viscosity decreases). The strain or creep

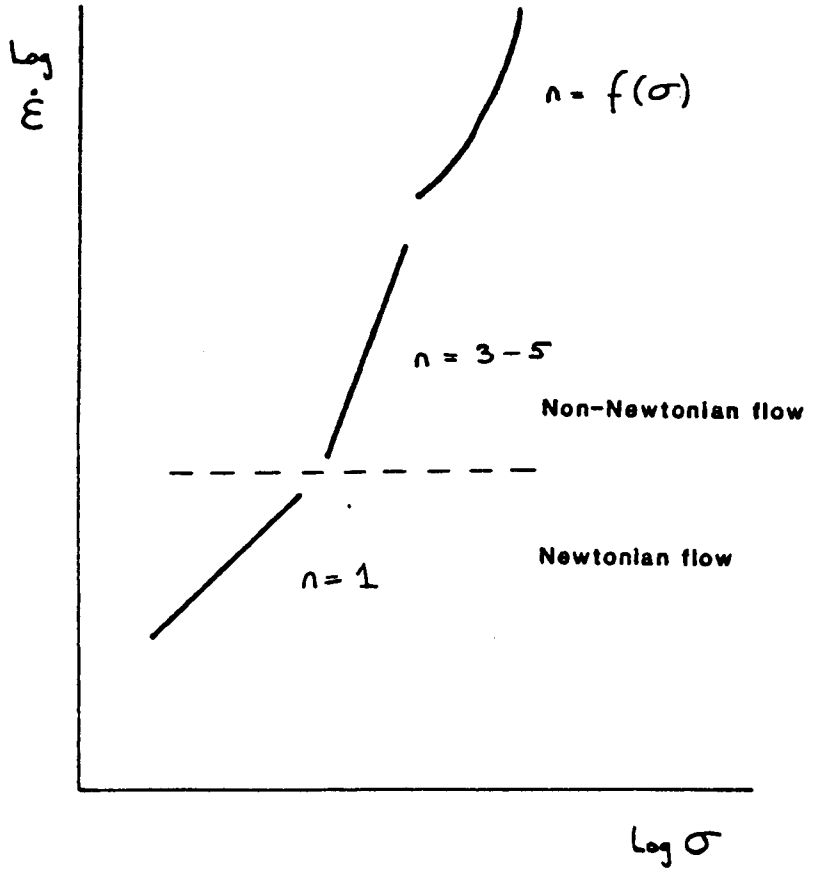

Figure 6.2 Viscous flow: log strain rate versus log stress. Slope n = 1, Newtonian flow; Slope n > 1, non-Newtonian flow.

rate is empirically expressed, for intermediate stresses, as a power function of σ:

$$\dot{\varepsilon} = \varepsilon_o \sigma^n \quad \text{for } T = \text{constant.}$$

where $n = \frac{\partial \ell n \dot{\varepsilon}}{\partial \ell n \sigma}$ and is the gradient of the stress-strain line as in i) above. n is an expression of the stress sensitivity of strain rate, and for intermediate stresses it commonly has a value between 3 and 5. (Figure 6.2)

Durham et al (1977) described non-Newtonian steady state flow as 'power law creep'.

6.1.3. Mechanisms of High Temperature Steady-State Flow.

Strain within a material undergoing high temperature steady-state flow (hot working) is caused by various mechanisms depending on the type of flow:

a) Newtonian Flow. (n=1). In Newtonian steady-state flow, strain is caused by the diffusional transport of matter between surfaces of crystals differently orientated with respect to stress. In other words the diffusional flow of matter between surfaces is stress induced.

Two main creep processes have been derived which are stress induced processes. Herring-Nabarro creep involves the diffusion of crystal atom vacancies through the grain between

two areas of its boundary: and Coble creep involves the diffusion of vacancies along the grain boundaries. A full explanation of these processes is given in Nicolas and Poirier (1976, Chapter 4). The Herring-Nabarro model has been further extended by Friedel (1964) and Nabarro (1967) to include the affect of different climb forces on diffusional transport.

b) Power Law Flow (n>1). The main process causing strain in conditions of power law flow is that of dislocation slip. The strain is due to the glide of dislocations in neighbouring parallel planes. As already discussed in section 6.1.1, steady-state creep can be attained only if recovery takes place. Weertman (1963) first proposed the model for creep by dislocation slip and called the process 'dislocation creep'. Nicolas and Poirier (1976) discuss the mechanisms of dislocation creep in detail.

Even though the strain is due to slip of dislocations in dislocation creep, the strain rate is still controlled by climb of the dislocations and thus by diffusion.

Dislocation creep is the most common mechanism for high temperature creep, Herring-Nabarro creep only occurring in materials extremely close to their melting point.

In both Newtonian and power law creep the strain rate is controlled by diffusion which can be expressed as a diffusion coefficient (D) for most materials, and is a function of stress. For power law creep the strain rate can be related

to the diffusion coefficient and the applied stress:

$$\dot{\varepsilon} = \dot{\varepsilon}_o \sigma^n D \qquad \text{where } n>1.$$

The above discussions show that for most crystalline materials at high to moderate relative temperatures (i.e. at lower crustal and upper mantle conditions) and intermediate shear stresses, plastic deformation occurs as a steady-state creep process for which $n>1$.

6.1.4 Recrystallisation Processes in Crystalline Materials Undergoing Steady-State Creep.

Experimental and natural studies have shown that in rocks undergoing steady-state power law creep, recrystallisation is an important process in the overall deformation process.

Recrystallisation could possibly be induced by either stress or strain. In both processes the driving force for recrystallisation is the difference in free enthalpy between the recrystallised and unrecrystallised states.

In stress induced recrystallisation (piezocrystallisation), the difference in free enthalpy is attributed only to the difference in elastic-strain energy between elastically anisotropic crystals in a favourable orientation and those in an unfavourable orientation in a non-hydrostatic stress

field. In piezocrystallisation the internal state of the crystals is the same before and after recrystallisation and they show no defects.

In strain induced recrystallisation (annealing), on the other hand, the difference in free enthalpy is attributed to the difference in stored plastic-strain energy due to the presence of dislocations generated during plastic flow and remaining trapped in the crystals; grain growth is due to the difference in total grain-boundary energy between a fine-grained and coarse-grained polycrystal.

A review of the various models which have been proposed for piezocrystallisation is given in Nicolas and Poirier (1976). Avé Lallemant and Carter (1970) presented piezocrystallisation as a mechanism for flow at high temperatures. The models of piezocrystallisation are mainly based on the work of Kamb (1959a). They rest on the assumption that the internal state of crystals is the same before and after recrystallisation, except with regard to elastic strain. Piezocrystallisation is thus incompatible with dislocation plastic flow and annealing recrystallisation as these processes lead to major internal crystal defects during crystal breakdown.

Avé Lallemant and Carter (1970) argue that piezocrystallisation is the operative mode of flow in upper mantle rocks (i.e. olivine rich tectonites), as the fabric observed in experimental studies and in natural rocks is the same as that predicted by the thermodynamic theory of Kamb (1959a) for

solids in the presence of an intercrystalline fluid. However, Nicolas and Poirier (1976) point out that Kamb (1959a) himself states that 'the type of preferred orientation expected in recrystallisation under stress is in most cases the same as would be expected in mechanical deformation of the same materials under the same uniaxial stresses'.

It would thus seem most likely that the main process of recrystallisation occurring in rocks undergoing steady-state power law creep is strain induced annealing recrystallisation which involves plastic strain and dislocation creep.

The annealing process causes the development of new, dislocation-free grains within a deformed polycrystal at the expense of strain hardened grains whose dislocation density is high. The annealing process involves nucleation and growth of new grains: either as a dynamic recrystallisation processes, which occurs during non-Newtonian steady-state creep (hot working) and acts as the softening process which competes with strain hardening (condition (iv) in section 6.1.1); or as a static crystallisation process, which occurs during stress-free high temperature annealing (cold working) of a material when the strain has exceeded a critical value. (i.e. condition (i) in section 6.1.1). Nicolas and Poirier (1976) review in detail the processes of annealing recrystallisation.

6.1.5 Expected Thin Section and Microstructural Features for Materials that have Undergone Deformation at Either Hot or Cold Working Conditions.

It is possible to determine the general conditions of deformation that a rock has undergone by studying the microstructures and thin section textures of the rock.

a) Rock which has undergone hot working (High temperature flow).

In the crystals of a rock that has undergone hot working, the grains will be divided into a polygonised substructure. This consists of slightly misorientated blocks (sub grains) which are relatively dislocation free, separated by dislocation walls.

At the grain boundaries the incompatability of deformation between neighbouring grains is relieved by diffusion accommodated by grain-boundary sliding. Localised grain-boundary migration often gives rise to a finer polygonisation at grain boundaries.

Recrystallisation, which is most likely to be annealing recrystallisation, occurs mainly at the grain boundaries where the strain energy is high.

In thin section these processes will produce mainly strain-free subgrains separated by sharp planar grain boundaries, and the presence of numerous polygonal neoblasts, the grain boundaries of which often intersect at 120^{o} triple points.

b) Rock which has undergone cold working

In crystals which have undergone cold working the dislocation densities are high with little evidence for dislocation climb or for recovery. In thin section the grains have highly undulose extinctions with kink banding a common feature. Recrystallisation only occurs rarely and is restricted to grain boundaries which are seen to be irregular under high magnifications.

c) Upper Mantle Rocks from the Studied Ophiolite Complexes Hot or Cold Working Regimes?

The thin section descriptions in Chapters 2-4 indicate that the Peridotite Unit, and possibly parts of the Lower Cumulate Unit, have undergone plastic deformation mainly under hot working conditions in all three areas of study.

Olivine is never seen to be kink banded and only the larger porphyroclasts have slightly undulose extinctions. Orthopyroxene is occasionally kink banded but more commonly the grains have been polygonised with variable amounts of recrystallisation.

The thin section textures and grain orientations are discussed in detail in Chapter 8.

6.1.6 Upper Mantle Flow - General Conditions

It is generally accepted that plastic deformation within the asthenospheric Upper Mantle, which occurs at shallow levels at a spreading axis, is a steady-state process. Cathles, III (1975) argues that the whole of the earth's Upper Mantle has a Newtonian viscosity of approximately 10^{22} poise except for a 75km thick low viscosity channel directly below the Moho, which has a viscosity of approximately 4×10^{20} poise. These results are based on isostatic adjustment studies of the earth.

Nicolas and Poirier (1976) summarize other studies on the viscosity of the earth's upper asthenosphere. All the results give a viscosity of between 10^{19} - 10^{22} poises for Newtonian flow conditions. (The viscosity remains constant in Newtonian flow).

Various calculations have been performed on the expected rate of shear in the asthenosphere (or creep rate) based on the lithospheric plate velocities and the thickness of the asthenosphere. (Summarized in Nicolas and Poirier, 1976) : -

$$\text{Creep rate} \quad \dot{\varepsilon} = u/t$$

where u = absolute plate velocity and t = thickness of asthenosphere. The results obtained lead to an estimated asthenospheric creep rate in the order of 10^{-15} to 10^{-13} sec^{-1}.

The theories discussed in sections 6.1.1 - 6.1.5 suggest that for asthenospheric mantle conditions, steady-state flow is most likely to be a power-law flow, as suggested by Twiss (1976), Durham et al (1977) and Nicolas (1976). Experimental work on the deformation of olivine (reviewed in section 6.2) also suggests that power law creep takes place in asthenospheric conditions with n between 3 and 5. (n = stress sensitivity of the strain rate: see section 6.1.2). The maximum creep rate attainable in laboratory experiments is 10^{-8} s^{-1} but extrapolation of the data down to asthenospheric creep levels (10^{-15} to 10^{-13} sec^{-1}) shows that power law creep is certainly possible in the asthenosphere (see section 6.2).

With power-law creep the viscosity does not remain constant as discussed above for Newtonian flow. In section 6.1.2 it was noted that as the shear stress increases the viscosity will decrease as :

$$\eta \text{ (Viscosity)} = \sigma/\dot{\varepsilon}$$

and thus the viscosity must be considered for a given strain rate or a given stress.

Nicolas and Poirier (1976) review the hypotheses and conclusions of recent studies on the theoretical flow mechanisms in the asthenosphere. (E.g. Carter et al, 1972; Kirby and Raleigh, 1973; Stocker and Ashby, 1973). These authors consider the various creep laws (Newtonian or power-law) and combine them with estimated mantle

geotherms. The viscosity is calculated for the various mechanisms of flow, and the mechanism for which the viscosity is lowest for given shear stresses and creep rates must be the dominant mechanism of flow.

Frost and Ashby (1981) have recently combined the work of previous investigations and have compiled deformation mechanism maps for olivine of various grain sizes. Figure 6.3 shows the deformation mechanism map for olivine for a grain diameter of 1mm. As can be seen, in asthenospheric conditions, the dominant mechanism of flow for olivine-rich rocks is power-law creep. As the grain size increases the field of power-law creep increases.

If one assumes that the dominant mechanisms for steady-state flow in mantle asthenospheric rocks is power-law creep, then the main process of flow will be by diffusion-controlled dislocation creep. (See section 6.1.3). This is the deformation of a crystal by slip along specific slip dislocation planes in a specific slip direction. The amount and direction of slip caused by the propagation of a dislocation on the slip plane is often expressed as a vector - the Burgers vector.

Within a crystal the energy of a dislocation is proportional to b^2 where b is the length of the Burgers vector. In orthorhombic crystals the length of the

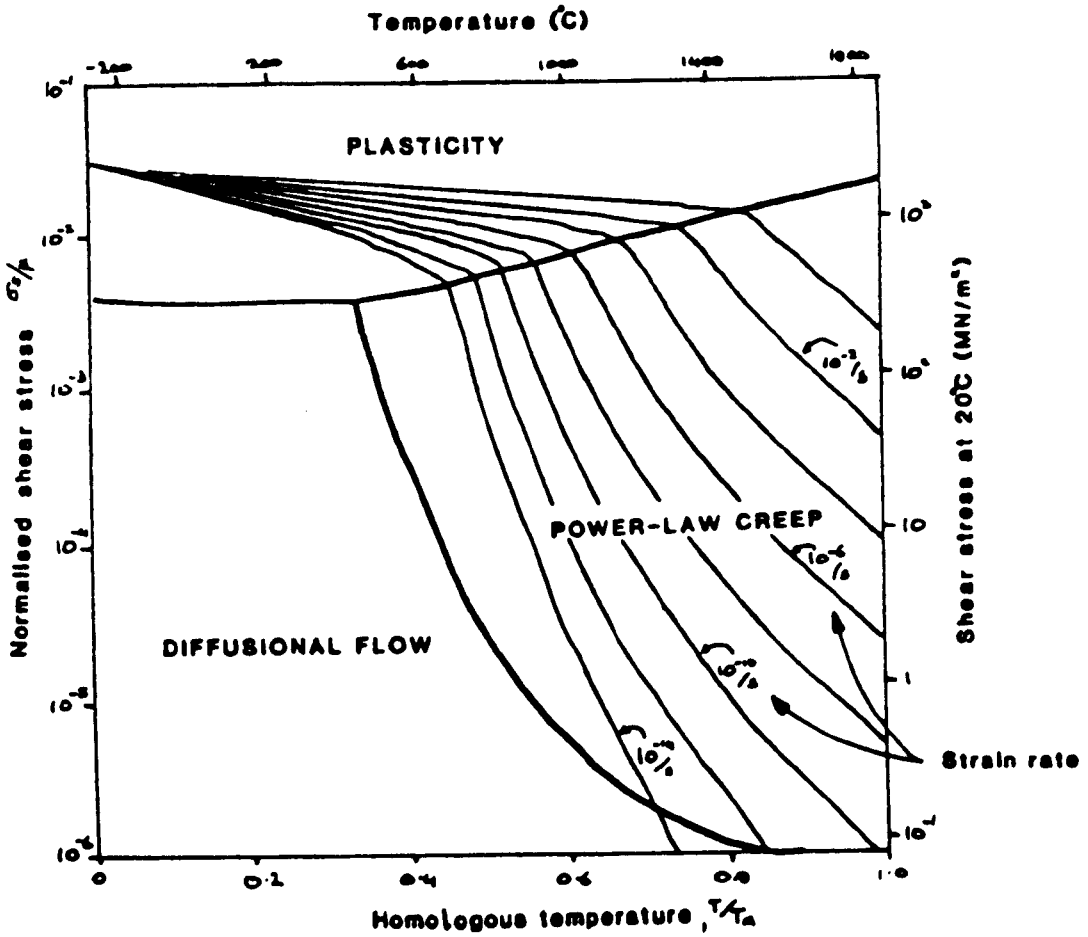

Figure 6.3 Deformation mechanism map for forsterite. (Stress versus temperature, grain diameter of 1 mm). (Modified from Frost and Ashby, 1981).

Burgers vector b is directly proportional to the dimensions of the lattice parameters of the unit cell. (As for olivine and orthopyroxene). Slip will most readily occur in the direction of lowest dislocation energy: i.e. in the direction of the smallest dimension of the unit cell. In these crystals the slip plane will be the densest crystallographic plane containing the slip direction.

Thus, if one assumes that olivine and orthopyroxene crystals of the Peridotite Units of the three areas studied have undergone power-law creep by diffusion-controlled dislocation creep, it should be possible to determine the operative slip planes and directions; and also what their orientations are with respect to each area. This is done by studying the crystallographic orientations of individual olivine and orthopyroxene grains within a thin section. This procedure is outlined in section 6.2 below.

6.2 The Application of the Theory of Asthenospheric Flow to Olivine and Orthopyroxene - Theoretical, Experimental and Observational Studies

In this section the crystallographic orientations of harzburgite minerals undergoing mainly dislocation creep flow processes are discussed.

6.2.1 Olivine

(a) Theoretical Slip Directions and Planes

Olivine is an orthosilicate and has full orthorhombic symmetry. The crystallographic habit and optical directions of forsterite are shown in Figure 6.4. Forsterite, the magnesium end-member of the olivine series, is the end-member closest to a typical Peridotite Unit olivine .

For forsterite the lattice parameters of the unit cell are:

a[100] = 4.76Å

b[010] = 10.21Å

c[001] = 5.99Å.

Dislocations with the [010] Burgers vector would have an energy approximately four times that of either the [100] or [001] Burgers vectors. The expected slip direction for olivine should thus be either [100] or [001].

The expected slip planes are (100), (011), (010) and $(0\bar{1}1)$, the most likely being (010). This is the only plane in which Si - O bonds do not have to be broken for slip to occur (Poirier,1975).

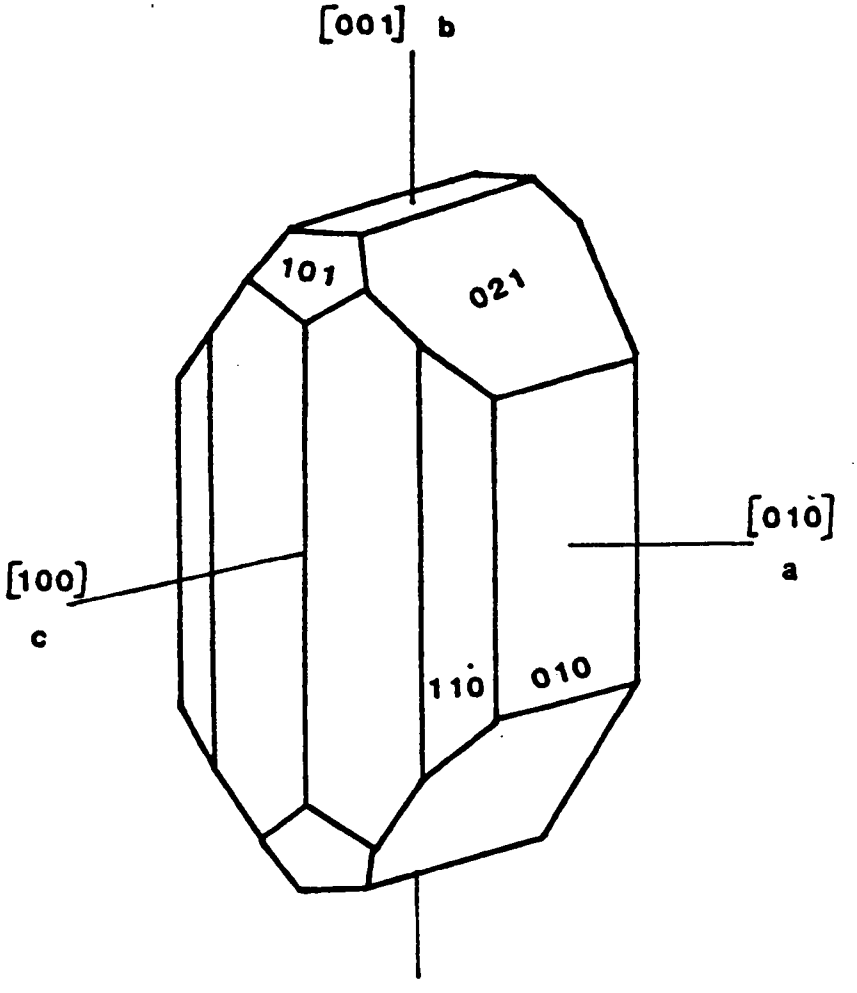

Figure 6.4 The crystallographic habit and optical directions of forsterite. (After Deer, Howie and Zussman, 1966).

(b) Experimental and Natural Studies on Olivine Slip Systems

An olivine crystallographic orientation was first recognised by Battey (1960) in a dunite from Dun Mountain, New Zealand. He showed that the olivine [100] crystallographic axis was parallel to the macroscopic fold axes and that [010] was perpendicular to the fold axes.

Initial experimental studies on olivine deformation were restricted to coaxial (irrotational) deformation. (Eg: Raleigh, 1968; Carter and Avé Lallemant, 1970; Green and Radcliffe, 1972; Nicolas et al, 1973). Carter and Avé Lallemant (1970) identified three major zones of different operative olivine slip systems, (Figure 6.5), from the experimental deformation of individual olivine crystals. Within the experimental conditions the slip system which is active largely depends on the temperature. At high temperatures the operative slip plane of olivine is (010) and the slip direction is [100]. At moderate temperatures the slip system is {0kl}[100], and at lower temperatures the dominant slip system is {110}[001].

The {0kl}[100] slip system was originally termed a 'pencil glide' type of movement (Raleigh,1968), but Nicolas and Poirier (1976) tie it down to a composite cross-slip type of movement on only a limited number of dense crystallographic planes such as (011), (010) and $(0\bar{1}1)$.

It must be noted here that all the experimental work on olivine slip systems has been carried out at much faster strain rates (greater than $10^{-8}sec^{-1}$) than the theoretically calculated asthenospheric strain rates (approximately 10^{-15} to $10^{-13}sec^{-1}$).

If the temperature-strain rate graph of Carter and Avé Lallemant (1970) is extrapolated back to asthenospheric strain rate, assuming that the boundaries between the different slip systems have a constant gradient, then the dominant slip system for dislocation slip of olivine at upper asthenospheric temperatures and pressures should be the (010)[100] slip system. (Figure 6.6)

In the study of the crystal slip systems which have been operative in natural peridotites from both ophiolite complexes and basalt zenoliths, which most probably have an asthenospheric origin, both the (010)[100] and {0kl}[100] olivine slip systems have been measured and related to the high temperature flow of the asthenosphere. (Eg: George, 1975 and 1978; Violette, 1980; Boudier and Coleman, 1980; Juteau et al, 1977; Girardeau and Nicolas, 1981; Prinzhoffer et al, 1980; Nicolas and Violette, 1982). The olivine [001] slip direction has rarely been observed in studies of natural rocks. Boudier and Coleman (1979) have measured the (110)[001] slip system as the operative slip system in the lowermost 2km of the southern Oman Mountains Peridotite Unit and relate it to a low temperature high stress environment present during sub-oceanic thrusting during obduction processes. Gueguen (1977) has observed the (110)[001] slip system in a few peridotite nodules from kimberlites which he relates to a late superimposed deformation.

Nicolas and Poirier (1976) have summarized the active slip systems of olivine determined from experimental and observational studies. They divide the slip systems into three purely qualitative domains depending on temperature and creep rate. Table 6.2 summaries these slip systems.

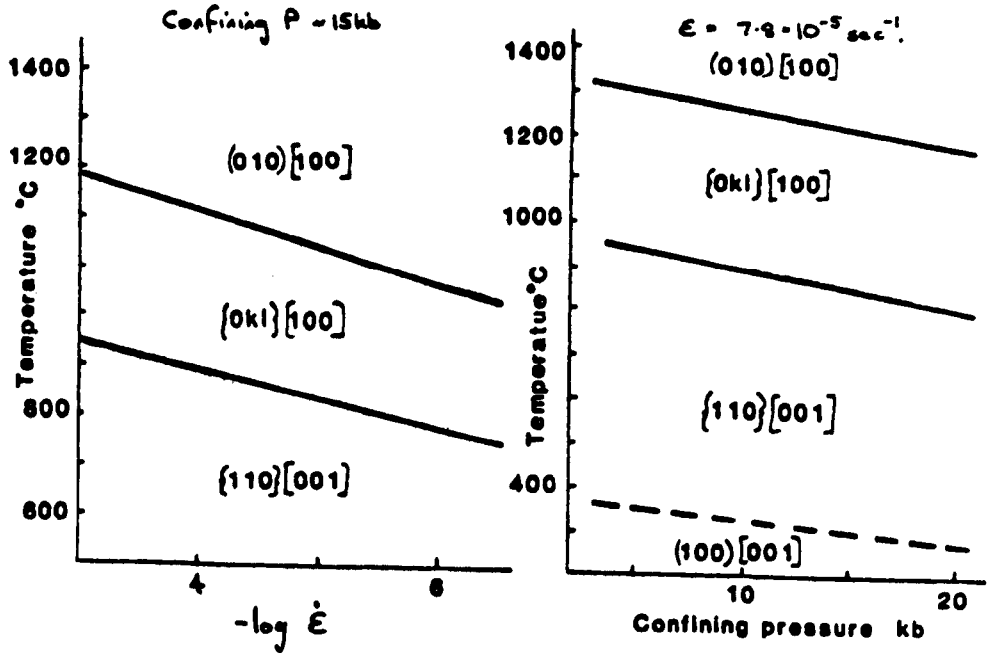

Figure 6.5 Predominant slip mechanisms in experimentally deformed olivine as a function of temperature and strain rate (a), and temperature and pressure (b). (After Carter and Avé Lallemant, 1970).

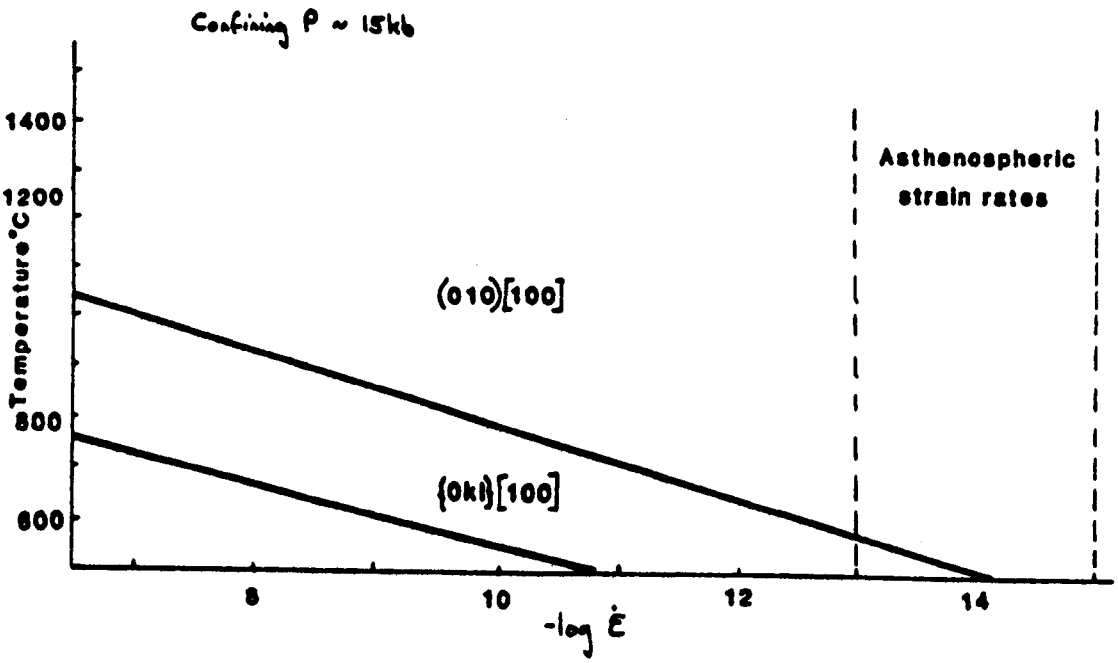

Figure 6.6 Figure 6.5 a) extended to more realistic asthenospheric strain rate values. (Modified from Carter and Avé Lallemant, 1970).

Low T High $\dot{\varepsilon}$	Medium T Medium $\dot{\varepsilon}$	High T Low $\dot{\varepsilon}$
(100) [001] + {110} [001] + (100) [010] -	(100) [001] {110} [001] + (100) [010] -	{110} [001] (010) [100] + {0kl} [100] + (001) [100] {101} [010] -

+ Common
- Uncommon

Table 6.2 Summary of active slip systems in olivine.

(From Nicolas and Poirier, 1976).

In the early coaxial deformation studies onolivine it was found that, for the (010)[100] slip system, the [010] olivine crystallographic axis was parallel to both the maximum compressive stress (σ_1) and strain (ε_1) axes. Both the syntectonic crystallisation process proposed by Avé Lallemant and Carter (1970) and the translation glide process proposed by Nicolas et al (1971) would give rise to the same orientations of olivine during coaxial deformation.

The syntectonic recrystallisation theory of Avé Lallemant and Carter (1970) involves a two stage process; firstly the nucleation of new grains at a host boundary, and secondly the growth of nuclei. The translation glide theory of Nicolas et al (1971) involves both intracrystalline gliding and intergranular slip.

Nicolas et al (1973) were the first workers to consider the effects of non-coaxial deformation on olivine. This was further developed by Poirier and Nicolas (1975) and Nicolas and Poirier (1976). Experiments on the deformation of olivine aggregates showed that the development of textures and crystallographic preferred orientations in porphyroclasts during an increasing strain is essentially a two stage process:

(i) 0% - 30% strain. In this strain field there is external rotation of initially anisometric grains which involves strong kinking and shortening in grains with the active slip direction close to σ_1. (ie. Mainly grain boundary sliding processes.)

(ii) Greater than 30% strain. Intercrystalline slip dominates in strains greater than 30%. At strains greater than 40% syntectonic recrystallisation becomes a major process occurring mainly at grain boundaries and in the highly strained domains of porphyroclasts.

In the 0% - 30% strain field the olivine grains rotate bodily, the [010] crystallographic axis rotating towards σ_1 to reach (010)[100] slip conditions. Intercrystalline (010)[100] slip does not become a major deformation process until the coefficient of resolved shear stress reaches its maximum value for the (010)[100] slip system (ie. until 30% strain is reached). Dislocation creep then dominates, the [100] crystallographic axis orientates parallel to the shear direction, and the [010] axis perpendicular to the shear plane.

In the field most authors have found that the lineation in mantle peridotites is parallel to the olivine [100] crystallographic axis which is sub-parallel to the minimum principal compressional strain axis (ε_3). Nicolas and Boudier (1975) point out that for irrotational deformation the [100] olivine axis is parallel to the ε_3 axis, but for rotational deformation (ie. simple shear) there is a slight angle between the [100] and ε_3 axes.

More recent experimental studies by Kunze and Avé Lallemant (1981) have shown that under mantle asthenospheric conditions the plastic strain can only be moderate because of recovery by syntectonic recrystallisation. They also propose that where grains are deformed by translation glide (ie. dislocation slip mechanisms) in a simple shear environment the olivine [100]

axis rotates towards ϵ_3 and not towards the shear direction as proposed by Nicolas and Poirier (1976).

For grains which have undergone syntectonic recrystallisation, Ross et al (1980) used the theories discussed in section 6.1.4 to determine the orientation of recrystallised grains with respect to stress and strain etc. The preferred lattice orientations are essentially controlled by the maximum principal compressional stress axis (σ_1) in that the [010] olivine axis is parallel to σ_1, and [100] parallel to σ_3.

Recent theoretical studies on the deformation of olivine at high temperatures and moderate stresses have been reviewed by Zeuch (1982). These studies, mainly by Twiss (1976) and Goetze (1978), propose that there is a transition from power-law flow dislocation creep mechanisms to non-linear grain-boundary creep mechanisms, resulting from the production of fine grain-sizes by dynamic recrystallisation.

Despite the production of find grain-sizes in experiments by Karato et al (1982), Zeuch and Green (1979) and Zeuch (1980) by dynamic recrystallisation, Zeuch (1983) finds no evidence for a transition to diffusional mechanisms in these experiments. Instead he concludes that deformation of olivine in the asthenosphere is dominated by dislocation creep with accompanying recovery by dynamic recrystallisation, as is proposed from the discussions in section 6.1.

Thus, in the mantle asthenospheric conditions of steady-state power-law creep, olivine deforms by dislocation creep processes with accompanying recovery by dynamic recrystallisation. Dislocation creep occurs along specific slip systems, the operative slip system largely being controlled by temperature. It is not possible to quantify the temperature ranges for each slip system because of the very low expected strain rates in the asthenosphere. Qualitatively, however, the highest temperature system is most likely to be (010)[100], and the moderate temperature system {0kl}[100]. The low temperature [001] slip direction would not be expected to be active in asthenospheric conditions.

In a simple shear environment the grains undergoing dislocation slip have their orientations controlled essentially by by principal compressive strain axes if the experimental work of Kunze and Avé Lallemant (1981) is accepted. Grains which have undergone syntectonic recrystallisation, on the other hand, have their orientations controlled by the principal stress axes (Ross et al, 1980). The relevance of this data in relation to the estimation of shear sense in a simple shear environment will be discussed in section 6.4.

6.2.2 Orthopyroxene (Enstatite)

(a) Theoretical Slip Directions and Planes

Enstatite is an orthorhombic chain silicate. The crystallographic habit and optical directions of enstatite are shown in Figure 6.7. The detailed crystallographic structure of enstatite is described in detail by Deer et al (1963).

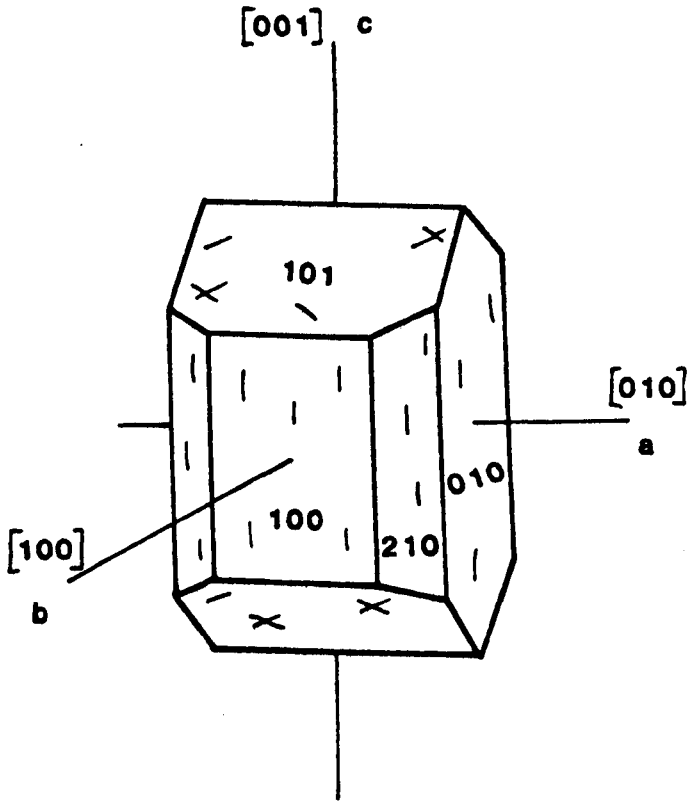

Figure 6.7 The crystallographic habit and optical directions of enstatite. (After Deer, Howie and Zussman, 1966).

The unit cell of enstatite has its shortest Burgers vector parallel to the [001] crystallographic direction in the (100) plane. (b = 5.2Å). The next shortest Burgers vector is on the (100) plane in the [010] crystallographic direction (b = 8.9Å); the longest Burgers vector (b = 9.73Å) is parallel to [100].

The [001] Burgers vector has by far the lowest energy and thus it can be predicted that the (100)[001] slip system is most likely to be the active slip system during dislocation creep.

(b) Experimental and Observational Studies on Enstatite Slip Systems

The existence of a (100)[001] glide system in enstatite was first recognised by Mügge (1898). His observations on natural rocks were confirmed experimentally by Turner et al (1960) and Griggs et al (1960). More recent work has been carried out by Green and Radcliffe (1972), Coe and Muller (1973) and Kohlstedt and Van der Sande (1973) at various temperature and pressure conditions. In all cases the (100)[001] slip system was the only operative system for dislocation creep processes.

Christensen and Lundquist (1982) have reviewed in detail the relationships of orthopyroxene to olivine orientations found by previous workers. The results are variable with some authors finding the expected relationship of orthopyroxene [001] parallel to olivine [100], and others finding no relationship between the two minerals.

This apparent anomaly may be explicable in terms of the intensity of shearing undergone by the rocks. Nicolas and Poirier (1976) use microstructural evidence to show that at high temperatures orthopyroxene will have a much higher creep resistance than olivine. In other words at fairly low stresses, olivine will deform by dislocation creep but orthopyroxene will not. It will be most likely to deform by grain boundary sliding processes. Only at higher stresses will orthopyroxene deform by dislocation creep, and only in these rocks will the orthopyroxene [001] axis be sub-parallel to the olivine [100] axis.

The high creep resistance of orthopyroxene will also inhibit polygonisation and recrystallisation processes (Green and Radcliffe, 1972). This is evident in harzburgite thin sections from the Peridotite Unit of all three areas, where it is uncommon to observe recrystallisation textures in orthopyroxene crystals.

6.2.3 Clinopyroxene and Plagioclase

Little work has been done on the plastic deformation of clinopyroxene and plagioclase. Nicolas and Poirier (1976) review that which has been done.

a) Clinopyroxene Clinopyroxene (enstatite) has a similar single low Burgers vector to orthopyroxene on the (100)[001] system. Experimental work has shown this to be the only slip system in enstatite. (Reviewed in Nicolas and Poirier, 1976).

Clinopyroxene will also have a high creep resistance similar to orthopyroxene.

b) Plagioclase. The plagioclase feldspars have a complex crystallography (Deer et al, 1963). In plastic deformation practically all plagioclase compositions deform by a combination of slip and twinning. Borg and Heard (1969,1970) are the only workers to have experimentally deformed plagioclase in plastic conditions. They report that slip occurs preferentially in the (010) plane but give no specific direction for slipping.

6.3 The Determination of the Last Active Crystal Slip Systems in Olivine and Orthopyroxene from Thin Sections.

There are a number of methods of determining the last active crystal slip system in grains from natural rocks. These

have been reviewed and described in detail by Nicolas and Poirier (1976) - (Chapter 9).

6.3.1 Methods Available

Five different methods have been used by various workers to determine the active crystal slip systems. A list of the methods is given below.

a) Optical determination. This method involves the direct observation of deformation lamellae and kink bands by the use of a polarizing microscope. In high temperature plastic flow only kink bands are present. In olivine these are often difficult to locate and measure accurately.

b) Universal Stage Determination. The use of a four-or-five -axis universal stage allows the direct determination of the crystallographic orientation of a grain. A comparison of the crystallographic orientation with the field measurement allows the slip system to be determined. (See section 6.3.2 below).

c) X-ray Determination. This method involves the same principals as the universal stage method in that the crystallographic orientation of a grain is determined and then the slip system is inferred from a comparison of the crystallographic results with the field structural orientations. A texture goniometer is used; its main drawback is that it can only be used on very fine-grained rocks; i.e. those with a grain diameter of less than 10μ.

d) The Observation of Substructures and Dislocations:

This method involves the direct observation of crystal defects by either dislocation decoration and etch pit studies or by X-ray topographic methods.

e) Transmission Electron Microscopy (T.E.M.) This technique allows the direct optical observation of crystal defects without the need for decoration or etch processes.

6.3.2. Method Used and Expected Results

a) Method Used.

In deciding on the best method of determining the active crystal slip systems of the minerals from Peridotite Unit specimens from all three areas of study, three points were considered:

i) The high degree of serpentinisation in most of the harzburgite and durite specimens collected. (Normally over 50%) - As described in chapters 2-4 serpentinisation partially masks the original textures by overprinting a serpentinite mesh-type texture on the rock. This makes it difficult to study the detailed internal defects of whole grains, especially of olivine, in most thin sections.

ii) The grain size of specimens to be studied - In most specimens the grain sizes of both olivine and orthopyroxene range from 0.1mm up to 1 cm. This grain size rules out the possibility of using the X-ray texture goniometer technique.

iii) The amount of time each method takes - as a large number of specimens had to be analysed it was important to find a method which was relatively fast. Etching or dislocation decoration techniques and T.E.M. methods require a great deal of sample preparation.

It was therefore decided to use the universal stage to determine the active crystal slip systems in olivine and orthopyroxene. For this technique the thin section does not have to be cut on a precise plane in relation to the structures present, nor is extensive sample preparation involved. On the other hand it does give a more accurate determination of the crystal slip systems than the unreliable method of studying kink bands, and every grain in a specimen can be measured as opposed to only the few grains in which kink bands can be seen.

A Zeiss four-axis universal stage was used to study the crystallographic orientations of olivine and orthopyroxene. The methodology of Phillips (1971) was used in operating the universal stage.

b) Expected Results for the Various Slip Systems from Universal Stage Work.

For each mineral type from each specimen, universal stage measurements enable the optic axes of each crystal to be determined. For both olivine and orthopyroxene (both of which are orthorhombic minerals) the three optic axes are sub-parallel to the crystallographic axes. Table 6.3

summarises the relationship between optic and crystallographic axes for both olivine and orthopyroxene.

The optic axes determined from the universal stage were directly plotted onto an equal area projection orientated parallel to the horizontal plane of the universal stage. The axes were then rotated back to their original 'in situ' field orientations and plotted on an equal area projection. The plotted projections for specimens from the three areas of study are presented in Chapter 7.

Olivine slip systems - expected crystallographic axes plots. The expected plots for both the (010)[100] and {0kl}[100] slip systems are shown in Figure 6.8.

For the (010)[100] slip system the [100] axis plots as a point cluster and is sub-parallel to the field slip lineation. The [001] axis plots as a cluster and lies approximately in the field foliation plane which also contains the [100] axis. The [010] axis plots as a cluster approximately perpendicular to both the slip lineation direction and the foliation plane.

In the {0kl}[100] slip system the [100] axis plots as a point cluster and is sub-parallel to the field slip lineation, as is the case for the (010)[100] slip system. Because the {0kl}[100] slip system involves slip on a number of different planes, the [010] and [001] axes will not plot as separate clusters, but will combine into a great-circle girdle pattern which intersects the foliation plane perpendicular to the slip direction. (See Figure 6.8).

Olivine		Orthopyroxene	
Optic Axis	Crystallographic Axis	Optic Axis	Crystallographic Axis
a	[0I0]	a	[0I0]
b	[00I]	b	[I00]
c	[I00]	c	[00I]

Table 6.3 The Relationship between the optic and crystallographic axes for olivine and orthopyroxene.

Orthopyroxene slip system - expected crystallographic axes plot. As described in section 6.2.2, orthopyroxene only has one active slip system in plastic flow conditions - the (100)[001] slip system. The expected crystallographic axes plots in relation to the field structures is shown in Figure 6.9. The [001] axis plots sub-parallel to the field slip lineation, the [010] axis lies approximately in the field foliation plane and perpendicular to the [001] axis and slip lineation direction, and the [100] axis plots approximately perpendicular to the field foliation plane. All the crystallographic axes plot as point clusters.

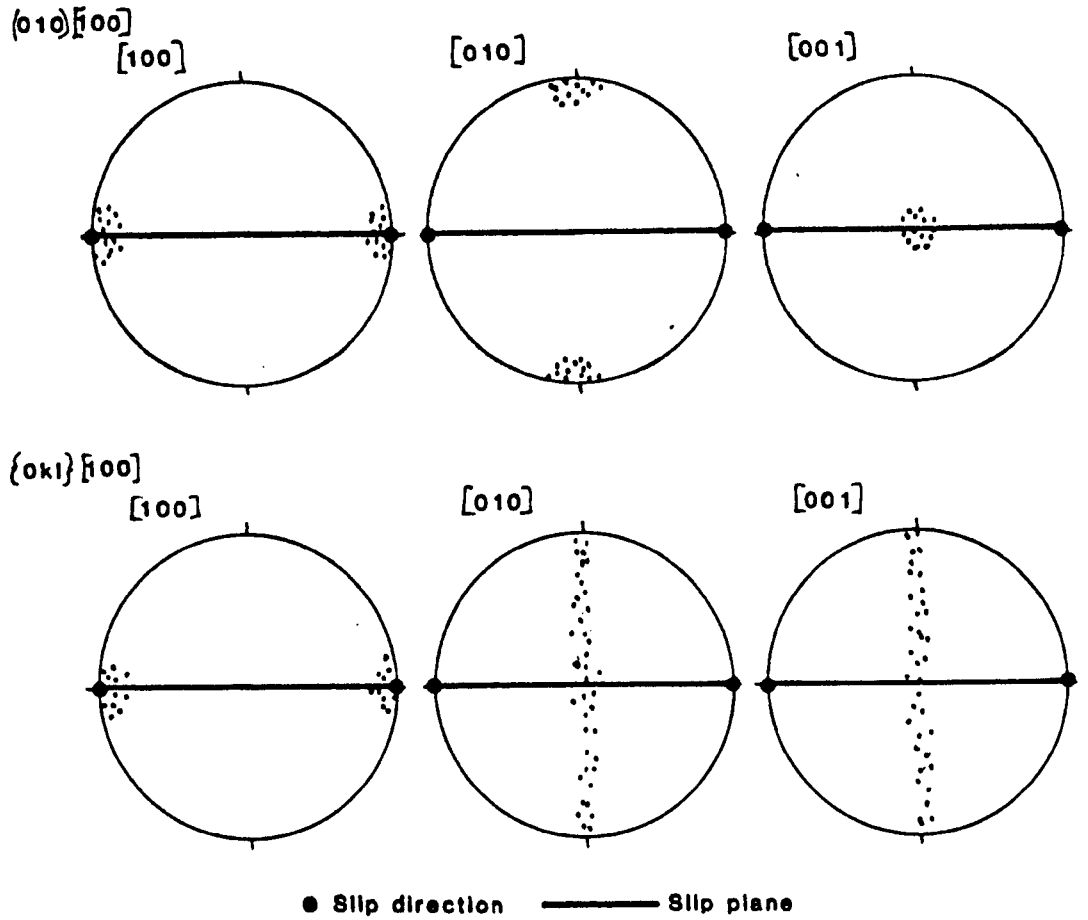

Figure 6.8 Expected crystallographic equal area plots for the olivine high and moderate temperature slip systems.

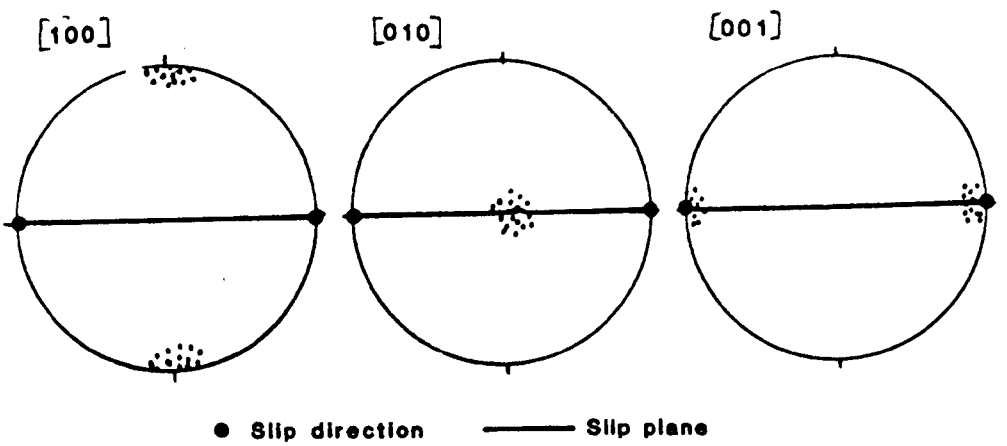

Figure 6.9 Expected crystallographic equal area plot for the orthopyroxene slip system.

6.4 Pure Shear or Simple Shear?

It should be possible to determine whether a specimen has undergone deformation in a pure shear environment or a simple shear environment, by studying the angular relationships between the crystallographic orientations and the shape orientations (ie. foliations and lineations) of olivine and orthopyroxene crystals.

6.4.1 Pure Shear

In specimens which have undergone pure or irrotational shear all the different structural elements will be coaxial and the total symmetry will be orthorhombic. For an olivine grain which has undergone pure shear in the (010)[100] slip system, the [100] axis will be parallel to the field lineation axis, the axis of minimum compressive stress (σ_3) and the axis of minimum compressive strain (ε_3). Figure 6.10 summarises the relationship between the different axes for pure shear.

6.4.2 Simple Shear

In a simple shear environment the different structural elements are not coaxial; the total symmetry is monoclinic. The asymmetry between the crystallographic lattice preferred orientation and the shape fabrics should enable a shear sense to be calculated for the simple shearing.

Nicolas et al (1972) first proposed that a shear sense can be determined from mantle rocks by determining the angular difference between the penetrative and kinematic elements in a rock. (Figure 6.11). (Penetrative elements are those which can be

directly measured in the field or on the microscope; ie. foliation, lineation, and shape-preferred orientations: kinematic elements are those which are related to the flow elements; ie. the crystallographic lattice fabric elements.)

According to the reasoning of Nicolas and Poirier (1976) (ie. that the olivine [100] axis rotates towards the shear direction in a simple shear regime) the shear sense can be defined by the angle between either the field lineation and the crystallographic slip direction, or the field foliation and the crystallographic slip plane. This is shown in Figure 6.11.

Some authors have determined the shear sense by using features within the grains in thin section as indicators of the kinematic axes. Darot and Boudier (1975) used the intersection of pyroxene cleavages with the crystal faces as a method of determining the shear sense. Girardeau and Nicolas (1981) used the obliquity between the extinction of olivine under crossed polars and the trace of the foliation plane. The drawback of these optical methods is that precisely cut sections are required which are perpendicular to the foliation plane and intersect the foliation plane parallel to the lineation trace (the XZ plane). In the determination of shear senses from the specimens collected for this study only the crystallographically defined slip planes have been used as kinematic elements.

The experimental results of Kunze and Avé Lallemant (1981) which suggest that the slip direction in a crystal undergoing dislocation creep rotates towards the minimum principal compressive strain axis (ε_3) rather than the shear direction,

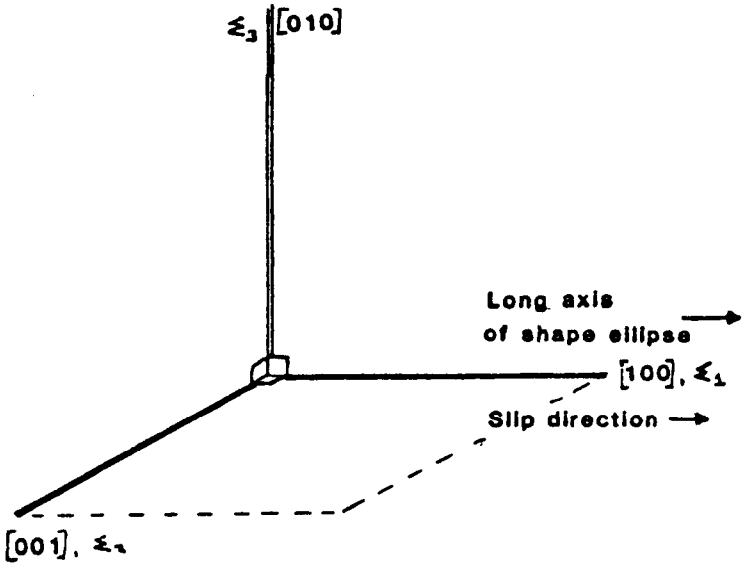

Figure 6.10 Relationship between the crystallographic and shape preferred orientation axes for pure shear in an olivine crystal undergoing high temperature shearing.

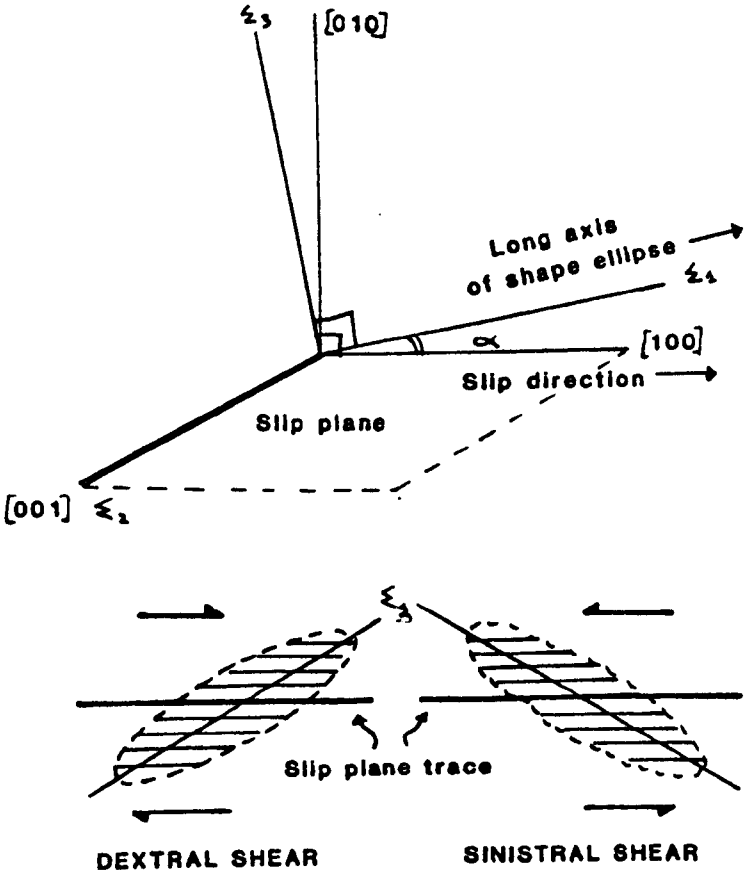

Figure 6.11 The relationship between the crystallographic and shape preferred orientation axes for simple shear - the determination of the shear sense.

(see section 6.2.1), are difficult to apply to rocks which have undergone simple shear in asthenospheric conditions. If the slip direction rotates towards parallelism with the ε_3 axis then it should also become parallel to the field lineations and foliation planes. If this is the case then there should be no angle between the kinematic and penetrative axes.

In most natural peridotites, however, an obliquity has been observed between the crystallographic lattice fabric and the field foliations and lineations. (Eg. Nicolas, 1973; Mercier and Nicolas, 1975.) This obliquity is also found in most experiments involving simple shear. These are reviewed by Bouchez et al (1983). All these experiments involve a single-slip hypothesis. This hypothesis considers minerals which have either a single slip plane, or many slip planes and a single slip direction (eg. {0kl} [100] slip system in olivine). The hypothesis has been tested for olivine in zones in which the kinematics were already known (Prinzhoffer and Nicolas, 1980) and there is an agreement that the fabric obliquity is what is expected.

The Von Mises (1928) condition demands that five independent slip systems operate if a polycrystal is to deform coherently by slip alone. If only one slip system operates, then the material must deform heterogeneously on the grain scale and other deformation mechanisms must be operative. As discussed in section 6.2, during deformation of olivine under high T/Tm conditions, obstacles to flow along the dominant slip system

are readily reduced by diffusion - assisted grain-boundary mobility. The single-slip hypothesis is thus largely applicable to olivine-rich rocks undergoing simple shear in asthenospheric conditions.

The single-slip hypothesis is directly challenged by the experiments of Kunze and Avé Lallemant (1981) because their results suggest an absence of asymmetry in the fabrics produced in a simple shear environment. Bouchez et al (1983) point out, however, that the experiments of Kunze and Avé Lallemant (1981) have not produced easily interpreted deformations as they involved punching and extrusion. Their experimental "shear zones" may in fact be close to a coaxial spinning history similar to that proposed by Means et al (1980), and thus their results are inconclusive.

The vast amount of evidence from natural peridotites as well as experimental evidence (reviewed above) suggests that the hypothesis of Nicolas and Poirier (1976) that, in a simple shear environment, the crystallographic lattice fabric rotates towards the shear direction, and not the ϵ_3 axis as proposed by Kunze and Avé Lallemant (1981), is more likely to be correct. This assumption only applies to high temperature deformation where the von Mises condition is not applicable due to the involvement of other deformation mechanisms.

In single-slip simple shear the amount of shearing that a rock has undergone can be quantitatively expressed by measuring the angle α between the slip direction and the mineral elongation or lineation direction. Shear is expressed either as the angle

of shear, θ, or the shear strain, γ. They are geometrically related to each other and to α, by the expression:

$$\gamma = \text{Tan } \theta = 2 \cot 2\alpha.$$

The relationship between shear strain, angular shear and the angle α for finite simple shear is shown in Figure 6.12.

The estimation of shear strain in the rocks studied for this thesis will be discussed in Chapter 7.

6.5 The Estimation of Shape Fabric Strength and Orientation in a Polycrystalline Aggregate.

In a simple shear environment, the expected behaviour of a polycrystalline aggregate undergoing single-slip is shown in Figure 6.13. As can be seen the elongation of individual crystals is approximately parallel to the foliation plane and lineation direction measured from the hand specimen or in the field.

Various techniques have been used to estimate shape preferred orientations and strengths in rocks. These are reviewed in detail in Chapter 8.

Once the elongation direction has been calculated it can be used along with, or instead of, the field lineations as penetrative elements of deformation. In a rock which has undergone a large amount of shear strain in an environment of a single shear direction, the shear angle, θ, should be directly relatable to the elongation value of the mean crystal shape ellipsoid in that the elongation will increase as the shear angle increases.

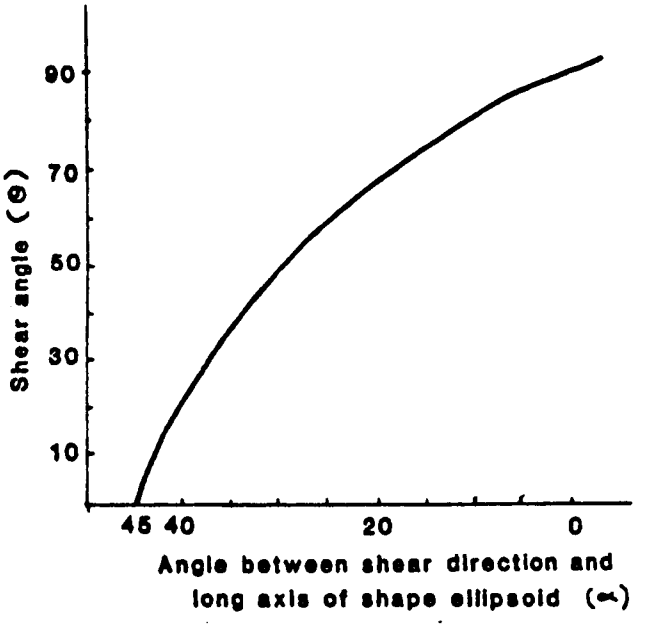

Figure 6.12 The relationship between angular shear and angle $\propto$ for finite simple shear. (From Nicolas and Poirier, 1976).

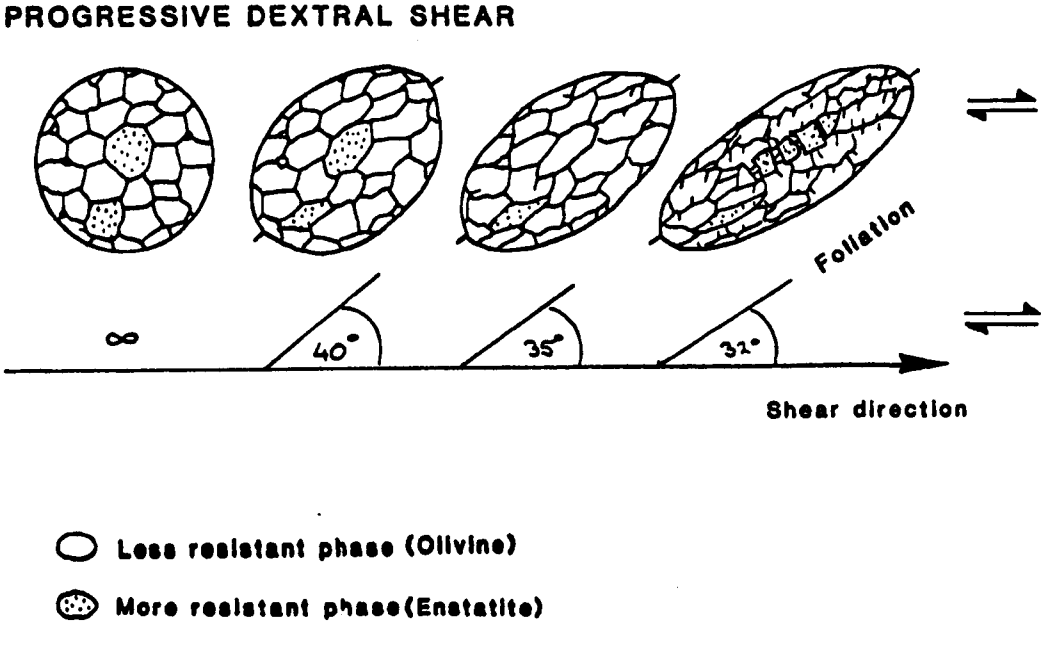

Figure 6.13 The expected behaviour of a polycrystalline aggregate undergoing simple shear. With a progressive deformation the slip directions in individual crystals tend to coincide with the shear plane. (Modified from Darot and Boudier, 1975).

This relationship will only hold for crystals undergoing dislocation slip processes. In most natural peridotites, diffusion along grain boundaries and recrystallisation processes have also occurred. When these other processes are a major part of the deformation event, only a weak shape fabric will be produced even though the crystallographic orientations show a strong slip direction point maximum.

If the direction of shearing changes during the deformational history of an area, as is thought to have happened in some of the areas of study in this thesis, then both the crystallographic and shape-preferred orientations will be drastically altered. The relation between a change in the shear direction and the crystallographic orientations is discussed in Chapter 7.

A detailed discussion of the relationship between a change in the shear direction, recrystallisation and shape preferred orientations of both olivine and pyroxene crystals is included in Chapter 8.

6.6 The Estimation of Applied Stress in Harzburgites and Dunites that have Undergone a Shearing Deformation.

If it is assumed that a peridotite has undergone deformation within a steady-state flow environment, then it is possible empirically to relate certain quantitative microstructural parameters to the applied stress.

6.6.1 Methods of Estimation of Applied Stress

Previous workers have used five methods to estimate the stress applied to a rock during its natural deformation:

(i) Subgrain size: The empirical relationship between sub-grain size and applied stress was determined by Weertman (1968). The empirical law can be expressed as follows:

$$d = K \frac{\mu b}{\sigma}$$

where d is the average subgrain diameter, K is a dimensionless constant of proportionality, μ is the average shear modulus, b is the Burgers vector of the active dislocations, and σ is the applied stress.

Within an olivine-rich rock care must be taken only to measure the sub-grains resulting from the fragmentation of the coarse grains into misorientated blocks and not those formed during post-deformational annealing processes. The former sub-grains usually have a diameter of between 50μm and 1mm; the latter sub-grains are usually less that 50μm thick and cannot be easily seen with an optical polarising microscope.

For olivine the value for K has been calculated as 800 by Raleigh and Kirby (1970). The values for the other two constant parameters have been listed by Frost and Ashby (1981):

$$\mu = 8.13 \times 10^{4} \quad MN/m^{2} \text{ at } 300°K; \; b = 6.0 \times 10^{-10} m.$$

The problem with the measurement of subgrains in a thin section is that it is often difficult to measure them accurately. The value of stress estimated from their measurement will also only give an approximation to the highest stress regime within the rock (Poirier and Guillope, 1979). A more useful possible indicator of stress is the size of neoblasts within the thin section as they will be more likely to give an estimation of the last stress regime that prevailed within the rock.

(ii) Neoblast size: The empirical relationship between neoblast size and applied stress is the same as that between sub-grain size and applied stress. The values of the constant parameters are, however, different.

The empirical law has been simplified to:

$$\sigma = KD^{-n}$$

by most authors where D is the mean neoblast diameter (μm) and K and n are derived constants.

Post (1977) used K = 19 and n = 0.67 ± 0.11, to calculate the applied stress in olivine crystals within a dunite. These values are based on the system being dry. Possibly more realistic values of K = 48, n = 0.79 for stress in the mantle, based on experimental evidence in a damp system, have been obtained by Ross et al (1980).

Avé Lallemant (1978) derived K and n for diopside and related the mean neoblast size to stress by the equation:

$$D = 60_{\sigma}^{-0.90}.$$

A similar equation was used by Ross and Nielsen (1978) for recrystallised enstatite where:

$$D = 46.77_{\sigma}^{-6.85}$$

Nicolas et al (1980) tentatively propose that the relationship:

$$d \text{ subgrain} = \tfrac{1}{2} D \text{ neoblast}$$

is valid for peridotite minerals, and that where serpentinisation is intense the measurement of sub-grain sizes may well be easier than neoblast sizes.

(iii) Dislocation Density: The commonly accepted empirical relationship bewteen the dislocation density within crystals and the applied stress is:

$$\sigma = K'_{\mu b\sqrt{\rho_t}}$$

where K' is a dimensionless constant, μ is the average shear modulus, b is the Burgers vector and ρ_t is the dislocation at the temperature of deformation. The empirical relationship is discussed in detail by Nicolas and Poirier (1976).

At high temperatures Kohlstedt and Goetze (1974) found $K' \simeq 5$ for olivine. Durham et al (1977), and Gueguen and Darot (1980) develop the use of dislocation densities for estimating stress for olivine.

(iv) The Curvature of Dislocation Segments: Nicolas and Poirier (1976) developed the empirical relationship between the curvature of dislocation segments and the applied stress. The formula:

$$R = \mu b/K\sigma$$

relates the radius of curvature of a segment of dislocation (R) to the applied stress using constants similar to those in methods (i), (ii) and (iii).

The problem with this method is that it will only give the effective stress acting on the dislocation, which will be determined only in part by the applied stress. The interaction with neighbouring dislocations will strongly affect the effective stress measurement.

(v) The Spacing Between Tilt Walls: Durham et al (1977) used the spacing between tilt walls within crystals as an indicator of the applied stress. The empirical relationship between tilt wall spacing and applied stress is similar to that for the dislocation densities.

6.6.2 The Method of Stress Estimation for this Study.

Green and Gueguen (1983) used the neoblast grain size equation of Post (1977), the tilt wall spacing of Durham et al (1977), and the dislocation densities of Durham et al (1977) and Gueguen and Darot (1980) to estimate the palaeostress within peridotite xenoliths from kimberlite pipes. All the three methods gave similar palaeostress values although the dislocation density results were slightly lower than those from the other two methods.

If the K and n values of Ross et al (1980) are used instead of the values of Post (1977) for the estimation of stress from neoblast size for olivine, the value of applied stress obtained is only very slightly lower than the minimum value calculated from Post (1977). The results are summarised in table 6.4.

In a review of the accuracy of the techniques available for the measurement of applied stress in natural rocks, White (1979) concluded that estimates are at present only qualitative. 'An extensive experimental programme is required before realistic quantitative estimates can be made.'

If, for the same rock type, the same technique of estimation of stress is used for each specimen, then at least relative values of stress can be obtained.

In methods (iii), (iv) and (v) lengthy laboratory techniques are required before measurements can be made, whereas in methods (i) and (ii) the grain sizes can be measured by the direct observation of thin sections using a polarising microscope.

In the present study a large number of moderately serpentinised dunite and harzburgite specimens are available for palaeostress determinations. In the light of the above considerations, the size of the neoblasts was used to estimate qualitatively the applied stress that the specimens had undergone during their last major deformation. The results obtained are discussed in Chapter 8. (Section 8.6).

Recrystallised grain size (Goetze 1975; Post 1977)	Tilt wall spacing (Durham et al 1977)	Dislocation density (Durham et al 1977; Gueguen and Darot 1980)
50-80MPa	80MPa	20-30MPa

Table 6.4 Results from different methods of palaeostress determination for olivines from a peridotite xenolith.

(From Gueguen and Darot, 1980).

6.7 Magmatic or Tectonic Orientations?

In the Peridotite Unit it is clear that both the harzburgites and dunites have been extensively tectonised with the development of a purely tectonic fabric. If an original cumulate texture existed prior to deformation, it certainly has no remnants in the Peridotite Units studied in this thesis.

In the Lower Cumulate Unit, however, in all the areas studied, the Peridotite Unit tectonism dies out upwards into the Lower Cumulate Unit. It is generally accepted that this unit has been formed by magmatic accumulation processes at the base of a magma chamber (see Chapter 1). It will be useful to distinguish between magmatic and tectonic orientation processes in the Lower Cumulate Unit in order to facilitate understanding of the interaction between cumulate and tectonic processes.

6.7.1 Magmatic Preferred Orientations

(a) Olivine Den Tex (1969) first determined how an individual olivine crystal will orient itself within a magma undergoing laminar flow. A crystal will orient itself so as to offer least resistance to the forces of movement. In other words, large crystal faces will show a marked preference for parallel orientation, the crystallographic axes becoming aligned either parallel to, or normal to, the magmatic flow lines depending on the turbulence of the flow.

The natural habits of an olivine crystal are shown in Figure 6.14. They are characterised by a pronounced development of {010}, {110} and {021} crystal forms. Brothers(1959, 1960, 1964) noted that the (010) face usually develops preferentially in an olivine crystal which has crystallised in a non-tectanic environment. This would align the [010] crystallographic axis of olivine perpendicular to the flow plane as Brothers (1959 and 1964) reported for both the Rhum and Skaergaard Complexes, and Jackson (1961) for the Stillwater Complex.

Den Tex (1969) points out that the olivine [010] axis will only be perpendicular to the igneous layering plane in a magma chamber in which the layers have formed by gravity settling from a stagnant magma. In a magma chamber undergoing convection and laminar igneous flow, the olivine crystals are most likely to form an imbrication fabric as shown in Figure 6.15. The individual crystals pile up at a low angle to the flow plane and dip in the sense of flow in a similar manner to the imbrication of pebbles in rapidly flowing rivers. Thus, by measuring the angular difference between the igneous flow plane and the olivine [010] axis, it should be possible to estimate the direction of igneous flow in the rock.

In natural systems, however, Den Tex (1969) notes that for olivine the {110} and {021} forms are just as likely to show a comparable tendency towards parallelism with the flow plane. This will cause the crystallographic plot not to be as straightforward to interpret as the paragraph above would suggest. However, on average, the olivine [010] axis should still plot approximately perpendicular to the igneous layering.

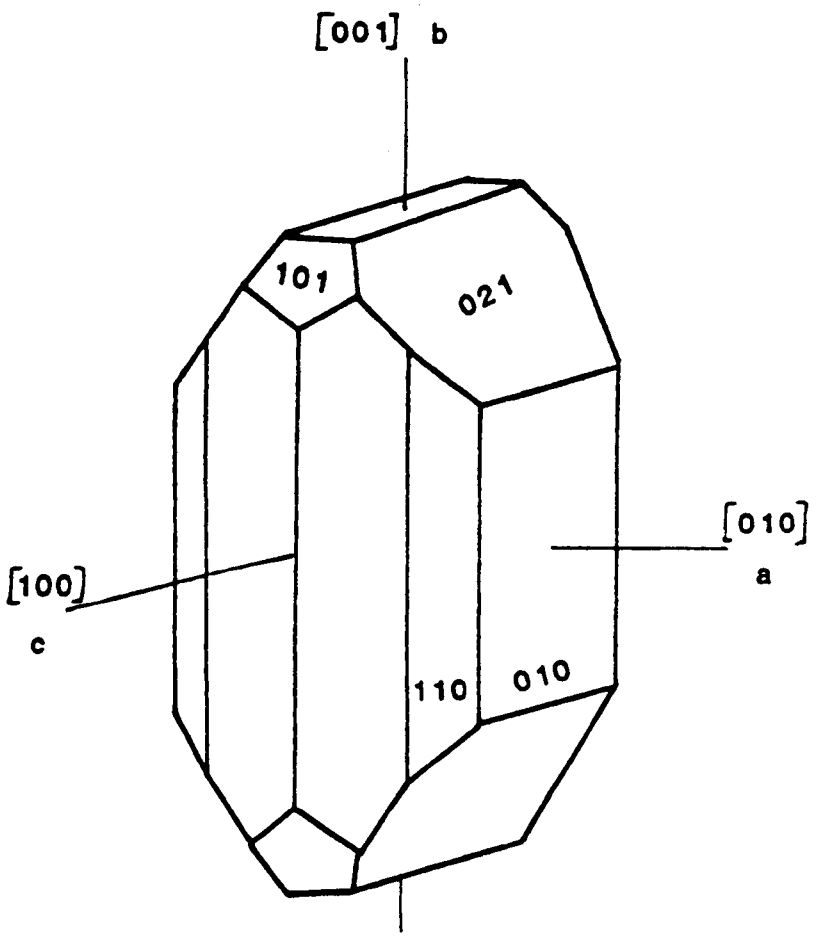

Figure 6.14 The natural habits of an olivine crystal. (Forsterite). (From Deer, Howie and Zussman, 1966).

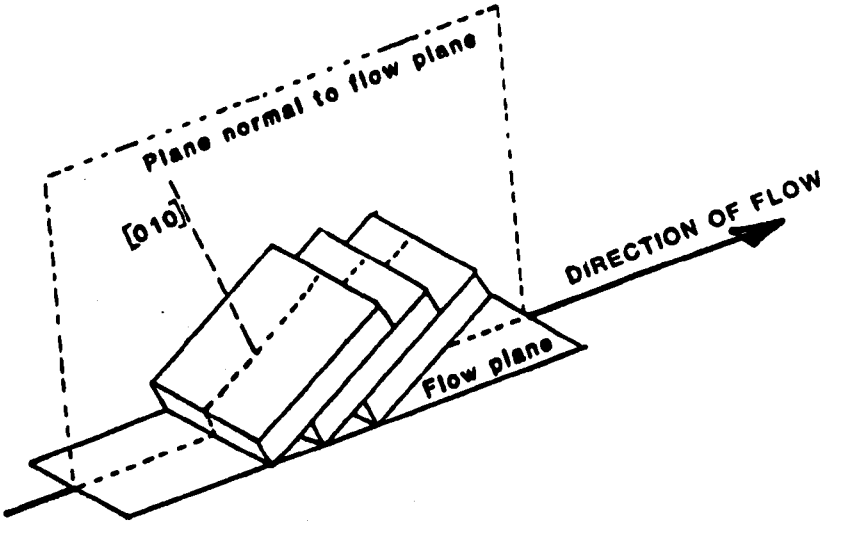

Figure 6.15 The formation of an imbrication fabric of idealised [010] tablets of olivine under laminar flow of the suspending magma. (From Den Tex, 1969).

In studies of the Oman Ophiolite, Browning (1982) and Smewing et al (1983) have used the crystallographic orientation of olivine to determine whether or not a cumulate has been tectonically deformed.

(b) Pyroxene No references have been found describing the expected magmatic orientation of pyroxene crystals. Using the same reasonings as for olivine, their orientation relative to a magmatic flow plane or igneous settling layering can easily be determined.

The natural habits of enstatite and diopside crystals are shown in Figure 6.16. In both, the forms {100} and {010} are conspicuous. Also conspicuous are the {210} form in enstatite and the {110} form in diopside.

The {100} form is by far the largest crystal face and thus in a magmatic environment it would be expected that the [100] crystallographic axis is approximately perpendicular to the igneous layering or flow plane.

6.7.2 Tectonic Orientations

The expected crystallographic orientations for olivine and ortho- and clinopyroxene have been discussed in detail in section 6.3 of this chapter.

Both the slip system of the pyroxenes ((100)[001]) and the high temperature olivine slip system ((010)[100]), yield the same crystallographic preferred orientations as would be expected in magmatic layering. ie. The (010) crystallographic plane

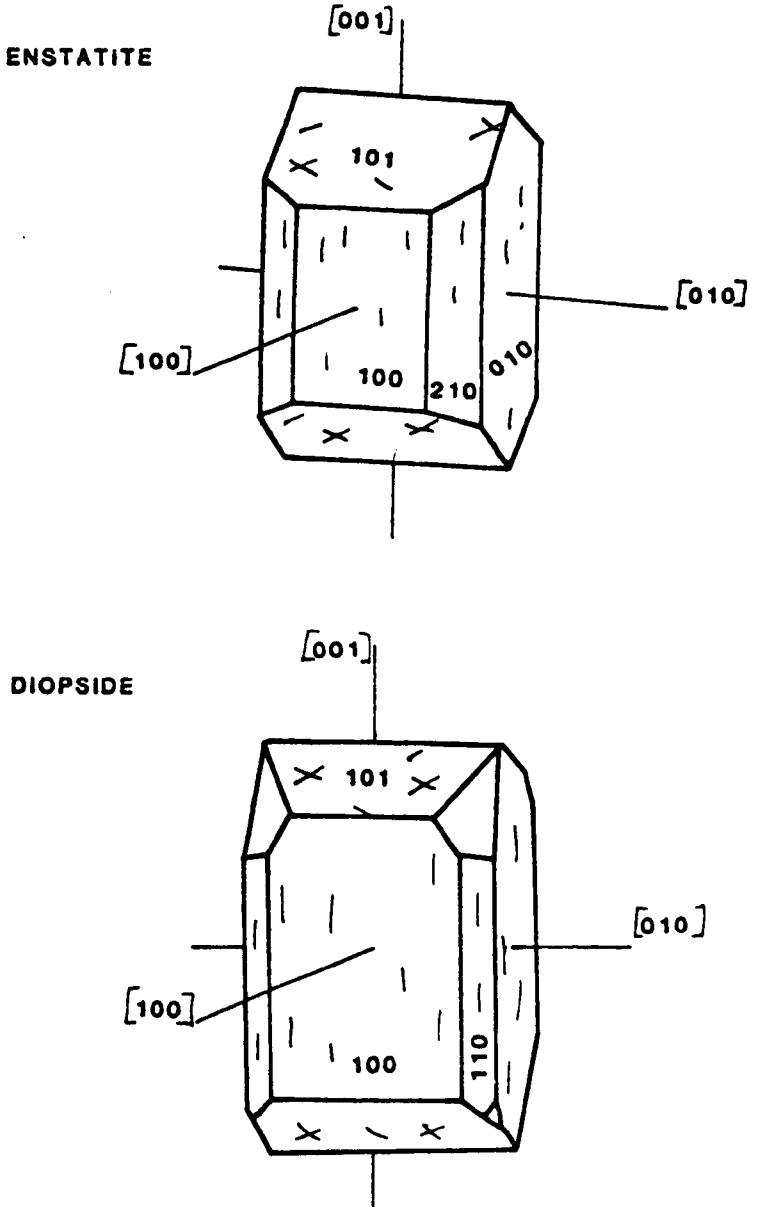

Figure 6.16 The natural habits of enstatite and diopside crystals. (From Deer, Howie and Zussman, 1966).

for olivine and the (100) crystallographic plane for pyroxene will be parallel to the slip plane in deformed crystals and to the igneous flow plane in undeformed magmatic crystals. This coincidence of tectonic and magmatic preferred orientations shows that great care must be taken in studying the crystallographic data in order that a tectonic orientation can be crystallographically distinguished from a magmatic orientation. Table 6.5 summarises the main differences in crystallographic trends between tectonic and magmatic orientations.

6.7.3 The Transition from Tectonic to Magmatic Orientations

The structural transition between tectonised and non-tectonised olivine-rich cumulates has not been studied in much detail by previous authors. Thayer and Jackson (1972) first introduced the hypothesis of 'crystal mush flow'. This is a process by which crystals can undergo large rotations while all the strain is accomodated by the intercumulus liquid, leaving the crystals undeformed.

George (1975, 1978) noted that much of the dunite of the Troodos Lower Cumulate Unit had probably undergone deformation by 'crystal mush flow'. He suggested that the synchronous deposition and deformation of magmatic sediments is an analagous process to the deposition of clastic sediments in basins undergoing penecontemporaneous deformation. In these sedimentary basins the transition between strongly deformed sediments and undeformed sediments is very gradual. As a similar gradual change was observed by George (1975, 1978) in the Troodos cummulates, he inferred that the magmatic settling of the cummulates occurred during deformation of the Peridotite Unit.

Olivine Crystallographic Axis	Magmatic Orientation	Tectonic Orientation
[100]	Girdle approx parallel to layering	Cluster approx parallel lineation within foliation plane
[010]	Dispersed cluster approx normal to layering.	Cluster approx normal to foliation plane for (010) [100] slip system. Girdle approx normal to foliation plane and lineation for {0kl} [100] slip system.
[001]	Girdle approx parallel to layering.	Cluster approx normal to lineation within foliation plane for (010)[100] slip system. Girdle approx normal to foliation plane and lineation for {0kl} [100] slip system.

Table 6.5 The main differences between tectonic and magmatic preferred orientations of olivine.

Thayer (1980) further develops the structural transition zone model by stating that in completely crystallised units in the lower part of the cumulate section, a penetrative subsolidus type of deformation is present. This grades upwards into crystal mush flow involving essentially grain-boundary sliding, and finally into fluid flow as the ratio of liquid to crystals increases. Arzi (1978) has calculated that for most rocks there exists a limit of partial melting, below which the rock can behave as a plastic solid and above which the rock cannot deform by solid-state deformation mechanisms. This boundary is termed the rheological critical melt percentage (RCMP) and for most rocks it has a value of 20% ± 10%.

It is difficult to determine whether a rock has or has not been deformed by crystal mush flow processes. The crystallographic orientations for both will be the same, as neither involves penetrative deformation. Thin section textures may give an indication as to whether the rock has been deformed, but the best method is probably to study the orientations of the large-scale layering features of the cumulate rocks and compare them with the foliation and lineations measured in the penetratively deformed cumulates below. If the layers and crystallographic orientations are sub-parallel to the underlying foliations, it would seem sensible to suggest that the layers have been formed in crystal mush flow conditions. This is the case for some areas of Oman, Shetland and Cyprus (See Chapters 2 - 4).

If there is a significant angular difference between the crystallographic orientations of the layered rocks and the underlying tectonically foliated rock, then the layered rocks were probably not deformed.

This relationship between large-scale crystallographic orientations between deformed and apparently underformed rocks will be discussed in detail for the three areas studied in Chapter 7.

6.8 Summary

The deformation of the asthenospheric mantle takes place by plastic flow in a steady-state regime. Steady-state is maintained by the interaction of strain hardening, recovery and annealing recrystallisation processes. Flow of the uppermost asthenospheric mantle at spreading centres is controlled by power-law flow conditions and for most stresses can be termed as a steady-state creep under hot-working conditions.

If the above assumptions are accepted then the type of shear environment of deformation can be determined from the relationship between penetrative and kinematic elements within the rock.

It is possible to estimate the applied palaeostresses within olivine rich rocks. An indication of the shear strain and preferred shape orientation of the various mineral types can also be estimated from suitable rock specimens.

Finally, it is possible to examine the structural transition zone within the Lower Cumulate Unit between deformed and undeformed rocks by studying relative crystallographic and field planar feature orientations.

In Chapter 7 the crystallographic orientations of samples collected from Oman, Cyprus and Shetland are presented and discussed in relation to a single shear direction and a change in the shear direction, as is thought to have occurred, from a study of the field structures from these areas (see Chapters 2 - 5).

A similar approach is adopted in Chapter 8 for the grain shape orientation studies from the three areas visited. In that chapter stress and shear strain estimations are also made.

Chapter 7

Crystallographic Orientations - Results and Interpretations.

CONTENTS

Chapter 7.

Specimens of tectonised harzburgite, olivine and olivine gabbro were collected from all three areas of study. Orientated thin sections were made from most of the samples collected, and the crystallographic orientation of olivine and occasionally orthopyroxene was determined using a four-axis universal stage. The procedures used are outlined in Section 6.3 of Chapter 6.

7.1 The Presentation of Results

In order that the crystallographic orientations can be directly compared with the local field structures, the results have been presented on Enclosures 16-23 which use the same base maps as Enclosures 1-15 described in Chapters 2-4. They have been rotated back to original field orientations, and each crystallographic axis is plotted on a lower hemisphere equal area projection. A separate lower hemisphere equal area projection showing the orientation of the foliation and lineation trends in the specimen (where measurable) is included with the three crystallographic axes plots for each specimen.

In a few of the wadi traverses of Oman and in a few localities of the Troodos Peridotite Unit, specimens were collected by John Smewing and Paul Browning of the Open University. The olivine crystallographic orientations were determined for these specimens by Nik Christensen of the University of Washington, Seattle, U.S.A.. John Smewing has kindly made the data available for this study. The results of these studies

are also included on the enclosures along with the results of the work carried out for this thesis.

The data of Christensen have been contoured using the Kamb (1959) method of contouring. This method essentially uses a counting circle of a large enough size so that it will repeatedly obtain densities close to the expected number for a randomly distributed population. This technique eliminates any points on an equal area net which are not within the main concentrations of data. An area is only significantly overpopulated if it has a population density greater than twice the expected number for a random distribution. The projections of Christensen are contoured at intervals of 0.5 of the expected number for a random distribution, so that regions above the fourth contour interval are overpopulated in comparison to a random distribution.

The crystallographic orientation data collected for this study has not been contoured. This is because only a limited number of crystals were measured from each specimen (usually 20) because of the high degree of serpentinisation of most specimens. The Kamb (1959) method of contouring would eliminate a lot of the data points as random distributions and a false impression would be gained of the true crystallographic orientations present. As will be discussed below, the odd scattered axes points not within the main concentrations of data are highly significant when considering the overall deformation history of the rock.

It would obviously be tedious to describe each individual crystallographic orientation for all the areas studied. Instead the main similarities and differences between crystallographic trends will be noted and then compared with the orientations of the field data. The Peridotite Unit and Lower Cumulate Unit will be considered separately.

7.2 Crystallographic Results from the Peridotite Units.

The crystallographic data has been interpreted in Table 7.1. The active slip system has been determined, where possible, as well as its relationship to the D1 or D2 deformation events.

A study of Table 7.1 and the associated enclosures shows that only a few specimens give a distinct slip system for olivine and pyroxene. Most of the crystallographic plots do not give one of the expected plots described for olivine and pyroxene slip systems in Section 6.3.2 of Chapter 6.

7.2.1 Expected Olivine Crystallographic Plots

In all areas, the crystallographic plots which indicate a strong crystal slip in only one direction are related to the D2 field structural orientations. This is best shown at the base of the Rajmi traverse (Enclosure 16) where the olivine crystallographic directions show a strong cluster pattern for specimens 02/30, 02/31, 02/34 and 02/37. In all of these cases the (010)[100] slip system has been the last active slip system in olivine, with the [100] slip direction sub-parallel to the field lineation.

Higher up in the Rajmi traverse specimens 01/41, 02/04 and 02/13 all indicate the olivine $\{0k1\}[100]$ slip system as the last active slip system, again with [100] slip direction parallel to the D2 related field lineation.

These D2 related, expected slip systems are sporadically present in all areas studied and have been indicated on Table 7.1.

Area	Specimen (from moho downwards)	D2 olivine slip system (Unless D1 only)	D2 Shear sense (Unless D1 only (On a horizontal plane)	D2 Shearing Intensity.
Rajmi	01/41	{0kl}[100]	Sinistral	Very high
	01/47	?	? Dextral	Low
	01/54	{0kl}[100]	Dextral	Moderate
	01/45	?{0kl}[100]	Dextral	Low
	01/43	{0kl}[100]	Dextral	Moderate
	02/13	{0kl}[100]	Sinistral	Moderate
	02/10	{0kl}[100]	Sinistral	High
	02/07	{0kl}[100]	Dextral	Very High
	02/06	?{0kl}[100]	Dextral	Moderate
	02/04	{0kl}[100].	Sinistral	Very High
	02/33	?	Dextral	Low
	02/34	(010)[100]	Dextral	High
	02/29	(010)[100]	Sinistral	Low
	02/30	(010)[100]	Sinistral	High
	02/31	(010)[100]	Sinistral	Moderate
	02/37	(010)[100]	Dextral	Very High
Ath Thuqbah	01/32	?	? Dextral	Very Low
	01/29	?{0kl}[100]	Dextral	Moderate
	01/28	{0kl}[100]	Dextral	High
	01/27	?{0kl}[100]	Dextral	Low
	02/14	{0kl}[100]	Sinistral	D1 only
	02/16	?(010)[100]	Sinistral	Moderate
	02/17	?	?	Low
Al Juwayf	02/41	{0kl}[100]	Dextral	Very High
A'Bal	02/42	(010)[100]	Dextral	High
Dhahr	02/43	?	Dextral	Low
Hayl Ada	02/103	?(010)[100]	? Sinistral	High
Sarami	02/88	?{0kl}[100]	?	D1 only
	02/91	?	?	D1 only
	02/93	(010)[100]	Sinistral	High
	02/96	(010)[100]	Dextral	High
	02/99	(010)[100]	Dextral	Moderate
Kanut	02/83	?{0kl}[100]	?	D1 only
	02/82	?	?	D1 only
	02/81	{0kl}[100]	Sinistral	D1 only
Hajir	02/79	?	?	Low
	02/78	{0kl}[100]	Dextral	Moderate
	02/76	?	?	Low
	02/73	?{0kl}[100]	?	Very Low
	02/69	(010)[100]	Dextral	High

Table 7.1 The interpretation of crystallographic data from the Peridotite Units.

Area	Specimen (from moho downwards)	D2 olivine slip system (Unless D1 only)	D2 Shear sense (Unless D1 only (On a horizontal plane)	D2 Shearing Intensity.
Al Abyad	02/46	{0kl}[100]	Sinistral	High
	02/51	?{0kl}[100]	Sinistral	Low
	02/55	{0kl}[100]	Dextral	High
	02/57	?{0kl}[100]	Sinistral	Moderate
	02/61	?(010)[100]	Sinistral	Low
	02/63	{0kl}[100]	Sinistral	High
	02/64	{0kl}[100]	Sinistral	Moderate
Troodos (Specimens from north to south)	10/51	?{0kl}[100]	Dextral	Low
	10/42	{0kl}[100]	Dextral	Moderate
	10/39	?{0kl}[100]	?	Low
	10/38	{0kl}[100]	Sinistral	High
	10/36	{0kl}[100]	Sinistral	High
	10/52	{0kl}[100]	Dextral	High
	10/32	?	?	Very Low
	10/55	?	?	Low
	10/31	{0kl}[100]	Dextral	Moderate
	10/19	{0kl}[100]	Dextral	High
	10/26	{0kl}[100]	Sinistral	High
	09/03	?{0kl}[100]	? Dextral	Low
	10/25	?{0kl}[100]	? Sinistral	Low
	10/27	{0kl}[100]	Dextral	High
	10/28	(010)[100]	Dextral	Moderate
	10/30	?	? Dextral	Low
Fetlar	05/02	?	?	Very Low
	05/03	{0kl}[100]	Sinistral	Moderate
Unst Clibberswick Hill	05/26	{0kl}[100]	Sinistral	Moderate
	05/25	(010)[100]	Sinistral	High
	05/24	?{0kl}[100]	? Dextral	Low
Little Heog	05/21	?(010)[100]	Dextral	Moderate
	05/31	?{0kl}[100]	? Sinistral	Low
	05/32	?{0kl}[100]	Dextral	Moderate
Muckle Heog	05/13	?{0kl}[100]	Sinistral	Moderate
	05/19	?	? Sinistral	Moderate
	05/12	{0kl}[100]	Dextral	Moderate
	05/18	(010)[100]	Sinistral	Moderate
Crussa Field	05/10A	{0kl}[100]	Sinistral	Very High
	05/10B	?	?	Very Low

* Shear sense defined on a vertical E-W plane looking northwards.

Table 7.1 The interpretation of crystallographic data from the Peridotite Units. (Continued)

7.2.2 Less Clear Olivine Crystallographic Plots

Most of the olivine crystallographic plots do not show a distinctive slip system as found in the specimens in Section 7.2.1. In order to study the abnormal crystallographic trends, care must first be taken to identify specimens which may have undergone active slip on one of the low temperature olivine slip systems. (See Section 6.2.1). In these specimens, the olivine [100] axis will most probably not form a distinctive cluster pattern: instead the low temperature olivine slip direction, the [001] axis, should show a strong cluster pattern. (Figure 7.1). In the specimens studied no such crystallographic orientations were found.

A close inspection of olivine crystallographic plots from the Peridotite Unit shows that in almost all cases, the [100] axis plot gives the most distinctive trends from a cluster to a girdle pattern. The [010] and [001] axes give much more scattered patterns, especially where the [100] axes form a girdle pattern. This implies that the active slip direction has always been [100] for olivine. (See below).

In most specimens where the olivine [100] axis does not form a simple strong cluster trend but instead a girdle pattern, an area is still identifiable on the [100] girdle where the [100] points are more concentrated into a cluster. This cluster within a girdle most probably indicates the last active slip direction as, in areas where this direction is clearly defined by other specimens with strong [100] cluster patterns, the cluster within a girdle is sub-parallel to the last active direction. This is shown on the Rajmi traverse (Enclosure 16) by comparing the crystallographic plots of specimen 02/06

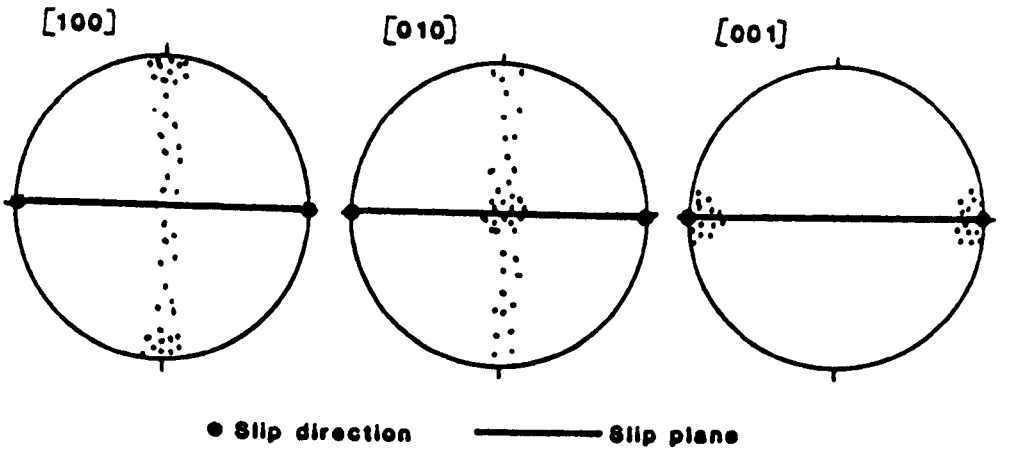

Figure 7.1 The expected crystallographic orientations for the olivine low temperature slip systems. (Equal area lower hemisphere projections).

([100] cluster within a girdle pattern) and specimen 02/07 ([100] cluster pattern): both [100] clusters are sub-parallel. Figure 7.2 summarizes the relationships between sepcimens 02/06 and 02/07.

The relationships observed in the [100] crystallographic plots from all of the areas studied suggests that, for most areas, the specimens have been deformed in a plastic shear flow environment in which the shear (slip) direction has changed. Figure 7.3 summarizes the expected [100] trends for a change in the shear direction. As can be seen, the stronger the shearing in the new direction, then the more likely it is for the [100] axes to plot as a cluster parallel to the shear direction.

The exact mechanisms of the rotation of grains into a new slip direction and the importance of recrystallisation of unfavourably orientated grains will be discussed in detail in Chapter 8.

At this stage it is possible to propose that the intensity of the last active slip direction determines the orientational variations of the olivine [100] axes. In a specimen which has undergone only a very small amount of shearing in the new direction (the D2 direction), a lot of the olivine grains which are crystallographically orientated towards the earlier shearing direction (D1), will be only slightly rotated towards the D2 slip direction, and very few grains will be recrystallised and grow in a favourable orientation for D2 shearing (i.e. [100] parallel to the D2 slip direction). If D2 shearing is more intense, more grains will break down and recrystallise

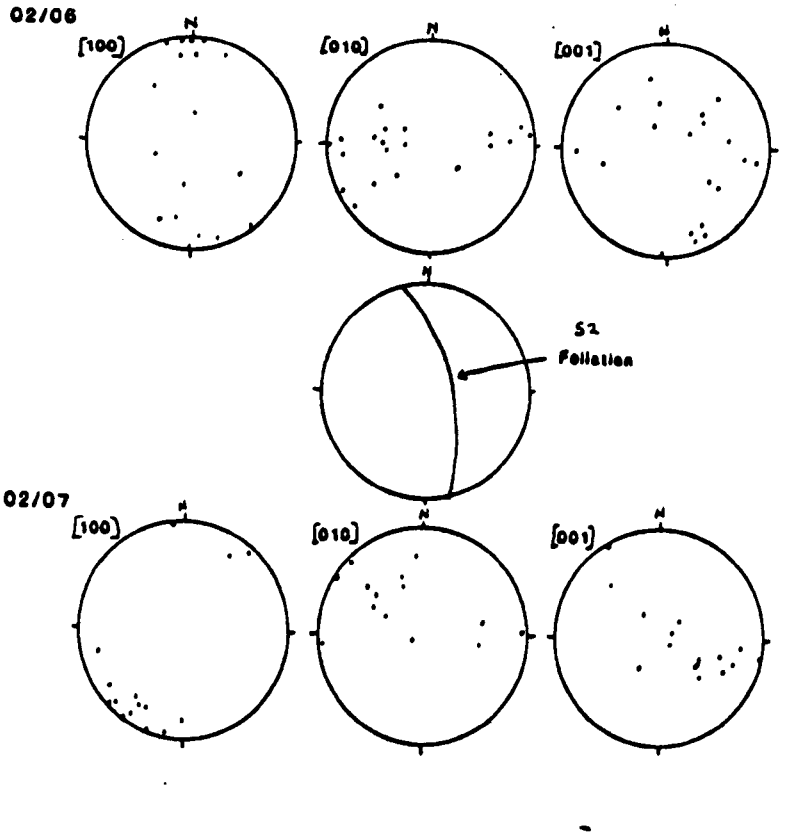

Figure 7.2 Crystallographic plots for specimens 02/06 and 02/07. The olivine [100] clusters for both specimens are parallel. (Equal area lower hemisphere projections).

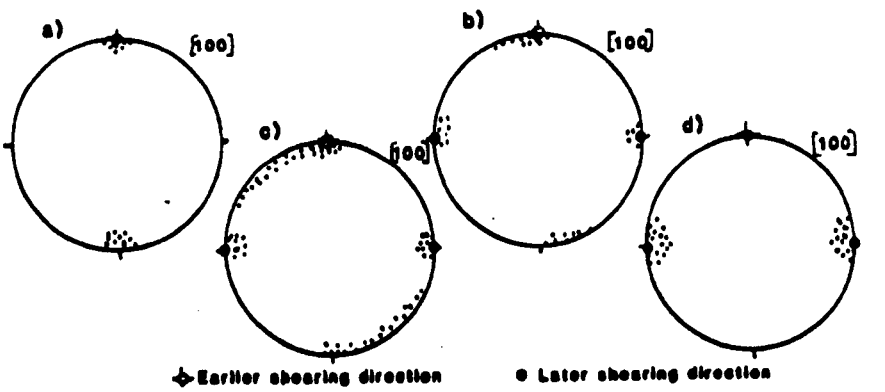

Figure 7.3 Progressive olivine [100] orientations for a change in the shearing direction. a) Earlier shearing direction only; b) Later shearing begins; c) Later shearing continues; d) Later shearing intense, earlier shearing trends destroyed. (Equal area lower hemisphere projections).

in the D2 shear direction, and those grains that do not break down will rotate much more than the example above towards the D2 shear direction. Thus, with an increase in D2 shearing, the [100] olivine axes will change from a cluster pattern parallel to the D1 shearing direction, to a girdle pattern between the D1 and D2 shearing direction, to a cluster pattern parallel to the D2 shearing direction. (See Figure 7.3). On the hand-specimen scale it can be seen that the Peridotite Unit has been deformed by simple shear as opposed to pure shear, (see below) and the angular relationship between the cluster and girdle patterns depends on the shear sense (Figure 7.4).

Most specimens show an intermediate [100] pattern with a partial girdle and a discernable D2 [100] cluster. This enables the D2 shearing direction to be fairly accurately defined for the majority of specimens and thus the determination of the shear sense if the rock has undergone deformation by simple shear.

The Kamb contoured data of Christensen give an accurate estimation of the D2 shear direction and the last active olivine slip system in areas which have undergone sufficiently intense D2 shearing. Specimen 01/45 from Rajmi shows a D2 cluster-slight girdle trend of olivine [100]. The equivalent specimen A-87 of Christensen shows an olivine {0kl}[100] slip system with the [100]axis parallel to the 01/45 D2 slip direction. (Figure 7.5).

In specimens which have undergone only a low intensity D2 shearing, however, the Kamb plot does not give an estimation of the D2 slip direction. Instead it only gives a mean value

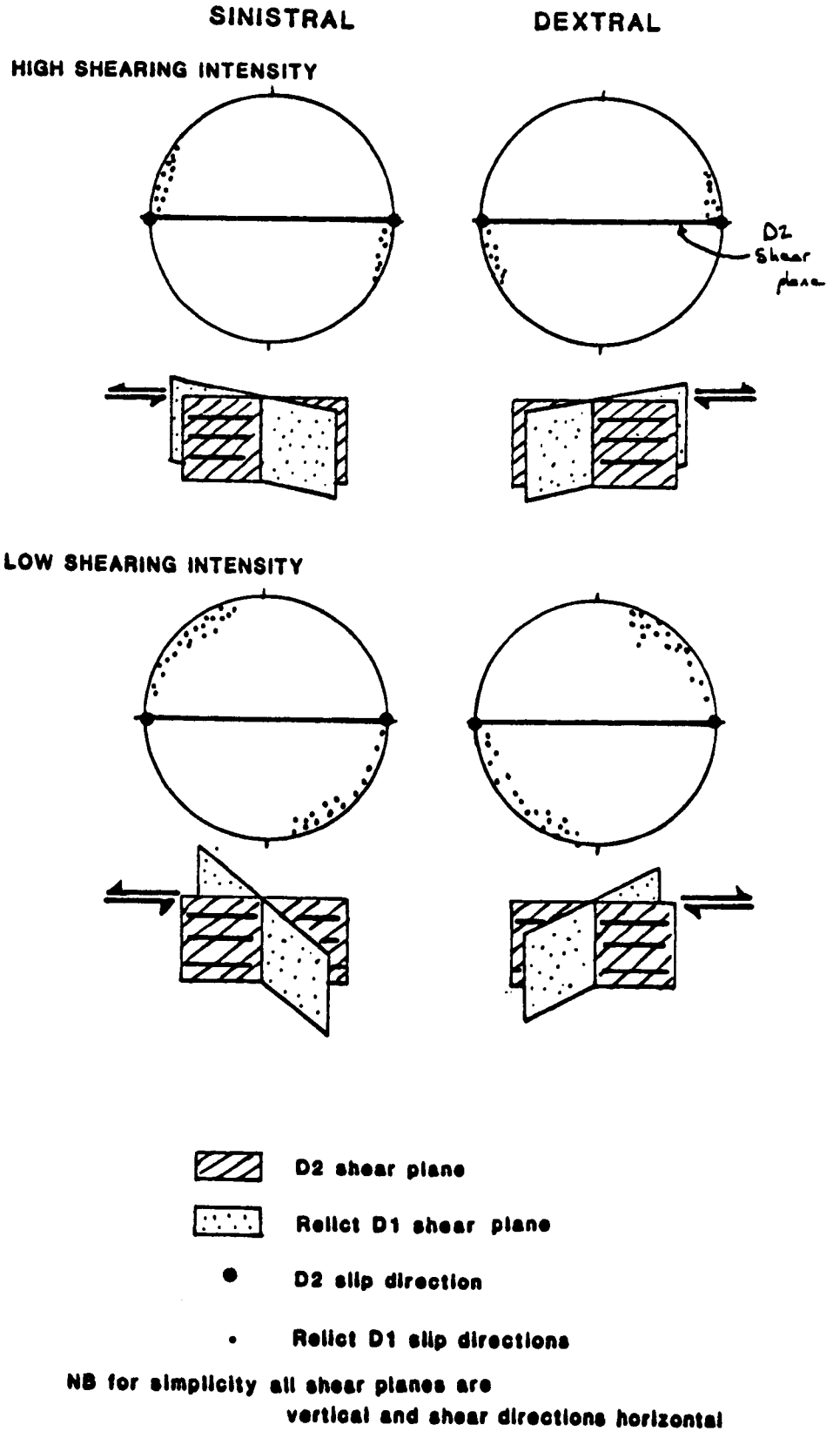

Figure 7.4 The angular relationship between the cluster and girdle patterns of olivine slip directions - dependence on shear sense. (Equal area lower hemisphere projections).

from all the [100] axes which has no structural meaning. Examples of this are specimens 02/16 and A-102 from the Ath Thuqbah area (Enclosure 17). The Kamb plot of A-102 shows a completely different mean [100] slip direction from that of the equivalent specimen 02/16. (See Figure 7.6). The D2 slip direction dips at a shallow angle towards the north, and the [100] plot of sample A-102 bears no relationship to this direction. In the Wadi Ath Thuqbah area the data of Christensen have been interpreted by Smewing et al (1983) to infer a main slip direction that dips towards the ENE instead of towards the north as proposed above from more detailed crystallographic studies.

The Kamb plotted data sometimes give a more girdle like pattern for the [100] axis which is more similar to the uncontoured data from the specimens collected for this study. E.g. Specimens 02/55 and A-2309 from Wadi Al Abyad. (See Enclosure 21). Specimen A-2306 from the Al Abyad area gives a two-point maximum [100] Kamb plot which Browning (1982) points out but does not explain. (Enclosure 21). The uncontoured crystallographic plot for this specimen would be expected to have a girdle pattern with possibly both D2 and D1 partial clusters. (The raw uncontoured plots of Christensen were not available for study).

7.2.3 Olivine Crystallographic Orientations and Field Structural Data.

A comparison of the crystallographic orientations, and the field foliations, lineations and thin section textures shows a strong correlation between the different data sets.

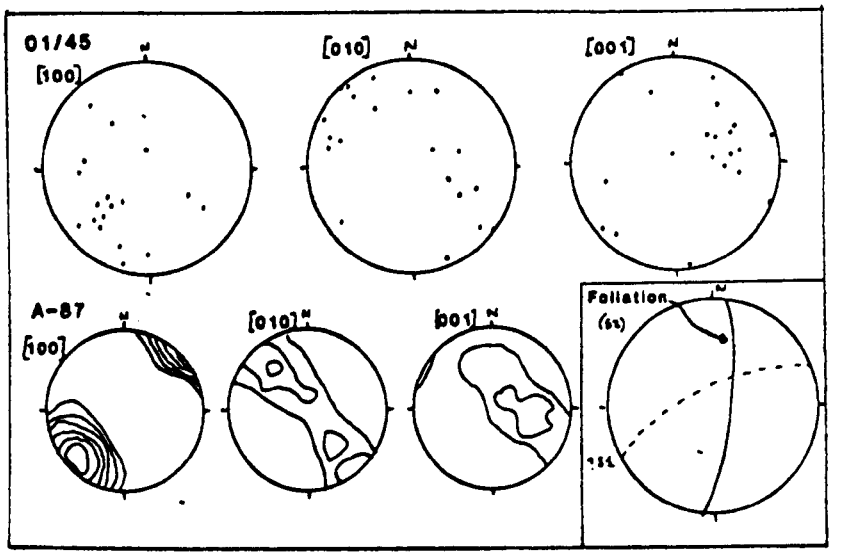

Figure 7.5 Olivine crystallographic plots of specimens 01/45 and A-87. (Equal area lower hemisphere projections). Specimen A-87 is Kamb contoured.

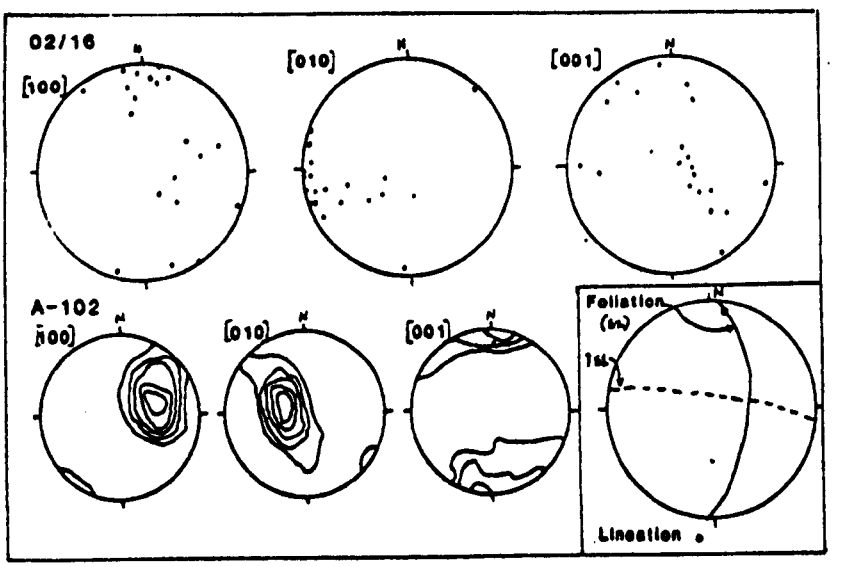

Figure 7.6 Olivine crystallographic plots of specimens 02/16 and A-102. (Equal area lower hemisphere projections). Specimen A-102 is Kamb contoured.

In areas of intense D2 shearing, such as at the base of the Rajmi traverse (Enclosures 2 and 16), the olivine [100] axes show strong cluster plots. These are sub-parallel to the field lineations which are defined by the alignment of chrome-spinel grains and identifiable orthopyroxene grains. (See Chapter 2). The D2 foliation planes have a constant trend and are similarly defined from spinel and orthopyroxene grains. They are sub-parallel to the olivine slip planes, the poles of which are defined by the olivine [010] axes for the (010)[100] slip system. (See Section 6.2.1). No relict D1 foliation planes or lineations have been preserved in these areas of intense D2 shearing. All the thin section textures are porphyroclastic to mosaic porphyroclastic.

In areas of weak D2 shearing such as between easting 230 and 250 in the Wadi Rajmi traverse, (Enclosures 2 and 16) the olivine [100] axes plot as girdle trends containing D2 clusters. Field lineations are difficult to measure in this area because of the low intensity of shearing. The D2 foliations are only sporadically developed and often relict D1 foliation planes are preserved; the poles of which form a girdle pattern. In both Cyprus and Shetland the D1 foliation has been preserved over large areas and shows an obvious folding type pattern around the D2 foliation plane. (i.e. the D1 foliation poles plot as a girdle pattern which includes the D2 foliation pole cluster). Such an obvious folding pattern is not so clear in areas of low intensity D2 shearing in the Peridotite Unit of Oman because of the scarcity of data from only one dimensional traverses.

However, a close examination of the data presented in Enclosures 1-8 would suggest a similar folding type pattern with relict D1 foliation planes in areas of low D2 shearing intensity.

A field lineation is measurable in some of these areas. It is of interest to note that the pattern of the lineation plots are the same as the olivine [100] axes from the same areas; for example compare the field lineation plots (Enclosure 7) with the various specimen [100] plots for the same areas of Wadi Al Abyad (Enclosure 21). This comparison shows that in areas of low D2 shearing intensity, some spinel grains are still sub-parallel to the earlier relict D1 shearing direction. This is possible as many spinel grains have most probably been crystallised prior to olivine growth and prior to either D1 or D2 shearing. (See thin section details in Chapter 2). Thus if an olivine crystal grows around a spinel grain orientating it parallel to the olivine shape elongation direction (i.e. the D1 foliation and lineation), and the olivine grain is not broken down and recrystallised, but only slightly rotated by the D2 shearing, then the spinel grain will preserve a rotated D1 orientation. If the olivine grain is recrystallised by D2 shearing, then any internal spinel grains will themselves become reorientated parallel to the new elongation direction. Thus the spinel grains act essentially as passive markers within the olivine crystals. (Figure 7.7). Chrome spinel in fact has a much more complex deformational history than that discussed above (see Christiansen, in press) with various crystallisation and deformational events. However, early spinel grains can be fairly easily identified by their elongate shape and regular size (See Chapter 2). The relationships between rotated and recrystallised olivine grains will be discussed in Chapter 8.

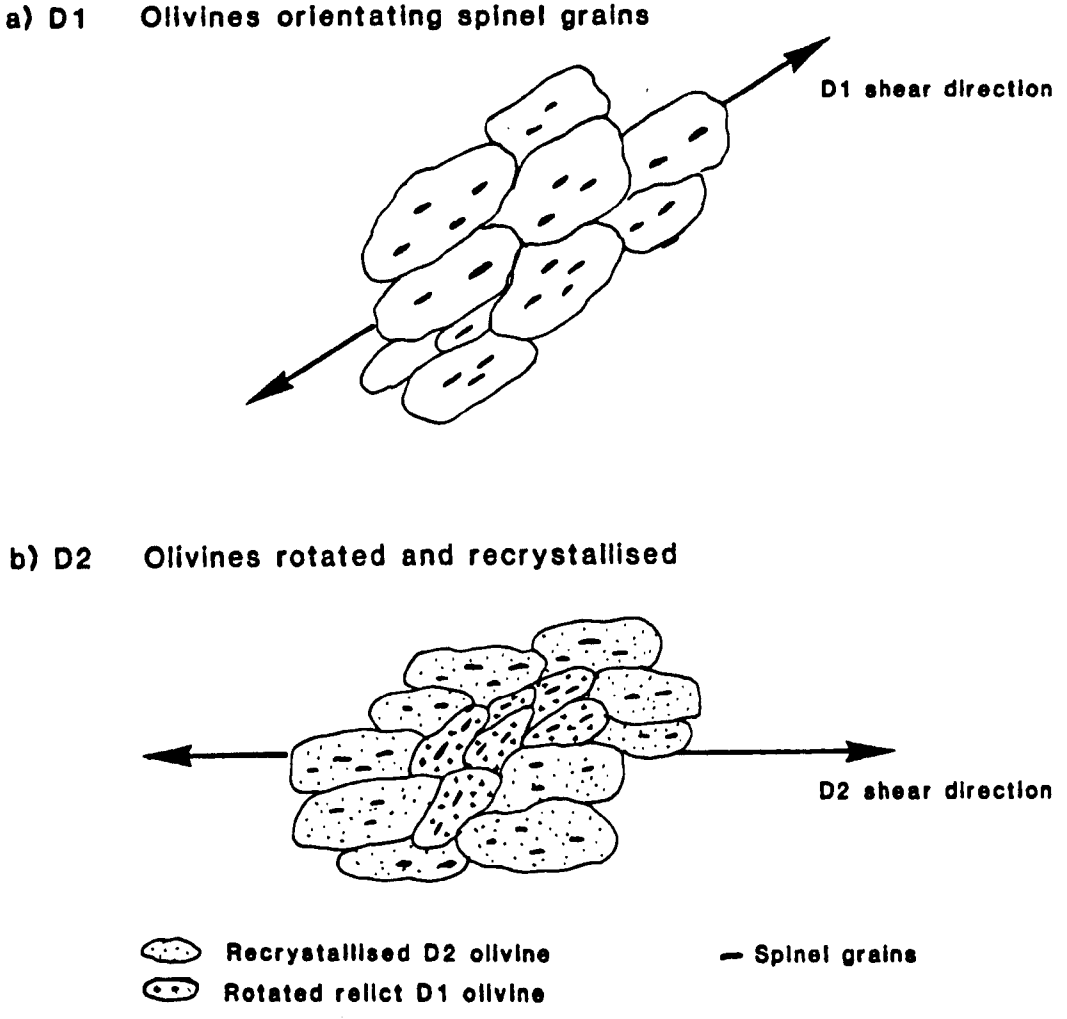

Figure 7.7 A sketch showing how spinel grains act as passive markers within olivine crystals and thus define a relict foliation in some grains.

The thin-section tectures in areas of low D2 shearing intensity vary from coarse to porphyroclastic.

In the topmost Peridotite Unit of the Wadi Sarami traverse and in Wadi Kanut no D2 shearing is apparent. The field foliations and lineations have constant trends over the whole area unaffected by D2 (see Enclosure 5 and Chapter 2). The olivine [100] axes, however, do not give the expected strong cluster patterns sub-parallel to the field lineations. Instead the [100] axes form very disperse clusters. This observation and the fact that all the specimens collected from this area except for 02/83, have coarse textures implies that extensive recrystallisation and grain growth has occurred in the olivines. Most of the olivines are extremely large (up to 5cm) and are unstrained (See plate 2.44, Chapter 2). This implies that annealing has occurred after the main D1 event but that the annealed crystallographic orientations are still partially controlled by the D1 shearing direction. The Sarami and Kanut areas are the only areas studied in which D2 shearing has not affected parts of the Peridotite Units.

7.2.4 Simple Shear and Shear Sense Determination.

On the whole, it is possible to define, for most specimens, a D2 slip direction, a D2 slip plane if the (010)[100] olivine shear system has been operative, a D2 foliation (S2) and a D2 lineation (L2 - a slip lineation). Where measurable these data have been plotted on an equal area projection next to the crystallographic axes plots on Enclosures 16-23.

It is clear on the hand-specimen scale that the shearing deformation can be considered a simple shear process. (See Section 6.4). In most specimens where the D2 slip direction is well defined by a strong olivine [100] axis cluster, a distinct angular relationship exists between the slip direction and the lineation. Using the theories discussed in Chapter 6 a shear sense has been calculated for suitable specimens. This data is included on Table 7.1.

Unfortunately the inaccuracy of the data does not enable a shear angle and thus a shear strain to be calculated for each specimen. It is only possible to qualitatively estimate the shear strain by considering the trends of the olivine [100] axes, the field lineations and foliations (see Section 7.2.5 below) and the thin section textures already described in this thesis. The possibility of using the crystal shape fabric as an indicator of the shearing intensity is discussed in Chapter 8. A qualitative estimation of the D2 shearing intensity for each specimen is included in Table 7.1 (i.e. Very low, low, moderate, high, very high).

7.2.5 Shear Folding

Detailed structural mapping on the scale of 1:250 in both Cyprus and Shetland (See Chapters 3 and 4, and Enclosures 28 and 30) has shown that the D1 foliation (S1) is folded about the D2 foliation (S2) on a small scale with the fold amplitude varying between 5 and 25 metres. The most obvious way for this folding pattern to have occurred is by shear folding. This type of folding occurs in environments which are deforming by progressive simple shear as is thought to have happened in the Peridotite

Units of the three ophiolites studied.

Figure 7.8 is taken from Hobbs et al (1976) and summarises the main principles of a shear folding model. For perfect shear folding to occur the strain must be a plane strain. However, in rocks within the Peridotite Unit, annealing recrystallisation is also a major process of deformation so that in the natural environment, the conditions of strain will not necessarily be of plane strain for all areas.

If an originally constantly trending lineation is deformed by shear folding, then the resulting lineations plot as a great circle trend which includes the slip lineation. (Figure 7.8). This is the trend observed in all areas in which the D2 shearing intensity has not been too great to destroy the relict D1 related lineations.

In all areas the D2 shear plane is parallel to the fold axial plane and the D2 shearing event is clearly associated with the folding pattern. A flexural slip or flow or any other folding type model can thus be ruled out as the mechanism of folding in the Peridotite Unit - in these cases earlier lineations only form great circle patterns after deformations if the earlier lineation was perpendicular to the fold axial plane prior to deformation. (See Hobbs et al, 1976). Otherwise small circle or other trends are formed.

In the shear folding model the different fold limbs are formed by a change in the sense of shearing. (Figure 7.8). If one shear sense is dominant in an area, then an asymmetric fold pattern is obtained as shown in Figure 7.9. The initial orientation of the S1 plane prior to deformation , the shear

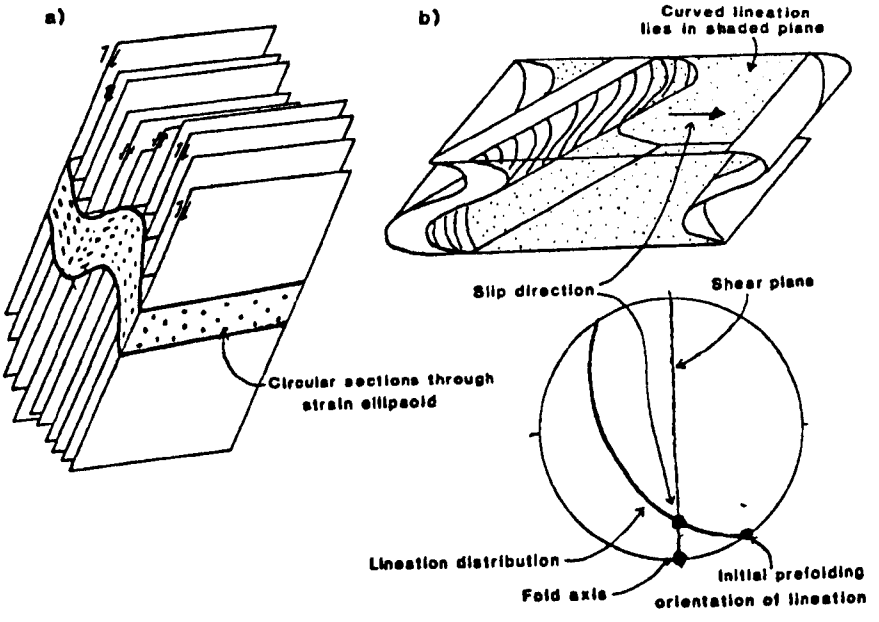

Figure 7.8 The main principles of a shear folding model. a) The production of similar folds by a change in the shear sense; b) The folding of an initially planar surface by shear folding and the deformation of an initially constantly trending lineation. (Modified from Hobbs et al, 1976).

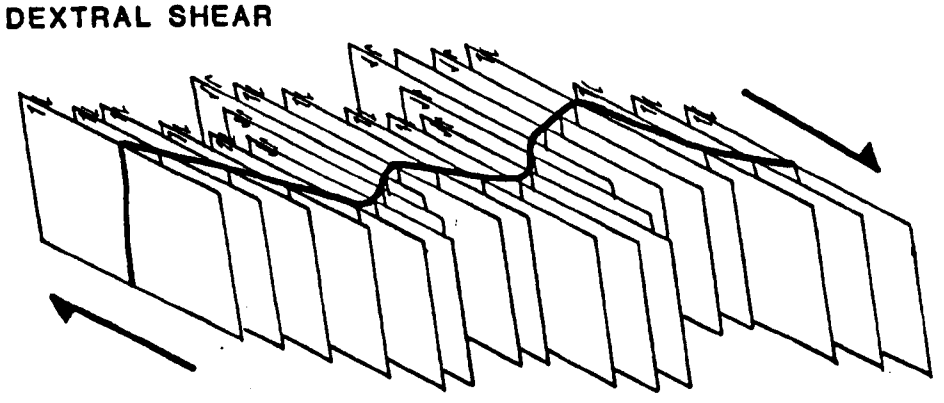

Figure 7.9 Production of an assymmetric fold pattern in an area of a dominant shear sense.

strain of the D2 deformation, and the D2 shear sense will determine the final orientation of the S1 plane in relation to the S2 plane (fold axial plane). Figure 7.10 summarises this and shows a graphical plot of the shear strain versus the angle between a line and the shear direction for different lines of various initial orientations. The theory behind this figure is discussed in Appendix 1 , and is used in section 7.2.6 to determine shear senses for the different areas.

In all three areas of study it is clear that the intensity of shearing and the sense of shearing rapidly change within very small areas. Three pairs of specimens were collected: 01/27 and 02/28 from Wadi Ath Thuqbah; 02/63 and 02/64 from Wadi Al Abyad; and 05/10A and 03/10B from Unst, Shetland. In all three cases the specimens were located only a few metres apart. Figure 7.11 shows that even though the specimens have been collected from essentially the same locality, their crystallographic plots give different deformational histories. In the Ath Thuqbah area specimen 01/28 gives a fairly strong olivine [100] cluster plot implying that the D2 deformation has been fairly intense, the 01/27 specimen shows a more girdle-like pattern for the [100] plot implying a less intense D2 deformation history. In Wadi Al Abyad a similar pattern is evident with specimen 02/63 implying an intense D2 and 02/64 a much less intense D2. In the Shetland specimens the variation in D2 intensity is even more marked with specimen 05/10A showing an intense D2 shearing, but specimen 05/10B showing very weak D2 shearing, with only a

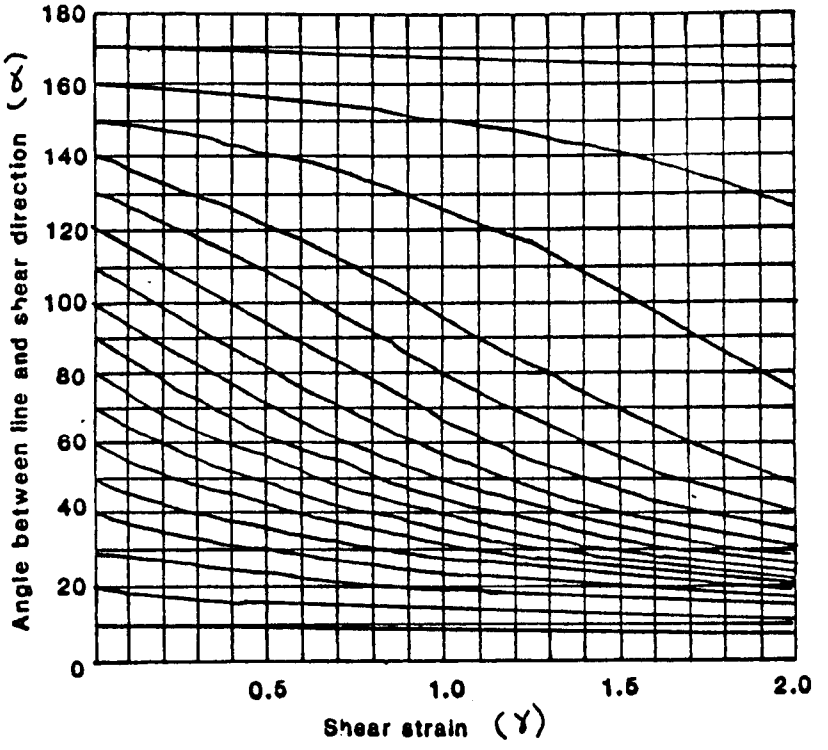

Figure 7.10 The relationship between shear strain and the initial orientation of a line with respect to the shear direction. (From Ramsay, 1967).

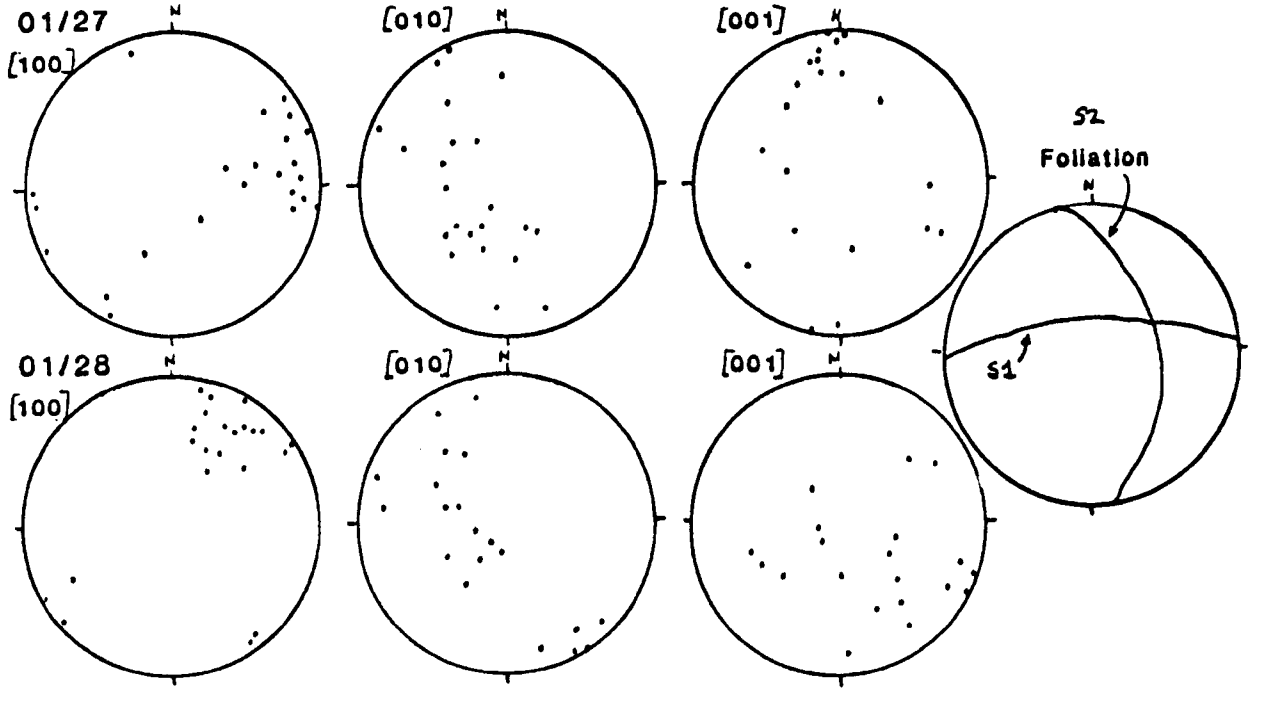

Figure 7.11 (See next page for caption)

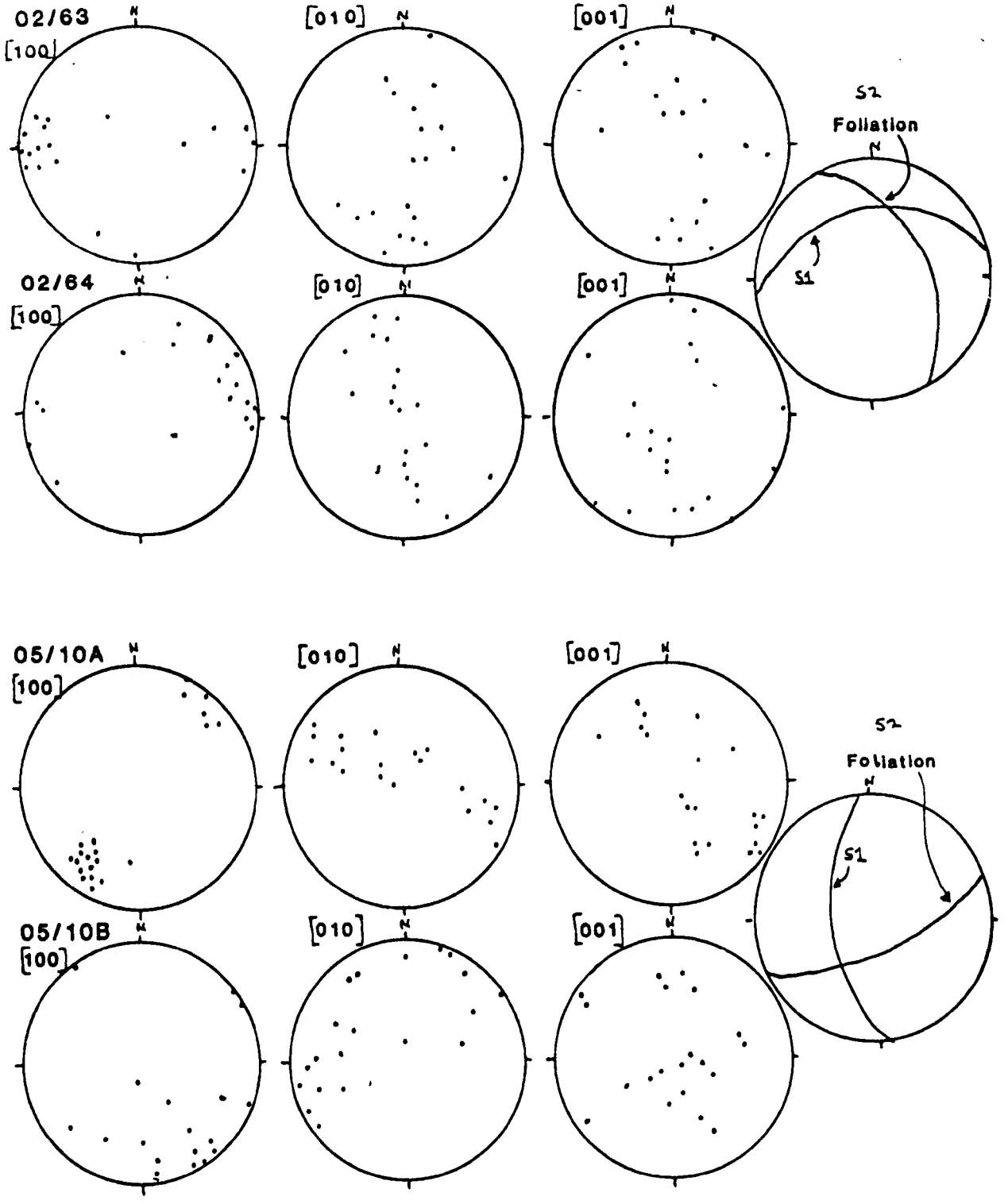

Figure 7.11 Equal area olivine crystallographic plots of specimens 01/27, 01/28, 02/63, 02/64, 05/10A and 05/10B.

few [100] axes parallel to the D2 slip direction with most preserving relict D1 slip directions which have been partially rotated by D2 shearing.

If the D2 deformation is essentially a simple shear type of deformation, then, if sufficient data is available, it should be possible to calculate the approximate orientation of the S1 plane before D2 deformation took place, and also the approximate shear strain, from the angles between the S2 and S1 planes from the same locality over a sizeable area. The theories and method of calculations for these relationships are discussed below.

7.2.6 Simple Shear and the Angular Relationships Between S1 and S2 Planes

(a) Simple Shear - Expected Structural Relationships

If a rock has been deformed by simple shear then the following relationships will always hold:

(i) The slip lineation (L2) associated with the simple shearing will always lie in the slip plane.

(ii) Where shear folding occurs the fold hinge axis will always lie in the slip plane but can make any angle with the slip lineation direction. This will depend on the orientation of the original layering or foliation plane prior to simple shearing taking place.

(iii) A constantly orientated lineation (L1) on the original layering or foliation plane (S1) will form a great circle trend after shearing has taken place. The slip lineation (L2) associated with the shearing will also lie on this great circle. The distribution of the earlier lineation (L1) on the great circle will depend on the initial orientation of the L1 lineation with respect to the shear direction and also on the intensity and sense of the shearing.

(iv) If the earlier foliation (S1) or layering plane had a constant orientation prior to deformation, then the poles to this plane will plot as a great circle trend after D2 shearing has taken place, the pi-pole girdle also including the shear plane pole (S2 foliation). The distribution of S1 poles will depend on the original S1 orientation and the intensity and sense of D2 shearing

as for the L1 distribution. The foliation pi-pole girdle orientation, however, bears no relation to the lineation great circle orientation for a shear folding environment.

Figure 7.12 demonstrates these relationships firstly for the simple case where the S1 plane was originally perpendicular to the D2 slip direction; secondly the case where the S1 was not originally perpendicular to the D2 slip direction but its pole still lay in the D2 slip plane; and thirdly the more general case where the S1 plane was not originally symmetrically oriented with respect to the D2 slip plane.

In all cases of simple shear there will be no differential strain on the shear planes themselves. On these planes the strain ellipsoid will be circular and thus there will be no change in any angular relationships within this plane during shearing deformation. Thus, in the cases considered in Figure 7.12, the line of intersection between the S1 plane and the D2 shearing plane will have a constant orientation before, during and after D2 shearing has taken place (Figure 7.13). This line is the same as the fold hinge axis in an area where shear folding has taken place.

The structural orientations described in Chapters 2 to 4 all conform to the orientations expected from deformation by a simple shear and shear folding type process.

(b) The Measurement of Angles between S1 and S2 Planes in a Rock which has undergone D2 Simple Shearing

It is important, when measuring angles between structural elements in a rock that has undergone simple shearing, that the angles are always measured on the plane which is parallel to the

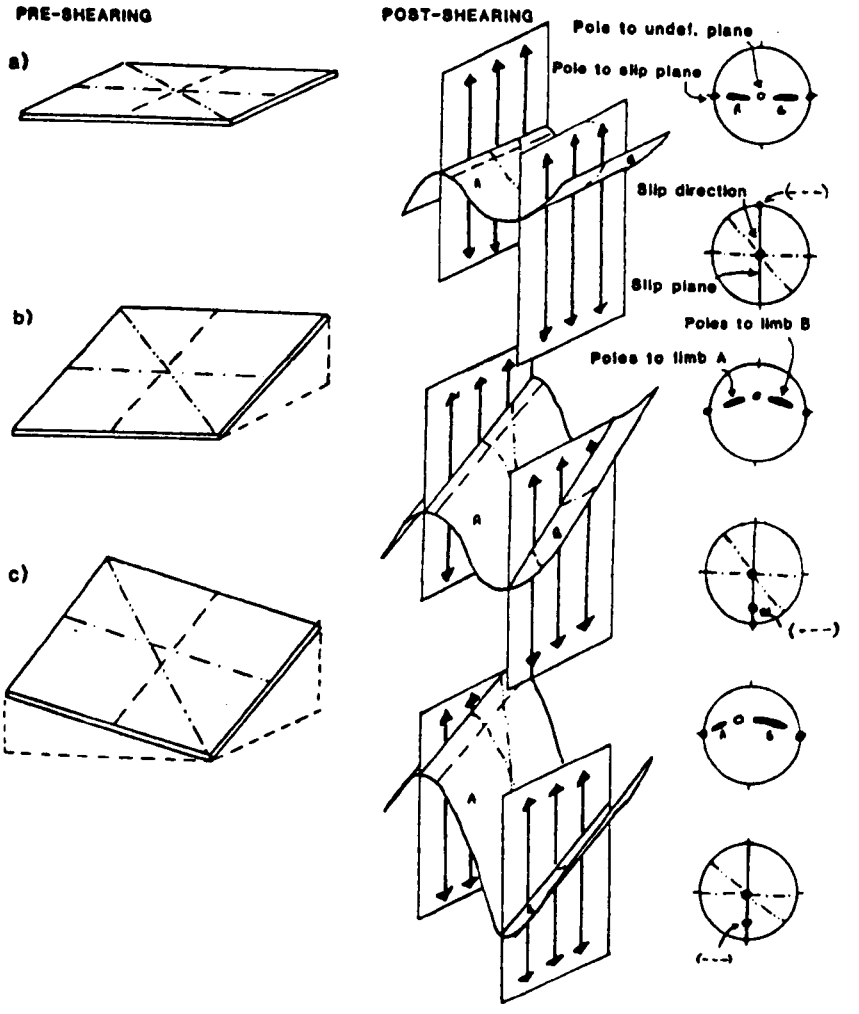

Figure 7.12 The deformation of an initially planar surface and constantly trending lineation by simple shear. a) S1 plane initially perpendicular to D2 slip direction; b) S1 plane initially not perpendicular to D2 slip direction but symmetrical to the D2 slip plane; c) S1 plane assymmetrical to the D2 slip plane and slip direction. (Equal area lower hemisphere projections).

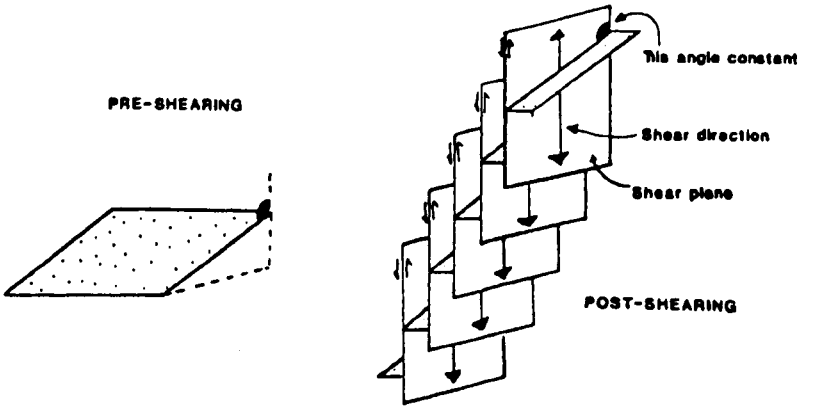

Figure 7.13 Sketch showing that the line of intersection between the S1 plane and D2 shearing plane will have a constant orientation before, during, and after D2 shearing. (Equal area lower hemisphere projections).

slip direction and perpendicular to the slip plane. This is termed the 'Y' plane and is approximately perpendicular to the intermediate principal finite strain axis. (Figure 7.14)

The angle between an S1 foliation plane and the shear deformation S2 foliation plane on the 'Y' plane can easily be estimated and can be related to the intensity of shearing as long as the following assumptions are made:

(i) The D2 deformation is by simple shear

(ii) The S2 plane is sub-parallel to the shear plane, and the L2 slip lineation is sub-parallel to the shear direction. (In a simple shear environment this is obviously not true; the angular difference between the S2 and the shear plane will typically be in the range of 0 to 30°. For the purposes of this study, however, accurate measurements of the shear plane and shear directions are not possible and for only semi-quantitative results this second assumption is reasonable.)

(iii) The S1 foliation plane and L1 lineation had a constant orientation over a large area prior to D2 shearing. In all Peridotite Unit areas studied, the S2 plane and L2 slip lineation have a constant orientation over a large area. In the Wadi Sarami and Kanut area where no D2 shearing has occurred see Section 7.2.3) the S1 foliation and L1 lineation have constant orientations. The evidence discussed in this and preceeding chapters suggests that the D1 structures have been formed by similar mechanisms to the D2 structures, the only difference being in the shear directions. It would thus seem a fair assumption that the D1 structures initially had constant orientations.

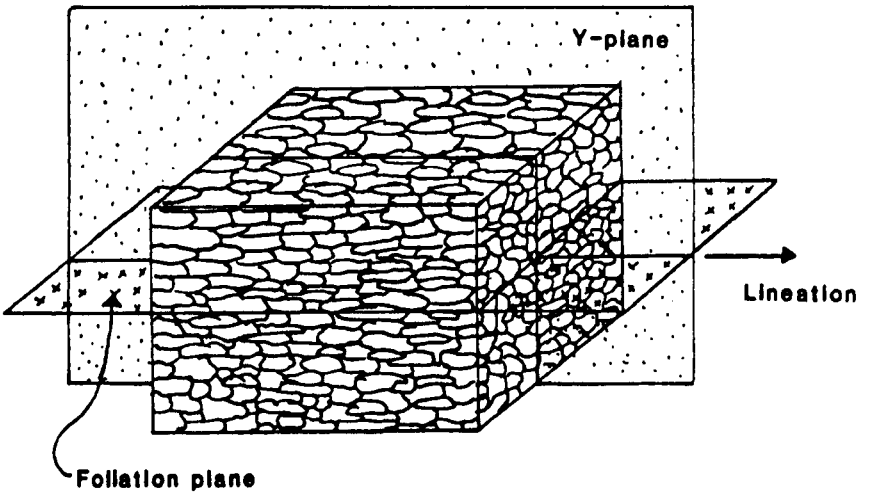

Figure 7.14 Penetrative foliation and mineral stretching lineation and their relationship to the 'Y' plane.

If these assumptions are accepted then it is possible to compare the S1 measurements from an area and relate their different orientations to variations in D2 shear sense and shear intensity.

Calculation of the angle between the S1 and S2 planes

As mentioned above the angle between the S1 and S2 planes must be measured on the 'Y' plane. In order to do this the 'Y' plane must firstly be defined. Figure 7.15 summarises how this is done. For a locality where a specimen has been collected and the slip direction determined, the'Y'plane is the great circle joining the slip direction with the pole to the slip plane. This great circle should intersect the S2 plane approximately in the vicinity of the L2 lineation, or at the intersection of the lineation great circle with the S2 plane where no L2 lineation is discernable. (Figure 7.15) The pole to the S2 plane should also be roughly within the 'Y' plane.

In most localities the D2 slip direction is not accurately known but an approximation of the 'Y' plane can still be made by using the structural data available. As the S2 and L2 orientations are fairly constant over large areas, a mean 'Y' plane can be calculated for the whole area of study.

The pole to the foliation pi-pole girdle will obviously plot on the S2 plane. The angle between this point and the intersection of the 'Y' plane with the S2 plane will remain a constant value for deformation by simple shear (as discussed above). Thus all S1 planes must intersect the S2 plane at this point (as is obvious from the pi-pole girdle).

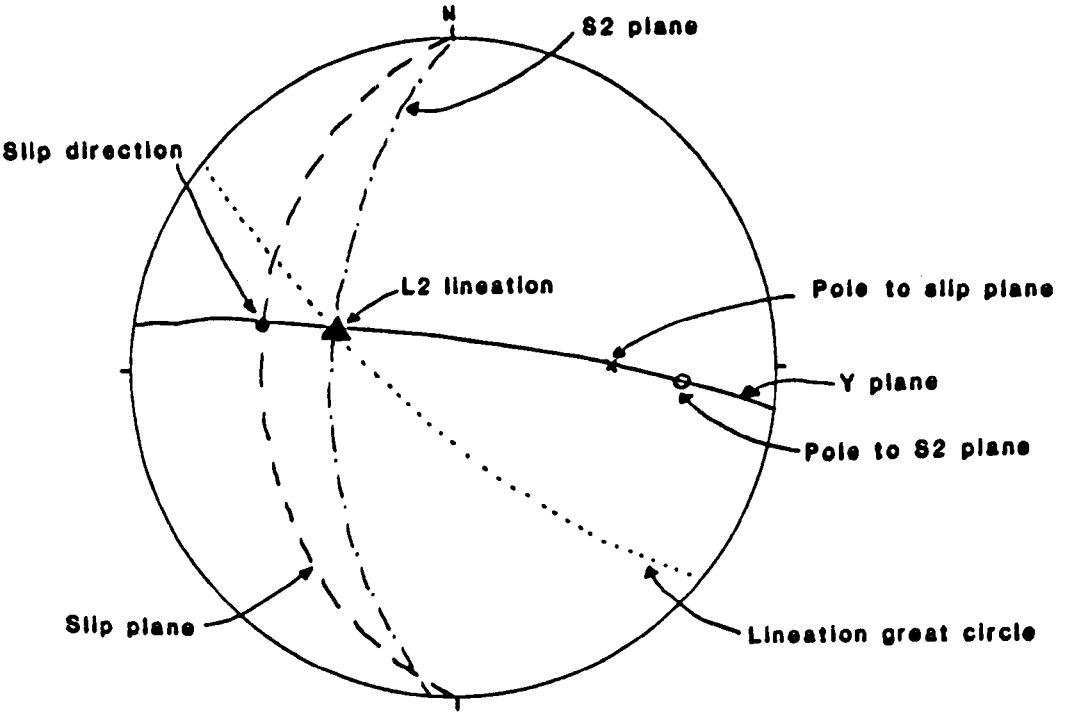

Figure 7.15 The definition of the 'Y' plane from the relationship between the different structural elements. (Equal area lower hemisphere projection).

If the 'Y' plane is graduated in 10^{o} intervals starting from its point of intersection with the S2 plane as is shown in Figure 7.16, then the angle between the S2 and S1 planes on the 'Y' plane can be read directly by plotting the S1 plane on the equal area projection and reading the value of the angle on the 'Y' plane at the intersection of the S1 plane with the 'Y' plane (see Figure 7.16), The value of the angle obviously depends on the shear sense as determined from crystallographic studies. This is made clear on Figure 7.16.

For individual samples for which the shear sense is known, the angle between the S2 and S1 planes can be directly measured. This gives, for each area, a range of angles for each shear sense. Where enough data is available,a rough estimation of the orientation of S1 before the D2 deformation is possible,as is shown in Figure 7.17. This, in effect, correlates the angle between the S2 and S1 plane with a shear sense and gives a rough estimation of the shearing intensity at each locality.

In order that a fairly quick estimation of the angle between the S2 and S1 plane on the 'Y' plane can be made, the approximate foliation pi-pole girdle can be graduated into angles as shown in Figure 7.18. This is done by joining each 10^{o} interval on the 'Y' plane with the pole to the pi-pole girdle, this giving a series of great circles, each representing an S1 plane at a specific angle from the S2 plane. The pole from each of these planes is then plotted on the pi-pole girdle thus giving a graduated pi-pole girdle for angles between the S2 and S1 planes on the 'Y' plane. (Figure 7.18)

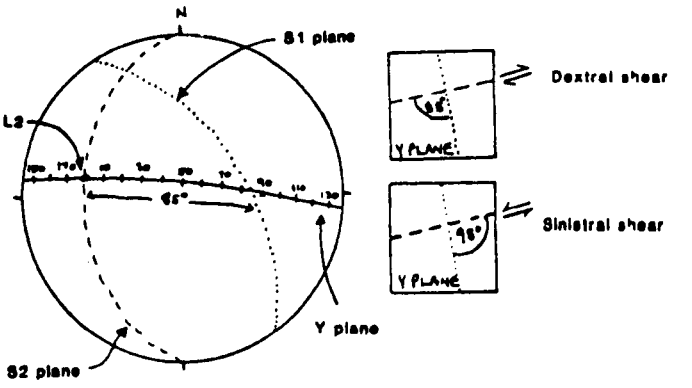

Figure 7.16 Graduation of the 'Y' plane and the calculation of the angle between the S2 and S1 planes on the 'Y' plane. (Equal area lower hemisphere projection).

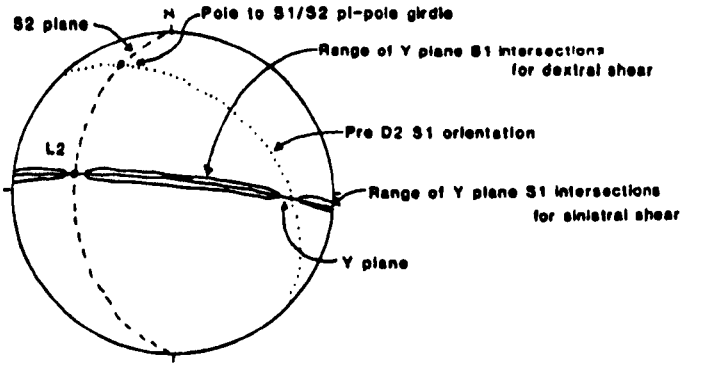

Figure 7.17 The estimation of the pre-D2 orientation of the S1 plane. (Equal area lower hemisphere projection).

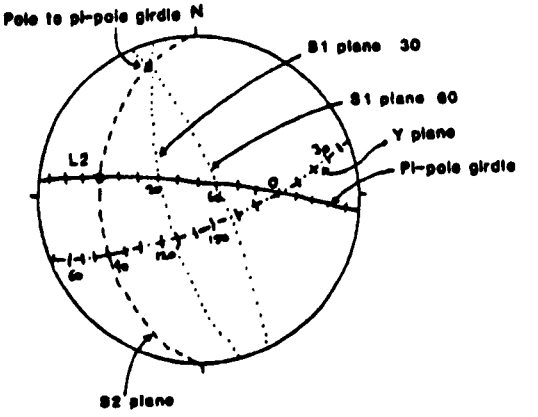

Figure 7.18 The graduation of the foliation pi-pole girdle from the orientation of the 'Y' plane and pole to the pi-pole girdle. (Equal area lower hemisphere projection).

Thus, with only minor rotations of individual S2 measurements towards the mean S2 pole for each area, the angle between the S1 and S2 planes can be estimated rapidly for each locality. The angles measured are then plotted on a histogram similar to that in Figure 7.19. This gives an indication of the range of shear intensities and also the dominant shear sense present within an area.

The histogram of the angle between the S1 and S2 planes on the 'Y' face can be directly related to Figure 7.10 as the angles measured are roughly equivalent to α on Figure 7.10 (the angle between a line of a known pre-D2 orientation and the shear direction). Once the shearing intensities derived from olivine crystallographic orientations and thin section textures have been taken into consideration, the histogram can be roughly qualified into the variation of shear intensity (γ). This is done by considering the range of α angles present for each area and the estimations of shear derived from the methods above, and correlating them with the graph in Figure 7.10. For shear values up to 1.0, the ideal initial orientation of the S1 planes before D2 deformation is between 70^{o} and 150^{o} for α, as these values give the largest variation in α for a change in the shear (γ). If the initial orientation of S1 is close to that of S2, then the orientation of S1 will hardly change with an increase in shear, and thus little information on the shear intensity can be gained from α (Figure 7.20).

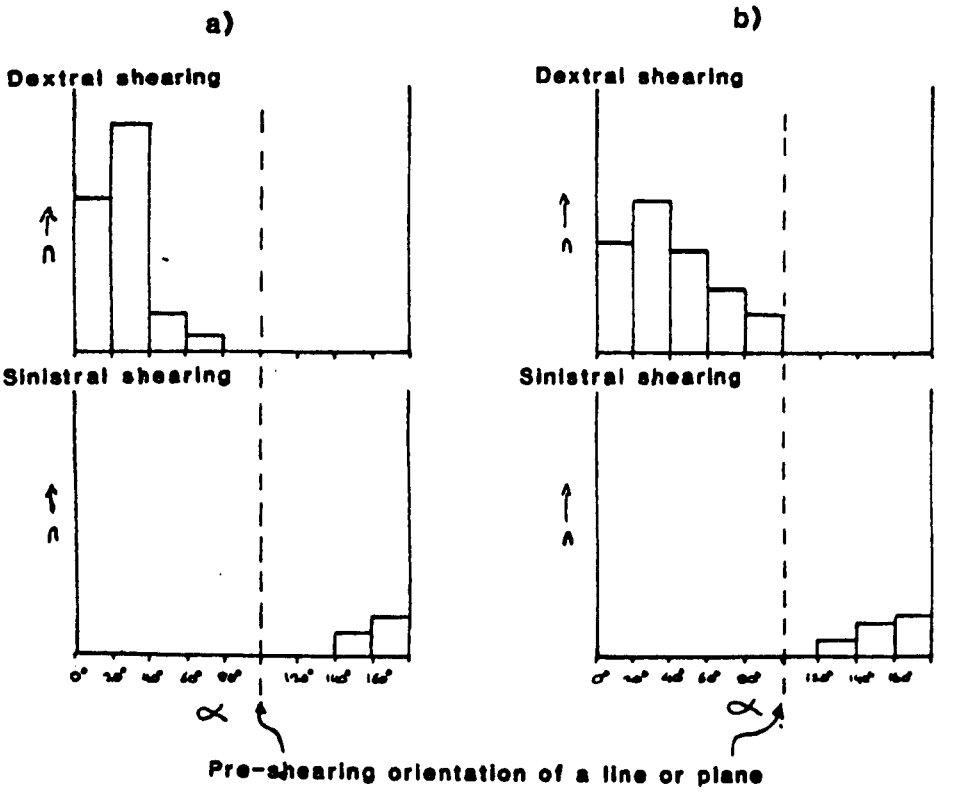

Figure 7.19 Typical histograms of α angles. a) Intense shearing; b) Weak shearing.

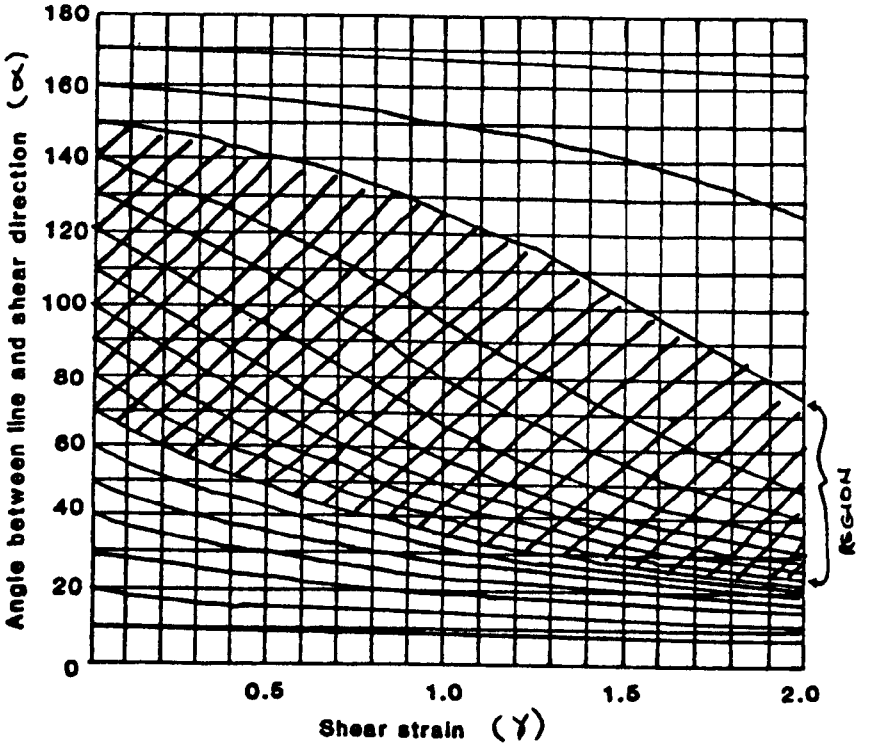

Figure 7.20 Figure 7.10 showing regions in which most information can be gained on the shear intensity. (Modified from Ramsay, 1967).

It must be stressed here that all these potential results are based on the assumptions made at the start of Section 7.2.6(b). However, as is shown below, the constant attitudes of the D2 structures from most Peridotite Unit areas do give fairly consistent results and it would seem that they are at least semi-quantitatively meaningful.

7.2.7 Estimates of Shearing Intensities from the Areas Studied

The theories and methods discussed in Section 7.2.6 have been used to estimate the dominant shear sense of D2 deformation for each area of Peridotite Unit studied. A mean foliation pi-pole girdle has been constructed and graduated with α angles for each area (Figure 7.21).

A careful study comparing the shear sense determined from crystallographic studies for each specimen with the α angle calculated from field measurements allows a range of α values to be obtained for each shear sense for each area. In Cyprus and Shetland where detailed two dimensional mapping was done and a large number of specimens were collected over relatively small areas, the α angle relation to shear sense can be determined fairly accurately. Figure 7.22 shows the distribution of α angles for each shear sense. It is clear from the estimation of shear intensities from textural and crystallographic evidence (Table 7.1) that the largest α angles measured for each shear sense indicate areas of very low D2 shearing, and that the S1 plane in these areas must be close to its original pre-D2 orientation.

a) Rajmi

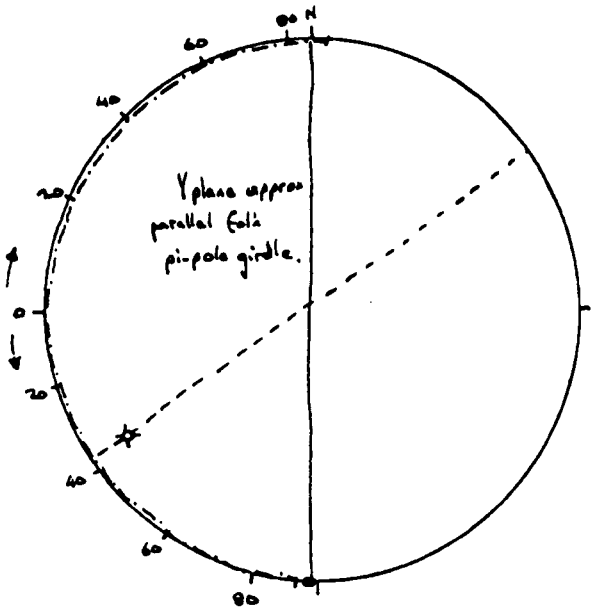

b) Ath Thuqbah

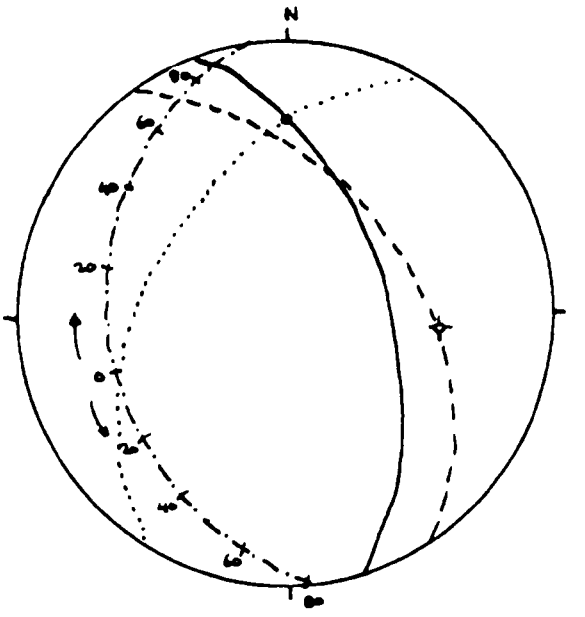

Foliation pi-pole girdle
S2 plane
? Pre-D2 S1 orientation
L2
?Pre-D2 L1 orientation
Y-plane

c) Sarami and Kanut

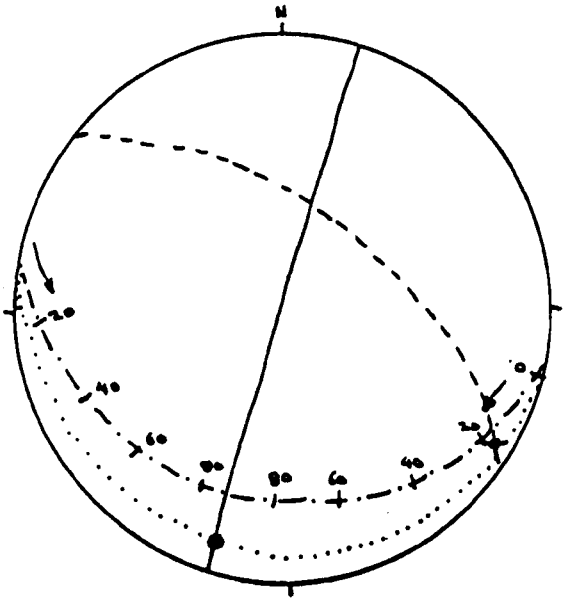

d) Hajir

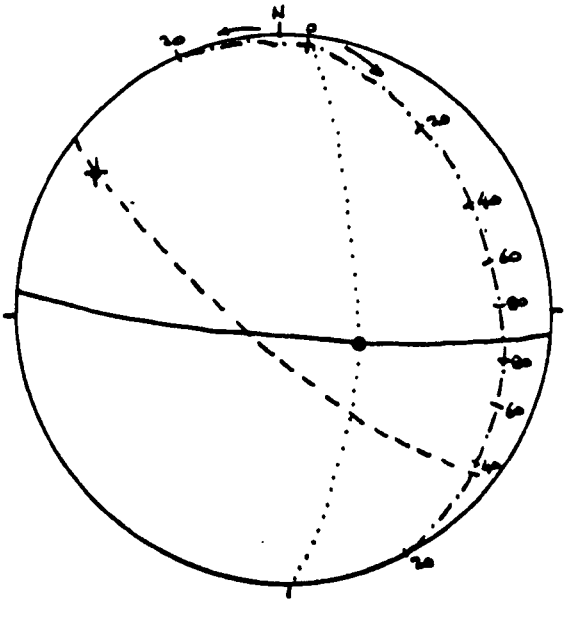

Figure 7.21 For caption see next page

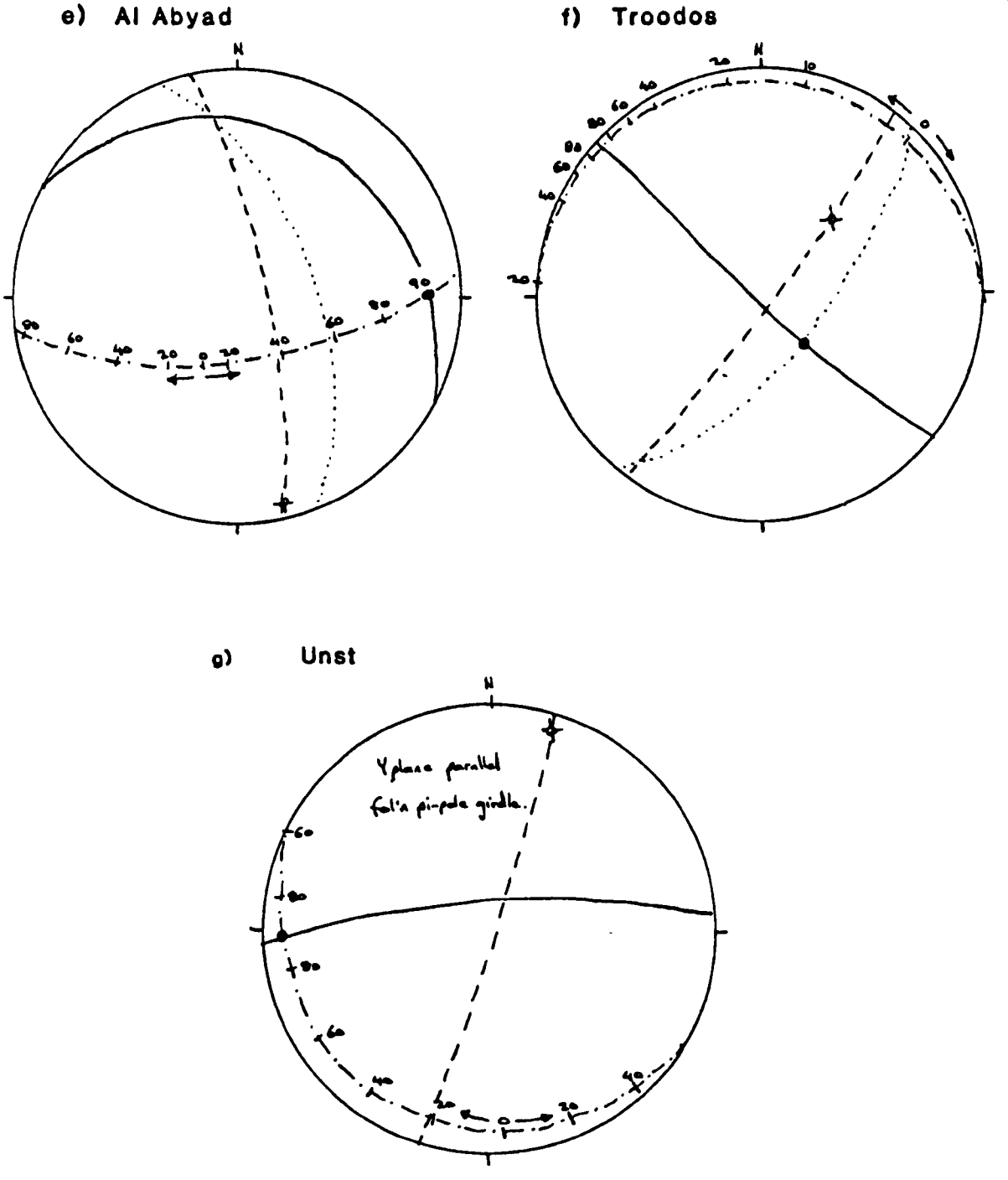

Figure 7.21 Mean foliation pi-pole girdles with graduations for each area studied. (Equal area lower hemisphere projections). Included are possible pre-D2 S1 and L1 orientations.

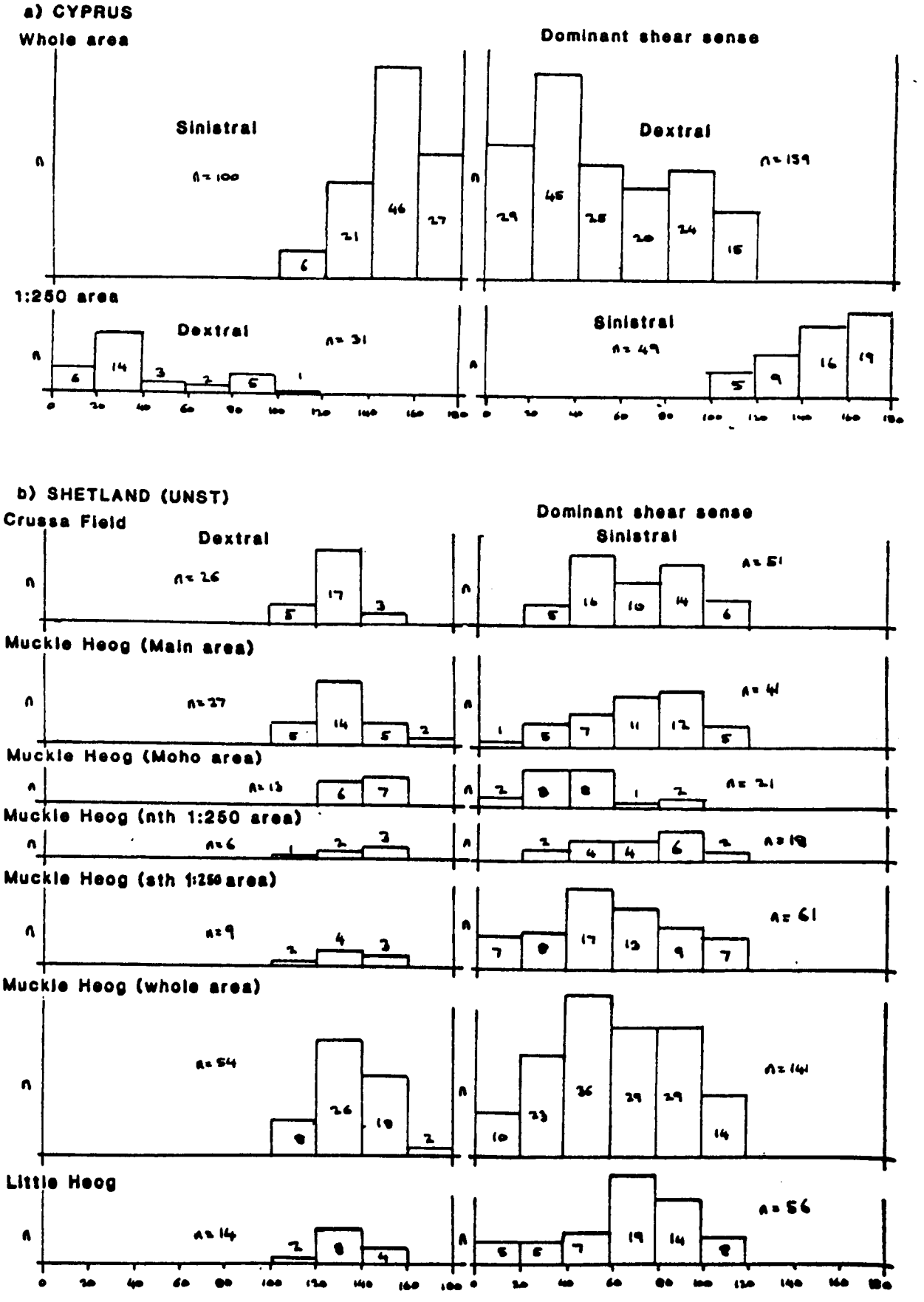

Figure 7.22 α histograms for the Cyprus and Shetland foliations.

Table 7.2 The major structural orientations and dominant shear senses for each Peridotite Unit Area.

Area	Approximate S2 attitude	Approximate D2 slip direction	Dominant D2 shear sense (on a horiz -ontal plane)	Variation in shearing intensity downwards from the moho.
Rajmi	090 80	180 00	Dextral	Highly variable with general increase downwards.
Ath Thuqbah	090 60	005 05	Dextral	Variable.
Sarami and Kanut	315 70	225 00	Sinistral	D1 only to high intensity D2 decreasing downwards
Hajir	200 70	150 60	Sinistral	Variable with general increase downwards.
Al Abyad	020 40	080 20	Sinistral[+]	Variable.
Troodos	225 80	135 60	Dextral	Variable.
Unst	360 80	275 20	Sinistral	Variable.

[+] Shear sense defined on a vertical E-W plane looking northwards.

In Oman where fewer specimens were collected and fewer detailed structural measurements made for each area, it is not worth constructing α-distribution histograms. However, similar comparisons between shearing intensities from specimens with α angles as for Cyprus and Shetland, allow an estimations to be made of the pre-D2 orientations of the S1 plane. The intersection between the pre-D2 S1 plane and the lineation or olivine [100] great circles gives an estimation of the original L1 slip lineation prior to D2 deformation. The pre-D2 S1 and L1 orientations are shown on Figure 7.21 for each area.

The data in Figure 7.21 allow the D2 shear sense to be determined for all areas where relict S1 foliations are still present. For Cyprus and Shetland, where an S1 foliation has been measured in most localities, the intensity of the D2 shearing as well as its sense has been calculated. The value of shear can be estimated from the value of the α angle as long as the pre-D2 S1 orientation is known (calculated from the graph in Figure 7.10).

The variations in shear sense for each area are shown in Enclosures 24-31. Enclosure 27 also includes estimations of the shear value for each shear sense. The major structural orientations and shear senses for each are summarised in Table 7.2.

It is clear that even from only small areas such as the 1:250 areas of Cyprus and Shetland (Enclosures 28 and 30) both senses of shear exist in the rocks. Zones can be defined of similar shear sense which indicate a shear folding pattern. However,

within small areas one shear sense predominates over the other, thus defining the dominant sense of shear in that area. In the relatively small Peridotite Unit areas of Cyprus and Shetland there is one predominant sense of shear over each area, although there are a few small localities within which the opposite sense of shear is dominant.

In the traverse sections of Oman both the dominant shear sense and the intensity of shearing vary through the sections. The major changes are summarised in Table 7.2. Table 7.2 and Enclosures 24-31 show that for Oman no correlation can be made between traverse areas. The D2 deformational features of each area are unique. The dominant shear sense, variation in intensity of shearing with depth from the moho plane, and also the direction of shearing is unique for each traverse area. This implies that the D2 events that took place in different individual areas of Oman are most probably not contemporaneous. The same probably follows for the D1 events.

This very important statement and the orientations of the D2 structural features from each area are considered in relation to an extensional or compressional environment in an oceanic spreading situation in Chapters 9 and 10.

7.2.9 Pyroxene Crystallographic Orientations

A study of the crystallographic orientation data of orthopyroxene shown in Enclosures 16 and 17 for Rajmi and Ath Thuqbah respectively, shows that the grains rarely orientate into a favourable direction for crystal shearing to occur.

As is described in Chapters 2-4 ,orthopyroxene commonly makes up only 15% of the modal constituents of a harzburgite. The textural descriptions have shown that the pyroxene crystals occur as either isolated individual grains or small isolated clots composed of a number of grains. This distribution of the grains and also the expected greater competency of orthopyroxene than olivine under mantle conditions (see Chapter 6), makes it difficult for orthopyroxene to slip in a similar manner to olivine. Instead the individual grains or clots act more passively as do the spinel grains. The grain shapes will define a foliation plane but the crystallographic orientations of the grains will rarely define the shear plane. Only in cases of intense shearing as in specimen 02/04 from Wadi Rajmi is the orthopyroxene [001] crystallographic axis parallel to the slip and shear directions as defined from the olivine [100] axes. In areas where the D2 shearing has been less intense,no distinct pattern is evident of the orthopyroxene [001] axes. A few of the grains may be favourably oriented for shearing to occur as in specimen 02/13 from Wadi Rajmi but most give a fairly random distribution (Figure 7.23).

Since little information about shear deformation is gained from the crystallographic orientations of orthopyroxene, only a few specimens have been measured. The main use of orthopyroxene is in defining a foliation plane within a specimen. This is considered in detail in Chapter 8.

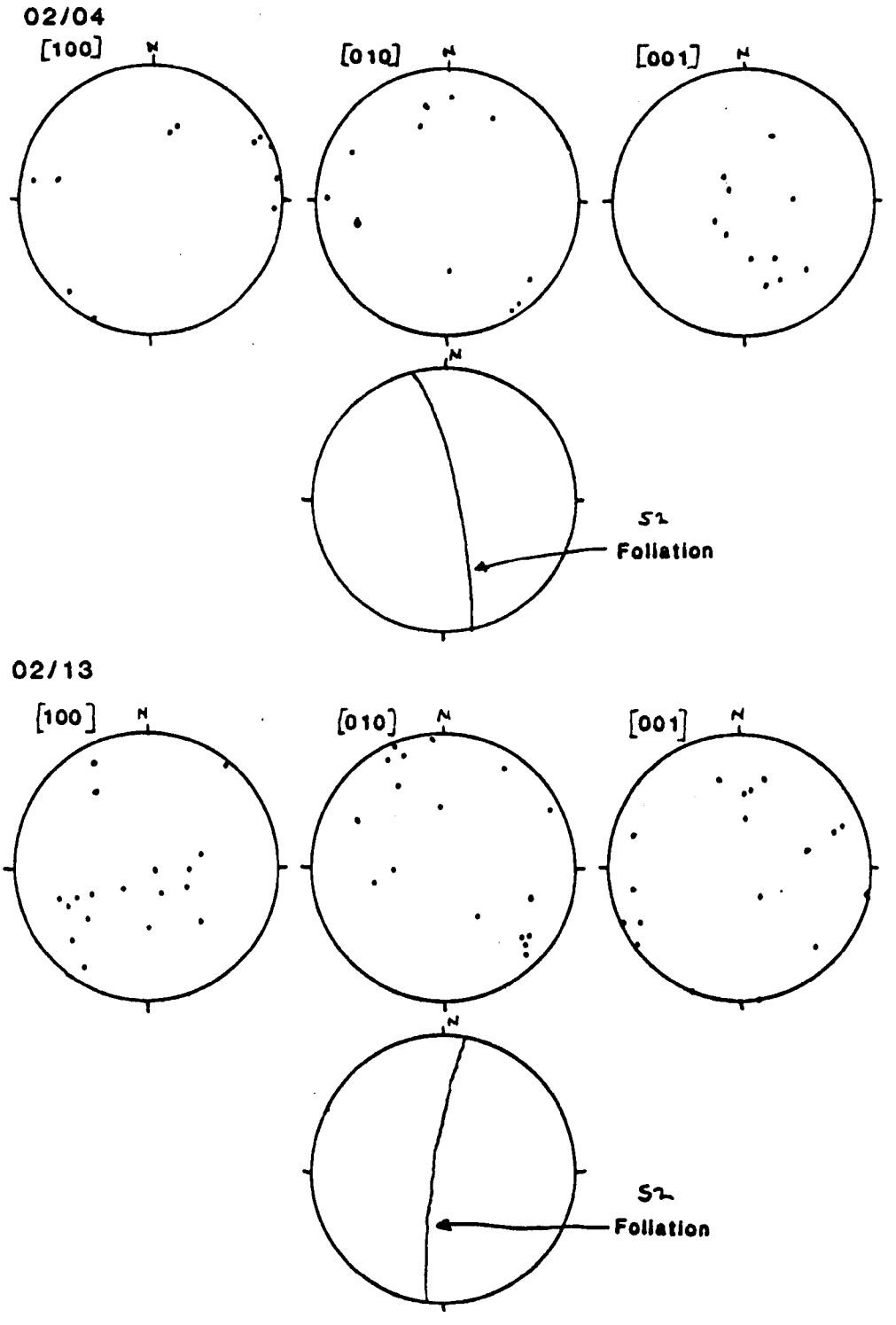

Figure 7.23 Orthopyroxene crystallographic orientations for specimens 02/04 and 02/13. (Equal area lower hemisphere projections).

7.3 Crystallographic Results From The Lower Cumulate Units

The crystallographic orientations of the Lower Cumulate Unit specimens studied are included with the Peridotite Unit results on Enclosures 16-23. The orientations are summarised and interpreted on Table 7.3. In most cases the interpretations as to whether a specimen has or has not been deformed by plastic shear agrees with the predictions from the field observations described in Chapters 2-4.

Only a few of the specimens collected have the expected cumulate crystallographic orientations of olivine described in Chapter 6. (i.e. [010] perpendicular to the layering, and [100] and [001] as girdles parallel to the layering.) Eg. Specimens 10/45 and 10/54 from Troodos (Figure 7.24). It is clear from textural and field evidence that other specimens which lack the expected olivine [010] perpendicular to the layering plane have not been deformed by plastic shear mechanisms. In these specimens the olivine crystallographic axes form no distinct pattern, e.g. specimen 02/87 form Sarami (Figure 7.25). The mechanisms of production of such crystallographic orientations is unclear, but it is certain that inter-crystalline shear in a preferred direction could not have occurred.

Specimens which have undergone plastic shear have fairly strong [100] clusters which have a similar orientation to the slip directions in the adjacent Peridotite Unit.

In a few of the areas, where the D2 shearing has been very weak and the olivine [100] axes in deformed harzburgite specimens give a girdle trend with no D2 slip direction cluster within the

Area	Specimen From moho upwards	[100] Distribution	Interpretation	
			Deformation by plastic shear	Cumulate Orientation [010] normal layering
Rajmi	01/35	Girdle	{0kl}[100]	No
	01/37	Dispersed Girdle	No	Unclear
Ath Thuqbah	02/28	Cluster	{0kl}[100]	No
	02/23	Dispersed	No	Unclear
Sarami	02/87	Dispersed	No	Unclear
Kanut	02/85	Dispersed	No	Unclear
Al Abyad	01/05	Dispersed cluster	{0kl}[100]	No
	01/06	Dispersed girdle	{0kl}[100]	No
	01/07	Cluster	{0kl}[100]	No
	01/08	Dispersed girdle	?	No
	01/20	Girdle	?	No
	01/22	Cluster	{0kl}[100]	No
	01/24	Girdle	{0kl}[100]	No
	01/26	Dispersed	No	Possible
Troodos (Specimens from north to south)	10/46	Dispersed girdle	?{0kl}[100]	?
	10/44	Girdle	{0kl}[100]	No
	10/45	Dispersed	No	Yes
	10/43	Dispersed girdle	No	Unclear
	09/05	Dispersed cluster	No	Yes
	10/07	Dispersed cluster	?	Unclear
	10/53	Dispersed cluster	{0kl}[100]	No
	10/54	Girdle	No	Yes
	09/02	Dispersed	No	Possibly
	09/04	Cluster	{0kl}[100]	No
	10/11	Dispersed	No	Possibly
Unst	05/08	Girdle	?	?
	05/34	Dispersed cluster	(010)[100]	No
	05/35	Dispersed girdle	{0kl}[100]	No

Table 7.3 The interpretations of crystallographic data from the Lower Cumulate Units.

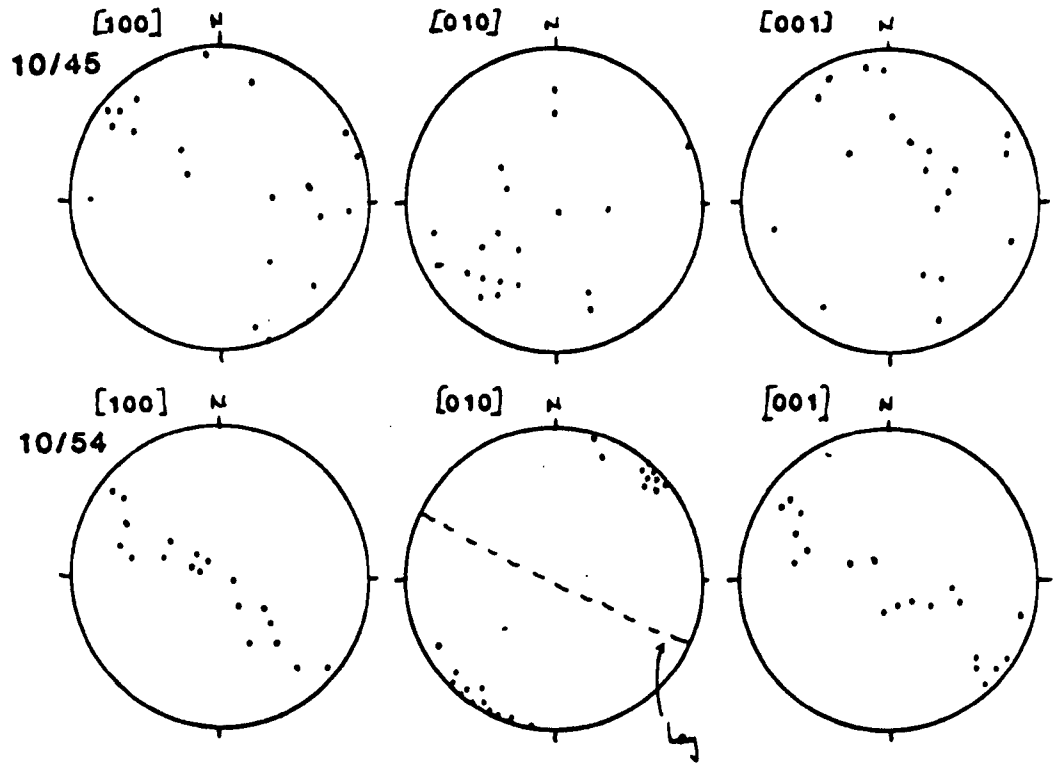

Figure 7.24 Olivine crystallographic orientations for specimens 10/45 and 10/54. (Equal area lower hemisphere projections).

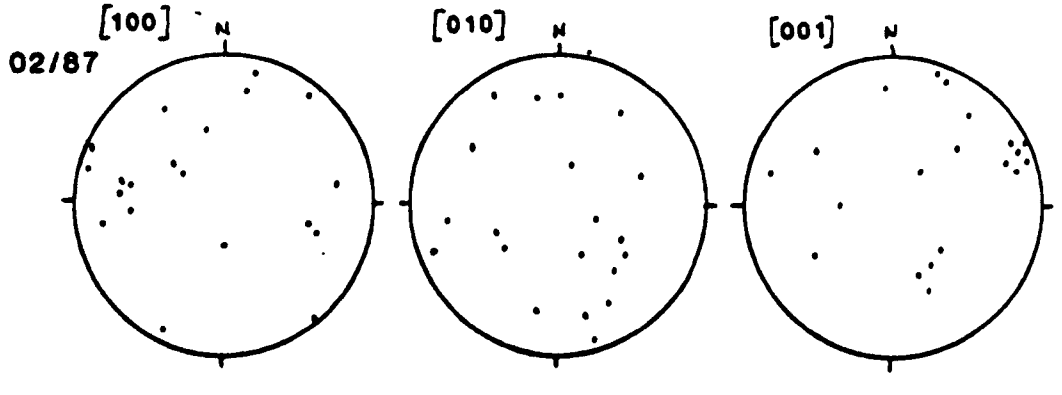

Figure 7.25 Specimen 02/87. Olivine crystallographic orientations. (Equal area lower hemisphere projections).

girdle, it is not possible to determine whether or not a Cumulate Unit specimen has been deformed. In this case the textural and field evidence must be relied on to determine whether or not the specimen has been deformed. In Table 7.3 such specimens have 'unclear' written on their interpretation.

The crystallographic results from the specimens collected by John Smewing and Paul Browning are also included on Enclosures 16-23 and Table 7.3.

The crystallographic interpretations of Table 7.3 and the field and textural data from Chapers 2-4 have been combined in Enclosures 24-31 to give estimations of shear sense and shear directions in areas of plastically deformed Lower Cumulate Unit for each area as well as the limit of plastic intercrystalline simple shear deformation. In all areas the directions of shearing in the plastically deformed Lower Cumulate Unit is the same as that in the adjacent Peridotite Unit.

It must be made clear that the limit to plastic deformation, as observed from the olivine crystallographic orientations, is not necessarily the limit of deformation but only of deformation by plastic shear processes involving intra-crystalline gliding and thus a penetrative deformation process. As discussed in Section 6.7.3 of Chapter 6 it is most likely that the rocks above this penetrative deformation limit have been deformed by 'crystal-mush flow' processes (i.e. Intra-crystalline movements). Unfortunately, it is not possible to determine from a study of the olivine crystallographic orientations, whether an olivine-rich rock has been deformed by crystal-mush flow processes or has not been tectonically deformed.

As mentioned in Chapters 2-4 and Section 6.7.3 of Chapter 6, the strong parallelism of the cumulate layers in Cumulate Unit areas immediately adjacent to the foliation and layering in areas which have undergone penetrative sub-solidus deformation, suggests that crystal mush flow processes have indeed been operative.

7.4 Summary of the Interpretations from Olivine Crystallographic Orientations

The results and interpretations presented in this chapter show that both the deformation events preserved in the Peridotite Unit can be considered as processes of simple shearing. It is clear that the intensity and the shear sense of the D2 deformation is variable both within and between areas. The direction of D2 shearing is fairly constant in a single area, but highly variable between areas.

The constant orientation of the D2 shearing directions within individual areas and their variability between areas most probably indicates that the D2 deformational events were not contemporaneous in the different areas of Oman. It is also evident that little time elapsed between the D1 and D2 events in some areas as in both Cyprus and Shetland both the S1 and S2 foliations extend roughly equal distances into the Lower Cumulate Unit.

The D1 and D2 structural orientations from each area will be interpreted in relation to an ocean spreading environment in Chapter 9. Their orientational differences with respect to the palaeo-ridge axis and palaeo-spreading direction of the crust will also be discussed.

Chapter 8

Crystal Size and Shape Orientation Studies

C O N T E N T S

Chapter 8

Various methods have previously been used to study the shape preferred orientation of grains in naturally deformed rocks. All the methods have involved either the detailed measurement of individual grains or the measurement of distances between grains.

In rocks containing suitable strain markers such as deformed fossils, whose pre-formed shape is known, the grain shape or fossil shape fabric can be directly related to the finite strain. However, in rocks without suitable strain markers, only the grain shape fabric can be measured and it cannot be interpreted in terms of finite strain.

In this chapter the methods appropriate for measuring grain shape fabric strengths in harzburgites and dunites are briefly reviewed and the most suitable techniques described. The results obtained are critically discussed taking simple shear processes and two deformational events into consideration. For this the crystallographic and shape fabrics in various specimens are compared and contrasted. Finally the grain sizes from suitable specimens are used to estimate the stress conditions prevalent during D2 shearing.

8.1 Methods of Grain Shape Fabric Strength Estimation Available for the Study of Peridotite Unit Rocks.

Five main methods have been used to estimate the grain shape fabric strength in rocks. They all estimate a two dimensional shape fabric. In order to obtain comparative values between specimens, all measurements must be carried out on the plane perpendicular to the

foliation and parallel to the lineation on the foliation plane (i.e. the 'Y' plane described in Chapter 7). All of these methods have been described in detail and critically discussed by Odling (1980). Here they are briefly described below and the major drawbacks of each method are identified.

8.1.1 Methods of Shape Fabric Strength Estimation.

a) Method 1. Ramsay (1967). A 'Centre to Centre' method.

This technique assumes that the length of a line from the centre of an object to the centre of one of its nearest neighbours is initially statistically independent of the line's direction. The shape fabric ratio is estimated directly from a graph of length of the centre to centre line, against the orientation of that line relative to a common azimuth. An accurate location of particle centres is required for this method.

b) Method 2. Dunnet (1969) and Dunnet and Siddans (1971). The Rf/θ method. An individual grain shape method.

This technique assumes homogeneous deformation of initially elliptical marker objects within their matrix. The long and short axis of each marker is measured and their ratio (Rf) is plotted as log Rf against the long axis orientation of each ellipse (θ). The shape of the array of points is interpreted to determine the strength of the shape fabric.

c) Method 3. Hext (1963). An individual grain shape method.

The method of Hext (1963) makes the assumption that the particles have an initial random orientation. The long and short particle axis ratios are measured as in method 2 above. These ratios are then directly related to the strain ellipse to give a direct

estimation of the strain. This technique has been further developed by Shimamota and Ikeda (1976).

d) Method 4. Fry (1979). A 'Centre to Centre' method.

This method measures the distribution of particle centres within a specimen. A distribution plot is constructed by placing each particle centre in turn on a central point of the plot and then marking in all other centres onto the plot. This produces a plot with an elliptically shaped central space surrounded by a random distribution of points. The central space defines the strain ellipse. This method gives a direct estimate of the bulk strain of the rock as opposed to the particle strain or shape fabric as determined by methods 1-3.

e) Method 5. Odling (1980). R_i method.

This technique measures the change in the number of particle-matrix interfaces per unit length in two perpendicular directions. One direction must be sub-parallel to the observed foliation. The number of particle-matrix interfaces can be directly related to the shape fabric strength as long as an initial random distribution of particles is assumed. Irregular grain shapes will obviously cause severe problems with this method.

In order to gain a more accurate estimation of the strength of the shape fabric, shape ellipsoids can be calculated from the shape ellipses of three perpendicular faces. Bell (1979) and Siddans (1980) used some of the methods described above to calculate a strain elliopoid from three mutually perpendicular faces and both authors showed that the faces need not be aligned with the structural features of the rock (i.e. X,Y and Z faces). Milton (1980) proved mathematically that in order to calculate a shape

ellipsoid, the three cut faces need not even be mutually perpendicular. It is best, however, to have as large an angle as possible between the three faces in order to reduce the errors arising from the calculations of the shape of the ellipsoid from the three ellipses. (R.F. Cheeney, pers. com., 1982).

8.1.2 Shape Fabric Strength Estimation in Peridotite Unit Rocks.

The two major drawbacks of the estimation of shape fabric strengths in harzburgites and dunites, apart from the obvious lack of knowledge on the initial pre-deformational fabric of the rocks, are serpentinisation and the often large grain sizes.

Serpentinisation of the harzburgites and dunites in all the areas studied is usually over 50% and quite commonly over 75%. (See Chapters 2-4). This in effect rules out the use of any centre to centre method for the estimation of the strength of shape fabric (methods 1 and 4) and also that of Odling (1980), method 5. Serpentinisation of the harzburgites commonly occurs in zones which separate small areas of relatively unserpentinised grains from each other. i.e. very few adjacent grains have been sufficiently preserved to measure enough distances between grain centres for the results to be statistically valid.

The large grain size of olivine in most harzburgite and dunite specimens (porphyroclasts normally between 2mm - 1cm) causes problems both with the centre to centre and the individual grain shape methods described above. In a conventionally sized thin section (2.5 x 5mm) there are often only a few olivine grains present. If this rock has been highly serpentinised, possibly only 10 grains can be made out sufficiently well for their long

and short dimensions to be measured. This is not an adequate number for the results from any of the methods discussed above to be statistically meaningful. Hanna and Fry (1979) state that a sample size of over 100 is required for all the methods. Larger thin sections could be made, but the size of the collected specimens limits the number which could practically be made. What is needed is a method of shape fabric strength estimation which involves the measurement of only a few individual grains from each specimen.

A favourable point concerning the estimation of shape fabric strength in harzburgites and dunites is that that the rocks can be considered as essentially monomineralic. As discussed in previous chapters spinel grains mainly behave as passive markers within the rocks, and in harzburgite, even in rocks with 20% pyroxene present, the pyroxene is distributed as small clots or individual grains within a monomineralic olivine matrix. Thus, the strength of the olivine shape fabric can be directly compared among most specimens from all the areas without having to take the effect of other mineral phases into account.

The strength of the shape fabric in harzburgites and dunites has been estimated from ophiolite complexes by Darot and Boudier (1975), Nicolas et al (1980) and Prinzhoffer et al (1980). All of these authors used individual grain shape dimension ratio methods to determine the grain shape ellipse for the 'Y' structural plane. They all used the grain shape ellipse as a direct substitute for the strain ellipse to estimate the strain. As will be discussed below, this is a very dubious substitution to make if the actual mechanisms of deformation are taken into account.

Poirier and Nicolas (1975) used the distribution of spinel grains within the harzburgites and dunites to estimate the strain. This method assumes that with an increase in strain the grains will become progressively scattered. Again these results must be seriously questioned as the studies in this thesis have shown that spinel is never randomly scattered in a harzburgite or dunite but more commonly forms dispersed clot like features or layers, and that there is often more than one phase of spinel present within the rock (S. Roberts, pers. com., 1983).

8.2 Method Used to Estimate the Strength of the Grain Shape Fabric Strength in Harzburgites and Dunites.

As mentioned in section 8.1.2 a method is required which measures the shapes of individual grains but only for a fairly small number of grains from each specimen.

Dr. R.F. Cheeney of the Geology Department of the University of Edinburgh has recently written a computer programme which gives an estimate of the best-fit shape ellipsoid from only a limited number of grains. This programme, called 'Ellipfit', has been used in this study to estimate the strength of the grain shape fabric from harzburgite and dunite specimens. It also calculates the orientations of the ellipsoid principal axes in relation to the orientation of the original specimen orientations in the field.

The 'Ellipfit' method involves the estimation of the best-fit shape ellipse for each of three or more faces, it then scales together the shape ellipses from each face to produce a best-fit shape ellipsoid for the specimen.

8.2.1 Laboratory Techniques.

As it is not possible to observe individual olivine grains on hand specimens, all the grain shape measurements were performed on thin sections. To distinguish individual grains the measurement had to be taken under crossed polarised light.

The 'Ellipfit' programme requires that six diameters are measured for each individual grain on each face. These diameters must be 30^{o} apart and be measured consistently for each grain on the same face. To do this a grid was made up which fitted into the microscope eyepiece in place of the cross-wires. Figure 8.1 shows an enlargement of this grid.

The grid zero axis is aligned parallel to the strike direction of the thin section (all the sections having previously been orientated with their original field orientations) and the microscope stage locked in position. The grid is now uniquely orientated with respect to the section orientation. (Figure 8.2). In order to keep the thin section constantly oriented it is moved only with a mechanical stage.

The diameters of each grain are measured by moving the section until the centre of the grid is positioned approximately in the centre of the grain. Each diameter is then measured using the graduation on the grid, starting with the zero axis and progressing anticlockwise around the grid until six diameters have been measured, each 30^{o} apart. This process is repeated for 15 grains (if 15 grains are measurable) on the same face.

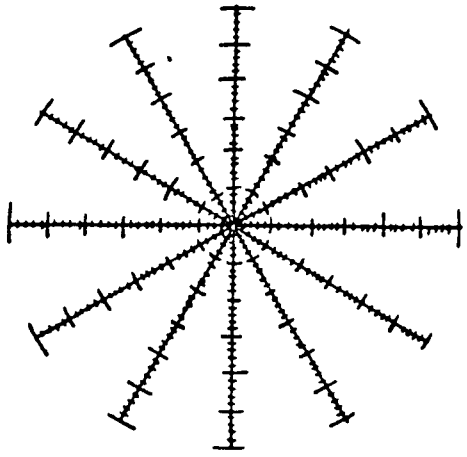

Figure 8.1 An enlargement of the 'Ellipfit' grid.

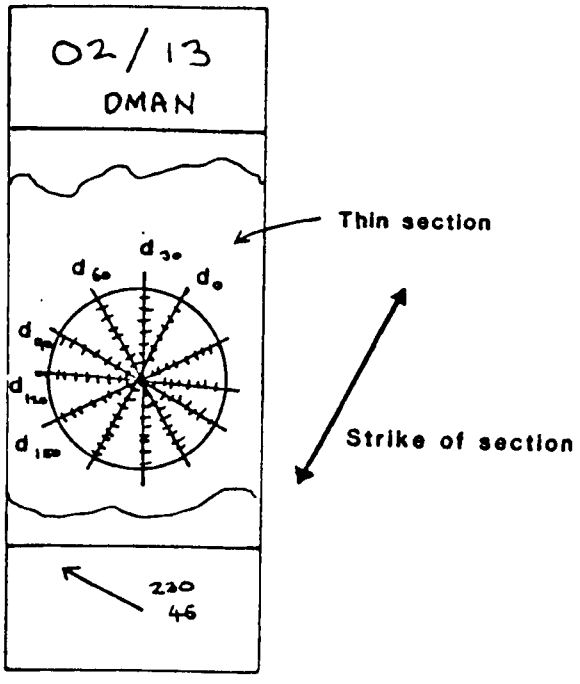

Figure 8.2 The alignment of the 'Ellipfit' grid with respect to the thin-section field orientation.

For each specimen three roughly perpendicular faces were cut and the procedure described above was carried out for each face. Thus, for each specimen, 45 grains in all were measured. Figure 8.3 shows an example of the raw data for a single specimen. The orientation of each face is given by the dip angle followed by the dip direction. The grain measurements are then input into the computer.

Care must be taken to ensure that the measurements are always made in an anticlockwise direction. Complications obviously arise when a section has been cut from the bottom face of an orientated specimen. (i.e. an overhanging face). In this case the measurements are still made in an anticlockwise progression but the orientation of the face must be carefully considered. Figure 8.4 shows the relationship of the orientation of a top face of a block to a bottom face, both of which are parallel. In all cases the face being measured must be viewed from the outside of the block. i.e. For a bottom face, because it is overhanging, the angle of dip of the face is the 180° complement of the dip angle of the top face. The dip direction of the overhanging face is the reverse of the top face. Thus in Figure 8.4 the orientation of the bottom face with a parallel top face orientation of 30/170 is 150/350.

8.2.2 The 'Ellipfit' Programme and the Plotting of Ellipsoid Shapes and Orientations.

The overall scheme of computation of the 'Ellipfit' programme is outlined in Table 8.1. More details of the programme are obtainable from Dr. R. F. Cheeney, Department of Geology, University of Edinburgh.

Olivine					
X FACE					299 82
d_0	d_{30}	d_{60}	d_{90}	d_{120}	d_{150}
9	9	12	13	10	8
10	15	11	10	10	8
13	15	16	24	17	15
29	23	20	16	23	31
16	23	25	23	26	19
15	17	15	12	10	12
23	20	21	22	22	20
16	14	12	16	15	14
23	23	12	10	10	11
10	9	8	6	5	8
11	11	10	13	11	10
22	25	28	25	22	24
13	24	21	17	8	9
26	24	25	26	24	26
14	12	12	11	11	11

Olivine					
Y FACE					129 12
d_0	d_{30}	d_{60}	d_{90}	d_{120}	d_{150}
8	9	7	9	8	7
15	12	10	9	9	11
16	15	11	12	12	16
20	19	13	13	22	19
21	17	11	9	9	12
18	13	11	10	10	13
12	12	8	12	12	11
21	22	12	11	10	12
13	12	10	9	10	12
16	14	14	11	12	16
7	8	8	7	9	8
17	21	19	13	13	15
13	12	14	12	9	10
30	18	15	16	15	17
13	11	11	9	7	10

Olivine					
Z FACE					022 92
d_0	d_{30}	d_{60}	d_{90}	d_{120}	d_{150}
11	11	11	10	9	10
21	18	26	31	24	21
16	19	21	14	10	11
12	14	15	12	11	10
15	16	17	18	14	16
9	8	9	12	11	10
13	12	17	16	19	15
31	30	24	27	24	24
8	8	10	17	14	11
21	23	30	27	25	22
20	19	15	17	22	21
16	13	13	19	20	19
13	14	18	18	15	13
9	12	12	11	12	9
15	17	14	15	16	15

Figure 8.3 The raw data of specimen 02/13.

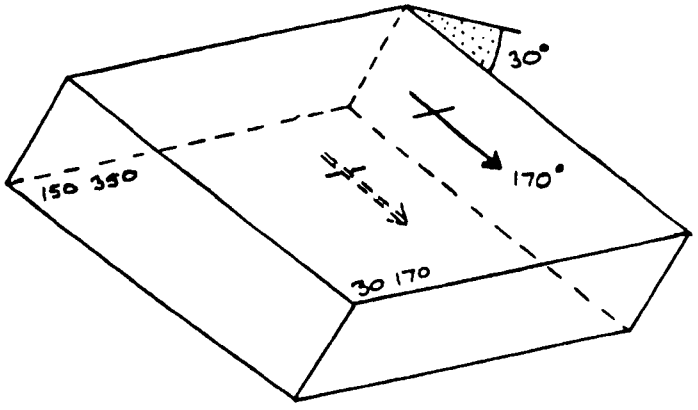

Figure 8.4 The relationship between the orientation of a top face to the orientation of a parallel bottom face.

THE ELLIPFIT PROGRAMME - R.F.CHEENEY, UNIVERSITY OF EDINBURGH

Overall scheme of computation:

I. Read data:
 I.I. Give a one line title and then state the number of plane faces on which measurements were made.
 I.2. For each face, give the angle of dip, the direction of dip and the number of elliptical sections measured.
 I.3. Follow this immediately with a list, section by section, of diameters at 30 degree intervals, starting in the strike direction and proceeding anticlockwise.
2. Process the data face by face:
 2.I. Calculate the best-fit ellipse to each section and output (with confidence intervals) the axial ratio and the direction of the long axis with respect to face coordinates.
 2.2. Normalise the area of the best-fit ellipse and scale the measured diameters.
 2.3. Aggregate the scaled diameters and repeat the calculations and output of section 2.I.
 2.4. Complete an analysis of variance for the face and output appropriate results.
3. Scale together the data from all faces.
 3.I. If three or more faces, starting at face I and cycling over all faces, calculate the direction of intersection of the current and next faces.
 3.2. Calculate the response in the intersection direction of the two faces and ratio to give an interim scaling factor.
 3.3. Calculate the closing error between the last and the first face and distribute uniformly over all faces.
4. Complete the 3D analysis.

Table 8.1 Summary of the Ellipfit Programme. (R.F. Cheeney, University of Edinburgh).

For each face, an analysis of variance is calculated for each grain and for the best-fit ellipse. The value of the residual variance shows how well the measurements from each grain fit into an ellipse. If these values are too high then the axial ratio for the calculated ellipse is not statistically meaningful. In the measurements carried out the residual variance for best-fit ellipses usually had acceptable values (10^{-3} or less).

A typical output for the final three dimensional analysis is shown in Figure 8.5. For each three dimensional analysis a residual variance is calculated, as well as a determinant on inversion, the value of which must be in the order of 10^3 for the results to be meaningful. The relevant results which enable the orientation and shape of the ellipsoid to be identified are the table of ellipsoid diameters and the table of principal values and principal axes orientations. (Figure 8.5). The data in these tables enables an equal area lower hemisphere projection to be constructed of the orientation of the principal axes of the ellipsoid as well as 0.95 cones of confidence around each axes. (Figure 8.6). This projection can then be directly compared with the crystallographic data and field data projections.

The shape of an ellipsoid has been represented on three different plots by various authors : -

1) The most used method is to plot the ratios of the principal axes on a two axis graph as shown in Figure 8.7. This is the Flinn plot and was originally proposed by Zingg (1935) and developed by Flinn (1962). In this plot the shape of the ellipsoid (i.e. prolate or oblate) determines how close to each axis the specimen will plot. The prolateness or oblateness of the ellipsoid can be represented by a dimensionless value K :

```
02/13 OLIVINE

THREE-DIMENSIONAL SYNTHESIS


DETERMINANT ON INVERSION = 2.259@  3
RESIDUAL VARIANCE = 4.067@ -3

SHAPE MATRIX ELEMENTS FOR AGGREGATE DIAMETERS,
RELATIVE TO USER'S COORDINATE SYSTEM:

  1.135@  0 -4.032@ -1  5.592@ -2
 -4.032@ -1  1.086@  0  4.460@ -2
  5.592@ -2  4.460@ -2  9.420@ -1

0.95 CONFIDENCE INTERVALS:
ELLIPSOID DIAMETERS, CONE SEMI-APICAL ANGLES, THETA
 8.384@ -1    8.126@ -1    7.890@ -1    10     5   -69
 1.071@  0    1.020@  0    9.753@ -1    15     9   -86
 1.302@  0    1.207@  0    1.130@  0    15     6     3

PRINCIPAL VALUES, AXES(PLUNGE.AZIMUTH) AND NUMBER OF ITERATIONS:

    1.514@  0     1.317      13
    9.615@ -1    75.051       0
    6.867@ -1    15.227      33

LODE'S PARAMETER: 0.149      ES: 0.281
```

Figure 8.5 Output of the 'Ellipfit' three-dimensional synthesis for specimen 02/13.

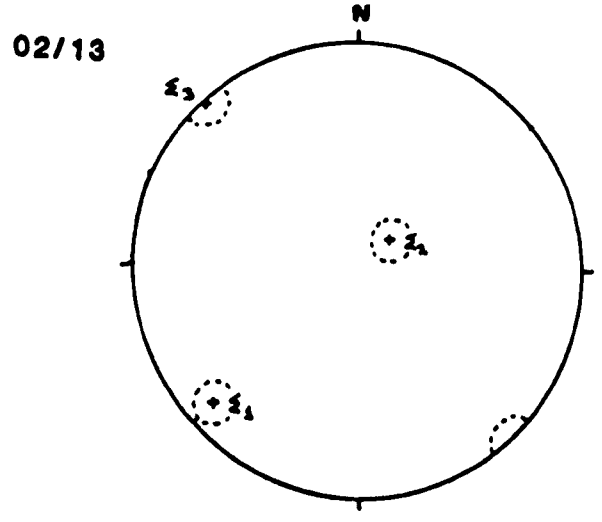

Figure 8.6 Lower hemisphere equal area projection of the principal shape axes and 0.95 confidence cones for specimen 02/13.

$$K = \frac{a-1}{b-1} \quad \text{where} \quad a = \frac{(1+\Sigma_1)}{(1+\Sigma_2)} \quad \text{and} \quad b = \frac{(1+\Sigma_2)}{(1+\Sigma_3)} .$$

The main drawback of this method of plotting is that for low deformation states the ellipsoids tend to have unnaturally close groupings.

Ramsay (1967) proposed that a more convenient method would be to plot the principal axes ratios as natural logarithms. This enables low deformation states to be more easily interpreted.

2) Harland and Bagley (1958) developed a triangular plot of the ellipsoid principal axes ratios. (Figure 8.8). The main disadvantage of this plot is its lack of symmetry which causes problems when determining deformation paths and also the precise ellopsoid shape.

3) Instead of using the principal axes ratios, the relative values of the principal axes can be directly plotted to determine the shape of the ellipsoid. Nadai (1963) first proposed this and used a three-axis plot, each axis representing a principal axis. Hsu (1966) fully developed these plots and used the natural logs of the principal axes (i.e. natural strains) as the axes of the plot. (Figure 8.9). The main advantage of the three-axes plot is that each of the principal axes can be considered simultaneously which allows an element of directional information to be preserved. This is lost in a Flinn plot. Owens (1974) also showed that the superposition of coaxial strains is represented on a three-axis plot by a simple vector addition on the plot itself. For a constant volume deformation, the strain history can be determined fairly readily from a three-axis plot by constructing a strain path from the origin through the data points.

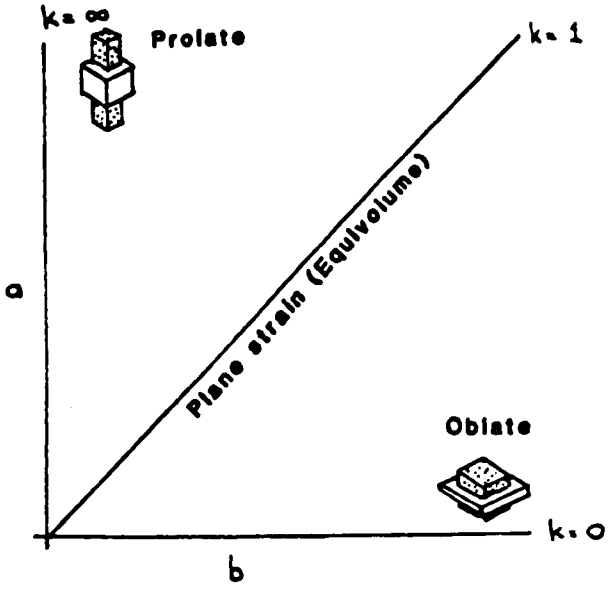

Figure 8.7 The Flinn plot.

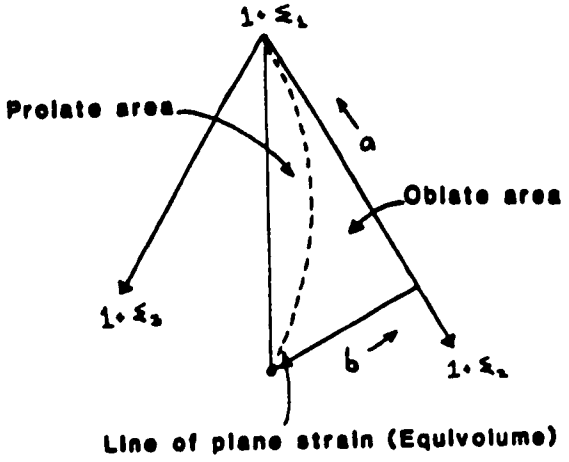

Figure 8.8 The Harland and Bagley triangular plot.

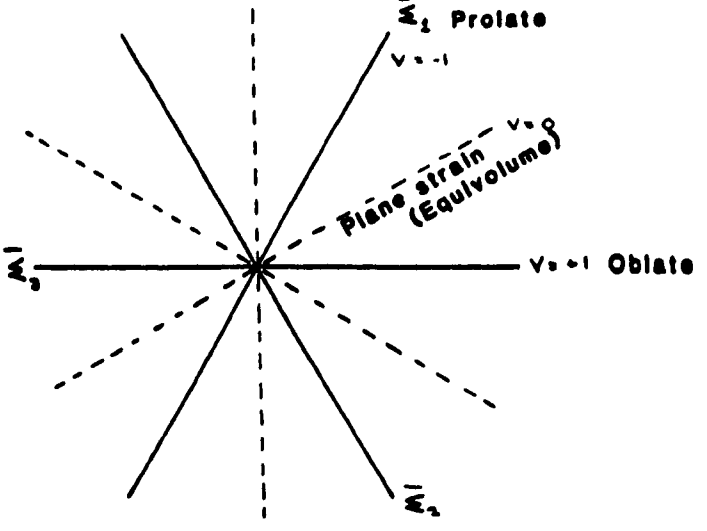

Figure 8.9 The Hsu three-axis plot.

The drawback of the three-axis plot is that the plotting of data on the plot can only be achieved by the rather laborious technique outlined by Owens (1974). However, the plotting procedure can be rapidly sped up by calculating two parameters which allow a direct plotting of the ellipsoid onto the diagram. The 'Ellipfit' programme calculates these two parameters. (Figure 8.10). :-

i) The straight line distance from the origin to the ellipsoid plot :

$$\bar{\Sigma}_s = \sqrt{\bar{\Sigma}_1^2 + \bar{\Sigma}_2^2 + \bar{\Sigma}_3^2} \qquad \text{where} \qquad \bar{\Sigma}_1, \bar{\Sigma}_2, \text{ and } \bar{\Sigma}_3$$

are the natural logs of the three ellipsoid principal axes. The value of $\bar{\Sigma}_s$ must be multiplied by 0.816 in order to draw a distance on the three-dimensional three-axis plot on a planar three-axis plot. (See Appendix 2).

ii) Lode's parameter (v) which is a measure of the oblateness or prolateness of the ellipsoid and is directly comparable with the 'K' value in a natural log Flinn ratio plot:

$$v = 2\left\{\frac{\bar{\Sigma}_2 - \bar{\Sigma}_3}{\bar{\Sigma}_2 - \bar{\Sigma}_3}\right\} - 1$$

For oblate ellipsoids 'v' has a positive value between 0 and 1, and for prolate ellipsoids 'v' has a negative value between 0 and -1.

Thus, the 'Ellipfit' programme enables both the shape and orientation of a shape fabric ellipsoid to be rapidly plotted for a large number of specimens. The main advantages of the 'Ellipfit' method over other methods of shape fabric estimation in the study of highly serpentinised rocks, are that only a

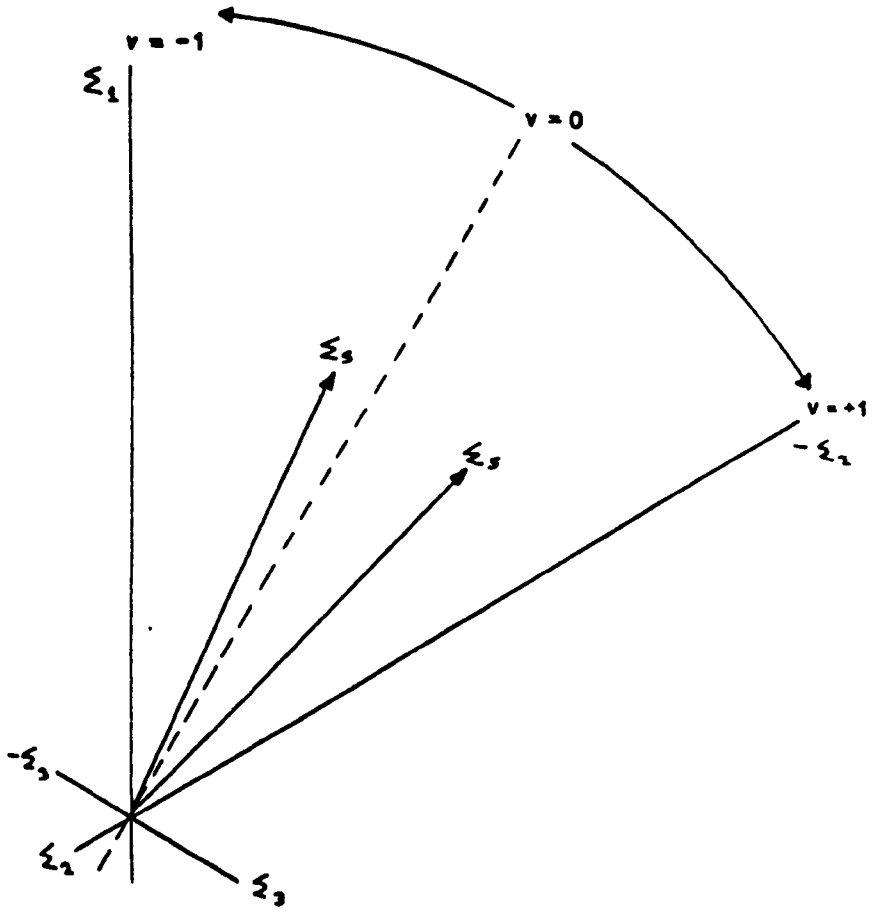

Figure 8.10 The plotting of data on a three-axis plot by use of the s and v parameters.

relatively small number of grains are required from each face and that the exact location of a grain centre is not required.

8.3 The Interpretation of Planar 3-axis Diagrams

As discussed in Chapters 6 and 7, it is most likely that the primary deformation of the Peridotite Unit was by shear processes involving plastic flow. This implies that there was essentially no volume change during deformation. If this is the case then the sum of the values of the natural logs of the principal axes of the shape ellipsoid equals zero. i.e : -

$$\bar{\Sigma}_1 + \bar{\Sigma}_2 + \bar{\Sigma}_3 = 0.$$

If it is accepted that there was no volume change then the values plotted on the 3-axis diagram can be directly compared with each other. The value of 'v' determines the shape of the ellipsoid and from this an idea can be gained of the style of deformation that each specimen shows.

The theories discussed in Chapter 6 and the evidence presented in Chapter 7 suggest that the rocks of the Peridotite Unit have undergone simple shearing, at least on hand specimen scale. If this is the case then the rock must have undergone a plane strain and the value of 'v' should be equal to zero. Thus for a simple shearing deformation only the value of $\bar{\Sigma}_s$ should vary with a change in the strength of shearing; 'v' will remain at zero.

For simple shear a succession of strain ellipsoids can be determined for a progressive increase in the shear strain. The six diameters for each value of shear strain are calculated by use of the Mohr construction. This has been done for shear strains

of 0.268, 0.577, 1.000, and 1.732 and 'v' and $\bar{\Sigma}_s$ calculated for each shear strain. (See Appendix 3). Figure 8.11 shows the values of $\bar{\Sigma}_s$ plotted against the shear strain. As would be expected the line joining the plotted points has a constant gradient. If the olivine crystals were all perfect spheres before deformation then this diagram would provide a direct correlation with the crystal ellipsoid shape and the particle shear strain of the deformation.

It is obviously impossible to determine the pre-deformational shape of olivines. The evidence discussed in Chapters 6 and 7 suggests that many of the crystals have undergone at least one recrystallisation event during deformation. For these crystals the orientation of the shearing direction and the sense of shearing will strongly control both their crystallographic and crystal shape orientations. If the crystal recrystallises during deformation then the crystal will preferentially grow into the direction which requires least energy for growth. (i.e. parallel to the minimum compressive stress axis, σ_3 : see Chapter 6). Thus, from the absolute beginnings of a new crystal onwards, it will grow in a preferential direction and no pre-deformational crystal shape can be defined.

If the shearing direction changes (i.e. D1 deformation is proceded by D2 deformation) then the crystals will have a preferred shape fabric prior to D2 deformation. However, the strength of the pre-D2 fabric will still depend on the D1 shear strain which, if there has been any subsequent D2 shearing, is impossible to quantify.

The angle between the D1 and D2 shearing directions will be another major factor determining the final D2 shape preferred orientation and fabric strength of the crystals. (Figure 8.12). If the angle between D1 and D2 shearing is small then the D1 shape and crystallographic fabric will be preferentially orientated in order that D2 shearing can continue on from D1 shearing without much change in the rate of grain breakdown, recrystallisation and growth. If, on the other hand, the angle between the D1 and D2 shearing directions is large, then very few of the grains will be crystallographically favourably orientated for D2 shearing to occur. Consequently, if the D2 shear strain is large enough, most of the grains will breakdown and recrystallise into more favourable orientations. i.e. The shape fabric will completely reform with D2 shearing, instead of starting with an initial preferably orientated fabric, as is the case where the angle between the D1 and D2 shearing directions is only small.

Before the shape fabric results from the collected specimens can be interpreted with any confidence, the D1/D2 angle, strength of D1 and D2 shearing, and thus the amount of grain recrystallisation compared with grain rotation must carefully be considered. In order to do this two relatively unserpentinised specimens were selected from the same area: one showing strong D2 shearing and the other only moderate D2 shearing. A detailed study of the crystallographic orientations and the grain shapes from each of the specimens was carried out and is described in section 8.4 below. As the specimens were selected from the same area it is reasonable to assume that the angle between the D1 and D2 shearing directions is the same for both specimens (see discussions in Chapter 7). Thus the controlling factor on the results is the D1 and D2 shearing strengths.

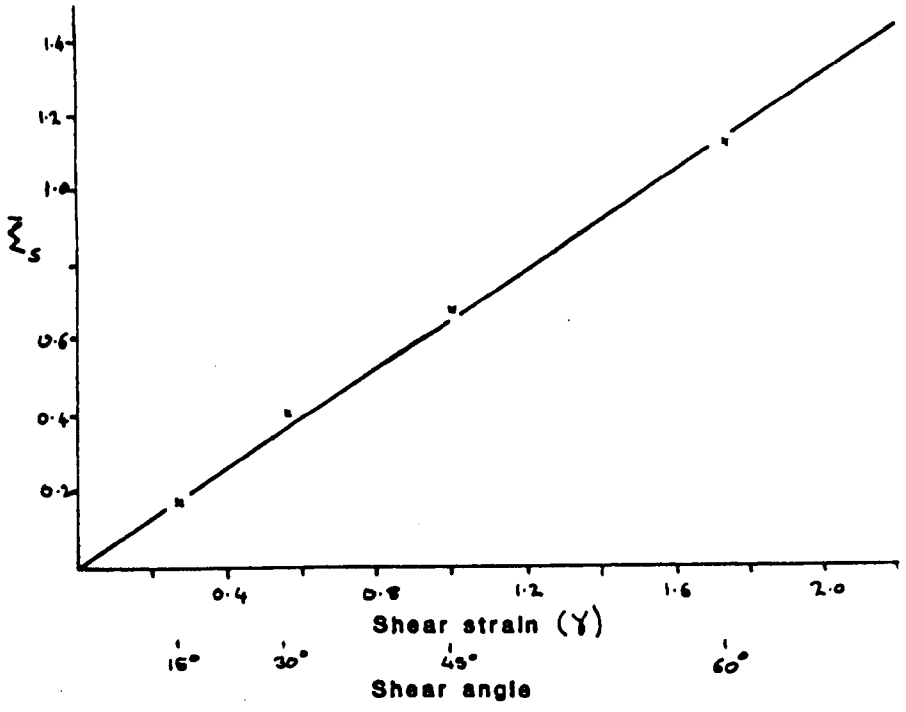

Figure 8.11 The correlation between ε_s and γ for homogeneous simple shear with no dilation.

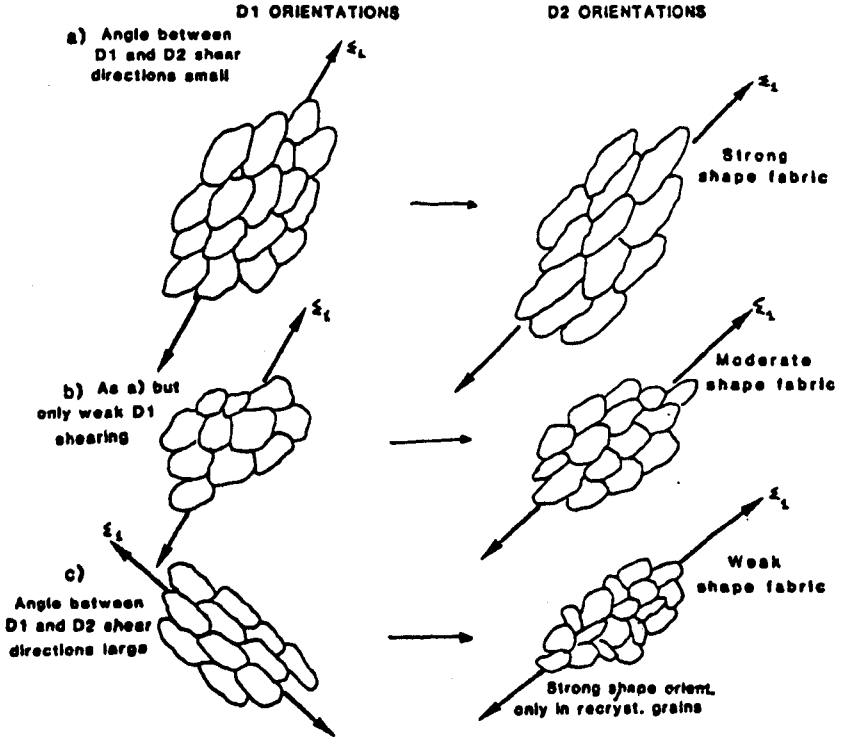

Figure 8.12 The relationship between the D1/D2 shear direction angle and the resulting D2 shape-preferred orientation and fabric strength.

8.4 Detailed Crystallographic and Shape Fabric Studies.

Detailed crystallographic and shape fabric studies were carried out on the relatively unserpentinised harzburgite specimens 01/45 and 02/10 of the upper section from the Wadi Rajmi traverse. (See Enclosure 2 for exact locations).

Before considering the results from these studies it is necessary to determine the expected shape fabrics for an olivine rich rock which had undergone a single simple shearing deformation event. These are summarised and contrasted with the expected crystal shape fabrics for a plane strain pure shearing deformation in Figure 8.13.

For simple shear the 'Y' face will show the strongest stretching and preferred orientation of the grains parallel to the foliation. The 'X' face will only show a slight stretching of the grains parallel to the slip direction (there will be no grain shape preferred orientation on the face which is parallel to the slip plane). The 'Z' face will show a slight stretching of the grains in a direction approximately parallel to the 'Y'-'Z' face intersection (See Figure 8.13). In a pure shearing case, on the other hand, the grains on the 'Z' face will be slightly elongated in a direction parallel to the 'X'-'Z' face intersection. (See Figure 8.13).

8.4.1 Specimen 01/45 - Moderate Intensity D2 Shearing.

In order to study the grain shapes of specimen 01/45 the orientation of the D2 slip direction and slip plane was first determined. To do this the crystallographic orientations of 125 olivine grains were measured. The results are plotted in Figure 8.14. As can be seen,

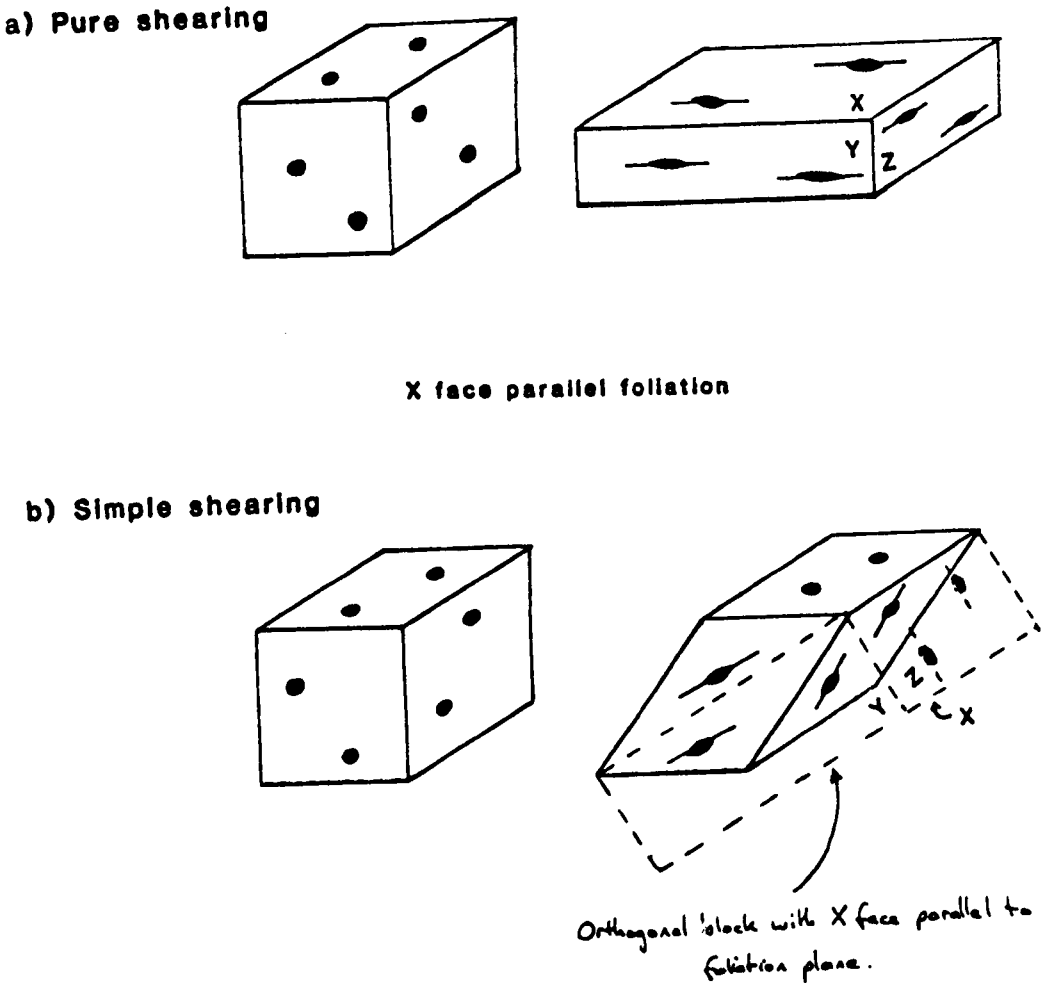

Figure 8.13 Expected shape fabrics for pure shearing and simple shearing. a) Pure shearing; b) Simple shearing.

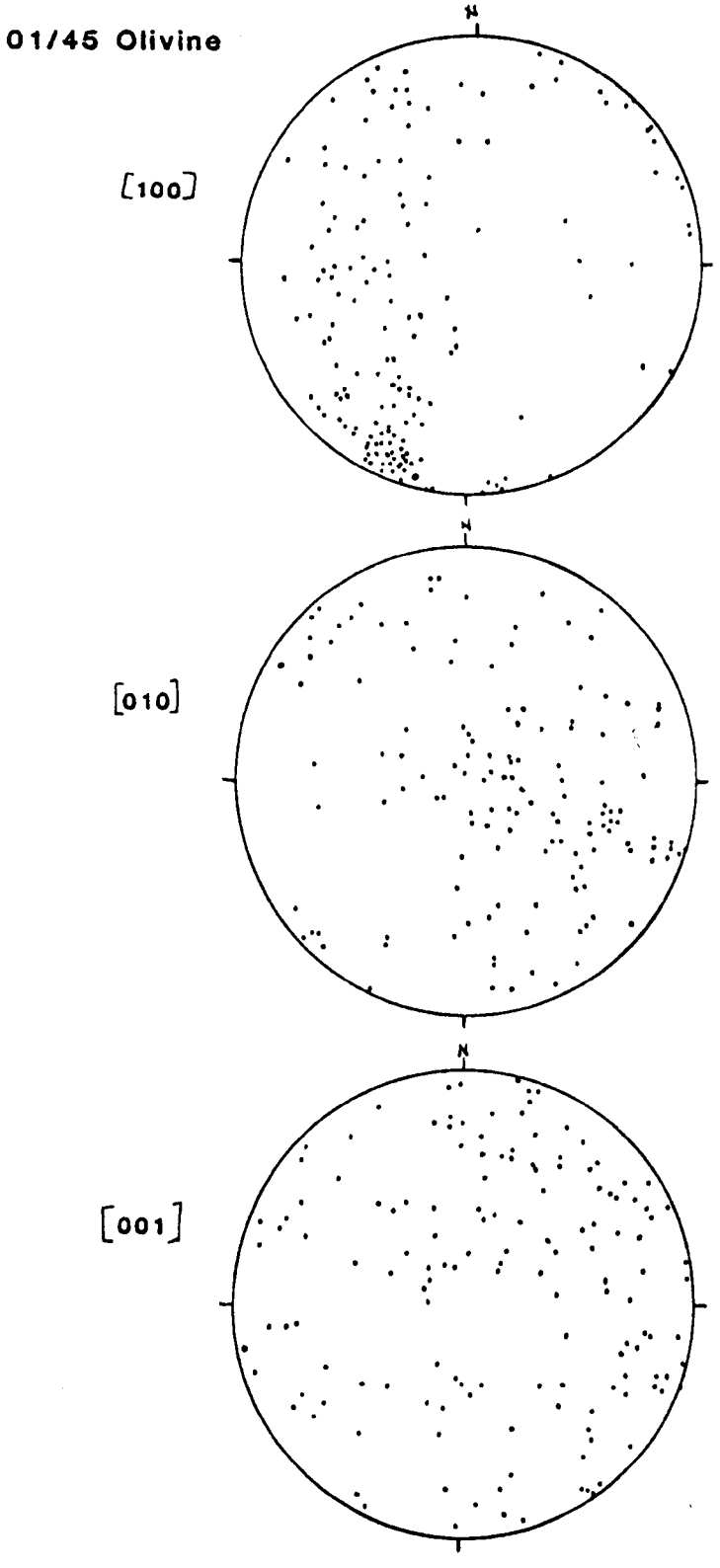

Figure 8.14 Olivine crystallographic orientations for specimen 01/45. (Equal area lower hemisphere projections).

the olivine [100] crystallographic axes give a great circle girdle trend with a fairly strong cluster dipping shallowly towards 215°. Following the discussions in Chapter 7, this cluster orientation can be taken to be the D2 slip direction of the olivine grains. A plot of the olivine [010] crystallographic axes associated with the D2 olivine [100] slip directions (Figure 8.15) shows that the active slip system of olivine during D2 deformation was the {0kl}[100] slip system. (See Chapter 7 for reasoning).

The hand specimen foliation plane dips 79° towards 303° and this defines the 'X' face. The angle between this plane and the D2 slip direction shows that the D2 deformation of the specimen is by a sinistral shear process. (Figure 8.16).

Three orthogonal faces were cut from specimen 01/45, each face representing the 'X', 'Y' and 'Z' faces in relation to D2 shearing (Figure 8.17). The spinel grain alignments are also plotted on Figure 8.17 and they define an S2 and a relict S1 plane. A $2cm^2$ area was then sketched from each face in order to study the olivine grain shapes of each face. These sketches are shown in Figure 8.18.

The olivine [100] plot suggests that the D2 deformation has been fairly strong as many olivine grains show a crystallographic preferred orientation with [100] parallel to the shearing direction. Some grains, however, have not been fully reorientated into the D2 shearing direction, but have been only partially rotated from their original D1 shearing orientations.

As shown in Chapter 7 the foliation pi-pole girdle for the Rajmi area is parallel to the D2 'Y' plane. The lineation great circle

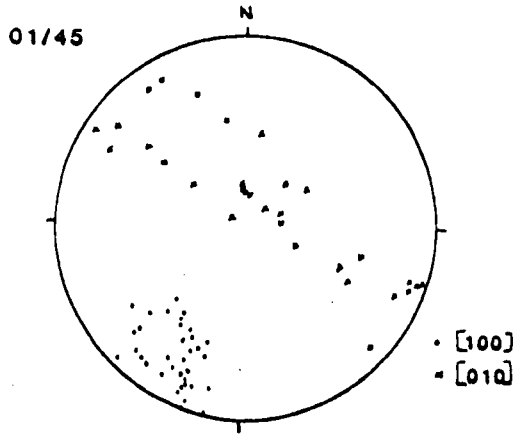

Figure 8.15 Olivine 100 cluster and related 010 girdle orientation for specimen 01/45.

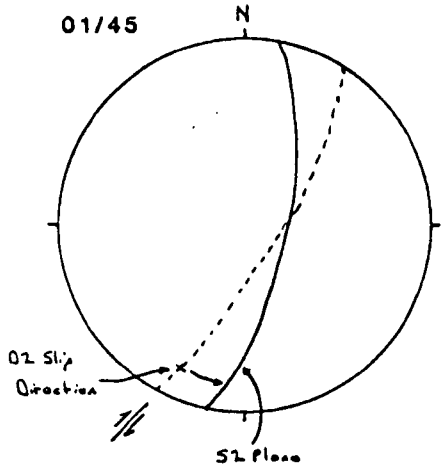

Figure 8.16 Sinistral shearing of specimen 01/45 from the angle between the foliation plane and slip direction. (Lower hemisphere equal area projection).

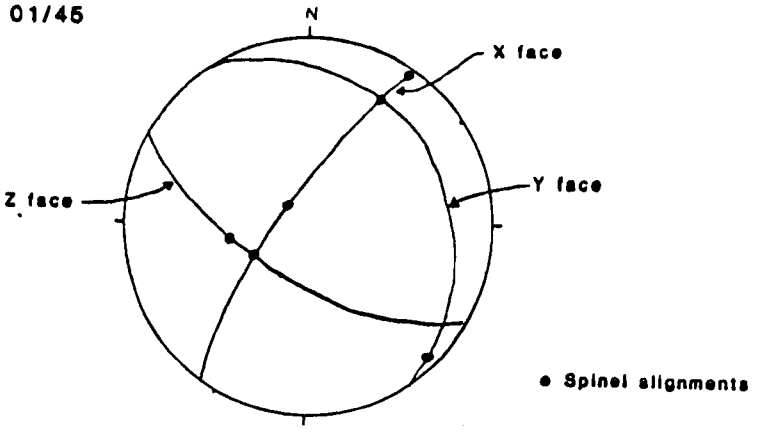

Figure 8.17 The orientation of the cut faces of specimen 01/45 and the spinel grain alignments on each face. (Lower hemisphere equal area projection).

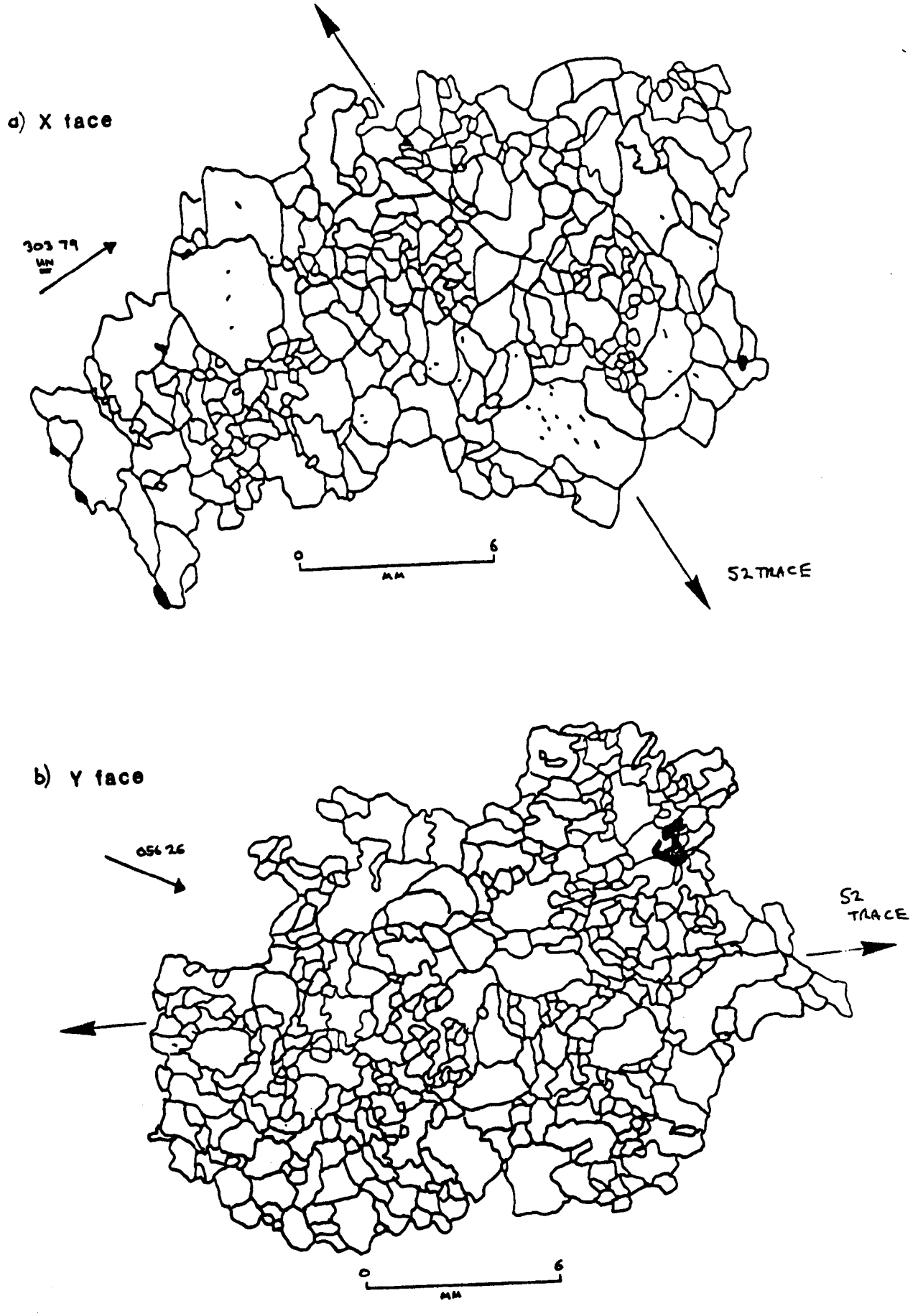

Figure 8.18 For caption see next page

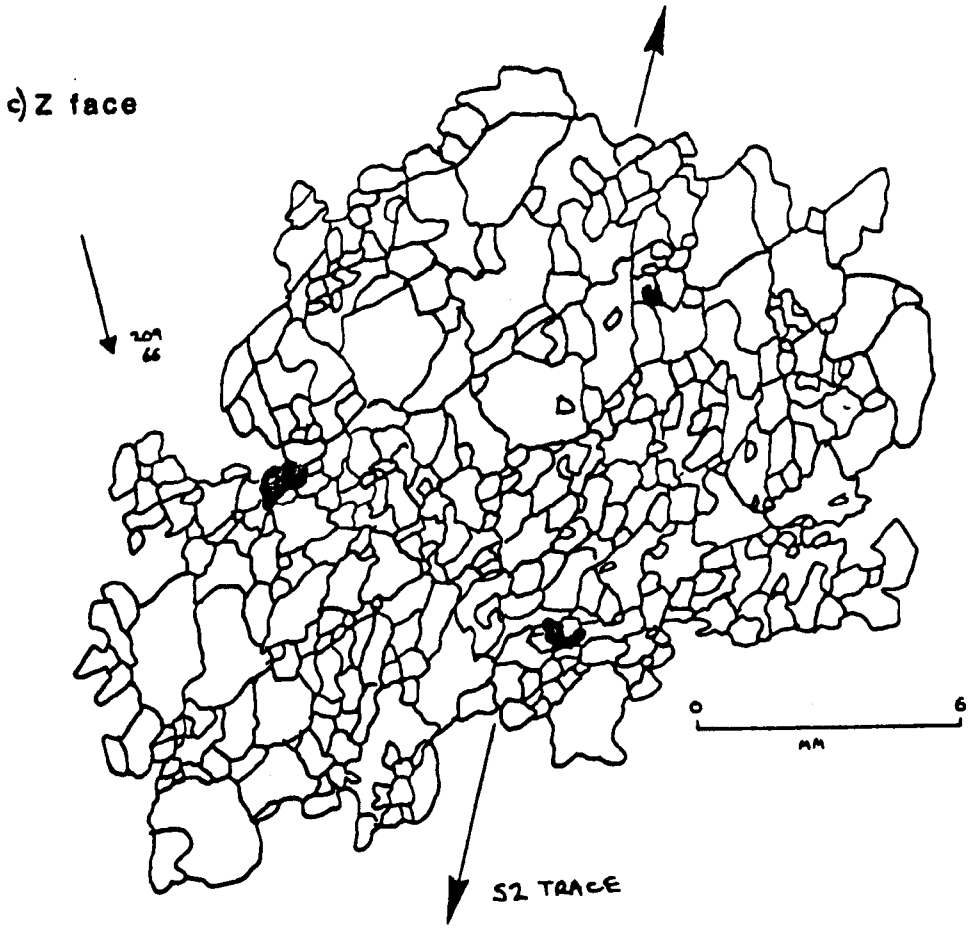

Figure 8.18 Sketches of each of the cut faces of specimen 01/45. a) 'X' face; b) 'Y' face; c) 'Z' face.

is also sub-parallel to the 'Y' plane. (Figure 8.19). This implies that the D1 shearing direction falls on the D2 'Y' plane, and thus all the partially rotated D1 olivine grains will have their [100] axes and also their shape elongation direction sub-parallel to the D2 'Y' plane.

The grain shapes of each face in Figure 8.18 reflect the [100] axis orientations always being parallel to the 'Y' plane. Various sample sizes of crystals were measured for each face and their diameters analysed by the use of the 'Ellipfit' programme. The axial ratios and long axes orientations for the mean ellipses of each face are shown in Table 8.2 for each sample size. The Σ_s and v values for the shape ellipsoid are also included. It is clear that the axial ratio values do not give true values for the D2 related shape orientation of crystals but that the partially rotated relict D1 grains strongly affect the values obtained. The predictions on the axial ratio values produced by simple shear, made from Figure 8.13, are that the 'Y' face axial ratio should be the largest, the 'Z' face intermediate, and the 'X' face close to unity. In Table 8.2 the 'Z' face axial ratios have the largest values for a sample number of 15 upwards, and the 'Y' face values are very low.

The coincidence of the foliation pi-pole girdle with the lineation and olivine [100] great circles implies that the 'Y' plane of the D1 shearing event has the same orientation as the 'Y' plane of the D2 shearing event. (See Figure 8.20). i.e. The D2 'Y' face should contain the maximum axial ratios for both D2 and relict D1 grains. This can be seen in the 'Y' face sketch in Figure 8.18 :

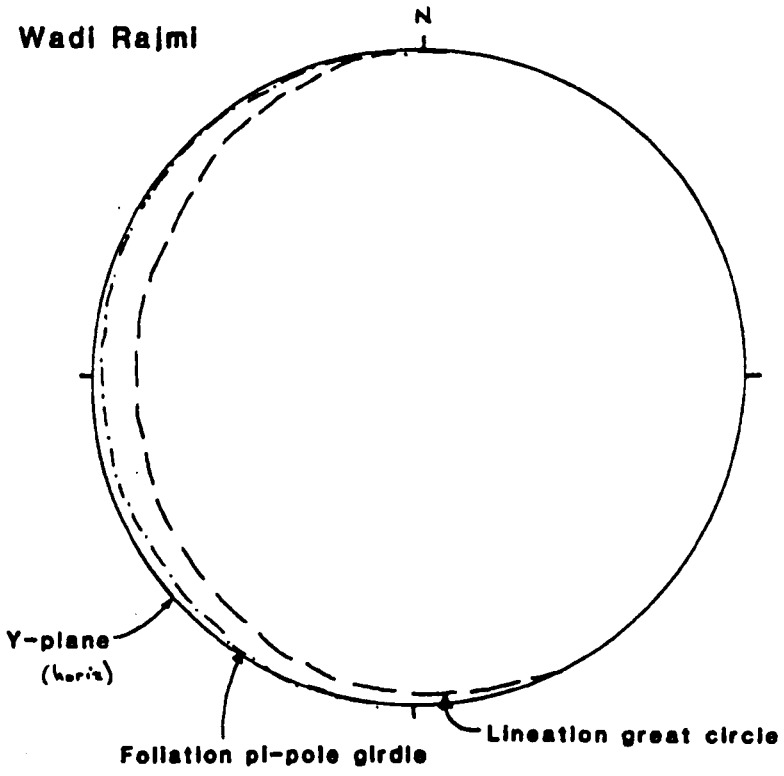

Figure 8.19 Equal area lower hemisphere projection of the mean foliation pi-pole girdle, 'Y' plane, and lineation great circle for the Wadi Rajmi area.

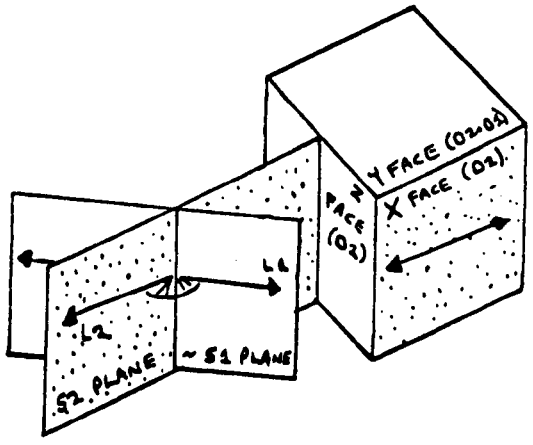

Figure 8.20 Sketch showing the coincidence of the 'Y' planes of both the D1 and D2 shearing events for specimen 01/45.

Table 8.2 Ellipfit results from specimen 01/45.

No.of crystals measured per face	X FACE				Y FACE				Z FACE				Ellipsoid Parameters	
	EAR	.95CI	MAD	.95CI	EAR	.95CI	MAD	.95CI	EAR	.95CI	MAD	.95CI	s	v
40	1.13	0.24	152	65	1.23	0.23	106	35	1.55	0.22	59	15	0.298	+0.870
20	1.19	0.18	168	34	1.22	0.14	82	24	1.45	0.15	60	13	0.288	+0.087
15	1.32	0.32	2	37	1.22	0.17	85	27	1.45	0.17	45	14	0.406	+0.331
10	1.66	0.53	1	32	1.13	0.23	87	60	1.46	0.13	44	11	0.507	-0.290
8	1.62	0.42	4	27	1.25	0.41	60	59	1.47	0.25	38	21	0.479	-0.375

EAR - Ellipse axial ratio

.95CI - .95 Confidence Interval

MAD - Major Axis Direction

there are many major axis directions. Thus, when grains are selected at random to measure their diameters, the axial ratio of the mean ellipse will be a mean of the axial ratios of both partially rotated relict D1 grains and recrystallised D2 grains. The value of the D2 axial ratio will thus be greatly underestimated.

The effect is not so marked for the D2 'X' and 'Z' faces as the axial ratio values for these faces will be lower for a simple shearing deformation (Figure 8.13).

Even though the mean axial ratio values bear no relationship to the D2 shearing intensity, the orientation of the major axis direction clearly does. The orientations shown in Table 8.2 are the same as those predicted from Figure 8.13 for D2 simple shearing. For a sample size of less than 15 grains per face the .95 confidence interval becomes rather large, especially for the 'Y' face, but for a sample size of over 15 grains it reaches more acceptable values.

It can therefore be concluded from this study that for a rock which has undergone only moderate D2 simple shearing, the values of the shape ellipse axial ratios and thus the shape ellipsoid parameters (v and Σ_s) have no relationship to the D2 shearing strength. The D2 shearing has, however, been sufficiently intense to orientate more olivine grains with their maximum shape axes parallel to the D2 trends than relict D1 olivine grains which have only been partially rotated. The orientation of the mean elipsoid Σ_1 axis will thus plot parallel to the expected D2 slip lineation direction. (Figure 8.21). The orientation of the Σ_2 and Σ_3 axes are not so certain. In specimens which have been

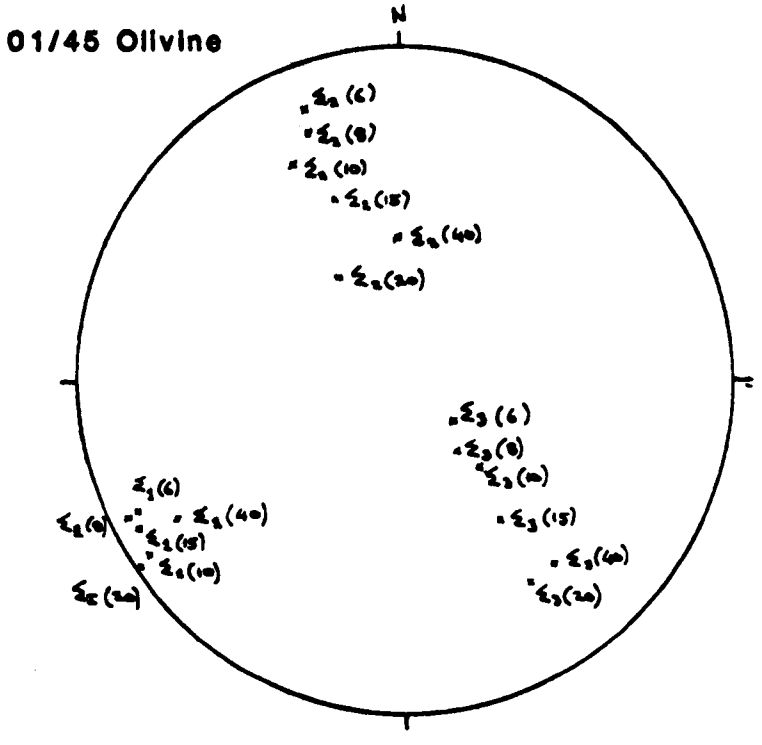

Figure 8.21 The orientations of the principal shape axes for different sample sizes. (Specimen 01/45, equal area lower hemisphere projection).

less strongly sheared by D2 deformation than specimen 01/45, even the orientation of the Σ_1 axis of the shape ellipsoid will not reliably define the L2 slip lineation direction.

As discussed in Chapter 6, recrystallisation most probably plays an important part in the overall deformation process of the Peridotite Unit. In order to study it in more detail the olivine grains from the 'Z' face of specimen 01/45 have been measured in detail crystallographically and dimensionally. The 'Z' face was chosen in order to minimise the effects of D1 on the shape of the crystals. This face is roughly sub-parallel to the relict S1 'X' face (see Figure 8.17) and thus any relict D1 grains should have an axial ratio close to unity.

Figure 8.22 shows the 'Z' face sketch with the measured grains segregated into grains of similar crystallographic orientation. The corresponding crystallographic orientation zones are shown on Figure 8.23. These figures show that the D2 crystallographically orientated grains have a fairly strong grain shape orientation with the long axis parallel to the expected D2 direction. The other grains, on the other hand, have a random orientation, some are elongate but many have no strong shape orientation.

Strongly strained olivine grains can easily be identified by their highly undulose extinction and/or their development of twinning. These grains are shown on the 'Z' face sketch on Figure 8.24 with their corresponding [100] orientations on Figure 8.25. They have a variable shape preferred orientation in relation to the D2 direction and have a large range of crystallographic orientations.

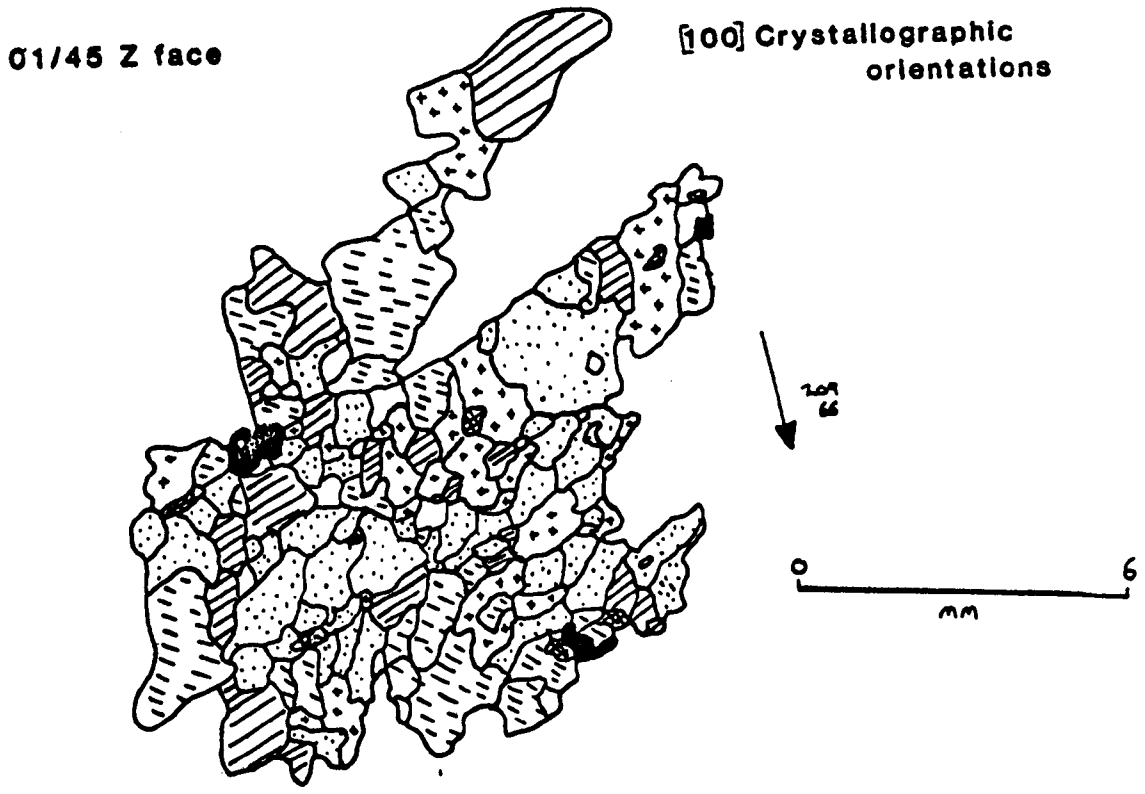

Figure 8.22 Specimen 01/45 'Z' face sketch showing the segregation of grains into grains of similar olivine [100] crystallographic orientation.

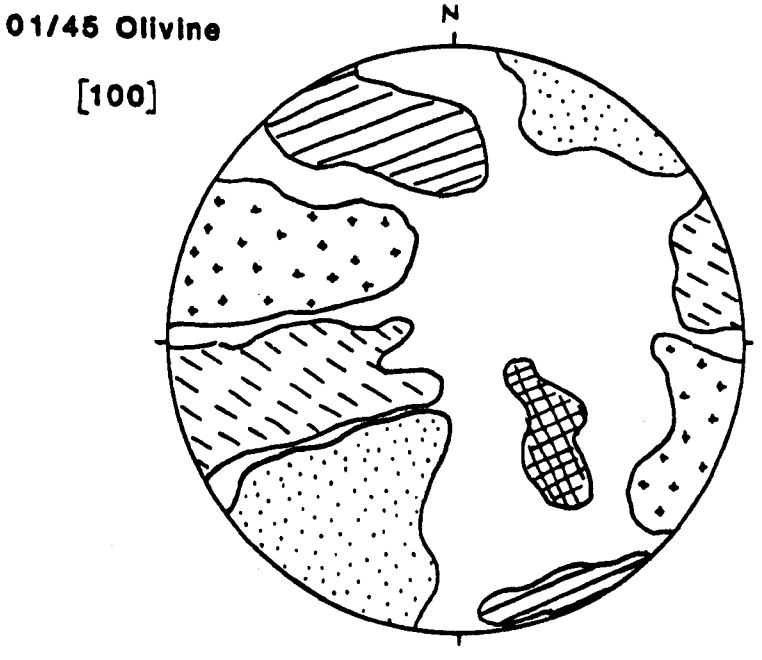

Figure 8.23 Equal area lower hemisphere projection of [100] orientations corresponding to the grain segregations of Figure 8.22.

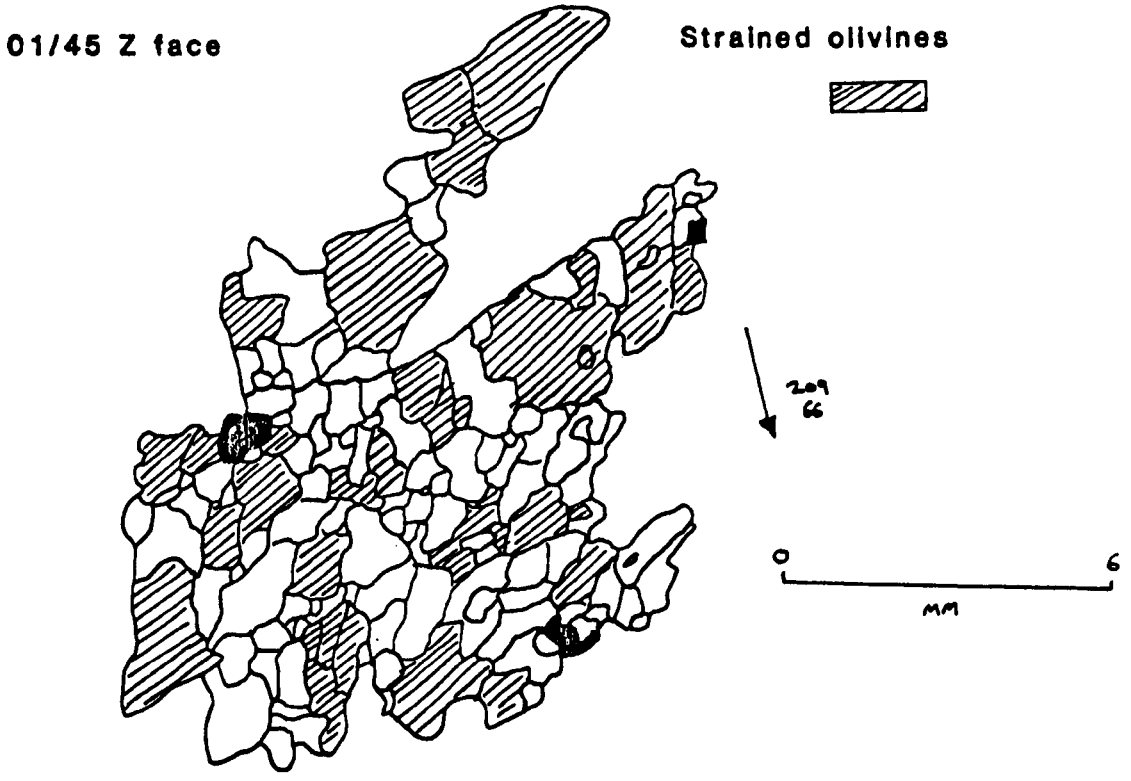

Figure 8.24 Specimen 01/45 'Z' face sketch showing highly strained olivine grains.

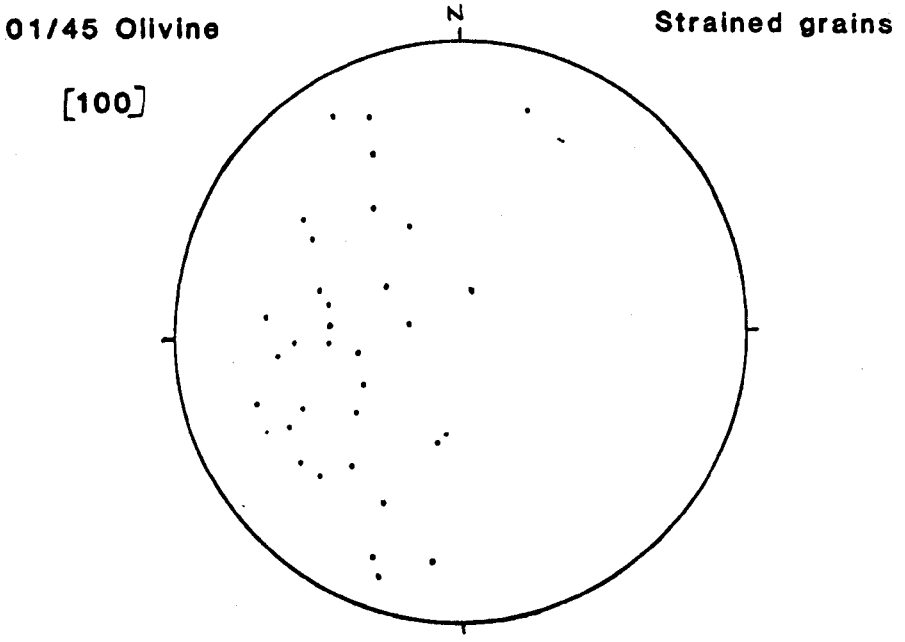

Figure 8.25 Equal area lower hemisphere projection of the [100] orientations of the highly strained olivine grains shown in Figure 8.24.

Unstrained, and thus most probably recrystallised grains, have also been identified and are shown in Figure 8.26 with their corresponding [100] orientations on Figure 8.27. These grains show a similar range of shape and crystallographic orientations to the highly strained grains.

The fact that both strained and unstrained grains have a similar range of crystallographic orientations suggests that the change from D1 to D2 shearing was transitional involving a gradual rotation of the shearing direction. This would account for the full range of crystallographic trends of the recrystallised grains; recrystallisation and grain growth taking place throughout the transitional shearing events.

The D2 shearing has both recrystallised and highly strained grains associated with it. This implies that the D2 shearing event was of a sufficiently long duration for grains to crystallise, grow, be strained, breakdown and recrystallise at least once.

The very fact that relict D1 olivine grains are preserved in the specimen shows that the D2 shearing cannot have had a high shear strain. Only some of the grains are recrystallised and reorientated parallel to the D2 shearing direction.

8.4.2 Specimen 02/10 - High Intensity D2 Shearing.

In contrast to specimen 01/45, specimen 02/10 has undergone an intense D2 shearing. The crystallographic orientations shown in Figure 8.28 have a strong olivine [100] cluster pattern developed parallel to the D2 slip direction with only a few grains plotting in the [100] girdle pattern which is well developed in specimen

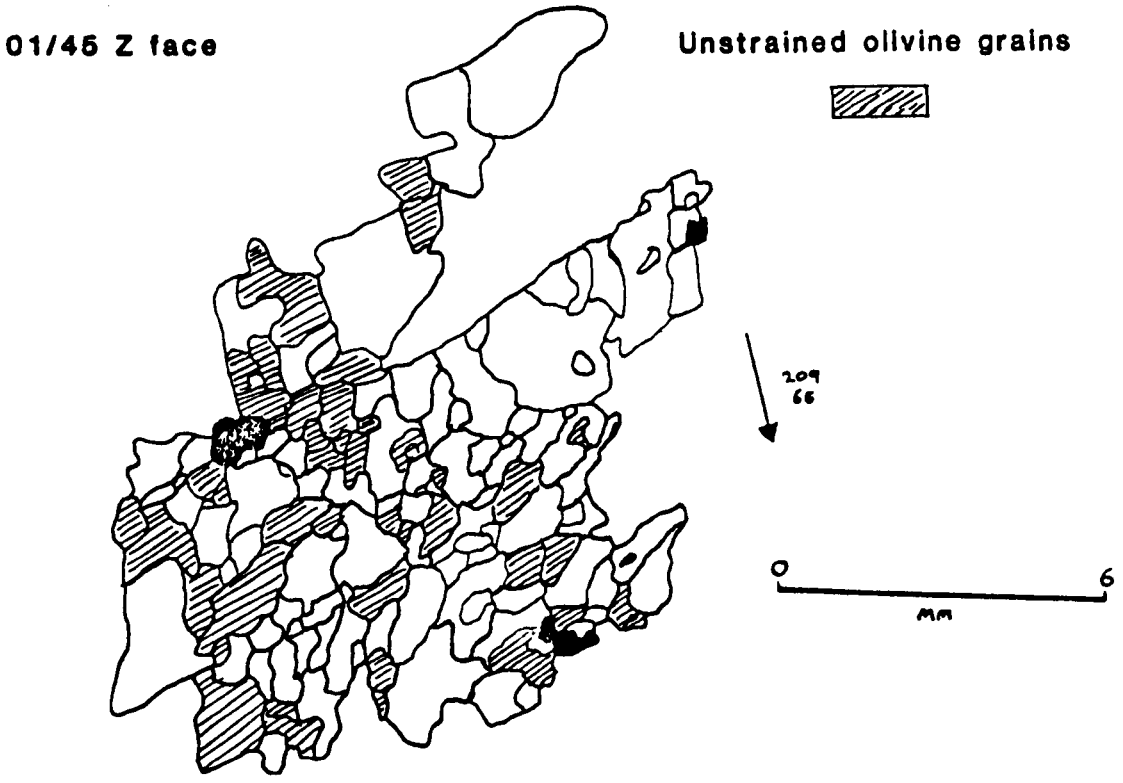

Figure 8.26 Specimen 01/45 'Z' face sketch showing unstrained olivine grains.

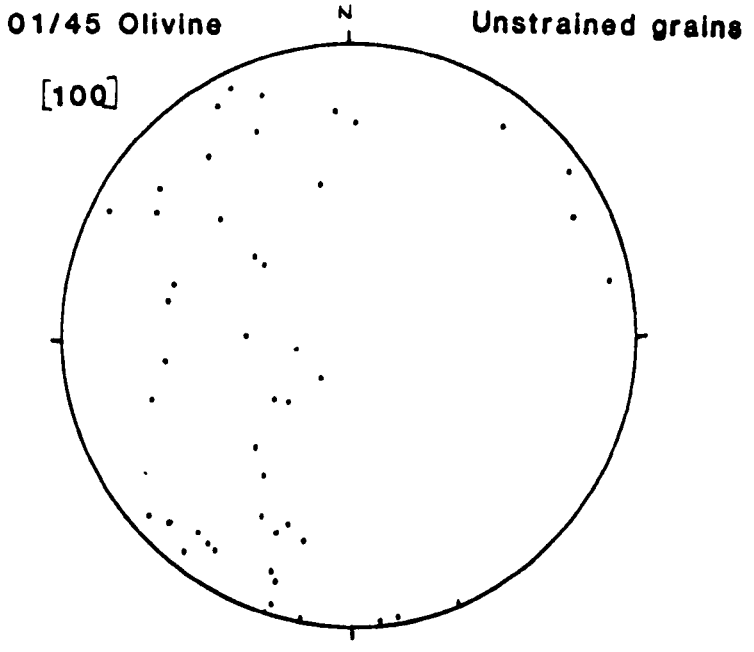

Figure 8.27 Equal area lower hemisphere projection of the [100] orientation of the unstrained olivine grains shown in Figure 8.26.

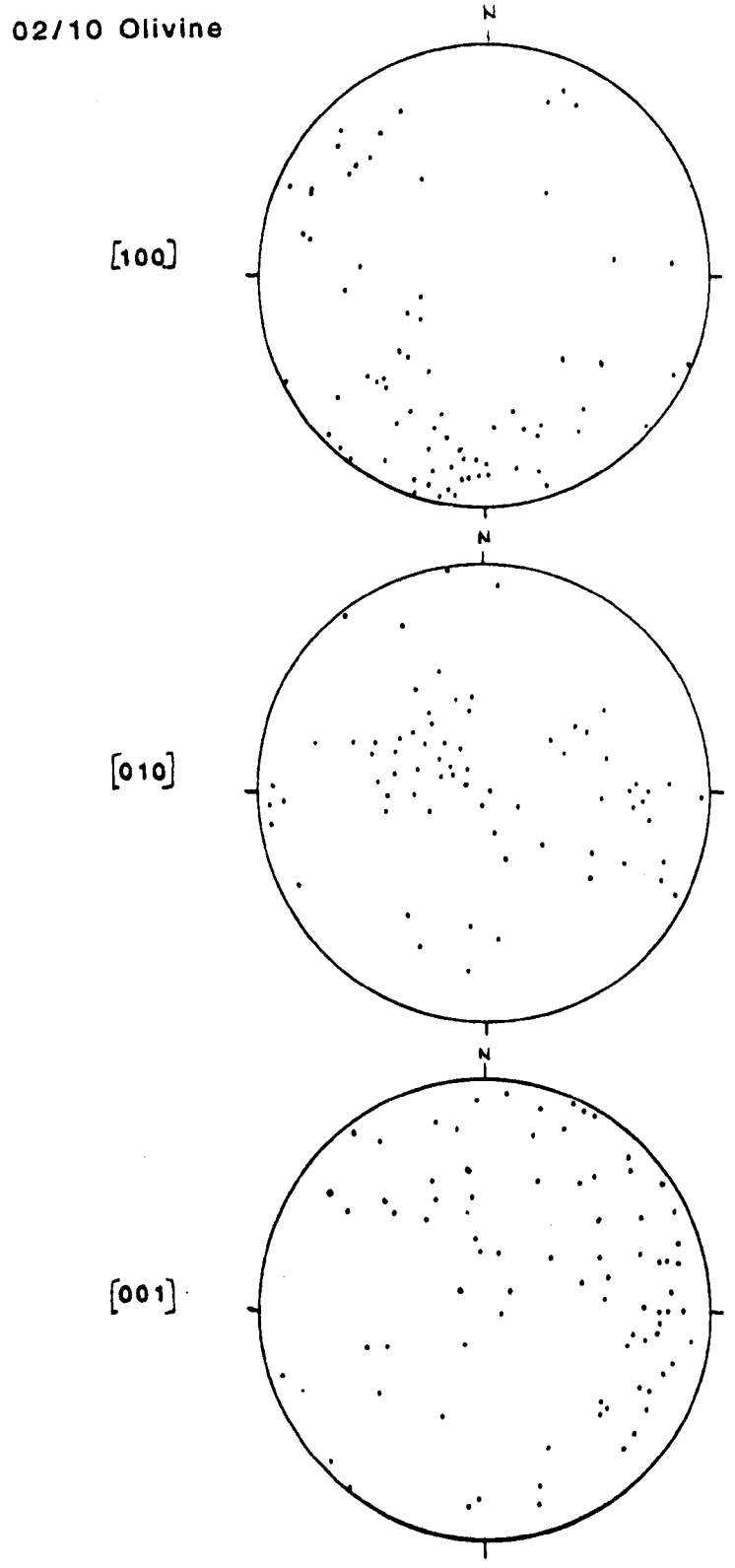

Figure 8.28 Olivine crystallographic orientations for specimen 02/10. (Equal area lower hemisphere projections).

01/45. The distribution of the olivine [010] axes suggests that the {0kl}[100] olivine slip system has been the active D2 slip system.

D2 related 'X', 'Y' and 'Z' faces were cut for specimen 02/10 and the spinel grain alignments measured for each face. (Figure 8.29). The spinel grains define an S2 plane approximately parallel to the 'X' face, but an S1 plane is not distinguishable.

The orientation of the [100] cluster and the S2 foliation plane ('X' face) implies that the D2 deformation has a sinistral shear sense with a shear direction dipping at a shallow angle towards 190^{o}. (See Figure 8.30).

Table 8.3 shows the results from an 'Ellipfit' study of 15 grains per face for specimen 02/10. The results conform to those expected for simple shearing with the 'X' face ellipse axial ratio close to unity, the 'Y' face axial ratio the largest, and the 'Z' face axial ratio only just larger than that of the 'X' face. (see Figure 8.13). The ellipsoid parameters thus give at least an estimation of the strength of D2 shearing : v is close to zero as is expected for simple shearing, and the Σ_s value of 0.100 gives a shear strain estimation of 0.15 when correlated with Figure 8.11. This is a very low shear strain and may well account for the few olivine grains of which the [100]axes are not preferably orientated in the D2 shearing direction but which plot as a girdle pattern. (Figure 8.28). The very fact that such grains exist implies that the Σ_s value will be an underestimate of the true D2 shear strain.

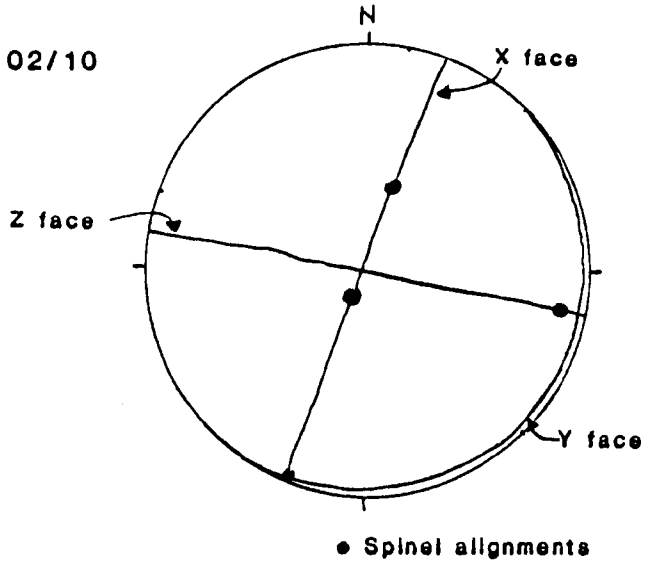

Figure 8.29 The orientation of the cut faces of specimen 02/10 and the spinel grain alignments on each face. (Lower hemisphere equal area projection).

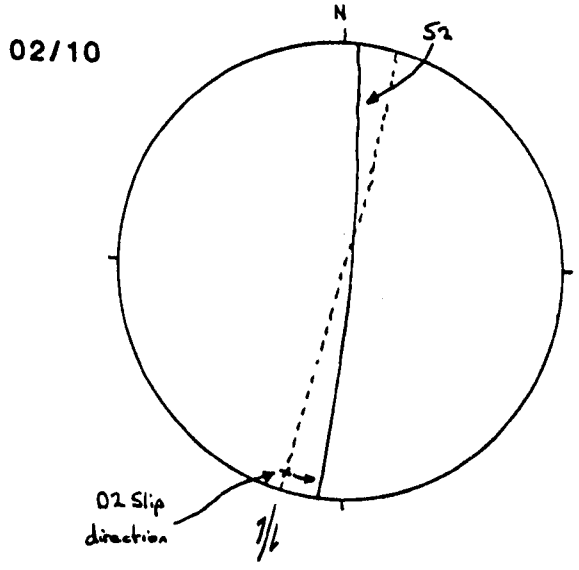

Figure 8.30 Sinistral shearing of specimen 02/10 from the angle between the foliation plane and slip direction. (Lower hemisphere equal area projection).

No of crystals measured per face	X FACE			Y FACE			Z FACE			Ellipsoid Parameters		
	EAR	.95	MAD .95	EAR	.95	MAD .95	EAR	.95	MAD .95	s	v	
15	1.00	0.19	70 00	1.25	0.13	157 18	1.08	0.17	131 72	0.100	0.067	

See Table 8.2 for legend

Table 8.3 Ellipfit results from specimen 02/10.

The orientation of the Σ_1 axis is sub-parallel to the D2 slip lineation direction as shown in Figure 8.31. The great circle joining the Σ_1 and Σ_2 axes is also sub-parallel to the S2 foliation plane. Both of these relationships are those expected for simple shearing.

A detailed study of recrystallisation and grain straining has been completed for the 'Z' face of specimen 02/10. A sketch of the 'Z' face showing the measured grains is shown in Figure 8.32. The olivine grains are segregated into grains of similar orientation. The corresponding grain [100] orientations are shown in Figure 8.33. In figure 8.34 both the highly strained and the completely unstrained olivine grains have been identified. As can be seen many of the grains which do not have their [100] axes orientated parallel to the D2 shearing direction are highly strained. Only 5 of these grains show no evidence of being strained to some degree.

Most of the olivine grains on the 'Z' face have the expected grain shape orientation for D2 simple shearing. (i.e. Their long axis is sub-parallel to the intersection of the 'α' face with the 'Z' face). These grains generally have a [100] plot parallel to the D2 shearing direction. They have a full range of deformation states from totally unstrained grains to highly strained grains. This is the same pattern that was noted for specimen 01/45, and again it implies that the grains which recrystallised into the D2 shearing direction have been strained and recrystallised at least once after initial crystallisation.

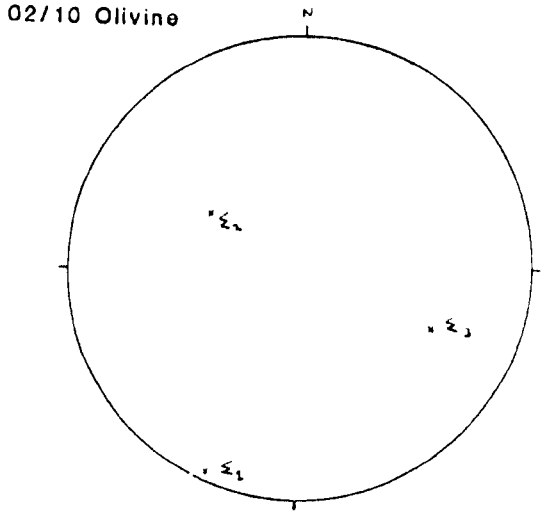

Figure 8.31 The orientation of the principal shape axes for specimen 02/10. (Equal area lower hemisphere projection).

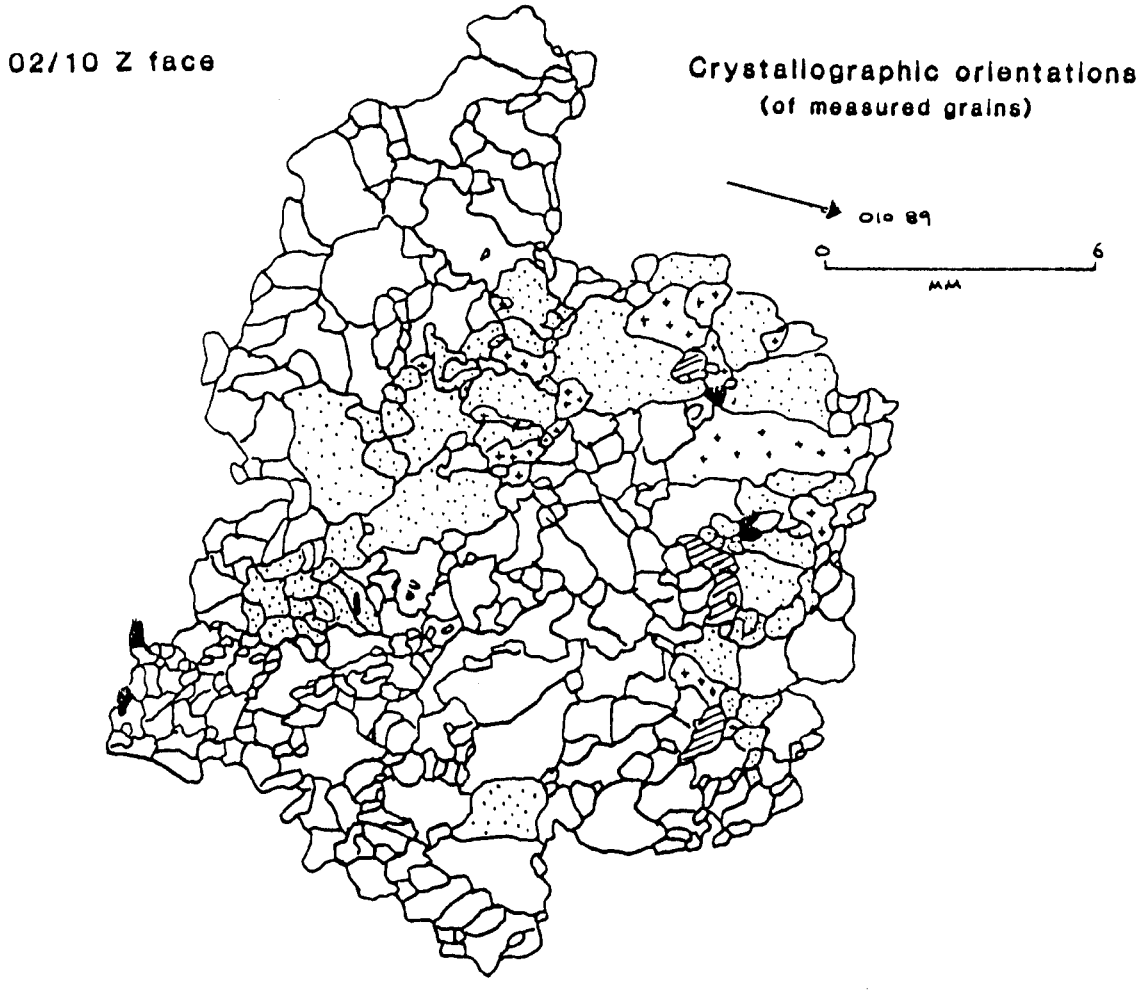

Figure 8.32 Specimen 02/10 'Z' face sketch showing the segregation of grains into grains of similar olivine [100] crystallographic orientation.

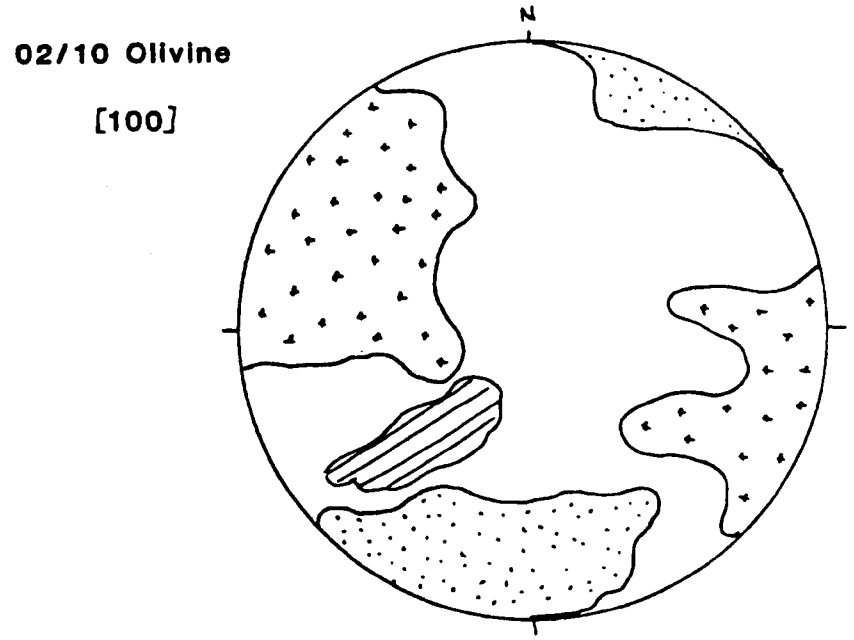

Figure 8.33 Equal area lower hemisphere projection of [100] orientations corresponding to the grain segregations of Figure 8.32.

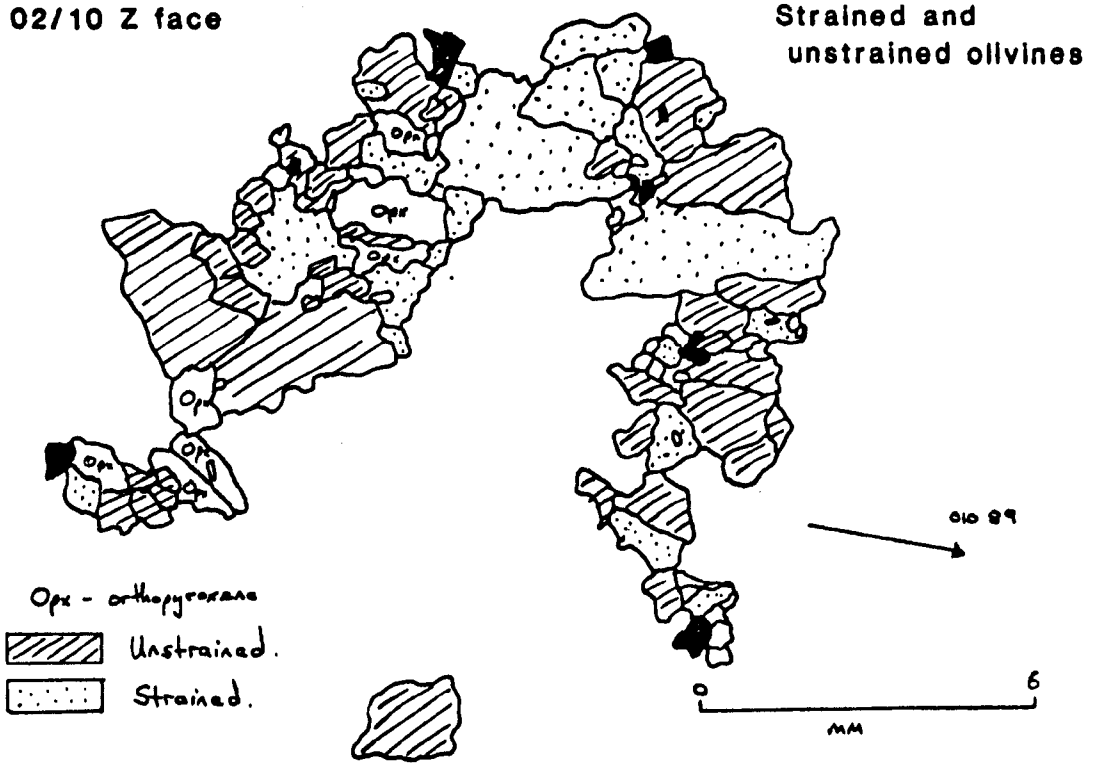

Figure 8.34 Specimen 02/10 'Z' face sketch showing the highly strained and unstrained olivine grains measured.

8.4.3 The Interpretation of the 'Ellipfit' Shape Ellipsoid Parameters.

The fact that the D2 deformation causes crystallisation, grain growth and straining, grain breakdown and recrystallisation and so on, all in the same deformational event, brings into question what the value of Σ_s really means. The studies on the 'Z' face of specimen 02/10 and also 01/45 show that this cyclical process is at different stages for different grains. In specimens similar to 02/10 which only, or at least mainly, have olivine grains orientated crystallographically parallel to the D2 shear direction, the Σ_s value will be a mean shape ellipsoid for the whole range of grains from neoblasts through to highly strained porphyroblasts. If the rock has undergone some degree of recovery after deformation then some of the olivine grains will grow as unstrained grains into shapes which are unrelated to deformation. In the calculation of Σ_s and v, these grains will affect the Σ_s and v values. i.e. If any recovery has taken place, the Σ_s value will tend to underestimate the shear strain of the deformation.

The studies discussed above show that it is not possible to distinguish relict D1, D2 or recovered grains from each other purely by examining the grain shapes and their strain states on various cut faces. If D2 has been of only a low intensity, then the calculated ellipsoid parameters and orientations from the measurement of 15 grains from each of three orthogonal faces are virtually meaningless. They are a measure of the mean olivine grain shape produced and controlled by a combination of D1 and D2 shearing strengths as well as any post-deformational recovery which has taken place. The value of the Lode's parameter, v, and Σ_s will depend on the different deformational shearing strengths

and also the angular difference between the two shearing directions.

In highly serpentinised grains, only the olivine neoblasts have been preserved sufficiently to enable Ellipfit measurements to be made for them. The highly strained grains are all too serpentinised for their original grain shapes to be made out. Thus, in these grains the Σ_s value is only for the neoblasts. The studies above show, however, that both D2 and relict D1 olivine neoblasts are preserved in rocks which have undergone only low intensity D2 deformation. It has also been proposed that there is a transitional change between the two deformational events in which olivine recrystallises in intermediate directions between the D1 and D2 slip directions. The Σ_s value, thus, still does not relate to only the D2 deformational event.

The only specimens for which Σ_s will vaguely relate to the D2 deformational event are those in which the D2 shearing has been sufficiently intense to breakdown and recrystallise, or at least fully rotate, all the olivine grains with their [100] crystallographic axes into parallelism with the D2 shearing direction. Even for these specimens it is not possible to identify and thus not possible to measure grains which have grown during recovery after D2 deformation has ceased. The Σ_s value thus only gives a very rough estimation of the D2 shear strain. It can, however, be used in a qualitative sense to compare the D2 shear strains between grains which have undergone fairly intense D2 shearing.

Suitable specimens for the estimation of Σ_s can only be chosen when all of the structural factors relating to that grain are taken into account. i.e. The olivine [100] crystallographic axes must plot as a cluster pattern; this cluster must be approximately

parallel to the D2 slip lineation as defined from both field and hand specimen measurements; the specimen should have a porphyroclastic to mosaic porphyroclastic texture (a coarse texture most probably implies that some post-D2 recovery has taken place) with the olivine grain shapes elongated parallel to the spinel D2 alignments on each face. Finally, once the mean shape ellipsoid parameters have been calculated, the Σ_1 axis must be parallel to the D2 slip lineation and the Lode's parameter, v, should be close to zero. If all of these relationships are present in a specimen then the value of Σ_s can be taken as a qualitative or semi-quantitative estimate of the D2 shearing strength. If one of the relationships is different from those described above, then the value of Σ_s cannot be even quantitatively related to the D2 shearing strength.

These factors have been applied to the specimens collected from the three areas of study and suitable specimens for Σ_s calculation identified. Their results are described in the next section.

8.5 D2 Shearing Strengths from Suitable Specimens.

The specimens deemed suitable for an estimation of the D2 shearing strength are listed on Table 8.4. As can be seen the value of the Lode's parameter is close to zero in all cases. The values of Σ_s obtained range from 0.100 up to 0.600. They are plotted on three axis diagrams for each area on Figure 8.35.

In all the three areas studied, the variation in Σ_s values corresponds well to the variation in shear intensities inferred from the field and crystallographic structural measurements and the textural descriptions. (See Table 7.1, Chapter 7).

Area	Specimen	Σ_s	v
RAJMI	02/07	0.276	+0.064
	02/I0	0.I00	+0.067
	02/I3	0.28I	+0.I49
	02/34	0.24I	+0.I54
ATH THUQBAH	02/28	0.234	+0.II2
FIZH DEEP MANTLE	02/43	0.595	-0.076
	02/I03	0.4I0	+0.020
SARAMI and KANUT	02/93	0.253	-0.I06
AL ABYAD	02/46	0.284	+0.020
	02/63	0.26I	-0.I46
UNST	05/I0A	0.207	+0.209
	05/25	0.487	+0.II3
	05/34	0.304	+0.II3
TROODOS	I0/I9	0.247	+0.I67
	I0/27	0.I72	-0.I82
	I0/36	0.I98	+0.2I0
	I0/42	0.I93	+0.065
	I0/53	0.II0	-0.II6
VOURINOS	08/0I	0.704	+0.I23

Table 8.4 Σ_s and v results for suitable specimens.

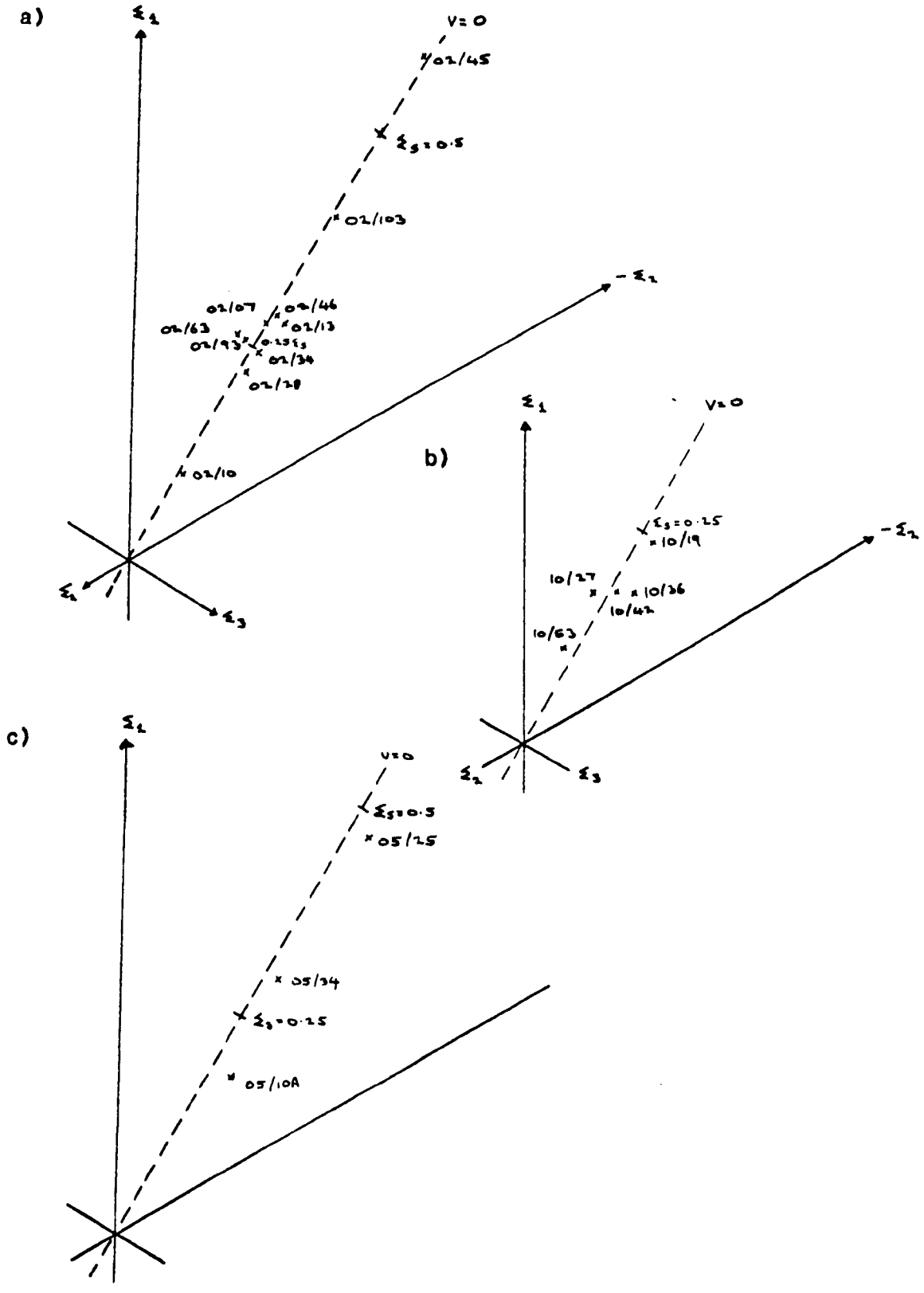

Figure 8.35 Three-axis shape diagrams of the specimens listed in Table 8.4. a) Oman areas; b) Cyprus area; c) Shetland area.

For Oman, the usual range of Σ_s values is between 0.230 and 0.284; most specimens lie between these two values. Higher shearing intensities are only preserved in specimens from the deep mantle areas of the Fizh structural block.

In the Troodos and Unst areas the Σ_s values conform well to the shearing intensity estimates made from the S1-S2 angles on the D2'Y' structural face. (See Chapter 7). As would be expected from its location (see Enclosure 10), specimen 10/53 has the lowest shearing intensity out of specimens studied from the Troodos area, as it is very close to the boundary where D2 penetrative shearing deformation dies out. The other specimens have similar values to most of the Oman specimens.

Only 3 specimens were suitable for measurement from Unst. They show a large range of Σ_s values with specimen 05/25 having the highest value of 0.487. It is from the Clibberswick Hill Block which is the stratigraphically lowest Peridotite Unit Block on Unst (See Chapter 4). The other Σ_s values are more similar to those obtained for most of the Oman specimens.

As discussed in Section 8.4 above, the direct correlation between Σ_s and shear strain for the simple shearing of a perfect sphere (see Figure 8.11), will give a gross underestimate for shear strains within the Peridotite Unit. The data used to construct Figure 8.11 assumed that a crystal does not change in volume and deforms purely by simple shear with no recrystallisation. The detailed study in Section 8.4 shows that grain breakdown and recrystallisation are a major part of the overall deformation process. Thus a single crystal which has started to crystallise during the D2 deformation may well start

to deform by simple shear processes; but, with an increase in bulk shear strain, the crystal may well start to break-down by sub-graining and eventually recrystallise as neoblasts. Thus the ξ_s value of a single crystal is constantly changing as is the strain state of that crystal. Every time it recrystallises, even though the bulk shear strain of the rock can be at a high value, the shear state of the individual crystal is effectively reset to zero shear strain at the start of recrystallisation. The Σ_s values calculated imply that recrystallisation occurs readily when the shear strain of the crystal has reached only about 0.4.

The Σ_s value for a specimen thus gives an average crystal shear strain value from those grains which have a fairly large crystal shear state (the porphyroblasts) and those which have a small crystal shear state (the neoblasts). This average crystal shear strain value is a gross underestimate of the bulk shear strain of the overall specimen. The bulk shear strain is more likely to be closer to the shear strain values estimated from the measurement of the S1/S2 angles for Troodos and Unst in Chapter 7.

8.6 Stress Estimations for D2 Shearing.

In order to obtain an estimation of the applied stress for D2 deformation, the specimens used to estimate the D2 shearing strain in Section 8.5 have been studied for the same reasons as discussed in Section 8.5. A mean olivine grain diameter was calculated by summing the six diameters of each grain for each face and dividing by the total number of diameters measured. The calculated diameters are shown in Table 8.5.

Area	Specimen	Mean Grain Diameter (mm)	$\sigma = 19D^{-0.5}$ (Post 1977) (bars) Min	Mean	Max	$\sigma = 48D^{-0.5}$ (Ross et al) (bars)
RAJMI	02/07	0.86	51	152	437	22
	02/10	1.16	41	124	369	17
	02/13	1.11	42	126	379	18
	02/34	0.80	53	158	455	23
FIZH DEEP MANTLE	02/43	0.72	59	171	483	26
	02/103	0.75	57	166	472	24
SARAMI and KANUT	02/93	1.05	44	131	391	19
AL ABYAD	02/46	1.17	41	122	368	17
	02/63	1.16	41	124	369	17
UNST	05/10A	0.74	58	167	475	25
	05/25	0.67	63	178	503	28
	05/34	0.81	53	157	452	23
TROODOS	10/19	0.83	52	155	446	23
	10/27	0.95	47	141	413	20
	10/36	1.34	36	112	341	16
	10/42	1.44	34	107	327	14
	10/53	0.86	51	152	437	22

Table 8.5 Palaeostress estimates for suitable specimens.

The equations of Post (1977) and Ross et al (1980), discussed in Chapter 6, have been used to calculate a value for the stress for each specimen. These values are included in Table 8.5. The relationships between the olivine neoblast size and the stress from the equations of Post (1977) and Ross et al (1980) are shown in Figure 8.36. For all of the equations, and especially that of Ross et al (1980), the value of the applied stress does not markedly vary with a change in grain size until a grain diameter of 0.7mm or less is reached. Thus, even though a large range of grain diameters were present in the specimens measured (see Table 8.5), the estimates of the applied stress do not vary very much. The variation in the stress estimates against the Σ_s value is shown in Figure 8.37 for the mean equation of Post (1977) and that of Ross et al (1980). For each equation, the stress estimates obtained generally show a slight increase in applied stress for an increase in the Σ_s value, as would be expected.

In the study of grain sizes, it is often difficult to distinguish neoblasts from sub-grains, as both commonly have straight extinction. Thus, the mean olivine grain diameters in Table 8.5 are neither the mean diameters of neoblasts nor of subgrains. Also, as discussed earlier in this Chapter, the deformation of olivine causes a cyclical pattern between recrystallisation, grain growth and grain breakdown of individual grains. A measurement of grains in a hand specimen will be the end result of the deformation and will include grains in all states of deformation. (i.e. Some grains will just have recrystallised whilst others will not yet have broken down. Some grains could have recrystallised and broken down many times.) The mean

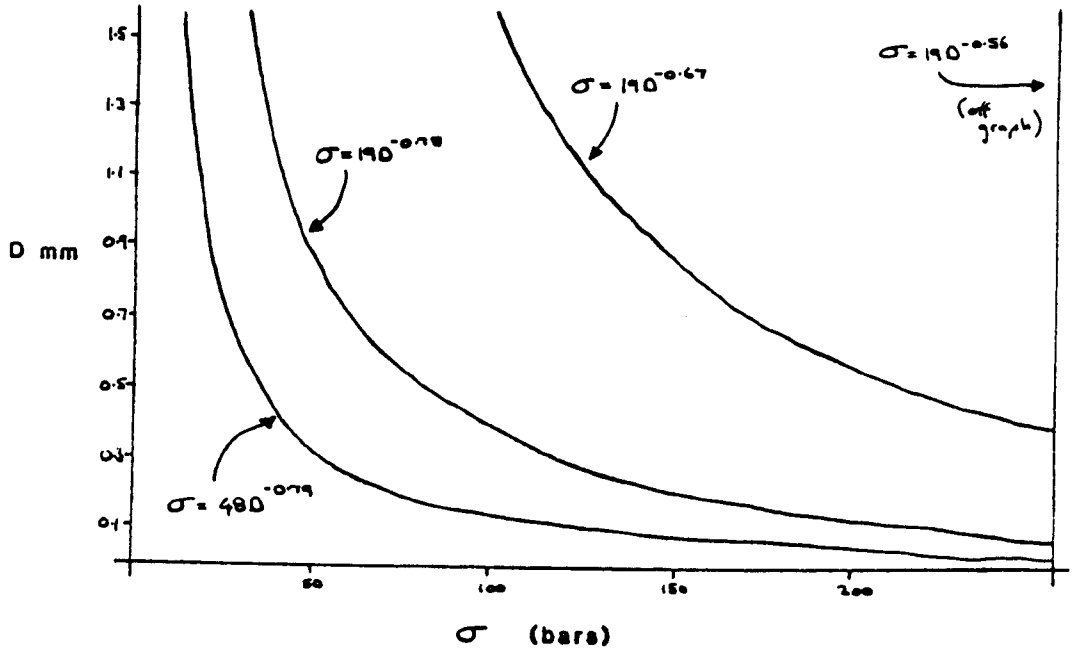

Figure 8.36 Stress versus neoblast diameter graph showing the dependence of grain size on the stress as calculated by Post (1977) and Ross et al (1980).

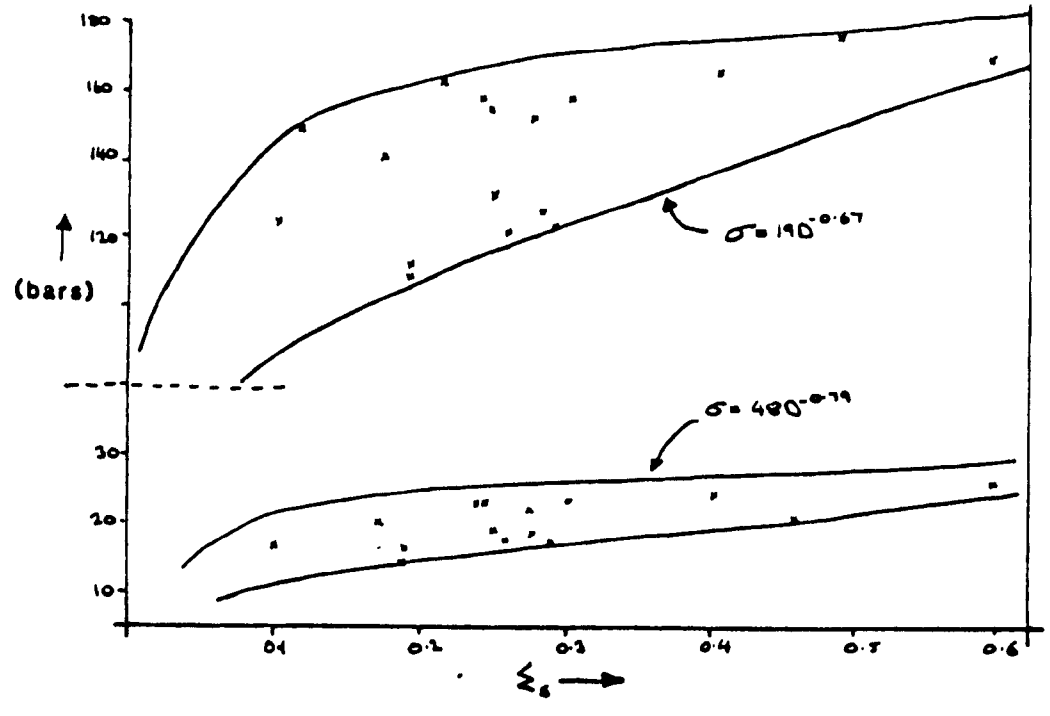

Figure 8.37 $\dot{\varepsilon}_s$ versus stress plot for the specimens of Table 8.5 calculated from the equations of Post (1977) and Ross et al (1980). See text for details.

olivine grain diameter will thus be a mean value from grains in all stages of the cyclical process. This will tend to overestimate the average neoblast grain size and thus underestimate the applied stress.

The calculated values for the applied stress can thus not be used as true quantitative values, but at least the specimens can be compared qualitatively for stress variations. The evidence would suggest that the applied stress for the second deformation was relatively constant over small areas in each of the Peridotite Units studied, and that the different shear strains and shear senses are produced by the heterogeneous reaction of the rocks to the applied stress. Some zones will be highly deformed whilst others will hardly be deformed at all and may even show an opposite sense of shearing. This is discussed further in Chapter 9.

8.7 Summary

The detailed studies discussed in this chapter have shown that the penetrative deformation of Peridotite Unit olivine-rich rocks is an extremely complex process. At all scales the deformation is heterogeneous. A whole traverse area can be divided up into zones of different shear senses. Where sufficient data are available, each of these zones can be divided into strongly and weakly sheared areas. (i.e. Cyprus).
The studies on thin section scales show that each olivine grain acts heterogeneously with respect to its neighbours, some growing whilst others are breaking down.

In the next Chapter the mean values of the structural parameters for each area will be considered with respect to the large-scale kinematic study of an ocean spreading setting (i.e. Mean D2 slip directions, mean shear senses etc.). It is important to bear in mind when considering the much larger scale regional kinematics that the actual D1 and D2 shearing deformations are extremely heterogeneous processes right down to the single grain scale.

PART 3

Overall Structural Synthesis and Models.

Chapter 9

Kinematic Interpretations for Each of the Areas Studied.

CONTENTS

Chapter 9.

In this chapter the structural data described and discussed in earlier chapters will be related to the orientation and position of a palaeo-spreading axis for each area. In order to do this, mean values of various structures will be calculated and then rotated to their original palaeo-spreading axis orientations by the use of a number of geometrical reference frames.

9.1 The Mean Structural Orientations for Each Area.

9.1.1 The Calculation and Diagrammatic Representation of Mean Structural Data.

In Chapter 7, a value for the pole to the foliation pi-pole girdle was estimated in order to calculate the angles between S1 and S2 planes. In order to verify and accurately calculate the mean value of the foliation pi-pole girdle, and to check on the non-randomness of, and whether the data is in, a girdle or cluster pattern, the foliation data from each area studied was analysed by a computer programme called 'Statis'. This has been written by Dr N H Woodcock of the Department of Geology, University of Cambridge, and, as well as contouring equal area plots, it also calculates the three principal eigenvalues and their ratios of the input structural data. Woodcock (1977) has shown how the eigenvalues and the eigenvalue ratios can be used to specify both the fabric shape and strength of data.

The 'Statis' programme derives eigenvalues from an orientation tensor method which was first proposed by Fara and Scheidegger (1963), Scheidegger (1964, 1965) and Watson (1965, 1966). This method is developed by Woodcock (1977). The three eigenvalues

computed from the individual observations have the relationship:

$$\lambda_1 + \lambda_2 + \lambda_3 = N$$

where $\lambda_{1,2 \text{ and } 3}$ are the principal eigenvalues and N is the number of observations made. This relationship is more meaningful when the eigenvalues are normalised to the form:

$$S_1 + S_2 + S_3 = 1.$$

where S is a normalised eigenvalue. Each of the eigenvalues are relatable to an eigenvector: the S_1 related eigenvector is an estimate of the distribution mean of the measurements; the S_3 related eigenvector is an estimate of the pole to the best fit pi-pole girdle; and the S_2 related eigenvector is perpendicular to both the S_1 and S_3 related eigenvectors.

Watson (1966) noted that perfect cluster distributions of data would have a normalised eigenvalue relationship of:

$$S_1 > S_2 = S_3$$

and that perfect great circle girdle distributions of data a relationship of :

$$S_1 = S_2 > S_3$$

Woodcock (1977) plotted the different eigenvalues or their ratios on similar diagrams to those used in the analysis of strain (see Section 8.2.2 of Chapter 8). He concluded that the logarithmic Flinn type plot of the ratio $\ln(S_1/S_2)$ plotted against $\ln(S_2/S_3)$ gives the most easily interpretable results. The tendency of a distribution to a girdle or a cluster can be quantified in a similar manner to the oblateness or prolateness

of a strain ellipsoid. In the case of the structural data with normalised eigenvalues of S_1, S_2 and S_3, the parameter K is equal to:

$$K = \ln(S_1/S_2) \; / \; \ln(S_2/S_3)$$

The variation of fabric shape with K is shown on Figure 9.1.

Woodcock (1977) points out that these fabric shape plots can only be used for those fabrics whose symmetry axes coincides with the eigenvectors (i.e. unimodal clusters, axially symmetric girdles, or some combination of the two). Where the fabric is monoclinic or triclinic then the symmetry axes may well not be coaxial with the eigenvectors. Before data can be interpreted by using fabric shape diagrams, the gross shape of the fabric must therefore be studied on an equal area projection to confirm that its symmetry is at least orthorhombic.

Woodcock (1977) also used the eigenvalue ratio of $\ln(S_1/S_3)$ which he termed the C parameter. On a fabric shape diagram this parameter is a measure of the distance away from the origin that a point plots and is effectively an estimation of the strength of the fabric. Values of C are also shown on Figure 9.1.

The Statis programme directly calculates both the C and K parameters for a data set. The mean attitudes and 0.95 cones of confidence of the data are calculated from the spherical Gaussian technique of Fisher (1953). A randomness factor, the R-value, is also computed by a method developed by Anderson and Stephens (1972).

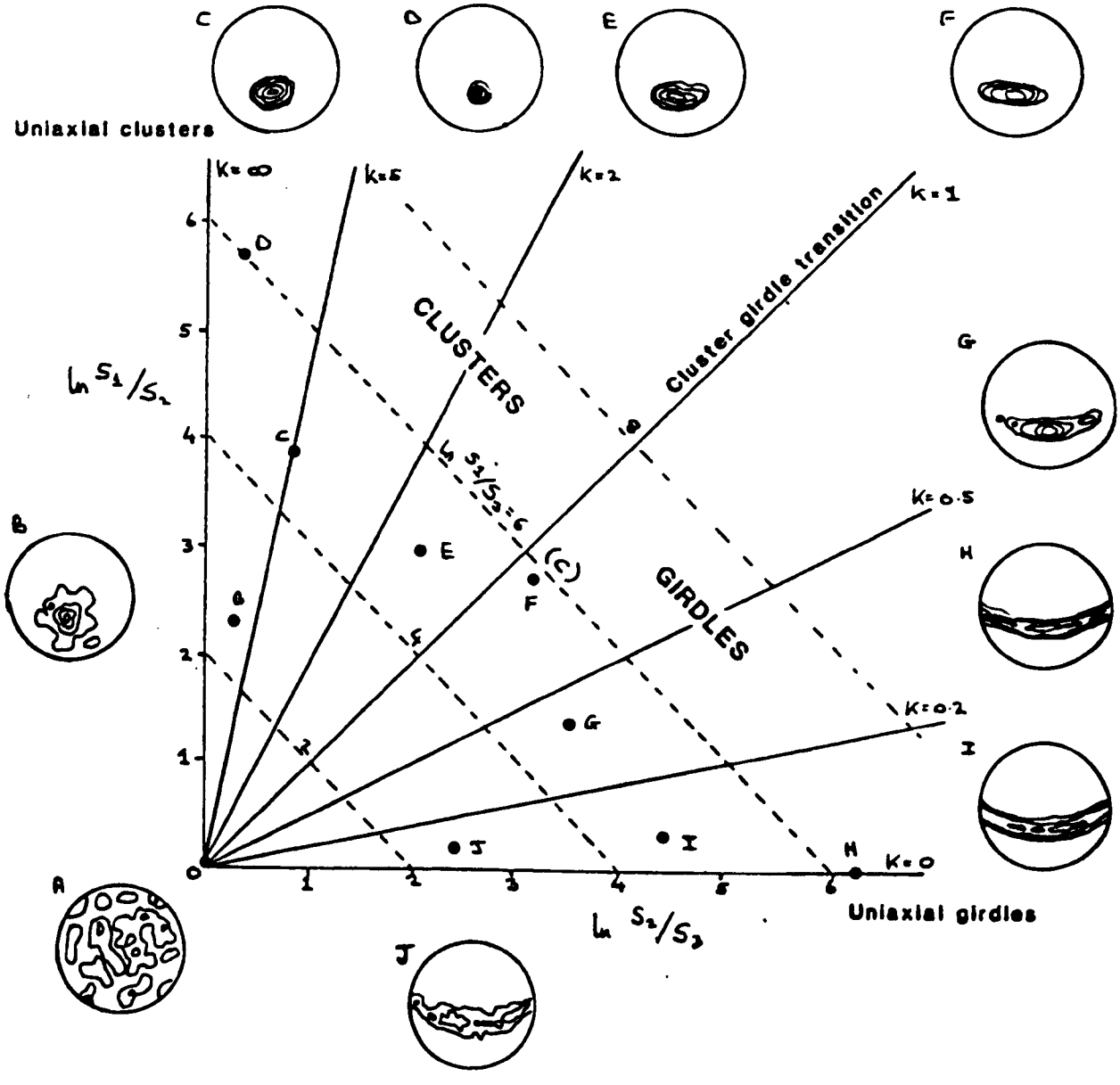

Figure 9.1 Two-axis logarithmic plot of ratios of normalised eigenvalues, with examples of fabric shapes in different parts of the graph. (After Woodcock, 1977).

In order to check whether or not the data collected is non-random, Woodcock (pers. com.) has determined two different methods of plotting data. The first method is to plot the C parameter against the sample size (N). For the data to be non-random, it must plot above the line shown in Figure 9.2 (for a 0.95 confidence level). The second method is to plot the S_1 normalised eigenvalue, against the randomness factor (R) divided by the sample size (N). This will produce a linear plot of the different data points, the value of R/N determining whether each data point has a random, girdle or cluster distribution. A Typical S_1 versus R/N plot with the critical values of R/N is shown in Figure 9.3.

If it is shown that the data is non-random, it can be plotted on a Flinn-type logarithmic plot in order to represent the shape of the distribution of points for each data set. (Figure 9.1). The drawback of the Flinn-type plot is that data sets with a low C parameter will not show a large spread over the diagram, even though there may be a large variation in their K parameters. This makes the variation in the shapes of the distribution of points for each data set difficult to interpret. A more useful method for plotting the data sets is to plot the C parameter versus the K parameter. This is effectively a two axis plot representing the strength of the preferred orientation along one axis (the C parameter) and the shape of the preferred orientation along the other axis (the K parameter). In this plot, even data sets with very low C parameters (as long as they have been shown to be non-random distributions from C versus N, and S_1 versus R/N plots) will have an easily identifiable preferred shape distribution (Figure 9.4).

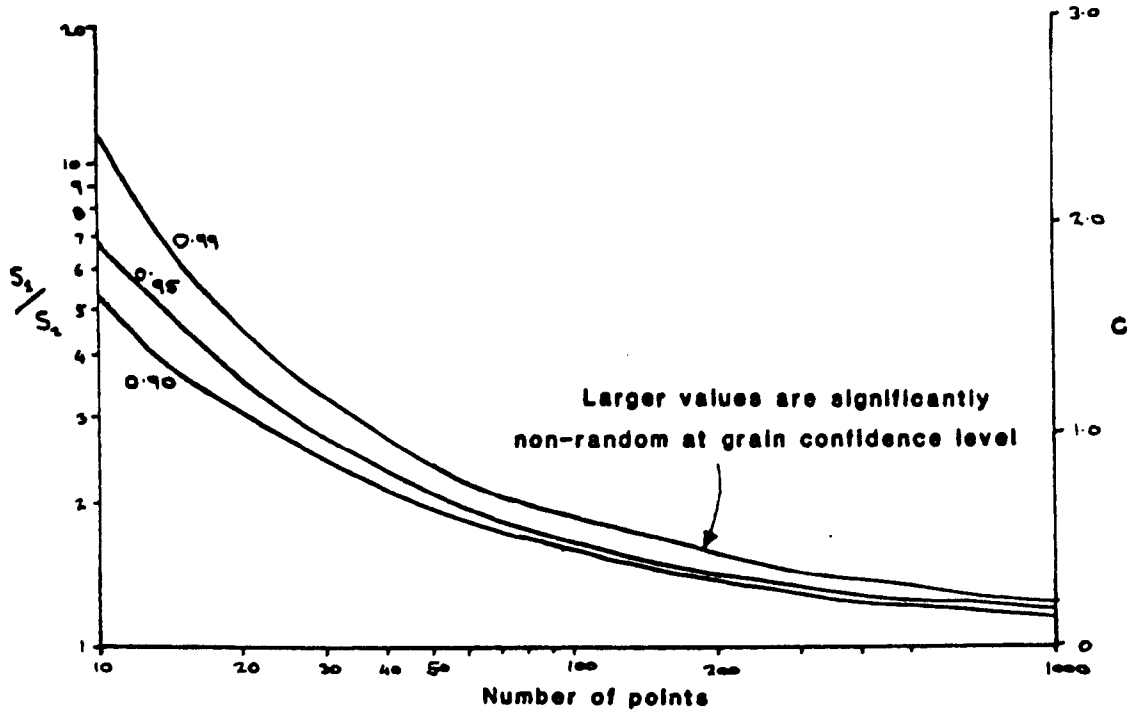

Figure 9.2 Critical values of the C parameter. Larger values are significantly non-random at given confidence levels. (Woodcock, pers. com.).

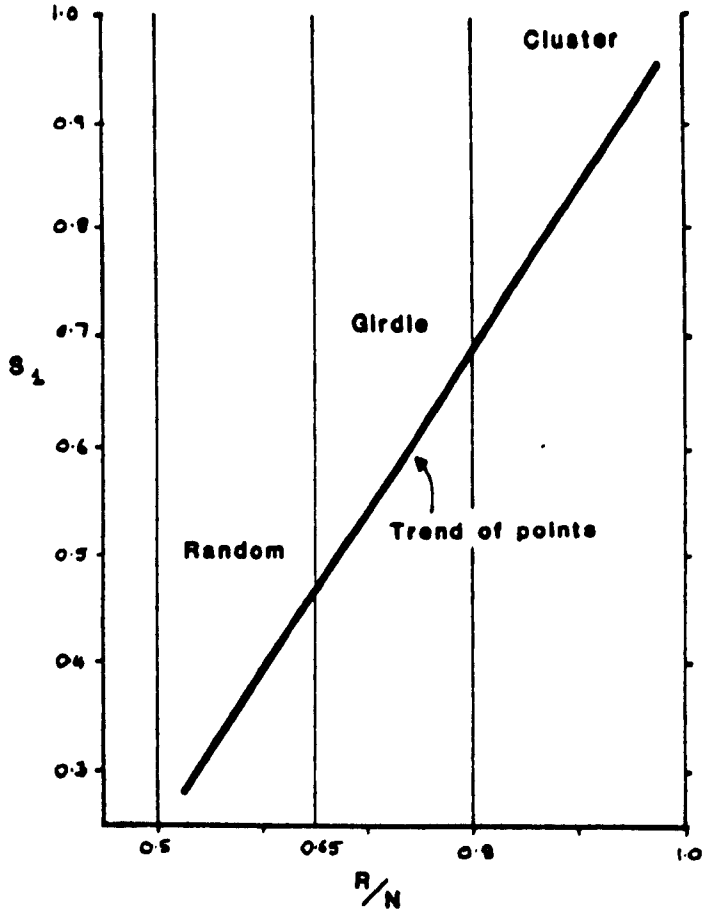

Figure 9.3 S_1 versus R/N plot with critical values. (Woodcock, pers. com.).

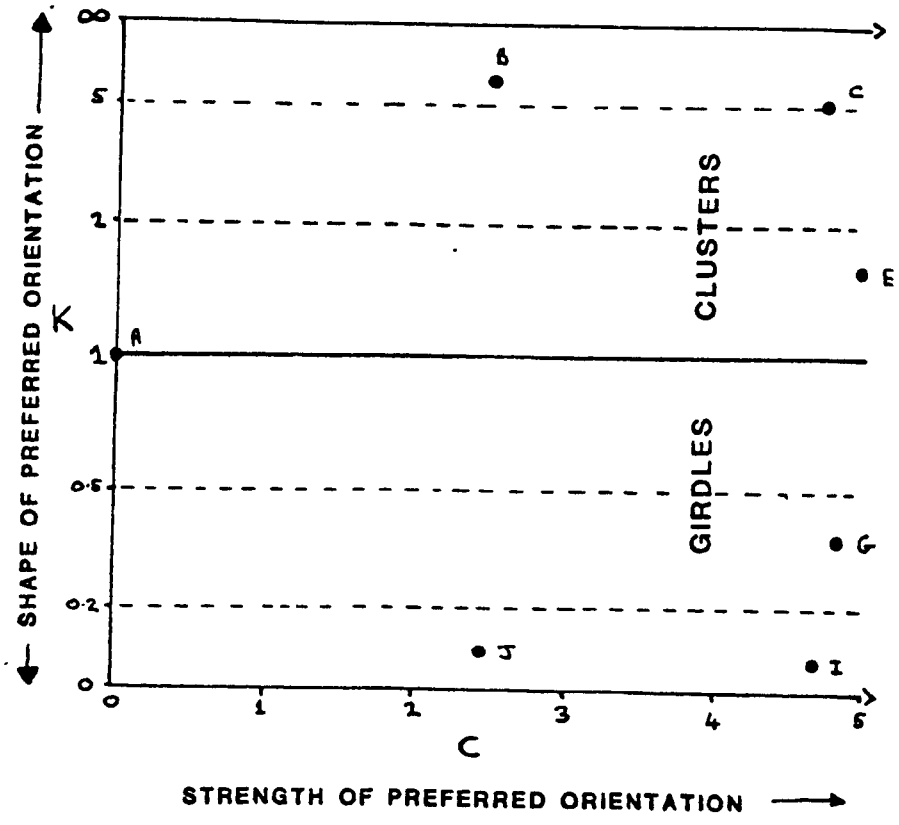

Figure 9.4 C versus K plot with critical values.

As will be shown below, C values of data sets collated from the areas studied are often low, and thus the K versus C plot has been used to interpret the shape fabric of the data.

9.1.2 Mean Foliation Data from the Areas Studied.

Table 9.1 summarises the various calculated parameters for the mean values of S1 and S2 planes from all of the areas studied. Each of the areas of structural data in Enclosures 2, 3, 5, 6, 7, 10 and 12 have been designated a code so that they can be referred to on Table 9.1. Theses codes are shown on the relevant enclosures. In order to represent this data diagrammatically, each data set has been numbered so that it can be easily identified on the various plots.

Figure 9.5 is a C versus N plot for all the data represented in Table 9.1. As can be seen, all the data are significantly non-random at 0.95 confidence levels. S_1 versus R/N plots for each of the areas studied (see Figures 9.6, 9.7 and 9.8) also show that all the data sets are non-random. In all areas there is also a clear distinction between the R/N values for S2 and S1 data sets; S2 poles always plotting as a cluster, and S1 poles usually plotting as a girdle pattern except in areas where no D2 shearing has occurred (Wadi Kanut and part of Wadi Sarami) when they plot as clusters.

As all the data-sets are non-random they can all be plotted on K versus C diagrams and be meaningful in terms of the shape distribution of the individual data points. K versus C plots for each of the areas studied are shown in Figures 9.9, 9.10 and 9.11. In all three areas almost all of the data-sets of S2 poles

Table 9.1 Statis results for the areas studied.

Area Code	Reference No. for plots	× Plane being considered.	Sample Size	● Mean Attitude	.95 Cone of confidence (degrees)	K	K/N	Natural Eigenvalue Ratios			S_1
								$\ln S_1/S_2$	$\ln S_2/S_3$	$\ln S_1/S_3$ (c)	
Rajmi											
M1&M7	1	S2	60	097 81	5.74	4.89	0.912	2.025	0.852	2.877	0.841
M1&M7	2	S1	60	122 88 (158 87)	13.91	0.22	0.640	0.402	1.185	1.587	0.534
M8&M9	3	S2	21	095 82	8.05	5.94	0.943	2.422	1.004	3.426	0.892
M8&M9	4	S1	20	126 88 (205 81)	23.06	0.23	0.681	0.415	1.173	1.588	0.536
M10&M11	5	S2	30	087 81	8.24	4.10	0.913	2.046	0.973	3.019	0.849
M12&M13	6	S2	44	054 61	7.94	0.93	0.883	1.528	1.590	3.118	0.793
C1&C4	7	S2	19	098 72	17.36	2.43	0.898	1.784	1.200	2.963	0.817
C1&C4	8	S1	20	325 87 (053 49)	17 37	0.86	0.789	1.075	1.177	2.252	0.691
C6&C8	9	Und	22	134 73 (064 46)	17.35	14.63	0.771	1.251	0.157	1.408	0.653
Ath Thuqbah											
M1&M2&M3	10	S2	40	087 63	7.10	2.56	0.912	1.946	1.207	3.153	0.843
M1&M2&M3	11	S1	32	013 66 (076 45)	17.49	0.23	0.687	0.413	1.182	1.595	0.536
C1	12	S2	30	094 48	8.27	3.03	0.913	1.952	1.097	3.049	0.841
C2&C3	13	Und	10	090 26	14.47	10.61	0.926	2.299	0.613	2.912	0.866
Sarami and Kanut											
Sarami											
M1	14	S1	22	033 62	12.57	5.89	0.865	1.818	0.629	2.448	0.801
M2	15	S2	20	313 72	7.39	11.86	0.954	2.711	0.781	3.492	0.912
C1	16	Und	10	034 55	14.42	8.23	0.926	2.214	0.688	2.903	0.859
Kanut											
M4&M5	17	S1	37	039 77	5.31	15.88	0.953	2.730	0.643	3.374	0.909
Part of C2	18	S1	12	046 72	10.75	9.98	0.947	2.576	0.796	3.372	0.901
C3 & Part of C2	19	Und	16	052 61	8.11	173.44	0.957	3.039	0.108	3.148	0.917

Table 9.1 Continued.

Area Code	Reference No. for plots	× Plane being considered.	Sample Size	● Mean Attitude	.95 Cone of confidence (degrees)	K	R/N	Natural Eigenvalue Ratios			S_1
								$\ln S_1/S_2$	$\ln S_2/S_3$	$\ln S_1/S_3$ (c)	
Musayfiyah											
M1	20	S2	12	345 87	14.46	3.47	0.908	1.983	1.032	3.016	0.843
C1	20a	Und	4	024 46	18.99	-	-	-	-	-	-
Hajir											
M1&M2&M3	21	S2	21	196 71	13.56	0.47	0.853	1.204	1.793	2.997	0.741
M1&M2&M3	22	S1	15	308 69 (258 69)	29.72	0.20	0.645	0.304	1.033	1.437	0.499
Al Abyad											
	23	S2	26	020 41	9.58	3.61	0.901	1.912	0.955	2.867	0.830
	24	S1	60	315 48 (018 25)	8.88	3.85	0.813	1.231	0.489	1.719	0.680
C1	25	S2& Und	112	041 34	2.61	7.02	0.963	2.874	1.222	4.102	0.932
Troodos											
M1&M2&M3	26	S2	85	225 90	4.75	11.24	0.914	2.160	0.520	2.681	0.845
M1&M2&M3	27	S1	65	129 90 (353 90)	9.17	1.53	0.789	1.008	0.760	1.768	0.651
M5&NthM4	28	S2	51	044 77	6.16	40.35	0.914	2.281	0.197	2.478	0.843
M5&NthM4	29	S1	59	126 85	8.00	2.66	0.845	1.397	0.764	2.161	0.734
M6&SthM4	30	S2	24	221 84	9.45	11.13	0.911	2.108	0.500	2.608	0.837
M6&SthM4	31	S1	26	297 89 (211 71)	17.15	0.35	0.741	0.594	1.202	1.796	0.582
M8&NthM7	32	S2	59	231 88	6.62	38.91	0.888	2.015	0.154	2.170	0.802
M8&NthM7	33	S1	29	316 90 (058 88)	13.86	1.77	0.795	1.140	0.790	1.930	0.683
M9&SthM7	34	S2	72	216 82	5.30	19.54	0.910	2.157	0.330	2.488	0.834
M9&SthM7	35	S1	45	124 88 (208 78)	11.48	0.63	0.779	0.851	1.143	1.994	0.640

Table 9.1 Continued.

Area Code	Reference No. for plots	Plane being considered. x	Sample Size	• Mean Attitude	.95 Cone of confidence (degrees)	K	R/N	Natural Eigenvalue Ratios $\ln S_1/S_2$	$\ln S_2/S_3$	$\ln S_1/S_3$ (c)	S_3
Troodos (cont.) M10&NthM12	36	S2	60	219 83	5.73	4.37	0.912	2.036	0.926	2.962	0.846
M10&NthM12	37	S1	38	305 87 (021 82)	12.09	1.39	0.792	0.998	0.803	1.801	0.652
M11&SthM12	38	S2	59	209 81	6.10	16.16	0.903	2.107	0.369	2.476	0.829
M11&SthM12	39	S1	109	305 90 (312 88)	12.21	2.38	0.808	1.196	0.677	1.873	0.687
C1	40	S2	80	049 71	6.15	10.96	0.871	1.771	0.368	2.139	0.776
C2	41	S2	45	047 79	7.99	21.49	0.879	1.922	0.240	2.163	0.793
C1&C2	42	S1	41	127 89 (041 72)	12 .71	1.10	0.760	0.858	0.813	1.683	0.623
Unst*											
Crussa Field	43	S2	87	174 87	5.25	19.22	0.894	1.986	0.283	2.269	0.806
Crussa Field	44	S1	77	094 87 (049 85)	8.47	0.80	0.786	0.902	1.039	1.941	0.645
Muckle Heog	45	S2	90	356 74	4.64	8.51	0.913	2.103	0.612	2.716	0.842
Muckle Heog	46	S1	58	095 82 (042 76)	11.28	0.89	0.737	0.754	0.818	1.572	0.596
Little Heog	47	S2	109	003 77	3.69	37.95	0.931	2.503	0.259	2.762	0.873
Little Heog	48	S1	49	074 82 (054 82)	11.80	0.65	0.753	0.755	1.003	1.758	0.609
Clibberswick Hill	49	S2	56	330 88	5.76	4.43	0.917	2.046	0.925	2.971	0.847
Clibberswick Hill	50	S1	54	061 85 (102 83)	9.70	1.79	0.803	1.084	0.738	1.822	0.667
CF&MH&LH	51	S2	286	358 81	2.72	12.17	0.903	2.044	0.440	2.485	0.824
CF&MH&LH	52	S1	184	089 84 (047 82)	5.97	0.72	0.753	0.774	0.965	1.739	0.611

* Emplacement related trends omitted from these data.

x Und. implies that the area has not been penetratively deformed by either D1 or D2. The values correspond to the cumulate layering plane.

• For S1 values that plot as girdles the mean attitude of the pole to the S1 pi-pole is given *in brackets.*

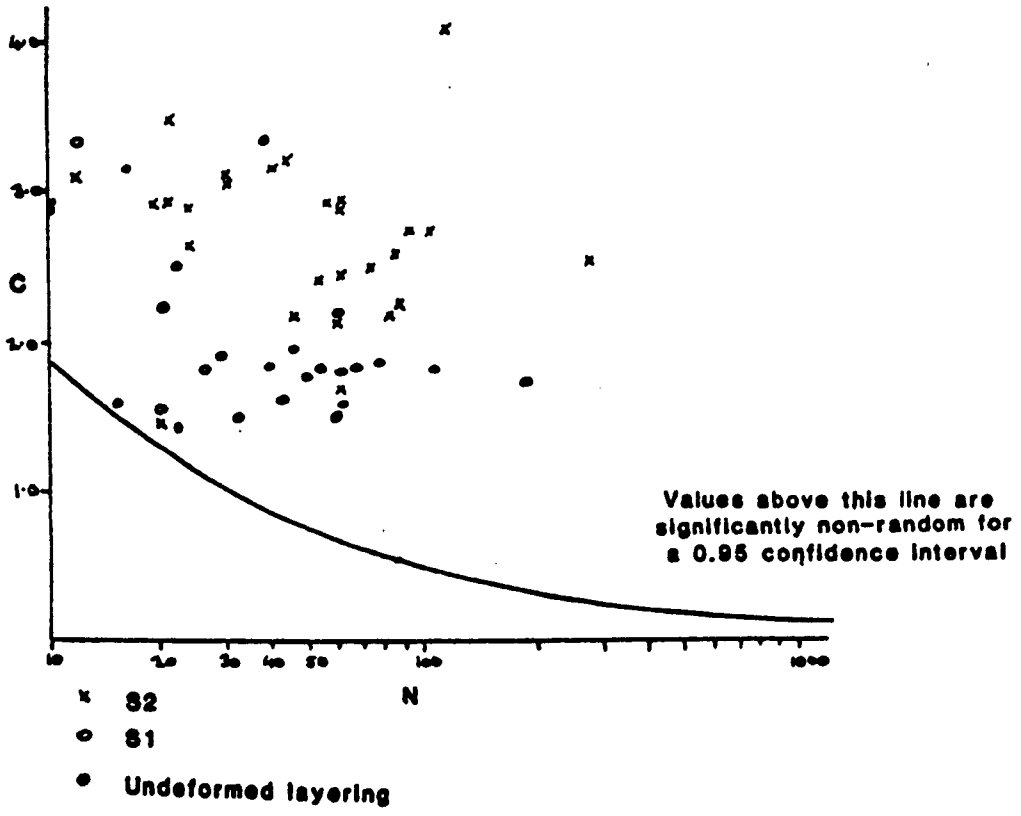

Figure 9.5 C versus N plot for the data sets of Table 9.1.

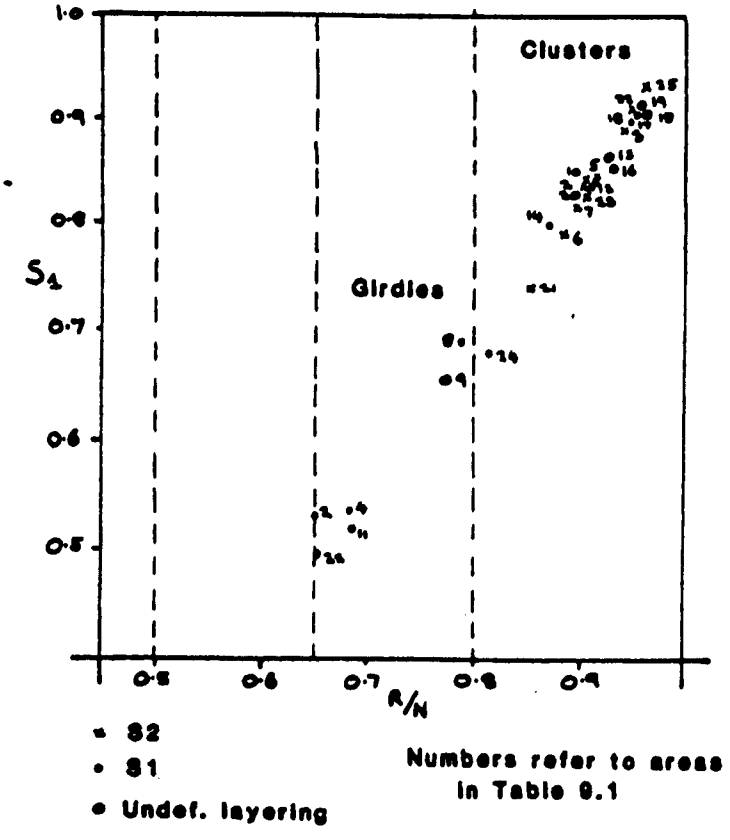

Figure 9.6 S_1 versus R/N plot for the Oman data sets of Table 9.1.

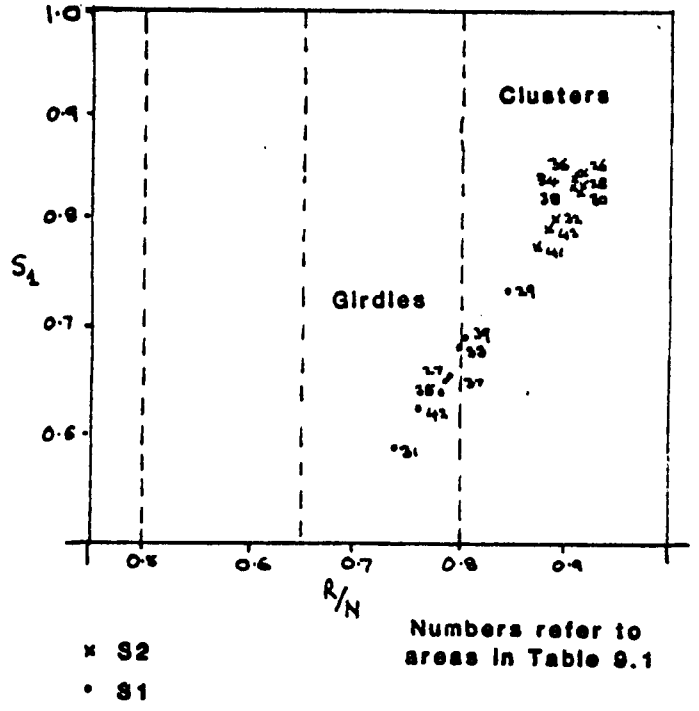

Figure 9.7 S_1 versus R/N plot for the Troodos data sets of Table 9.1.

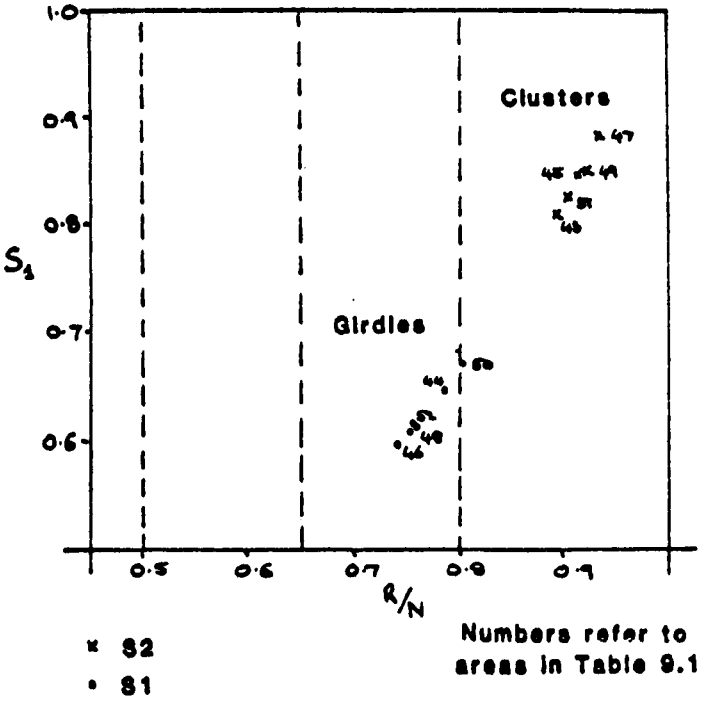

Figure 9.8 S_1 versus R/N plot for the Unst data sets of Table 9.1.

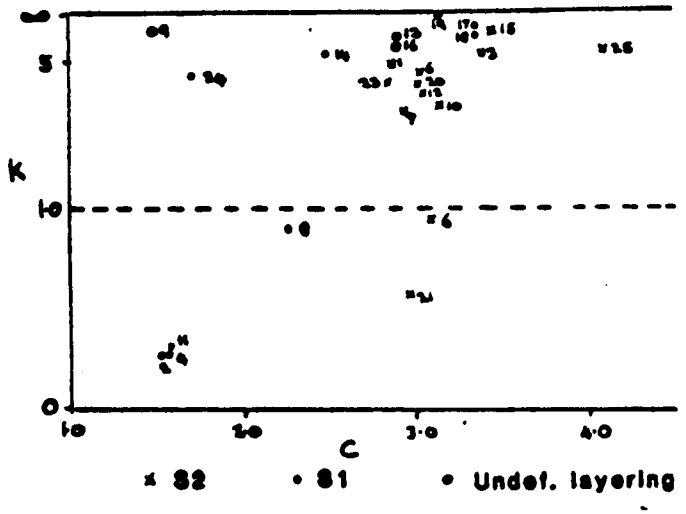

Figure 9.9 K versus C plot for the Oman data sets of Table 9.1.

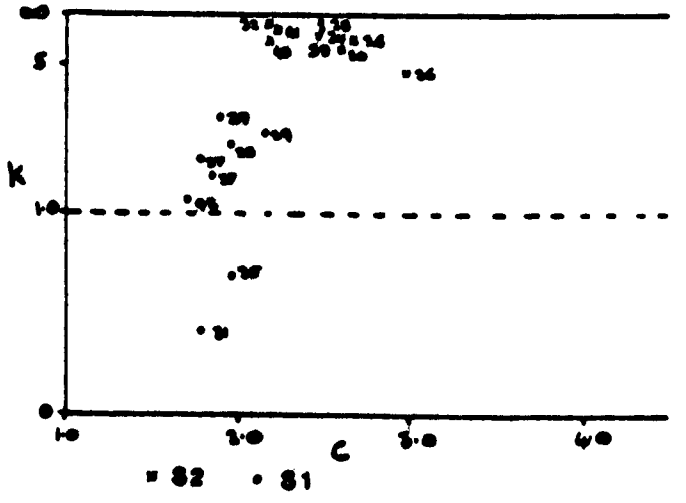

Figure 9.10 K versus C plot for the Troodos data sets of Table 9.1.

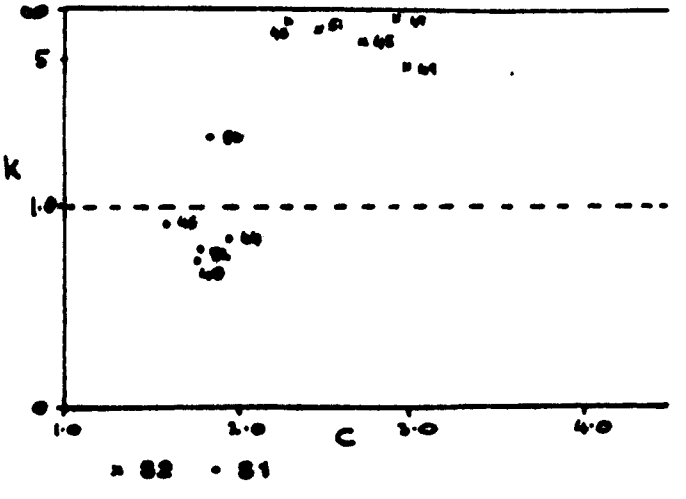

Figure 9.11 K versus C plot for the Unst data sets of Table 9.1.

have K values greater than 2.5 and C values greater than 2. This shows that the S2 poles plot as well developed clusters for almost all of the areas, and that the calculated mean attitude of the S2 planes can be reliably used as a mean value for each area in kinematic studies.

The only data-sets of S1 poles that can be used to estimate the mean attitude of the S1 foliation before D2 shearing occurred are those of the Wadi Kanut and Wadi Sarami areas which have K values greater than 5 and C values greater than 2.5. The other S1 pole data-sets have a large range of K values, and values of C between 1.5 and 2. The range of K values indicates that in some areas the S1 poles plot as great circles and in others tend towards clusters, with a range of girdle distributions in between for most areas. This is especially well shown in the Troodos area plot (Figure 9.10). The fairly low C values show that the S1 pole girdle and cluster patterns are fairly dispersed and not so precisely defined as the S2 pole clusters.

A study of the mean S2 attitudes calculated for the areas of each enclosure shows that they have very similar values for all of the areas within each enclosure. The same is seen for the mean S1 attitudes of the Wadi Sarami and Kanut enclosure (Enclosure 5). This enables a mean S2 and/or S1 attitude to be calculated for each enclosure area. These calculated values are shown in Table 9.2.

The results discussed in Chapter 7 show that there is usually only a very small angle (0-20^{o}) between the shear plane and the related foliation plane. The mean S2 or S1 foliation plane calculated for each area can thus be used as an estimation of

Table 9.2 Mean structural attidues for each of the areas studied.

Area	Mean S2 orientation	Mean D2 slip direction	Mean pre-D2 D1 orientation	Mean pre-D2 D1 slip direction	Mean undeformed complete layer orientation	Dike orientation (Plate-shortzontal)	Directed dyke orientation (strike)	Rotation axis attitude	Angle of rotation
Rajmi	097 81	186 06	(146 90)	(238 14)	134 73	065 40	180 112	155	40
Ath Thuqbah	087 63	004 15	(024 69)	(096 43)	090 26	080 30	165	170	30
Şarami and Kanut	313 72	217 06	033 62	118 08	040 57	044 52	180	135	52
Hajir	196 71	146 64	(218 72)	(303 17)	(020 40)	(010 40)	152	100	40
Al Abyad	020 41	084 24	(076 78)	(163 10)	* 041 34	018 50	130	100	52
Troodos	223 88	134 62	(127 86)	(044 50)	?	285 90	180	015	90
Unst	358 81	273 27	(107 87)	(018 08)	?	170 90	?	080	90

* Deformed

All readings in direction of dip and angle of dip unless otherwise stated.

( ) Uncertain values.

the mean D2 or D1 shearing plane for each area.

9.1.3 Mean Shearing Directions from the Areas Studied.

As was made clear in Chapters 2 - 4, lineations are difficult to measure in many of the areas studied. Where they have been identified, their orientations strongly reflect the olivine [100] orientations measured from hand specimens. (See Chapter 7). The detailed olivine crystallographic analysis of specimens enables a D2 and/or D1 slip direction to be determined for each individual specimen. As a large number of specimens from each area studied were analysed, a range of D2 slip directions can be obtained for each area.

Figure 9.12 shows equal area projections of the D2 slip directions for each specimen from each area. The mean S2 plane from each enclosure area has also been plotted on each projection. In most areas the D2 slip directions plot as a cluster pattern close to the mean S2 plane.

If it is assumed that the mean S2 plane is also the mean D2 shearing plane, then the D2 shear direction must lie on the S2 plane. This direction has been calculated for each area by estimating the line on the S2 plane which falls closest to the centre of the cluster of [100] slip directions. An estimation of the D2 shear direction is thus possible for each area studied. These shear directions have been plotted on equal area projections in Figure 9.12 and included in Table 9.2.

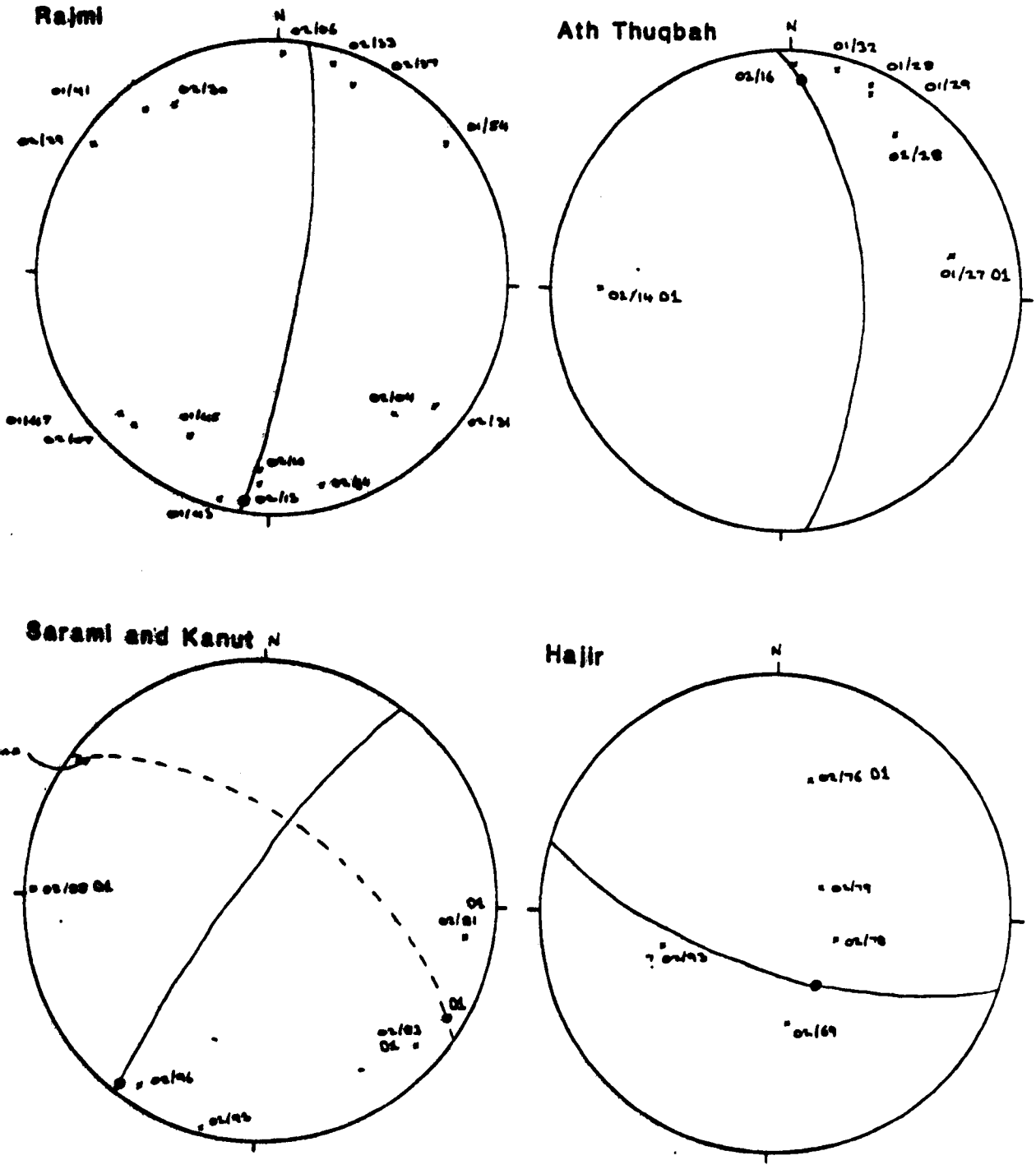

Figure 9.12 See next page for caption

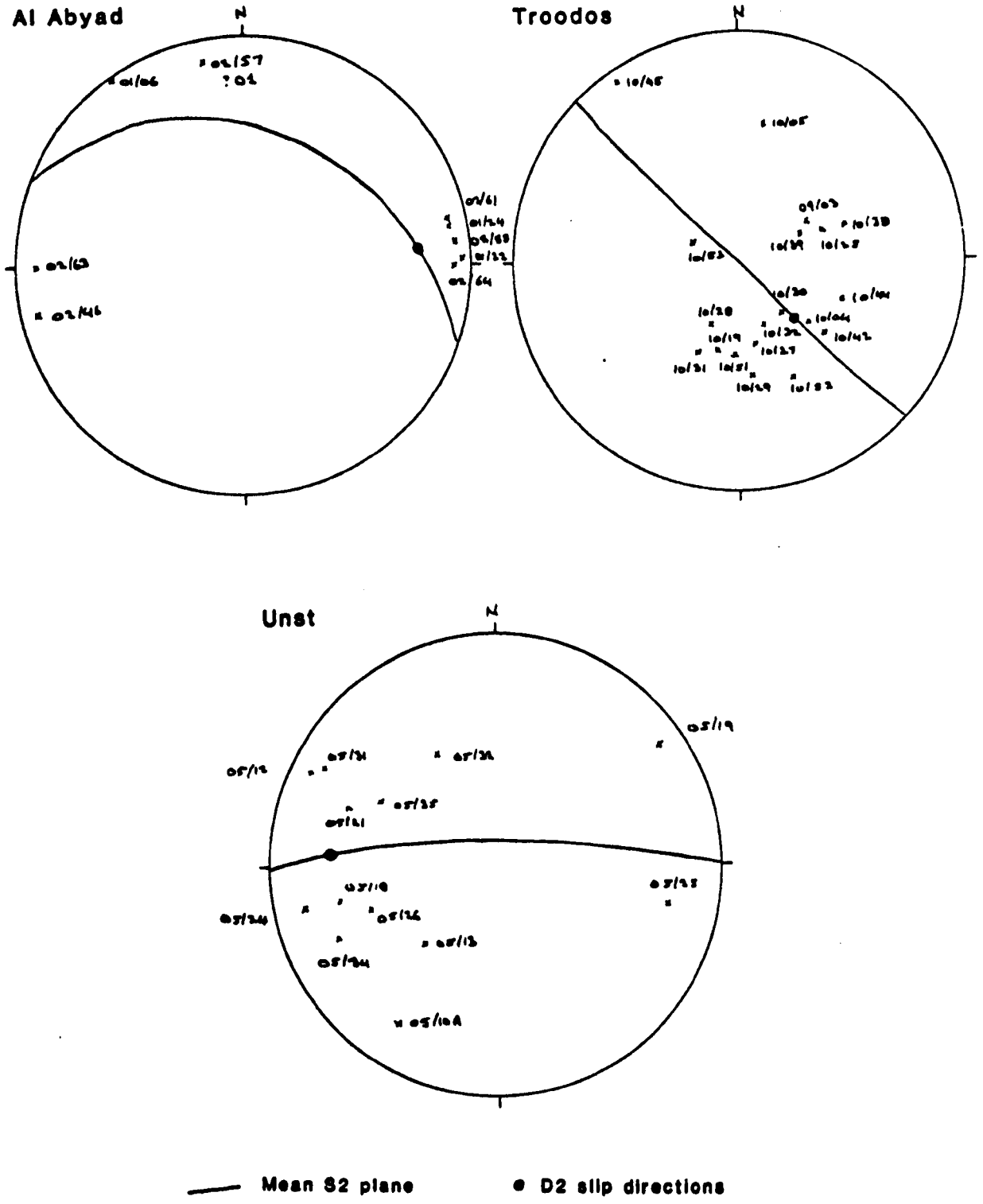

Figure 9.12 D2 slip directions as determined from the crystallographic study of olivine grains for each area. The mean S2 plane is included on each equal lower hemisphere projection for each area.

9.2 The Determination of a Palaeohorizontal Plane, a Palaeo-Spreading Axis and Spreading Direction for Each Area.

In order to relate the D1 and D2 shearing planes and directions to processes at present-day oceanic spreading centres certain reference frames have to be determined from the studied ophiolite complexes. Firstly the palaeohorizontal plane must be defined, and secondly the strike of the ridge and the side of the ridge which the ophiolite represents.

9.2.1 The Determination of the Palaeohorizontal Plane.

Various lithological features could be used to determine the palaeohorizontal plane in an ophiolite complex:

i) The depositional planes of the sediments and volcanics at the stratigraphically highest levels of an ophiolite complex.

ii) A plane perpendicular to the dip of the dykes from the Sheeted Dyke Complex.

iii) Magmatic layering planes from the Cumulate Unit.

iv) The major lithological contact between the residual mantle and the overlying cumulate sequence. i.e. The petrological moho.

The advantages and disadvantages of using each of these horizons in determining the palaeohorizontal plane have been discussed in detail by Smewing et al (1983).

The main problem with using either the volcanic or cumulate layering planes is that even over only small areas they have a highly variable orientation. The topography of present day sea floors at accretionary margins is often highly undulating and thus the depositional planes in pillowed volcanics can frequently be steeply dipping. This is borne out by the detailed study of flow orientations within the pillow lavas of the Oman Ophiolite which show dramatic changes over short distances. (Smewing et al, 1983).

The detailed study of cumulate layering orientations in Oman by Browning (1982) and in this study has shown that they have highly variable attitudes in some areas indicating either the ends of localised magma chambers or internal flow or slump features within magma chambers. Prinzhoffer et al (1980), Girardeau and Nicolas (1981), and Nicolas and Violette (1982) all used major lithological boundaries within the cumulate sequence as a palaeohorizontal plane. This assumption is based on models of magma chambers beneath accretionary centres which show the plane of magmatic layering inclined towards the ridge but lithological boundaries as horizontal. (Greenbaum, 1972; Casey and Karson, 1981). In all the three areas studied in this thesis this relationship clearly does not hold.

In ophiolites where the Sheeted Dykes Unit has been well preserved (as in Oman and Cyprus) it is fairly easy to determine a mean dyke strike and dip direction, and thus to define a palaeohorizontal plane that is perpendicular to the dyke dip. In most present day spreading centres, it would seem that the majority of the dykes within the Sheeted Dyke Complex have been intruded sub-vertically. However, Harper (1982) and Searle and Panayiotou (1979) showed for the Josephine Ophiolite, Oregon, and the Troodos Ophiolite respectively, that some sheeted dykes have low and highly variable angles to the

gross lithologic layering of the ophiolite. Thus, before a palaeohorizontal plane can be defined from the orientation of the sheeted dykes, the dykes must be studied in detail in order that only those dykes which have been intruded sub-vertically are used. In some ophiolites this may be difficult. The main problem with using the plane perpendicular to the dip of the sheeted dykes as a palaeohorizontal plane is that the dykes often outcrop a considerable distance from the structures of interest in the Peridotite and Lower Cumulate Units. Emplacement or uplift events could easily have disorientated the Sheeted Dykes with respect to the Peridotite Unit (as has certainly happened in the Troodos Ophiolite: see Chapter 3). In some incomplete ophiolites which have a large outcrop of the lower ophiolite sequence, the Sheeted Dyke Complex is absent (as in the Shetland Ophiolite); this obviously makes this method of determining the palaeohorizontal useless.

In the three ophiolite complexes studied, the only lithological feature which has a constant attitude over large areas is the petrological moho. (i.e. the boundary between the Peridotite Unit and the Lower Cumulate Unit). The model for mantle flow at oceanic spreading centres derived by Nicolas and Violette (1982) requires the moho plane to be steeply dipping and also folded on a large scale in areas of diapirically spreading asthenosphere. In the areas studied, however, the moho plane has clearly not been folded on a large scale (see Chapters 2 - 4). It would thus appear a fair assumption that, in the ophiolites studied, the moho plane is the most reliable indicator of the palaeohorizontal.

In complete ophiolite sequences where little internal disorientation has taken place by emplacement events (as in Oman), the reliability

of using the moho plane as a palaeohorizontal can be checked against the attitude of the dykes in the Sheeted Dyke Complex. This is done for the Oman Ophiolite in Section 9.3 of this chapter.

9.2.2 The Determination of a Palaeo-Spreading Axis and Spreading Direction.

Four parameters have been considered by Nicolas and Violette (1982) and Smewing et al (1983) in order to determine the orientation of the palaeo-ridge direction and also the side of the ridge on which the ophiolite had originally been formed:

i) The strike and one-way chilling directions of the Sheeted Dyke Complex.

ii) The strike of transcurrent faults.

iii) The trend of mineral lineations within the Peridotite Unit.

iv) The inclination of the foliation planes within the Peridotite Unit with respect to a palaeohorizontal plane.

Parameters ii) and iii) will only give a palaeo-ridge strike and not a spreading direction. Parameter ii) assumes that transcurrent faults in ophiolites can be interpreted as transform faults with the palaeo-ridge strike perpendicular to them. However, in most ophiolites there is little evidence that transcurrent faults are relicts of transform faults. Even if they are, studies from modern oceans show that it cannot be assumed that the palaeo-ridge is perpendicular to them.

The results discussed in this thesis show that the trends of mineral

lineations within the Peridotite Unit are highly variable between different areas of the Oman Ophiolite. They thus cannot be reliably used to infer a palaeo-ridge strike.

Girardeau and Nicolas (1981) used the inclination of the foliation planes within the Peridotite Unit to determine both a palaeo-ridge strike and a spreading direction for the Bay of Islands Ophiolite in Newfoundland. They assumed that the foliation planes within the Peridotite Unit are the relics of the asthenospheric flow plane and that this flow plane dips away from the ridge axis. They also showed that for the Bay of Islands Complex, the cumulate layers in the Cumulate Unit dip in the opposite direction to the Peridotite Unit foliations; i.e. towards the ridge axis. Sleep (1975) modelled an accretionary centre on the basis that the angle of inclination of the mantle flow plane with respect to the palaeo-horizontal depends on the spreading rate. (A 10^{o} angle gives a spreading rate of 5cm yr^{-1}; a 25^{o} angle gives 1cm yr^{-1}). The results of the S2 foliation orientations for the areas studied for this thesis certainly do not comply with the Bay of Islands model and thus cannot be used for determining the palaeo-ridge orientations.

The most favourable parameter for determining both the palaeo-ridge strike and the spreading direction is the sheeted dykes. Both Nicolas and Violette (1982) and Smewing et al (1983) come to this same conclusion. The mean strike of the sheeted dykes can be assumed to be sub-parallel to the ridge strike; and the one-way chilling direction of the dykes can be used to determine the spreading direction, and hence on which side of the ridge axis the ophiolite complex was formed.

9.2.3 Palaeohorizontal Planes and Ridge Directions for the Areas Studied.

a) The Oman Ophiolite: As already mentioned in Chapter 2 the Sheeted Dyke Complex of the northern Oman Ophiolite has been studied in detail by Lippard (1981). He shows from dyke chilling statistics that the ophiolite has been formed on the SW flank of a roughly NW-SE striking ridge. The strikes of the sheeted dykes for each ophiolite block studied are shown in Figure 9.13. In the Fizh Block there are two main strikes, the NW-SE strike being related by Smewing (1980) to a leaky transform zone, and the N-S strike a normal ocean-spreading situation. Both these trends are considered in the section below. (Section 9.3). In the other blocks the strike of the dykes follows the arcuate shape of the Oman Mountains. The dyke strike directions are included on Table 9.2.

The moho plane has a fairly constant dip for each of the blocks studied. This is taken to represent the palaeohorizontal and has been marked on Enclosures 2 - 8 and included on Table 9.2.

b) The Troodos Ophiolite: As discussed in Chapter 3, the main sheeted dyke trend of the Troodos Ophiolite is N-S. The spreading direction has been proposed to be west to east by Kidd and Cann (1974) and Kidd (1977), but this is based on only a few measurements and cannot be used as statistical evidence for the spreading direction.

The moho plane has constant orientation in the Mount Olympus area of the Troodos Ophiolite. This is marked on Enclosure 10 and included in Table 9.2.

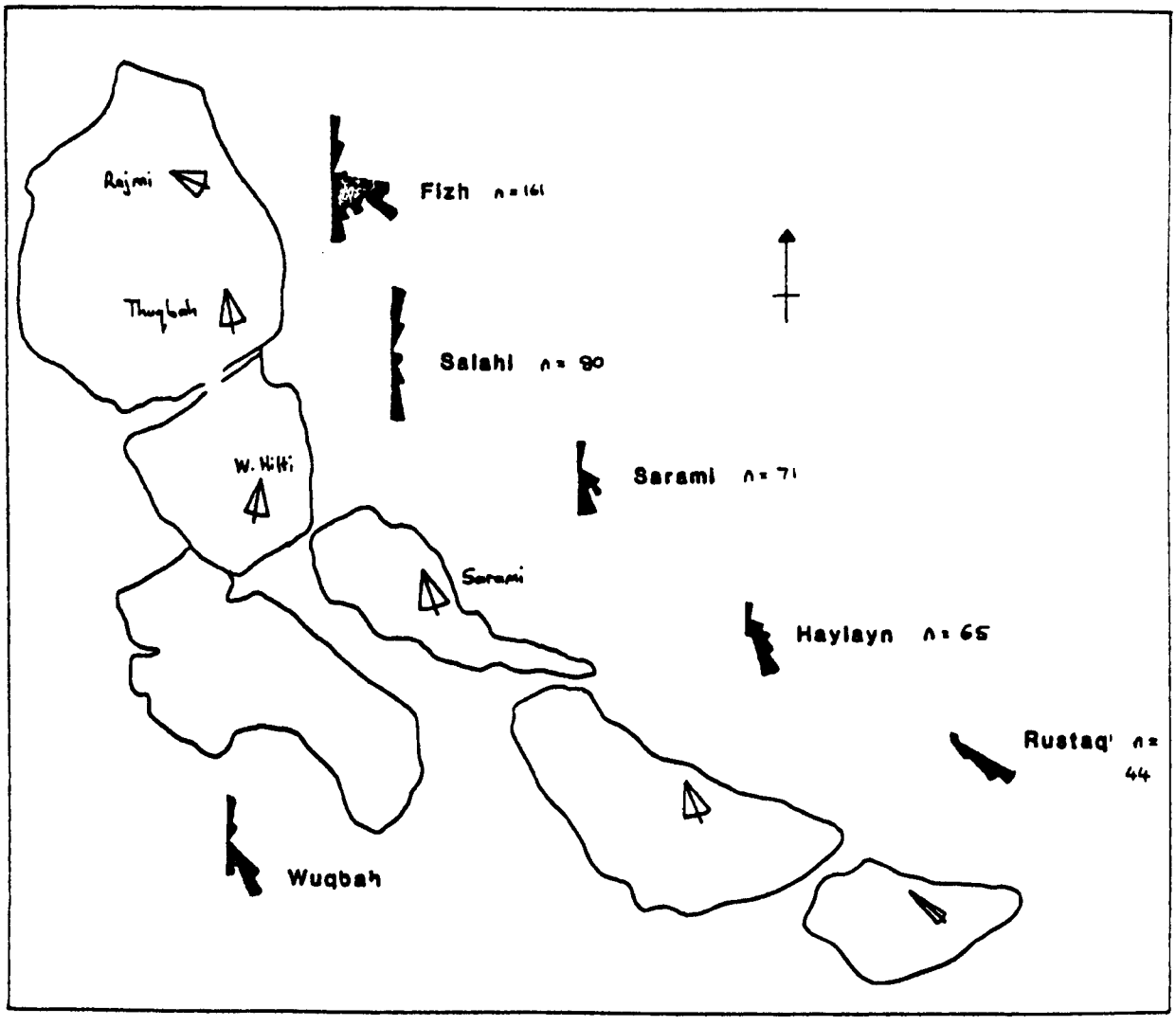

Figure 9.13 The Sheeted Dyke strikes for the ophiolite blocks in the Northern Oman Mountains. (From Lippard, 1981).

c) The Shetland Ophiolite: No Sheeted Dyke Unit outcrops in the Shetland Ophiolite. Thus neither a palaeo-ridge orientation nor a spreading direction can be determined. The moho plane has a constant orientation in each of the ophiolite blocks studied. This is marked on Enclosure 12 and included in Table 9.2.

9.3 The Rotation of the Mean Structural Orientations of Each Area Back to their Original Ocean Spreading Orientations.

The most simple way to rotate the mean structural data of Table 9.2 back to a palaeohorizontal is to merely rotate the moho plane back to a horizontal along a horizontal rotation axis. This axis is parallel to the strike of the moho plane. All the other data is then rotated on the same axis by the same angle of rotation as the moho plane.

Figures 9.14 - 9.20 shows the rotation of the data in Table 9.2 back to an original ocean spreading orientation for each area. Two equal area projections are shown for each area, one with the unrotated data and the other with the data after rotation.

In some of the Oman areas where the mean angle of dip of the Sheeted Dyke Complex is known, the orientation of the dykes have been plotted and rotated. (Figures 9.14, 9.15, 9.16 and 9.17). In all of these areas the sheeted dykes rotate to a near-vertical orientation except where minor warping due to emplacement has occurred. This fact and the parallelism of the rotation axes of each area to the general arcuate shape of the Oman Mountains (implying that the rotation axes are perpendicular to the direction of emplacement) indicate that the rotations performed for each area

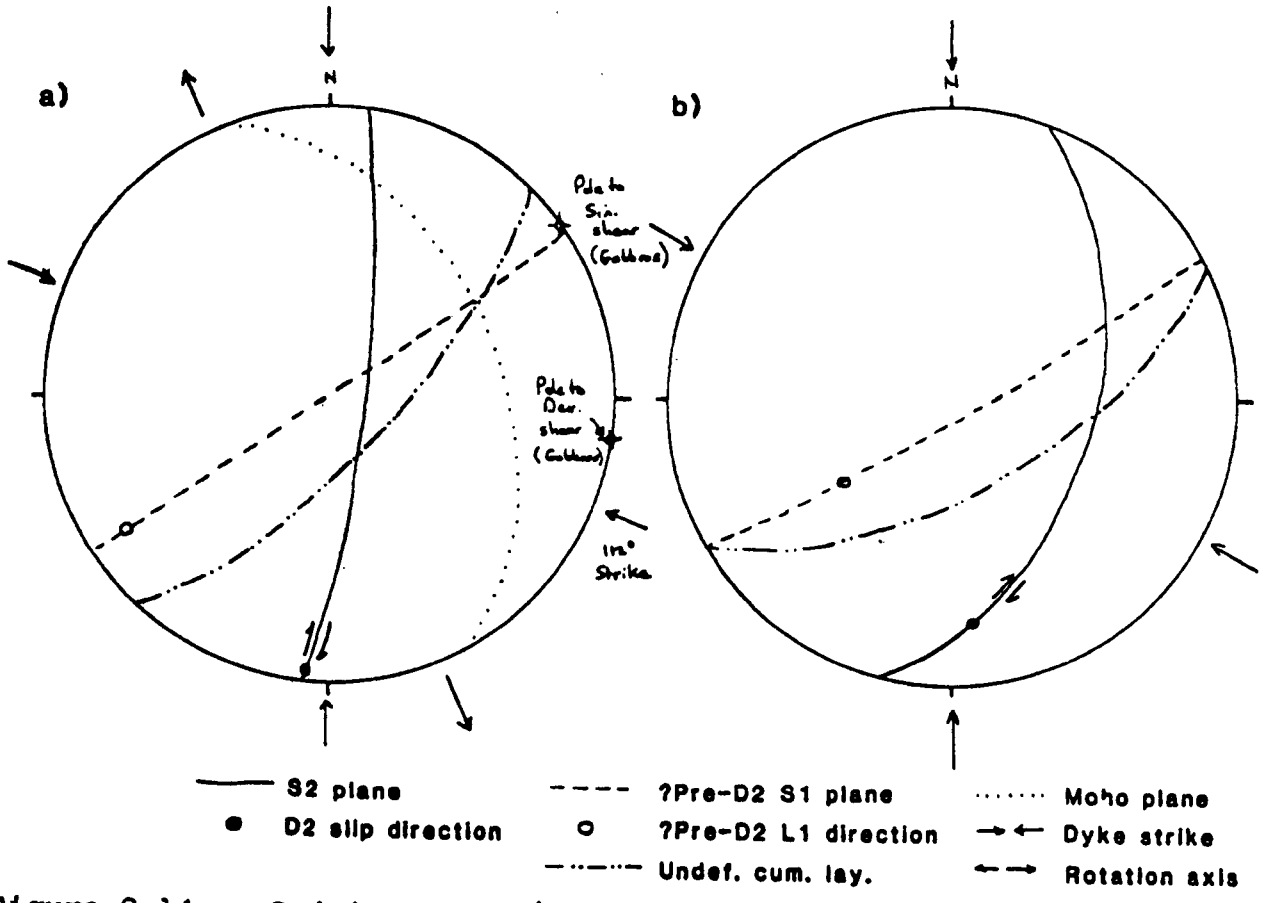

Figure 9.14 Rajmi area. a) The data of Table 9.2 with the rotation axis marked; b) The data rotated back ocean spreading orientations. (As in Table 9.3). (Equal area lower hemisphere projections).

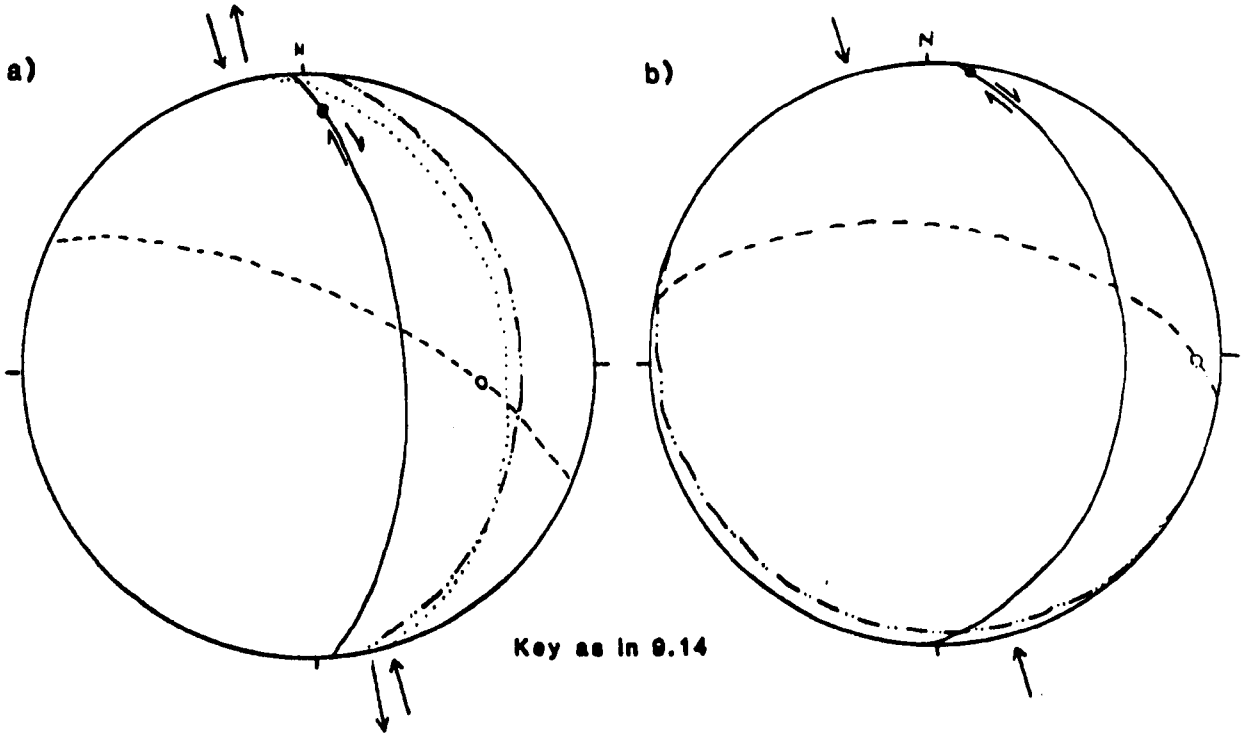

Figure 9.15 Ath Thuqbah area. a) The data of Table 9.2 with the rotation axis marked; b) The data rotated back to ocean spreading orientations. (As in Table 9.3). (Equal area lower hemisphere projections).

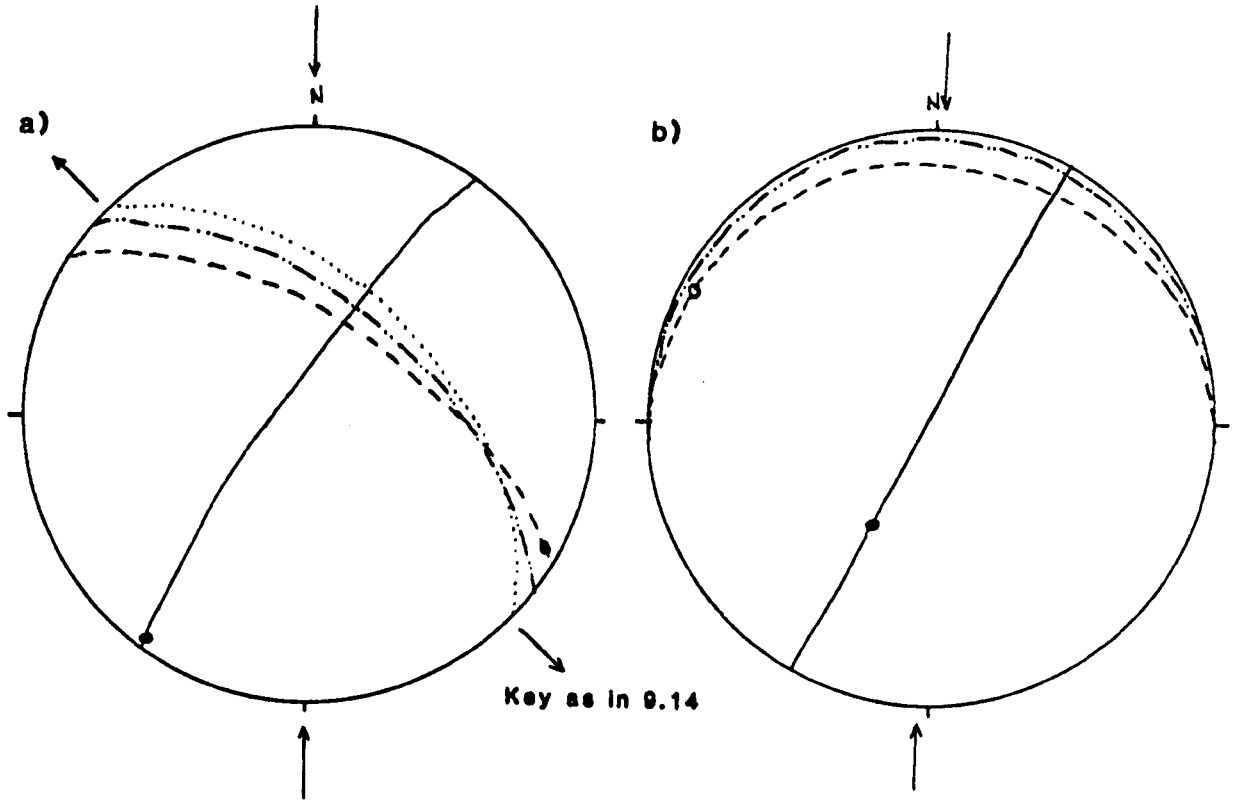

Figure 9.16 Sarami and Kanut areas. a) The data of Table 9.2 with the rotation axis marked; b) The data rotated back to ocean spreading orientations. (As in Table 9.3). (Equal area lower hemisphere projections).

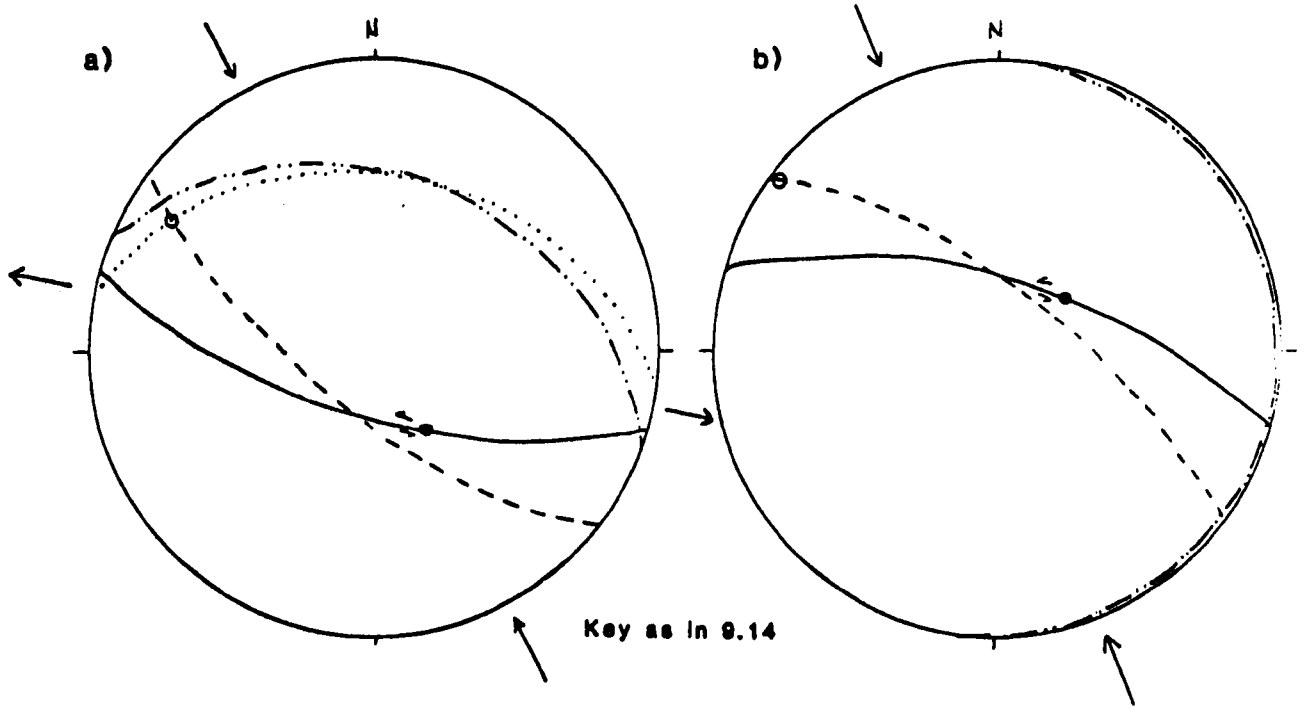

Figure 9.17 Hajir area. a) The data of Table 9.2 with the rotation axis marked; b) The data rotated back to ocean spreading orientations. (As in Table 9.3). (Equal area lower hemisphere projections).

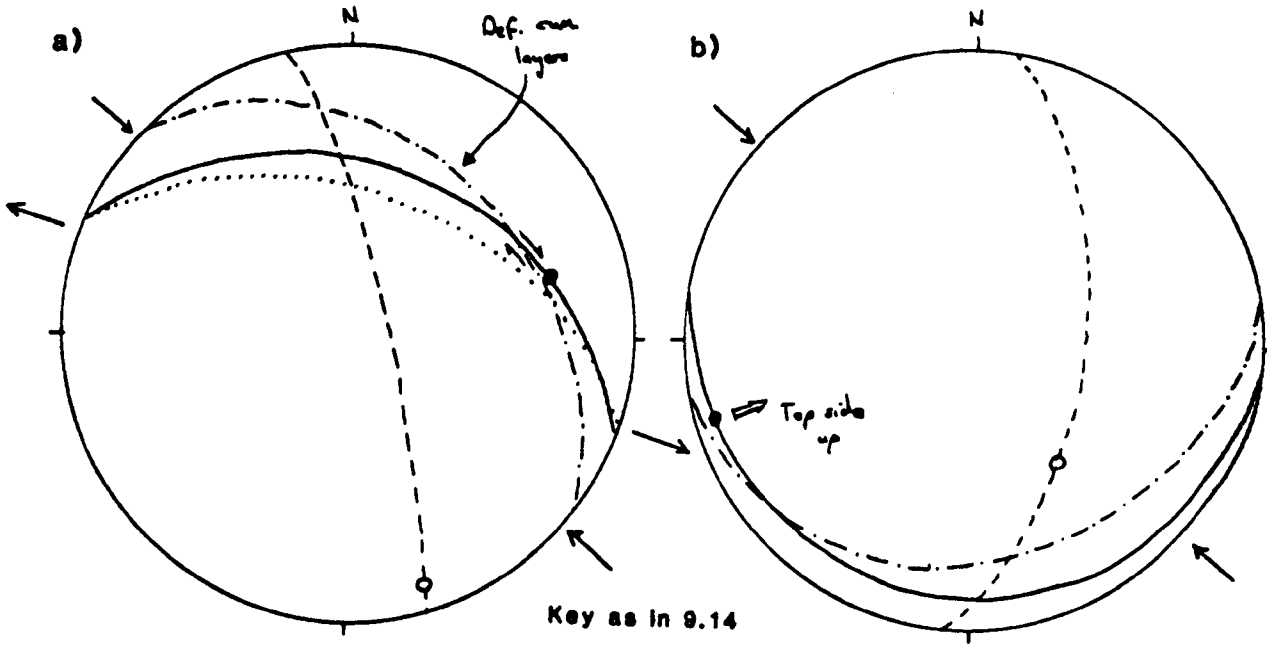

Figure 9.18 Al Abyad area. a) The data of Table 9.2 with the rotation axis marked; b) The data rotated back to ocean spreading orientations. (As in Table 9.3). (Equal area lower hemisphere projections).

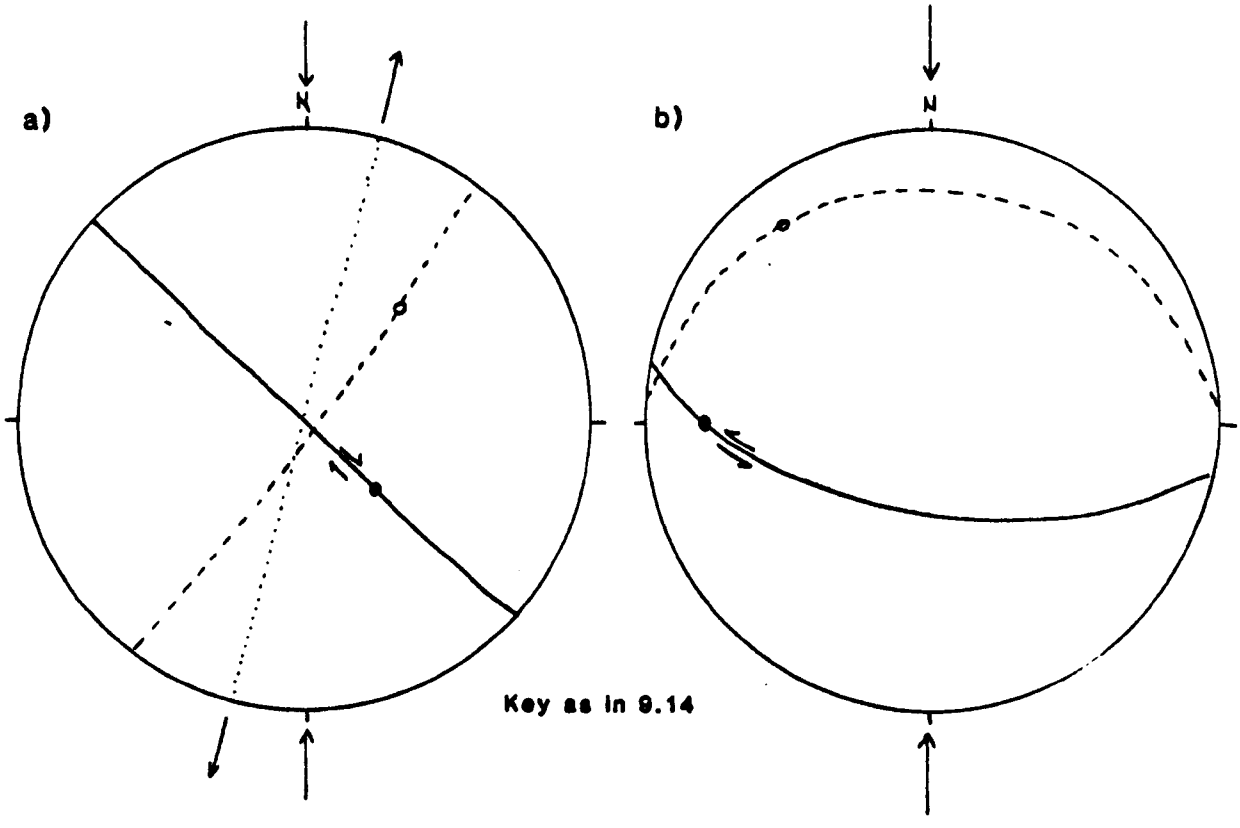

Figure 9.19 Troodos area. a) The data of Table 9.2 with the rotation axis marked; b) The data rotated back to ocean spreading orientations. (As in Table 9.3). (Equal area lower hemisphere projections).

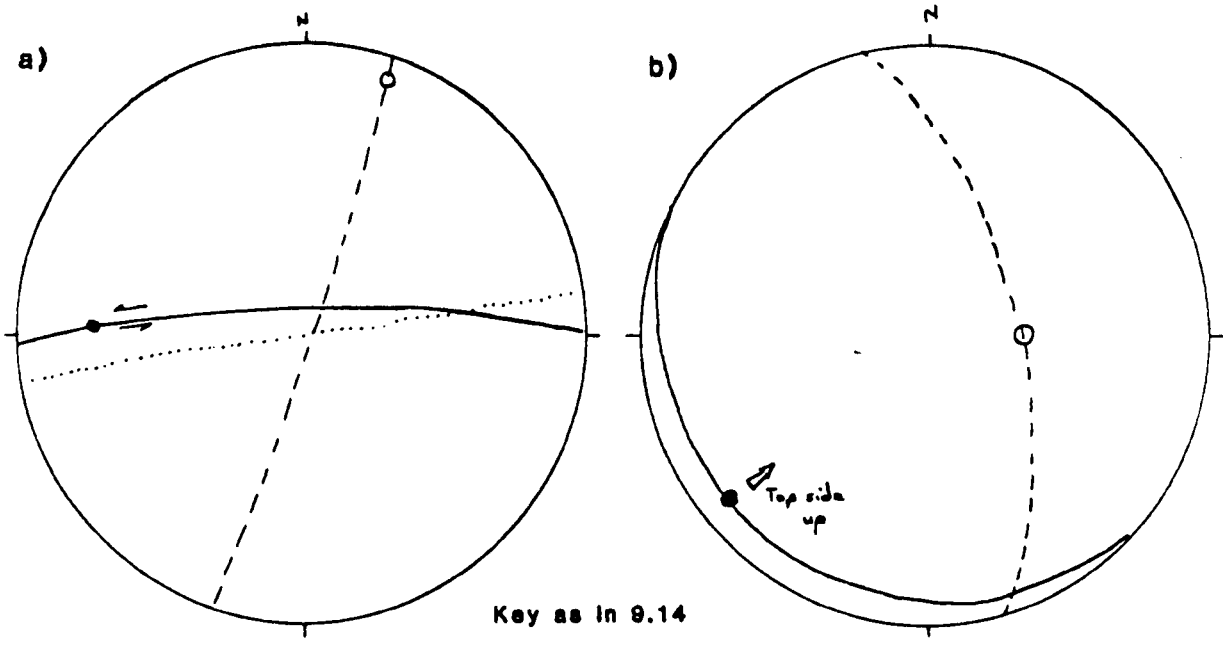

Figure 9.20 Unst area. a) The data of Table 9.2 with the rotation axis marked; b) the data rotated back to ocean spreading orientations. (As in Table 9.3). (Equal area lower hemisphere projection).

fairly realistically rotate the data back to pre-emplacement orientations.

In all the figures, the mean sheeted dyke strike is marked except for Unst. In the Rajmi area, both the dyke orientations previously discussed are shown (Figure 9.14).

In order to facilitate comparisons between the different areas of Oman, all the dyke strikes have been rotated to a N-S direction. (i.e. about a vertical rotation axis). The resulting data orientations are shown in Table 9.3. Figure 9.21 shows an equal area projection of D2 mean structural orientations for a horizontal moho and a N-S striking ridge axis.

The mean orientations of Table 9.3 have been diagrammatically represented in Figure 9.22. Also shown are the dominant senses of D2 shearing calculated for each area (See Chapter 7).

It is clear from Table 9.3 and Figures 9.14-9.22 that neither the D2 nor D1 related structures have a common orientation between areas. Each of the ophiolite blocks studied in Oman, and the complexes of Troodos and Unst have unique S2 plane orientations and D2 shearing directions with respect to the ridge axis and ocean spreading direction inferred from the Sheeted Dyke Complex. This shows that no simple relationship can be inferred between the spreading direction of the oceanic crust and the underlying Peridotite Unit structures.

The S2 planes vary from a sub-horizontal orientation in some areas to a sub-vertical orientation in others. The D2 shearing direction in the S2 plane is also highly variable between areas and has no obvious relationship with the orientation of the S2 plane with

Table 9.3 Mean structural attitudes relative to a horizontal moho and a N-S striking ridge axis.

Area	S2 plane	D2 slip direction [Upper surface shear direction]	S1 plane	S1 slip direction	Undeformed cumulate plane	Spreading direction
Rajmi 1.	108 49	175 25 [175 25]	150 84	235 50	150 63	E- W
Rajmi 2.	169 49	238 25 [238 25]	212 84	304 50	212 63	
Ath Thuqbah	108 33	024 05 [204 175]	024 52	107 08	035 08	E- W
Sarami and Kanut	297 88	210 56 [Unclear]	355 15	295 05	360 05	E- W
Hajir	040 67	077 63 [077 63]	241 71	330 01	310 05	E- W
Al Abyad	233 12	302 04 [122 176]	145 33	192 48	+212 24	E- W
Troodos	190 62	268 22 [088 158]	002 24	320 18	-	? W- E
Unst*	209 10	231 10 [051 170]	075 64	092 62	-	?

1. N-S dyke strike
2. 112° dyke strike

* No ridge strike or spreading direction calculable.

+ Deformed cumulate planes.

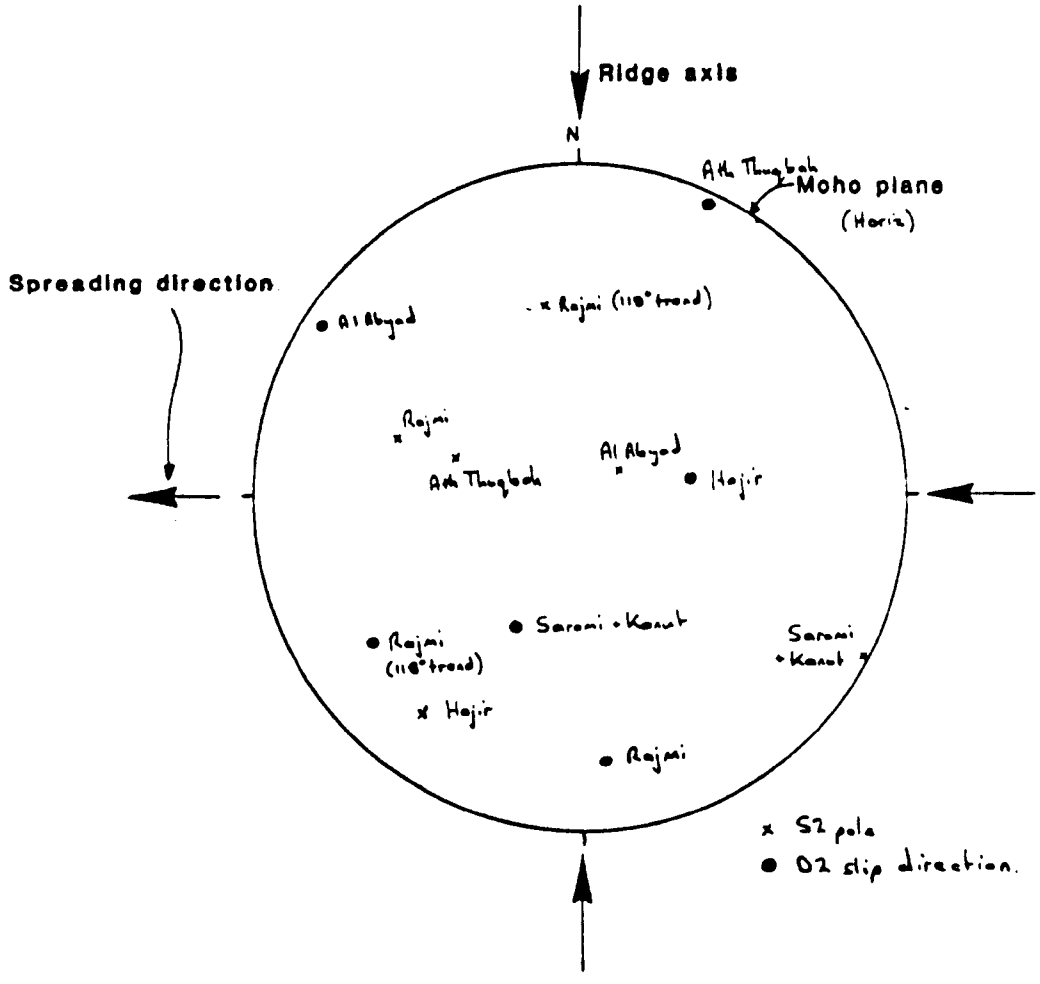

Figure 9.21 Equal area lower hemisphere projection of mean S2 poles and D2 slip directions for all the Oman areas.

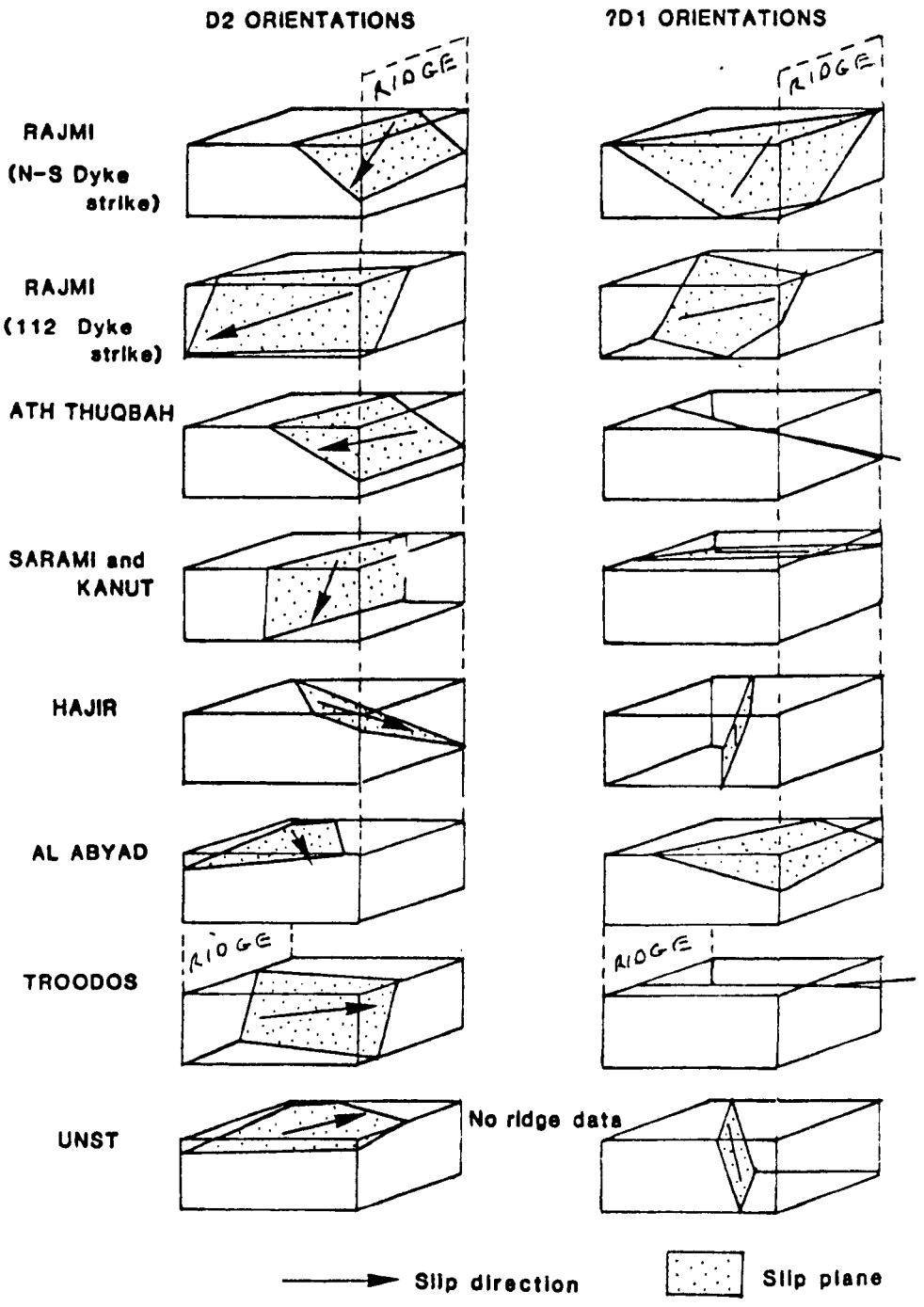

Figure 9.22 Diagrammatic representations of the data in Table 9.3. (not to scale).

respect to the ridge axis and spreading direction.

The possible orientations of major slip surfaces in the Lower Cumulate Units of the Rajmi and Al Abyad areas are included in Figures 9.14. These have been determined from small scale shear measurements (Riedel shears). (See Chapter 2). In both areas the major slip surfaces have fairly steep dips and variable strikes after rotation (see Figures 9.14(b) and 9.18(b)). The small-scale shears are late-stage ductile features as they disrupt D2 related fabrics. (See Chapter 2). They are thus not formed by the main asthenospheric mantle deformation episodes and may well be related to late stage transform fault movements. Sufficient data is not available for a detailed study of these sheer zones.

In the next chapter, various models of the kinematic behaviour of the Peridotite Unit, with respect to an ocean ridge axis and associated spreading direction, will be discussed in the light of the evidence presented above.

Chapter 10

The Kinematic Behaviour of the Uppermost Asthenospheric Mantle at a Spreading Centre.

CONTENTS

10.1 The Kinematic Behaviour of the Uppermost Mantle Beneath a Spreading Centre - Generalised Models.

Very little is known about the geometry and kinematics of plastic flow in the uppermost mantle beneath spreading centres. Two main models have been derived, mainly from heat flow studies.

(i) The "dyke-intrusion" model of McKenzie (1967) and of Cann (1970, 1974) in which a narrow vertical intrusion of partially molten mantle material feeds the crustal magma chamber and fills the gap created due to spreading (Figure 10.1). The residual mantle material is plated onto the off-axis residual mantle material just as with the intrusion of dykes. A vertical flow structure is thus laterally frozen into the cooling uppermost mantle. This relict vertical flow structure can then be rotated due to off-axis subsidence in the oceanic crust, resulting in a moderately inclined mantle foliation away from the ridge (Figure 10.1).

(ii) The "right-angle turn" model of Lanseth et al (1966). This model involves the vertical upwelling of mantle asthenosphere at a ridge axis with a right-angled turn of the flow to a horizontal orientation at the limit between the asthenosphere and lithosphere (Figure 10.2).

These models have been critically discussed by Bottinga and Allègre (1976), Bottinga and Steinmetz (1979) and Nicolas and Violette (1982). Nicolas and Violette (1982) conclude that both models are plausible. Parker and Oldenburg (1973) predicted that the lithosphere rapidly thickens away from a ridge axis and that this is consistent with the Langseth et al (1966) model.

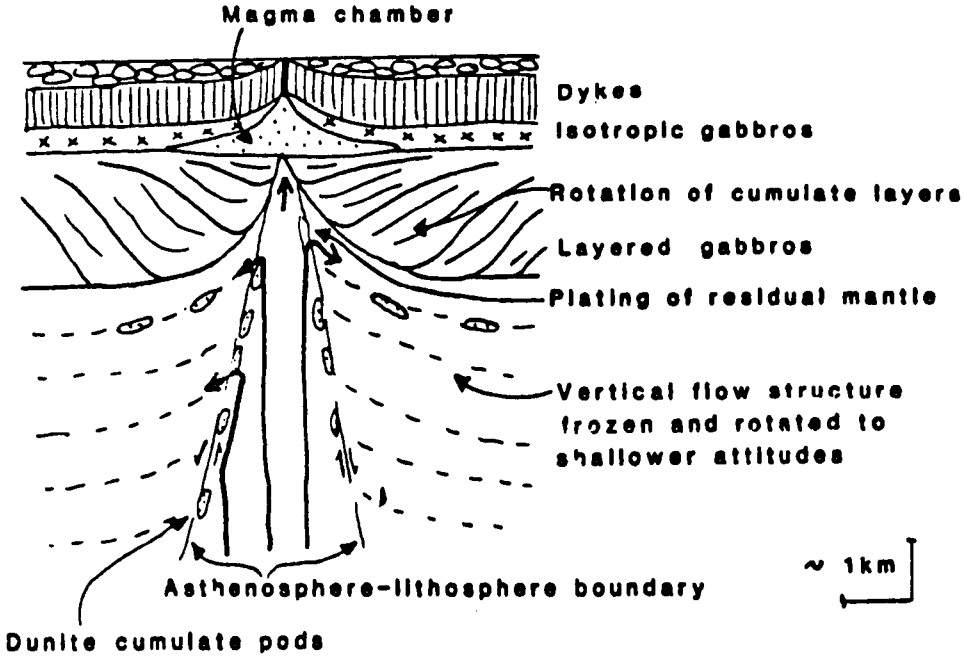

Figure 10.1 A simplified "dyke-intrusion" model. (Modified from McKenzie, 1967, and Cann, 1970 and 1974).

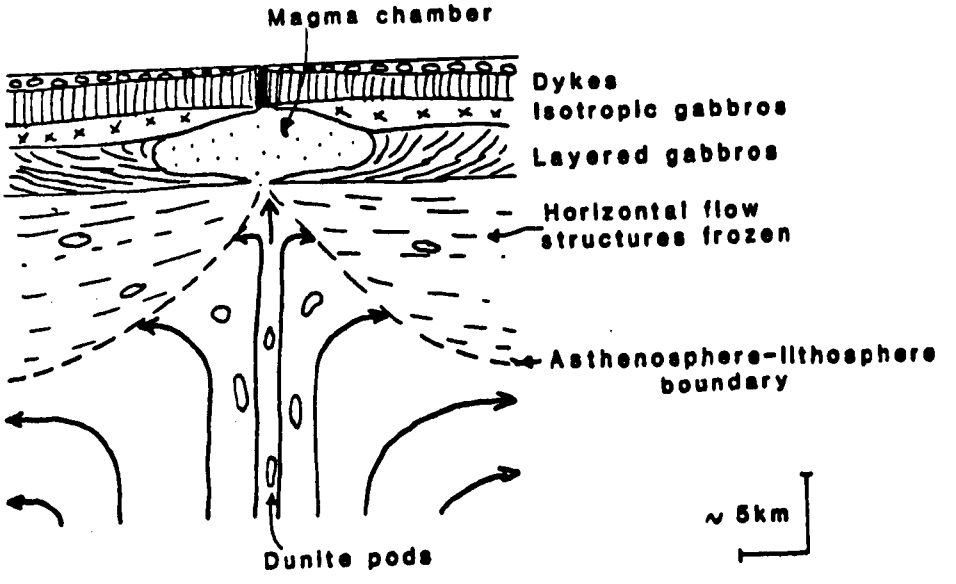

Figure 10.2 The "right-angle turn" model. (Modified from Langseth et al, 1966).

A review of the dynamics of ocean ridge centres by Sleep and Rosendahl (1979), however, shows that the rate of thickening of the oceanic lithosphere away from a spreading axis is largely dependent on the spreading rate (Figure 10.3). In fast spreading ridges (5cm yr^{-1}) the asthenosphere-lithosphere (the 1185°C isotherm in Figure 10.3) boundary has a very shallow dip, and it is difficult to visualise how the "dyke-intrusion" model could be possible in such a situation. The diapirically rising asthenospheric mantle material would be too ductile to be confined to a narrow injection zone directly beneath the ridge axis. In a slow spreading ridge (1cm yr^{-1}) environment, however, the asthenosphere-lithosphere boundary has a steep dip. In this situation the rising mantle material is most probably confined to a narrow conduit directly beneath the ridge axis and thus a "dyke intrusion" model is more plausible than in a fast-spreading ridge environment. The "right-angle" turn model is plausible for both fast-and slow-spreading ridges.

10.2 Models of Upper Mantle Flow at Spreading Centres Derived from the Structural Study of Ophiolite Complexes.

Very few studies have been published that deduce the flow pattern of the uppermost mantle beneath a spreading centre from the structural study of ophiolite complexes. These have been reviewed by Nicolas and Violette (1982).

The only general model that has been proposed which encompasses the structural data from a large number of ophiolite complexes, is that of Nicolas and Violette (1982). They use the structural

a) 5cm/yr

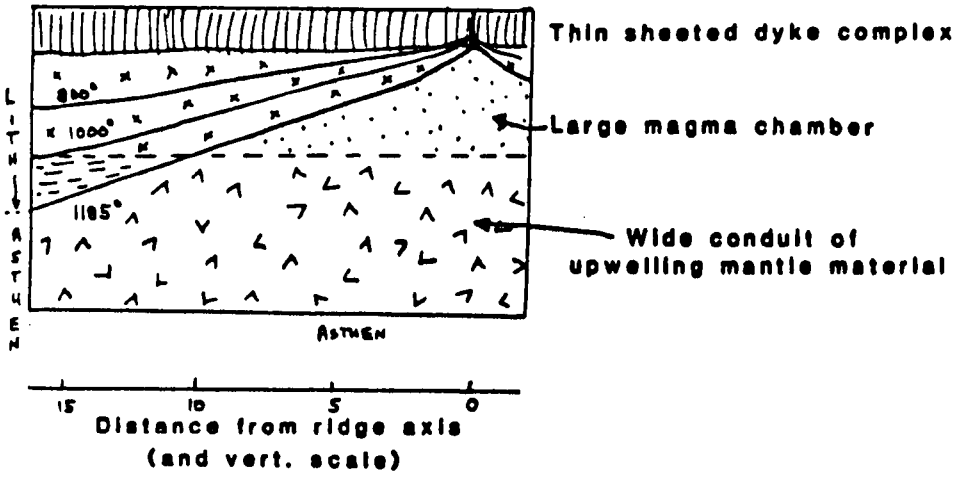

b) 1cm/yr

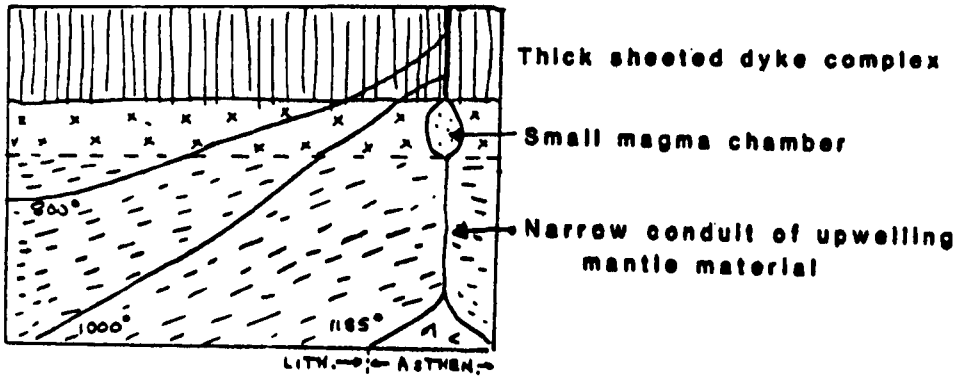

Figure 10.3 The dependence of the rate of thickening of the lithosphere on the spreading rate. a) Fast spreading ridge; b) Slow spreading ridge. (Modified from Sleep and Rosendahl, 1979).

measurements from eleven ophiolite complexes and distinguish two oceanic situations from them:

(i) A horizontally spreading asthenosphere illustrated by the Table Mountain massif (Newfoundland).

and (ii) A diapirically spreading asthenosphere illustrated by the Acoje ophiolite (Phillipines).

Each oceanic situation has been characterised by a comparative study of various structural and petrological parameters between each ophiolite complex. In the Table Mountain type, the mantle foliation has a homogeneous, regular and sub-horizontal orientation over large areas. The moho plane is horizontal and has no large-scale folds. Chromite deposits are rare and the mantle is chemically depleted. In the Acoje type, the mantle foliation is inhomogenous and has a sub-vertical orientation, the moho plane is folded, and important economical chromite deposits are found as well as a less depleted mantle.

Nicolas and Violette (1982) combine the two ophiolite types into a single model of asthenospheric flow. They propose a model similar to that derived by Vogt (1976) where the vertical mantle flow at a diapir centre diverges horizontally in every direction, including that parallel to the ridge. At about 50km from the diapir centre the mantle flow becomes progressively perpendicular to the ridge due to the damming effect of transform faults. Figure 10.4 summarises the model of Nicolas and Violette (1982).

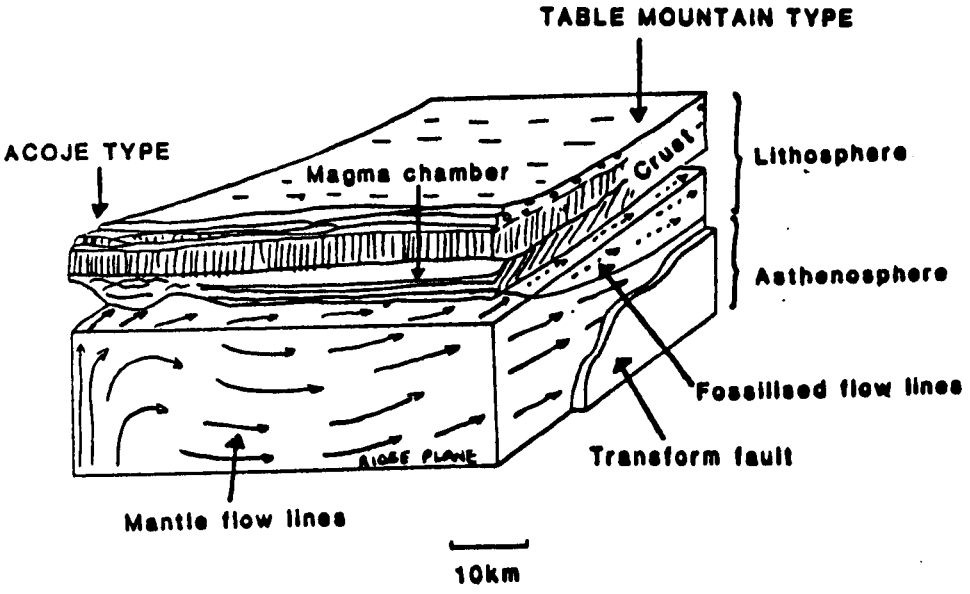

Figure 10.4 The ridge model of Nicolas and Violette (1982) resulting from local uprising of mantle flow (Acoje type) followed by horizontal divergence and progressive channelling by transform faults (Table Mountain type).

Nicolas and Violette (1982) propose that the mantle structures ovserved from an ophiolite complex can be used to determine the position at which the ophiolite complex was formed: ie. close to a diapiric uprise centre (Acoje type) or close to transform zones (Table Mountain type).

10.3 Ductile Mantle Structures - Relicts of Asthenospheric Flow?

In the Nicolas and Violette (1982) model, it is assumed that all the mantle structures observed from the eleven ophiolites are asthenospheric flow structures, and that once the residual mantle has cooled sufficiently (below 1000°C according to Nicolas and Violette (1982)) it cannot deform by ductile means. The discussions in Chapters 6 and 7 would agree with this assumption.

The limit to mantle ductile flow has arbitrarily been taken as the asthenosphere-lithosphere boundary. There is no evidence for what happened to the asthenospheric mantle before it passed through the asthenosphere-lithosphere boundary preserved in ophiolite complexes, as only those flow structures present in the mantle at the point of transition from asthenosphere to lithosphere will be fossilised. Thus the vertical diapiric uprise of mantle material at an ocean spreading centre can only be inferred in models of mantle asthenospheric flow. If the residual mantle material has passed through the asthenosphere-lithosphere boundary in an ocean-spreading environment prior to the ophiolite obduction and/or emplacement, then only the ductile flow structures associated with the movement of the residual mantle away from a diapiric centre will be preserved. Relict

vertical flow structures associated with the diapiric uprise could only be preserved if the ophiolite is obducted very soon after its formation as oceanic crust. In such a case the mantle residuum is still in a ductile state (and thus asthenospheric) and it may preserve vertical flow structures. However, the obduction and emplacement of an ophiolite with a still ductile mantle will cause the mantle to be deformed by ductile processes thus destroying any relict vertical flow structures present prior to obduction.

The only way by which vertical structures associated with the diapriric uprise of material could be preserved is in an extremely slow spreading environment (less than $\frac{1}{2}$cm yr^{-1}) where there is only a narrow conduit of rising asthenospheric mantle. In this situation the edges of the conduit within the uppermost mantle could also define the asthenosphere-lithosphere boundary and thus the only ductile flow which could occur in the uppermost mantle would be a vertical flow (ie. the model of Cann (1970, 1974)).

Nicolas and Violette (1982) do not take into account the variation in spreading rates in their ridge model. They relate the Acoje type ophiolites to vertically uprising mantle material prior to horizontal spreading, and include the Troodos complex as an Acoje type ophiolite. As will be discussed below, there is strong evidence to suggest that the main foliation within the Troodos Complex has been formed during horizontal flow of the mantle material away from a diapiric centre.

10.4 Diapiric Uprise or Horizontal Spreading Flow? - Evidence from the Ophiolites Studied in this Thesis.

In all of the three areas studied, there is evidence to show that the major flow structures observed in the lower ophiolite sequences are related to the flow of asthenospheric mantle away from diapiric uprise centres, and not to the flow of the diapirically upwelling mantle at uprise centres. The evidence is two-fold: firstly the existence of two ductile deformational events in most areas; and secondly the fact that the ductile deformation extends into the Lower Cumulate Unit in most areas.

(i) Two Deformational Events. In all of the ophiolite complexes studied, two ductile deformational events have been distinguished. In the areas where D2 shearing has occurred, the S2 plane is usually easy to measure in the field. The S1 plane, on the other hand, is often difficult to identify (see Chapter 7). Previous workers in these areas have only measured the most prominent foliation plane (usually the S2 plane). In the Troodos Ophiolite the prominent foliation plane has been interpreted as the S1 plane by George (1975, 1978) and has been used by Nicolas and Violette (1982) in their study. The evidence presented in Chapters 3 and 7 of this study show that this prominent foliation plane is the S2 plane and thus could not have been formed by the vertical rise of material in a mantle diapir.

The northern Oman Ophiolite and Shetland Ophiolite have not been studied by Nicolas and Violette (1982).

(ii) Ductile Deformation of the Lower Cumulate Unit.

In the three ophiolite complexes studied both the D1 and D2 ductile deformations extend into the Lower Cumulate Unit. Nicolas and Prinzhoffer (1983) argue that the dunites that outcrop between the main harzburgites and layered gabbros are residual in origin and thus imply that the ductile shearing structures do not extend into the oceanic crust.

In Oman, however, the evidence discussed in Chapters 2 and 7, shows that in some areas the lowermost layered gabbros have been extensively deformed by both the D1 and D2 shearing events. In Wadi Al Abyad the D2 shearing extends at least 1km into the layered gabbros.

In Cyprus and Shetland, the D1 and D2 shearing dies out in the dunites of the Lower Cumulate Unit. If these dunites were residual material, and thus were part of the mantle sequence, then they would be expected to contain a tectonic foliation over their whole extent, as they would have gone through the same deformation processes as the residual harzburgites below. No harzburgites from ophiolite complexes have ever been reported as being udeformed by ductile deformation processes. It would thus seem most reasonable to consider the massive dunites of Cyprus and Shetland as cumulate and not as residual in origin.

The fact that the base of the Lower Cumulate Unit is deformed by both D1 and D2 shearing in all three areas studied, implies that both the D1 and D2 events must have occurred when the lowermost cumulates were in a solid deformable state and thus

after they had moved slightly off-axis. In other words the D1 and D2 deformation occurred during flow away from the diapiric uprise centres situated along the ridge axis and not during vertical flow within a mantle diapir itself.

A model must thus be derived which involves at least two different shearing events that occur during slightly off-axis flow of the asthenospheric mantle material.

10.5 A Two-Shearing Model for the Off-Axis Flow of Asthenospheric Mantle.

The structural data presented in this thesis shows that there are at least two shearing events occurring in the asthenospheric mantle after diapiric uprise has occurred. The evidence from Oman shows that the D1 and D2 events need not be the same events in different areas and that in some areas only one deformational event has occurred.

The most obvious way to produce two shearing events is to have two different centres of diapiric uprise in the same ridge section (Figure 10.5). The residual mantle material flows away from each diapiric uprise centre in all directions including that parallel to the ridge axis (as proposed by Nicolas and Violette (1982)). In the area between the two uprise centres the two diverging flow systems will meet and interact with each other. If the diapiric uprise centres are active at different times, then the youngest centre will produce the D2 flow planes which will shear fold the D1 flow planes from the earlier diapiric uprise centre.

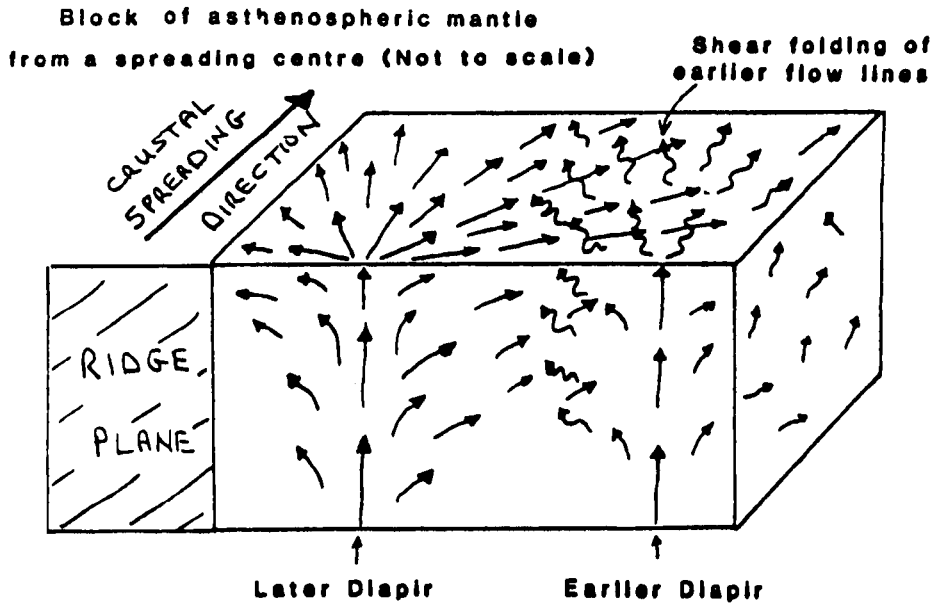

Figure 10.5 Two adjacent centres of diapiric uprise causing two diverging flow areas which interact to form areas preserved that have undergone two ductile shearing events - the flow or shear interaction model.

The intensity of the D2 shearing will depend on two main factors. Firstly the original proximity of the ophiolite to the diapiric centre when the uppermost mantle was going through the asthenosphere to lithosphere transition, and secondly on the crustal spreading rate. If the ophiolite was originally close to the diapiric centre, then the shearing away from the diapiric centre will be intense compared to an area more distant from it. In a slow spreading ridge environment the magma input into the crustal magma chambers is slow compared to a fast spreading ridge environment. This slow input would give a less intense shearing pattern away from the diapiric uprise centre. However, this is complemented by the fact that in a slow spreading environment the dip of the asthenosphere-lithosphere boundary is much steeper than for fast spreading (see Figure 10.3), and thus the diverging flow lines from the diapiric centres will be fossilised much nearer to the diapiric centres.

The detailed work on the Cumulate Unit of Oman by Browning (1982) shows that the variation in strike of the cumulate layers can be interpreted as a result of cumulation from magma chambers of finite length beneath the ridge axis. This fits in well with the suggestion that the mantle material diapirically uprises in a number of centres along the ridge axis.

There is no reason why the planes of diverging flow from each diapiric centre should be horizontal. The mean orientations of S1 and S2 planes discussed in Chapter 9 would certainly imply this, assuming they have been formed by the method described above.

The S1 and S2 planes also show no consistency in their shear sense. This can be explained by the possibility of surges of residual material away from the rising diapir at differing depths, thus varying both the shear intensities and shear senses within the diverging mass of material.

Another factor which will have a strong influence on the orientation of the D1 and D2 structures is the presence of transform faults. There is clear seismological evidence that transforms extend into the asthenospheric mantle areas along ridge axes. (Francis, 1981; Project ROSE Scientists, 1981.) Nicolas and Violette (1982), in their model, used the proposal of Vogt and Johnson (1975) that transform movements, have a damming effect on the mantle flow and thus rotate the flow perpendicular to the ridge axis. The transform zones may also cause a steepening of the flow planes.

A model for the kinematic behaviour of the uppermost asthenospheric mantle at a spreading centre is shown in Figure 10.6. It is based on the interaction of flow planes diverging away from localised diapiric uplift centres and also on the presence of transform zones.

It is not possible to accurately position each of the areas studied in this model, as the whole system is dynamic and each area studied will have been produced in a unique setting. Figure 10.7 shows suggested settings for the different areas studied based on the model in Figure 10.6.

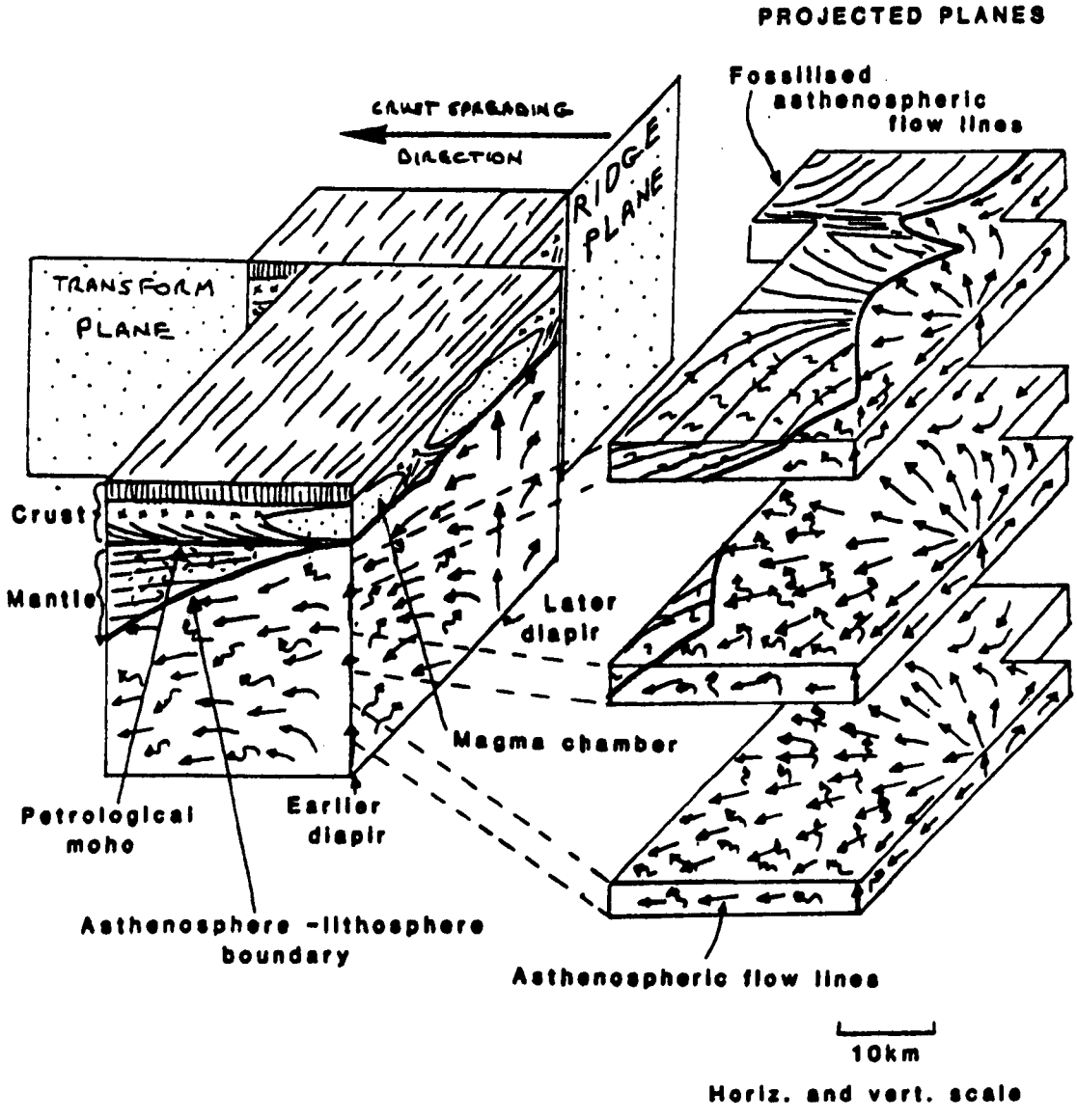

Figure 10.6 A model for the kinematic behaviour of the uppermost asthenospheric mantle derived from the results described in Chapters 2 to 9.

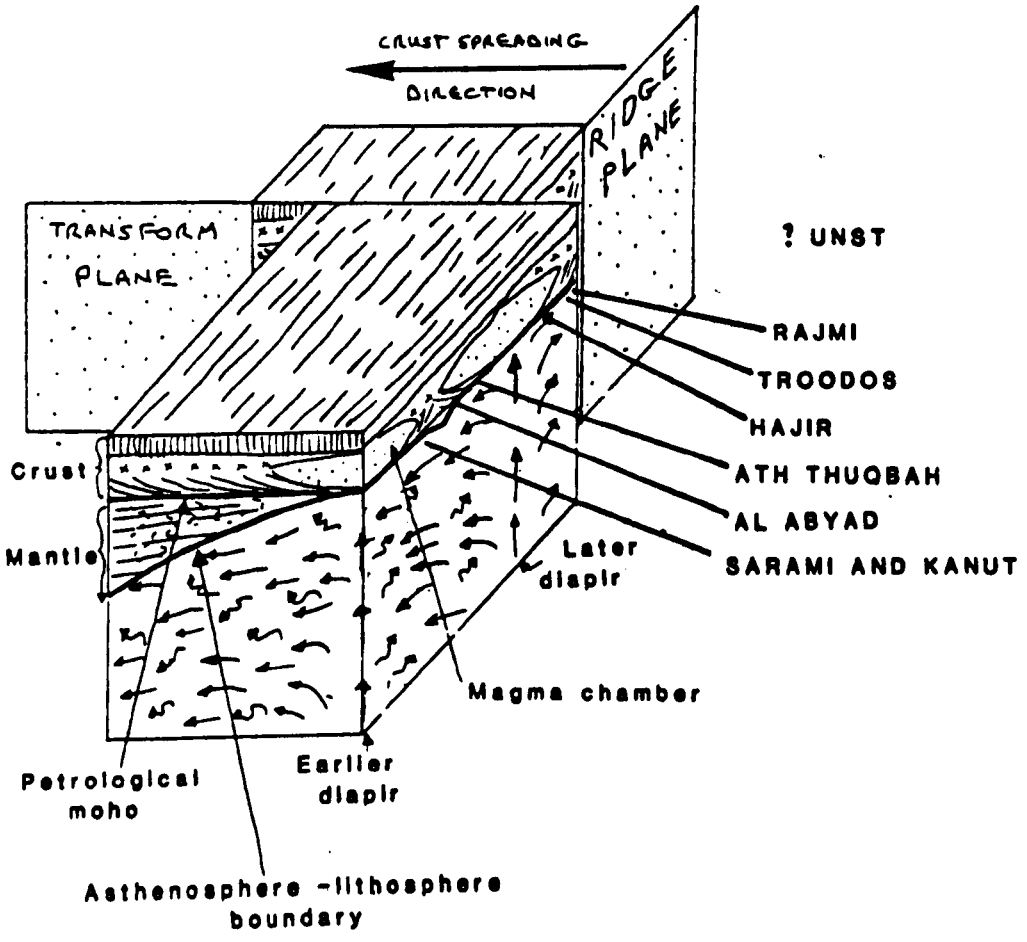

Figure 10.7 Possible settings for the different areas studied at an ocean spreading centre, based on the model in Figure 10.6.

10.6 Present-Day Spreading Centres - Evidence for Asthenospheric Flow of Residual Mantle Material?

The only evidence that can be obtained from present day ocean studies for asthenospheric flow at spreading centres is from the results obtained from seismic refraction studies of the oceanic lithosphere.

Hess (1964) first proposed that the uppermost mantle beneath the oceans is seismically anisotropic as a result of a preferential orientation of its constituent olivine crystals. Verma (1960) showed, from laboratory studies that the olivine [100] cyrstallographic axis gives a relatively high seismic velocity (9.87km sec^{-1}) whereas the [010] and [001] axes give lower seismic velocities (7.73km sec^{-1} and 8.65km sec^{-1} respectively).

Francis (1969) points out that seismic refraction studies at sea will only provide information about the top 3-4kms of oceanic mantle material, and thus will record a fossil anisotropy produced by the [100] slip of olivines at or close to spreading centres whilst the mantle is still undergoing ductile deformation. Both Christensen and Smewing (1981) and Peselnick and Nicolas (1978) correlate the seismic anisotropy of Oman and the Antalya Complex (Turkey) respectively to the seismic anisotropy observed in present day ocean studies.

The main drawback of the seismic anisotropy studies of present-day oceans is that they give only an average value over a large area and cannot show up the detailed relationships of asthenospheric

mantle flow which can be demonstrated from the study of ophiolite complexes. The mean seismic anisotropy of large areas is, however, fairly variable between different oceanic areas. The slow spreading Mid-Atlantic ridge (approximately 1.5cm yr^{-1}) gives very low seismic anisotropies compared to the fast spreading East Pacific Rise (4.4cm yr^{-1}). (Francis, 1969.) In both areas the fast seismic direction is roughly perpendicular to the ridge axis.

This correlates well with the predictions of the model in Section 10.5. In slow-spreading ridges, such as the Mid-Atlantic ridge, the magma chambers are only small and sporadic and the mantle feeder conduits are a narrow zone. (See Figure 10.3.) This will give a mantle asthenospheric flow pattern of a highly divergent nature except at the vicinity of transform zones where the flow will be perpendicular to the ridge axis. The fossilised seismic anisotropy will thus only give a weak preferred orientation for the fast velocity approximately perpendicular to the ridge axis. This is shown in Figure 10.8. In fast spreading ridges the magma chambers are large and the mantle feeder conduit a wide zone. (See Figure 10.3.) The magma chambers are also more abundant along ridge strike which implies that there are more diapiric uprise centres. This will give rise to a much larger fossilised seismic anisotropy than for slow spreading ridges (Figure 10.8).

The evidence of seismic anisotropy studies thus does not provide direct proof for the model of Section 10.5 but at least it does agree with what the model predicts.

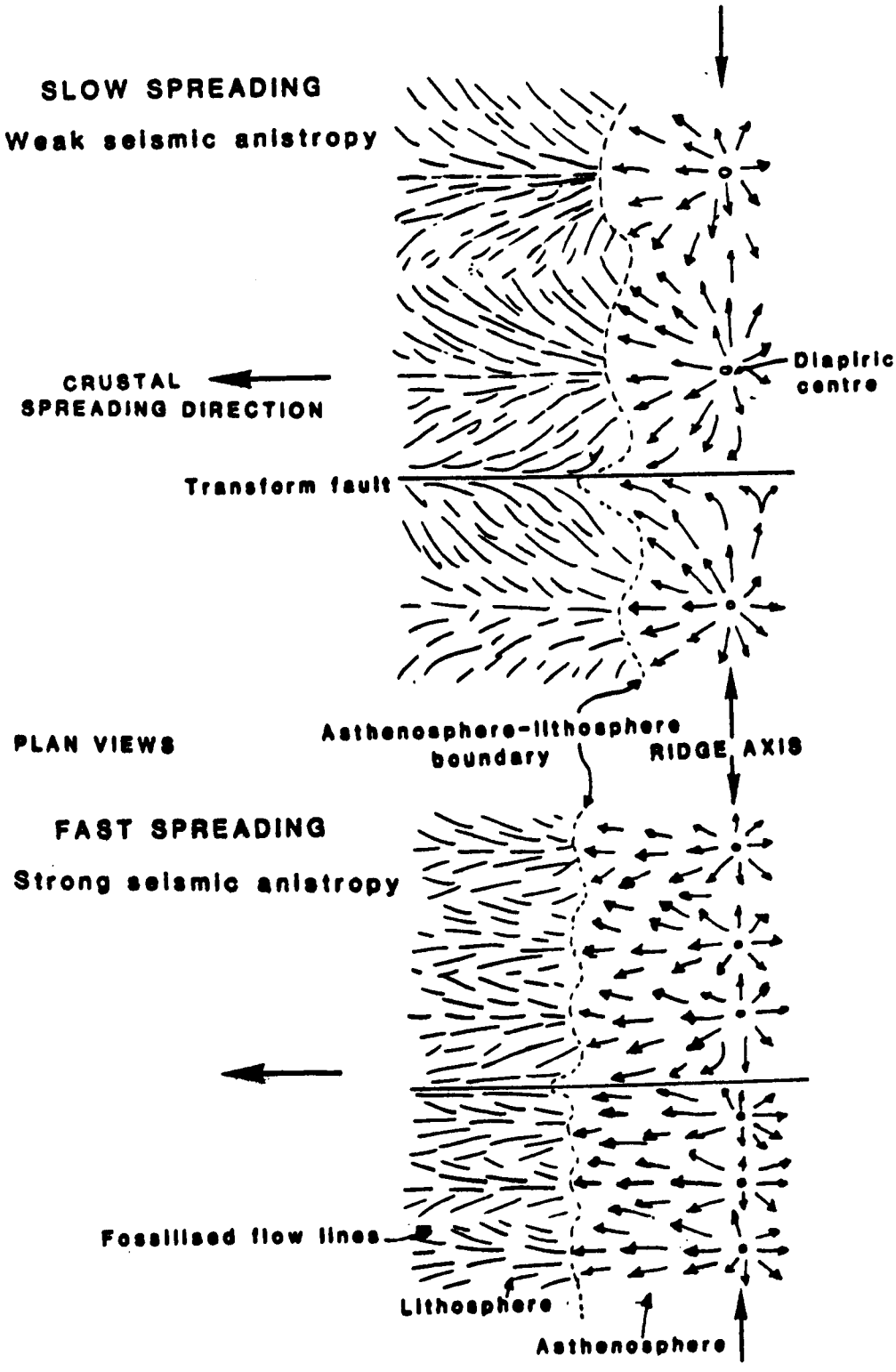

Figure 10.8 Variations on the value of the seismic anisotropy depending on the spreading rate.

10.7 The Driving Mechanism of Plate Tectonics - Do Structural Studies from Ophiolites Help?

It is generally agreed that some or all of the mantle is undergoing convection (Alvarez, 1982). The exact driving force for the motion of the plates, however, is uncertain. The forces generated in or by the plates themselves are obviously important, in particular slab pull, ridge push and sliding of the plate away from the elevated ridge. (Forsyth and Uyeda, 1975).

A problem which could possibly be solved from ophiolite studies, is whether the oceanic lithospheric plates become decoupled from the asthenosphere and thus whether the lithosphere can be driven by the in-plate forces alone.

Unfortunately, an ophiolite sequence only includes no more than 15km thickness of mantle material. This will have been rapidly transformed from ductile asthenospheric mantle to more brittle lithospheric mantle very close to the ridge axis. If the lithosphere is decoupled from the asthenosphere then it would be expected that the lithosphere-asthenosphere boundary would be a major ductile shear zone. The fossilised ductile foliations in the lithospheric mantle should thus be parallel to lithosphere-asthenosphere boundary, and the foliations fossilised close to a ridge axis should dip at a moderate angle away from the ridge axis.

The structures summarised in Chapter 9 for the areas studied certainly do not show this relationship. Whether it holds for asthenospheric structures fossilised into the lithosphere at deeper levels than ophiolites sample, cannot be ascertained. The results presented are therefore inconclusive regarding lithospheric-asthenospheric decoupling. They merely apply to the very localised near-ridge area where the asthenospheric mantle reaches shallow levels and cannot be related to normal off-axis oceanic lithosphere and asthenosphere.

10.8 Mid-Ocean Ridge or Back Arc Basin? - Evidence from the Structural Study of Lower Ophiolite Sequences.

Geochemical evidence (reviewed in Chapters 2-4) from the three ophiolite complexes studied suggest that they all have been formed in a back-arc basin setting.

As only the uppermost mantle is sampled in ophiolite complexes, only the ductile asthenospheric structures formed at or very close to the ridge axis are preserved. Thus, as mentioned in Section 10.7, only the ridge-related processes will be preserved in the mantle sequences.

As both mid-ocean ridges and back arc basins involve spreading of oceanic crust, it would seem logical to assume that similar ridge-related processes are occurring in the uppermost mantle beneath the spreading centre. It is thus not possible to discriminate a back arc basin ophiolite from a mid-ocean ridge ophiolite from the ductile structures within mantle sequences in ophiolites.

Appendices

Appendix 1 The Determination of the Pre-shearing Orientation of a Line for Simple Shearing Deformations.

In a simple shearing deformation, Ramsay (1967) has shown that it is possible to determine mathematically the relationship between the angle that a line makes with the shear plane before and after deformation.

From Figure A.1 it can be seen that the relationship between a line originally making an angle α with the shear plane and its new angle α' after simple shearing has taken place, is:

$$\cot \alpha' = \cot \alpha + \gamma$$

where γ is the shear strain. The graphical solution to this equation is shown in Figure 7.10.

Appendix 2 The Conversion Factor for Plotting the Three-Dimensional Value of $\bar{\Sigma}_s$ on a Planar Diagram.

Figure A.2 shows a unit cube of the $\bar{\Sigma}_1$, $\bar{\Sigma}_2$ and $\bar{\Sigma}_3$ reference axes with the space diagonal ($\bar{\Sigma}_s$). In order to project these orthogonal reference axes onto a plane which has reference axes $\bar{\Sigma}_1$, $\bar{\Sigma}_2$ and $\bar{\Sigma}_3$ which subtend angles of 120^o, each axes must be projected through an angle whose cosine is $\sqrt{2/3}$. Thus, the projection of any natural strain coordinate onto one of these axes is $\sqrt{2/3}\ \bar{\Sigma} = 0.816\bar{\Sigma}$.

Appendix 3 The Use of a Mohr Diagram to Calculate the Diameters of a Strain Ellipsoid for Homogeneous Simple Shear with no Dilation.

This method has been derived by Dr. R F Cheeney (University of

Edinburgh). (pers. com.). Figure A.3 shows the λ_1, λ_3 plane for a rock that has undergone simple shear (λ_1 and λ_3 are two of the principal quadratic elongations, $\lambda_2 = 1$ for the plane strain). The shear strain (γ) is defined from the angle of shear (ψ):

$$\gamma = -\tan \psi.$$

and the major axis of the strain ellipse makes an angle θ with the shear surface. (measured acticlockwise positive).

The Mohr diagram for the strained state is shown in Figure A.4. Cheeney (pers.com) has derived the relationship from the Mohr diagram which calculates the λ_1 (maximum principal quadratic elongation) and λ_3 (minimum principal quadratic elongation) values from the value of the shear strain (γ):

$$\lambda_1 = 1 + \gamma^2/2 + \gamma\sqrt{1 + \frac{\gamma^2}{4}}$$

and $$\lambda_3 = 1 + \gamma^2/2 - \gamma\sqrt{1 + \frac{\gamma^2}{4}}\ .$$

The θ angle is also relatable to γ by the equation :

$$\theta = \frac{1}{2} \arctan\left(\frac{2}{\gamma}\right)\ .$$

Thus for any state of homogeneous plane simple shear without dilation, the Mohr circle diagram for the principal plane containing λ_2 and λ_3 can be constructed. To this, supplementary circles for the principal planes containing the λ_1, λ_2 and λ_2, λ_3 can be added, and thus the strain state in any direction can be obtained.

Table A.1 shows the values of ψ, γ, λ_1, λ_3 and θ for ellipsoids at various states of strain, along with the values of v and Σ_s for each strain ellipsoid, calculated from the six diameters from each principal plane.

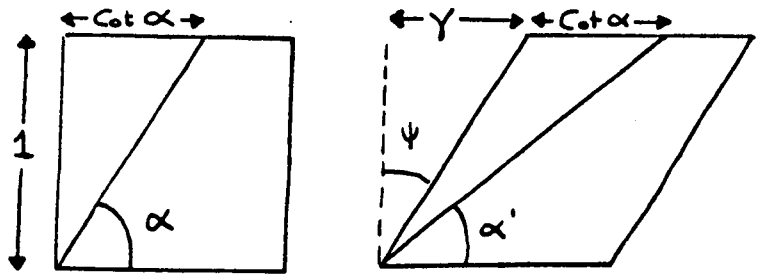

Figure A.1

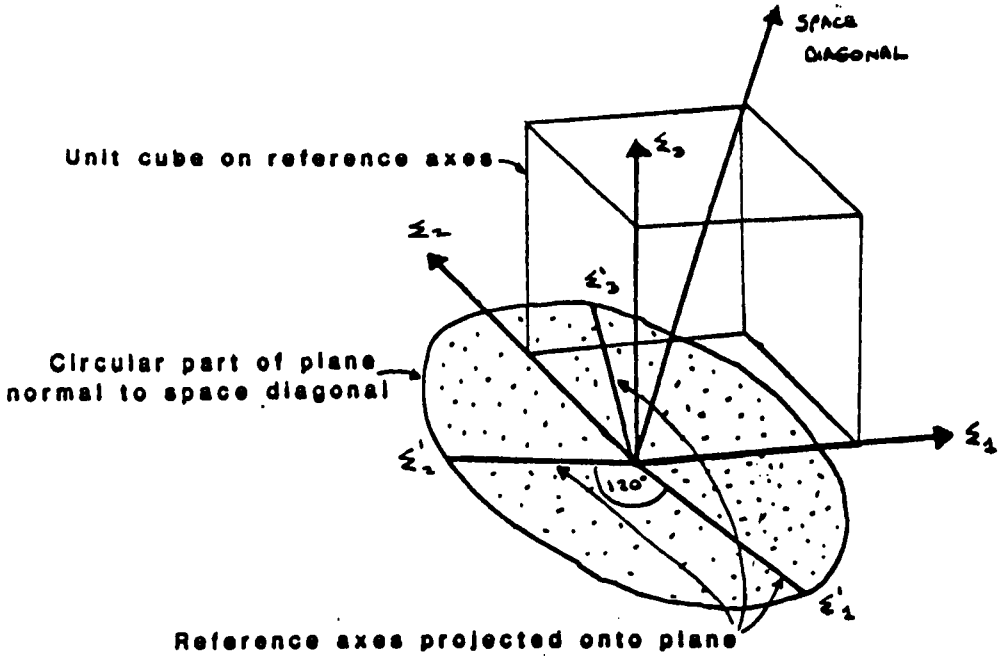

Figure A.2

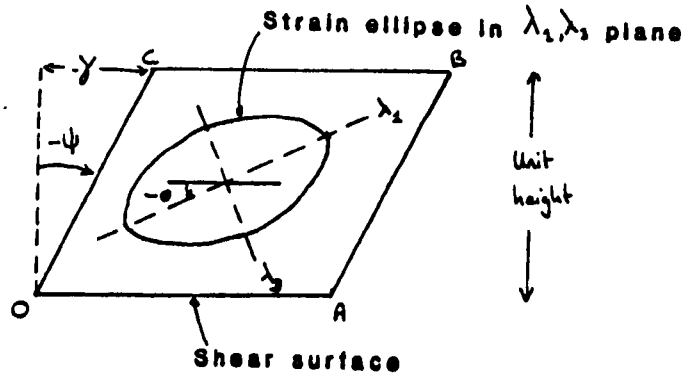

Figure A.3

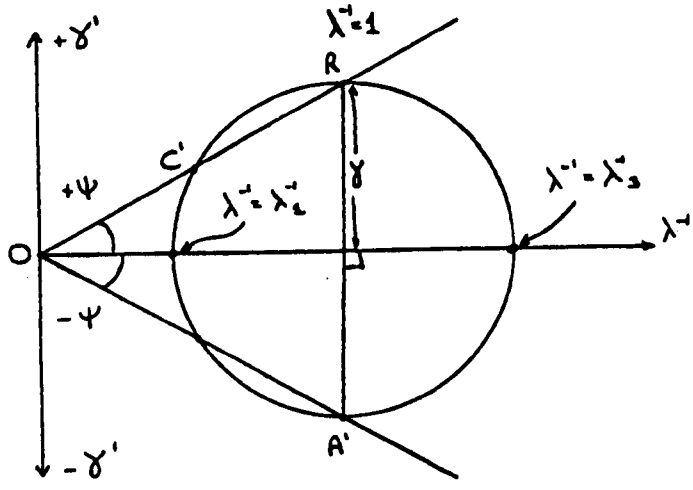

Figure A.4

Angle of Shear	-I5°	-30°	-45°	-60°
Shear Strain	-0.268	-0.577	-I.000	-I.732
λ_1	I.306	I.768	2.6I8	4.79I
λ_3	0.766	0.566	0.382	0.209
Θ	4I°	37°	32°	25°
Lode's Parameter	-0.0I2	0.00I	0.00I	-0.008
Σ_s	0.I86	0.40I	0.676	I.I05
Σ_s X 0.8I6	0.I52	0.327	0.552	0.902

Table A.1

References

Alabaster, T., Pearce, J.A., Mallick, D.J., & Elboushi, I, 1980. The volcanic stratigraphy and location of massive sulphide deposits in the Oman ophiolite. In "Ophiolites" Proc. Int. Oph. Symp. Cyprus 1979, Panayiotou, A (ed). 751-757.

Alabaster, T., Pearce, J.A., & Malpas, J. The volcanic stratigraphy and petrogenesis of the Oman Ophiolite Complex. C.M.P. 81, 168-183.

Allen, C.R. 1975. The petrology of a portion of the Troodos Plutonic Complex, Cyprus. Ph.D. Thesis Cambridge (Unpub).

Alvarez, W. 1982. Geological evidence for the geological pattern of mantle returnflow and the driving mechanism of Plate Tectonics. J. Geop. Res, 87, 6698-6710.

Amin, M.S. 1954. Notes on the ultrabasic body of Unst, Shetland Islands. Geol. Mag., 91, 399-406.

Anderson, T.W. & Stephens, M.A. 1972. Tests for randomness of directions against equatorial and bimodal alternatives. Biometrika, 59, 613.

Anderton, R., Bridges, P.H., Leeder, M.R. & Sellwood, B.W. 1979. A dynamic stratigraphy of the British Isles. George Allen & Unwin, London. 301pp.

Anonymous, 1972, Penrose Field conference on ophiolites. Geotimes. 17, 24 - 25.

Arzi, A.A. 1978. Critical Phenomena in the rheology of partially melted rocks. Tectonophysics, 44, 178-184.

Augustilithus, S.S. 1979. Atlas of the textural patterns of basic and ultrabasic rocks and their genetric significance. de Gruyter, Berlin, 393pp.

Avé Lallemant, H.G. 1975, Mechanisms of preferred orientations of olivine in tectonite peridotite. Geology, 3, 653-656.

Avé Lallemant, H.G. & Carter, N.L. 1970. Syntectonic recrystallisation of olivine and modes of flow in the upper mantle G.S.A. Bull., 81, 2203-2220.

Avé Lallemant, H.G., Mercier, J-C.C., Carter, N.L. & Ross, J.V., 1980. Rheology of the upper mantle: inferences from peridotite xenoliths. Tectonophysics, 70, 85-113.

Bailey, E.H. 1981. Geological map of Muscat - Ibra area, Sultanate of Oman. J. Geop. Res., 86 Pocket Map.

Battey, M.H. 1960. The relationship between preferred Orientation of olivine in dunite and the tectonic environment. A.J.S., 258, 716-727.

Bell, A.M. 1979. Factorisation of finite strains in three dimensions - a computer method. J. Struct. Geol. 1, 163-167.

Benson, W.N. 1926. The tectonic conditions accompanying the intrusion of basic and ultrabasic igneous rocks. Nat. Acad. Sci. Mem., 19 Mem 1, 90pp.

Borg I.Y. & Heard, H.C. 1969. Mechanical twinning and slip in experimentally deformed plagioclase. Cont. Min. Pet., 23. 128-135.

Borg, I.Y. & Heard, H.C. 1970. Experimental deformation of plagioclase. In "Experimental and natural rock deformation'. Paulitsch Ed., Springer, Berlin, 375-403.

Bottinga, Y & Allegre, C.J. 1978. Partial melting under spreading ridges. Phil. Trans. R. Soc. Lond. A. 288, 501-525.

Bottinga, Y. & Steinmetz, L. 1979. A geophysical, geochemical, petrological model of the oceanic lithosphere. Tectonophysics, 55, 311-348.

Bouchez, J.L., Lister, G.S. & Nicolas, A., 1983. Fabric asymmetry and shear sense in movement zones. Geol. Rund. 72, 401-419.

Boudier, F. & Coleman, R.G. 1981. Cross section through the peridotite in the Samail ophiolite, southern Oman mountains. J. Geop. Res. 86. 2573-2592.

Brongniart, A. 1827. Classification et caractères mineralogique des roches homogenes et heterogenes. Levrault, F.G. Paris.

Brothers, R.N. 1959. Flow orientations of olivine. Am. J. Sci. 257, 574-584.

Brothers, R.N. 1960. Olivine nodules from New Zealand. Intern. Geol. Congr. 21st. Copenhagen, Rept. Session, Norden, 13. 68-81.

Brothers, R.N. 1964. Petrofabric analysis of Rhum and Skaergaard layered rocks. J. Petrol., 5, 255-274.

Brown, G.C. & Mussett, A.E. 1981. The inaccessible earth. George Allen and Unwin, London. 235pp.

Browning, P. 1982. The Petrology, Geochemistry, and structure of the plutonic rocks of the Oman ophiolite. Ph.D. Thesis. O.U. (Unpub).

Browning, P. & Smewing, J.D. 1981. Processes in magma chambers beneath spreading axes: evidence from magmatic associations in the Oman ophiolite. J. Geol. Soc. Lond., 138, 279-280.

Browning, P. & Lippard, S.J. 1982. Wadi Hawasina-Rustaq Oman Geological Ophiolite Project Map 4/5. Open University.

Campbell, I.H. 1977. A study of macro-rythmic layering and cumulate processes in the Jumberland intrusion, Western Australia. J. Pet., 18, 183-213.

Cann, J.R. 1970. New model for the structure of the oceanic crust. Nature, 226, 928-930.

Cann, J.R. 1974. A model for oceanic crustal structure developed. Geophys. J.R. Astron. Soc., 39. 169-187.

Carter, N.L.; Baker, D.W.; George. R.P. Jr. 1972. Seismic anisotrophy, flow, and constitution of the upper mantle. 'Flow and Fracture of Rock'. Am. Geop. Union. Geop. Mono., 16, 167-190.

Carter, N.L. & Ave Lallemant, H.G. 1970. High temperature flow of dunite and peridotite. G.S.A. Bull. 81, 2181-2202.

Casey, J.F. & Karson, J.A. 1981. Magma chamber profiles from the Bay of Islands ophiolite complex. Nature, 292, 295-301.

Cassard, D.; Nicolas, A., Rabinovitch, M., Moutte, J., Leblanc, M. & Prinzhoffer, A. 1981. Structural classification of chromite pods in southern New Caledonia. Economic Geology. 76. 805-831.

Cathles, L.M. III. 1975. The viscosity of the earth's mantle Princeton University Press, Princeton, New Jersey. 386pp.

Christensen, N.I. & Lundquist, S.M. 1982. Pyroxene orientation within the upper mantle. Geol. Soc. Bull., 93, 279-288.

Christensen, N.I. & Smewing, J.D. 1981. Geology and seismic structure of the northern section of the Oman ophiolite. J. Geop. Res. 86, 2545-2555.

Christiansen, F.G. (in prep.) Deformation fabric and micro-structures in ophiolitic chromitites and host ultramafics, Sultanate of Oman.

Coe, R.S. & Muller, W.F. 1973. Crystallographic orientation of clinoenstatite produced by deformation of orthoenstatite. Science, 180, 64-66.

Coleman, R.G. 1977. Ophiolites, ancient oceanic lithosphere? Springer-Verlag. 229pp.

Darot, M. & Bondier, F. 1975. Mineral lineations in deformed peridotites: kinematic meaning. Petrologie, I, (no.3) 225-236.

Deer, W.A., Howie, R.A. & Zussman, J. 1966. An Introduction to the rock forming minerals. Longman. 528pp.

Den Tex, E. 1969. Origin of ultramafic rocks, their tectonic setting and history: a contribution to the discussion of the paper "the origin of ultramafic and ultrabasic rocks" by P.J. Wyllie. Tectonophysics, 7 (5-6), 457-488.

Dewey, J.F. & Kidd, W.S.F. 1977. Geometry of plate accretion. G.S.A. Bull, 88, 960-968.

Dick, H.J.B. 1977. Part melting of the Josephine Peridotite I, the effect of mineral composition and its consequence for geobarometry. Am. J. Sci., 277, 801-832.

Dick, H.J.B., & Sinton, J.M. 1979. Compositional layering in alpine peridotites: evidence for pressure solution creep in the mantle. J. Geol. 87, 403-416.

Dickey, J.S. Jnr. 1975. A hypothesis of origin for podiform chromite deposits. Geochim. Cosmochim. Acta., 39, 1061-1074.

Dietz, R.S. 1961. Continent and ocean basin evolution by spreading of the sea. Nature, 190, 854-857.

Duncan, R.A. & Green, D.H. 1980. Role of multistage melting in the formation of oceanic crust. Geology 8, 22-26.

Dunnett, D. 1969. A technique of finite strain analysis using elliptical particles. Tectonophysics. 7, 117-136.

Dunnett, D. & Siddans, A.W.B. 1971. Non-random sedimentary fabrics and their modification by strain. Tectonophysics, 12. 307-325.

Durham, W.B., Goetze, C. & Blake, B. 1977. Plastic flow of oriented single crystals of olivine. II. Observations and interpretations of the dislocation structures. J. Geop. Res. 82, 5755-5770.

Fara, H.D. & Scheiddeger, A.E. 1963. An eigenvalue method for the statistical evaluation of fault plane solutions of earthquakes. Bull. Seis. Soc. Am. 53, 811-816.

Fisher, R. 1953. Dispersion on a sphere. Proc. Roy. Soc. A 217, 295-305.

Flinn, D. 1952. A tectonic analysis of the Muness phyllite block of Unst and Uyea, Shetland. Geol. Mag., 89, 263-272.

Flinn, D. 1956. On a deformation of the Funzie conglomerate, Fetlar, Shetland. J. Geol., 64. 480-505.

Flinn, D. 1958. On the nappe structure of N.E. Shetland. Q.J.G.S. Lond., 114. 107-136.

Flinn, D. 1961. On deformation at thrust planes in Shetland and in Jotunheim area of Norway. Geol. Mag., 98. 245-256.

Flinn, D. 1970. Some aspects of the geochemistry of the metamorphic rocks of Unst and Fetlar, Shetland. Proc. Geol. Ass., 81, 509-527.

Flinn, D., Frank, P.L., Brook, M. & Pringle, I.R. Basement - cover relations in Shetland. In "The Caledonides of the British Isles". Geol. Soc. Lond., pp.109-115.

Forsythe, D. & Uyeda, S. 1975. On the relative importance of the driving forces of plate motion. Geophys. J.R. Astron. Soc., 43, 163-200.

Fox, P.J., Detrick, R.S., Purdy, G.M. 1979. Evidence for crustal thinning near fracture zones: implications for ophiolites. "Ophiolites" Proc. Int. Oph. Symp. Cyprus. 161-168.

Francis, T.J.B. 1969. Generation of seismic anisotropy in the upper mantle along mid-ocean ridges. Nature 221, 162-165.

Francis, T.J.G. 1981. Serpentinization faults and their role in the tectonics of slow spreading ridges. J. Geop. Res. 86, 616-622.

Friedel, J. 1964. Dislocations. Pergamon, London.

Frost, H.J. & Ashley, M.F. 1981. Deformation mechanism maps for ceramics. Cambridge University Report. (Unpub).

Fry, N. 1979. Random joint distribution and strain measurement in rocks. Tectonophysics 60, 89-105.

Garson, M.S. & Plant, J.A. 1973. Alpine type ultramafic rocks and episodic mountain building in the Scottish Highlands. Nature Phys. Sci., 242, 34-38.

Gass, I.G. 1960. The geology and mineral resouces of the Dhali area. Cyprus Geol. Surv. Dept. Mem. No. 4., 116pp.

Gass, I.G. 1968. Is the Troodos Massif of Cyprus a fragment of Mesozoic Ocean Floor? Nature, 220. 39-42.

Gass, I.G. 1980. The Troodos massif: Its role in the unravelling of the ophiolite problem and its significance in the understanding of constructive plate margin processes. In "Ophiolites" Proc. Int. Oph. Symp. Cyprus., 1979. Panayiotou (Ed). 23-35.

Gass, I.G. & Masson-Smith, D. 1963. The geology and gravity anomalies of the Troodos massif, Cyprus. R.Soc. London Phil. Trans. A 255, 417-467.

Gass, I.G. & Smewing, J.D. 1973. Intrusion, extrusion and metamorphism at constructive margins: Evidence from the Troodos Massif, Cyprus. Nature, 242, 26-29.

Gass, I.G. & Smewing, J.D. 1980. Ophiolites: Obducted Oceanic lithosphere. In "The Sea, Volume 7: The Oceanic Lithosphere". Emiliana, C. (Ed). Wiley, New York, 339-361.

Gealey, W.K. 1977. Ophiolite obduction and geologic evolution of the Oman Mountains and adjacent areas. Bull. Geol. Soc. Am., 88, 1183-1191.

George, R.P.J. 1975. The internal structure of the Troodos ultramafic complex, Cyprus. Ph.D. Thesis (Unpub) State University, New York (Stony Brook). 196pp.

George, R.P. Jr. 1978. Structural petrology of the Olympus Ultramafic Complex in the Troodos Ophiolite, Cyprus. G.S.A. Bull. 89, 845-865.

Girardeau, J. & Nicolas, A. 1981. The Structures of two ophiolite massifs, Bay-of-Islands, Newfoundland: a model for oceanic crust and upper mantle. Tectonophysics, 77, 1-34.

Glennie, K.W., Boeuf, M.G.A., Hughes-Clarke, M., Moody-Stuart, M., Pilaar, W.F.H. & Reinhardt, B.M. 1973. Late Cretaceous nappes in Oman mountains and their geological evolution. Am. Ass. Pet. Geol. Bull., 57, 5-27.

Goetze, C. 1978. The mechanisms of creep in olivine. Phil. Trans. R. Soc. London. Ser. A., 288, 99-118.

Graham, G.M. 1980 Structure and sedimentology of the Hawasina window, Oman mountains. Unpublished Ph.D. Thesis. (O.U.). 422pp.

Green, H.W. & Gueguen, Y. 1974. Origin of kimberlite pipes by diapiric upwelling in the upper mantle. Nature, 249, 617-620.

Green, H.W. & Radcliffe, S.V. 1972. Deformation processes in the upper mantle. "Flow and fracture of rock". Am. Geop. Union. Geop. Mono, 16, 139-156.

Greenbaum, D. 1972. Magmatic process at ocean ridges: evidence from the Troodos massif, Cyprus. Nature, Phys. Sci., 238, 18-21.

Greenbaum, D. 1977. The chromitiferous rocks of the Troodos ophiolite complex, Cyprus. Econ. Geol, 72, 1175-1194.

Griggs, D.T., Turner, F.J. & Heard, H.C. 1960. Deformation of rocks at 500^{0} to 800^{0}C in rock deformation, Griggs & Handin Ed., Geol. Soc. Am. Mem., 79, 39-104.

Gueguen, Y. 1977. Dislocation in mantle peridotite nodules. Tectonophysics, 39. 231-254.

Gueguen, Y. & Darot, M. 1980. Microstructures and stresses in naturally deformed peridotites. Rock Mech. Suppl., 9. 159-162.

Hanna, S.S. & Fry, N. 1979. A comparison of methods of strain determination in rocks from S.W. Dyfed and adjacent areas. J. Struct. Geol. 1, 155-162.

Hargreaves, R.B. (Ed). 1980. Physics of magmatic processes, Princeton University Press, Princeton, New Jersey. 585pp.

Harland, W.B. & Bagley, M.B. 1958. Tectonic regimes. Geol. Mag. 95, 89-104.

Harper, G.D. 1982. Evidence for large-scale rotation at spreading centres from recrystallisation textures in olivine - bearing xenoliths Tectonophysics, 82, 25-44.

Hart, E.W. 1970. A phenomenological theory for plastic deformation of polycrystalline metals. Acta Metall., 18. 599-610.

Harte, B. 1977. Rock nomenclature with particular relation to deformation and recrystallisation textures in olivine bearing xenoliths. J. Geol. 85, 279-288.

Hess, H.H. 1955. Serpentinites, orogeny and epeirogeny. In "Crust of the Earth" Geol. Soc. Am. Spec. Paper., 62. 391-408.

Hess, H.H. 1960. Carribean Research Project: Progress Report. Bull. Geol. Soc. Am., 71, 235-240.

Hess, H.H. 1962. History of ocean basins, in petrologic studies: a volume to honour A.F. Buddington. G.S. Am., 599-620.

Hess, H.H. 1964. Seismic anistropy of the uppermost mantle under oceans. Nature, 203. 629-631.

Hext, G.R. 1963. The estimation of seond-order tensors, with related tests and designs. Biometrika, 50, 353-373.

Hobbs, B.E., Means, W.D. & Williams, P.F. 1976. An outline of structural geology. John Wiley & Sons Inc. 571pp.

Hopson, C.A., Coleman, R.G., Gregory, R.T., Pallister, J.S. & Bailey, E.H., 1981. Geologic section through the semail ophiolite and associated rocks along a muscat - Ibru Transect. S.E. Oman mountains. J. Geop. Res. 86, 2527-2544.

Hsu, T.C. 1966. The characteristics of coaxial and non-coaxial strain paths. J. Strain Anal. 1, 216-222.

Irvine, T.N. 1980. Magmatic infiltration metasomatism, double-diffusive fractional crystallisation, and adcumulus growth in the Muskox intrusion and other layered intrusions in "Physics of magmatic processes". Hargreaves, R.B. (Ed). Princeton University Press, 325-384.

Jackson, E.D. 1961. Primary textures and mineral associations in the ultramafic zone of the Stillwater Complex, Montana. U.S. Geol. Surv. Prof. Paper, 358, 1-106.

Jackson, M. 1979. Structures des filons dans les massifs de peridotite: mecanismes d'injection et relations avec la deformation plastique. These Doct. Spec. Univ. Nantes. (Unpub).

Jackson, E.D. Green, H.W. II & Moores, E.M. 1975. The Vourinos ophiolite,Greece: cyclic units of lineated cumulates overlying harzburgite tectonite. Geol. Soc. Am. Bull., 86, 390-398.

Jackson, E.D. & Thayer, T.P. 1972. Some criteria for distinguishing between stratiform, concentric and alpine peridotite - gabbro complexes. 24th I.G.C. Section 2. 289-296.

Juteau, T., Nicolas, A., Dubessy, J., Fruchard, J.C. & Bouchez, J.L. 1977. Structural relationships in the Antalya ophiolite complex, Turkey: possible model for an oceanic ridge. G.S.A. Bull, 88, 1740-1748.

Kamb, W.B. 1959a. Ice petrofabric observations. J. Geop. Res., 64, 1891-1909.

Kamb, W.B. 1959b. Theory of preferred orientation developed by crystallisation under stress. J. Geol., 67. 153-170.

Karato, S.1., Toriurui, M. & Huju, T. 1982. Dynamic recrystallisation and high temperature rheogoly of olivine in : S. Akimoto and M.H. Manghnani (Ed) High Pressure Research in Geophysics. Proceedings of US-Japan seminar, Hakone, Japan, January, 1981. Center for Academic Publications, Tokyo, pp171-189.

Key, R.M. 1972. A study of the metamorphic histories of the Saxa Vord, Valla Field and Lamb Hoga Blocks of north-east Shetland. Ph.D. Thesis (Unpub). University of Liverpool.

Kidd, G.W. 1977. A model for the process of formation of the upper oceanic crust. Geophys. J.R. Astr. Soc., 50. 149-183.

Kidd, G.W. & Cann, J.W. 1974. Chilling statistics indicate an ocean floor spreading origin for the Troodos complex, Cyprus. Earth Planet. Sci. Lett., 24, 151-155.

Kirby, S.H. & Raleigh, C.B. 1973. Mechanisms of high temperature, solid state flow in minerals and ceramics and their bearing on the creep behaviour of the mantle. Tectonophysics, 19, 165-194.

Kohlstedt, D.L. Goetze, C. 1974. Low stress, high temperature creep in olivine single crystals. J. Geop. Res., 79, 2045-2051.

Kohlstedt, D.L. & Van Der Sande, J.B. 1973. Transmission electron microscopy investigation of the defect microstructure of four natural orthopyroxenes. Contr. Mineral and Petrol, 42, 169-180.

Kunze, F.R. & Ave Lallemant, H.G. 1981. Non-coaxial experimental deformation of olivine. Tectonophysics 74, T1-T13.

Langseth, M.G., Le Pichon, X., & Ewing, M. 1966. Crustal structures of midocean ridges. J. Geop. Res., 71, 6351-6356.

Leblanc, M. 1978. Petrographie et geochimie des chromites de Nouvelle Caledonie; essai sur l'evolution des peridotites et la genese des corps chromiferes. Acad. Sci. Paris comptes rendus, 287, 771-774.

Lees, G.M. 1928. The geology and tectonics of Oman and parts of south - eastern Arabia. Quart. J. Geol. Soc. Lond., 84(4), 585-670.

Lippard S.J. (Ed) 1980. Wadi Jizi Oman geological ophiolite project map 2. Open University.

Lippard, S.J. 1981. Sheeted dyke analysis N. Oman (Unpub).

Lippard, S.J. & Rothery, D.A. (Eds). 1981. Wadi Ahin - Yangul Oman geological ophiolite project map 3. Open University.

Lippard, S.J. & Rothery, D.A. 1983. Open University Oman ophiolite project, memoir map. Open University.

Loney, R.A., Hommelberg, G.R. & Coleman, R.G, 1971. Structure and petrology of the alpine type peridotite at Burro mountain, California. U.S.A. J. Pet., 12, 245-309.

Malpas, J. 1977. Petrology and tectonic significance of Newfoundland ophiolites with examples from the Bay of Islands. North Am. ophiolites Bull., 95, 13-23

McKenzie, D.P. 1967. Some remarks on heat flow and gravity anomalies. J. Geop. Res., 72, 6261-6273.

McKenzie, D.P. 1969. Speculations on the consequences and causes of plate motions. Geophys. J.R. Astr. Soc., 18, 1-32.

McQuillin, R. & Brooks, M. 1967. Geophysical surveys in the Shetland Islands. Inst. Geol. Sci. (U.K). Geophys. Paper 2, 22pp. HMSO.

Means, W.D., Hobbs, B.E., Lister, G.S. & Williams, P.F. 1980. Verticity and non-coaxiality in progressive deformations. J. Struct. Geol. 2, 371-378.

Menzies, M. & Allen, C. 1974. Plagioclase lherzolite residual mantle relationships within two eastern Mediterranean ophiolites. Cont. Min. Pet. 45, 197-213.

Miller, J.A. & Flinn, D. 1966. A survey of the age relations of Shetland Rocks. Geol. J. 5, 95-116.

Milton, N.J. 1980. Determination of the strain ellipsoid from measurement on any three sections. Tectonophysics, 64, T19-T27.

Moores, E.M. & Vine, F.J. 1971. The Troodos Massif, Cyprus and other ophiolites as oceanic crust: evaluation and implications. Phil. Trans. R. Soc. Lond. A 268, 443-466.

Morgan, W.J. 1972. Deep mantle convection plumes and plate motions. Bull. Am. Assoc. Pet. Geol. 56, 203-213.

Mykura, W. 1976. British regional geology Orkney and Shetland. Edinburgh: HMSO. 149pp.

Mügge , D. 1898. Uber translation und verwandte erscheinungen in kristallen. Neues Jahrb. Min. Geol. Pal., 1, 71-158.

Nabarro, F.R.M. 1967. Steady state diffusional creep. Phil. Mag., 16, 231-237.

Nadai, A. 1963. Theory of flow and fracture of solids. Vol 2. pp.705. New York, McGraw-Hill.

Nicolas, A. 1976. Flow in upper-mantle rocks: some geophysical and geodynamic consequences. Tectonophysics 32, 93-106.

Nicolas, A., Bouchez, J.L., Boudier, F., & Mercier, J.C. 1971. Textures, structures and fabrics due to solid state flow in some European lherzolites. Tectonophysics, 12, 55-86.

Nicolas, A., Bouchez, J.L. & Boudier, F. 1972. Interpretation cinematique des deformations plastiques dans le massif de lherzolite de Lanzo (Alpes Piemontaises) - Comparaison avec d'autres massifs. Tectonophysics 14, 143-171.

Nicolas, A., Boudier, F. & Boullier, A.M. 1973. Mechanisms of flow in naturally and experimentally deformed peridotites. A.J.S. 273, 853-876.

Nicolas, A. & Boudier, F. 1975. Kinematic interpretation of folds in alpine-type peridotites. Tectonophysics 25, 233-260.

Nicolas, A. & Poirier, J.P. 1976. Crystalline plasticity and solid state flow in metamorphic rocks. John Wiley & Sons. 444pp.

Nicolas, A, Boudier, F., Bouchez, J.L. 1980. Interpretation of peridotite structures from ophiolitic and oceanic environments. Am. J. Sci. 280A [Jackson volume] 192-210.

Nicolas, A. & Jackson, M. 1982. High temperature dykes in peridotites: origin by hydraulic fracturing. J. Pet., 33, 568-587.

Nicolas, A. & Violette, J.F. 1982. Mantle flow at oceanic spreading centres: models derived from ophiolites. Tectonophysics 81, 319-339.

Nicolas, A. & Prinzhofer, A. 1982. Cumulative or residual origin for the transition zone in ophiolites: structural evidence. J. pet., 24, part 2, 188-206.

Odling, N.E. 1980. Structural, textural and metamorphic studies in the Lewisian of Gairloch, N.W. Scotland. Ph.D. (Unpub). Edinburgh.

O'Hara, M.J., Saunders, M.J. & Mercy, E.L.P. 1975. Garnet-peridotite primary ultrabasic magma and eclogite: interpretation of upper-mantle processes in kimberlite. Phys. Chem. Earth, 9, 571-604.

Owens, W.H. 1974. Mathematical model studies on factors affecting the magnetic anistropy of rocks. Tectonophysics. 24, 115-131.

Pallister, J.S. 1981. Structure of the sheeted dyke complex of the semail ophiolite near Ibra, Oman. J. Geop. Res., 86, 2661 - 2672.

Pallister, J.S. & Hopson, C.A. 1981. Semail ophiolite plutonic suite: field relations, phase variation, cryptic variation and layering, and a model of a spreading ridge magma chamber. J. Geop. Res. 86, 2593-2644.

Parker, R.L. & Jackson, M. 1982. High temperature dykes in peridotites: origin by hydraulic fracturing. J. Pet. 33, 568-587.

Pearce, J.A., Alabaster, T., Shelton, A.W., Searle, M.P. 1981. The Oman ophiolite is a Cretaceous arc-basin complex: evidence and implications. Phil. Trans. R. Soc. Lond. A300, 299-317.

Peselnick, L. & Nicolas, A. 1978. Seismic anistropy in an ophiolite peridotite: application to oceanic upper mantle. J. Geop. Res., 83, 1227-1235.

Phemister , J. 1963. Geological survey of Great Britain (Scotland) Quarter inch sheets 1 and 2. Ordnance Survey.

Phillips, W.R. 1971. "Mineral Optics" pp171-230. W.H. Freeman and Co., San Fransisco .

Poirier, J.P. 1975. On the slip systems of olivine, J. Geop. Res., 80, 4059-4061.

Poirier, J.P. & Nicolas, A. 1975. Deformation induced recrystallisation due to progressive misorientation of subgrains, with special reference to mantle peridotites. J. Geol., 83, 707-720.

Poirier, J.P. & Guillope, M. 1979. Deformation induced recrystallisation of minerals. Bull. Mineral. 102, 67-74.

Post, R.L. 1977. High temperature creep of Mt. Burnet dunite. Tectonophysics, 42, 75-110.

Prichard, H.M. 1982. The chromite of the Shetland ophiolite. A reappraisal in the light of new theory and techniques. A report for the Commission of European Communities. Open University. 264pp.

Prichard, H.M. & Spray, J.G. (In prep). The Shetland ophiolite N.E. Scotland: evidence for Lower Ordovician tectonic displacement from an island arc setting.

Prinzhoffer, A., Nicolas, A., Cassard, D., Moutte, J., Leblanc, M., Poirier, J.P., & Robinovitch, M., 1980. Structures in the New Caledonia peridotites- gabbros: implications for oceanic mantle and crust. Tectonophysics, 69, 85-112.

Prinzhoffer, A. & Nicolas, A. 1980. The Bogota Peninsula, New Caledonia: a possible oceanic transform fault. J. Geol., 88, 387-398.

Project ROSE Scientists, 1981. Microearthquake activity on the Orozocofracture zone: preliminary results from project ROSE. J. Geop. Res., 86, 3783-3790.

Raleigh, C.B. 1968. Mechanisms of plastic deformation of olivine. J. Geop. Res., 73, 5391-5406.

Raleigh, C.B. & Kirby, S.H. 1980. Creep in the upper mantle. Min. Soc. Am. Spec. Pap., 3, 113-121.

Ramsay, J.G. 1967. Folding and fracturing of rocks. McGraw-Hill Book Compary. 568pp.

Read, H.H. 1934. The metamorphic geology of Unst in the Shetland Islands. Mineral Mag., 23, 519-540.

Read, H.H. 1936. The metamorphic history of Unst, Shetland. Proc. Geol. Ass., 47, 283-293.

Reinhardt, B.M. 1969. On the genesis and emplacement of ophiolites in the Oman mountains geosyncline. Schweiz. Min. Pet. Mitt., 49/1, 1-30.

Robertson, A.H.F. 1977a. The Moni melange, Cyprus: an olistostrome formed at a destructive plate margin. J. Geol. Soc. Lond., 133, 447-466.

Robertson, A.H.F. 1977b. Tertiary uplift history of the Troodos Massif, Cyprus. Geol. Soc. Amer. Bull., 88j 1763-1772.

Robertson, A.H.F. & Woodcock, N.H. 1980. Tectonic setting of the Troodos massif in the east Mediderranean. In Proc. Int. Oph. Symp. Cyprus, Panayiotou A. (Ed). 36-49.

Robertson, A.H.F. & Woodcock, N.H. 1983. Genisis of the Batinah melange above the semail ophiolite, Oman. J. Struct. Geol. 5, 1-17.

Ross, J.V., Mercier, J-C.C., Avé Lallemant, H.G., Carter, N.L. & Zimmerman, J. 1980. The Vourinos ophiolite complex, Greece: the tectonic suite. Tectonophysics, 70, 63-83.

Ross, J.V. & Nielson, K.C. High temperature flow of wet polycrystalline enstatite. Tectonophysics 44, 233-261.

Rothery, D.A. 1982. The evolution of the Wuqbah Block and the application of remote sensing in the Oman ophiolite. Ph.D. Thesis. O.U. (Unpub). 414pp.

Scheidegger, A.E. 1964. The tectonic stress and tectonic motion direction in Europe and Western Asia as calculated from earthquake fault plane solutions. Bull. Seis. Soc. Am. 54, 1519-1528.

Scheidegger, A.E. 1965. On the statistics of the orientation of bedding planes, strain axes and similar sedimentological data. U.S. Geol. Surv. Prof. Paper, 525-C, 164-167.

Searle, M.P. 1980. The metamorphic sheet and underlying volcanic rocks beneath the semail ophiolite in the northern Oman mountains of Arabia. Ph.D. Thesis. O.U. (Unpub). 213pp.

Searle, M.P. & Malpas, J. 1981. Structure and metamorphism of rocks beneath the semail ophiolite of Oman and their significance in ophiolite obduction. Trans. R. Soc. Edinburgh., 71, 247-262.

Searle, D.L. & Panayiotou, A. 1980. Structural Implications in the evolution of the Troodos Massif, Cyprus. "Ophiolites". Proc. Int. Oph. Symp. Cyprus , 1979 Panayiotou, A. (Ed). 50-60.

Shelton, A. & Gass, I.G. 1980. Rotation of the Cyprus microplate. In "Ophiolites" Int. Oph. Symp. Cyprus, 1979, Panayiotou, A. (Ed). 61-65.

Shimamoto, T. & Ikeda, Y. 1976. A simple algebraic method for strain estimation from deformed ellipsoidal objects. I. Basic theory. Tectonophysics, 36. 315-337.

Siddans, A.W.B. 1980. Analysis of 3-D homogeneous, finite strain using ellipsoidal objects. Tectonophysics, 64, 1-16.

Simonian, K.O. & Gass, I.G. 1978. The Arakapas fault belt, Cyprus: a fossil transform fault. Geol. Soc. Amer. Bull., 89, 1220-1230.

Sleep, N.H. 1975. Formation of oceanic crust: some thermal constraints, 80, No 29, 333-334.

Sleep, N.H. & Rosendahl, B.R. 1979. Topography and tectonics of mid-ocean ridge axes. J.G.R. 84, 6831-6839.

Smewing, J.D. 1975. Metamorphism of the Troodos massif, Cyprus. Ph.D. Thesis (Unpub). O.U. 267pp.

Smewing, J.D. 1979. The Sumeini-shinas Area. Oman Geological ophiolite Project Map 1. Open University.

Smewing, J.D. 1980. An upper cretaceous ridge transform intersection in the Oman ophiolite. In "Ophiolites" Proc. Int. Ophiolite Symp. Cyprus, 1979, Panayiotou (Ed)., 407-413.

Smewing, J.D. 1981. Mixing characteristics and compositional differences in mantle-derived melts beneath spreading axes: evidence from cyclically layered rocks in the ophiolite of north Oman. J. Geop. Res. 86. 2645-2659.

Smewing, J.D., Christensen, N.I., Bartholomew, I.D., & Browning, P. 1983. The structure of the oceanic upper mantle and lower crust in the northern section of the Oman ophiolite. (in press). Spec. pub. Geol. Soc. Lond. "Ophiolites and Oceanic Lithosphere".

Steinmann, F. 1905. Geologische beobachtungen in den Alpen. II die schardt'sche uber faltungstheorie und die geologische bedeutung der tiefsecabsatze und der ophiolitischen massengesteine: Ber. Nat. Ges. Freiburg, i, Bal. 16. p. 44-65.

Stocker, R.A. & Ashby, M.F. 1973. On the rheology of the upper mantle. Rev. Geop. & Space Phys., 11, 391-426.

Streckeisen, A. 1976. To each plutonic rock its proper name. Earth Sci. Review, 12, 1-33.

Sturt, B.A., Roberts, D. & Fumes, H. 1983. A conspectus of Scandinavian Caledonian ophiolites. (In press). J. Geol. Soc. Lond. Spec. Pub. on ophiolites and oceanic lithosphere.

Suen, C.J., Frey, F.A. & Malpas, J. 1979. Bay-of-Islands ophiolite suite, Newfoundland, petrological and geochemical characteristics with emphasis on rare-earth element geo-chemistry. Earth and Planetary Sci. Lett., 45, 337-348.

Swarbrick, R.E. 1980 The Momonia complex of S.W. Cyprus: a Mesozoic continental margin and its relationship to the Troodos complex. In "Ophiolites". Proc. Int. Oph. Sym. Cyprus, 1979. Panayiotou (Ed). 86-92.

Thayer, T.P. 1960. Some critical differences between alpine-type and stratiform peridotite-gabbro complexes. 21st. Int. Geol. Cong. Copenhagen, Repts. 13. 247-259.

Thayer, T.P. 1980. Syncrystallisation and sub-solidus deformation in ophiolitic peridotite and gabbro. A.J.S., 280-A, 269-283.

Thayer, T.P. & Jackson, E.D. 1972. A classification of igneous rocks by their history of crystallisation and emplacement. U.S. Geol. Survey. Prof. Paper. 800-B, 79-83.

Turner, F.J., Heard, H.C. & Griggs, D.T. 1960. Experimental deformation enstatite and accompanying inversion to clino-enstatite. Int. Geol. Congress XXI Sess. Copenhagen, XVIII, 399-408.

Twiss, R.J. 1976. Structural superplastic creep and linear viscosity in the earth's mantle. Earth and Planetary Sci. Lett., 33, 86-100.

Verma, R.K. 1960. Elasticity of some high density crystals. J. Geop. Res. 65, 757-766.

Vine, F.J. & Matthews, D.H. 1963. Magnetic anomalies over oceanic ridges. Nature, 199, 947-949.

Violette, J-F. 1980. Structure des ophiolites des Phillipines et de Chypre. - Ecoulement asthenospherique sous les zones d'expansion oceaniques. Ph.D. Thesis. Universite de Nantes (Unpub). 152pp.

Vogt. P.R. 1976. Plumes, subaxial flow and topography along the mid-oceanic ridge. Earth and Planetary Sci. Lett., 29, 309-325.

Vogt, P.R. & Jackson, G.L. 1975. Transform faults and longitudinal flow below the mid-ocean ridge. J. Geop. Res. 80, 1399-1428.

Watson, G.S. 1965. Equatorial distributions on a sphere. Biometrika 52, 193-201.

Watson, G.S. 1966. The statistics of orientation data. J. Geol., 74, 786-797.

Weertman, J. 1968. Dislocation climb theory of steady state creep. Trans. Amer. Soc. Metals, 61, 681-694.

White, S.H. 1979. Difficulties associated with paleostress estimates. Bull. Mineral, 102, 210-215.

Williams, H. & Smyth, W.R. 1973. Metamorphic aureoles beneath ophiolite suites and alpine peridotites: tectonic implications with West Newfoundland examples. A.J.S., 273, 594-621.

Wilson, R.A.M. 1959. The geology of the Xeros-Troodos area. Cyprus. Geol. Surv. Dept. Mem. No.1., 135pp.

Woodcock, N.H. 1977. Specification of fabric shapes using an eigenvalue method. G.S.A. Bull., 88, 1231-1236.

Woodcock, N.H. & Robertson, A.H.F. 1982. Stratigraphy of the Mesozoic rocks above the Semail ophiolite, Oman. Geol. Mag. 119, 67-76.

Zeuch, D.H. 1980. The dislocation substructure of experimentally deformed synthetic dunite. Ph.D. Diss. Univ. California, Davis, California.

Zeuch, D.H. 1983. On the inter-relationship between grain size sensitive creep and dynamic recrystallisation of olivine. Tectonicphysics, 93, 151-168.

Zeuch, D.H. & Green, H.H.W., 1979. Experimental deformation of an "anhydrous" synthetic dunite. Bull. Mineral, 102, 185-187.

Zingg, T. 1935. Beitrag zur schotteraralyse. Schweiz. Min. Pet. Mitt., 15, 39-140.